A NONLINEAR/INELASTIC ROOFTOP

TUNED MASS DAMPER FRAME

by

Jerod Greg Johnson

A dissertation submitted to the faculty of
The University of Utah
in partial fulfillment of the requirements for the degree of

Doctor of Philosophy

Department of Civil and Environmental Engineering

The University of Utah

May 2012

The University of Utah Graduate School

STATEMENT OF DISSERTATION APPROVAL

The dissertation of **Jerod Greg Johnson**

has been approved by the following supervisory committee members:

Chris P. Pantelides	, Chair	**12/12/2011** Date Approved
Steven F. Bartlett	, Member	**12/12/2011** Date Approved
Rebecca M. Brannon	, Member	**12/12/2011** Date Approved
Lawrence D. Reaveley	, Member	**12/12/2011** Date Approved
Paul J. Tikalsky	, Member	**12/12/2011** Date Approved

and by **Paul J. Tikalsky**, Chair of the Department of **Civil and Environmental Engineering**

and by Charles A. Wight, Dean of The Graduate School.

ABSTRACT

Reduction of a building's response to earthquake ground motion has been the focal point behind considerable research and structural engineering innovation in recent decades. For many years, engineers have understood that altering a structure's fundamental period offers the greatest opportunity for reducing its response to seismic ground motion. Innovations such as base isolation have been developed which enable a building's fundamental period to be out-of-phase with the soil dependent dynamic properties of the site, the result being a significant reduction of seismic accelerations, forces and overall damage. Other approaches utilize highly ductile structural frames which offer the benefit of sustaining service loads while being subjected to significant lateral distortion. Such systems enable lengthening of the fundamental period of the structure during nonlinear response which typically reduces the acceleration response. Furthermore, ductile systems utilize creative methods to dissipate earthquake energy in a stable manner to prevent the earthquake input energy from causing damage at sensitive regions of structural assemblies. Creative applications of mass and stiffness utilized as penthouse enclosures at the rooftop of structures offer the potential for changing a building's structural dynamic properties. This method has been termed a rooftop tuned mass damper frame (RTMDF). The incorporation of specific yielding mechanisms within these structures offers the potential of further modifying a structure's dynamic properties while also introducing methods for increased energy dissipation. The net

result of this method is an inexpensive retrofit measure to improve the seismic performance of existing structures. The method also offers the potential for improving the expected performance of new structures or reducing construction costs of the seismic system.

This research investigates the effectiveness of buckling restrained braces in rooftop tuned mass damper frames for reducing seismic response. This approach could be implemented for a relatively low cost at the roof of the suited structure. It will have the benefit of introducing designated yielding members (DYM's) for seismic energy dissipation in a controlled manner and will create an opportunity to lengthen the fundamental period of the original structure. These effects are complementary and offer the potential for reduction of seismic acceleration response and reduction of earthquake demand on the base structure.

TABLE OF CONTENTS

Page

Page

ACKNOWLEDGEMENTS

The author acknowledges Dr. Larry Reaveley for his passion for research and continuous encouragement, Dr. Chris Pantelides for effective teaching in countless classes and Stephanie, Logan, Brigham, Sydney and Lyndsey Johnson for years of patience, tolerance and support in this endeavor.

1 INTRODUCTION

Over the past 80 years, seismic resistant design for the built environment has emerged to be among the greatest structural engineering innovations of the modern age. In developed societies with modern infrastructure, major earthquakes claim significantly fewer lives when compared to prior generations. Humankind's understanding of earthquake mechanisms and seismic ground motions is continually advancing. Furthermore, the understanding of how buildings respond to earthquakes continues to increase. This understanding offers the opportunity for specific and deliberate design of structures to mitigate potential loss. Despite the innovations and improvements in the field of earthquake engineering, major earthquakes still claim lives and billions of dollars in repair costs following large events. This is true even in developed areas of the world. An example of this is the Northridge 1994 Earthquake, which despite striking at a well-developed area with modern infrastructure, holds the distinction of being the most costly earthquake in the history of the United States.[1] The repair costs associated with this event were certainly associated with structural systems but to an even larger degree for nonstructural elements and components along with building contents. Consequently, new technologies, innovations, and improved design methods are always under development and construction procedures are continually improving. The research presented herein demonstrates the potential for the creative adaptation of existing technologies to reduce earthquake demand for either new construction or as a seismic rehabilitation strategy.

The approach is to utilize a nonlinear/inelastic rooftop tuned mass damper frame (NRTMDF) which will double as the penthouse enclosure, a common feature utilized for many structures to house mechanical equipment. The research will focus on two key aspects of the rooftop tuned mass damper frame which dramatically affect the performance of the global structure. First, the NRTMDF will enable the lengthening of the building's fundamental period. The reduction of earthquake response due to a lengthened period is a well established fact for most seismically active regions of the world and is even found within the prescriptive requirements of contemporary codes for new construction.[2] Figure 1.1 illustrates this concept using the response spectrum developed from a N-S component of the acceleration record of the May 18, 1940 El Centro Earthquake. Figure 1.2 also demonstrates this for the spectrum representing a typical design scenario. As shown, a lengthened period results in a decrease of the acceleration response. Second, the NRTMDF offers the opportunity for introducing a deliberate earthquake input energy dissipating mechanism within the structure. Earthquake input energy that is dissipated in a controlled and stable yielding mechanism will not be free to propagate through the structure and cause damage either directly or by triggering progressive failure. In fact, all of the energy dissipated in the yielding mechanism may be considered as a net seismic energy reduction (reduced seismic demand) on the base structure.

In a fundamental sense the lengthening of a period enabled by the NRTMDF can be observed through examination of simple inverted pendulum systems. Figure 1.3 demonstrates a single degree of freedom system with the structural mass (m) and stiffness (k) represented accordingly. Classical dynamic theory predicts the frequency (ω) of this

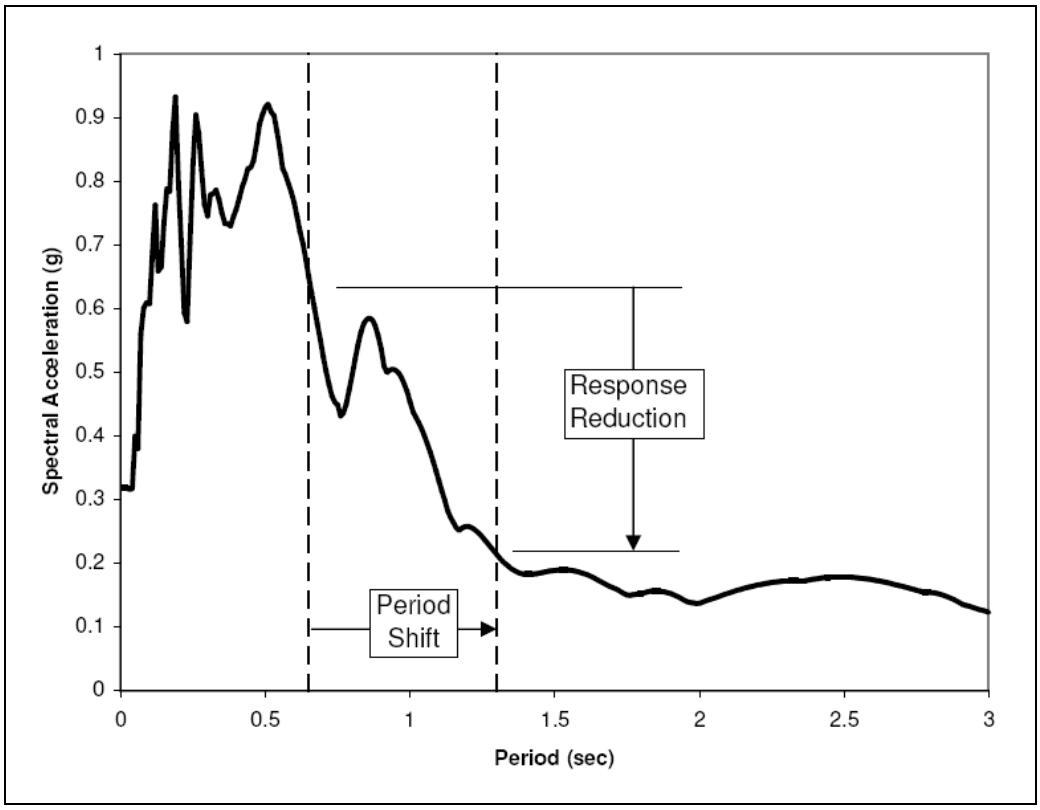

Figure 1.1 El Centro 1940 N-S Component 5% Damped Response Spectrum

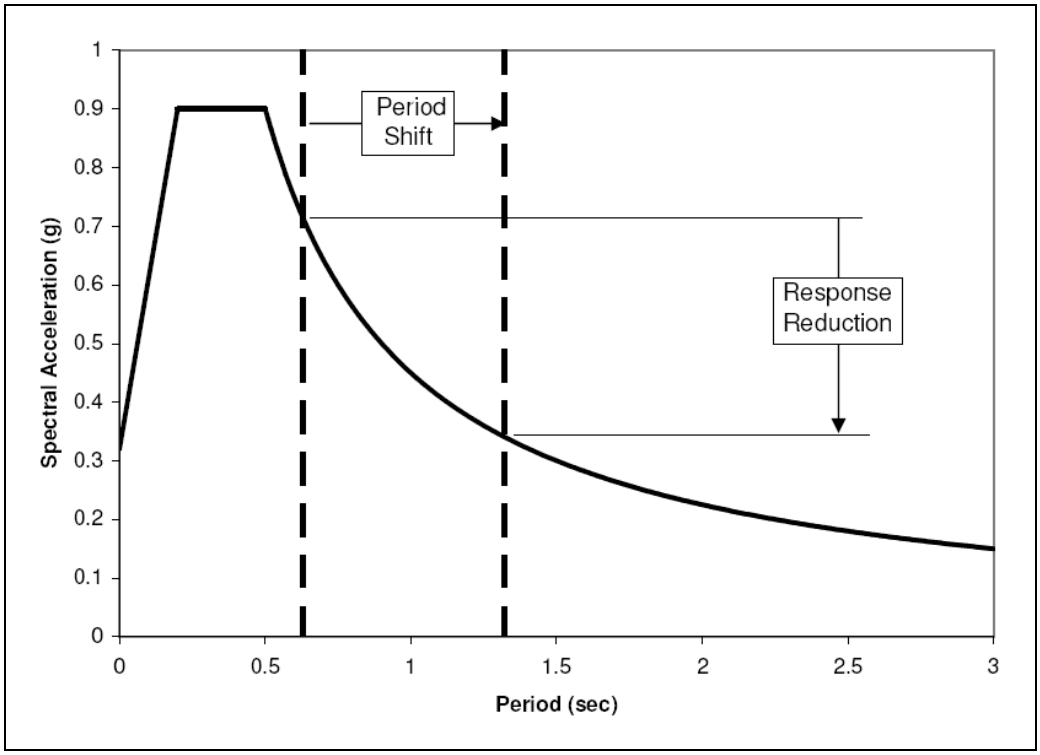

Figure 1.2 5% Damped Design Spectrum with Period Shift

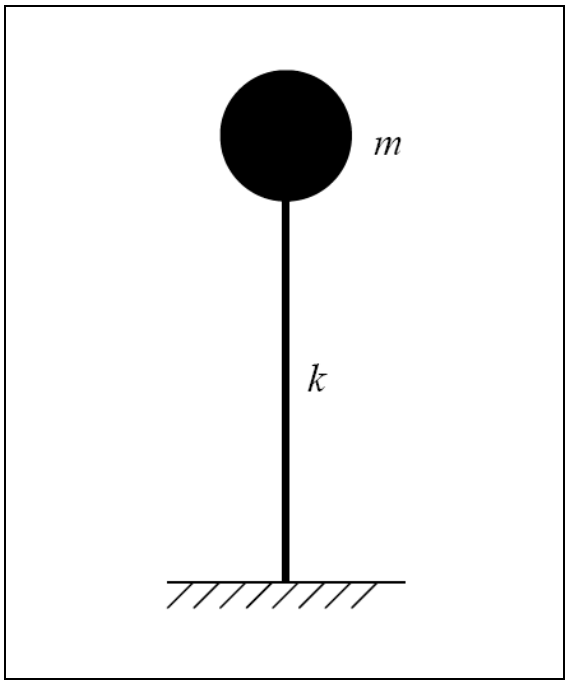

Figure 1.3 Inverted Pendulum System

system through eigenvalue solution presented in Equation 1-1. From this the frequency can be converted to the structural period and the relationship can be derived as presented in Equation 1-2.

$$\det\left[k - \omega^2 m\right]=0 \qquad \text{Eq. 1-1}$$

$$T = 6.28\sqrt{\frac{m}{k}} \qquad \text{Eq. 1-2}$$

Fundamentally, Equation 1-2 demonstrates that period lengthening can be enabled with an increase in mass and/or a decrease in stiffness. Since alteration of mass or stiffness in an existing structure is not often a pragmatic approach, the NRTMDF enables an effective lengthening of period with the addition of mass at the penthouse and softening effect by virtue of the reduced effective stiffness of the NRTMDF as compared to the typical story stiffness of the structure. This approach is conceptually demonstrated with the simplified representation of Figure 1.4 which depicts the inverted pendulum system

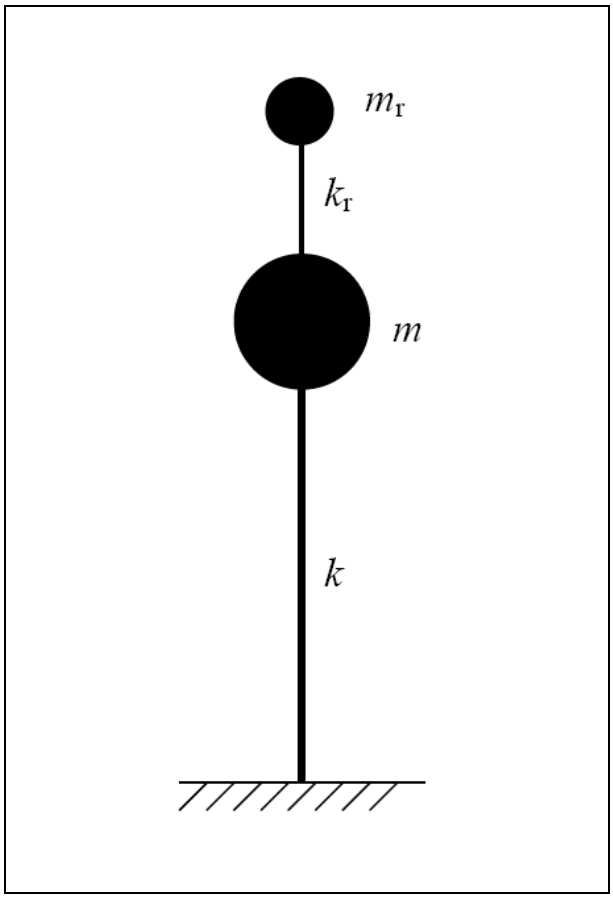

Figure 1.4 Inverted Pendulum with NRTMDF

altered with the NRTMDF with mass represented as m_r and stiffness represented as k_r. For this, the mass and stiffness are represented with the simple matrices of Equations 1-3 and 1-4 with the mass and stiffness of the NRTMDF represented as 1/10 the mass and stiffness of the original (undamped) system.

$$M = \begin{bmatrix} m & \\ & m/10 \end{bmatrix} \qquad \text{Eq. 1-3}$$

$$K = \begin{bmatrix} 11k/10 & -k/10 \\ -k/10 & k/10 \end{bmatrix} \qquad \text{Eq. 1-4}$$

Solving for fundamental frequencies using Equation 1-1 yields a fundamental (mode 1) period represented by Equation 1-5 and a mode 2 period represented by Equation 1-6.

$$T_1 = 7.35\sqrt{\frac{m}{k}} \qquad \text{Eq. 1-5}$$

$$T_2 = 5.36\sqrt{\frac{m}{k}} \qquad \text{Eq. 1-6}$$

Hence, the approach utilizing fundamental concepts demonstrates the potential for lengthening of fundamental (mode 1) period that can be enabled using the NRTMDF. Likewise, this demonstrates the development or enhancement of mode 2 behavior which creates a counteracting inertial effect where the NRTMDF moves opposite the primary structure as depicted in Figure 1.5.

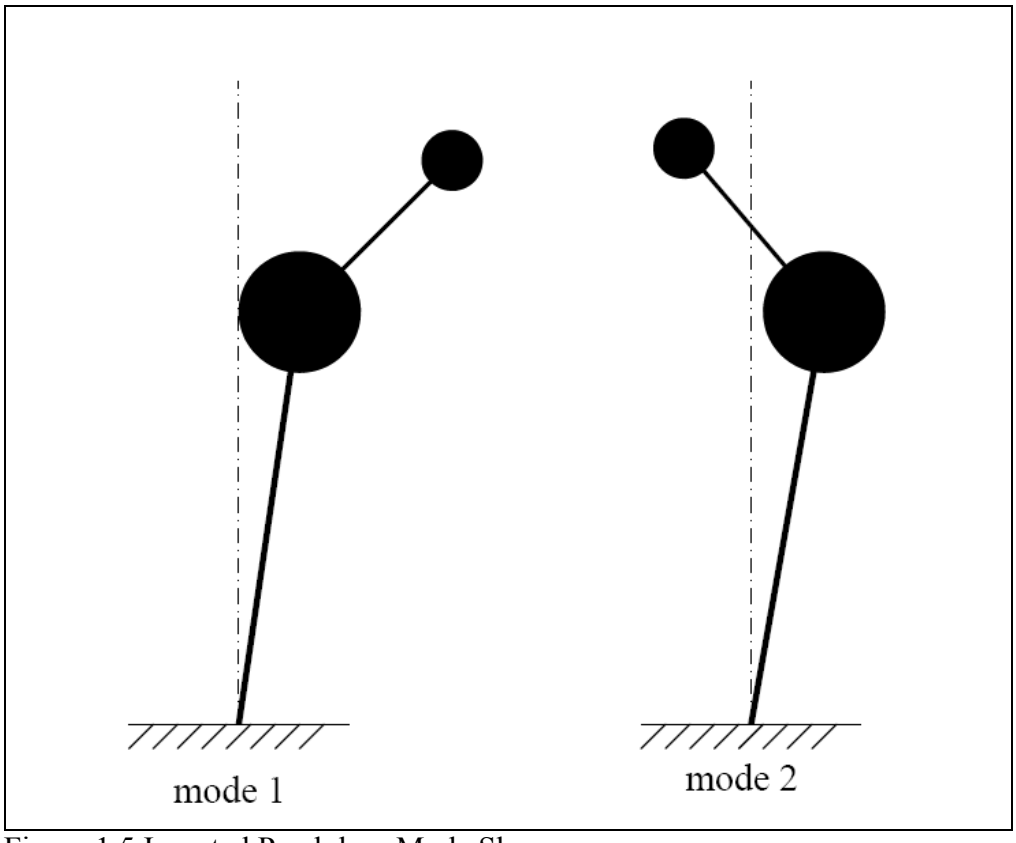

Figure 1.5 Inverted Pendulum Mode Shapes

The concept of requiring ductility in structural systems has been a feature of building codes for many years. When properly incorporated, ductility has the effect of creating increased hysteretic damping within the system. This can be qualitatively represented as a diminished response spectrum as shown in Figure 1.6 which also demonstrates the effect of nonlinear period shift enabled due to the softening effect driven by ductile behavior of the NRTMDF. When considered in tandem, the nonlinear period shift and increased hysteretic damping provide an effective approach for response reduction.

Code developers have realized that requiring ductile behavior is the most economically viable approach for building safe structures in regions of moderate to high

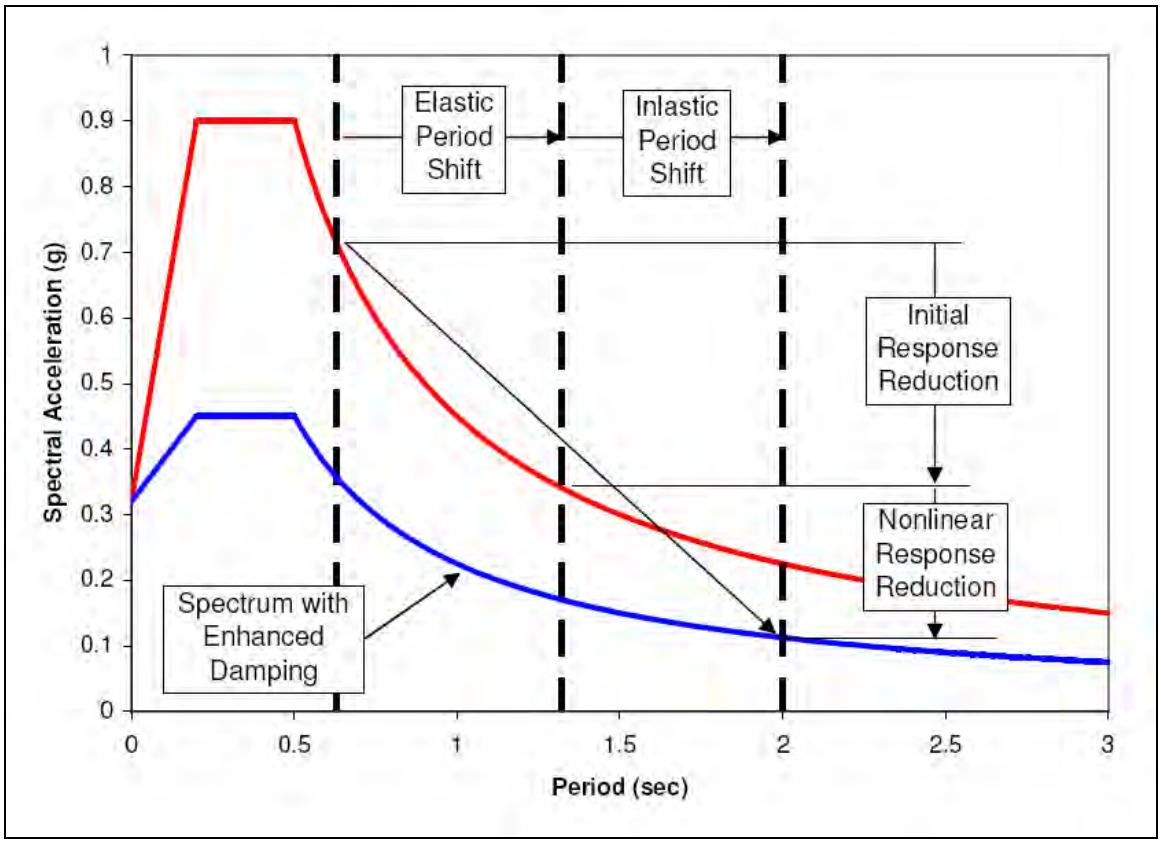

Figure 1.6 Design Spectra with Enhanced Damping and Period Shifts

seismicity. The concept of ductility in structural systems has long been understood but only recently have the behaviors of ductile yielding mechanisms become the focal point behind high performance seismic systems, particularly within the context of performance based seismic design (PBSD). Whereas past prescriptive codes typically addressed ductility on a global scale for the structural system, contemporary codes show more tendencies toward specific energy dissipating and yielding mechanisms. Current PBSD methods typically account for specific and deliberate elements to dissipate energy in a stable and controlled manner. Common among such systems is the special moment frame, which under contemporary codes and PBSD procedures, utilizes specific and deliberate design and detailing to accommodate plastic hinging of the beam near the beam-column connections of a building. Eccentric braced frames incorporate ductility with a shear link in a beam driven by axial forces from connecting braces. Buckling restrained braces (BRB's) focus ductility into a yielding core.[3,4] Perforated plate connections enable ductility with shear distortions through a perforated plate fuse.[5] These systems offer the benefit of symmetric hysteretic behavior while dissipating energy through cyclic action in a stable, localized, controlled and targeted manner. Among these, the buckling restrained braced frame has emerged as one of the most promising ductile seismic concepts in recent years. It offers the benefit of performing hysteretically with the axial element lengthening and shortening elastically and inelastically. Upon being subjected to reversing cycles of strain, BRB's dissipate considerable seismic energy as the braces experience repeated cycles of elasto-plastic tension and compression. This is demonstrated in the idealized hysteretic relationship of Figure 1.7, which is meant to represent typical BRB Behavior. For this, the effective energy

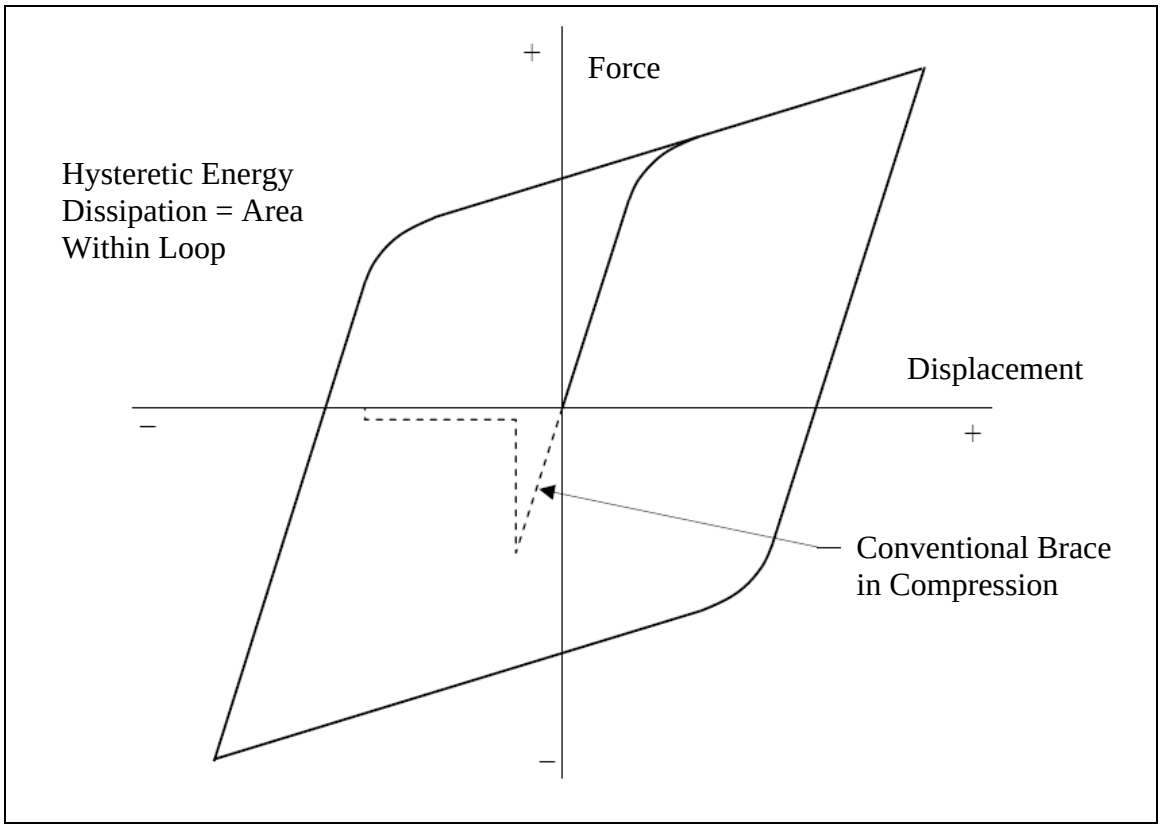

Figure 1.7 Typical Buckling Restrained Brace Hysteretic Behavior

dissipated within each cycle can be quantified as the area within the hysteresis loop. The effectiveness of the BRB stems from axial loading action of the yielding core, enabling it to maintain the advantages of a stiff initial lateral system while still remaining capable of significant ductile behavior when subjected to high loads. As such, significant ductility is introduced into the frame while minimizing drifts and associated effects of geometric nonlinearity (P-Delta). Hence, this technology is deemed the most effective and stable approach for introducing designated yielding members in the NRTMDF frame.

Figure 1.8 depicts the adaptation of the BRB as the mechanism for targeted energy dissipation of a Nonlinear/Inelastic Rooftop Tuned Mass Damper Frame. Figure 1.9 shows the basic geometry of the buckling restrained braces which enables the favorable hysteretic properties qualitatively demonstrated in Figure 1.7.

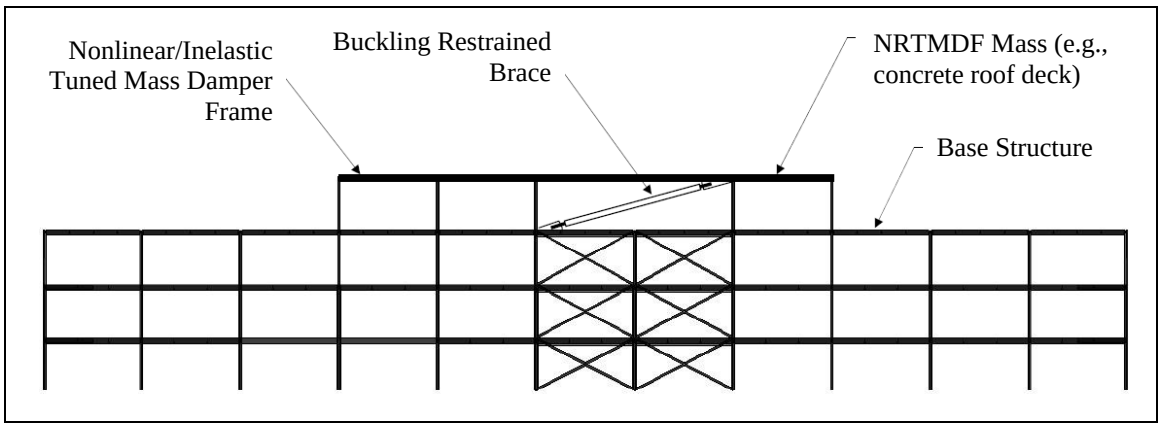

Figure 1.8 Typical Building Geometry with NRTMDF

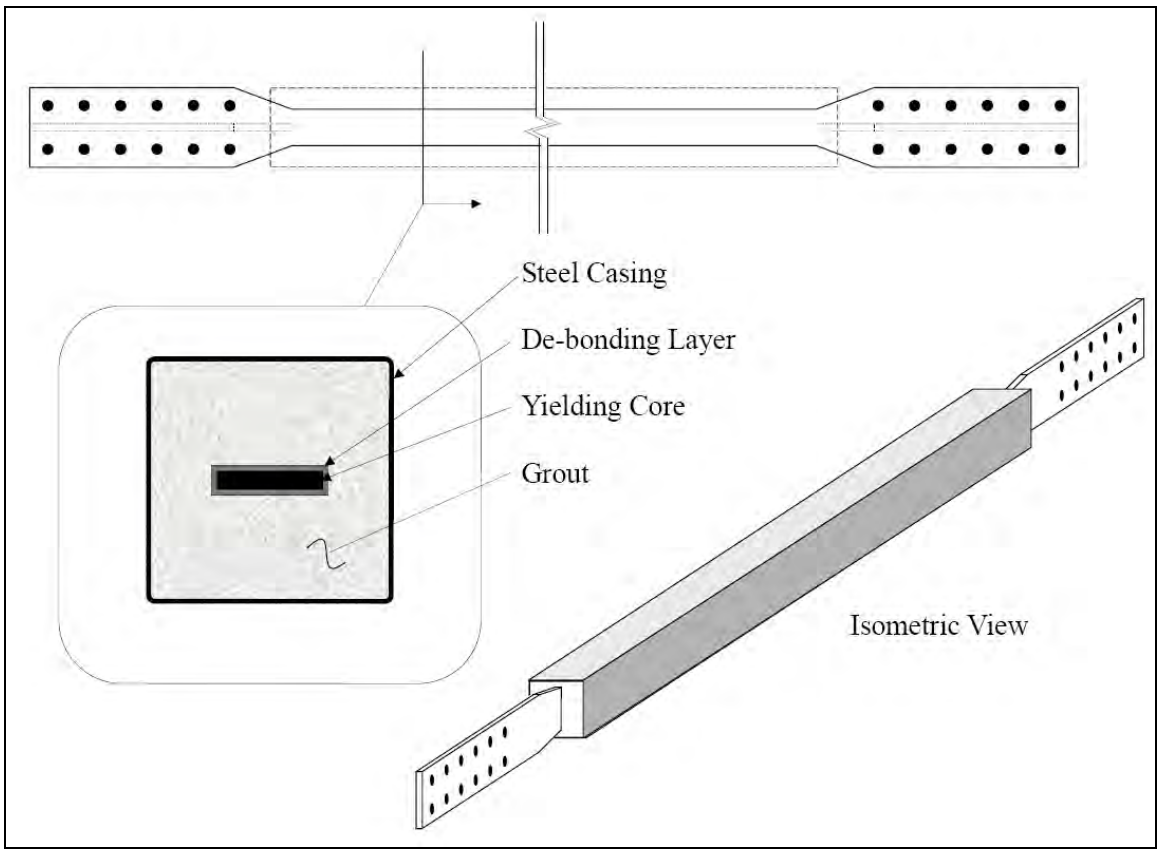

Figure 1.9 Basic Buckling Restrained Brace Components

Recent efforts have resulted in the development of specific design procedures called "Performance Based Plastic Design" (PBPD) which specify the design of highly ductile, yet sufficiently stiff and strong lateral systems. This is enabled, in large part, through the development of designated yielding members (DYM).[6] The objective for this approach is to control the level of damage in accordance with a specific performance objective and is deemed far more effective and reliable than the conventional, prescriptive, code-driven approach of applying the '*R*' factor to account for ductility in the global system still present in current codes for new construction. Whereas the traditional approach is an indirect accounting of nonlinearity through the global system, the PBPD approach enables ductility through a direct (potentially sacrificial) element design approach for the designated yielding member. The balance of the frame is then designed to remain elastic. Studies have shown that the PBPD procedure is a far more direct and reliable approach for achieving optimal performance of seismic force resisting systems. For the research presented herein, the introduction of a DYM at the NRTMDF follows the PBPD approach. It introduces a specific and deliberate mechanism through which earthquake energy is channeled. This energy is then dissipated at a specific location in a safe and effective manner thereby minimizing damage to the global structure. This allows for performance consistent with specific performance objectives in accordance with the methods of Performance Based Seismic Design (PBSD).

The incorporation of designated yielding members to reduce and control structural response to seismic motion is not a new concept. The March 2007 edition of *Steel Construction Today & Tomorrow* features a paper compiled by Okada addressing Energy Balance Seismic Design.[7] For this procedure, the application of members acting

hysteretically is directly accounted for in the overall evaluation approach. In fact, hysteretic behavior of designated members with significant action occurring only during large, rare events is a key component of this method. Once the designated yielding (damping) devices become mobilized, their energy is quantified and counted within the cumulative energy capacity of the entire system. The research herein outlined follows the same approach. The NRTMDF will mobilize in a large seismic event. When this happens, it will become a mechanism for dissipating significant seismic energy. For a given earthquake record, this energy (plastic strain energy) can be quantified and will effectively be counted as energy no longer free to cause damage to the primary structural system.

In general, a benefit of ductile systems is found in their ability to lengthen the fundamental period of the structure. For relatively stiff soil sites located near rupturing faults, longer period structures generally respond with a reduced acceleration response when compared to short period structures. This is due to matching of frequency contents which yields a higher structural response when sites and structures are closer to matching and lower response when frequency contents between the two become more displaced. Hence, a structure whose frame yields due to seismic inertial forces will undergo a period shift that will typically lessen the seismic acceleration response and reduce the event's overall impact for stiff and moderately stiff sites. Engineers have long understood this to be true and have developed systems such as seismic base isolation to deliberately lengthen a building's fundamental period.[8,9] In the author's past research the potential of increasing the fundamental period and thereby lowering seismic response by utilizing a mass tuned damper in the form of a limber frame atop relatively stiff buildings was

investigated.[10, 11] The research indicated that a reduction in seismic response was possible for a set of well suited specific parameters including the input ground motion and the dynamic properties of the original structure.

The NRTMDF method is theorized to develop multiple period shifts (period lengthening within the structure. First is the period shift enabled by the elastic behavior of the NRTMDF and its initial stiffness. As the NRTMDF mobilizes and the elastic limitations of the BRB yielding cores are breached, a second period shift is introduced which is transient and is based upon the degraded stiffness of the BRB members strained beyond their elastic range to a maximum drift within the analysis. This effective stiffness is calculated simply as the maximum BRB force divided by its displacement. The multiple periods may be characterized as T_o (the initial undamped fundamental period), T_e (the period due to the initial elastic behavior of the NRTMDF), and T_p (the period due to plastic behavior of the NRTMDF with degraded stiffness due to nonlinear behavior). While the NRTMDF is expected to enable the multiple period shifts for any structure to which it is added, it is theorized that the actual values of the calculated periods and the associated reductions in spectral acceleration will be the greatest indicator of the effectiveness of the NRTMDF approach. For this research, it is hypothesized that for structures with relatively low fundamental periods, the NRTMDF approach may not enable period shifts large enough to drive a significant reduction in spectral acceleration response. Also, for structures with relatively long fundamental periods, spectral accelerations may already be relatively low and attempts to further reduce the spectral acceleration by virtue of period lengthening may not enable a significant reduction but may in fact result in NRTMDF displacements beyond practical limitations. In summary,

Figure 1.10 illustrates this concept and the hypothesis that structures within a certain range of initial fundamental period are thought to be the candidates for which the NRTMDF approach will be most effective. The values associated with the range of expected effectiveness are unique to each site and its associated acceleration response spectrum and for this case are presented with respect to the design spectrum of Figure 1.6.

For the author's dissertation research, the objective is to investigate the application of designated yielding frame members (buckling restrained braces) incorporated in rooftop tuned mass damper frames to determine the feasibility and effectiveness of this approach for reducing seismic response. The methods for measuring performance demonstrated within this research are aimed toward the quantification of

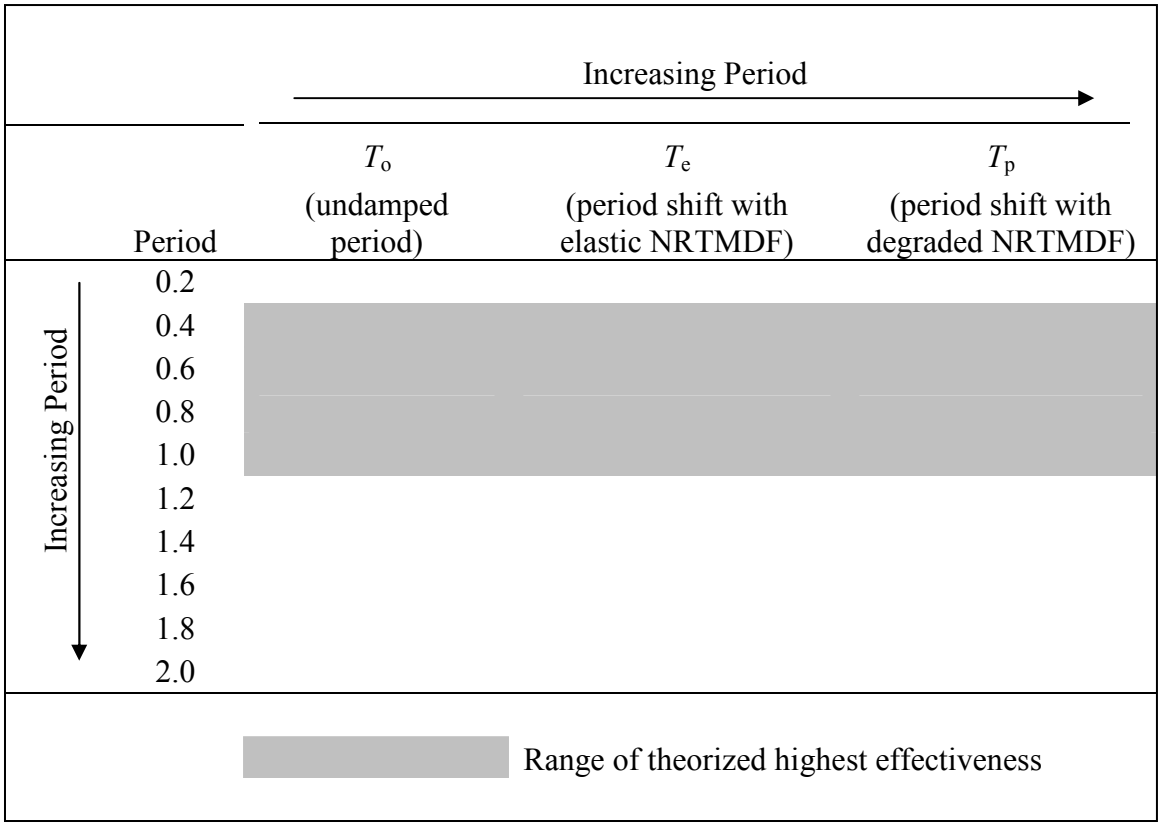

Figure 1.10 Conceptual Range of Theorized Highest Effectiveness

structural demand and the reduction thereof utilizing the NRTMDF approach. This method would introduce a new and inexpensive alternative for the mitigation of damage caused by earthquakes. This translates to safer structures with lower repair costs following a large event or less expensive new structures. It also translates to reduced ancillary costs associated with failure of and bracing for nonstructural elements and components since the approach not only reduces demands on the structure itself but on all of the building systems within the structure. This study represents a new tool and a new avenue of study for researchers and engineers to consider in an attempt to mitigate the costly effects of significant earthquakes.

2 LITERATURE REVIEW

The concept of tuned mass dampers to reduce a structure's response to a forcing function is not new. However, the stochastic nature of an earthquake acceleration record as a forcing function does not lend itself well to the classical theory of structural dynamics and tuned mass dampers. Hence, fundamental dynamic theory found in many texts presents strategies toward tuned mass dampers for reducing structural response for steady state forcing functions applied to the structure such as those induced by machinery or components of the mechanical system. Chopra (1995) outlines the theory behind a vibration absorber or tuned mass damper for a simple spring-and-mass system subjected to a steady state forcing function and demonstrates that when properly tuned, the response amplitude of the main system may be reduced to near zero.[12]

Chopra also addresses the utilization of tuned mass dampers for the 59 story Citicorp Center in midtown Manhattan.[13] Utilization of an 820 kip block of concrete at the structure's 59th floor as a movable damping mass reportedly reduces oscillations by as much as 40%, thus easing much of the discomfort experienced by occupants during high winds. Another example is the Tuned Sloshing Damper (TSD) which, according to Robinson, Gamble and Myslimaj, provides structural damping with a mechanism of viscous liquid flow between partially filled tanks.[14] The tank is designed so that the liquid surface wave has a fundamental frequency tuned to be at or near the fundamental frequency of the building. With internal baffles and multidirectional fins such a device

carries a high degree of potential tuning thereby enabling the system frequency to match that of the original structure and provide optimal response reduction. According to these authors, values of damping approximately 1% to 2% of critical may be increased to as much as 3% to 4%, an increase that provides a significant reduction in structural response. For geographic regions where seismic forces are significant, these authors suggest higher mode effects may be significant and may complicate the tuning of the system for optimal performance.

Past research has indicated utilization of tuned mass dampers can be an effective measure for the general suppression of structural vibrations.[15,16] These results notwithstanding, research from various authors indicates unfavorable results regarding the effectiveness of tuned mass dampers for reducing structural vibrations resulting from seismic motion. Kaynia, Veneziano and Biggs investigated the effectiveness of passive tuned mass dampers for seismic applications and concluded tuned mass dampers did not appear to be effective for reducing seismic response.[17] Sladek and Klingner also studied the effect of a prototypical tuned mass damper addressing both linear and nonlinear behavior of a prototype structure subjected to the N-S component of the El Centro 1940 ground motion and likewise concluded such an approach did not appear useful for seismic applications.[18]

More contemporary research referenced in the following paragraphs and elaborated upon within the context of this research supports the utilization and effectiveness of tuned mass damping systems for the reduction of seismic response. Wong and Johnson concluded that the application of multiple tuned mass dampers at various stories in a structure holds the potential for significantly reducing plastic energy

demand and damage on the base structure.[19] Also, the tuned mass dampers hold the potential for dissipating significant seismic energy. While plastic energy demand increased at the roof level for this study, the analytical study demonstrated reductions in demand for the balance of the structure with energy reductions of more than 70% in some plastic hinges. Figure 2.1 demonstrates the results and presents the demand reduction at the moment frame joints for the test structure.

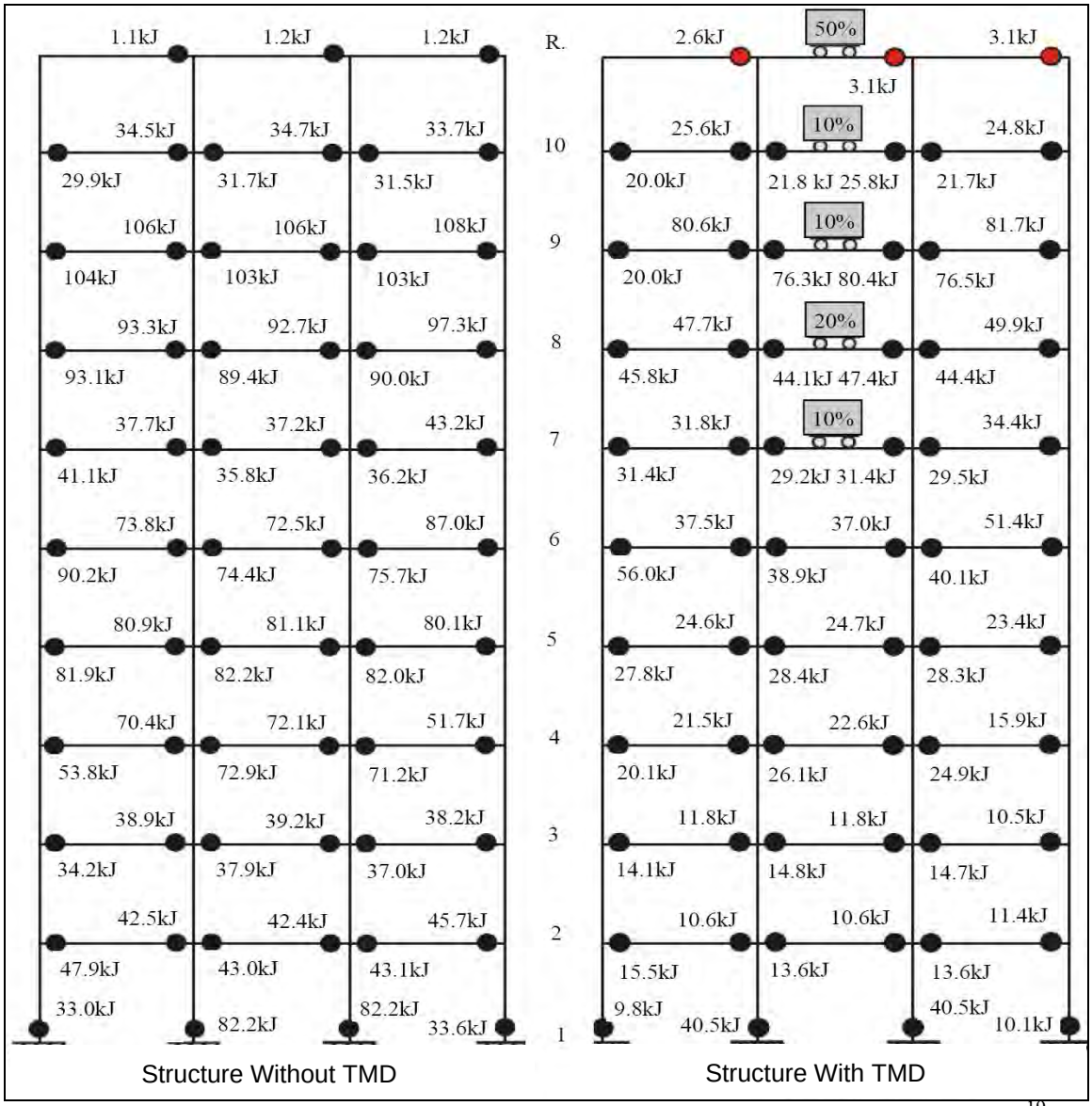

Figure 2.1 Reduction in Plastic Energy Demand with Multiple Tuned Mass Dampers[19]

The utilization of tuned mass dampers applied solely at the roof of a structure was investigated by Nawrotski in a research study conducted in 2006.[20] For this study a rooftop mass was applied to the test structure with helical steel spring devices with integrated dampers (Figure 2.2). Nawrotski reports a reduction in rooftop displacements by 40% between the undamped and damped structures as shown in Figure 2.3 and an increase in effective damping from 5% to 15%.

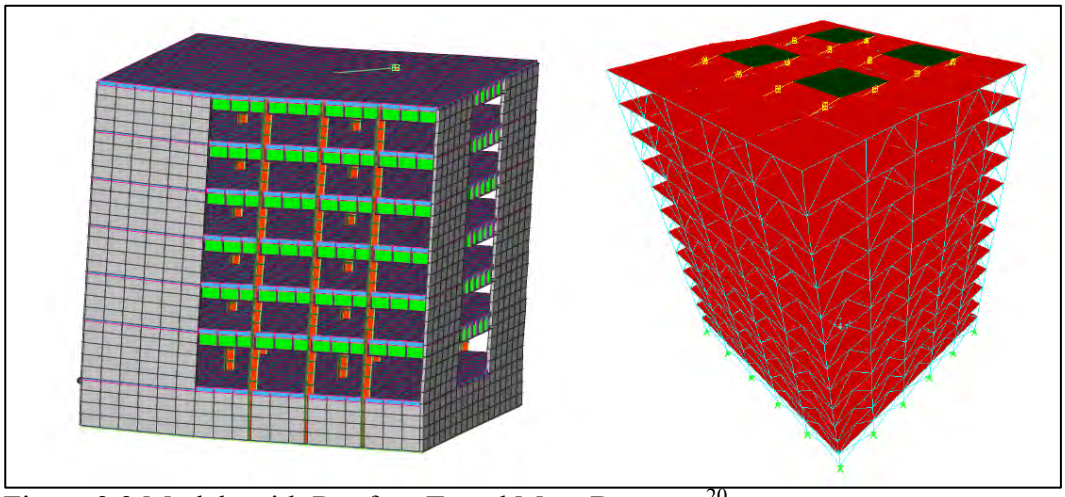

Figure 2.2 Models with Rooftop Tuned Mass Dampers[20]

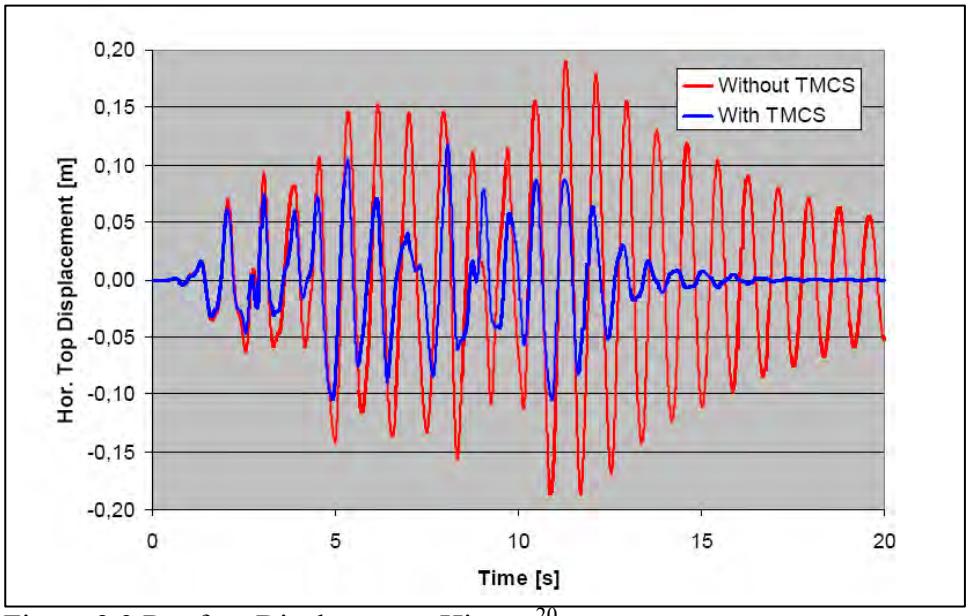

Figure 2.3 Rooftop Displacement History[20]

The utilization of rooftop structures for reducing seismic response was investigated by Villaverde on two separate occasions. In 1998, his study introduced the possibility and effectiveness of using a rooftop structure as mass for a passive tuned damper.[21] His analytical model consisted of an isolated rooftop structure resting upon laminated rubber bearings as shown in Figure 2.4. Viscous dampers were used in addition to the laminated rubber bearings to create a highly damped vibration absorbing mechanism at the roof level. One analytical model was used for the study, consisting of a stiff moment frame. The test structure was a five-story, one-bay, two-dimensional model consisting of one uniform steel shape for all columns and one uniform steel shape for all beams. The ground motion for the study was a modified version of the Secretaria de Comunicaciones y Transportes (SCT) accelerogram, recorded during the Mexico City1985 earthquake. The accelerogram was tuned so that the dominant period of ground motion matched the period of the undamped structure. Villaverde reported reductions in peak response parameters as high as 84% for the damped structure. Though reductions this high seem extraordinarily large, they are not irrational in consideration of the ground motion which was tuned to resonate with the undamped test structure. Nevertheless, Villaverde's conclusions demonstrate a reduction in seismic response for selected structures and ground motions is possible with tuned mass dampers in the form of a rooftop mass and stiffness enhanced with viscous dampers.

Villaverde re-visited the rooftop isolation system in 2005 utilizing steel oval elements in lieu of laminated rubber bearings and viscous dampers.[22] The steel oval elements act in a nonlinear hysteretic fashion to effectively de-couple the rooftop structure while also dissipating seismic energy as shown in Figure 2.4. Peak rooftop

Figure 2.4 Rooftop Damper Structures[21,22]

displacements are reduced by as much as 55% according to scale model testing of the approach. This approach is characterized as a simple and inexpensive method to protect some buildings against earthquake effects including a reduction in the amount of structural and nonstructural damage accompanying a large earthquake.

A practical application of the upper story damping system concept was demonstrated with the base isolated addition of two stories above the original three-story structure of the China Basin Landing in San Francisco shown in Figure 2.5.[23] For this project, the base isolation of the new stories above the original structure created an altered structure with a longer fundamental period and introduced new energy dissipation and performance that showed that the structure with the base isolated addition had a

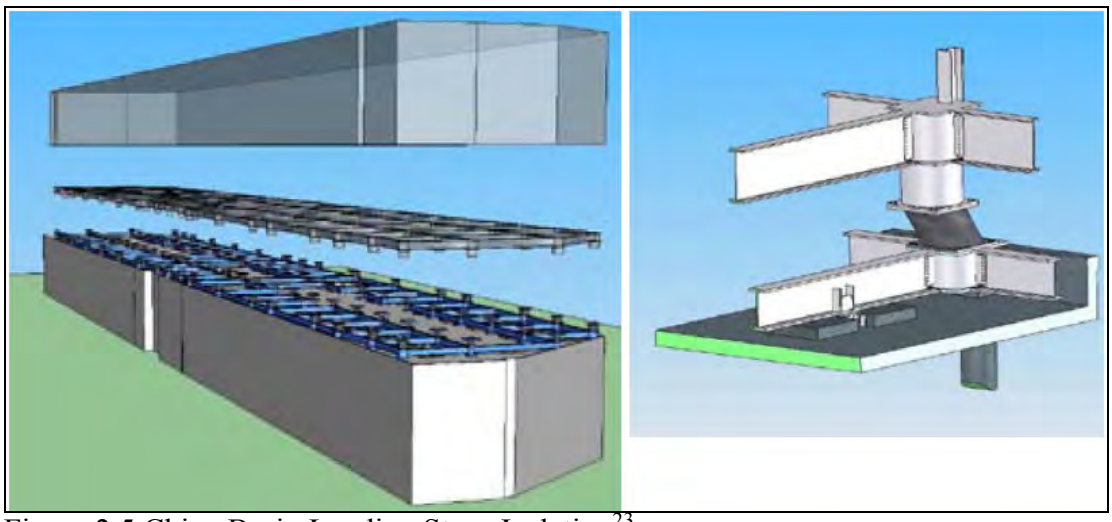

Figure 2.5 China Basin Landing Story Isolation[23]

higher reliability than the base structure without the addition. This illustrates the beneficial effect that the upper story mass damping structural system can have on the overall performance of a building. Furthermore, designers of this system indicated this may be the future direction of engineering for additions in high seismic areas.

The author's prior research demonstrates the potential for rooftop frames as a tuned mass damping system.[10,11] Figures 2.6 and 2.7 depict models from the past study for both the undamped and damped cases. When the addition of the rooftop frame shifts the structure from a region of resonance with the theoretical ground motion to a region where the frequency of the ground motion and the frequency of the structure are far apart, a reduction in seismic response may be achieved. Figure 2.8 demonstrates results from the study for the N-S component of the El Centro 1940 accelerogram and illustrates the reduction in peak rooftop displacement along with limber behavior of the rooftop frame. Table 2.1 summarizes the results for the complete suite of acceleration records included

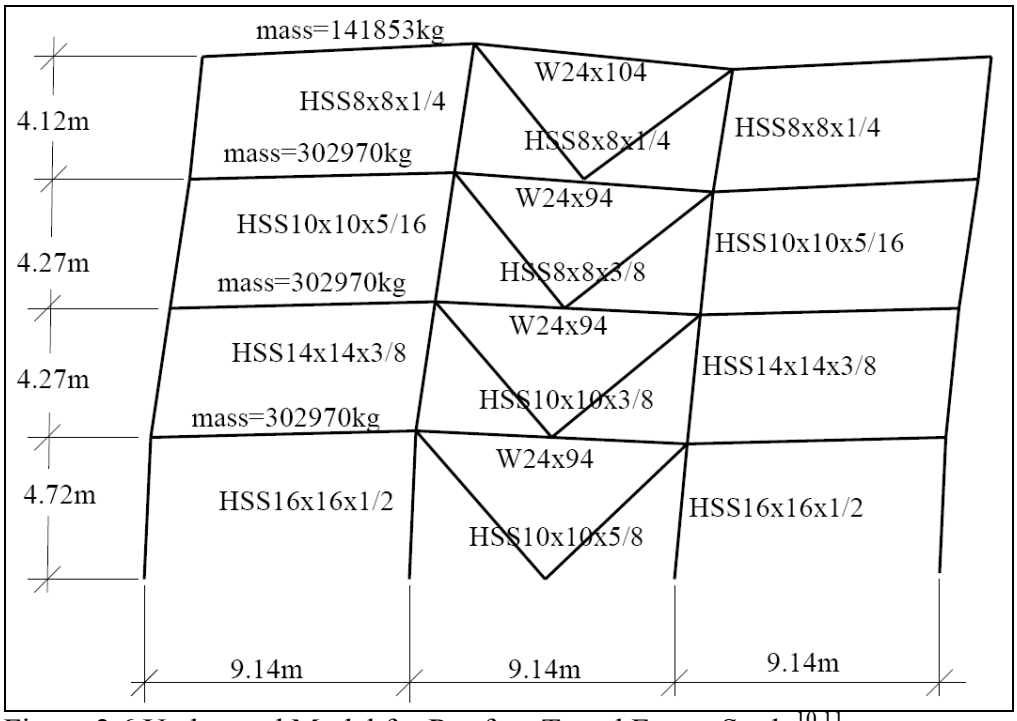

Figure 2.6 Undamped Model for Rooftop Tuned Frame Study[10,11]

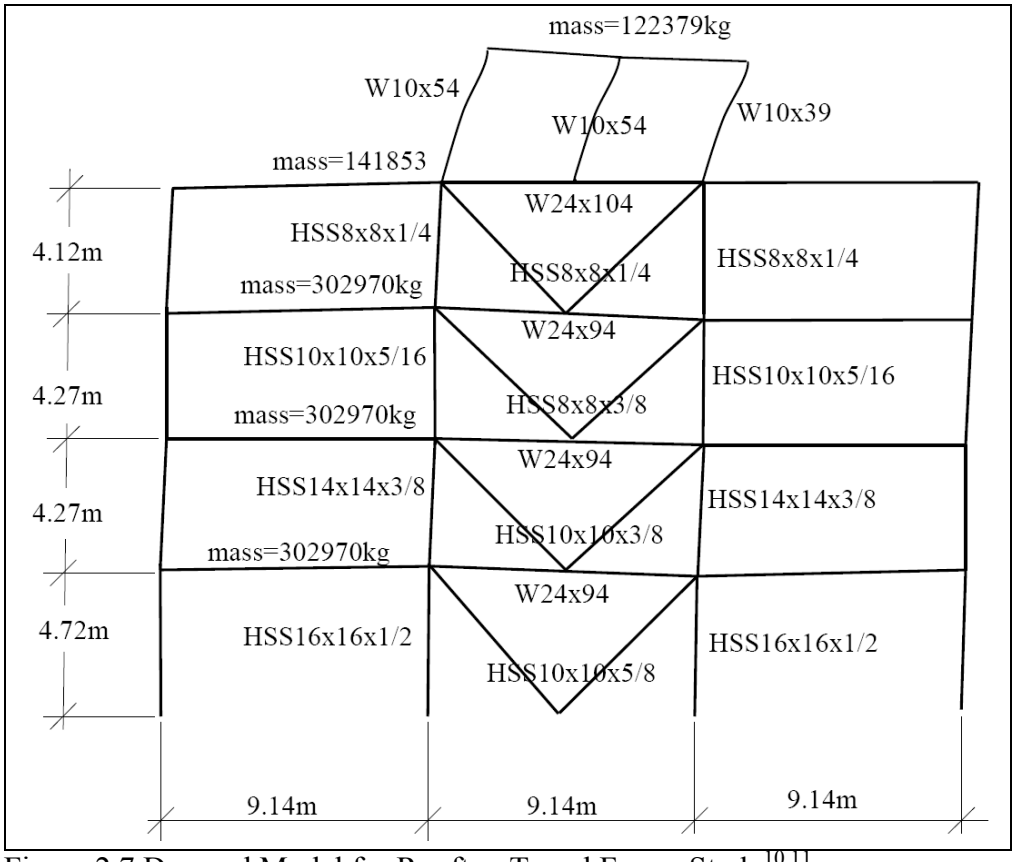

Figure 2.7 Damped Model for Rooftop Tuned Frame Study[10,11]

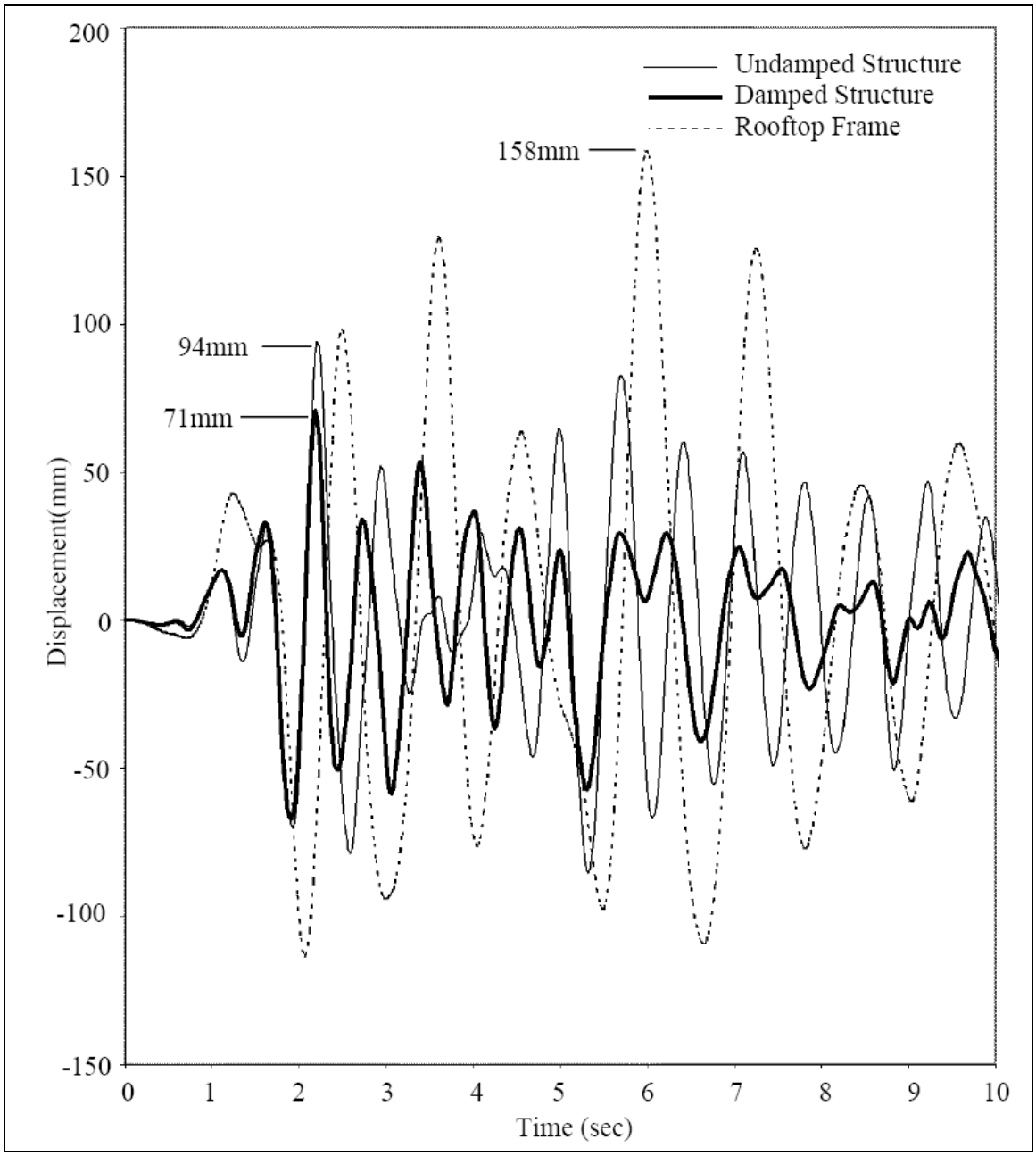

Figure 2.8 Undamped, Damped Rooftop and Rooftop Damper Displacement for N-S El Centro 1940 acceleration record[10,11]

Table 2.1 Time History Analysis Summary[10,11]

	Peak Rooftop Displacement (mm)			Peak Base Shear kN		
Record	U	D	Change	U	D	Change
El Centro	94	71	-24%	4261	4026	-6%
Loma Prieta	84	68	-19%	4924	4132	-16%
Kobe	246	132	-46%	12099	6334	-48%
Northridge	106	81	-24%	4878	4533	-7%
San Fernando	50	58	16%	2967	2576	-13%

U - Undamped
D - Damped

within the study. Though this approach cannot be effective for an arbitrary structure and any arbitrary ground motion, the research suggests that many structures are candidates for the rooftop frame damping system. Consideration of the site's dynamic soil properties and the dynamics of the original structure must be evaluated on a case by case basis. This approach is characterized as a relatively inexpensive method of improving the expected seismic performance and/or reducing the seismic demand for the existing or new structure under consideration.

3 METHOD OF ANALYSIS

3.1 Analysis Objectives

Analyses conducted with respect to the nonlinear/inelastic rooftop tuned mass damper frame (NRTMDF) serve the purpose of assessing the feasibility of this approach for reducing structural response to earthquake ground motion. In addition, the analyses serve to quantify the effectiveness of the approach and to determine combinations of structures and ground motion characteristics for which the approach is most effective.

3.2 Structures Used for Analyses

For the analyses, ten actual structures were chosen and analytically modeled to represent a broad array of lateral force resisting systems and structural geometries (Figures 3.1 through 3.10). The structures have lateral force resisting systems of steel braced frames, steel eccentric braced frames, concrete shear walls or steel moment frames. The structures range from 2 to 9 stories and have fundamental periods from 0.25 seconds to 2.0 seconds as summarized in Table 3.1. The structures have generally plan symmetrical lateral for system and as such, the analytical models demonstrate little torsional behavior. The structures were designed according to the provisions of various versions of the Uniform Building Code and the International Building Code (edition dependent upon the year of construction).[24,25] It is believed that all of the structures were constructed in accordance with the designs represented in project record drawings.

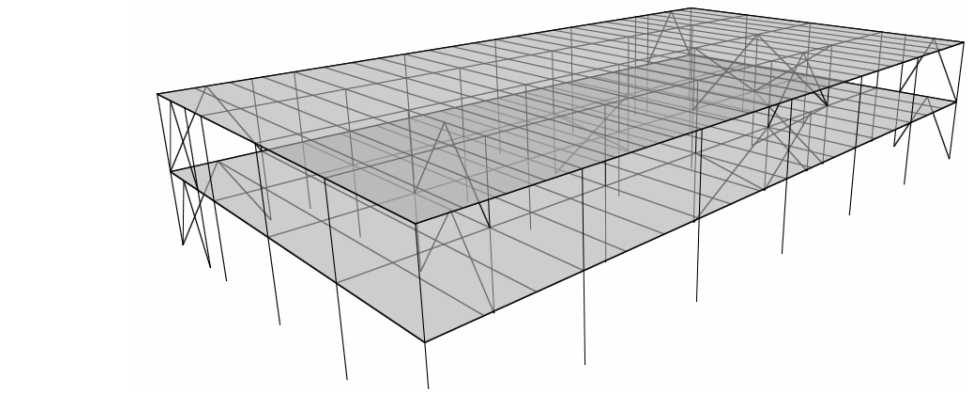

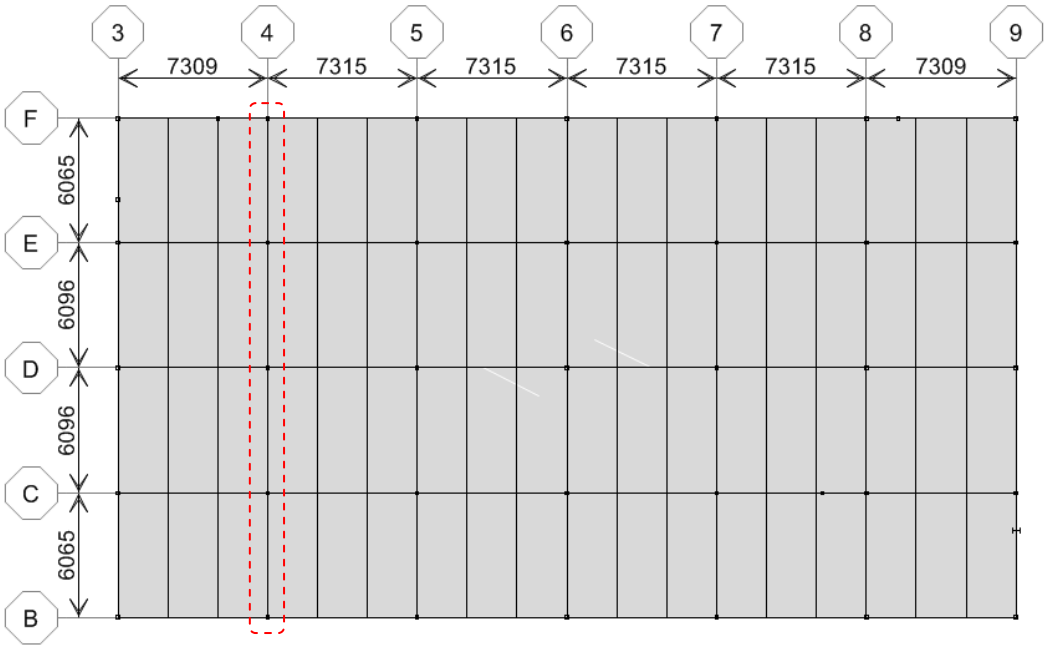

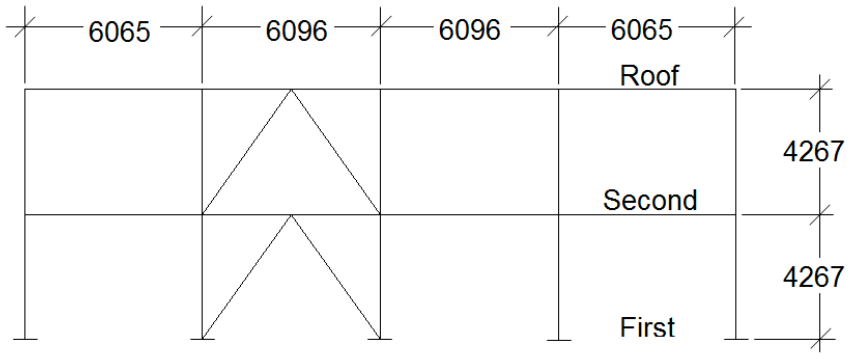

Note: All dimensions in millimeters

Figure 3.1 Building BF-1 3D, Plan and Section at Gridline 4

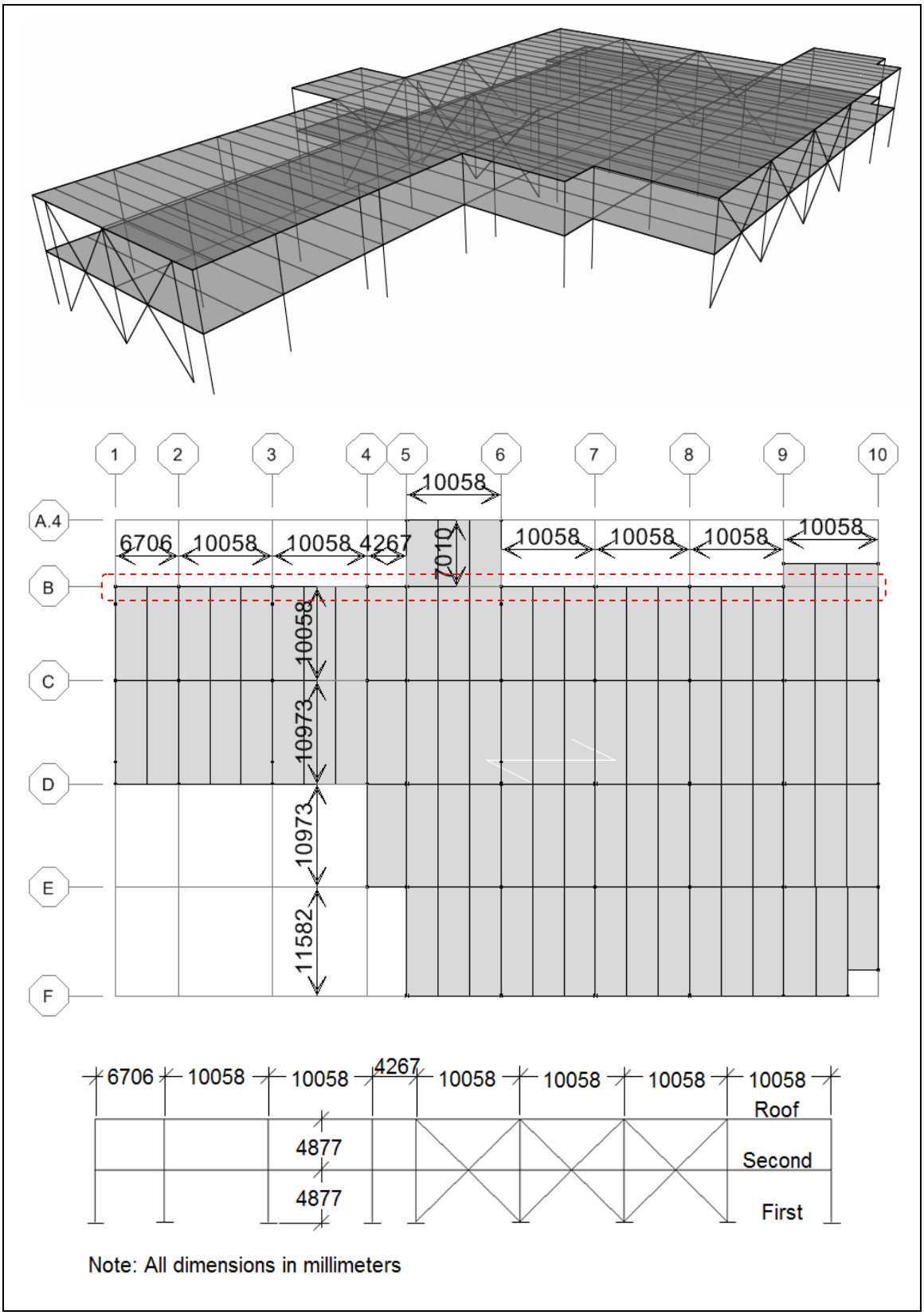

Figure 3.2 Building BF-2 3D, Plan and Section at Gridline B

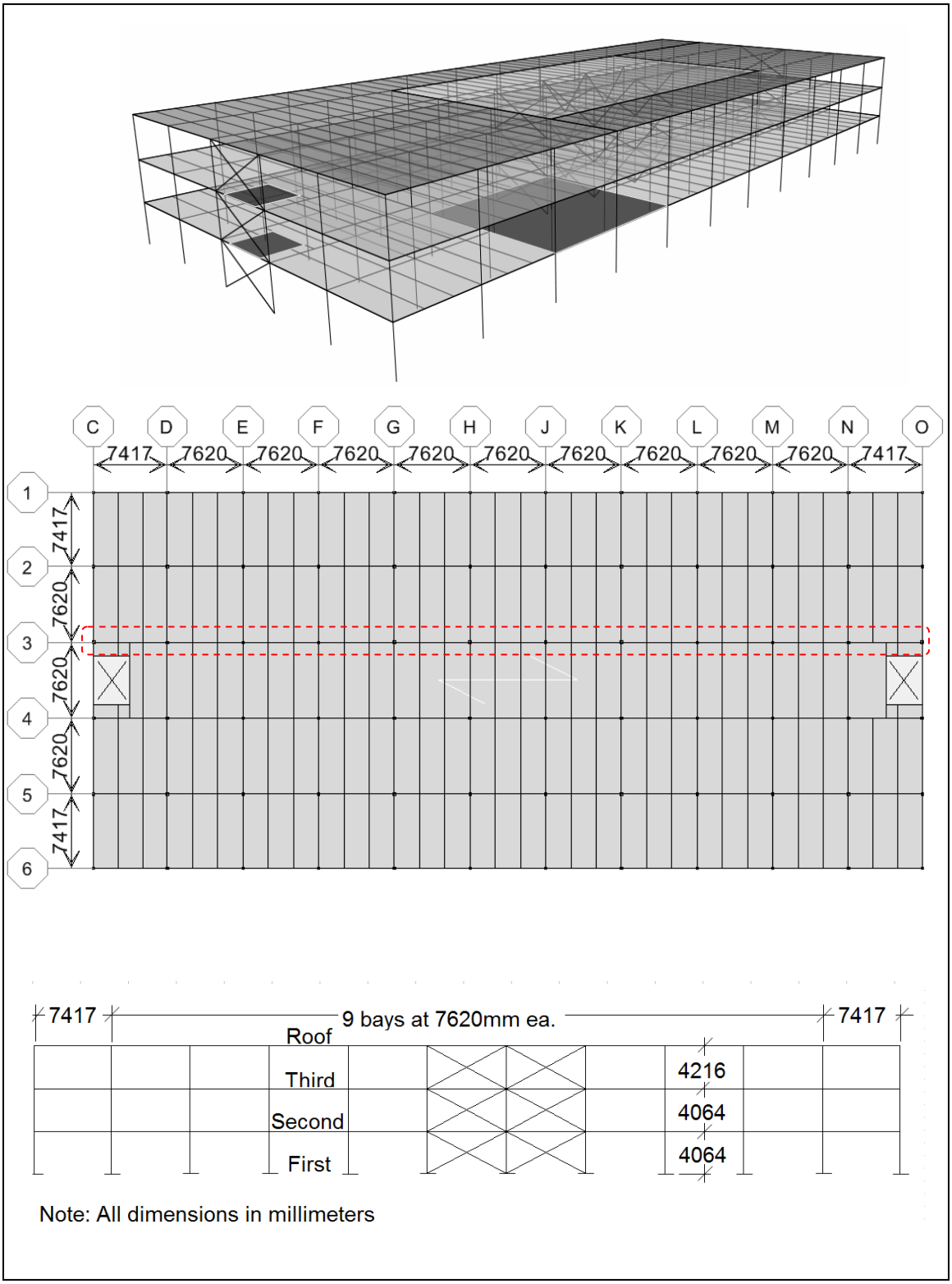

Figure 3.3 Building BF-3 3D, Plan and Section at Gridline 3

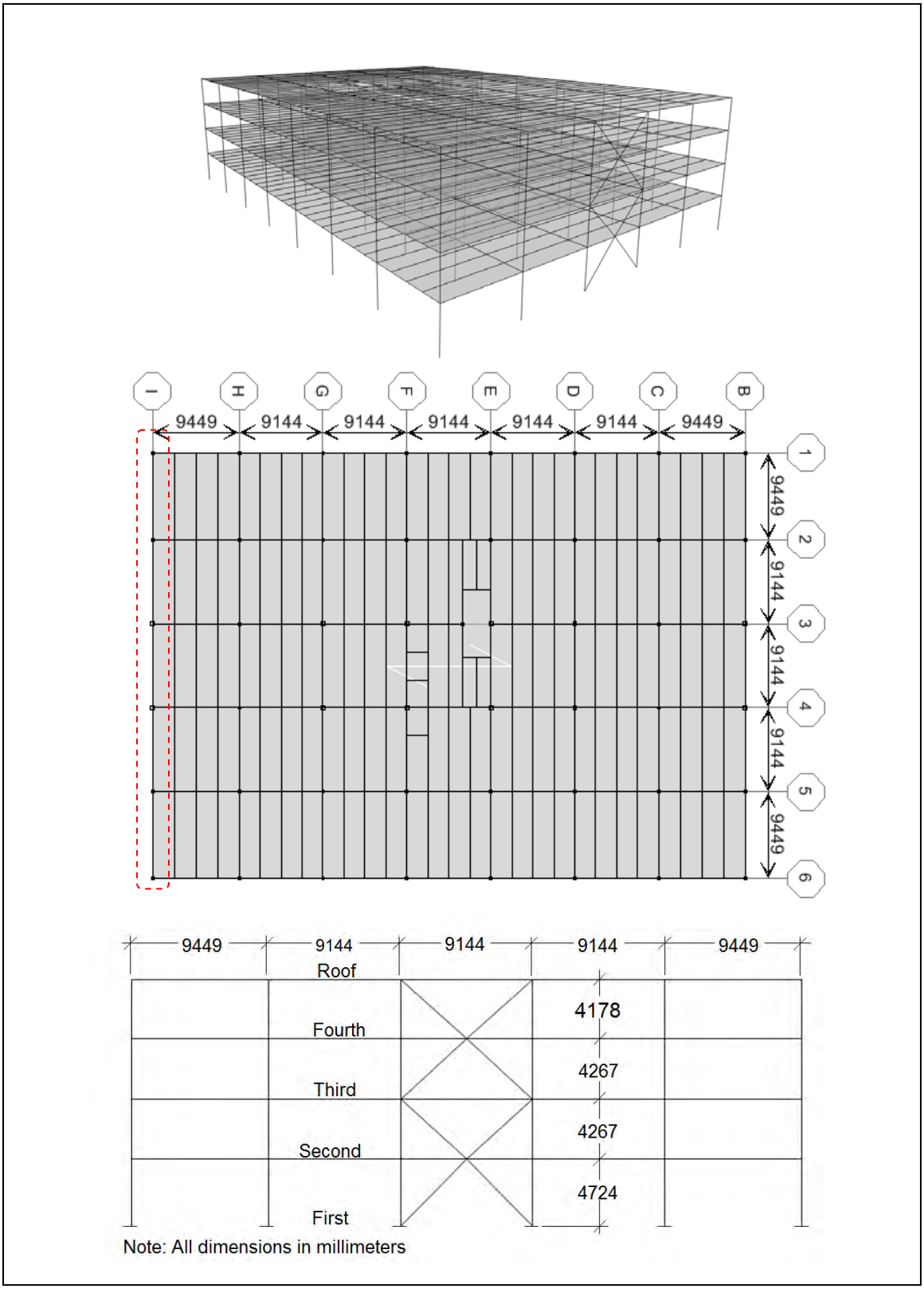

Figure 3.4 Building BF-4 3D, Plan and Section at Gridline I

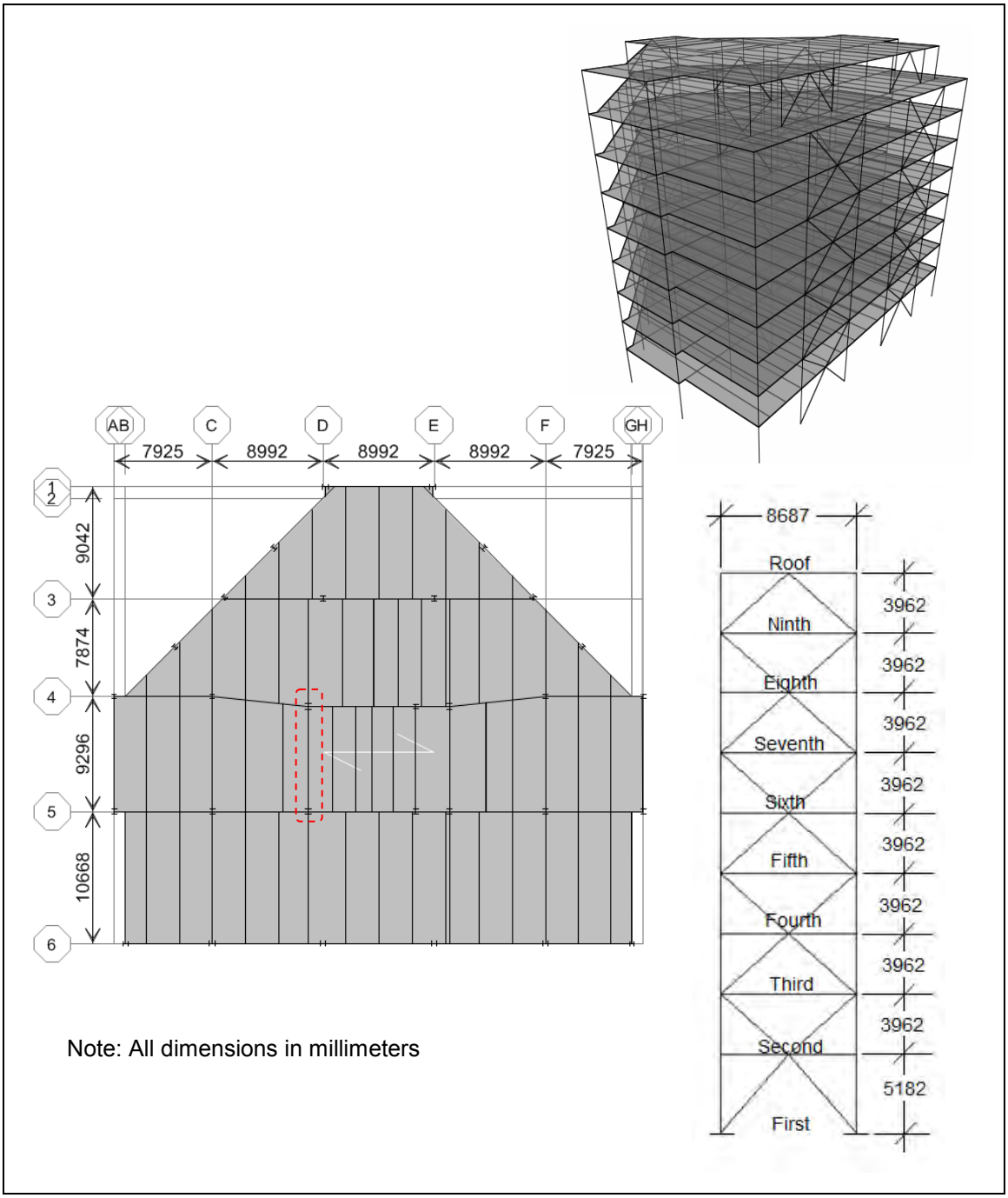

Figure 3.5 Building BF-5 3D, Plan and Section at Gridline D

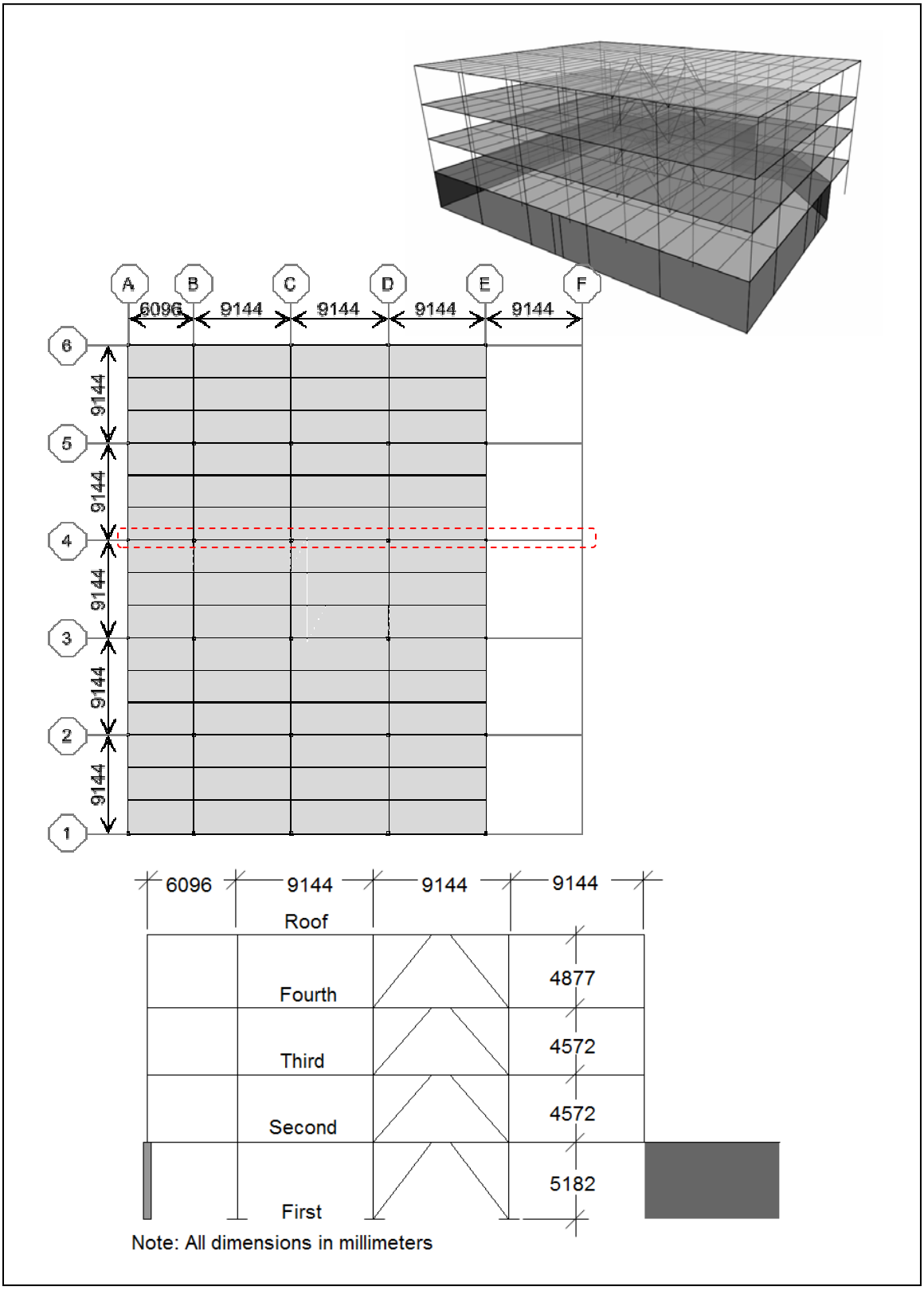

Figure 3.6 Building EBF-1 3D, Plan and Section at Gridline 4

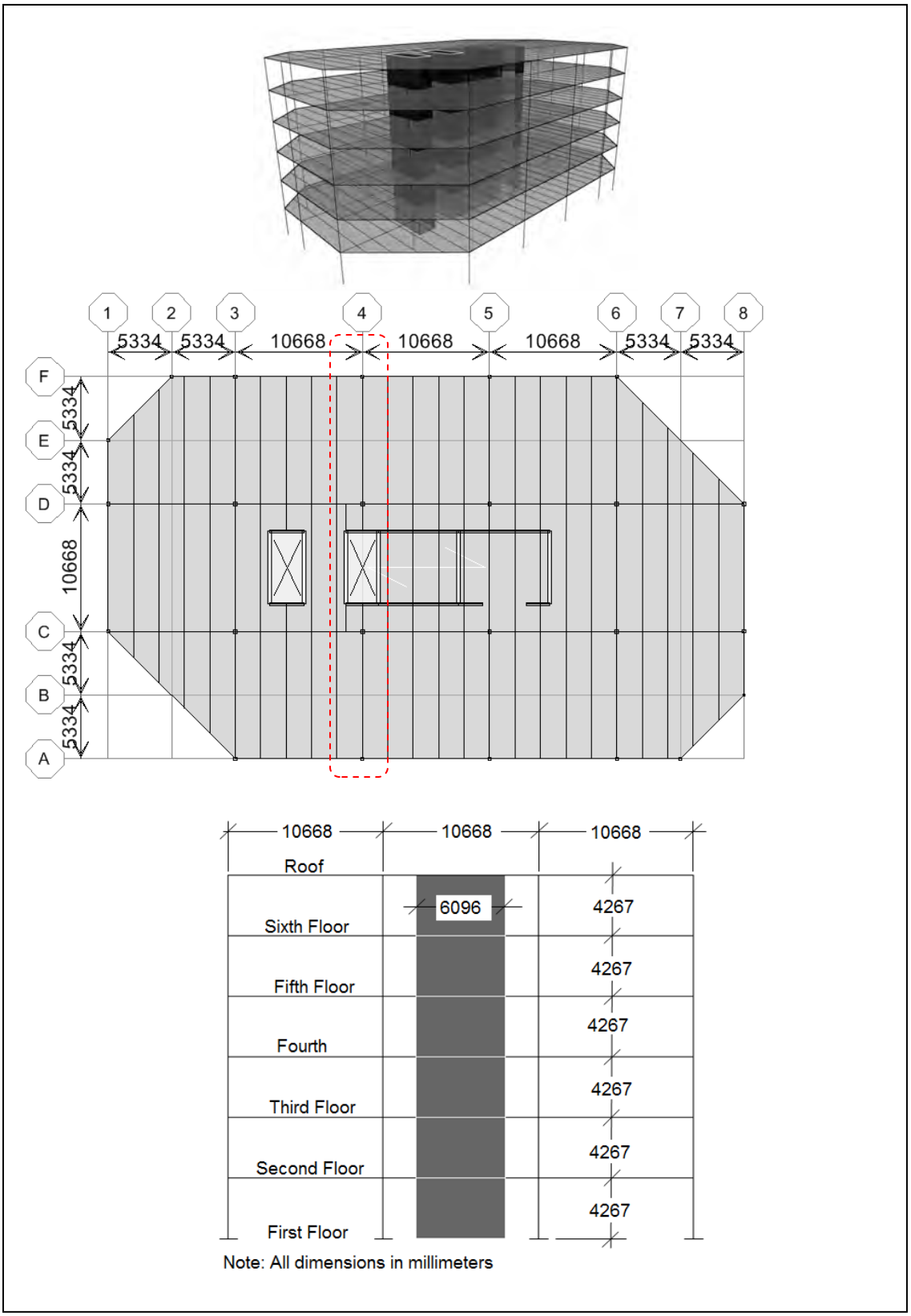

Figure 3.7 Building SW-1 3D, Plan and Section at Gridline 4

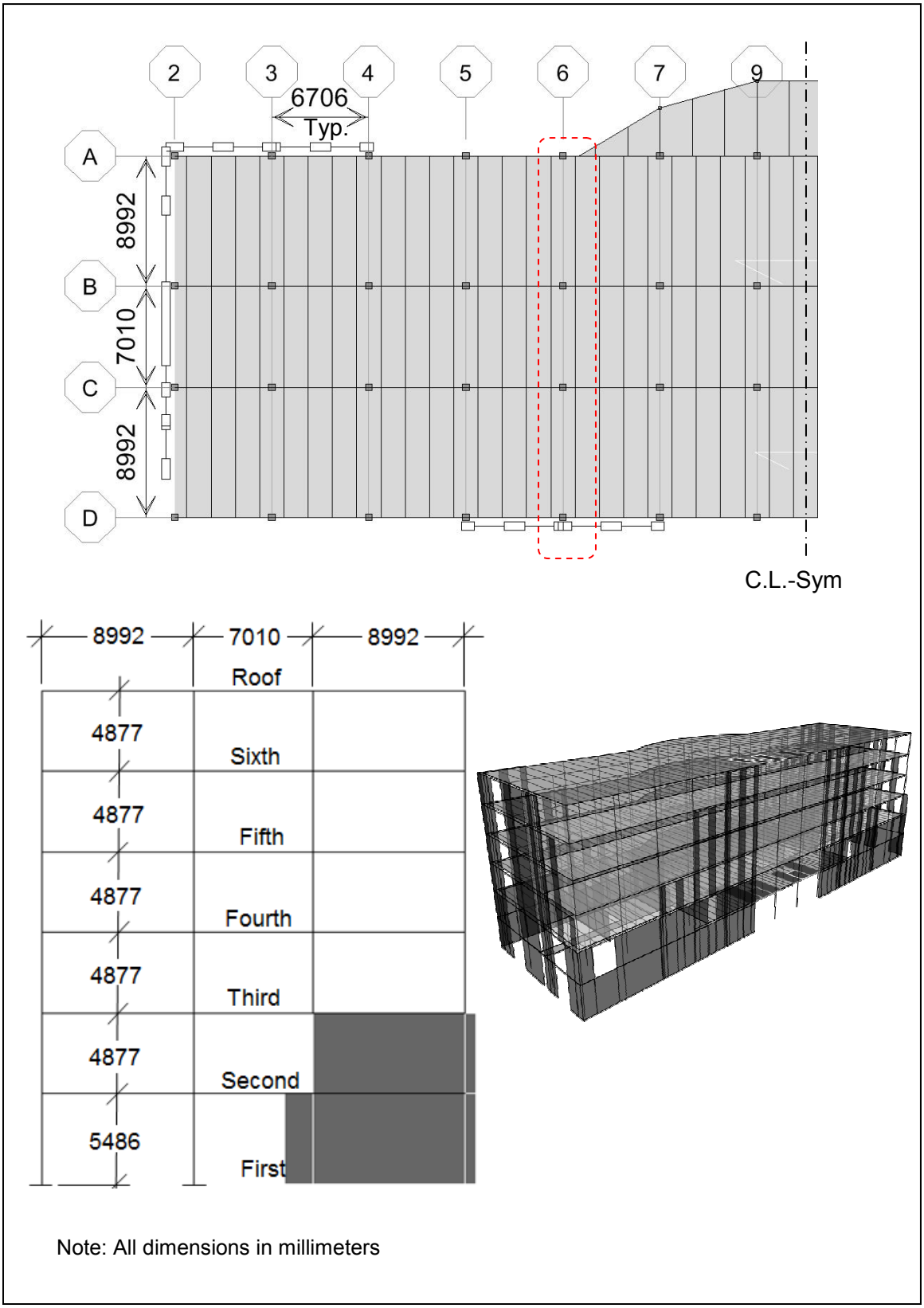

Figure 3.8 Building SW-2 3D, Plan and Section at Gridline 6

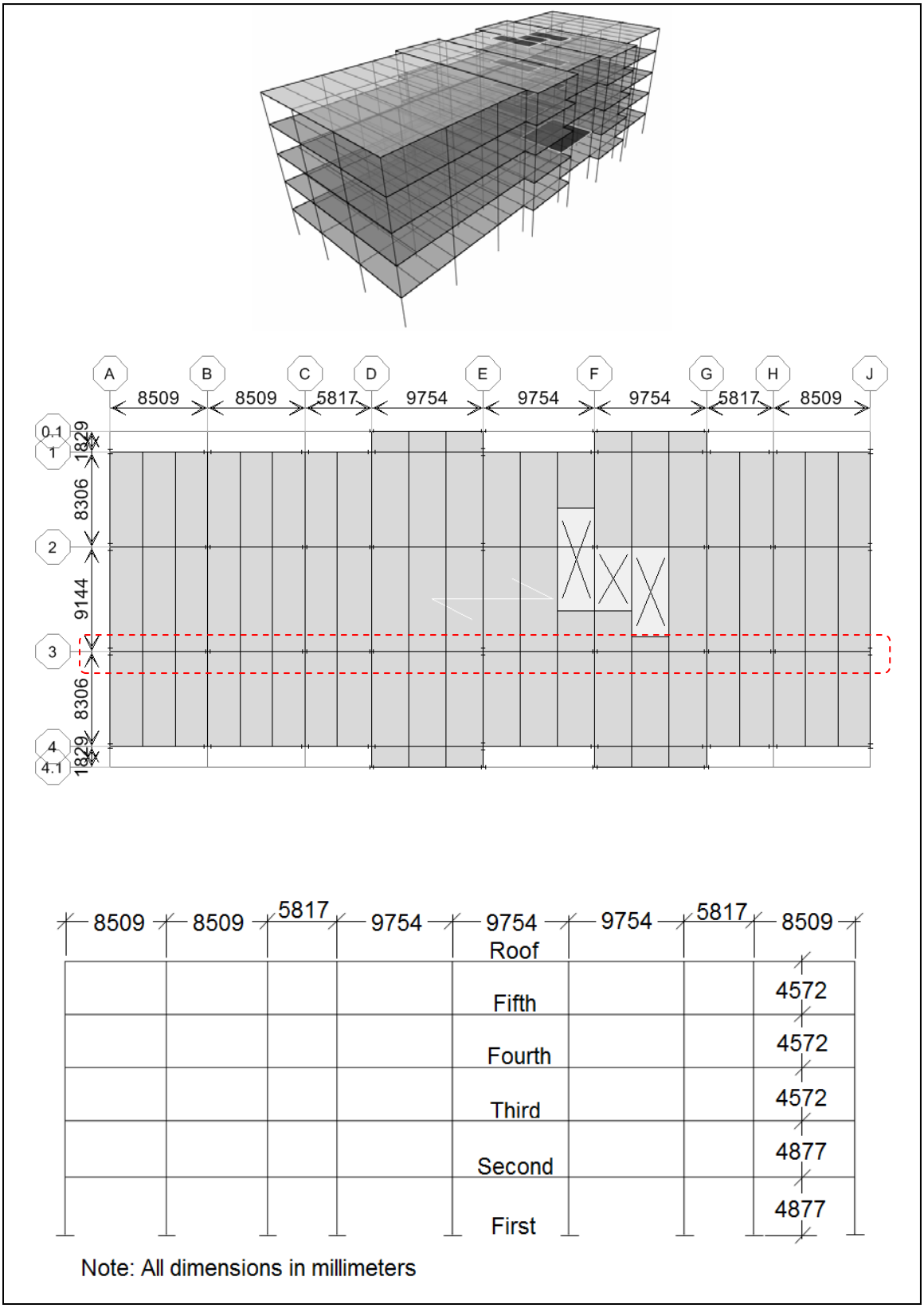

Figure 3.9 Building MF-1 3D, Plan and Section at Gridline 3

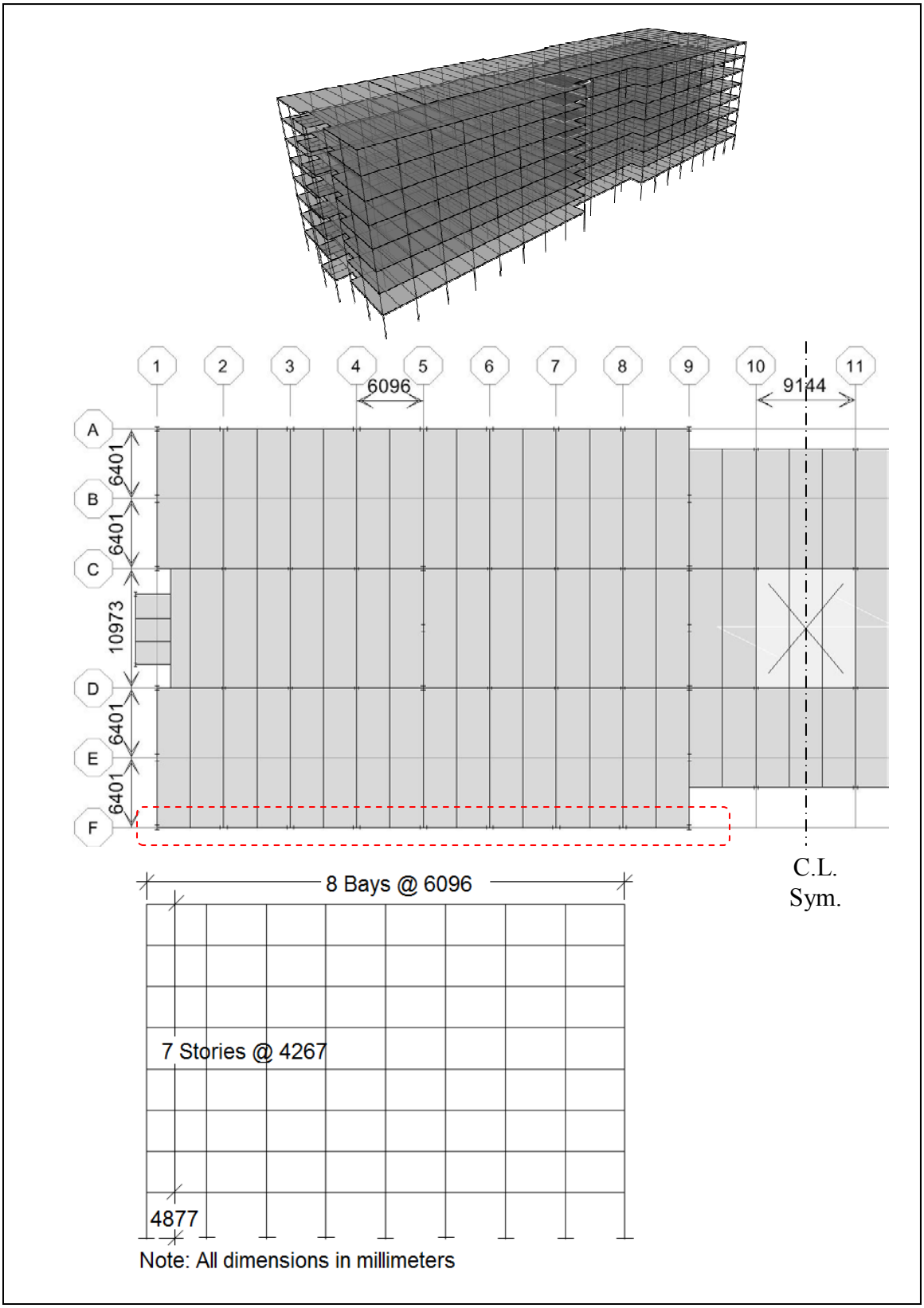

Figure 3.10 Building MF-2 3D, Plan and Section at Gridline F

Table 3.1 Summary of Structures

Designation	No. Stories	Lateral System	Use	Period (sec)
BF-1	2	Braced Frame	Office Building	0.25
BF-2	2	Braced Frame	Educational/Research	0.30
BF-3	3	Braced Frame	Office Building	0.40
BF-4	4	Braced Frame	Office Building	0.63
BF-5	9	Braced Frame	Office Building	1.05
EBF-1	4	Ecc. Braced Frame	Computation Facility	0.54
SW-1	6	Shear Wall	Office Building	0.35
SW-2	6	Shear Wall	Research Facility	0.41
MF-1	5	Moment Frame	Office Building	1.40
MF-2	8	Moment Frame	Office Building	2.00

3.3. Modeling Protocol

Analytical studies for the ten structures were conducted utilizing conventional dynamic modeling approaches along with state-of-the-art finite element analysis applications (ETABS, SAP2000, Perform 3D, all produced and distributed by CSI Berkeley). Conventional dynamic modeling approaches included simplified models with single lumped masses representing each story level (m_i) and single elements representing the stiffness of each floor (k_i). Figure 3.11 depicts a simplified model for building BF-4, with the NRTMDF. For the simplified models the rooftop damper frame is represented with a damper mass (m_R) and the effective stiffness of the damper frame (k_{er}). The simplified analyses utilized modal superposition techniques with spreadsheets and visual basic algorithms (Microsoft Excel). This approach fundamentally solves the acceleration history for each mode shape utilizing the traditional equation of motion:

$$ku + c\dot{u} + m\ddot{u} = p(t) \qquad \text{Eq. 3-1}$$

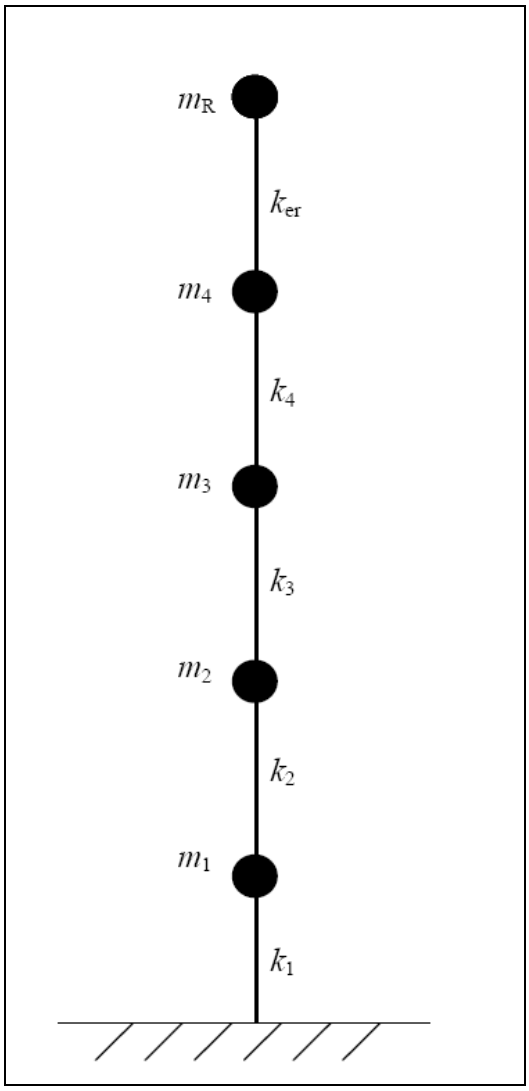

Figure 3.11 Simplified Model for BF-4 with NRTMDF

where the stiffness (k), modal damping (c) and inertial forces (m) combine with respective displacement, velocity and acceleration values to balance with the forcing function $p(t)$ reflecting the acceleration history. Additional simplified models as well as full three dimensional analytical models were developed with ETABS, SAP 2000 and Perform 3D, all distributed by CSI Berkeley (Figures 3.1 through 3.11). These applications solve for the linear motion of the structure through direct solution methods utilizing the mathematical stiffness, damping and mass matrices for each structure at each

time interval through the acceleration history. For nonlinear analyses, similar approaches utilize following the fundamental equation:

$$fs(u,\dot{u}) + c\dot{u} + m\ddot{u} = p(t) \qquad \text{Eq. 3-2}$$

For this method, the stiffness component (*fs*) becomes altered with a modified stiffness matrix reflecting the nonlinear behavior of various elements within the system. At each time interval, nonlinearity is incorporated as it becomes triggered through the element force-displacement hysteretic relationship coupled with changes in direction reflected in the sign of element deformational velocity. This requires an iterative approach at each relatively small time interval (0.005 to 0.025 seconds) where nonlinearity is triggered which then drives the analysis toward a numerically stable solution incorporating modified stiffness properties. Though a corroboration between the advanced three dimensional models and the simplified models could be demonstrated, the advanced models enabled the incorporation of nonlinearity of the rooftop tuned mass damper frames along with element nonlinearity (where triggered) of the elements of the lateral force systems of the structures. This provides the most realistic assessment of the behavior of the rooftop frames and their effect on the original structures. Two-dimensional analyses were deemed acceptable for the purposes of this research since torsional behavior was not significant and since the performance and effectiveness of the NRTMDF can be successfully embodied with lateral motions applied in only one primary direction. While analyses in both primary directions would be expected in an actual design scenario, it would compound the requirements and output for analyses herein

presented without changing the results qualitatively or quantitatively to a significant degree. Hence, each model was analyzed in a specific direction to test the concept of the NRTMDF.

3.4 Analyses Acceleration Records

Ground motion acceleration records selected for the time history analyses reflect a broad array of earthquake magnitudes, soil conditions, distance to source and rupture mechanisms. The motions were taken from the SAC Phase 2 project ground motion database and include actual records along with artificially generated records.[26] The accelerations developed as part of the SAC Phase 2 project are deemed suitable for analyses of this nature as they were developed by SAC expressly for the purpose of performing response spectra and time history analyses in topical investigations, case studies, and trial applications for the SAC Phase 2 Steel Project. Table 3.2 summarizes the ground motions for the analyses and Figures 3.12 through 3.20 depict the acceleration response spectrum developed for each record along with the envelope of all spectra. The spectra demonstrate an extremely broad array of frequency content in addition to an extremely broad range of spectral acceleration magnitudes.

Though such a broad array of motions would not be required for analyses pertaining to any specific site, they were considered prudent for the purposes of determining the outer boundaries of motions for which the NRDMDF approach is effective as well as the nature of motions and structures for which the nonlinear/inelastic rooftop tuned mass damper frame approach is most effective.

The wide array of structure models coupled with the diverse array of ground motions represent a broad approach to both structures and ground motions. With this, the

Table 3.2 Summary of SAC Ground Motions

History	Magnitude	dist (km)	History	Magnitude	dist (km)
LA01	6.9	10	BO05	4.3	8.4
LA02	6.9	10	BO06	4.3	8.4
LA04	6.5	4.1	BO13	5.9	96
LA12	7	12	BO16	5.9	98
LA15	6.7	7.5	BO18	5.9	118
LA18	6.7	6.4	BO19	5.9	132
LA20	6	6.7	BO20	5.9	132
LA21	6.9	3.4	BO21*	6.5	30
LA22	6.9	3.4	BO22*	6.5	30
LA23	7	3.5	BO25*	6.5	30
LA25	6.7	7.5	BO33	5.9	96
LA28	6.7	6.4	BO34	5.9	96
LA30	7.4	1.2	BO35	5.9	98
LA37*	7.1	1.5	BO36	5.9	98
SE04	6.2	15	NF01	7.4	1.2
SE05	6.5	56	NF02	7.4	1.2
SE08	6.5	80	NF11	7.3	1.1
SE10	6	6.7	NF12	7.2	1.1
SE12	7.1	80	NF15	6.7	6.4
SE18	8	42	NF16	6.7	6.4
SE19	8	42	LASS1A	NA	NA
SE21	7.1	8.5	LASS1B	NA	NA
SE25	6.5	56	LASS1C	NA	NA
SE26	6.5	56	LASS1E	NA	NA
SE30	8	42	LASS2A	NA	NA
SE31	8	42	LASS3B	NA	NA
SE32	8	42	LASS3C	NA	NA
SE36	7.4	66	LASS4C	NA	NA

LA - Los Angeles *Simulated

SE - Seattle

BO - Boston

NF - Near Field

LASS - Los Angeles Soft Site
(modified versions of 10%/50-Year records with broadly representative soft soil conditions using SHAKE and SUMDES applications)

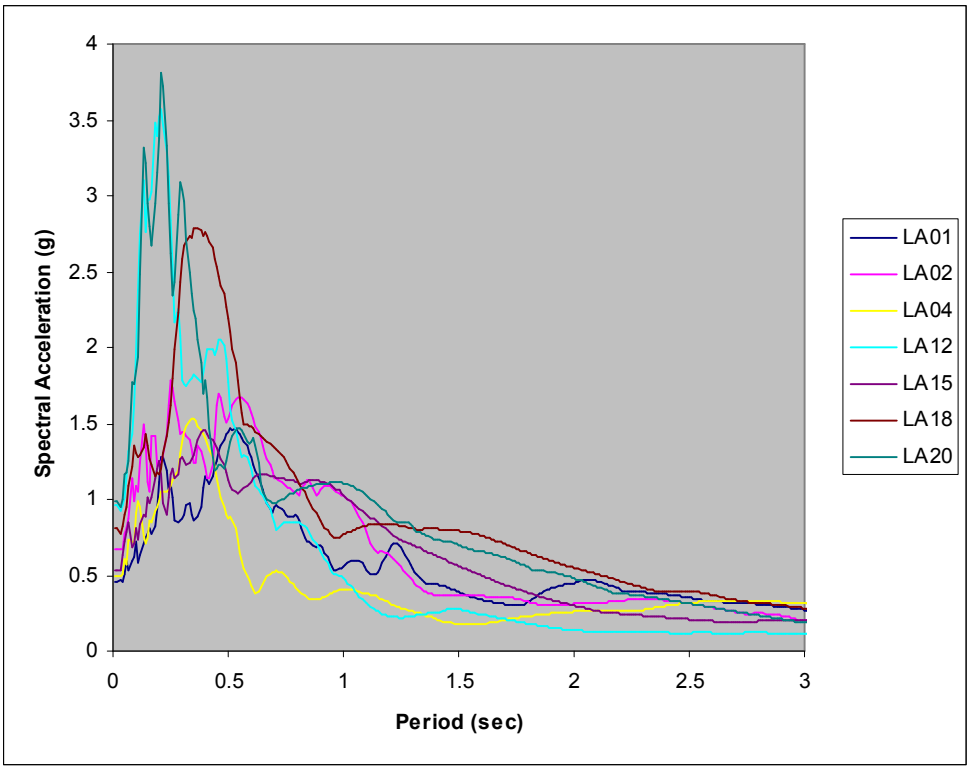

Figure 3.12 SAC Spectra Los Angeles 10% in 50-Year, 5% Damped

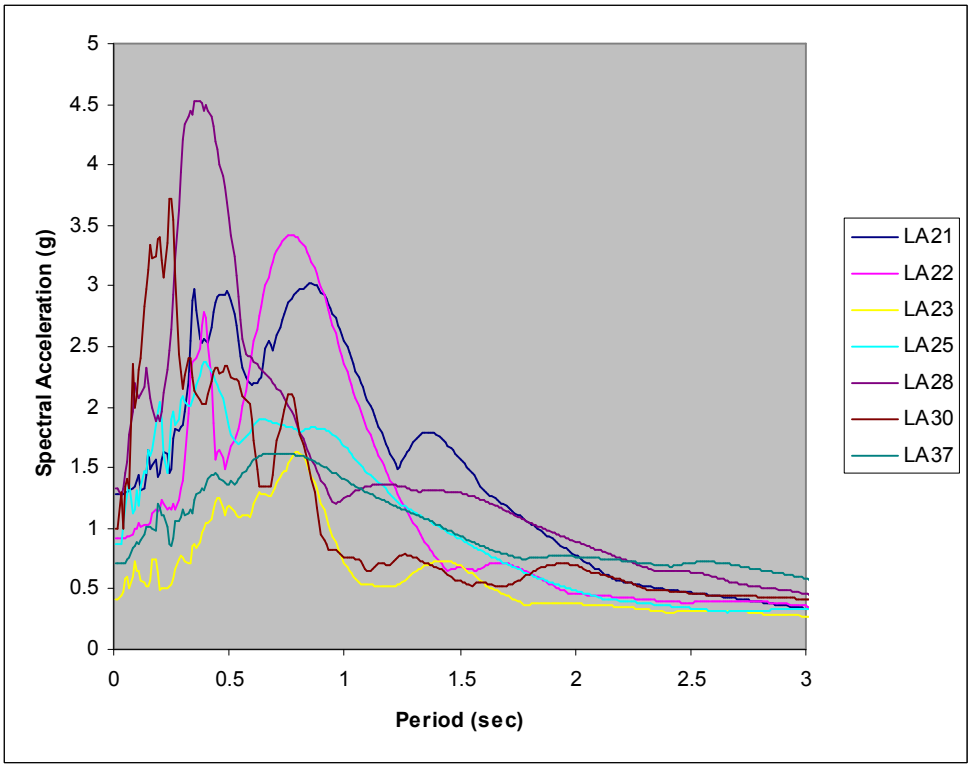

Figure 3.13 SAC Spectra – Los Angeles 2% in 50-Year, 5% Damped

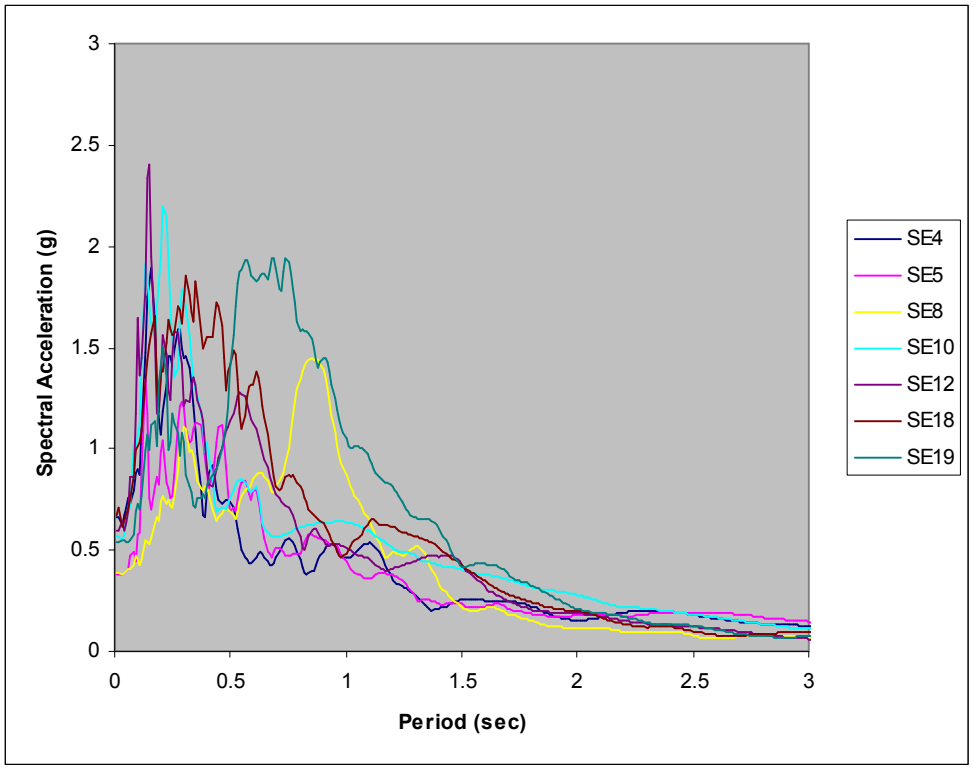

Figure 3.14 SAC Spectra Seattle 10% in 50-Year, 5% Damped

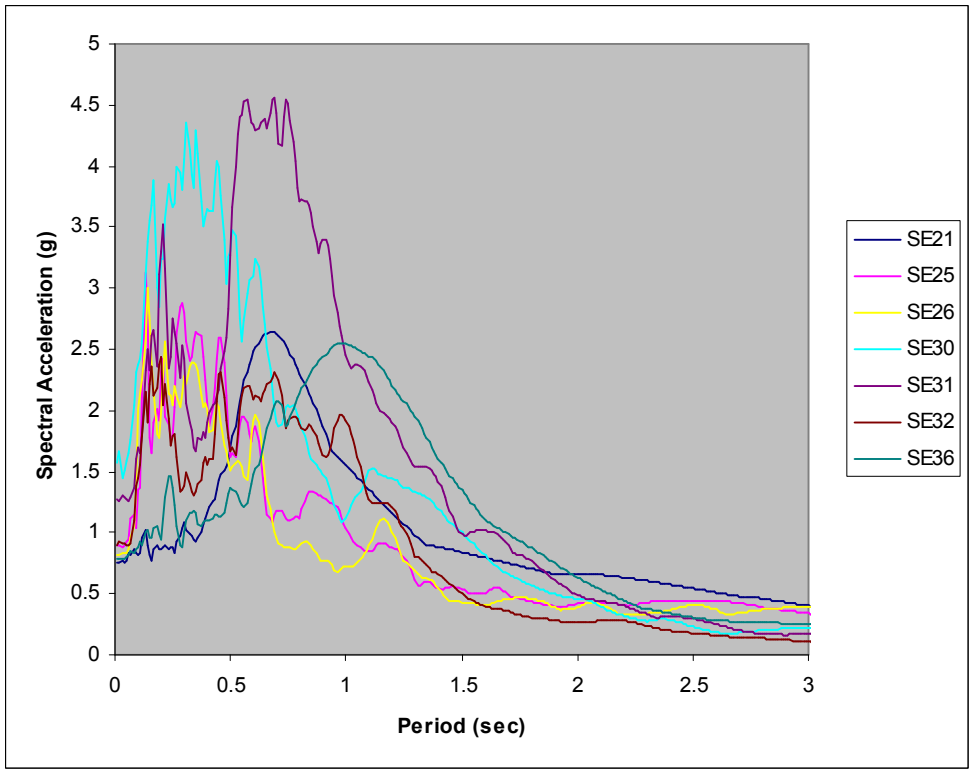

Figure 3.15 SAC Spectra Seattle 2% in 50-Year, 5% Damped

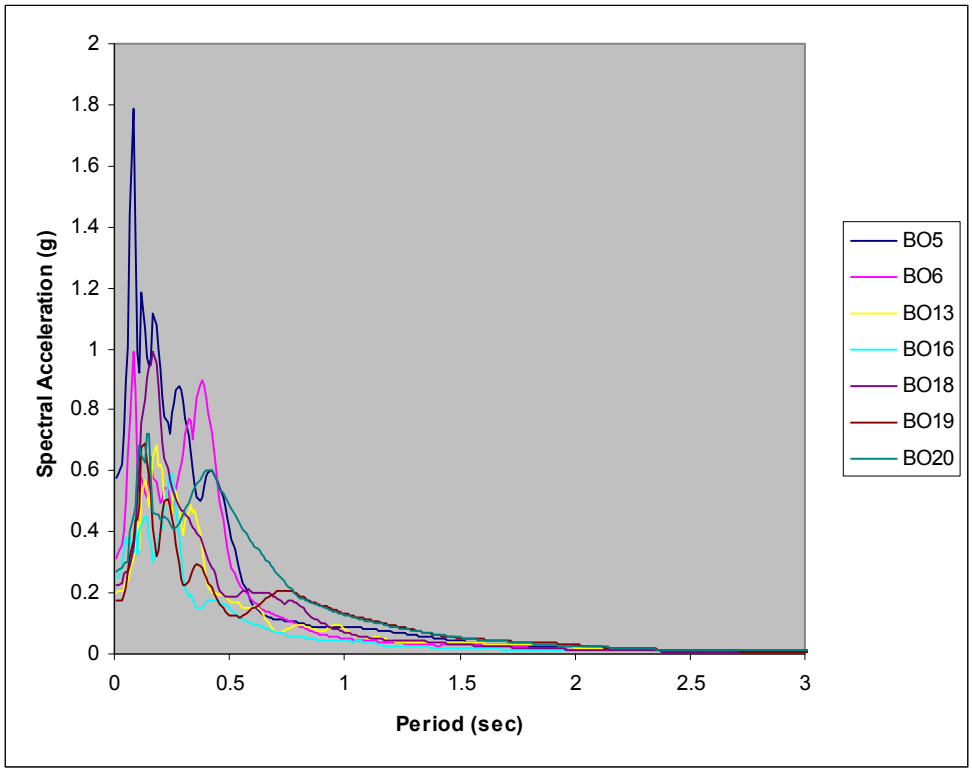

Figure 3.16 SAC Spectra Boston 10% in 50-Year, 5% Damped

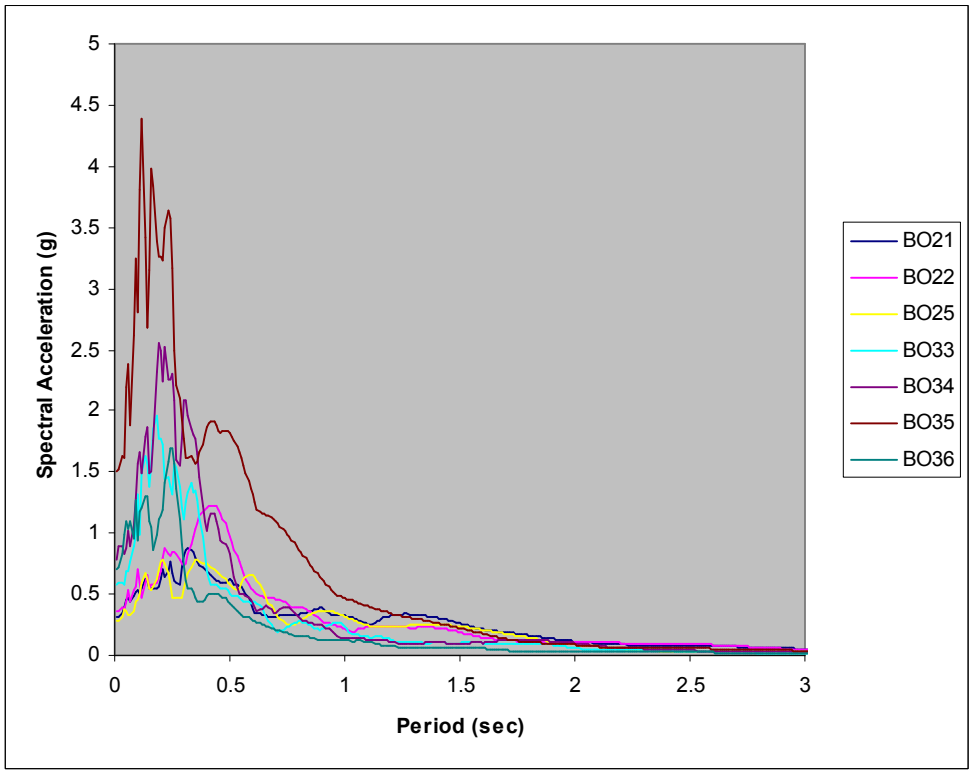

Figure 3.17 SAC Spectra Boston 2% in 50-Year, 5% Damped

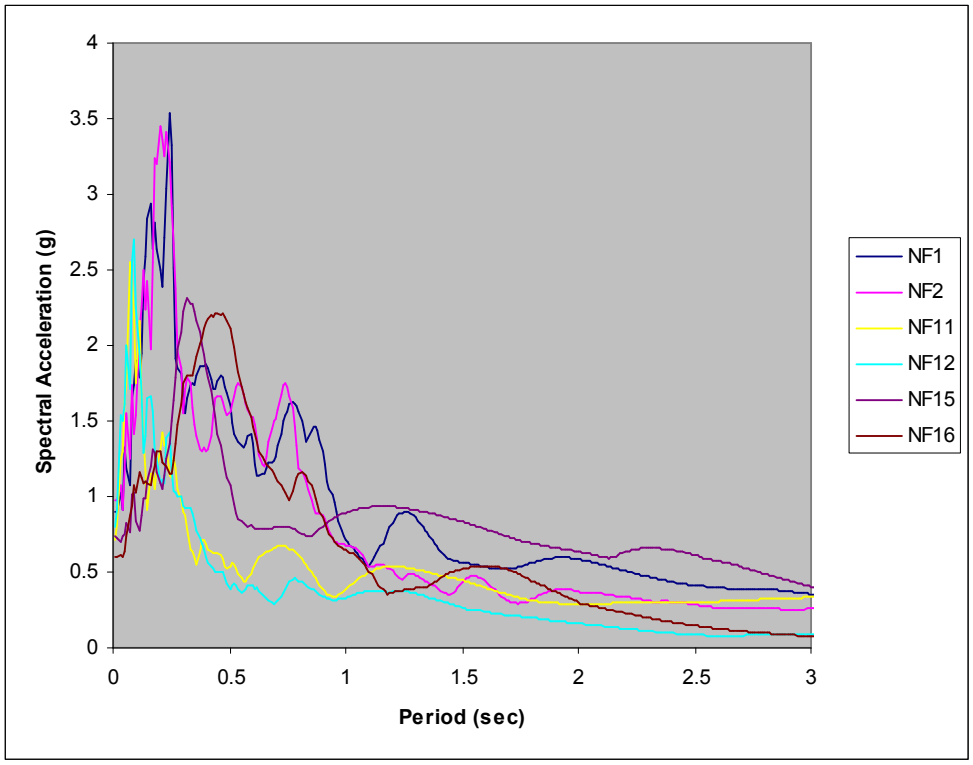

Figure 3.18 SAC Spectra Near Field, 5% Damped

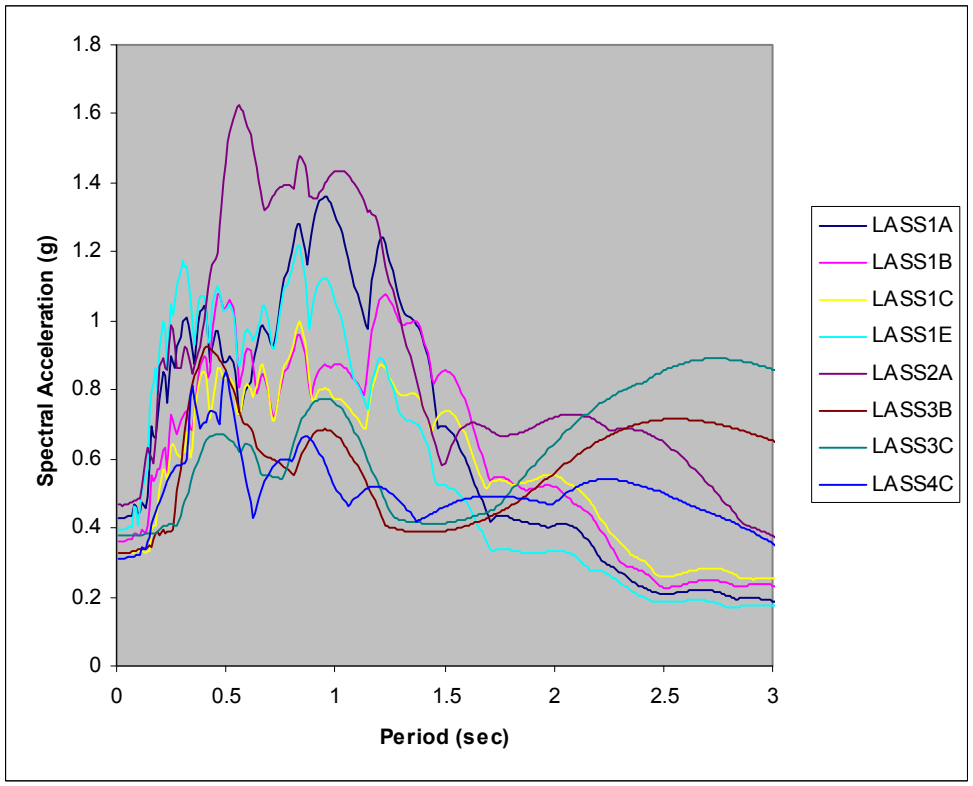

Figure 3.19 SAC Spectra Soft Sites, 5% Damped

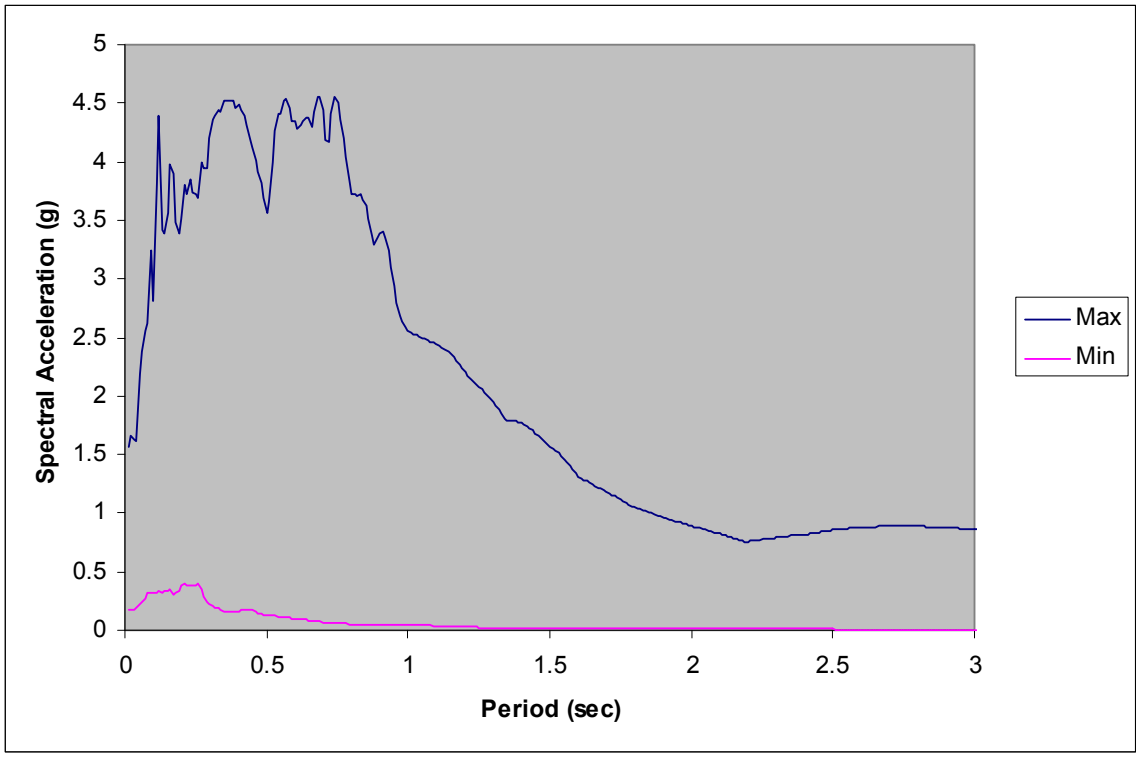

Figure 3.20 SAC Spectra Envelope, 5% Damped

analyses establish the range of structures and ground motions for which the nonlinear/inelastic rooftop tuned mass damper frame may be deemed effective as shown hereafter.

3.5 Time History Analysis Approach

Selection of linear and nonlinear time history analyses methods enabled the most direct and rational approach for assessing the effectiveness of the rooftop tuned mass damper frames. Conventional methods such as equivalent static procedures and even dynamic response spectrum procedures address element nonlinearity in indirect, and sometimes in an inaccurate manner. Furthermore, nonlinear time history procedures enable the direct quantification of the performance of the rooftop damper and the original structure including peak transient performance parameters along with overall

performance parameters such as energy demand and energy dissipated. Additionally, conventional response spectrum procedures are deemed less effective since modal combination techniques account only for scalar quantities associated with peak response parameters (all modal contributions are positive) and are indirect with respect to the development of a composite peak response parameters based on typical modal combination techniques (SRSS and CQC modal combination methods). The nonlinear time history approach directly accounts for the counteracting effects associated with mode 2 response depicted in Figure 3.21. The beneficial effects of amplified mode 2

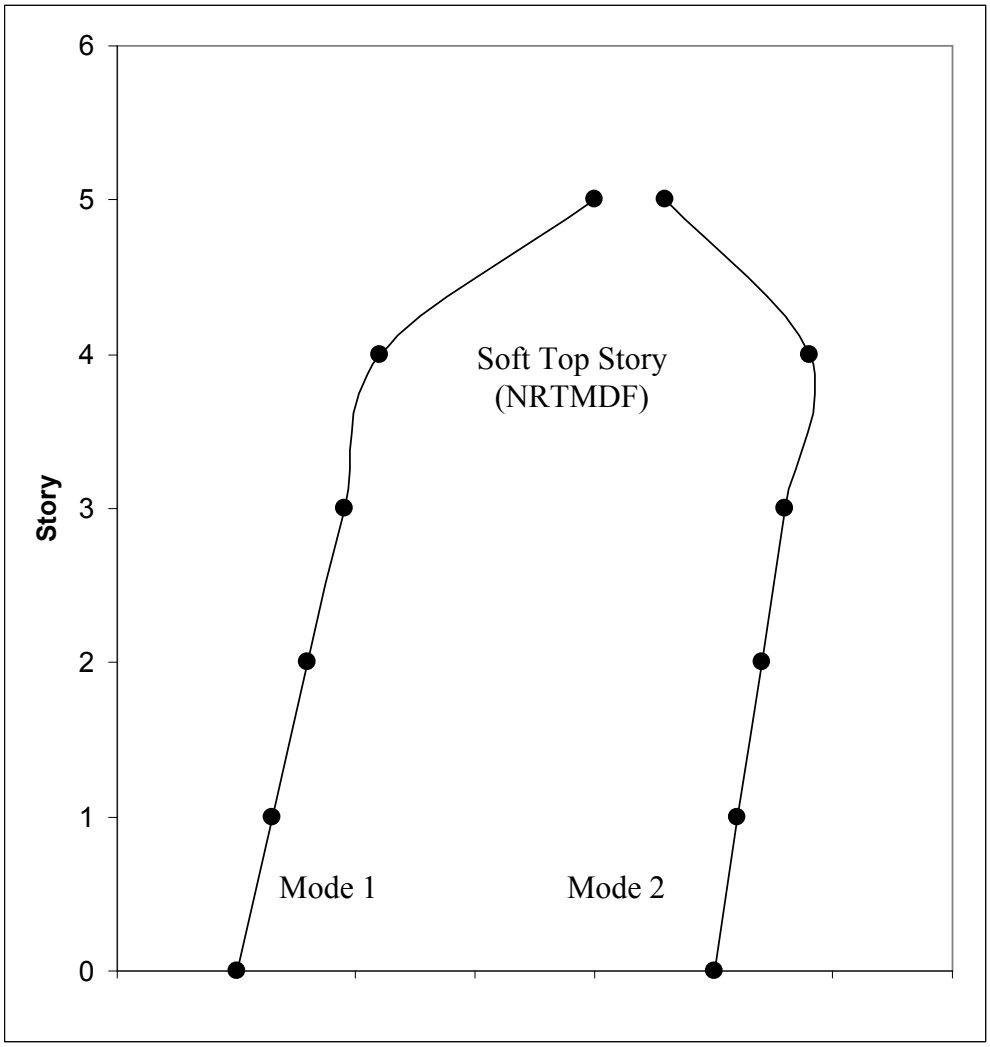

Figure 3.21 BF-4 Simplified Model Representations of Mode 1, Mode 2

response will be demonstrated hereafter as the NRTMDF develops into a counteracting inertial effect to the motion of the base structure. Such behavior may not accurately be captured using static or response spectrum analyses methods. Other approaches utilized within the context of this study include nonlinear static pushover analyses which may indicate whether damper mobilization is likely to occur prior to yielding of the original structure.

3.6. NRTMDF Modeling Parameters

Modeling parameters for buckling restrained braces within the NRTMDF were based upon current guidelines for modeling the behavior of buckling restrained bracing elements.[27] In particular, the primary performance parameters of the BRB elements affecting the behavior of the global system include elastic stiffness, effective stiffness, yield strength, post yield stiffness ratio and maximum capable nonlinear strain (ductility) in both tension and compression. Design of the NRTMDF requires the utilization of a strategy that tracks these key parameters in conjunction with the mass selected for inertial resistance of the NRTMDF frame. For this study, effective stiffness of the penthouse BRB represented the most convenient parameter for tracking performance through the parametric optimization studies and the selection of the effective parameters to enable the highest effective reduction in seismic response. Figure 3.22 depicts the hysteretic backbone of a typical BRB, assumed to behave symmetrically in tension and compression with degraded effective stiffness reflected from progressively higher levels of inelastic strain.

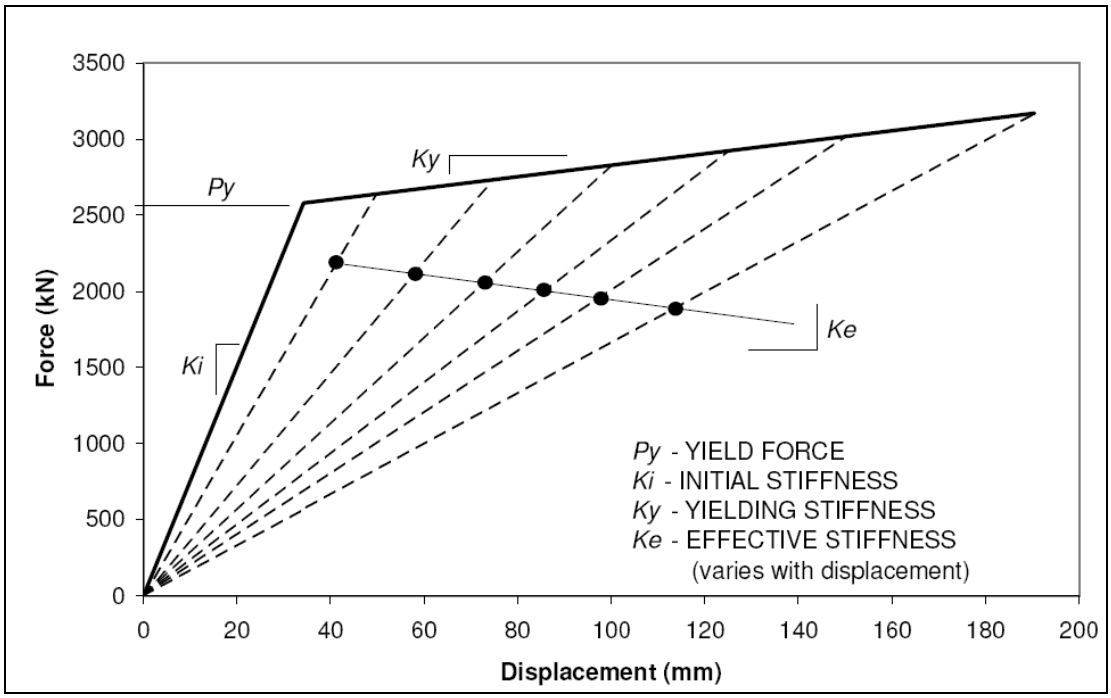

Figure 3.22 Typical NRTMDF Hysteretic Backbone

While analytical approaches may ultimately enable the development of an effective approach for optimization, the stochastic nature of input ground motions precludes this as a pragmatic possibility for the time history analyses. Determination of effective properties for the NRTMDF is most likely achieved by trial and error. This approach is reflected in this study. Nevertheless, the comprehensiveness of this study has identified useful approximations the key parameters of the NRTMDF which may be utilized as a starting point for selection of effective properties. For example, 5% the average story stiffness serves as starting point for assessing an effective NRTMDF stiffness.

3.7 Rational Design Approach

Beyond the broad analysis approach utilizing the SAC ground motions, each of the ten test structures was subjected to a rational design scenario utilizing a suite of

ground motions representing hard, medium, and soft soil conditions. The purpose of this was to address the performance-based design protocol outlined in the ASCE 41 Standard, *Seismic Rehabilitation of Existing Buildings* for each soil classification.[28] As such, the hard soil conditions reflect Type C soil, medium conditions reflect Type D and soft conditions reflect Type E which is also consistent with NEHRP (National Earthquake Hazards Reduction Program) criteria. Within these classifications, ground motions were also selected with distances from source of 0 to 10km, 10 to 30km and 30 to 50km+ as indicated in Tables 3.3 through 3.5. The purpose with this was to include motions representing the various distances from source to capture the attenuation and near source effects resulting from seismic waves propagating through the varying soil conditions.

ASCE 41 prescribes a standard for seismic performance termed the Basic Safety Objective (BSO). The BSO is defined as structural capacity sufficient to enable a Life Safety level of performance for an earthquake having a 10% probability of exceedence in a 50-Year period. Also the BSO includes a Collapse Prevention level of performance for an earthquake having a probability of exceedence of 2% in 50-Years. For convenience, these seismic events are termed Basic Safety Earthquake 1 (BSE-1) and Basic Safety Earthquake 2 (BSE 2) respectively. For each of the three soil conditions (Hard, Medium, Soft), 7 records for BSE-1 and 7 records for BSE-2 were selected from the SAC inventory. This is consistent with provisions addressed in ASCE 41 reflecting the Basic Safety Objective and time history analysis procedures. Tables 3.3, 3.4, 3.5 summarize the records selected for this analysis and Figures 3.23 through 3.34 depict the acceleration response spectra for each record along with the average of the spectra compared to the prescribed code design spectra. The respective records were scaled in

Table 3.3 Hard Site Ground Motions

Basic Safety Earthquake (BSE-1), 10% in 50-Year Recurrence (R = 474 years) Target Magnitude (Mw) 6.5 to 7.0					
Distance (km)	Record	Station	Distance (km)	Mw	PGA(g)
0 to 10	LA20	North Palm Springs, 1986	6.7	6.0	0.99
	BO7	Nahanni, 1985	6.7	6.9	0.09
10 to 30	SE04	Morgan Hill 1984 Gilroy	15	6.2	0.66
	LA12	Loma Prieta, 1989, Gilroy	12	7.0	0.97
30 to 50+	SE05	West. Washington, Olympia, 1949	56	6.5	0.38
	SE06	West. Washington, Olympia, 1949	56	6.5	0.35
	SE12	Puget Sound, Wa., Olympia, 1949	80	7.1	0.60
			Average	6.6	0.58

Basic Safety Earthquake (BSE-2), 2% in 50-Year Recurrence (R = 2475 years) Target Magnitude (Mw) 7.0 to 7.5					
Distance (km)	Record	Station	Distance (km)	Mw	PGA(g)
0 to 10	LA28	1994 Northridge	6.4	6.7	1.33
	LA30	1974 Tabas	1.2	7.4	0.99
	LA39	Palos Verdes (Simulated)	1.5	7.1	0.50
10 to 30	LA33	Elsyian Park (Simulated)	10.7	7.1	0.78
	SE39	Shallow Interplate (Simulated)	15	7.9	0.58
30 to 50+	SE25	1949 Olympia	56	6.5	0.90
	SE30	1985 Valparaiso	42	8.0	1.57
			Average	7.2	0.95

Table 3.4 Medium Site Ground Motions

Basic Safety Earthquake (BSE-1), 10% in 50-Year Recurrence (R = 474 years) Target Magnitude (Mw) 6.5 to 7.0					
Distance (km)	Record	Station	Distance (km)	Mw	PGA(g)
0 to 10	LA13	Northridge, 1994, Newhall	6.7	6.7	0.68
	LA14	Northridge, 1994, Newhall	6.7	6.7	0.66
	LA18	Northridge, 1994, Sylmar	6.4	6.7	0.82
10 to 30	LA02	Imperial Valley, 1940, El Centro	10	6.9	0.68
	SE03	Morgan Hill, 1984, Gilroy	15	6.2	0.39
30 to 50+	SE15	Eastern Wa., Tacoma County, 1949	60	7.1	0.29
	SE18	Llolleo, Chile 1985	42	8.0	0.67
			Average	6.9	0.60

Basic Safety Earthquake (BSE-2), 2% in 50-Year Recurrence (R = 2475 years) Target Magnitude (Mw) 7.0 to 7.5					
Distance (km)	Record	Station	Distance (km)	Mw	PGA(g)
0 to 10	LA23	1989 Loma Prieta	3.5	7.0	0.42
	LA24	1989 Loma Prieta	7.5	7.0	0.47
	SE23	1992 Erzincan	2.0	6.7	0.61
10 to 30	LA31	Elsyian Park (Simulated)	17.5	7.1	1.30
	LA32	Elsyian Park (Simulated)	17.5	7.1	1.19
30 to 50+	SE28	1965 Seattle	80	7.1	1.39
	SE32	1985 Valparaiso	42	8.0	0.90
			Average	7.1	0.90

Table 3.5 Soft Site Ground Motions

Basic Safety Earthquake (BSE-1), 10% in 50-Year Recurrence (R = 474 years) Target Magnitude (Mw) 6.5 to 7.0					
Distance (km)	Record	Station	Distance (km)	Mw	PGA(g)
0 to 10	SE01	Long Beach, Vernon CMD Bldg.	1.2	6.5	0.17
	LA03	Imperial Valley, 1979, Array #05	4.1	6.5	0.68
	LA15	Northridge, 1994, Rinaldi RS	7.5	6.7	0.53
10 to 30	LA09	Landers, 1992, Yermo	25	7.3	0.52
	LA10	Landers, 1992, Yermo	25	7.3	0.36
30 to 50+	LA07	Landers, 1992, Barstow	36	7.3	0.42
	SE07	West. Washington, Seattle Army B., 1949	80	6.5	0.29
			Average	6.9	0.43

Basic Safety Earthquake (BSE-2), 2% in 50-Year Recurrence (R = 2475 years) Target Magnitude (Mw) 7.0 to 7.5					
Distance (km)	Record	Station	Distance (km)	Mw	PGA(g)
0 to 10	LA38	Palos Verdes (Simulated)	1.5	7.1	0.78
	LA40	Palos Verdes (Simulated)	1.5	7.1	0.63
	SE24	1992 Erzincan	2.0	6.7	0.54
10 to 30	LA35	Elsyian Park (Simulated)	11.2	7.1	0.99
	LA36	Elsyian Park (Simulated)	11.2	7.1	1.10
30 to 50+	SE33	Deep Interplate (Simulation)	65	7.9	0.80
	SE36	1978 Miyagi-Oki	66	7.4	0.78
			Average	7.2	0.80

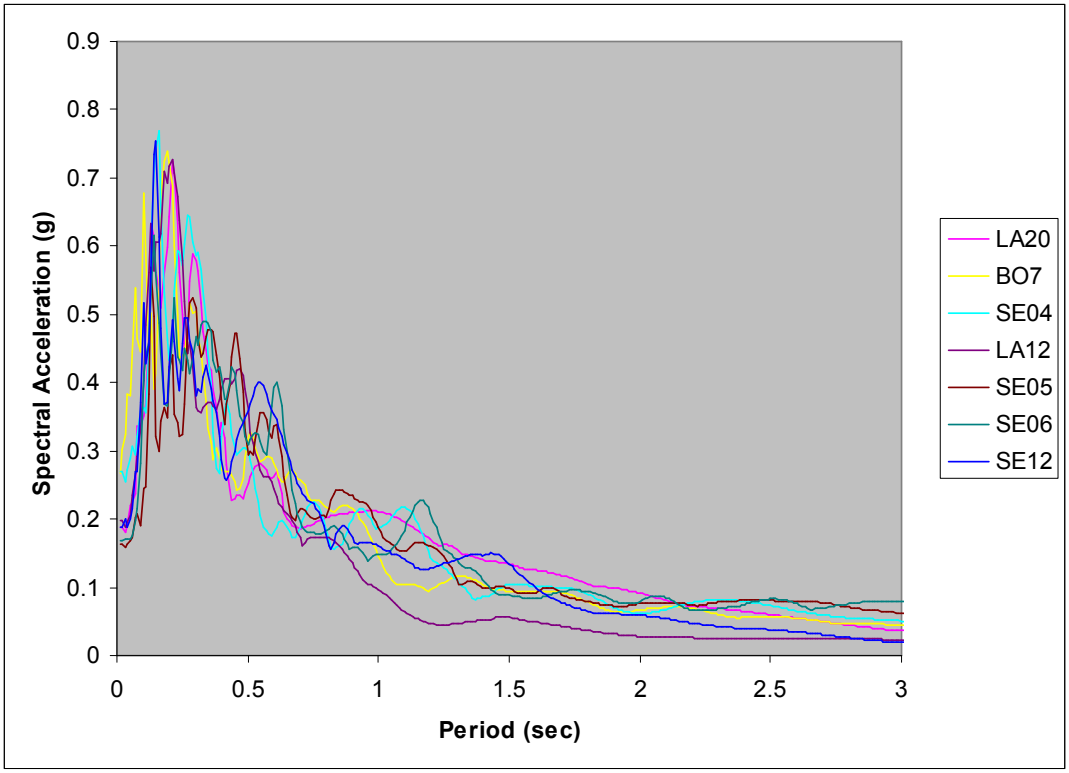

Figure 3.23 Hard Site Spectra for BSE-1, 5% Damped

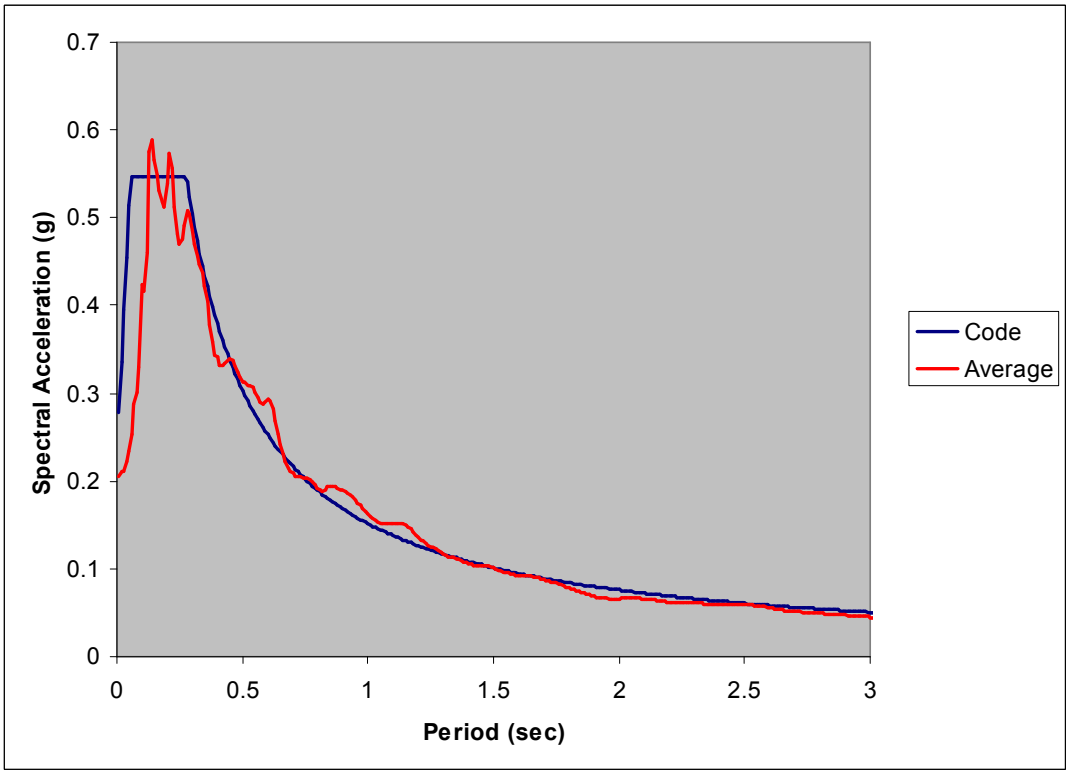

Figure 3.24 Hard Site Average and Code Spectra for BSE-1

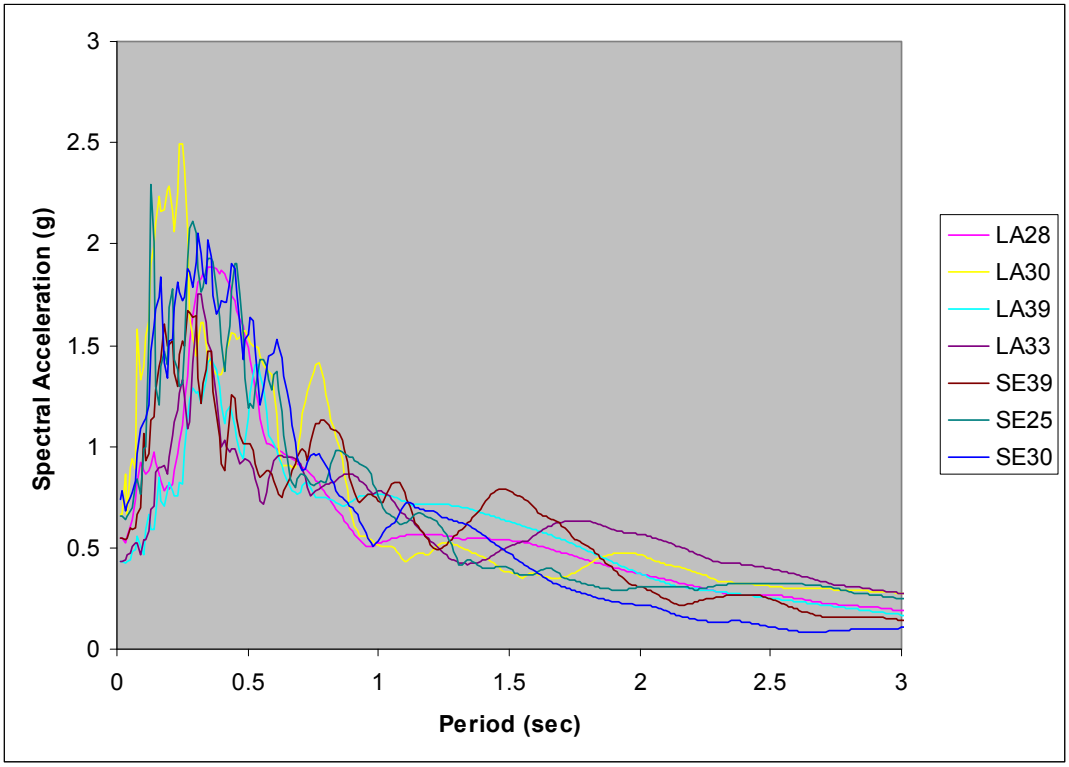

Figure 3.25 Hard Site Spectra for BSE-2, 5% Damped

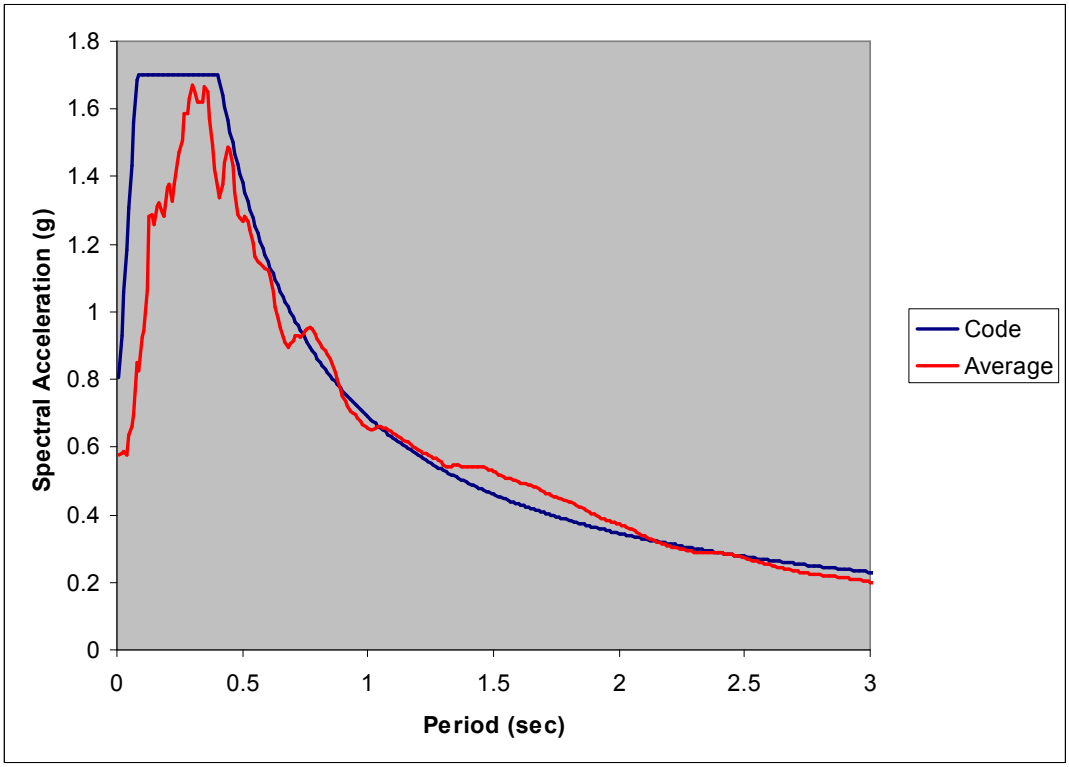

Figure 3.26 Hard Site Average and Code Spectra for BSE-2

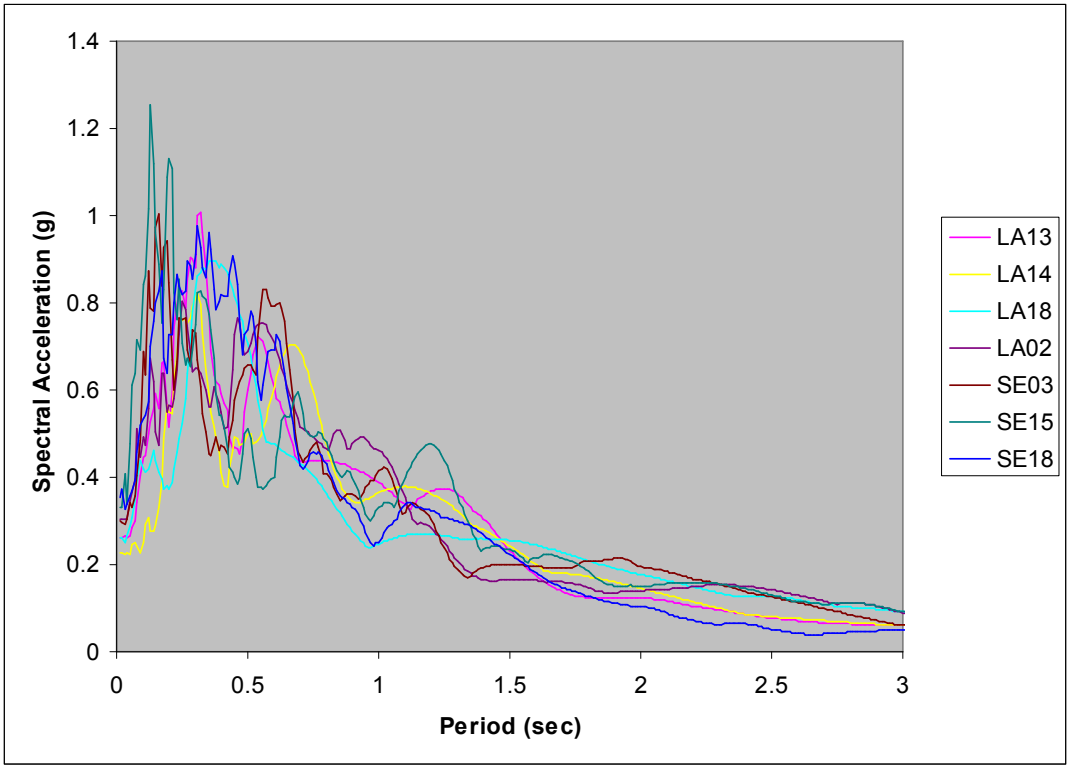

Figure 3.27 Medium Site Spectra for BSE-1

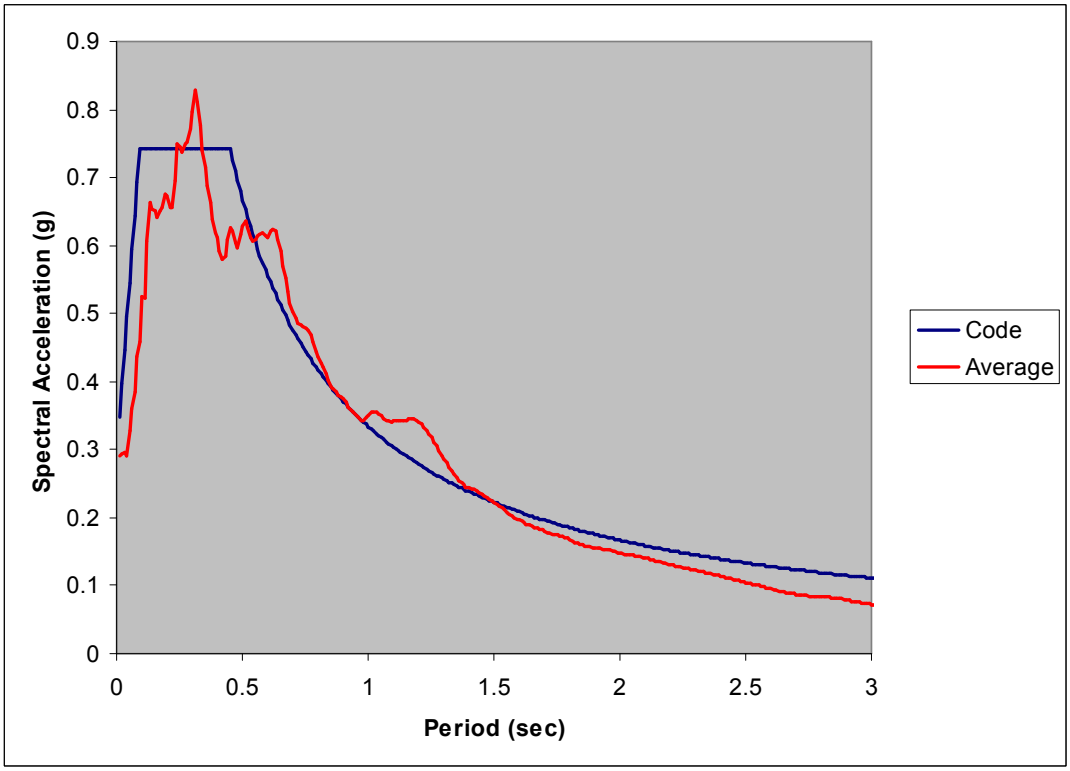

Figure 3.28 Medium Site Average and Code Spectra for BSE-1

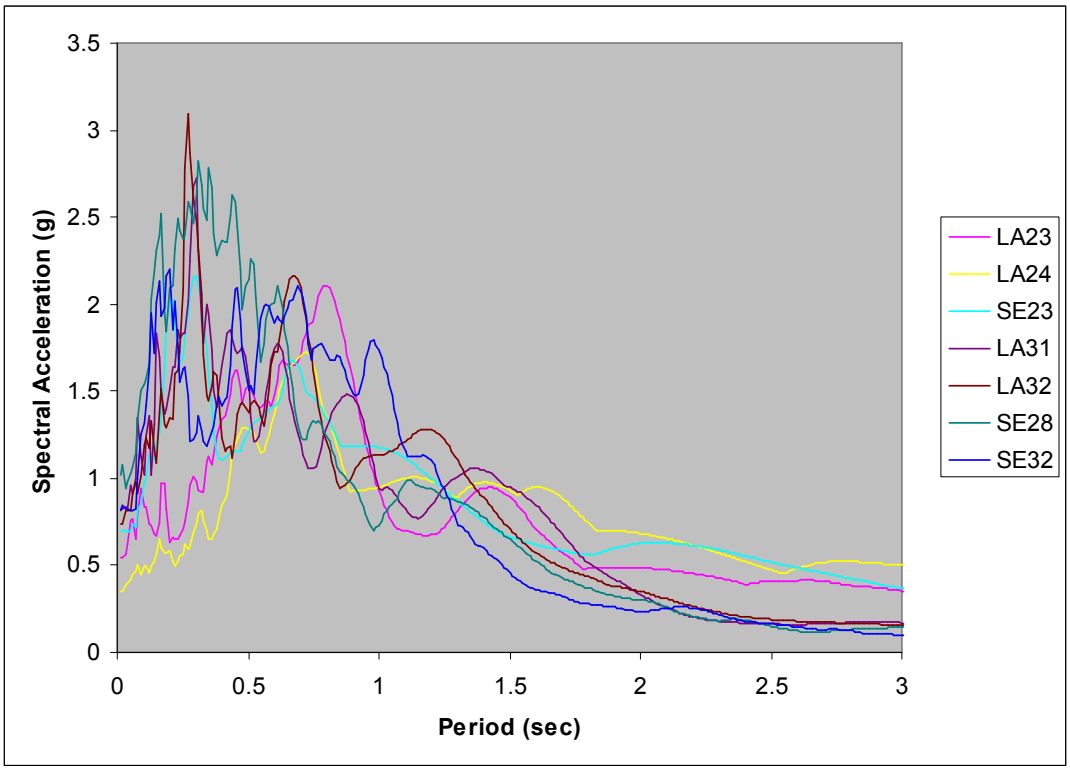

Figure 3.29 Medium Site Spectra for BSE-2, 5% Damped

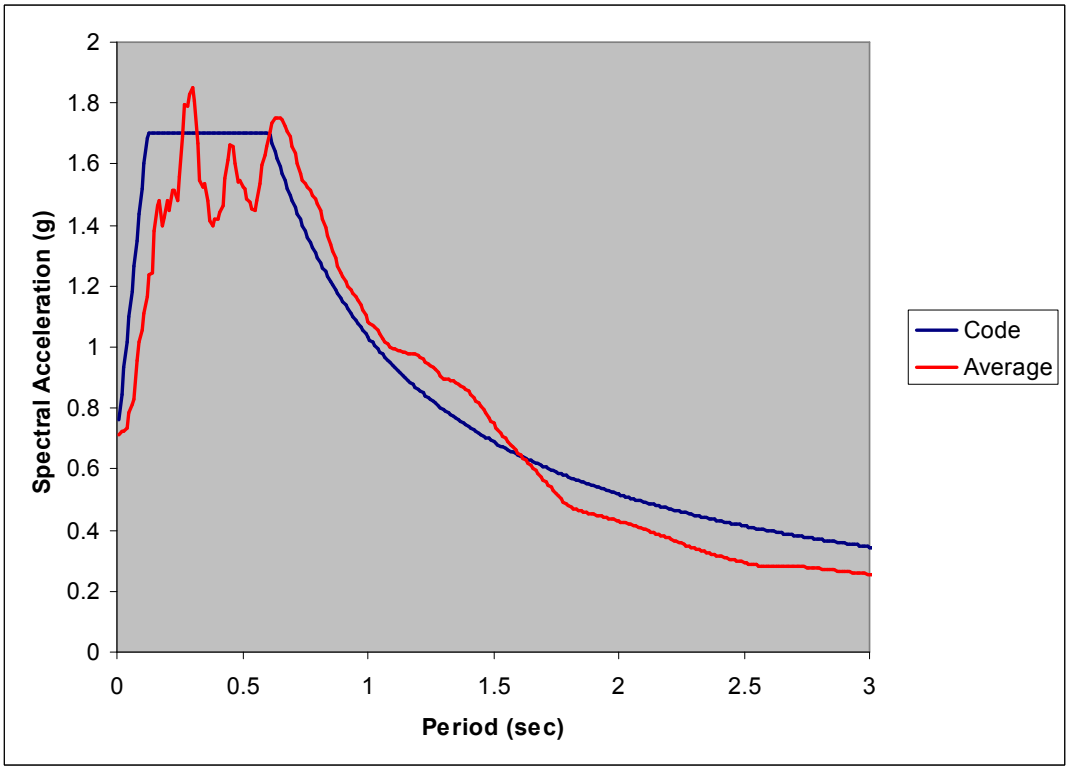

Figure 3.30 Medium Site Average and Code Spectra for BSE-2

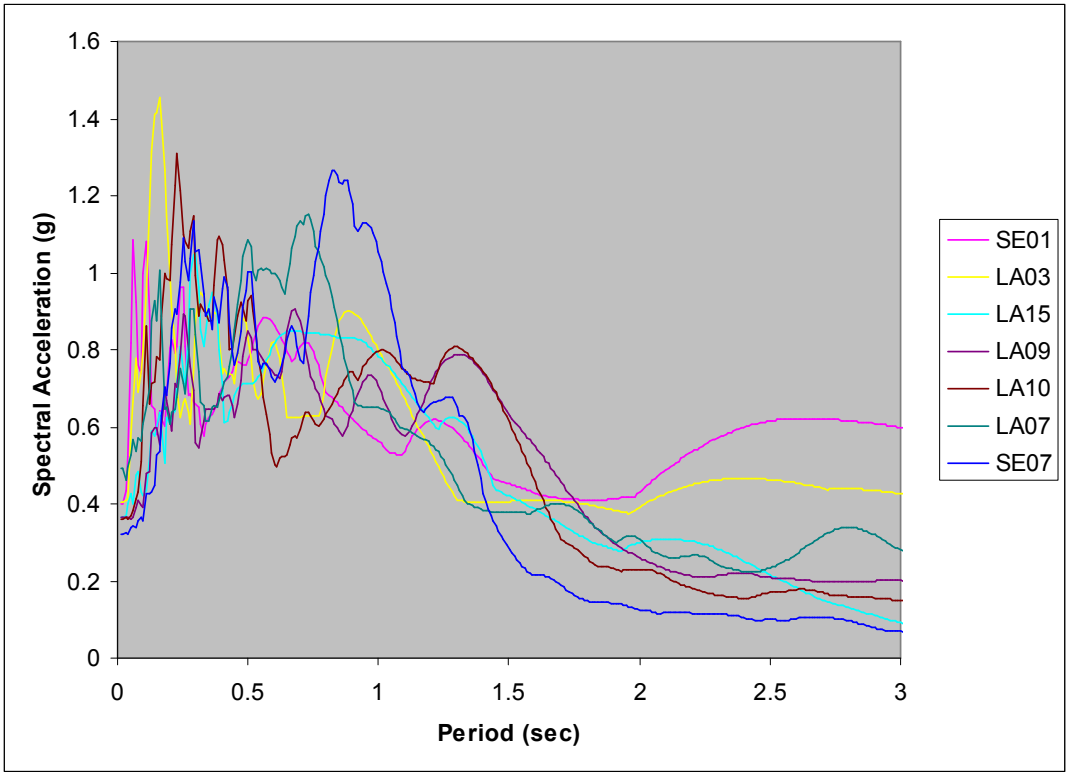

Figure 3.31 Soft Site Spectra for BSE-1, 5% Damped

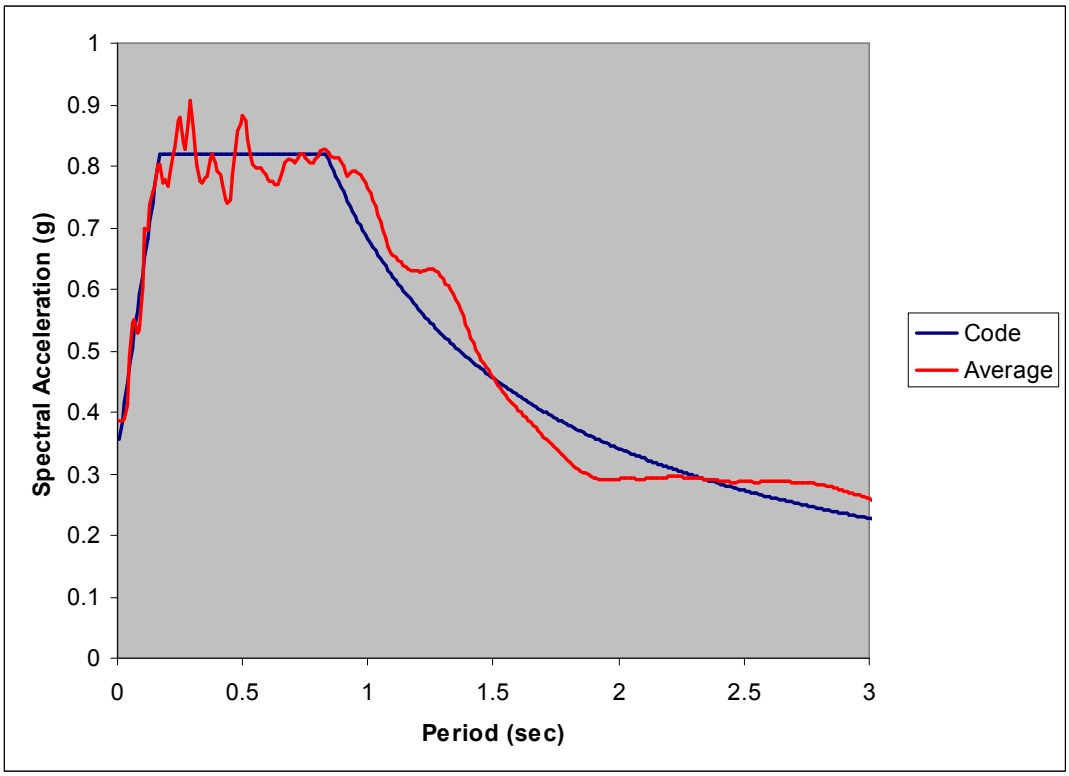

Figure 3.32 Soft Site Average and Code Spectra for BSE-1

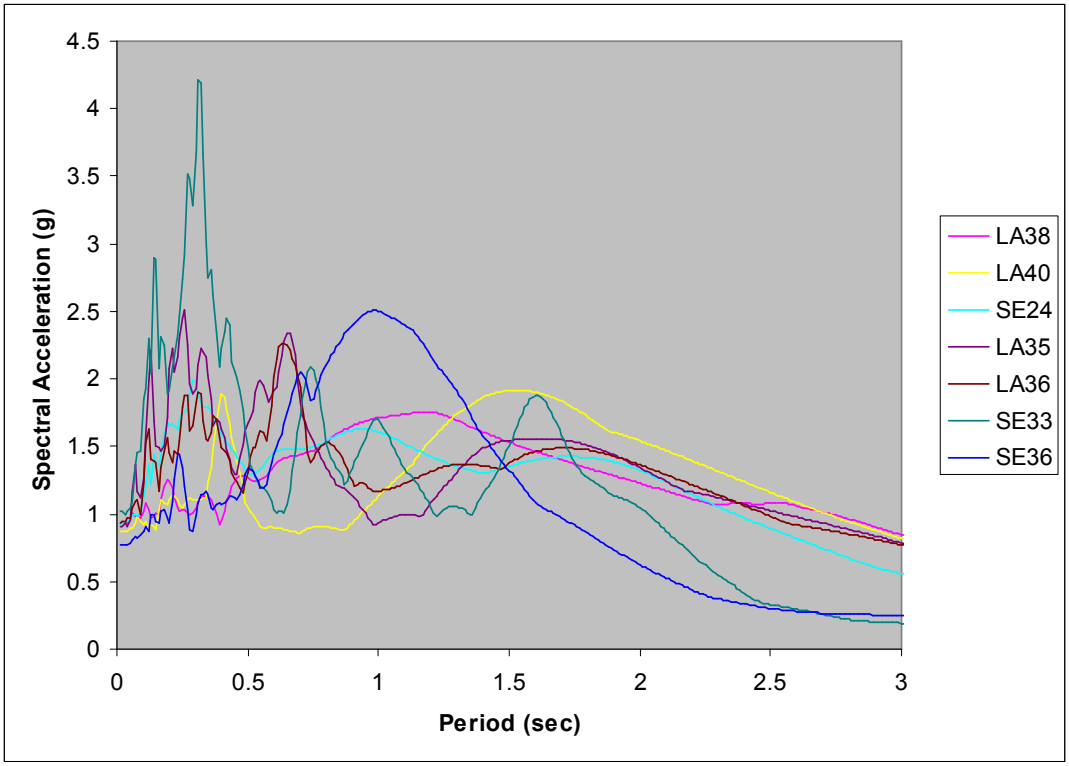

Figure 3.33 Soft Site Spectra for BSE-2

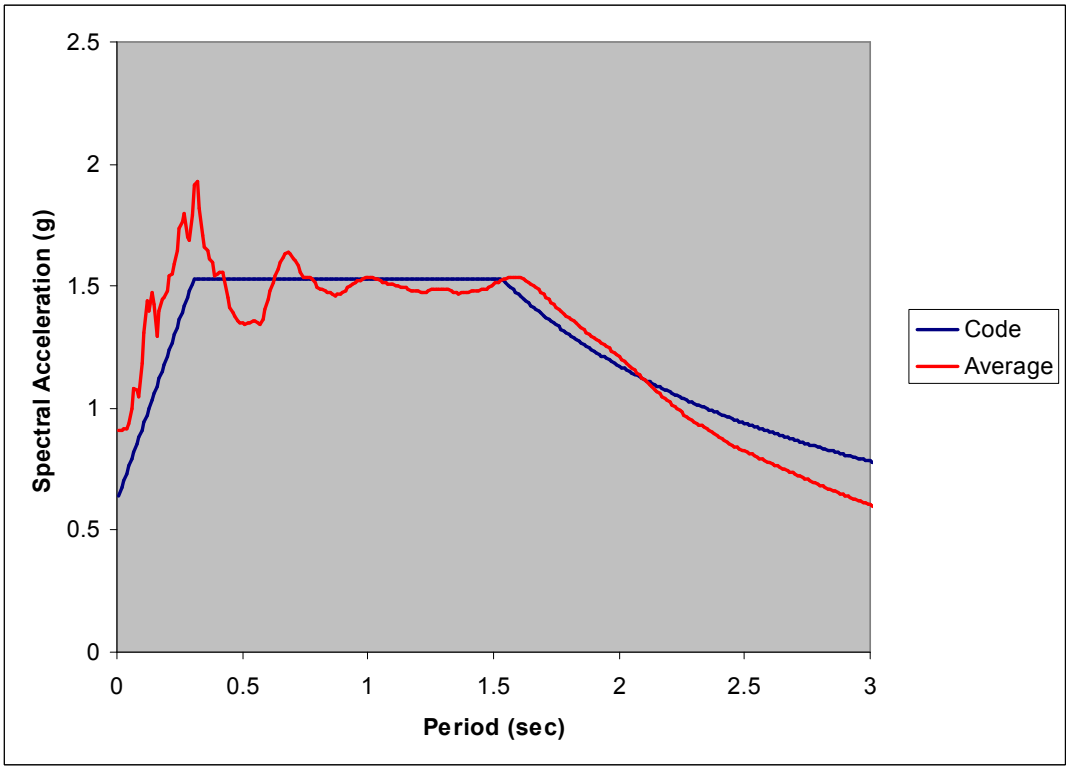

Figure 3.34 Soft Site Average and Code Spectra for BSE-2

accordance with standard procedures to coincide with spectra prescribed by ASCE 41 for the suite of structures. Common spectra were selected for BSE-1 (10% in 50-Year event) and BSE-2 (2% in 50-Year event) owing to proximity of the model building sites which results in similar mapped spectral acceleration values. Furthermore, utilizing site specific unique spectra and scaling the selected motions to these values for each of the test structures would have unnecessarily compounded the quantity of analysis input motions by a factor of 10 while only slightly changing the analysis output results with no significant change in qualitative output. The motions, as characterized, are deemed sufficient for assessing the effectiveness of the NRTMDF approach and satisfying the objectives of the research. The results of these analyses corroborate the findings of the earlier studies by Johnson, Pantelides and Reaveley and reflect the appropriateness and extent of effectiveness of the NRTMDF approach for each structure and each suite of motions reflecting each of the three soil conditions.[11]

Recent web based tools developed by the Pacific Earthquake Engineering Research Center (PEER) have enabled the automated selection of ground motions based on spectra input by the user.[29] This tool has the capability of filtering ground motion selection on the basis of magnitude, fault type, record duration, distance to rupture plane, average shear wave velocity in the top 30m of the ground at the recording station (Vs_{30}) and pulse type. For BF-4, ground motions were derived from the PEER website reflecting the Basic Safety Objective and a medium soil condition. This was selected since medium soils represent the predominant condition reflecting typical sites. Building BF-4 was selected as the most typical structure represented within the study. The purpose of this analysis effort is to demonstrate the application of the PEER tools with

respect to the NRTMDF, its analysis, design and optimization. Table 3.6 summarizes the ground motions identified using the PEER website and Figures 3.35 through 3.38 depict the spectra for BSE-1 and BSE-2 along with the spectra prescribed by ASCE 41 derived from current mapped spectral acceleration values.

3.8 Effective Performance and the Basic Safety Objective (BSO)

An effective NRTMDF configuration may be realized for any specific ground motion or performance objective; however, this is unrealistic in most scenarios since the specific nature of future ground motions can never truly be determined. For this reason, code prescriptive methods typically require a suite of ground motions representing the expected motions at a specific site correlating to the predetermined performance

Table 3.6 Ground Motions from PEER Website

Distance (km)	Records for BSE-1	Distance (km)	Mw	PGA (g)	Vs30 (m/s)
0-10	NGA_158IMPVALL.H-AEP_FP	0.3	6.53	0.272	274.5
	NGA_184IMPVALL.H-EDA_FN	5.1	6.53	0.417	202.3
	NGA_184IMPVALL.H-EDA_FP	5.1	6.53	0.444	202.3
10-30	NGA_719SUPERST.B-BRA_FN	17	6.54	0.158	208.7
	NGA_730SPITAK.GUK_FP	24	6.77	0.189	274.5
30-50+	NGA_947NORTHR.ARC_FP	39.7	6.69	0.082	308.6
	NGA_1094NORTHR.SOR_FP	51.7	6.69	0.069	308.6

Distance (km)	Records for BSE-2	Distance (km)	Mw	PGA (g)	Vs30 (m/s)
0-10	NGA_1605DUZCE.DZC_FP	6.6	7.14	0.519	276
	NGA_1615DUZCE.1062_FN	9.2	7.14	0.245	338
10-30	NGA_850LANDERS.DSP_FP	21.8	7.28	0.166	345.4
	NGA_881LANDERS.MVH_FN	17.3	7.28	0.144	345.4
	NGA_1602DUZCE.BOL_FN	12	7.14	0.784	326
30-50+	NGA_838LANDERS.BRS_FP	34.9	7.28	0.086	370.8
	NGA_1776HECTOR.12149_FP	56.4	7.13	0.077	345.4

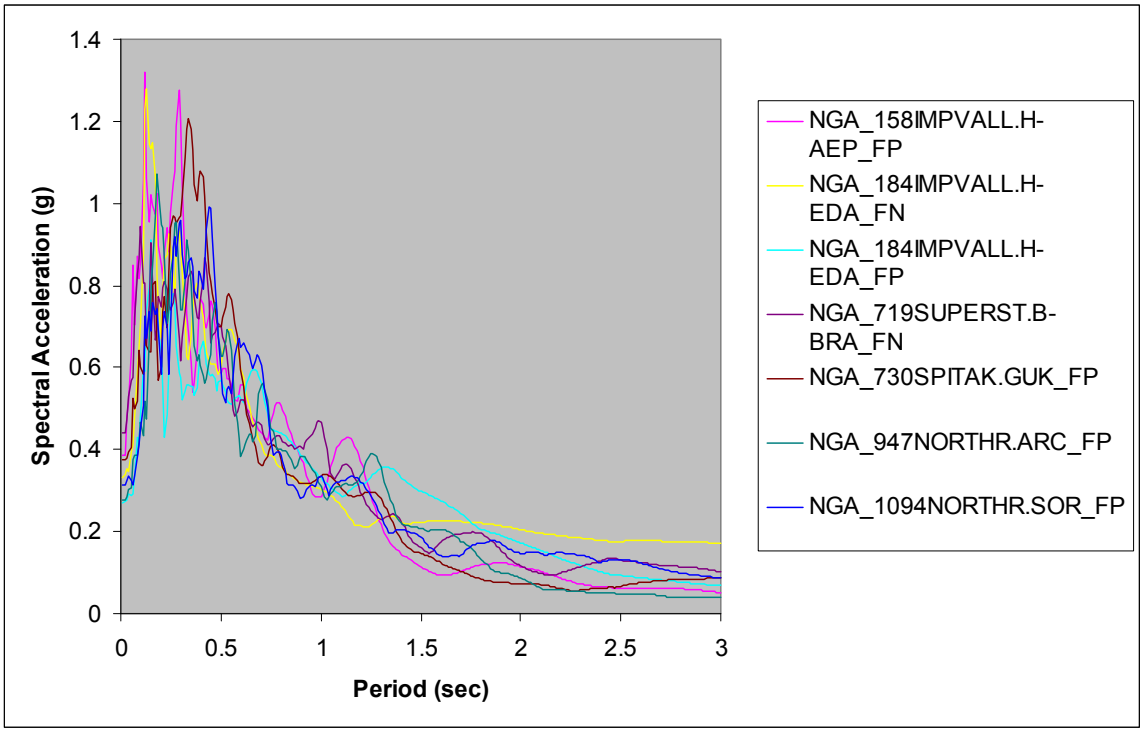

Figure 3.35 PEER Spectra for BSE-1, 5% Damped

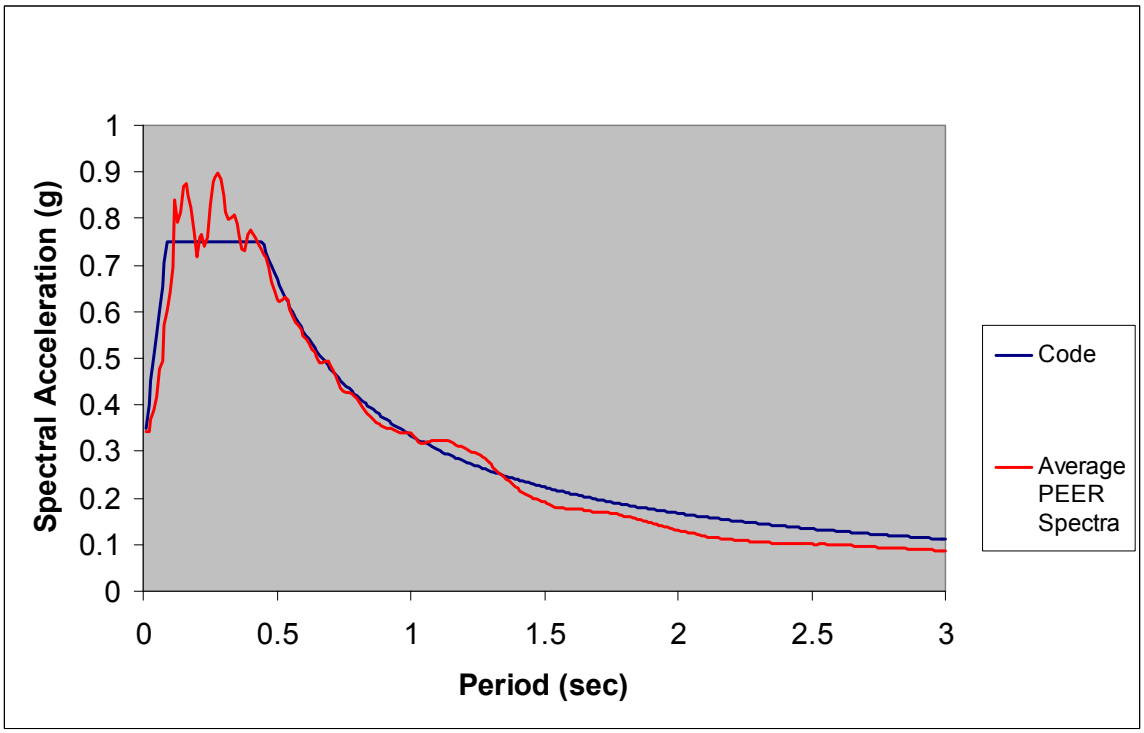

Figure 3.36 Average PEER and Code Spectra for BSE-1

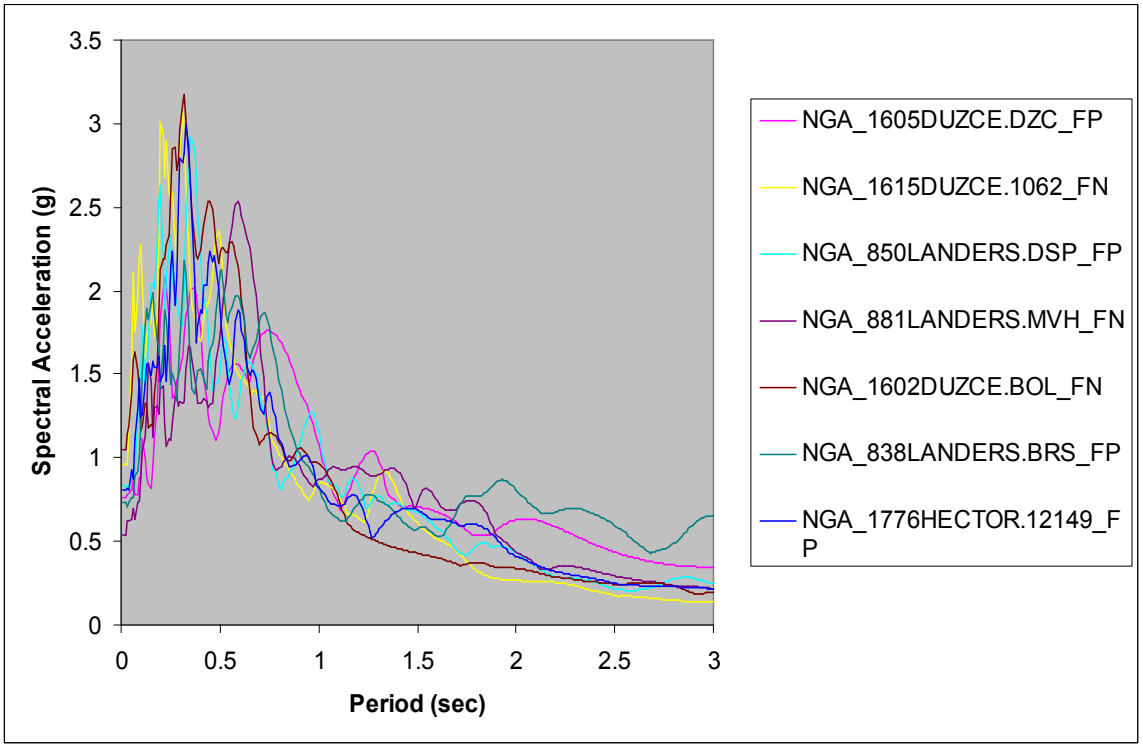

Figure 3.37 PEER Spectra for BSE-2, 5% Damped

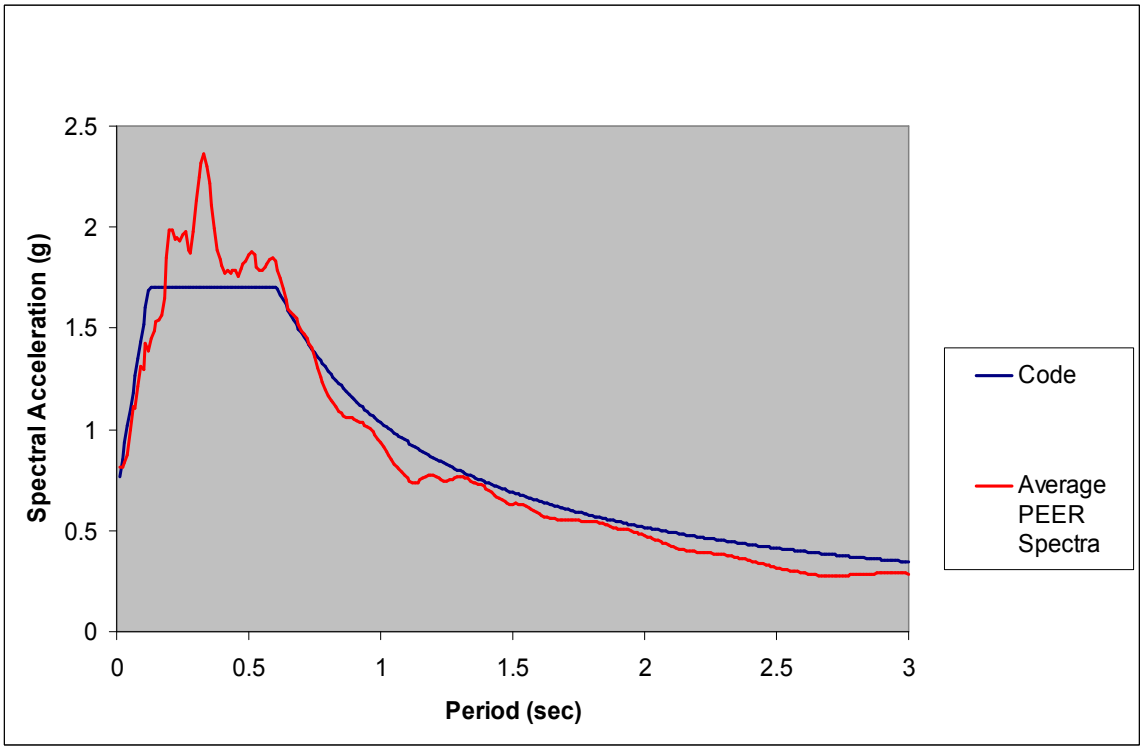

Figure 3.38 Average PEER and Code Spectra for BSE-2

objective. An effective solution for the NRTMDF solution may be realized and may result in favorable performance based on the average (or peak) response for this scenario. When multiple performance objectives are being considered, an effective NRTMDF solution may be determined for any single objective, but the effective properties of the NRTMDF determined may result in diminished performance for competing/parallel performance objectives. An example of this is the BSO (Basic Safety Objective) undertaken within the context of this study (Table 3.7). While an effective solution may be realized for the suite of motions representing a 2% in 50-Year event (BSE-2), this may come at the expense of an effective solution for the 10% in 50-Year event (BSE-1) and vice versa. Hence, a rational approach is to determine a solution that, although may not be most effective for either case, is satisfactory for both and yields a diminished response in the parameters of interest. It also follows that favorable performance may be realized

Table 3.7 Performance Objectives vs Ground Motions

		Ground Motion		
		50%/50-Year	10%/50-Year	2%/50-Year
Seismic Performance	Operational			
	Immediate Occupancy			
	Life Safety			
	Collapse Prevention			

Basic Safety Objective

Peripheral Performance Objectives

for ground motions representing a single performance objective, but this may result in unsatisfactory performance for other objectives that might be sought. To address this, a common rational approach is to seek a design solution for common performance objectives (ground motions) and to verify that unfavorable behavior does not follow suit for other peripheral objectives (e.g., a 50% in 50-year ground motion). Also, engineers may pursue a multi objective effective design which utilizes a weighted averaging of effective performance parameters in an effort to achieve the targeted performance considering the multiple objectives.

Following the Basic Safety Objective, effective performance for this study has been realized based on the average of output parameters for both the BSE-1 and BSE-2 earthquakes. While properties could be determined for each earthquake suite individually, such property selection for one earthquake suite may come at the expense of the other. Oftentimes, a valid approach for this is to identify which performance objective is most critical and then to verify that performance is not seriously compromised using the ground motions for other performance objectives of interest. For instance, the NRTMDF may be tuned for effective performance for BSE-2. It may then not perform effectively for BSE-1. Likewise, effective performance of the NRTMDF for BSE-1 may not yield effective performance of the NRTMDF for BSE-2. For this study, average reduction in performance parameters for BSE-1 and BSE-2 has been sought. It would follow suit to run a check using a different ground motion, such as a 50%/50-Year event simply to verify that peak output parameters have not increased, thereby putting a building in greater jeopardy for a smaller but more frequent event. Such an approach is approximated with the broad-based SAC ground motions utilized within this study.

While many ground motions contain accelerations reflecting a large, rare (2% in 50-year) event, others reflect smaller accelerations which may coincide with a small, frequent event (50% in 50-Years).

3.9. Energy Based Procedures

Analysis procedures for historic and even contemporary building codes contain protocols driven toward assessment of performance on the basis of peak transient output parameters (displacement, drift, and base shear). While this approach is generally effective, it is typically based on 5% inherent critical damping from both structural and nonstructural sources (as prescribed by current building codes) and it does not account for hysteretic energy dissipation on a structure throughout the duration of the transient event. Structural elements subject to repeated cycles of elastic and inelastic strain suffer strength degradation and fatigue that cannot be accounted for by assessing system effectiveness on the basis of peak output parameters alone. For example, a structure that yields only once will not suffer the same damage as it would for yielding multiple times. Furthermore, repeated cyclic motion creates increased demand on nonstructural elements, components and systems which most often represent a larger financial investment than does the structural system itself. Recent research has led to the development of protocols to account for this. Park and Ang introduced the concept of a damage index to account for seismic performance using energy methods accounting for behavior through the complete history of the earthquake.[30] Others including Amador, Teran-Gilmore utilize similar approaches gauging seismic performance based on a combination of peak transient displacement and total energy demand.[31] Accumulated energy demand on a structure for a given acceleration record is a parameter readily reported by most modeling

applications. Energy conservation principals require that all energy entering the system must be accounted for. Accumulated input energy must equal the sum of dissipated plus other embodied (potential or kinetic) energy. For most conventional structural analysis applications and modeling methods, the energy input into a system is dissipated by inherent system damping and by hysteretic demand on structural elements. Ideally, the inelastic hysteretic demand occurs at specific locations on designated yielding members. These may include shear links, plastic flexural hinge locations, braces yielding in tension or buckling in compression (or yielding in both tension and compression for buckling restrained braces) or confined areas of reinforced concrete assemblies. Once the hysteretic behavior of these elements is established for a given acceleration record, the total energy demand can be balanced and quantified. For this approach, it is common to reduce inherent damping (due to nonstructural systems) to 2% to 3% of critical. For assessing the effectiveness of the NRTMDF, the total energy demand for elements between the damped and undamped structures may be compared to demonstrate the diminished hysteretic demand on the structure enabled by using the rooftop damping system (NRTMDF). Reductions in energy demand may be compared directly to gauge the effectiveness (or lack thereof) of the rooftop frame. Other approaches accounting for energy in combination with peak output parameters such as damage index calculations can also demonstrate the overall effectiveness of the approach.

The concept of a damage index (D) is an approach gaining favor for assessment of seismic performance accounting for both peak transient behavior and hysteretic energy demand. Park and Ang developed the concept of damage index on an elemental basis as the peak displacement (δ_M) compared by ratio to the maximum capable displacement

(δ_u) accounting for nonlinear behavior of the element.[32] To this, energy demand is quantified by adding the ratio of total element energy demand (E) and the idealized elasto-plastic energy dissipated represented by the product of yield force (Q_y) and maximum capable displacement (δ_u). The fundamental damage index becomes:

$$D = \frac{\delta_M}{\delta_u} + \frac{\beta}{Q_y \delta_u} \int dE \qquad \text{Eq. 3-3}$$

For this, β is a factor accounting for the cyclic loading effect reflecting an inverse relationship to the structure's ability to demonstrate favorable hysteretic performance. The parameter β is determined by setting the energy portion of Eq. 3-3 to unity and solving directly for β; it serves to normalize the approach by quantitatively assessing the appropriate contribution of energy dissipation to the composite damage index calculation. The values for E, Q_y and δ_u are established from the nonlinear static pushover curve for the structure, where E represents the total area under the static pushover curve in both directions; Q_y and δ_u are the yield strength and maximum capable displacement determined from the pushover analysis. Equation 3-3 was originally developed for the assessment of damage on an element by element basis. Once calculated for the global system (including an assumed value for inherent damping), a composite damage index is then derived yielding a result reflecting a unity relationship where unity equates to the point of structural failure. Park and Ang suggest that a damage index (D) of 0.4 or less typically means that the structure is recoverable. Values between 0.4 and 1.0 reflect significant damage. For this, the structure may have performed sufficiently to address

Life Safety and Collapse Prevention concerns, but recovery would likely be an economic impracticality.

Adaptation of the damage index concept yields an approach to account for peak transient demand as well as total energy demand for a given structure and ground motion for this study. While calculating a damage index for every element and ground motion is beyond pragmatic limitations, a global adaptation of the concept is deemed a useful approach for gauging the effectiveness of the NRTMDF. Pushover analyses methods as prescribed by the ASCE 41 standard provide a convenient approach for determining the yield strength (Q_y) and the maximum capable displacement (δ_u) for each of the ten test models. Figure 3.39 depicts the pushover curve for BF-5 with these parameters indicated. Nonlinear time history analyses for each structure and ground motion enable

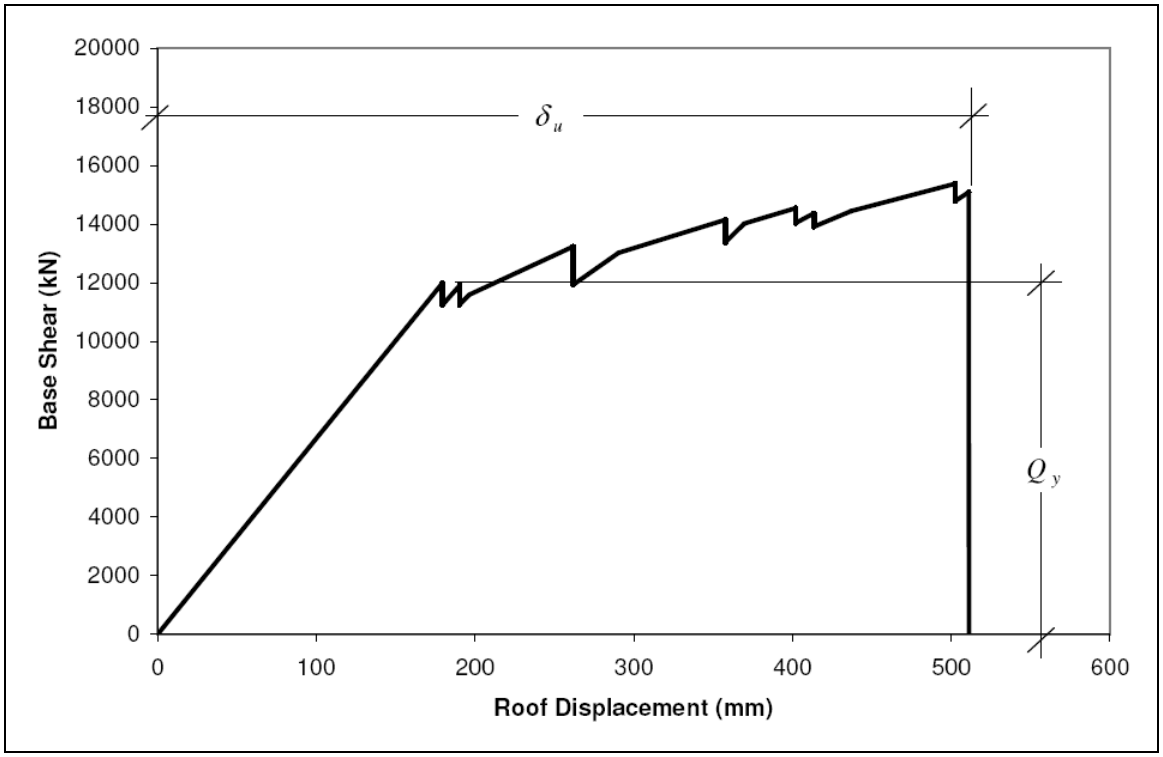

Figure 3.39 Nonlinear Pushover Diagram for BF-5

the quantification of input energy, peak displacement and energy demand represented by modal damping and element hysteretic behavior.

Supplemental to the examination of peak transient output parameters, damage index calculations are utilized herein to demonstrate the effectiveness of the NRTMDF for the complete time history of each acceleration record of the Basic Safety Objective.

Fardis utilizes an adapted version of the Park and Ang energy approach with claims of higher accuracy with respect to the damage index calculation model.[33] Fardis explains that the Park and Ang method falls short of accurately predicting structural failure based on statistical analyses of 169 reinforced concrete test specimens, 128 of which were tested with uniaxial loading and 41 with biaxial loading. Of the 169 specimens, 130 were tested to failure, defined as an abrupt change in the hysteretic relationship (loss of stiffness) while 39 were tested to near failure, representing behavior akin to Collapse Prevention (threshold of failure) level of performance. For these specimens, the calculated average damage index fell well below 1.0 indicating that the Park and Ang mathematical approach is too liberal in its predictions of favorable performance. For the Fardis approach, the damage index (D_E) is derived entirely from energy relationships:

$$D_E = \frac{\max E_d + \beta \int dE_h}{E_{d,u}} \qquad \text{Eq. 3-4}$$

For this, the value max E_d represents the peak value of member deformation energy up to the instant of interest in response, taken as the end of the time history analysis. The value

dE_h is taken as the total energy dissipated up to that instant and $E_{d,u}$ is the deformation energy in monotonic loading up to failure (area under the pushover curve).

The Fardis method and the Park and Ang method reflect an accounting of energy on an element by element basis which is then mathematically accumulated to develop the damage index for the complete structure. For the analyses herein represented, rational adaptations of these energy methods are demonstrated for each global structure. Comprehensive analysis would predicate calculation of damage indices on an element by element basis followed by the global damage index calculation for each structure and ground motion. Most computer applications are capable of reporting hysteretic energy on an element by element basis as well as the total hysteretic energy developed for the complete time history. However, element by element calculation of damage indices is deemed non pragmatic for the broad nature of this study. In lieu of this, the concept is adapted to the nonlinear static pushover analysis of the undamped base structure (structure without the NRTMDF). The associated hysteretic energy for the complete structure is then estimated by determining the area under the pushover curve up to the peak displacement calculated from the nonlinear time history analyses for both the undamped and damped structures. This rational adaptation of the energy methods to the global structures using pushover relationships coupled with nonlinear time history modeling enables the calculation of damage indices and comparison of the resulting values between the damped and undamped structures. This achieves the aim of measuring the global performance of the undamped and damped structures for the complete time domain of each record. Coupled with the analyses of peak output

parameters, this overall approach is considered acceptable for the assessment of the effectiveness of the NRTMDF.

3.10 Equivalent Damping Calculation

A tool akin to the energy methods for demonstrating the performance of the NRTMDF is the calculation of an equivalent damping ratio for the undamped and damped test models. Priestley, Seible and Calvi (1996) developed a procedure for assessment of equivalent damping as a modified ratio of energy dissipated per cycle (A_h) and the elastic strain energy (A_e) at peak displacement.[34] The developed relationship is represented by the following equation:

$$\xi_{eq} = \frac{A_h}{4\pi A_e} \qquad \text{Eq. 3-5}$$

For this approach it is necessary to model the nonlinear behavior of the system so that the hysteretic energy may be calculated. While nonlinear time history methods presented in this research enable the development of projected hysteresis loops for individual nonlinear elements they do not enable the development of a composite hysteretic relationship representing the global structure which can be conveniently adapted to this approach. Therefore, the approach for assessing the aforementioned energy parameters for this research follows the piecewise monotonic loading approach (nonlinear pushover analysis) which enables the development of the global force-displacement relationship necessary for the energy calculations. Once the projected peak displacements are determined, they can be applied to the hysteretic relationship to determine the hysteretic

damping energy (A_h) and the strain energy (A_e) which is derived from the effective stiffness of the system:

$$K_{eff} = \frac{V_m}{\Delta_m} \qquad \text{Eq. 3-6}$$

where V_m is the base shear on the force-displacement relationship corresponding to the maximum projected displacement Δ_m. Figure 3.40 depicts the load displacement relationship for BF-5 and the parameters utilized for the equivalent damping calculation. For the damped test structure the total hysteretic energy dissipated by the system (A_h) includes the energy dissipated in hysteretic action of the NRTMDF at its peak displacement (Δ_m) which is taken as the area within the NRTMDF hysteretic diagram up to the peak NRTMDF displacement.

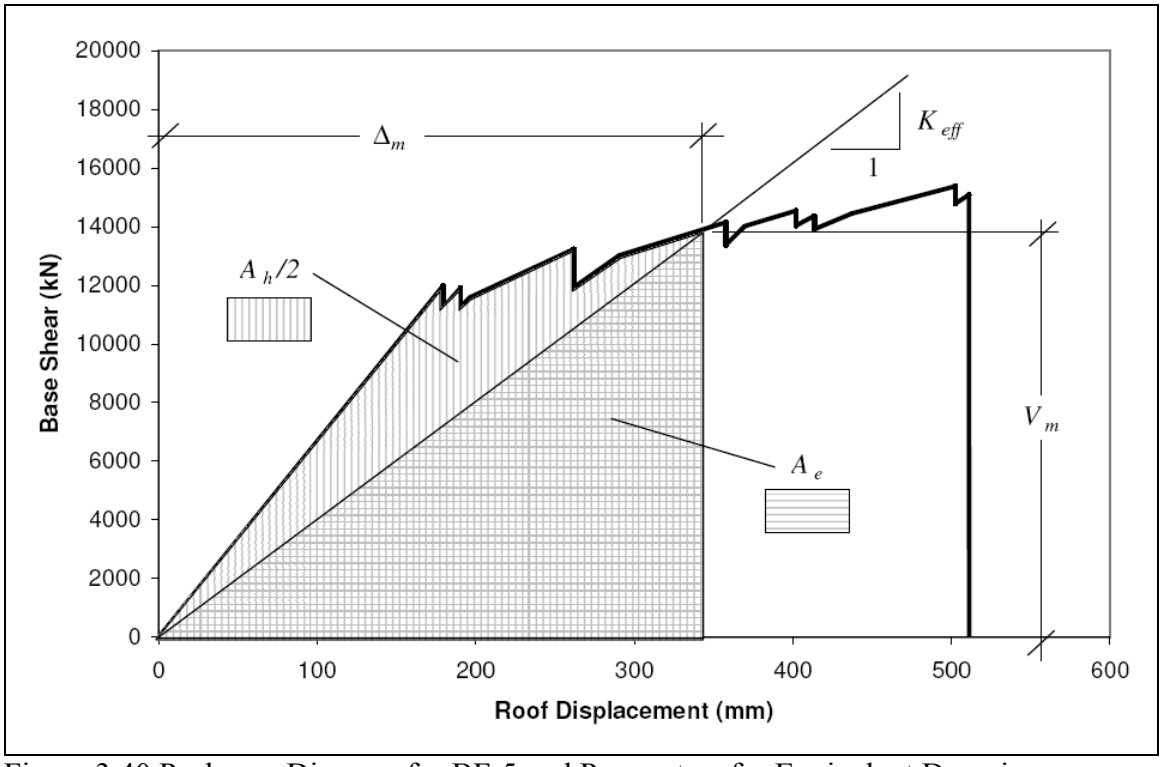

Figure 3.40 Pushover Diagram for BF-5 and Parameters for Equivalent Damping

The calculation of an equivalent damping ratio provides an effective demonstration of the change in energy dissipating behaviors in the structures as the NRTMDF becomes a mechanism for shifting fundamental dynamics and a tool for targeted energy dissipation.

3.11. Nonstructural Elements and Components

Damage assessment of global structural assemblies using damage indices and peak transient parameters may be useful for assessing a structure's expected performance for a given acceleration record. However, structural systems oftentimes comprise only about 20% to 25% of a building's total embodied financial investment for typical structures. For structures with contents of unusual value, this amount could be far less. Clearly, if structural systems fail an entire building may be compromised. Conversely, a structural system may perform well but nonstructural damage may still be severe enough to compromise a major portion of a building's value. Seismic stabilization of nonstructural elements and components is an issue which gains attention with each major event. Current codes for new construction require specific and deliberate design and detailing of seismic bracing for nonstructural elements and components. Within this context, economically feasible innovations which hold the promise of reducing damage to nonstructural elements and components become very attractive to building owners and other stakeholders. Whether an innovation is effective for reducing nonstructural damage may be difficult to assess since the design and detailing for such assemblies does not always fall within the purview of building designers. To address this, prescriptive requirements of contemporary codes require design forces for bracing nonstructural elements and components following procedures meant to replicate response

spectra that may develop within the building.[35] These procedures use a baseline input parameter, the short period design site spectral acceleration (S_{ds}) which is modified by assembly response and ductility coefficients and then by geometric parameters reflecting the amplification of acceleration observed with increasing height within the structure (accelerations within the building increase with height). If the accelerations can be reduced, damage to nonstructural elements and components may be mitigated.

The time history analysis methodology for this study provides convenient assessments of floor spectra which may be used to qualitatively gauge the forces acting on nonstructural elements and components. The acceleration response spectra may be developed for the damped and undamped structures which may then be directly compared. Though specific forces may not be calculated, an examination of the spectra demonstrates the effectiveness of the NRTMDF approach. Such comparisons are developed within the results portion of this study. The potential benefits of an effective NRTMDF are expected to reach far beyond the quantified structural parameters outlined in this study. Where the analysis indicates benefits that may be realized in the structural system with the NRTMDF, the nonstructural systems are also expected to benefit, perhaps even more than the primary structure.

3.12 Summary of Analyses

In summary, the overall phases of analyses embodied in this research are:

- Phase I – simplified (pendulum) elastic analyses for test models using spreadsheets and visual basic algorithms. NRTMDF modeled and optimized using effective stiffness properties.

- Phase II – Simplified (pendulum) nonlinear analyses for test models using CSI applications (ETABS Version 9) plus corroboration between simplified and full three dimensional models. Determination of effective properties for NRTMDF based on effective stiffness parameters and actual nonlinear properties. Utilization of nonlinear static pushover analyses of damped structures to verify mobilization of NRTMDF prior to initiation of nonlinearity of the base structure.
- Phase III – Nonlinear time history of test models following a rational design scenario utilizing suites of ground motions representing the ASCE 41 approach reflecting hard, medium and soft sites. Utilization of CSI Berkeley Applications (Version 14 of SAP 2000 corroborated with Version 4.03 of Perform 3D). Supplemental analysis of test structure BF-4 demonstrating the usage of the PEER Ground Motion Database web application.
- Damage index calculations to determine NRTMDF effectiveness throughout the time domain for each record of the Basic Safety Objective.
- Equivalent damping calculations using nonlinear analysis approaches to demonstrate the change in energy dissipating behaviors between the undamped and damped structures.
- Comparison of floor spectra for damped and undamped structures to assess effectiveness of the NRTMDF with respect to nonstructural elements and components following ground motions and other performance parameters from the Basic Safety Objective.

4 RESULTS OF BROAD-BASED LINEAR ELASTIC ANALYSES

Linear elastic analysis methods provide a reflection of predominant analysis methods generally used by practitioners. While these methods alone are insufficient for adequately characterizing the performance of the NRTMDF, they may serve to identify whether a particular structure and a suite of anticipated ground motions may be viable candidates for this approach. The linear elastic analyses include the previously identified ground motions derived from the SAC suite summarized in Table 3.2 which represent hard, medium and soft soil conditions. Tables 4.1 through 4.10 summarize the results of the linear elastic analysis and the change in peak output parameters enabled by the NRTMDF. For these, iterative algorithms were utilized to solve for effective mass and stiffness values of the NRTMDF for each structure and the suite of SAC ground motions. Solving for effective mass and stiffness for individual specific motions is not pragmatic for a design scenario because of the unique signature of each individual record. Nevertheless, effective parameters may be determined for records of similar magnitude and frequency content which may be indentified and characterized by the acceleration response spectra for the records in question. Tables 4.1 through 4.10 list the changes in peak response parameters enabled by the NRTMDF. The values of peak transient parameters for the undamped and damped cases are listed in the Appendix B.

Table 4.1 BF-1 Linear Analyses Results

Undamped Parameters:	Damped Parameters:
Mode 1 Period = 0.25 sec	Mode 1 Period = 0.49 sec
Mode 2 Period = 0.12 sec	Mode 2 Period = 0.24 sec
Mode 1 Mass = 95.8%	Mode 1 Mass = 18.1%
Mode 2 Mass = 4%	Mode 2 Mass = 78.3%
NRTMDF Mass = 58826 kg	NRTMDF Eff. Stiffness = 10.51 kN/mm

Acc. History	Peak Base Shear change	Peak Roof Disp. change	Damper Disp. (mm)	Acc. History	Peak Base Shear change	Peak Roof Disp. change	Damper Disp. (mm)
LA01	-4.6%	-1.3%	107	BO05	-6.4%	-10.3%	40
LA02	-16.4%	-23.2%	142	BO06	-18.3%	-29.9%	37
LA04	-14.9%	-13.3%	77	BO13	-2.4%	-5.7%	19
LA12	-10.0%	-14.1%	190	BO16	-11.1%	-14.0%	21
LA15	-19.6%	-17.2%	93	BO18	-9.1%	-15.0%	19
LA18	-25.2%	-17.0%	174	BO19	-1.7%	-7.7%	18
LA20	1.7%	-0.5%	129	BO20	-6.1%	-0.4%	42
LA21	36.7%	61.3%	221	BO21	-9.0%	-6.7%	52
LA22	7.3%	22.4%	115	BO22	-9.9%	-0.4%	92
LA23	5.7%	31.8%	84	BO25	5.8%	5.2%	51
LA25	-19.6%	-17.2%	151	BO33	-2.4%	-5.8%	56
LA28	-25.3%	-17.1%	283	BO34	-15.3%	-17.1%	85
LA30	-15.8%	-16.5%	206	BO35	4.8%	-1.3%	199
LA37	7.1%	22.3%	100	BO36	-11.1%	-14.0%	59
SE04	-5.6%	-1.4%	85	NF01	-6.1%	-9.1%	179
SE05	-6.8%	-6.0%	64	NF02	-9.0%	-12.7%	169
SE08	7.1%	16.5%	59	NF11	1.5%	-1.5%	52
SE10	1.7%	-0.5%	75	NF12	0.3%	-4.2%	55
SE12	-22.6%	-24.7%	99	NF15	-25.4%	-28.9%	84
SE18	2.5%	1.1%	113	NF16	0.7%	4.5%	171
SE19	0.3%	8.0%	91	LASS1A	-16.0%	-14.1%	63
SE21	19.1%	44.0%	109	LASS1B	-14.7%	-7.0%	78
SE25	-6.8%	-6.1%	148	LASS1C	-17.1%	-10.7%	63
SE26	-2.3%	-4.1%	147	LASS1E	-19.0%	-19.0%	82
SE30	2.4%	1.1%	265	LASS2A	-3.7%	5.0%	92
SE31	0.4%	8.1%	214	LASS3B	19.8%	51.2%	59
SE32	-12.2%	-8.5%	141	LASS3C	3.6%	26.9%	44

Table 4.2 BF-2 Linear Analyses Results

Undamped Parameters	Damped Parameters
Mode 1 Period = 0.3 sec	Mode 1 Period = 0.77 sec
Mode 2 Period = 0.12 sec	Mode 2 Period = 0.29 sec
Mode 1 Mass = 99%	Mode 1 Mass = 14.2%
Mode 2 Mass = 1%	Mode 2 Mass = 84.9%
NRTMDF Mass = 201642 kg	NRTMDF Eff. Stiffness = 13.76 kN/mm

Acc. History	Peak Base Shear change	Peak Roof Disp. change	Damper Disp. (mm)	Acc. History	Peak Base Shear change	Peak Roof Disp. change	Damper Disp. (mm)
LA01	-9.0%	-10.1%	142	BO05	-2.9%	-8.5%	32
LA02	1.1%	6.2%	205	BO06	-8.0%	-9.9%	30
LA04	-7.4%	-7.7%	76	BO13	-1.0%	-1.6%	17
LA12	4.6%	5.0%	180	BO16	6.3%	0.0%	17
LA15	-5.7%	-5.7%	208	BO18	-2.6%	-1.4%	40
LA18	-5.5%	-5.8%	256	BO19	11.2%	17.0%	36
LA20	-1.6%	-2.0%	189	BO20	-12.5%	-14.6%	44
LA21	-7.2%	-1.7%	514	BO21	-7.7%	-8.7%	72
LA22	-6.0%	12.9%	579	BO22	-9.7%	-13.5%	81
LA23	0.8%	2.6%	275	BO25	-12.9%	-12.8%	52
LA25	-5.7%	-5.7%	338	BO33	-1.0%	-1.6%	50
LA28	-5.4%	-5.7%	416	BO34	-12.5%	-14.3%	71
LA30	-4.0%	-8.1%	360	BO35	-1.8%	-7.7%	170
LA37	-8.6%	-10.6%	269	BO36	6.3%	0.0%	48
SE04	-1.3%	-3.1%	90	NF01	-2.7%	-5.8%	295
SE05	-4.8%	-6.1%	89	NF02	1.0%	-2.0%	256
SE08	-5.5%	-6.1%	209	NF11	-4.1%	-6.4%	110
SE10	-1.6%	-2.0%	109	NF12	5.0%	5.5%	82
SE12	0.8%	-0.8%	131	NF15	-4.4%	-2.7%	172
SE18	-9.5%	-11.3%	165	NF16	-10.9%	-13.2%	195
SE19	-4.7%	1.9%	312	LASS1A	-6.5%	-6.9%	194
SE21	12.3%	21.4%	415	LASS1B	-3.6%	-0.8%	145
SE25	-4.8%	-6.0%	207	LASS1C	6.7%	13.3%	148
SE26	-9.2%	-12.3%	188	LASS1E	-5.4%	-5.2%	196
SE30	-9.6%	-11.4%	387	LASS2A	0.9%	4.7%	237
SE31	-4.7%	1.8%	732	LASS3B	-0.5%	6.6%	96
SE32	3.3%	6.6%	351	LASS3C	8.3%	18.4%	87
SE36	17.7%	35.5%	335	LASS4C	-3.5%	2.7%	103

Table 4.3 BF-3 Linear Analyses Results

Undamped Parameters	Damped Parameters
Mode 1 Period = 0.41 sec	Mode 1 Period = 0.79 sec
Mode 2 Period = 0.18 sec	Mode 2 Period = 0.38 sec
Mode 1 Mass = 82.4%	Mode 1 Mass = 24.3%
Mode 2 Mass = 8.6%	Mode 2 Mass = 60.7%
NRTMDF Mass = 449616 kg	NRTMDF Eff. Stiffness = 33.27 kN/mm

Acc. History	Peak Base Shear change	Peak Roof Disp. change	Damper Disp. (mm)	Acc. History	Peak Base Shear change	Peak Roof Disp. change	Damper Disp. (mm)
LA01	-29.7%	-16.8%	174	BO05	-18.3%	-39.2%	53
LA02	8.0%	12.7%	215	BO06	-12.1%	-20.1%	59
LA04	-12.8%	-17.3%	114	BO13	18.5%	15.5%	27
LA12	-23.8%	-30.0%	192	BO16	-29.3%	-29.0%	19
LA15	-12.2%	-14.7%	220	BO18	-7.2%	2.8%	43
LA18	-17.2%	-21.8%	306	BO19	25.3%	13.6%	43
LA20	-19.8%	-16.1%	231	BO20	-20.1%	-21.1%	72
LA21	-17.5%	-9.9%	601	BO21	-14.5%	-18.4%	80
LA22	-13.1%	-22.3%	654	BO22	-18.7%	-26.4%	120
LA23	-4.6%	6.1%	313	BO25	-24.1%	-25.1%	86
LA25	-12.2%	-14.7%	358	BO33	18.5%	15.5%	79
LA28	-17.3%	-21.8%	498	BO34	-6.4%	-8.5%	112
LA30	-25.2%	-15.6%	414	BO35	-22.4%	-26.3%	221
LA37	-17.6%	-12.6%	317	BO36	-29.3%	-29.0%	54
SE04	-28.4%	-25.3%	95	NF01	-14.4%	-8.5%	299
SE05	16.2%	0.9%	122	NF02	-6.3%	-3.2%	283
SE08	6.3%	20.6%	232	NF11	9.1%	20.3%	94
SE10	-19.9%	-16.2%	133	NF12	17.0%	9.6%	97
SE12	-0.6%	7.9%	170	NF15	-3.0%	-4.2%	208
SE18	-23.9%	-27.0%	208	NF16	-18.4%	-21.6%	237
SE19	-10.4%	20.4%	341	LASS1A	-1.9%	9.4%	210
SE21	-12.6%	26.6%	450	LASS1B	-0.3%	13.5%	165
SE25	16.3%	0.9%	285	LASS1C	3.1%	17.6%	168
SE26	-14.5%	-22.1%	228	LASS1E	2.3%	16.1%	209
SE30	-23.8%	-27.0%	489	LASS2A	5.0%	26.2%	255
SE31	-10.3%	20.5%	801	LASS3B	-20.0%	-15.3%	99
SE32	8.2%	9.3%	402	LASS3C	-8.4%	5.1%	87
SE36	18.3%	58.9%	375	LASS4C	-20.8%	-7.2%	117

Table 4.4 BF-4 Linear Analyses Results

Undamped Parameters	Damped Parameters
Mode 1 Period = 0.63 sec	Mode 1 Period = 0.96 sec
Mode 2 Period = 0.26 sec	Mode 2 Period = 0.57 sec
Mode 1 Mass = 81.3%	Mode 1 Mass = 32.2%
Mode 2 Mass = 11.4%	Mode 2 Mass = 51.6%
NRTMDF Mass = 359591 kg	NRTMDF Eff. Stiffness = 19.7 kN/mm

Acc. History	Peak Base Shear change	Peak Roof Disp. change	Damper Disp. (mm)	Acc. History	Peak Base Shear change	Peak Roof Disp. change	Damper Disp. (mm)
LA01	-10.1%	-22.2%	284	BO05	13.3%	14.7%	38
LA02	-14.5%	-20.8%	397	BO06	2.0%	-11.4%	31
LA04	18.2%	17.2%	159	BO13	-11.6%	-22.9%	34
LA12	-4.1%	-7.8%	324	BO16	-2.9%	-11.7%	23
LA15	-11.4%	-12.7%	426	BO18	-32.4%	-31.8%	48
LA18	-10.8%	-23.9%	436	BO19	-29.8%	-21.0%	64
LA20	-9.8%	-0.5%	433	BO20	-16.9%	-26.9%	83
LA21	-4.4%	10.4%	1047	BO21	37.2%	32.8%	133
LA22	-48.3%	-28.7%	995	BO22	29.2%	-6.4%	133
LA23	-41.9%	-43.1%	354	BO25	-20.2%	-23.5%	156
LA25	-11.4%	-12.7%	694	BO33	-11.6%	-22.9%	98
LA28	-10.8%	-24.0%	710	BO34	-10.6%	-18.6%	101
LA30	23.9%	-15.9%	380	BO35	-21.8%	-27.2%	332
LA37	-16.9%	-15.4%	532	BO36	-3.0%	-11.7%	67
SE04	7.4%	7.1%	193	NF01	-3.2%	-30.4%	373
SE05	3.5%	-3.6%	226	NF02	-5.8%	-15.7%	263
SE08	-34.9%	-9.4%	406	NF11	-26.6%	-26.5%	104
SE10	-9.9%	-0.5%	250	NF12	-13.9%	1.9%	149
SE12	-15.8%	-27.3%	213	NF15	19.6%	6.2%	281
SE18	-32.9%	-39.8%	279	NF16	-18.2%	-31.2%	347
SE19	-27.6%	-40.6%	479	LASS1A	-0.4%	26.5%	420
SE21	-41.6%	-36.3%	761	LASS1B	-12.2%	5.2%	285
SE25	3.4%	-3.6%	528	LASS1C	-22.9%	-2.3%	255
SE26	-27.6%	-43.3%	320	LASS1E	-16.1%	14.0%	374
SE30	-32.9%	-39.9%	656	LASS2A	-13.6%	-5.3%	461
SE31	-27.6%	-40.5%	1125	LASS3B	-2.0%	-5.8%	230
SE32	-35.0%	-25.5%	681	LASS3C	-0.9%	12.4%	228
SE36	-8.3%	16.1%	803	LASS4C	19.0%	32.0%	203

Table 4.5 BF-5 Linear Analyses Results

Undamped Parameters	Damped Parameters
Mode 1 Period = 1.04 sec	Mode 1 Period = 1.46 sec
Mode 2 Period = 0.44 sec	Mode 2 Period = 0.83 sec
Mode 1 Mass = 68.7%	Mode 1 Mass = 44.3%
Mode 2 Mass = 14.3%	Mode 2 Mass = 29.6%
NRTMDF Mass = 426337 kg	NRTMDF Eff. Stiffness = 14.45 kN/mm

Acc. History	Peak Base Shear change	Peak Roof Disp. change	Damper Disp. (mm)	Acc. History	Peak Base Shear change	Peak Roof Disp. change	Damper Disp. (mm)
LA01	-33.0%	-5.2%	325	BO05	-10.2%	-16.8%	55
LA02	-27.5%	-43.6%	425	BO06	9.5%	-6.4%	41
LA04	-15.5%	-31.6%	198	BO13	-8.6%	-28.5%	39
LA12	-5.1%	-21.6%	244	BO16	-24.6%	-25.9%	24
LA15	-37.1%	-25.2%	518	BO18	25.9%	-20.4%	46
LA18	-19.2%	24.7%	458	BO19	-36.7%	-38.5%	77
LA20	-21.1%	-5.0%	544	BO20	-15.3%	-22.3%	76
LA21	-8.6%	-18.7%	1191	BO21	-20.2%	-13.2%	215
LA22	-30.2%	-50.2%	1120	BO22	-19.6%	-10.8%	165
LA23	65.8%	57.2%	599	BO25	-19.7%	10.4%	200
LA25	-37.1%	-25.2%	843	BO33	-8.5%	-28.4%	111
LA28	-19.2%	24.6%	746	BO34	15.0%	30.4%	113
LA30	-1.4%	20.7%	522	BO35	-32.6%	-21.8%	268
LA37	-14.4%	-27.7%	722	BO36	-24.6%	-25.9%	69
SE04	-22.9%	-44.7%	132	NF01	58.7%	38.1%	518
SE05	-10.4%	-0.3%	234	NF02	4.1%	-16.2%	355
SE08	-10.1%	-39.2%	439	NF11	17.3%	23.8%	268
SE10	-21.1%	-5.0%	314	NF12	-16.4%	-1.3%	200
SE12	15.9%	-0.3%	359	NF15	-22.9%	25.8%	522
SE18	-26.9%	-12.0%	271	NF16	19.0%	30.7%	506
SE19	-21.2%	-27.7%	590	LASS1A	-36.5%	-32.5%	686
SE21	13.7%	-28.6%	894	LASS1B	-21.9%	6.9%	583
SE25	-10.4%	-0.3%	546	LASS1C	-16.3%	11.9%	495
SE26	-31.6%	-6.5%	363	LASS1E	-37.6%	-38.1%	584
SE30	-26.9%	-12.0%	636	LASS2A	-35.6%	-42.4%	578
SE31	-21.1%	-27.7%	1385	LASS3B	-9.6%	-23.5%	225
SE32	-42.0%	-52.2%	705	LASS3C	-22.0%	-27.7%	212
SE36	-44.5%	-33.3%	1260	LASS4C	1.5%	32.7%	276

Table 4.6 EBF-1 Linear Analyses Results

Undamped Parameters	Damped Parameters
Mode 1 Period = 0.55 sec	Mode 1 Period = 1.28 sec
Mode 2 Period = 0.22 sec	Mode 2 Period = 0.52 sec
Mode 1 Mass = 89.2%	Mode 1 Mass = 18.6%
Mode 2 Mass = 9.2%	Mode 2 Mass = 40.9%
NRTMDF Mass = 458861 kg	NRTMDF Eff. Stiffness = 13.01 kN/mm

Acc. History	Peak Base Shear change	Peak Roof Disp. change	Damper Disp. (mm)	Acc. History	Peak Base Shear change	Peak Roof Disp. change	Damper Disp. (mm)
LA01	-17.9%	-31.2%	316	BO05	10.1%	8.5%	43
LA02	-21.1%	-26.7%	271	BO06	4.3%	4.9%	22
LA04	6.9%	1.2%	172	BO13	-12.7%	-20.1%	26
LA12	-2.3%	-18.8%	179	BO16	-5.0%	-6.3%	21
LA15	-4.7%	-12.5%	394	BO18	-16.8%	-25.6%	28
LA18	20.2%	23.8%	371	BO19	-10.1%	-19.0%	46
LA20	-14.4%	-6.7%	418	BO20	-9.9%	-22.4%	64
LA21	2.6%	6.1%	824	BO21	-1.5%	13.1%	147
LA22	-31.1%	-33.5%	526	BO22	2.5%	-10.8%	116
LA23	-8.4%	-18.0%	284	BO25	-5.0%	-19.1%	117
LA25	-4.7%	-12.5%	642	BO33	-12.7%	-20.1%	73
LA28	20.2%	23.8%	603	BO34	-1.6%	1.6%	83
LA30	-6.2%	-22.0%	380	BO35	-2.6%	-26.6%	231
LA37	-14.8%	20.2%	531	BO36	-5.0%	-6.3%	59
SE04	12.4%	-8.7%	141	NF01	3.9%	9.9%	428
SE05	-27.4%	-28.4%	167	NF02	-7.5%	-27.4%	217
SE08	-28.1%	-21.8%	230	NF11	7.2%	19.7%	231
SE10	-14.4%	-6.7%	241	NF12	-8.5%	7.4%	161
SE12	-15.4%	-28.9%	213	NF15	45.1%	58.0%	381
SE18	1.1%	0.7%	324	NF16	3.0%	-4.9%	245
SE19	-25.2%	-35.4%	378	LASS1A	2.7%	29.3%	478
SE21	-19.1%	-25.3%	604	LASS1B	22.5%	34.9%	420
SE25	-27.4%	-28.3%	389	LASS1C	21.5%	33.1%	358
SE26	-15.5%	-12.3%	361	LASS1E	17.6%	17.4%	367
SE30	1.1%	0.7%	760	LASS2A	-27.8%	-26.4%	520
SE31	-25.2%	-35.4%	887	LASS3B	1.4%	2.0%	194
SE32	-35.0%	-32.1%	494	LASS3C	2.8%	8.3%	187
SE36	-10.5%	36.2%	881	LASS4C	19.6%	32.5%	210

Table 4.7 SW-1 Linear Analyses Results

Undamped Parameters	Damped Parameters
Mode 1 Period = 0.35 sec	Mode 1 Period = 0.97 sec
Mode 2 Period = 0.16 sec	Mode 2 Period = 0.34 sec
Mode 1 Mass = 65.5%	Mode 1 Mass = 13.2%
Mode 2 Mass = 14.2%	Mode 2 Mass = 55.7%
NRTMDF Mass = 465902 kg	NRTMDF Eff. Stiffness = 20.94 kN/mm

Acc. History	Peak Base Shear change	Peak Roof Disp. change	Damper Disp. (mm)	Acc. History	Peak Base Shear change	Peak Roof Disp. change	Damper Disp. (mm)
LA01	-9.7%	-12.3%	151	BO05	-14.8%	-2.2%	44
LA02	1.5%	0.7%	311	BO06	-13.6%	-17.1%	46
LA04	-7.2%	-8.8%	103	BO13	-4.6%	-10.7%	28
LA12	-6.4%	-10.0%	172	BO16	-6.3%	0.7%	19
LA15	-10.2%	-11.9%	311	BO18	-2.9%	-6.0%	40
LA18	-0.6%	-1.4%	273	BO19	-5.6%	-28.7%	51
LA20	-10.0%	-10.2%	296	BO20	-10.1%	-6.3%	56
LA21	-0.4%	3.7%	755	BO21	7.4%	6.5%	112
LA22	-2.5%	7.9%	675	BO22	-10.5%	-13.5%	93
LA23	-20.7%	-14.2%	221	BO25	-13.9%	-18.7%	99
LA25	-10.2%	-11.9%	507	BO33	-4.6%	-10.7%	79
LA28	-0.7%	-1.4%	445	BO34	-1.5%	-6.3%	97
LA30	4.1%	-5.2%	210	BO35	-12.2%	-6.0%	161
LA37	-12.8%	-3.0%	369	BO36	-6.2%	0.7%	54
SE04	-5.1%	2.0%	129	NF01	-4.2%	-6.5%	242
SE05	-8.2%	-12.2%	145	NF02	3.8%	-0.3%	190
SE08	-10.5%	5.1%	302	NF11	1.8%	-7.6%	80
SE10	-10.0%	-10.2%	171	NF12	-2.2%	8.8%	106
SE12	-0.5%	-8.8%	150	NF15	3.2%	7.2%	258
SE18	-13.2%	-18.2%	167	NF16	-8.8%	-10.2%	188
SE19	-2.3%	11.3%	320	LASS1A	4.0%	-1.4%	362
SE21	6.2%	25.1%	452	LASS1B	-2.4%	3.8%	241
SE25	-8.2%	-12.2%	338	LASS1C	-13.3%	-8.1%	223
SE26	-3.5%	-15.4%	228	LASS1E	-2.8%	-5.8%	309
SE30	-13.2%	-18.2%	391	LASS2A	-5.4%	36.3%	366
SE31	-2.3%	11.4%	751	LASS3B	-8.6%	-4.0%	167
SE32	3.5%	11.2%	542	LASS3C	0.3%	12.8%	189
SE36	12.7%	34.7%	662	LASS4C	2.1%	11.6%	171

Table 4.8 SW-2 Linear Analyses Results

Undamped Parameters	Damped Parameters
Mode 1 Period = 0.41 sec	Mode 1 Period = 0.97 sec
Mode 2 Period = 0.18 sec	Mode 2 Period = 0.4 sec
Mode 1 Mass = 63.4%	Mode 1 Mass = 15.3%
Mode 2 Mass = 16.1%	Mode 2 Mass = 51.92%
NRTMDF Mass = 1545298 kg	NRTMDF Eff. Stiffness = 72.11 kN/mm

Acc. History	Peak Base Shear change	Peak Roof Disp. change	Damper Disp. (mm)	Acc. History	Peak Base Shear change	Peak Roof Disp. change	Damper Disp. (mm)
LA01	-6.9%	-14.0%	150	BO05	-10.1%	-20.9%	59
LA02	-7.1%	1.0%	352	BO06	1.5%	-10.6%	68
LA04	-6.3%	-11.4%	136	BO13	25.3%	15.9%	30
LA12	-11.2%	-23.1%	179	BO16	-22.5%	-22.2%	20
LA15	-9.2%	-11.4%	299	BO18	-1.5%	-18.9%	38
LA18	-2.9%	-2.2%	317	BO19	-7.8%	-3.6%	53
LA20	4.9%	-18.1%	304	BO20	-6.8%	-8.0%	68
LA21	-12.5%	11.9%	761	BO21	5.4%	7.5%	111
LA22	15.8%	14.0%	712	BO22	-6.7%	-16.0%	124
LA23	-5.4%	-5.1%	241	BO25	-5.8%	-20.5%	108
LA25	-9.2%	-11.4%	486	BO33	25.3%	15.9%	86
LA28	-2.9%	-2.2%	515	BO34	-18.9%	-16.9%	96
LA30	-23.4%	-14.2%	241	BO35	-13.5%	-9.4%	195
LA37	-15.5%	0.6%	398	BO36	-22.5%	-22.2%	58
SE04	-29.6%	-24.2%	143	NF01	-21.1%	-6.3%	256
SE05	-13.0%	-4.9%	150	NF02	-7.1%	-13.9%	205
SE08	-3.7%	-2.5%	295	NF11	-3.8%	-0.8%	94
SE10	4.9%	-18.2%	175	NF12	-12.2%	16.9%	109
SE12	0.7%	-5.0%	162	NF15	5.2%	14.1%	235
SE18	-12.9%	-18.2%	167	NF16	-10.0%	-16.6%	228
SE19	-17.9%	-0.5%	328	LASS1A	-9.1%	3.6%	393
SE21	-18.2%	-1.8%	485	LASS1B	-5.4%	-1.3%	272
SE25	-13.1%	-4.9%	349	LASS1C	-4.1%	-0.7%	250
SE26	2.2%	-13.8%	270	LASS1E	-6.5%	-4.1%	341
SE30	-12.9%	-18.2%	393	LASS2A	-11.3%	8.7%	408
SE31	-17.9%	-0.4%	770	LASS3B	-9.9%	-13.9%	179
SE32	8.2%	14.3%	582	LASS3C	-9.8%	3.5%	195
SE36	-4.3%	49.2%	694	LASS4C	-3.3%	6.4%	178

Table 4.9 MF-1 Linear Analyses Results

Undamped Parameters	Damped Parameters
Mode 1 Period = 1.4 sec	Mode 1 Period = 2.43 sec
Mode 2 Period = 0.57 sec	Mode 2 Period = 1.25 sec
Mode 1 Mass = 80.7%	Mode 1 Mass = 30.4%
Mode 2 Mass = 10.7%	Mode 2 Mass = 37.83%
NRTMDF Mass = 552112 kg	NRTMDF Eff. Stiffness = 4.9 kN/mm

Acc. History	Peak Base Shear change	Peak Roof Disp. change	Damper Disp. (mm)	Acc. History	Peak Base Shear change	Peak Roof Disp. change	Damper Disp. (mm)
LA01	10.5%	5.1%	749	BO05	12.7%	-13.0%	48
LA02	3.8%	43.1%	727	BO06	-30.7%	-44.1%	26
LA04	22.5%	39.7%	520	BO13	-27.9%	-37.3%	31
LA12	-21.7%	-17.1%	347	BO16	16.2%	-27.3%	19
LA15	-7.8%	-28.5%	676	BO18	-19.1%	-19.9%	31
LA18	-14.2%	-28.8%	1054	BO19	-6.7%	-18.5%	58
LA20	-10.1%	-27.0%	961	BO20	-6.6%	2.0%	61
LA21	-34.3%	-36.7%	1466	BO21	-15.2%	-30.8%	291
LA22	21.6%	16.4%	1078	BO22	-26.2%	-18.6%	252
LA23	-35.2%	-32.0%	691	BO25	-33.3%	-44.8%	177
LA25	-7.8%	-28.5%	1101	BO33	-27.8%	-37.3%	88
LA28	-14.2%	-28.8%	1714	BO34	-47.3%	-40.0%	113
LA30	12.5%	12.6%	1021	BO35	-10.0%	-14.5%	233
LA37	-10.0%	-10.8%	1377	BO36	15.9%	-27.4%	56
SE04	-1.3%	0.9%	352	NF01	10.5%	1.3%	1054
SE05	10.0%	12.8%	347	NF02	14.8%	14.9%	663
SE08	11.3%	-16.1%	349	NF11	0.9%	-0.4%	599
SE10	-10.2%	-27.0%	554	NF12	-14.5%	-26.3%	341
SE12	-33.2%	-40.8%	384	NF15	-17.3%	-18.6%	1201
SE18	-12.7%	-26.1%	436	NF16	-21.3%	-48.2%	425
SE19	-11.2%	-29.1%	423	LASS1A	-18.4%	-32.0%	887
SE21	-5.4%	-6.8%	1200	LASS1B	-25.3%	-39.2%	881
SE25	10.0%	12.8%	811	LASS1C	-26.7%	-30.1%	839
SE26	2.6%	14.4%	878	LASS1E	-22.4%	-33.3%	667
SE30	-12.7%	-26.1%	1023	LASS2A	14.1%	32.7%	1537
SE31	-11.1%	-29.0%	995	LASS3B	58.9%	90.1%	1261
SE32	7.6%	-7.5%	652	LASS3C	78.5%	119.8%	1429
SE36	-6.9%	-22.0%	1395	LASS4C	39.5%	48.4%	1049

Table 4.10 MF- 2 Linear Analyses Results

Undamped Parameters	Damped Parameters
Mode 1 Period = 2 sec	Mode 1 Period = 3.53 sec
Mode 2 Period = 0.77 sec	Mode 2 Period = 1.79 sec
Mode 1 Mass = 79.1%	Mode 1 Mass = 36.6%
Mode 2 Mass = 10.9%	Mode 2 Mass = 46.27%
NRTMDF Mass = 2498806 kg	NRTMDF Eff. Stiffness = 10.51 kN/mm

Acc. History	Peak Base Shear change	Peak Roof Disp. change	Damper Disp. (mm)	Acc. History	Peak Base Shear change	Peak Roof Disp. change	Damper Disp. (mm)
LA01	-46.3%	-47.6%	888	BO05	1.4%	-9.1%	44
LA02	-31.6%	-26.8%	624	BO06	2.0%	1.9%	48
LA04	-20.3%	-13.4%	1052	BO13	-3.7%	-13.4%	47
LA12	-6.3%	39.3%	479	BO16	-28.3%	-37.2%	16
LA15	-4.7%	-27.1%	679	BO18	-18.6%	-3.6%	28
LA18	-18.4%	-32.5%	1273	BO19	-10.8%	-12.8%	44
LA20	-30.1%	-40.9%	1031	BO20	-3.4%	-11.9%	50
LA21	-7.9%	-17.4%	1610	BO21	7.9%	-19.3%	246
LA22	-19.1%	20.3%	1518	BO22	-14.0%	-42.6%	172
LA23	2.5%	-20.2%	892	BO25	31.7%	15.6%	165
LA25	-4.7%	-27.1%	1105	BO33	-3.7%	-13.3%	133
LA28	-18.4%	-32.5%	2070	BO34	1.3%	-15.2%	171
LA30	-9.0%	-17.2%	1488	BO35	-8.0%	-22.5%	153
LA37	-21.0%	-16.9%	2183	BO36	-28.3%	-37.1%	46
SE04	-17.8%	-12.9%	419	NF01	-24.8%	-26.9%	1311
SE05	-28.1%	-26.9%	424	NF02	-5.3%	1.8%	1151
SE08	-15.0%	-15.2%	238	NF11	29.5%	30.7%	1238
SE10	-30.1%	-41.0%	595	NF12	1.8%	-19.8%	373
SE12	-19.7%	-25.1%	296	NF15	-23.0%	-31.0%	1494
SE18	-12.3%	-17.5%	361	NF16	5.7%	-8.0%	595
SE19	-1.7%	0.7%	607	LASS1A	-23.8%	-32.6%	724
SE21	-30.5%	-17.4%	1701	LASS1B	-25.3%	-41.0%	904
SE25	-28.1%	-26.9%	990	LASS1C	-21.5%	-41.3%	936
SE26	12.8%	-2.1%	1199	LASS1E	-19.3%	-29.2%	635
SE30	-12.2%	-17.4%	847	LASS2A	-19.7%	-37.3%	1243
SE31	-1.8%	0.8%	1426	LASS3B	-33.7%	1.4%	2245
SE32	-17.7%	-14.4%	421	LASS3C	-35.6%	-4.8%	2684
SE36	-0.6%	-18.2%	1133	LASS4C	-36.4%	-46.3%	1142

Early approaches for optimization of NRTMDF properties (mass and stiffness) primarily followed a trial and error approach. A minimum of two analysis runs demonstrated directional trends that could be followed to reach effective properties. For instance, an incremental increase in stiffness (5% to 10%) oftentimes resulted in a decrease in peak base shears and rooftop displacement. Continuation of the incremental increase would eventually result in a reversal of the trend of diminishing base shear or displacement result thereby enabling the identification of an effective value for the variable analysis parameter (e.g., stiffness). Attempts to determine the most suitable mass and stiffness of the NRTMDF (producing the greatest reduction in transient response parameters) for a unique and specific ground motion at times yielded an impractical NRTMDF mass result with masses as high as 50% to 90% of the total undamped building mass. Therefore NRTMDF mass was targeted at a value of approximately 15% of the total structural mass as an initial value. Such a magnitude is thought to be practical inasmuch as it may be accommodated within many structures without requiring significant retrofitting to support the added gravity load. Furthermore an NRTMDF mass value of 15% enables the development of inertial forces from the rooftop damper sufficient to develop an altered seismic response (see Section 5.5 for further information regarding NRTMDF mass). The NTRMDF masses determined for each structure for the SAC motion suite are indicated in Tables 4.1 through 4.10. Upon applying the mass of the NRTMDF, stiffness was selected following the iterative analysis approach described previously. Increases or decreases of stiffness within the context of a design scenario can often be determined when considering a target period or displacement as reflected by the design acceleration or displacement spectra in question.

Results reported are change in peak transient base shear, change in peak transient rooftop displacement and damper displacement. Additional parameters including NRTMDF stiffness (taken as an elastic stiffness value for the linear analyses presented in this section), period changes, and modal participation ratios for each structure for the first two modes of the damped and undamped structures are also presented in Tables 4.1 through 4.10. The second mode is included for the undamped and damped structures since its modal participation becomes significant for the damped structure. The results are also shown diagrammatically on the response spectra of Figures 4.1 through 4.8, therein demonstrating the period shifts for the first two modes of each structure driven by the NRTMDF along with the correlating change in spectral acceleration response.

4.1 Discussion of Linear Elastic Analysis Results

The linear elastic analyses corroborate the earlier research Johnson, Pantelides and Reaveley and reflect a fundamental validity to the approach.[10,11] While the approach does not offer a comprehensive solution for reduction of seismic response, it offers the potential for response reduction when the NRTMDF drives a shift in periods that correlate to favorable changes in spectral acceleration response. This can be observed in the spectra developed for the SAC ground motions shown in Figures 4.1 through 4.8. As a specific example, consider BF-4 and the LA23 ground motion. Undamped mode 1 and mode 2 periods are 0.63 and 0.26 seconds respectively with 81.3% mass participation in mode 1 and 11.4% participation in mode 2 (Table 4.4). For the damped structure, mode 1 and mode 2 periods are 0.96 and 0.57 seconds respectively with 32.2% mass participation in mode 1 and 51.6% participation in mode 2. For BF-4 and the LA23 motion, linear elastic methods yield a reduction in base shear of 41.9% and a reduction of 43.1% in peak

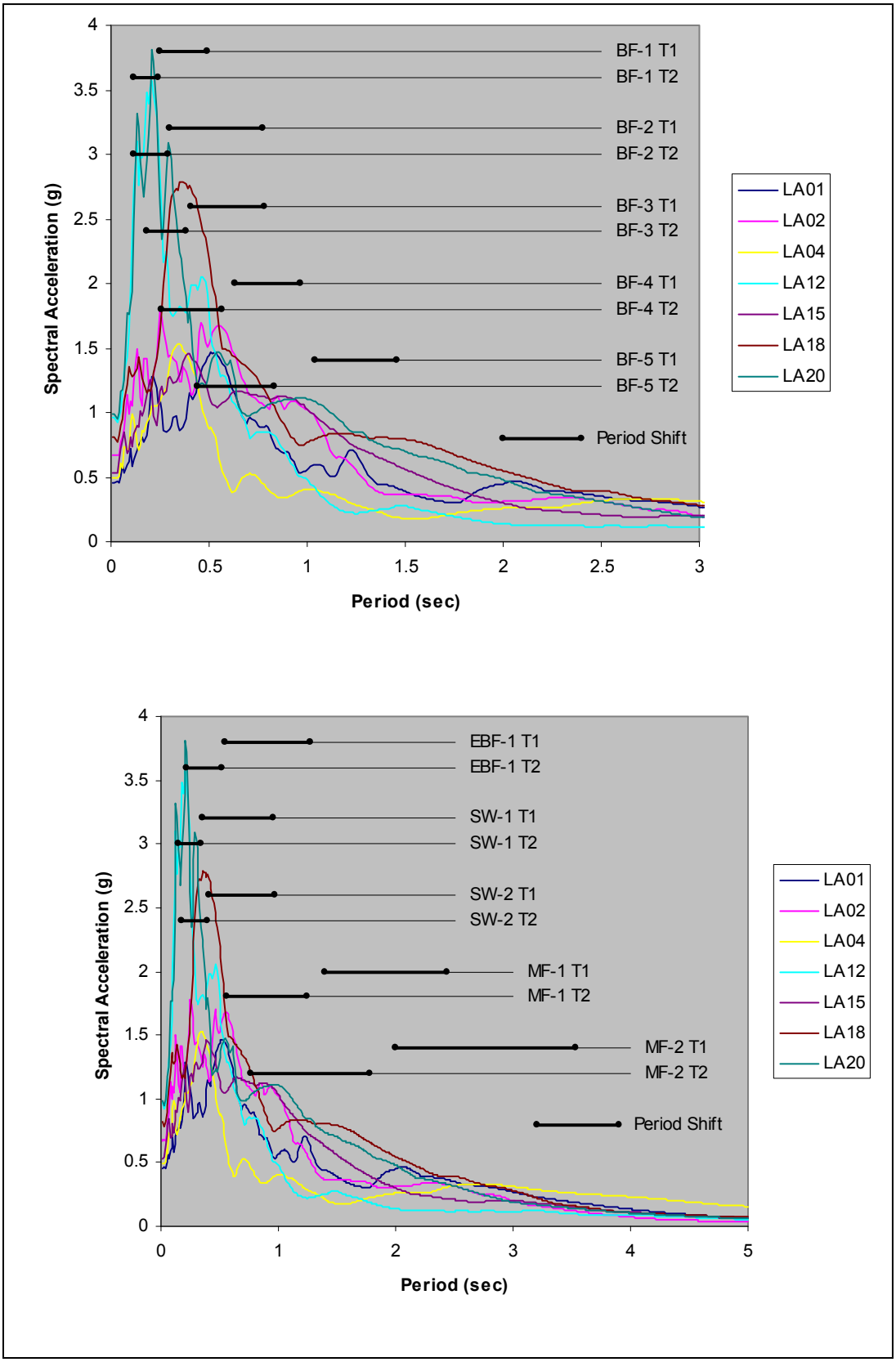

Figure 4.1 LA 10% in 50-Year Spectra with Period Shifts

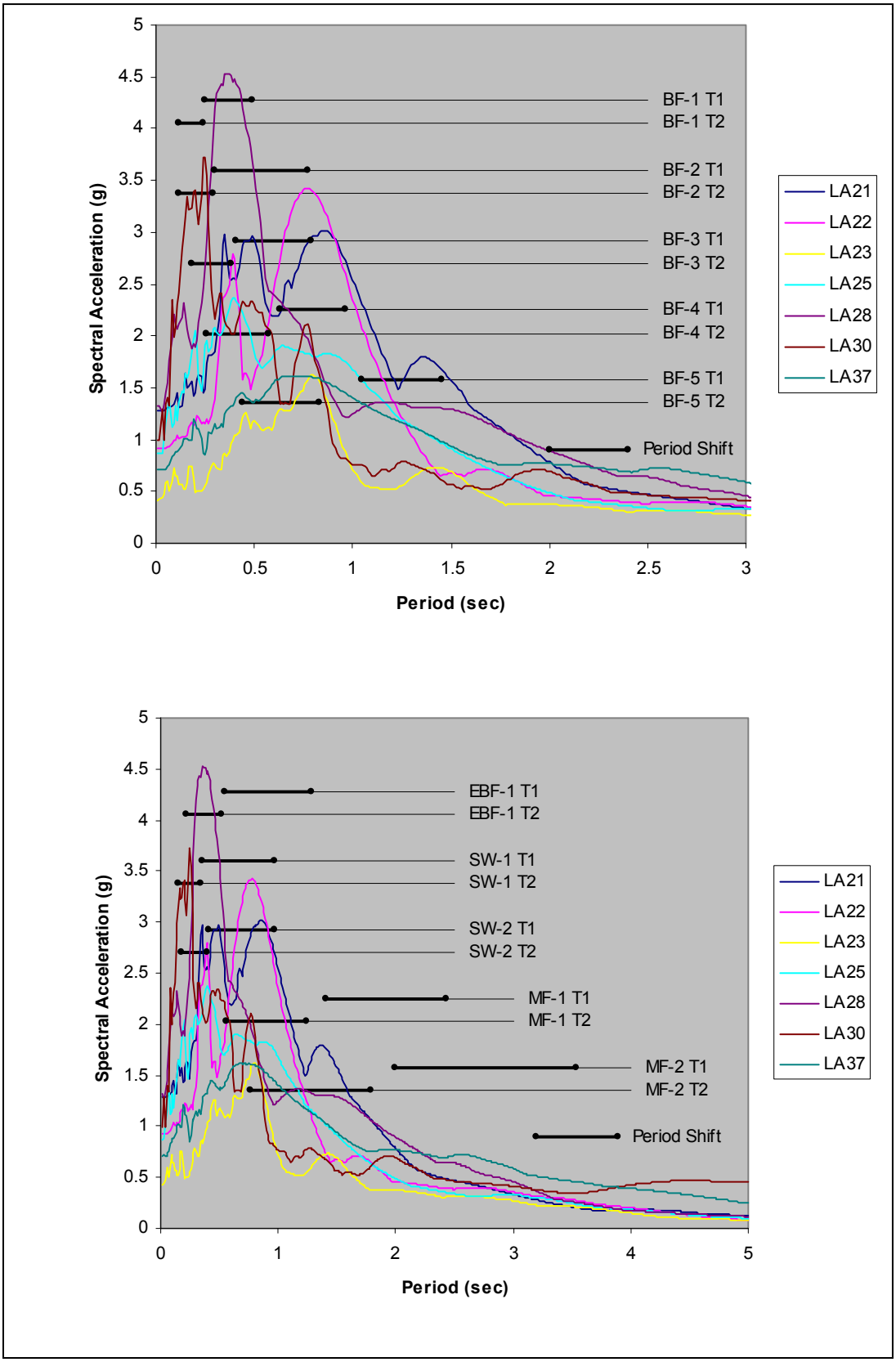

Figure 4.2 LA 2% in 50-Year Spectra with Period Shifts

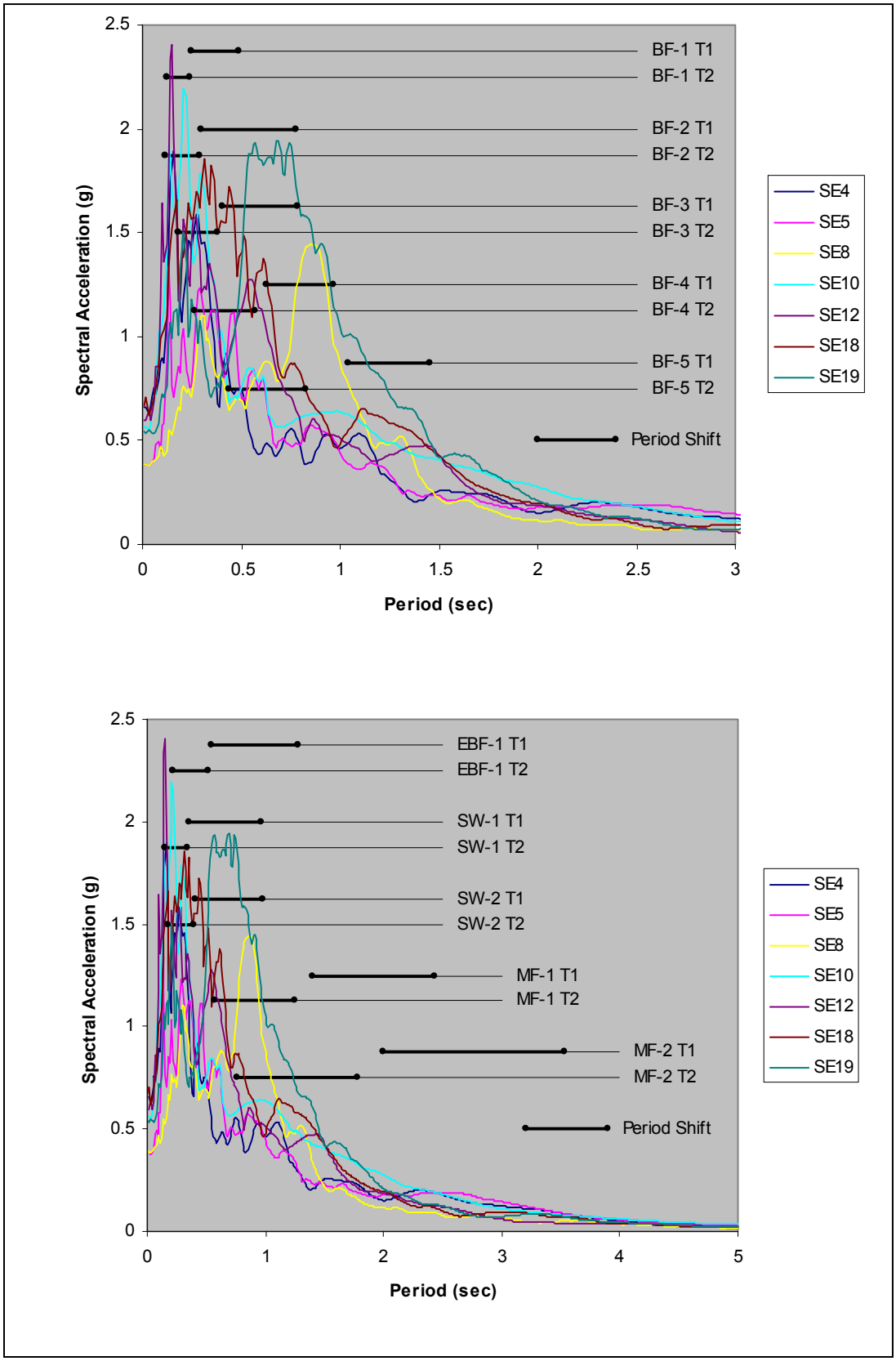

Figure 4.3 SE 10% in 50-Year Spectra with Period Shifts

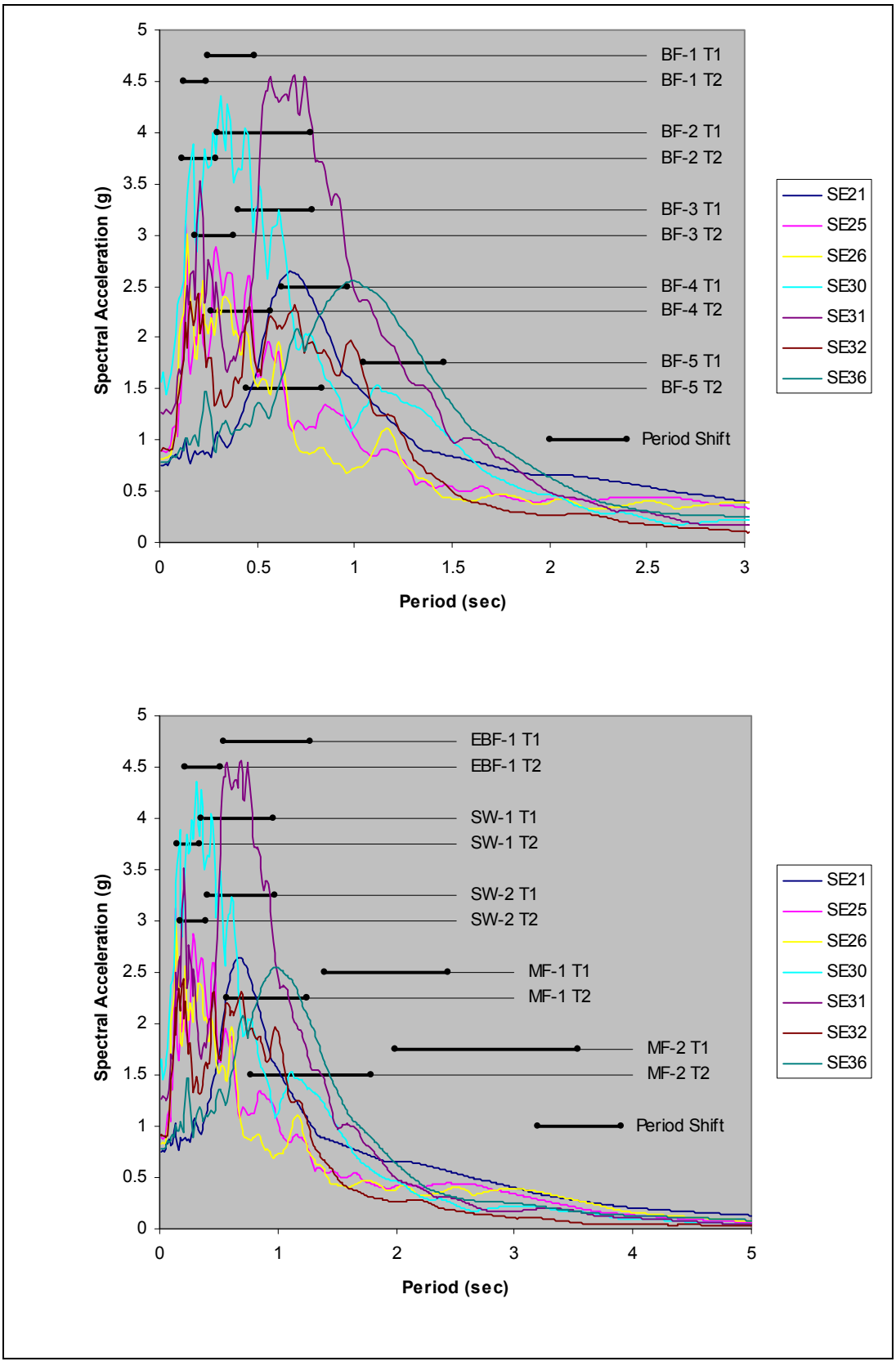

Figure 4.4 SE 2% in 50-Year Spectra with Period Shifts

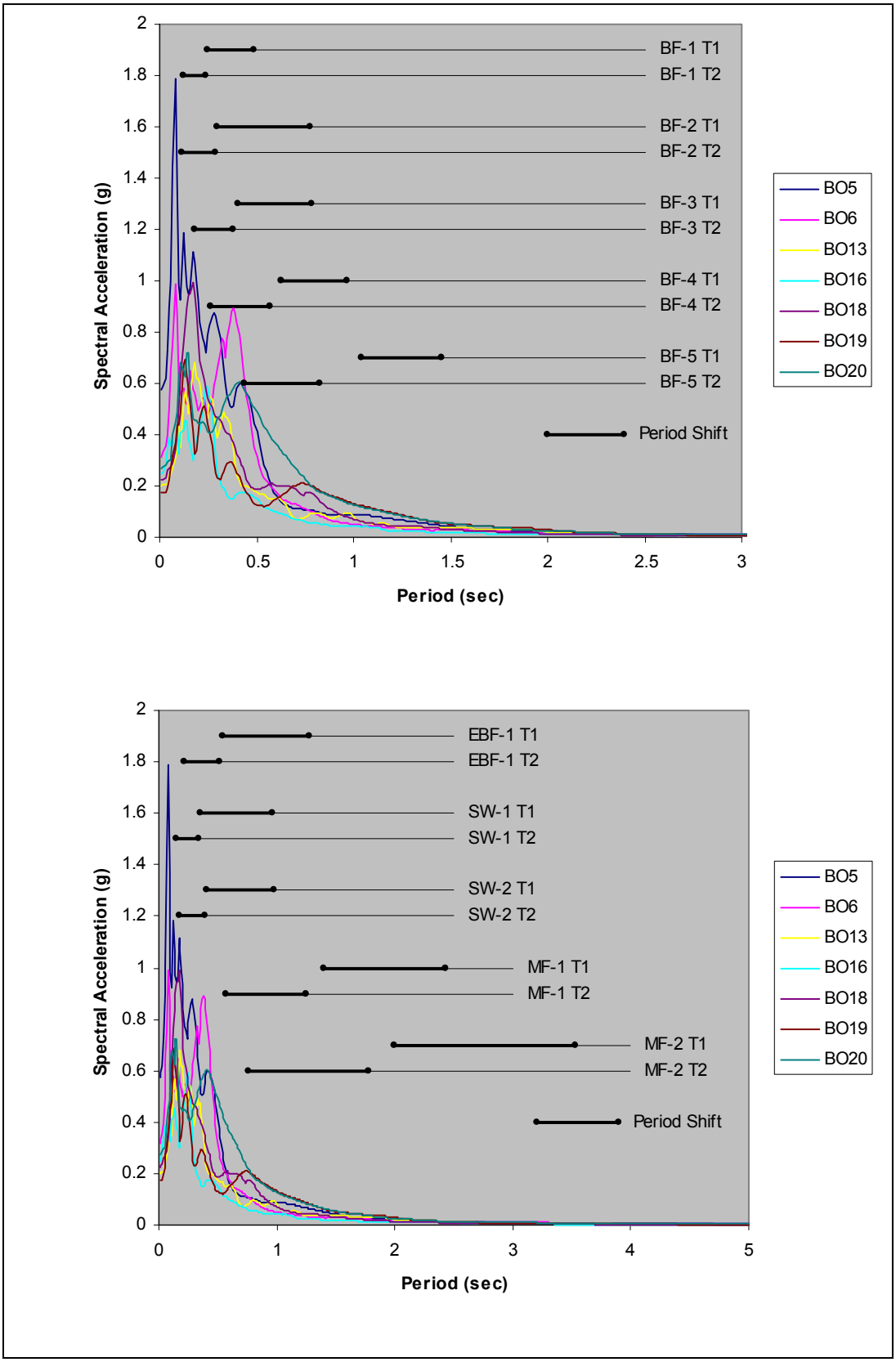

Figure 4.5 BO 10% in 50-Year Spectra with Period Shifts

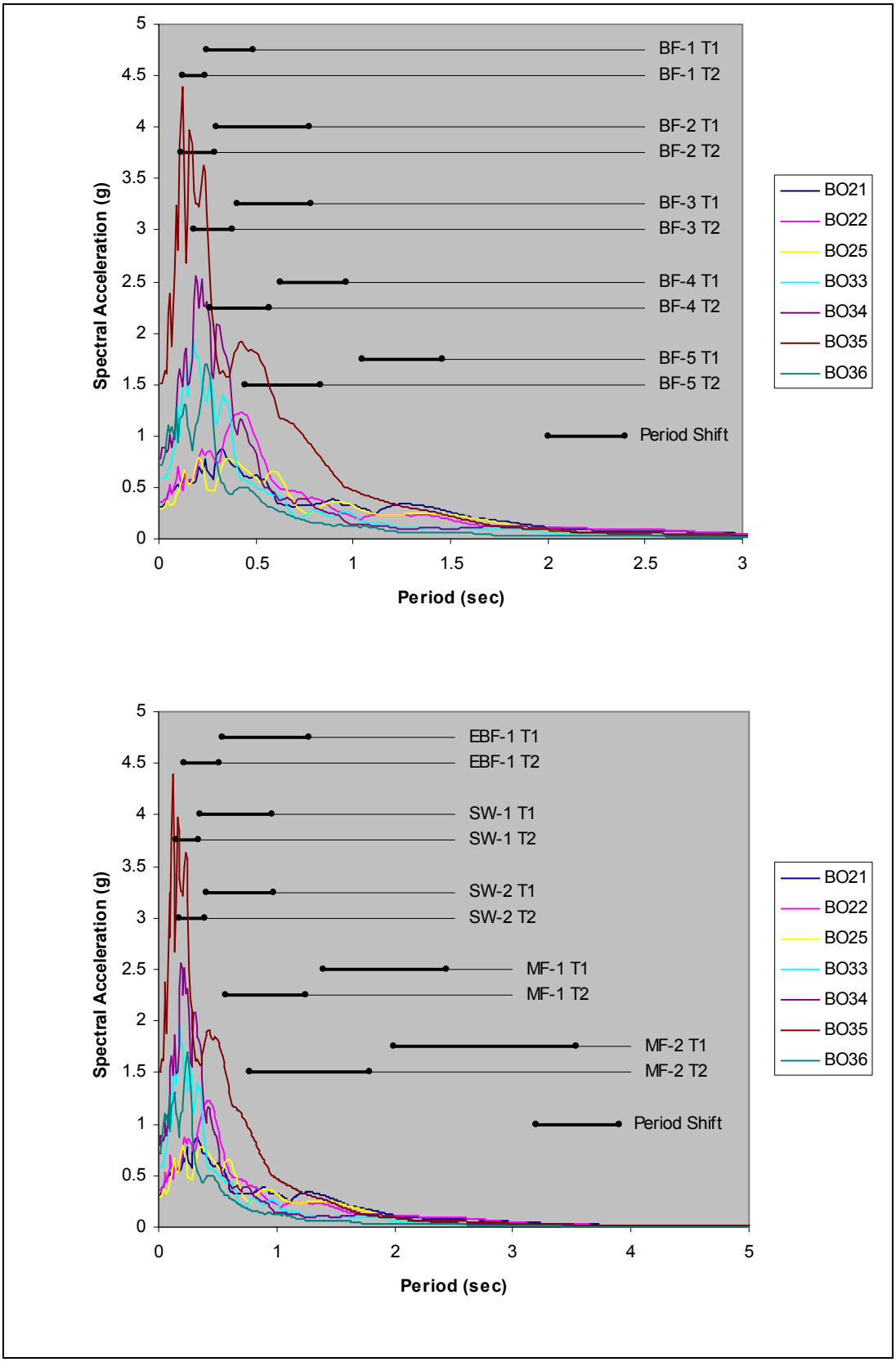

Figure 4.6 BO 2% in 50-Year Spectra with Period Shifts

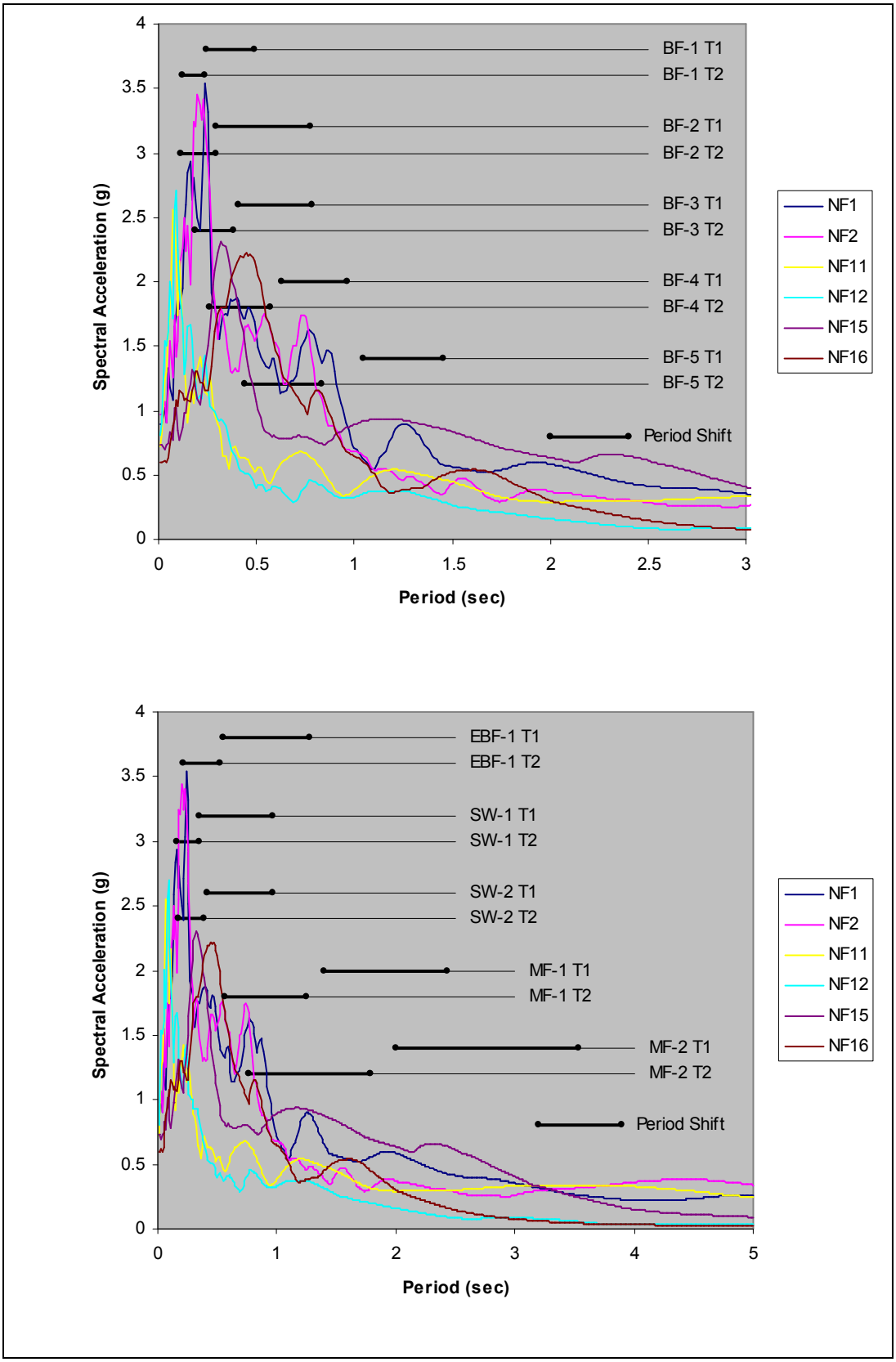

Figure 4.7 Near Field Spectra with Period Shifts

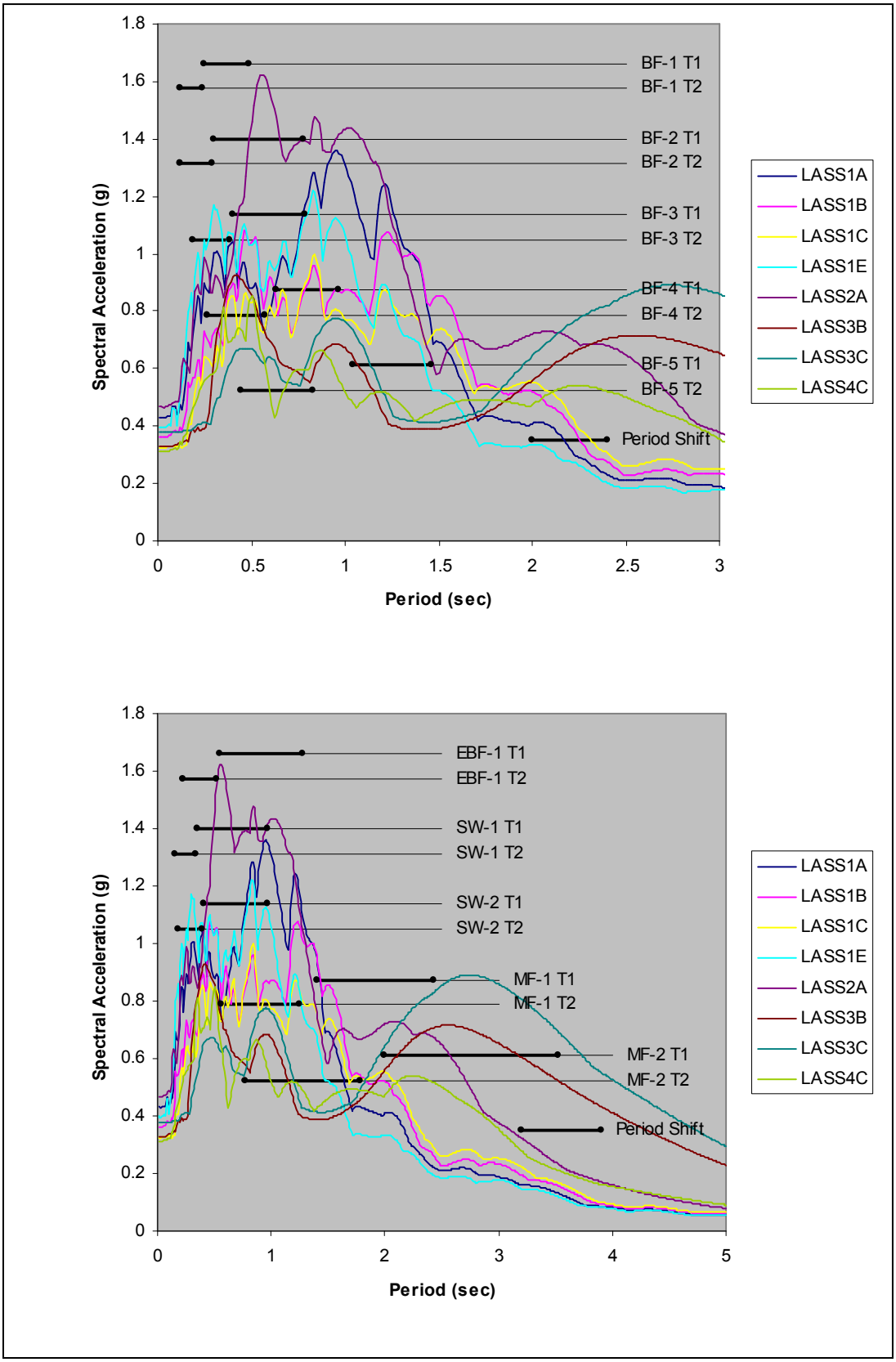

Figure 4.8 Soft Site Spectra with Period Shifts

displacement at the roof level of the structure. Figures 4.9 and 4.10 depict the time history response for these parameters. These reductions are attributable to two phenomena driven by the NRTMDF. First, the mode 1 period shift from 0.63 to 0.96 seconds correlates to a reduction from 1.30g to 0.88g in the spectral acceleration ordinates as shown in Figure 4.11. Second, the NRTMDF forces increased participation of mode 2 which, as postulated previously, drives a scenario of opposing inertial forces between the NRTMDF and the building below thereby reducing its response. As demonstrated in Figure 4.11, the spectral acceleration ordinate for the mode 2 period shift increases from 0.58g to 1.08g. This enhances performance (diminishes peak transient responses) since it introduces a counteracting inertial effect with the NRTMDF moving opposite the building below. This example reflects the concept that the NRTMDF not

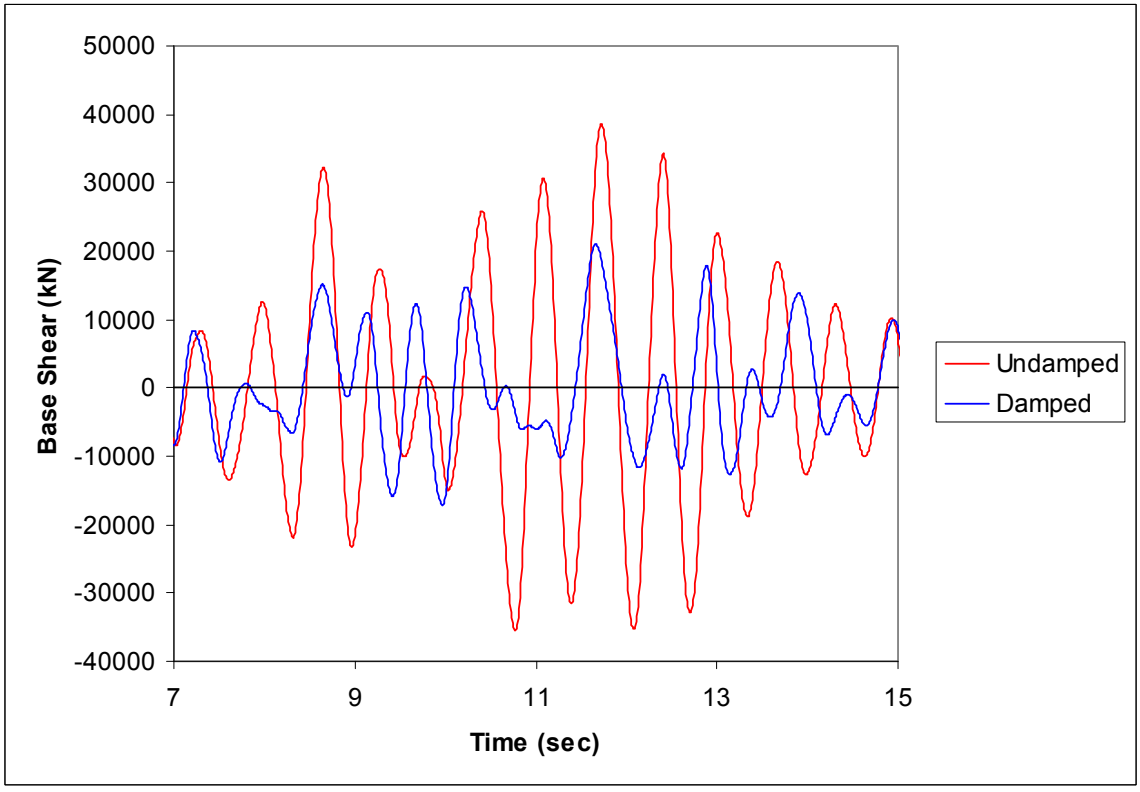

Figure 4.9 Base Shear Responses for Damped and Undamped BF-4, LA23 Motion

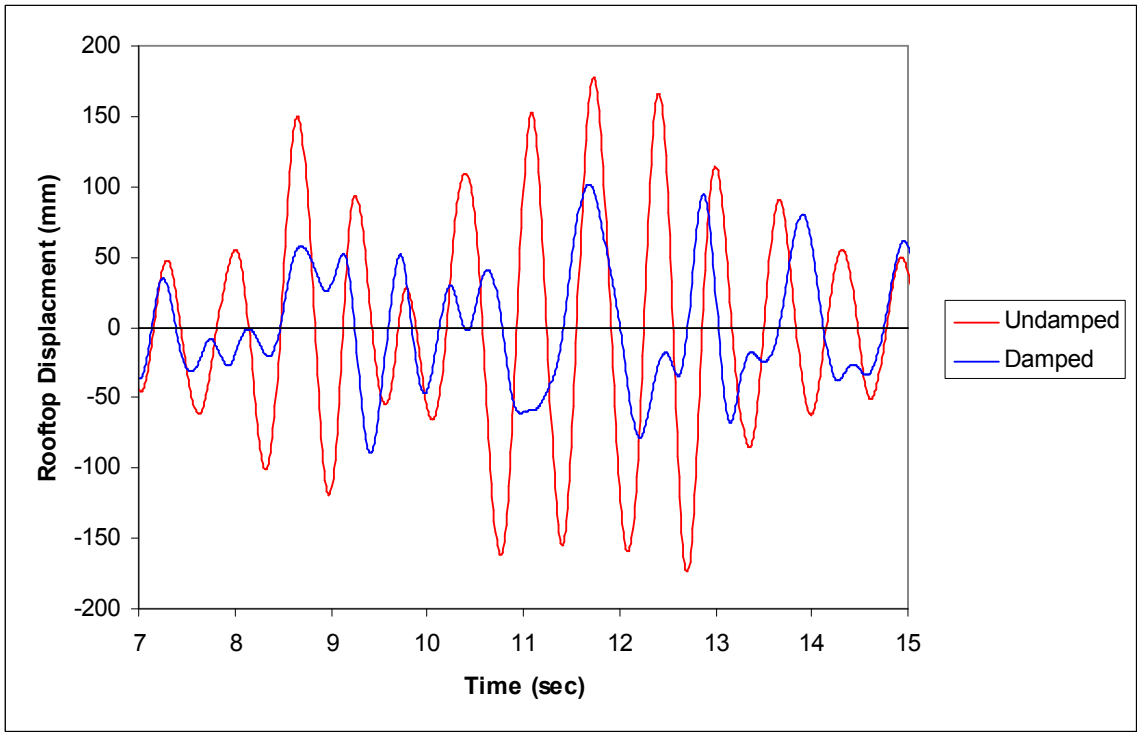

Figure 4.10 Rooftop Responses for Damped and Undamped BF-4, LA23 Motion

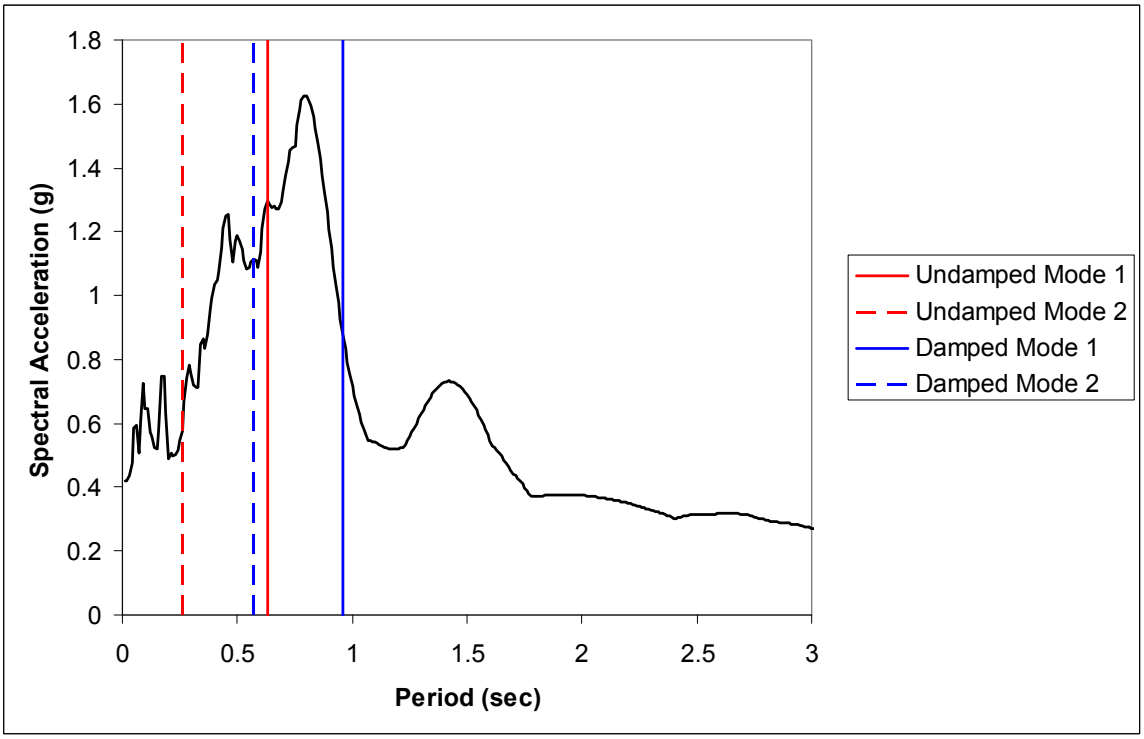

Figure 4.11 LA23 Spectrum (5% Damped) with BF-4 Undamped and Damped Periods

only changes the fundamental mode, but all other modes. In fact, the introduction of the NRTMDF creates a scenario where mode 2 becomes significant (see mode 2 participation factors indicated in Tables 4.1 through 4.10 for the damped models). Observation of modal participation for the undamped structures reflects the idea that the fundamental mode governs, as is presumed following most code driven analysis procedures for mid and low-rise structures. The introduction of the NRTMDF creates what contemporary codes would characterize as a mass and stiffness irregularity at the top of the structure with behavior that can only be captured by considering higher mode effects. As demonstrated, the higher mode effect for the models is manifest as a significantly increased mode 2 participation factor along with a beneficial counteracting inertial effect. Alternatively, consider the LA04 motion and BF-4. Figure 4.12 demonstrates mode 1 and mode 2 period shifts driven by the NRTMDF. As shown in this figure, the period shift for mode 1 results in spectral acceleration ordinates of nearly the same value (0.39g) between the undamped and damped cases. For mode 2, the spectral acceleration ordinate decreases with the period shift from 1.13g to 0.54 g. Hence, the beneficial counteracting inertial forces of mode 2 become diminished and the NRTMDF does not produce a reduced seismic response in BF-4 for this motion. The net result is an increase in peak base shear of 18.2% and increase in peak rooftop displacement of 17.2%. Figures 4.13 and 4.14 depict the base shear and rooftop displacement responses for this structure and motion. As an additional consideration, an increase of total mass of approximately 10% due to the NRTMDF exacerbates the unfavorable response since it contributes to the inertial mass for mode 1 and mode 2 thereby amplifying the unbeneficial behavior of each.

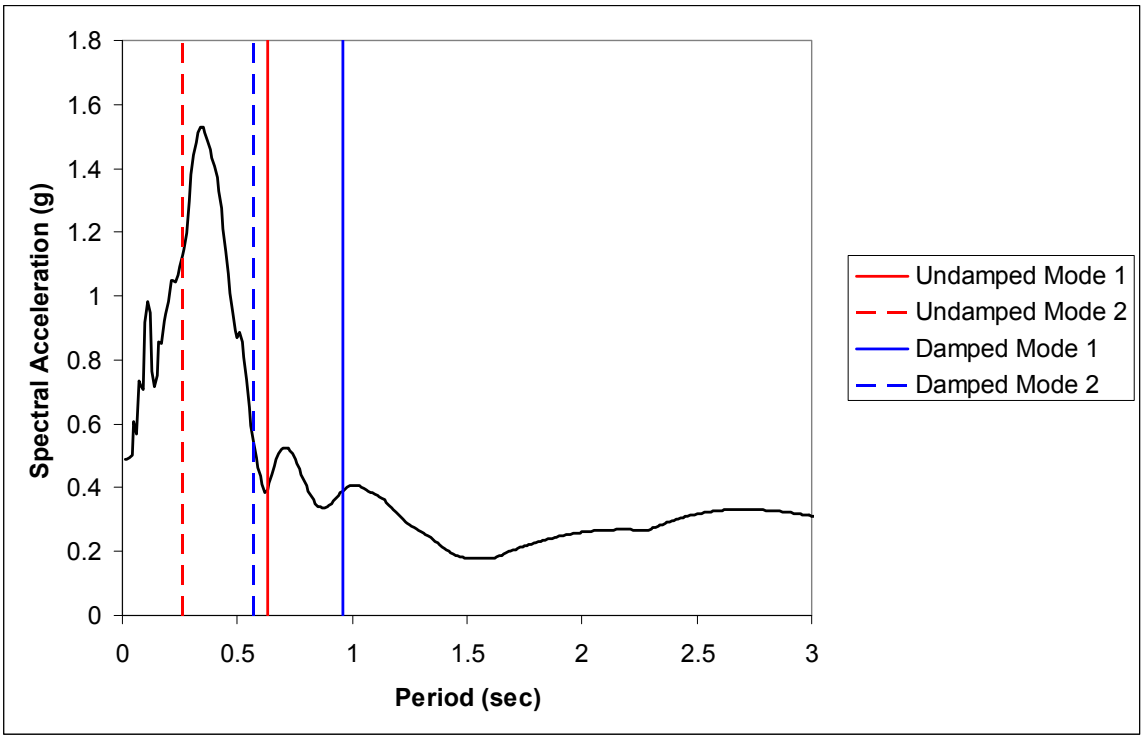

Figure 4.12 LA04 Spectrum (5% Damped) with BF-4 Undamped and Damped Periods

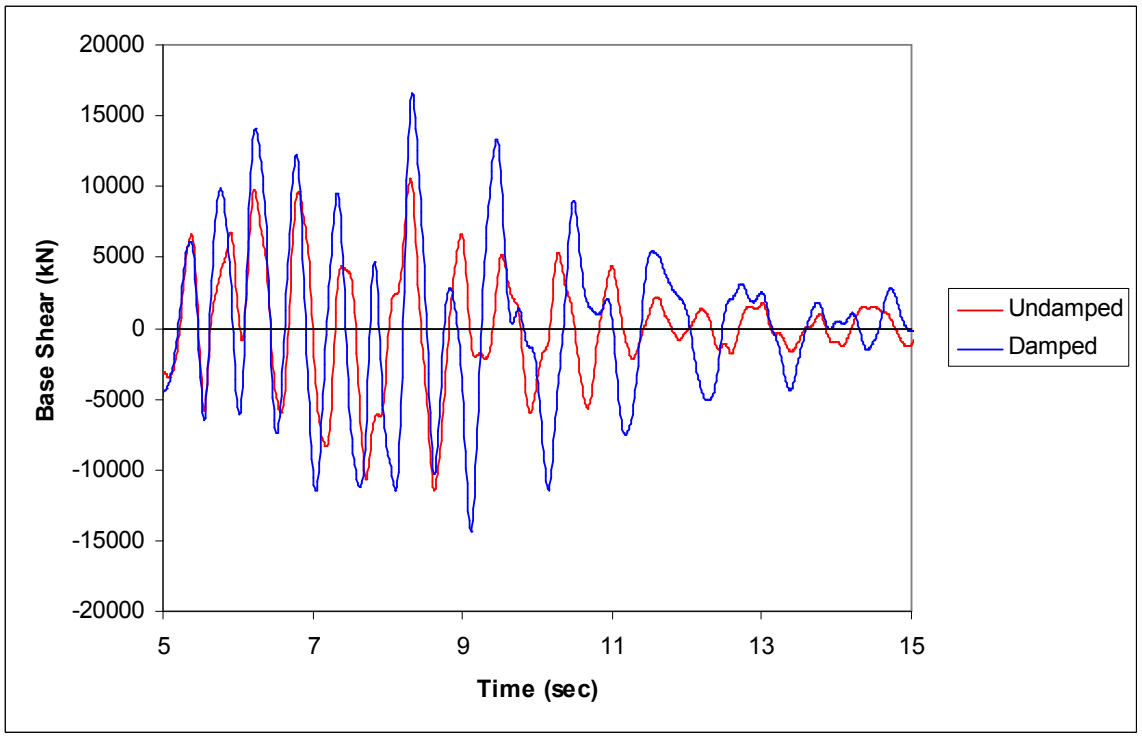

Figure 4.13 Base Shear Responses for Damped and Undamped BF-4, LA04 Motion

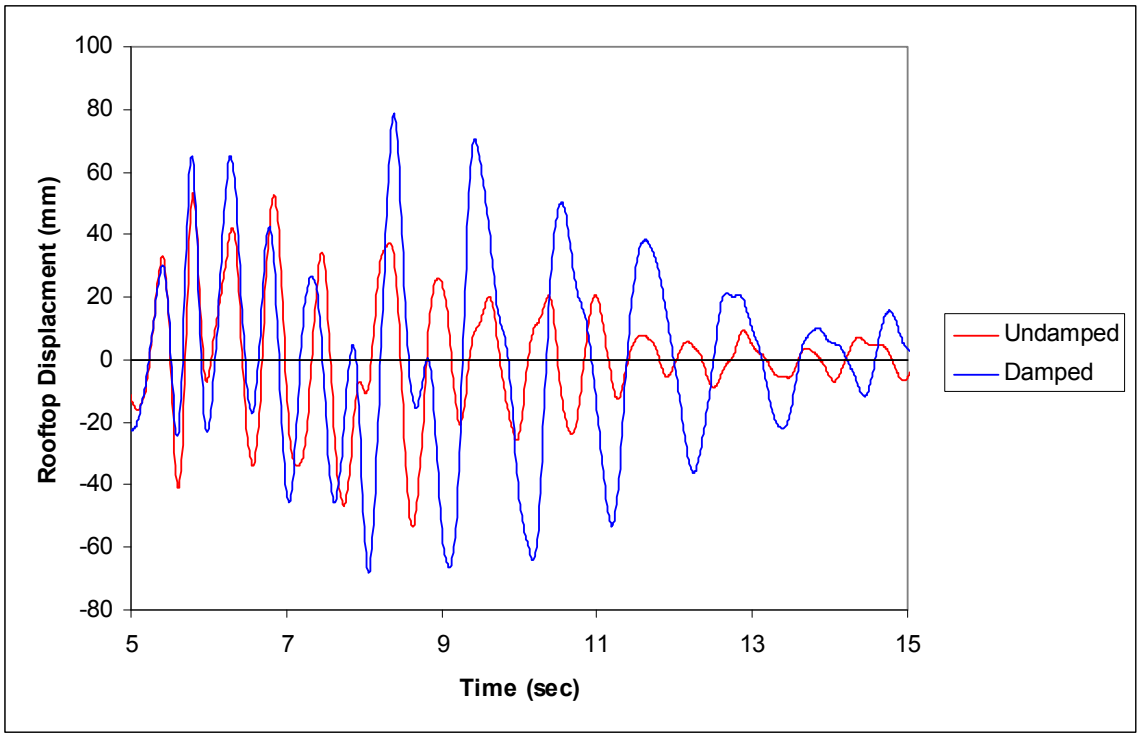

Figure 4.14 Rooftop Responses for Damped and Undamped BF-4, LA04 Motion

Qualitative observations of the period shifts for each structure in relation to the SAC acceleration spectra corroborate the results of the linear time history analysis for each building. Table 4.11 lists the average change in peak base shear, rooftop displacement and NRTMDF displacements for each structure using the SAC ground motions. While these average parameters do not demonstrate major changes in response, they reflect general trends in performance alterations enabled by the NRTMDF. Examination of changes in response for individual records in Tables 4.1 through 4.10 indicate significant changes for some specific records which typically correspond to significant changes in spectral acceleration ordinates driven by primary period shifts summarized in these tables and in Figures 4.1 through 4.8.

Table 4.11 Change in Average Peak Output Parameters and Peak NRTMDF Displacement for Linear Elastic Analyses

Structure	Change in Peak Base Shear	Change in Peak Rooftop Displacement	Peak NRTMDF Displacement (mm)
BF-1	-5.2%	-1.6%	104
BF-2	-3.7%	-1.7%	193
BF-3	-8.8%	-5.1%	224
BF-4	-10.9%	-12.4%	346
BF-5	-13.4%	-11.5%	430
EBF-1	-4.8%	-5.1%	312
SW-1	-4.9%	-2.8%	243
SW-2	-6.9%	-4.8%	259
MF-1	-16.0%	-10.8%	671
MF-2	-13.3%	-17.8%	814

4.2 Fundamental Conclusions of Linear Elastic Analyses

The linear elastic results demonstrate three distinct general trends that may be observed with the suites of buildings and ground motions. First, for structures of relatively short fundamental periods of 0.3 seconds or less (BF-1, BF-2, which are two stories), shifts in period driven by an effective NRTMDF design do not enable a significant reduction in spectral acceleration response. This notwithstanding, the results for these structures demonstrate trends of effectiveness for the approach. For shorter period structures, the original undamped structures typically have periods correlating to the regions of spectra where positive slopes may generally be observed. The result is that shifting periods are more likely place the structure at a region of increased spectral acceleration response. Fundamentally, the linear elastic analysis methods demonstrate less likelihood for beneficial performance due to the NRTMDF for cases such as this.

The second general trend that may be observed from the linear elastic analysis methods is that for buildings of medium fundamental periods ranging from 0.3 to 1.2

seconds (BF-3, BF-4, BF-5, EBF-1, SW-1, SW-2 which range from 3 to 6 stories except for BF-5 which is 9 stories), shifts in fundamental periods are more likely than short or long fundamental period structures to result in changes in spectral acceleration ordinates yielding a diminished structural response. For these, mode 1 period shifts may typically result in a decrease in the spectral acceleration ordinate when examining the correlating spectra. The mode 2 period shifts may typically result in an increase in the spectral acceleration ordinate which drives mode two behaviors with the NRTMDF inertial effects offsetting the inertial effects in the original structure.

The third general trend applies to structures with relatively long fundamental periods, typically greater than 1.2 seconds (MF-1, MF-2). For these, undamped fundamental periods are typically beyond the range of resonance with most firm sites and records. As such, the fundamental period shift, particularly for mode 1, does not result in a significant reduction in the spectral acceleration ordinate since the undamped structural period is typically beyond primary site periods to begin with. Likewise, the mode 2 period shift does not typically result in an increase, but a decrease in the spectral acceleration ordinate thereby precluding the beneficial mode 2 counteracting inertial behavior driven by the NRTMDF.

Figure 4.15 depicts the period ranges of these general trends and conclusions reflected for a typical firm site (Type D Soil). These trends, the accompanying conclusions and the associated period ranges for each of the trends become altered for sites and spectra representing less typical conditions such as soft sites and bedrock to near field effects. Also noteworthy for longer period structures is the correlating spectral displacement ordinate for both mode 1 and mode 2 of the damped structures.

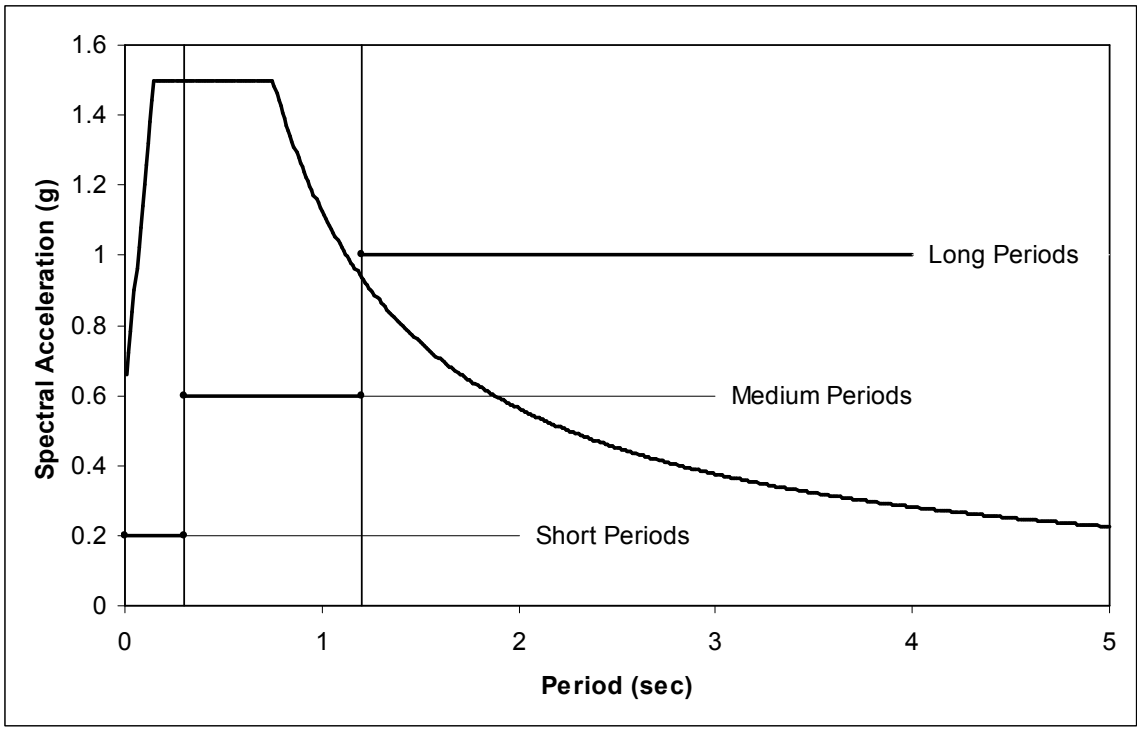

Figure 4.15 General Trends and Period Shifts for Firm Site Acceleration Spectrum

Longer periods typically translate to larger displacements particularly for soft sites. This is demonstrated in the analyses and in the displacement spectrum shown in Figure 4.16 reflecting the LASS3C (soft site) ground motion. The higher displacements are reflected in the NRTMDF drift calculations for MF-1 and MF-2 which have average peak values of 671mm and 814mm respectively (Tables 4.9 and 4.10) and peak drift calculations for MF-2 of 2,684mm (LASS3C motion). While the analysis demonstrates the potential for reduced response, the projected behavior indicates that these structures are not likely viable candidates for the approach. Likewise, for any structure with a relatively long period, effective damper properties (mass, effective stiffness) would likely result in a very limber NRTMDF with a propensity toward very high displacements and probable

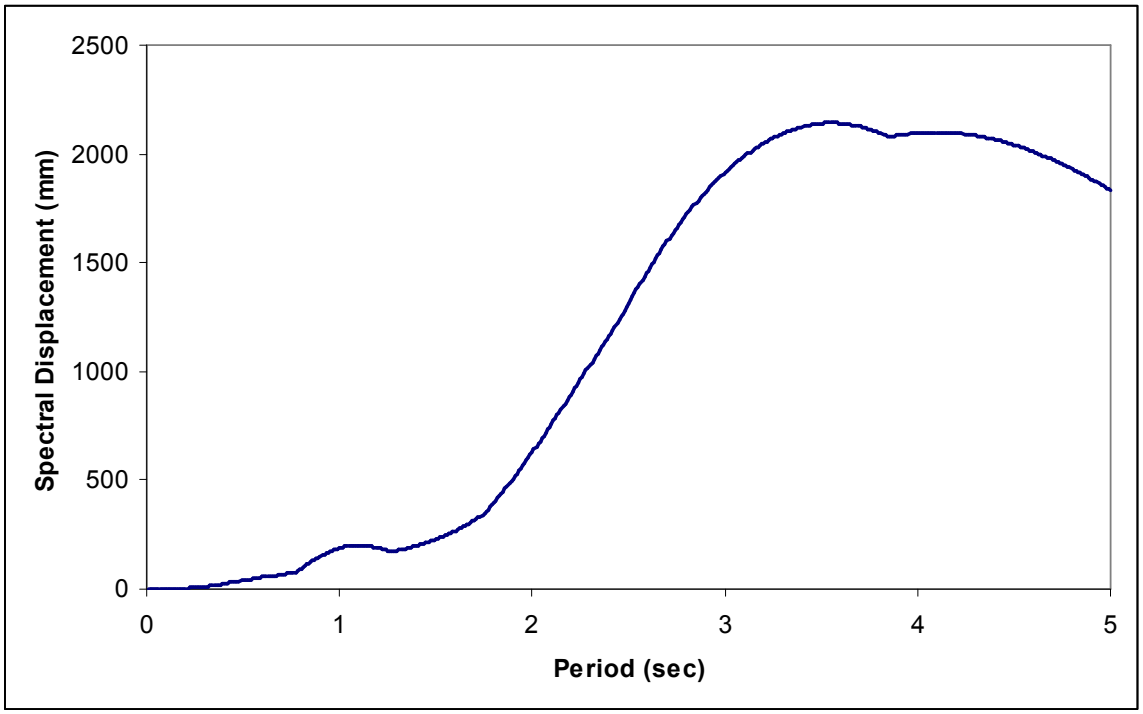

Figure 4.16 Displacement Spectrum for LASS3C Ground Motion

instabilities due to geometric nonlinearity, excessive strain or other behaviors associated with extreme drift including damage to nonstructural elements and components.

4.3 Limitations of Linear Elastic Analyses

The linear elastic methods for assessing the effectiveness of the NRTMDF are thought to be effective for identifying whether a given structure might be a candidate which could benefit from this approach. The linear methods should be considered an initial screen of a building and site to gain an understanding of basic trends of behavior. These methods are only rough approximations for truly characterizing the behavior of the structures and the effectiveness and performance of the NRTMDF. Benefits of the linear elastic approaches are found in their simplicity. Shortcomings for these methods include, but are not limited to:

- Lack of accounting for actual structural damping and targeted hysteretic energy dissipation.
- Non apparent effects of unidirectional impulses caused by near-field effects.
- No accounting for mechanisms and alteration of stiffness and accompanying period shifts due to yielding of the NRTMDF.
- Innaccurate accounting for NRTMDF displacement behavior and whether it remains within practical limitations.
- Inability to predict whether active nonlinearity in the NRTMDF is achieved prior to yielding of the base structure where active nonlinearity is defined as the development of inelastic hysteretic behavior of the buckling restrained braces of the NRTMDF.
- The linear methods will likely underestimate the NRTMDF mass necessary to develop effective inertial forces between the primary building and NRTMDF (see Section 5.5).

Linear Elastic methods inherently account for damping and energy dissipation solely by classical modal damping methods with either the damping component included within the SDOF component of modal superposition techniques or by use of a damping matrix which effectively diminishes structural response as a function of velocity. For linear elastic methods, these are the only approaches enabling energy to escape the system. Nonlinear behavior has long been recognized as the primary method for developing damped behavior associated with significant ground motions. While linear elastic methods are useful, they do not provide a means to account for nonlinear behavior that is observed and in fact generally expected when significant ground motions occur.

As a fundamental result, linear elastic methods cannot accurately predict base shears, story drifts, displacements and other performance parameters when the structure is subjected to a motion that would push its materials beyond their capable elastic range.

A unidirectional pulse can have a profound effect on nonlinear hysteretic behavior. Such pulses are most often observed with near-field ground motions and may be manifest as a peak transient behavior which is far greater in one direction than the other. Pulses may be caused by a sudden unidirectional fault rupture or by unidirectional superposition of propagating seismic waves. This behavior is not cyclical but drives a pulse of seismic energy in only one direction. This leads to significant lack of balance in hysteretic relationships and may cause permanent nonlinear deformations from which a structure potentially might not recover. This phenomenon is virtually non-apparent using linear elastic methods with the only clue of its presence being elastic displacements which might be much larger in one direction than the other. This can be observed for the LA04 ground motion for some of the buildings in this research for which linear elastic methods predict a damper displacement significantly higher in one direction than the other as shown for BF-5 in Figure 4.17.

Conventional linear elastic methods account for nonlinear behavior by virtue of prescribed multipliers and divisors when considering displacements and base shears respectively, for design purposes. While these provisions recognize that structural softening occurs due to material yielding, they do not directly account for the degradation of stiffness due to inelastic strains which result in shifts (increases) in fundamental periods. Such shifts typically result in a reduced spectral acceleration response. The result is that linear elastic methods typically predict unrealistically large base shears and

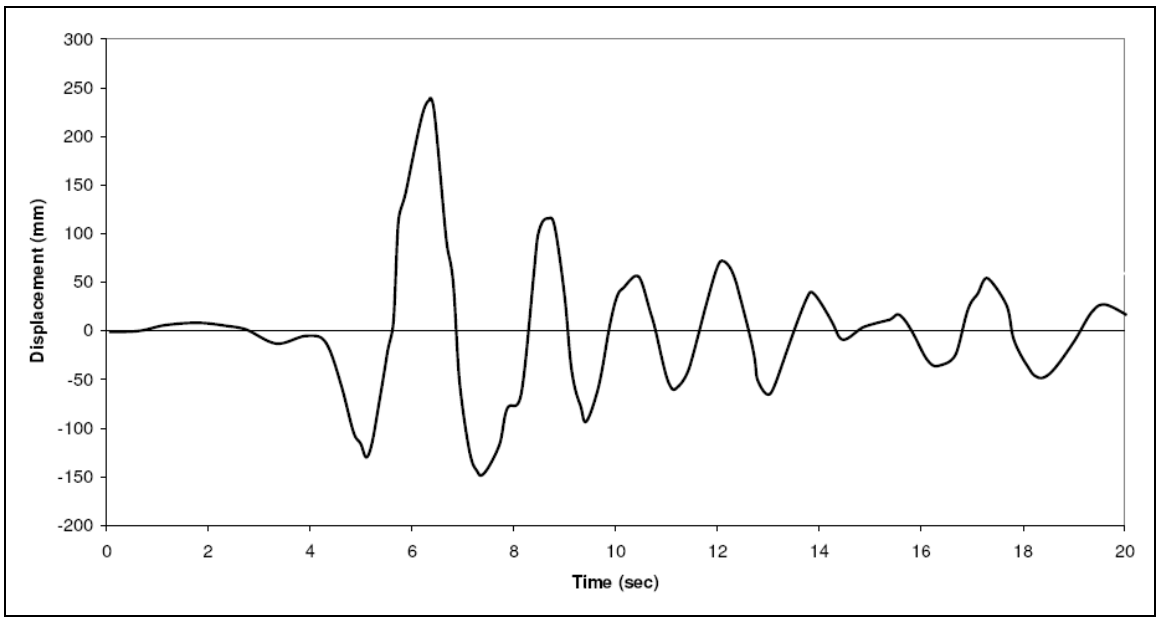

Figure 4.17 Rooftop Damper Displacement for BF-5, LA04 Ground Motion

element forces along with underestimated calculations of predicted of drifts, displacements, element strain and other peak transient responses.

The NRTMDF models examined within this research are expected to experience relatively large drifts and displacements. The magnitudes of displacements are expected to be in ranges of behavior where both material and geometric nonlinearity (P-Delta effects) are expected to be significant. While linear elastic methods may address geometric nonlinearity, they do not address the accompanying material nonlinearity and maximum capable inelastic behaviors of various elements and components.

While conclusions may be drawn by examining the effective stiffness of the NRTMDF using linear elastic methods, the results of the nonlinear inelastic methods shown hereafter will demonstrate that direct relationships between elastic stiffness of the NRTMDF for linear elastic methods and the effective stiffness of the NRTMDF for nonlinear inelastic methods cannot be drawn. This is due to a time domain requirement

of the NRTMDF to effectively mobilize and develop significant nonlinear hysteretic behavior. This time domain is typically beyond the stand-alone periods of the NRTMDF based on elastic methods. At best, the linear elastic methods may serve to develop a range of values for initial stiffness (K_i) and effective stiffness (K_e) of the NRTMDF (see Figure 3.22). Typically, the stiffness of the NRTMDF using linear elastic methods will fall somewhere between K_i and K_e (minimum stiffness based on peak NRTMDF displacement) based on the nonlinear inelastic methods.

4.4 Conclusions for Linear Elastic Analyses

Linear elastic methods have inherent limitations that would preclude their practical use as the sole method for assessing the effectiveness of an NRTMDF and its ability to alter seismic response for a given structure and ground motion. Nevertheless, these methods are thought to be effective as a preliminary tool for assessing whether a structure may be a viable candidate for the approach. While the results herein presented for linear elastic analysis procedures are deemed insufficient, there are correlations that will be shown with these results and the results of the nonlinear inelastic analysis methods presented hereafter. Overall, consistencies will be shown that will demonstrate that when linear elastic methods demonstrate a reduction in seismic response, the nonlinear inelastic methods will also typically demonstrate a reduction in seismic response though the magnitudes of performance parameters will be different. Likewise, correlations will also be demonstrated when increases in structural response are observed for both the linear elastic methods and the nonlinear inelastic methods.

In summary, linear elastic methods may be used as a qualitative tool for assessing whether a structure is a viable candidate for this approach. Linear elastic methods can be

used for quantitative analyses but only with sufficient understanding of the limitations. General conclusions of the broad based linear analyses for the NRTMDF approach are:

- The NRTMDF method is an effective approach for lengthening a structure's fundamental period.
- The fundamental period shift enabled by the NRTMDF is an effective approach for reducing the acceleration response shorter period structures (1.2 seconds or less) located on firm sites (Type D or firmer soil) which is the predominant condition for most sites.
- For higher period structures (1.2 seconds or more) the NRTMDF can enable lengthening of the fundamental period, but for firm sites, the reduction in acceleration response is not significant since the spectral acceleration ordinate of the undamped structure is relatively low to begin with.
- The NRTMDF approach lengthens the periods of higher modes (mode 2) which can introduce beneficial counteracting inertial effects.
- Unlike conventional approaches, use of the NRTMDF introduces significant higher mode response which must be accounted for in the analysis. Whereas the first mode may account for roughly 70% to 95% of total seismic mass using conventional approaches, the NRTMDF approach reduces mode 1 participation by roughly half while doubling the participation of mode 2.
- NRTMDF mass must be of sufficient magnitude to enable the NRTMDF to develop sufficient inertial mass to counteract the inertia of the structure below. Studies presented herein indicate NRTMDF mass of approximately 10% to 15%

of total building mass is effective for linear analysis approaches (see Section 5.5 for further information).

- Linear analysis methods predict peak output parameters (displacement, drift and base shear) thought to be far beyond the magnitudes of those of more realistic nonlinear analysis methods.
- Modal analysis of a structure along with qualitative comparison of the fundamental period and the site response spectrum serves as an effective tool for determining whether a lengthened fundamental period (approximately 2x the undamped period) will likely result in a reduction of the spectral acceleration response. Such a reduction reflects the potential for the overall reduction in seismic response.
- Time history analysis is the most suitable analysis method for the NRTMDF approach since it accounts for counteracting inertial effects (positive and negative motions) introduced with significant higher mode effects. Since response spectrum and static methods only account for the positive accumulation of modal response effects, they cannot capture the counteracting dynamics and inertia.
- While linear analysis methods are believed an inadequate approach for detailed analysis and design of the NRTMDF, they are believed to serve as an adequate preliminary assessment tool for identifying whether structure and site are suitable for the approach.

5 RESULTS FOR BROAD-BASED NONLINEAR INELASTIC ANALYSES

Nonlinear inelastic analysis methods provide a realistic assessment of the NRTMDF and the potential reductions in seismic response it induces in the base structure. Furthermore, these analysis methods enable rational assessments of stability and energy dissipation of the NRTMDF. Other issues accounted for within the context of nonlinear analysis methods include the effects of unbalanced directional effects of the original ground motion (unidirectional pulses). Also, assessment of effective nonlinear mobilization of the NRTMDF becomes possible with nonlinear analysis. This issue becomes important since the fundamental nonlinear dynamics of the NRTMDF frame are likely to be significantly out-of-phase with the original ground motion frequency content to the degree that careful tuning of the damper is required to ensure the development of active nonlinearity for effective performance. The nonlinear inelastic analysis approach addressed in this chapter utilizes the same ground motions as the linear elastic analysis derived from the SAC database.

Tables 5.1 through 5.10 list the results of the nonlinear inelastic analyses for the ten test models and the SAC ground motion suite. Values listed are the changes in peak output parameters (base shear and rooftop displacement). The calculated values for these are found in Appendix C. Unlike the linear elastic analysis approach, this approach

Table 5.1 BF-1 Nonlinear Analyses Results

NRTMDF Properties

Mass = 88239 kg
Damper Yield Strength = 605.5 kN
Initial Stiffness = 31.67 kN/mm
Average Effective Stiffness = 7.94 kN/mm*
Initial Damped Period = 0.38 sec
Average Peak Damped Period = 0.68 sec

Acc. History	Peak Base Shear change	Peak Roof Disp. change	Damper Disp. (mm)	Acc. History	Peak Base Shear change	Peak Roof Disp. change	Damper Disp. (mm)
LA01	-0.7%	-22.0%	56	BO05	-5.1%	-16.7%	33
LA02	-1.9%	-36.8%	98	BO06	-10.3%	7.3%	34
LA04	-0.3%	-10.3%	76	BO13	-14.2%	-22.3%	20
LA12	-1.3%	-15.1%	98	BO16	-37.2%	-46.4%	14
LA15	-0.1%	-2.2%	100	BO18	-21.4%	-27.4%	24
LA18	-0.5%	-11.6%	123	BO19	-13.2%	-29.8%	19
LA20	-1.6%	-20.5%	109	BO20	4.0%	17.1%	30
LA21	1.0%	24.8%	318	BO21	-21.1%	-24.6%	45
LA22	0.7%	21.1%	236	BO22	-0.3%	-13.4%	73
LA23	18.3%	39.9%	51	BO25	28.2%	34.8%	55
LA25	-0.7%	-12.7%	189	BO33	-0.9%	-22.5%	65
LA28	-0.3%	-4.7%	250	BO34	-1.6%	-24.3%	64
LA30	-2.3%	-21.9%	193	BO35	-2.0%	-20.3%	113
LA37	0.6%	22.5%	153	BO36	-2.0%	-40.7%	41
SE04	-1.1%	-26.1%	57	NF01	-3.2%	-32.3%	126
SE05	2.1%	-16.2%	57	NF02	-1.9%	-21.7%	95
SE08	5.4%	-4.5%	36	NF11	-0.7%	-20.5%	62
SE10	-1.1%	-23.0%	58	NF12	-1.7%	-44.8%	40
SE12	-1.4%	-35.0%	56	NF15	-0.6%	-15.5%	129
SE18	-1.1%	-24.2%	79	NF16	0.0%	-0.4%	90
SE19	-0.6%	-17.2%	48	LASS1A	-0.2%	-7.3%	82
SE21	1.0%	37.6%	96	LASS1B	-11.9%	-11.8%	55
SE25	-1.1%	-20.7%	117	LASS1C	-7.5%	3.8%	50
SE26	-1.4%	-23.7%	134	LASS1E	-0.8%	-24.6%	75
SE30	-1.1%	-11.2%	187	LASS2A	-0.1%	-3.2%	54
SE31	-1.0%	-13.2%	245	LASS3B	20.6%	43.4%	42
SE32	-0.6%	-10.6%	131	LASS3C	14.7%	31.2%	30
SE36	0.0%	-0.5%	84	LASS4C	-15.3%	-4.3%	39

*Effective stiffness at average of peak NRTMDF displacement from each record

Table 5.2 BF-2 Nonlinear Analyses Results

NRTMDF Properties

Mass = 366618 kg
Initial Stiffness = 77.82 kN/mm
Initial Damped Period = 0.49 sec
Damper Yield Strength = 2439.5 kN
Average Effective Stiffness = 23.23 kN/mm*
Average Peak Damped Period = 0.81 sec

Acc. History	Peak Base Shear change	Peak Roof Disp. change	Damper Disp. (mm)	Acc. History	Peak Base Shear change	Peak Roof Disp. change	Damper Disp. (mm)
LA01	-4.5%	-10.5%	97	BO05	-17.9%	-41.1%	40
LA02	-4.4%	-21.5%	136	BO06	-13.1%	-57.1%	30
LA04	-14.8%	-36.3%	77	BO13	-0.8%	-3.1%	22
LA12	-2.0%	-20.3%	130	BO16	3.8%	18.4%	16
LA15	-11.8%	-28.2%	123	BO18	-8.1%	-27.7%	20
LA18	-2.5%	-17.6%	229	BO19	22.1%	28.3%	17
LA20	-5.5%	-32.3%	149	BO20	-1.2%	-4.1%	45
LA21	-0.2%	-1.4%	469	BO21	-17.2%	-41.9%	43
LA22	1.4%	12.7%	259	BO22	-3.3%	-8.4%	79
LA23	3.7%	9.1%	87	BO25	-3.0%	-9.7%	42
LA25	-2.7%	-22.6%	231	BO33	-3.9%	-8.0%	69
LA28	-2.8%	-11.4%	441	BO34	-10.9%	-48.3%	72
LA30	-1.3%	-10.0%	151	BO35	0.2%	2.0%	186
LA37	1.3%	3.8%	205	BO36	6.0%	14.1%	44
SE04	-2.6%	-20.6%	64	NF01	-1.3%	-14.6%	125
SE05	-14.5%	-30.7%	60	NF02	-1.1%	-12.0%	97
SE08	-9.8%	-20.1%	72	NF11	-5.9%	-12.9%	61
SE10	-9.3%	-42.6%	73	NF12	-15.6%	-34.0%	54
SE12	-5.3%	-18.6%	68	NF15	-3.2%	-26.9%	191
SE18	-2.5%	-22.2%	96	NF16	-2.9%	-25.7%	137
SE19	-1.5%	-3.0%	89	LASS1A	-12.4%	-26.5%	63
SE21	5.0%	13.8%	177	LASS1B	0.2%	0.6%	82
SE25	-3.9%	-25.0%	136	LASS1C	2.5%	7.2%	58
SE26	-3.7%	-31.4%	140	LASS1E	-14.1%	-27.8%	80
SE30	-5.5%	-25.9%	250	LASS2A	1.9%	4.3%	112
SE31	-2.3%	-16.7%	374	LASS3B	0.9%	2.5%	66
SE32	2.2%	20.1%	158	LASS3C	9.8%	34.7%	56
SE36	11.8%	30.1%	208	LASS4C	-4.4%	-13.0%	58

*Effective stiffness at average of peak NRTMDF displacement from each record

Table 5.3 BF-3 Nonlinear Analyses Results

NRTMDF Properties

Mass = 374683 kg
Damper Yield Strength = 1829.6 kN
Initial Stiffness = 76.27 kN/mm
Average Effective Stiffness = 13.67 kN/mm*
Initial Damped Period = 0.58 sec
Average Peak Damped Period = 1.09 sec

Acc. History	Peak Base Shear change	Peak Roof Disp. change	Damper Disp. (mm)	Acc. History	Peak Base Shear change	Peak Roof Disp. change	Damper Disp. (mm)
LA01	-0.4%	-19.6%	162	BO05	-29.3%	-56.1%	32
LA02	-0.6%	-26.8%	140	BO06	-35.6%	-72.1%	29
LA04	-1.0%	-42.1%	110	BO13	-6.2%	-1.0%	23
LA12	-1.3%	-36.0%	140	BO16	-26.7%	-31.7%	13
LA15	-0.6%	-25.1%	255	BO18	-0.2%	0.4%	32
LA18	-0.7%	-15.9%	403	BO19	6.7%	-23.3%	21
LA20	-0.8%	-26.6%	171	BO20	-25.2%	-42.0%	47
LA21	-1.1%	-25.7%	458	BO21	-11.9%	-43.3%	49
LA22	-1.7%	-39.1%	375	BO22	-0.9%	-44.4%	82
LA23	-0.1%	-6.8%	216	BO25	-2.9%	-29.7%	79
LA25	-0.8%	-21.4%	432	BO33	16.1%	-26.0%	55
LA28	-0.8%	-11.3%	706	BO34	-0.5%	-27.1%	55
LA30	-0.9%	-23.6%	290	BO35	-0.7%	-21.1%	155
LA37	-0.1%	-4.1%	360	BO36	-30.0%	-36.5%	40
SE04	-0.3%	-18.7%	53	NF01	-1.2%	-36.5%	172
SE05	-0.2%	-14.9%	130	NF02	-0.2%	-8.0%	179
SE08	-0.1%	-11.1%	132	NF11	7.6%	-37.9%	79
SE10	-0.7%	-36.8%	93	NF12	6.7%	-25.3%	52
SE12	-0.1%	-6.2%	121	NF15	-0.6%	-18.6%	325
SE18	-1.2%	-44.2%	159	NF16	-0.7%	-20.4%	166
SE19	0.1%	4.3%	141	LASS1A	-0.1%	-7.2%	115
SE21	-0.1%	-3.8%	239	LASS1B	-0.2%	-14.8%	107
SE25	-1.0%	-29.7%	313	LASS1C	-0.1%	-5.0%	105
SE26	-0.4%	-11.0%	274	LASS1E	-0.2%	-10.8%	93
SE30	-1.9%	-31.1%	346	LASS2A	-0.1%	-7.5%	171
SE31	-0.5%	-16.7%	515	LASS3B	-0.5%	-33.3%	96
SE32	-0.4%	-16.0%	269	LASS3C	0.0%	0.7%	77
SE36	0.2%	10.5%	369	LASS4C	-4.4%	-33.7%	60

*Effective stiffness at average of peak NRTMDF displacement from each record

Table 5.4 BF-4 Nonlinear Analyses Results

NRTMDF Properties

Mass = 719186 kg
Damper Yield Strength = 2307.9 kN
Initial Stiffness = 82.25 kN/mm
Average Effective Stiffness = 12 kN/mm*
Initial Damped Period = 0.9 sec
Average Peak Damped Period = 1.63 sec

Acc. History	Peak Base Shear change	Peak Roof Disp. change	Damper Disp. (mm)	Acc. History	Peak Base Shear change	Peak Roof Disp. change	Damper Disp. (mm)
LA01	-0.9%	-35.5%	193	BO05	51.5%	16.8%	37
LA02	-1.2%	-35.4%	252	BO06	37.6%	-15.4%	26
LA04	5.0%	39.3%	176	BO13	-21.4%	-27.3%	21
LA12	-0.7%	-28.8%	160	BO16	11.5%	-22.1%	17
LA15	-0.2%	-7.7%	483	BO18	-54.0%	-18.6%	27
LA18	-0.7%	-20.1%	360	BO19	-24.9%	29.9%	32
LA20	-0.5%	-17.9%	336	BO20	-25.2%	-29.8%	51
LA21	-1.2%	-23.3%	652	BO21	18.9%	0.9%	81
LA22	-1.1%	-18.6%	580	BO22	-18.8%	-30.2%	108
LA23	-1.2%	-43.0%	212	BO25	-28.6%	-43.3%	69
LA25	-0.5%	-13.3%	749	BO33	-30.6%	-27.1%	77
LA28	-0.9%	-16.0%	700	BO34	-21.8%	-22.9%	88
LA30	-0.4%	-12.3%	586	BO35	-0.9%	-29.9%	235
LA37	-0.3%	-7.8%	614	BO36	1.6%	-19.4%	43
SE04	-0.1%	-4.7%	121	NF01	-0.4%	-14.5%	321
SE05	-0.5%	-32.1%	143	NF02	-0.6%	-20.2%	248
SE08	-0.6%	-31.6%	155	NF11	-0.2%	-15.5%	132
SE10	-0.3%	-18.5%	196	NF12	-24.2%	4.9%	73
SE12	-1.1%	-45.4%	211	NF15	-0.3%	-15.9%	337
SE18	-5.3%	-62.9%	179	NF16	-1.0%	-30.6%	251
SE19	-2.0%	-49.5%	351	LASS1A	-0.3%	-13.8%	348
SE21	-1.1%	-18.9%	632	LASS1B	-0.3%	-17.9%	253
SE25	-1.1%	-30.2%	380	LASS1C	-0.3%	-15.3%	276
SE26	-2.4%	-56.1%	244	LASS1E	-0.5%	-26.0%	248
SE30	-2.4%	-36.5%	400	LASS2A	-1.2%	-37.0%	277
SE31	-2.3%	-25.3%	608	LASS3B	-0.2%	-10.5%	253
SE32	-2.1%	-44.9%	356	LASS3C	0.1%	10.0%	270
SE36	-1.0%	-29.0%	714	LASS4C	-14.6%	57.4%	175

*Effective stiffness at average of peak NRTMDF displacement from each record

Table 5.5 BF-5 Nonlinear Analyses Results

NRTMDF Properties

Mass = 775159 kg
Damper Yield Strength = 1491.8 kN
Initial Stiffness = 61.49 kN/mm
Average Effective Stiffness = 6.35 kN/mm*
Initial Damped Period = 1.48 sec
Average Peak Damped Period = 2.44 sec

Acc. History	Peak Base Shear change	Peak Roof Disp. change	Damper Disp. (mm)	Acc. History	Peak Base Shear change	Peak Roof Disp. change	Damper Disp. (mm)
LA01	-34.0%	-27.4%	310	BO05	-22.8%	-31.2%	25
LA02	11.6%	-44.7%	410	BO06	7.7%	-25.7%	26
LA04	-22.6%	-32.7%	184	BO13	11.5%	-11.4%	14
LA12	-40.3%	-37.8%	234	BO16	-36.0%	-29.9%	14
LA15	33.8%	-24.9%	597	BO18	1.0%	-48.0%	32
LA18	-16.4%	-15.1%	540	BO19	-38.7%	-41.8%	36
LA20	83.6%	-28.4%	590	BO20	-20.8%	-33.9%	54
LA21	-0.1%	-20.7%	1011	BO21	-39.8%	-4.8%	152
LA22	-0.1%	-12.8%	1053	BO22	-48.4%	-12.9%	76
LA23	-10.1%	-7.6%	371	BO25	-25.5%	-1.0%	202
LA25	-0.1%	-20.7%	889	BO33	-8.4%	-13.7%	47
LA28	-3.6%	-16.2%	986	BO34	-10.7%	-8.4%	75
LA30	-2.8%	6.4%	815	BO35	-30.3%	-28.8%	308
LA37	-3.6%	-26.0%	1080	BO36	-36.0%	-30.6%	39
SE04	-42.8%	-47.1%	116	NF01	12.4%	0.9%	753
SE05	-38.4%	-21.6%	145	NF02	-17.9%	-33.6%	444
SE08	-44.5%	-50.6%	205	NF11	10.4%	24.1%	460
SE10	-31.4%	-29.8%	330	NF12	-23.8%	-7.7%	153
SE12	-37.5%	-45.6%	154	NF15	-15.7%	-2.7%	689
SE18	-37.9%	-24.0%	253	NF16	-20.6%	-8.6%	418
SE19	18.0%	-27.1%	394	LASS1A	50.2%	-41.0%	547
SE21	-3.6%	-27.0%	1135	LASS1B	-35.2%	-33.2%	394
SE25	33.7%	-35.7%	400	LASS1C	-35.9%	-23.2%	428
SE26	-32.5%	-43.6%	466	LASS1E	16.8%	-40.3%	393
SE30	71.4%	-44.1%	540	LASS2A	-3.6%	-27.8%	947
SE31	-0.1%	-14.6%	899	LASS3B	-6.3%	-1.0%	533
SE32	-7.5%	-49.9%	526	LASS3C	-0.1%	2.5%	781
SE36	-0.1%	-24.9%	1214	LASS4C	-21.3%	23.6%	327

*Effective stiffness at average of peak NRTMDF displacement from each record

Table 5.6 EBF-1 Nonlinear Analyses Results

NRTMDF Properties

Mass = 705943 kg
Damper Yield Strength = 1623.4 kN
Initial Stiffness = 57.4 kN/mm
Average Effective Stiffness = 8.87 kN/mm*
Initial Damped Period = 0.96 sec
Average Peak Damped Period = 1.87 sec

Acc. History	Peak Base Shear change	Peak Roof Disp. change	Damper Disp. (mm)	Acc. History	Peak Base Shear change	Peak Roof Disp. change	Damper Disp. (mm)
LA01	-10.8%	-43.3%	213	BO05	-18.4%	-5.0%	37
LA02	-11.6%	-41.7%	272	BO06	20.7%	-3.7%	28
LA04	-2.1%	-15.6%	197	BO13	-7.0%	7.7%	21
LA12	-6.4%	-26.0%	158	BO16	1.2%	-27.3%	14
LA15	0.7%	3.5%	416	BO18	-29.1%	-30.4%	20
LA18	-4.0%	-14.1%	396	BO19	-19.6%	66.4%	35
LA20	-7.7%	-30.9%	307	BO20	-10.7%	-36.4%	51
LA21	-4.6%	-12.8%	694	BO21	-2.7%	-23.6%	78
LA22	-6.1%	-20.9%	452	BO22	-5.4%	-35.0%	74
LA23	-8.4%	-42.2%	207	BO25	10.1%	-32.6%	90
LA25	-1.0%	-3.4%	524	BO33	33.8%	-25.2%	59
LA28	-3.6%	-11.3%	737	BO34	-3.0%	-26.2%	85
LA30	-8.9%	-26.8%	575	BO35	-8.4%	-29.2%	235
LA37	-0.2%	-1.0%	659	BO36	1.0%	-48.4%	38
SE04	-1.4%	-11.8%	145	NF01	-4.6%	-19.8%	385
SE05	-5.1%	-32.0%	139	NF02	-12.3%	-42.6%	314
SE08	-4.3%	-30.1%	189	NF11	1.8%	19.2%	199
SE10	-4.5%	-28.1%	144	NF12	-65.1%	21.7%	88
SE12	-12.9%	-55.6%	149	NF15	2.7%	16.2%	323
SE18	-9.6%	-46.8%	137	NF16	-8.2%	-27.8%	208
SE19	-16.4%	-54.7%	291	LASS1A	-0.9%	-5.5%	345
SE21	-9.0%	-27.7%	667	LASS1B	-5.1%	-28.7%	227
SE25	-10.7%	-34.9%	307	LASS1C	-1.8%	-12.6%	262
SE26	-9.1%	-34.1%	214	LASS1E	-4.3%	-24.2%	242
SE30	-8.4%	-22.2%	396	LASS2A	-11.0%	-40.9%	321
SE31	-8.8%	-35.9%	443	LASS3B	-1.8%	-12.1%	308
SE32	-13.9%	-43.7%	272	LASS3C	1.5%	12.1%	293
SE36	-3.9%	-18.2%	557	LASS4C	1.1%	8.5%	166

*Effective stiffness at average of peak NRTMDF displacement from each record

Table 5.7 SW-1 Nonlinear Analyses Results

NRTMDF Properties

Mass = 931797 kg
Damper Yield Strength = 4352.5 kN
Initial Stiffness = 265.18 kN/mm
Average Effective Stiffness = 42.95 kN/mm*
Initial Damped Period = 0.54 sec
Average Peak Damped Period = 0.98 sec

Acc. History	Peak Base Shear change	Peak Roof Disp. change	Damper Disp. (mm)	Acc. History	Peak Base Shear change	Peak Roof Disp. change	Damper Disp. (mm)
LA01	-0.2%	2.5%	129	BO05	3.1%	-55.5%	29
LA02	1.8%	-17.6%	140	BO06	5.2%	-74.3%	22
LA04	7.0%	-58.1%	73	BO13	2.5%	-57.1%	20
LA12	5.5%	-37.3%	108	BO16	-4.6%	13.5%	15
LA15	2.2%	-21.1%	188	BO18	1.3%	-34.9%	16
LA18	4.4%	-21.7%	310	BO19	0.9%	-32.1%	13
LA20	6.3%	-34.7%	145	BO20	1.4%	-27.0%	34
LA21	8.2%	-38.8%	403	BO21	2.7%	-39.3%	29
LA22	6.3%	-34.6%	282	BO22	3.6%	-40.9%	63
LA23	-0.1%	2.0%	139	BO25	1.6%	-23.4%	44
LA25	2.9%	-17.9%	327	BO33	6.6%	-56.9%	58
LA28	3.2%	-15.0%	586	BO34	8.9%	-62.5%	54
LA30	4.7%	-28.3%	167	BO35	1.5%	-10.8%	168
LA37	-1.6%	16.0%	293	BO36	-0.4%	8.3%	34
SE04	3.5%	-36.6%	47	NF01	3.3%	-24.1%	159
SE05	3.9%	-42.2%	101	NF02	4.0%	-33.1%	147
SE08	0.2%	-2.9%	98	NF11	-1.1%	20.1%	51
SE10	5.3%	-47.0%	70	NF12	1.3%	-20.4%	55
SE12	3.1%	-28.9%	89	NF15	5.4%	-32.4%	261
SE18	6.6%	-46.0%	128	NF16	3.9%	-26.1%	156
SE19	-3.1%	49.7%	128	LASS1A	0.3%	-3.7%	74
SE21	-2.3%	30.3%	214	LASS1B	-0.3%	4.7%	90
SE25	9.0%	-47.0%	165	LASS1C	-0.6%	10.2%	85
SE26	7.8%	-41.6%	173	LASS1E	0.9%	-10.7%	85
SE30	-218.9%	-43.6%	231	LASS2A	-1.4%	19.4%	155
SE31	-1.6%	11.6%	429	LASS3B	0.7%	-10.1%	86
SE32	-1.8%	17.1%	210	LASS3C	-1.9%	39.7%	73
SE36	-1.1%	11.8%	304	LASS4C	1.8%	-25.8%	45

*Effective stiffness at average of peak NRTMDF displacement from each record

Table 5.8 SW-2 Nonlinear Analyses Results

NRTMDF Properties

Mass = 2163421 kg
Damper Yield Strength = 7623 kN
Initial Stiffness = 700.5 kN/mm
Average Effective Stiffness = 87.02 kN/mm*
Initial Damped Period = 0.58 sec
Average Peak Damped Period = 1.12 sec

Acc. History	Peak Base Shear change	Peak Roof Disp. change	Damper Disp. (mm)	Acc. History	Peak Base Shear change	Peak Roof Disp. change	Damper Disp. (mm)
LA01	-1.7%	-17.4%	175	BO05	-3.2%	-51.7%	30
LA02	-2.7%	-25.7%	142	BO06	-5.7%	-77.2%	27
LA04	-5.3%	-46.0%	107	BO13	-0.4%	-17.2%	16
LA12	-6.4%	-38.2%	131	BO16	-91.5%	-32.4%	10
LA15	-2.7%	-22.1%	253	BO18	-0.8%	-25.3%	22
LA18	-3.2%	-15.3%	394	BO19	-0.5%	-20.2%	15
LA20	-3.9%	-25.0%	172	BO20	-1.5%	-28.0%	38
LA21	-5.1%	-26.4%	435	BO21	-2.6%	-42.2%	39
LA22	-7.6%	-38.6%	372	BO22	-4.8%	-45.9%	77
LA23	-1.5%	-16.4%	176	BO25	-1.6%	-23.7%	74
LA25	-3.9%	-21.2%	422	BO33	-2.1%	-34.7%	54
LA28	-0.1%	-10.4%	732	BO34	-3.7%	-37.6%	58
LA30	-4.7%	-26.5%	295	BO35	-3.3%	-19.4%	147
LA37	-1.0%	-8.9%	340	BO36	-1.8%	-36.7%	27
SE04	-3.2%	-35.4%	59	NF01	-3.8%	-25.1%	205
SE05	-1.2%	-16.3%	116	NF02	-1.9%	-17.5%	161
SE08	-0.2%	-2.7%	115	NF11	-1.9%	-29.5%	73
SE10	-3.7%	-38.4%	97	NF12	-1.5%	-26.4%	49
SE12	-0.5%	-6.6%	133	NF15	-2.1%	-14.5%	327
SE18	-5.9%	-43.6%	154	NF16	-4.1%	-23.1%	181
SE19	0.0%	0.5%	171	LASS1A	-0.6%	-7.1%	141
SE21	-0.4%	-3.5%	272	LASS1B	-1.0%	-13.5%	109
SE25	-4.9%	-31.8%	240	LASS1C	-0.2%	-3.5%	105
SE26	-2.4%	-15.3%	216	LASS1E	-1.2%	-13.6%	121
SE30	-2.4%	-34.4%	278	LASS2A	-0.4%	-4.7%	201
SE31	-3.8%	-23.0%	527	LASS3B	-2.9%	-36.3%	120
SE32	-2.9%	-20.6%	251	LASS3C	0.0%	0.3%	106
SE36	0.3%	3.8%	423	LASS4C	-1.4%	-22.7%	64

*Effective stiffness at average of peak NRTMDF displacement from each record

Table 5.9 MF-1 Nonlinear Analyses Results

NRTMDF Properties

Mass = 799207 kg
Damper Yield Strength = 947.7 kN
Initial Stiffness = 31.36 kN/mm
Average Effective Stiffness = 3.31 kN/mm*
Initial Damped Period = 1.96 sec
Average Peak Damped Period = 3.1 sec

Acc. History	Peak Base Shear change	Peak Roof Disp. change	Damper Disp. (mm)	Acc. History	Peak Base Shear change	Peak Roof Disp. change	Damper Disp. (mm)
LA01	-43.3%	-24.7%	399	BO05	-19.3%	-15.6%	34
LA02	-40.1%	10.4%	443	BO06	-5.1%	-12.8%	16
LA04	-15.6%	26.2%	410	BO13	27.0%	5.0%	20
LA12	4.1%	-24.2%	198	BO16	-29.8%	-17.6%	12
LA15	3.5%	-21.7%	456	BO18	41.0%	-37.9%	19
LA18	-10.9%	-20.1%	689	BO19	-4.7%	-30.1%	31
LA20	-30.9%	-23.1%	707	BO20	-5.9%	-18.4%	50
LA21	-9.7%	-26.1%	1127	BO21	70.1%	-50.3%	196
LA22	-16.6%	1.2%	874	BO22	5.3%	-35.9%	148
LA23	-42.2%	-47.8%	599	BO25	24.9%	-46.0%	131
LA25	-2.4%	-18.0%	887	BO33	-0.3%	-16.2%	72
LA28	-7.5%	-21.0%	1181	BO34	22.8%	41.5%	70
LA30	-19.8%	-13.6%	1142	BO35	13.9%	-29.0%	234
LA37	-1.0%	-11.9%	1558	BO36	-29.8%	-21.2%	34
SE04	-65.8%	4.0%	223	NF01	-19.8%	-17.3%	998
SE05	31.7%	-23.7%	106	NF02	-39.9%	-18.3%	543
SE08	105.7%	-36.5%	153	NF11	19.2%	-16.4%	754
SE10	-28.1%	-28.6%	385	NF12	245.9%	-29.7%	285
SE12	-4.9%	-64.9%	162	NF15	16.2%	-18.6%	955
SE18	-46.8%	-51.1%	239	NF16	-24.0%	-22.3%	428
SE19	-51.9%	-36.1%	355	LASS1A	-5.5%	-43.9%	399
SE21	-20.8%	-1.0%	1449	LASS1B	-28.7%	-50.9%	498
SE25	-30.2%	-34.9%	388	LASS1C	-12.6%	-45.8%	474
SE26	-33.3%	-30.4%	472	LASS1E	-24.2%	-48.5%	342
SE30	-17.2%	-30.1%	699	LASS2A	-40.1%	-13.2%	984
SE31	-19.9%	-25.7%	828	LASS3B	-12.1%	39.5%	1124
SE32	-38.6%	-31.7%	508	LASS3C	34.0%	41.9%	3273
SE36	-18.2%	-15.9%	1237	LASS4C	8.5%	-16.1%	699

*Effective stiffness at average of peak NRTMDF displacement from each record

Table 5.10 MF-2 Nonlinear Analyses Results

NRTMDF Properties

Mass = 2776448 kg
Damper Yield Strength = 2439.5 kN
Initial Stiffness = 136.93 kN/mm
Average Effective Stiffness = 10.43 kN/mm*
Initial Damped Period = 2.54 sec
Average Peak Damped Period = 3.72 sec

Acc. History	Peak Base Shear change	Peak Roof Disp. change	Damper Disp. (mm)	Acc. History	Peak Base Shear change	Peak Roof Disp. change	Damper Disp. (mm)
LA01	-14.3%	-46.0%	799	BO05	-22.8%	-13.5%	27
LA02	-1.3%	-6.5%	544	BO06	13.6%	20.4%	21
LA04	-15.2%	15.3%	753	BO13	-32.6%	-31.7%	12
LA12	-8.0%	9.1%	256	BO16	-0.4%	15.0%	8
LA15	-6.1%	-25.1%	551	BO18	-8.6%	-39.3%	16
LA18	-6.1%	-23.5%	1007	BO19	-21.6%	-49.7%	22
LA20	-8.9%	-33.0%	863	BO20	-7.1%	-33.6%	44
LA21	-4.7%	-16.7%	1472	BO21	-17.5%	-20.9%	102
LA22	2.7%	11.7%	1074	BO22	-6.0%	-10.5%	107
LA23	-5.2%	-22.2%	785	BO25	-5.1%	-30.5%	133
LA25	-7.1%	-26.5%	1034	BO33	-34.8%	-38.4%	47
LA28	-3.1%	-24.6%	1786	BO34	-19.2%	-49.3%	50
LA30	-2.1%	-7.9%	1862	BO35	-12.9%	-23.5%	205
LA37	-4.3%	-16.9%	1930	BO36	-0.7%	9.9%	25
SE04	-26.8%	11.0%	266	NF01	-6.9%	-26.0%	1141
SE05	-36.8%	-25.4%	198	NF02	-1.5%	-6.2%	1229
SE08	-28.7%	-36.1%	160	NF11	3.3%	17.5%	998
SE10	5.7%	-35.1%	421	NF12	-34.4%	-34.1%	146
SE12	-29.6%	-45.1%	183	NF15	-5.6%	-21.3%	1318
SE18	-38.2%	-47.3%	155	NF16	-2.6%	-33.6%	361
SE19	-43.9%	-23.6%	339	LASS1A	-12.5%	-42.5%	492
SE21	-3.4%	-12.4%	1530	LASS1B	-13.2%	-46.4%	585
SE25	-9.2%	-33.9%	758	LASS1C	-13.6%	-48.1%	628
SE26	19.2%	-37.6%	620	LASS1E	-26.9%	-40.7%	436
SE30	-7.6%	-28.5%	632	LASS2A	-9.8%	-34.1%	956
SE31	-4.1%	-16.6%	842	LASS3B	-0.4%	-1.6%	2100
SE32	-6.5%	-18.1%	434	LASS3C	-2.5%	-9.8%	2605
SE36	-7.6%	-26.8%	969	LASS4C	-9.3%	-34.7%	941

*Effective stiffness at average of peak NRTMDF displacement from each record

utilizes a somewhat higher mass for the NRTMDF equal to approximately 15% to 20% of the total building mass. The same rationale for this applies regarding the capability of the structure to support the added gravity load of the NRTMDF while this magnitude of mass is sufficient to provide inertial effects capable of altering the primary structure's dynamics. Furthermore, the results of the analyses demonstrate that this quantity of mass is sufficient to develop active nonlinear mobilization of the NRTMDF. For more information regarding NRTMDF mass see Section 5.5.

Iterative approaches were utilized to determine the near optimal stiffness of the NRTMDF. These were comprised primarily of trial and error analyses pursuing trends of increasingly favorable behavior based on observation of peak output parameters (e.g. rooftop displacement). This method was thought to be acceptable in consideration of the stochastic nature of the ground motions which precluded the development of an analytical optimization approach. These approaches were similar in nature to those of the linear elastic methods but yielded different results owing to the nature of altered behavior accounted for with nonlinear analysis methods. Additional iterative analysis approaches for the nonlinear analysis were required beyond those of the linear analysis methods to account for geometric constraints of the NRTMDF. Among these, the spatial geometry of the NRTMDF predicates a maximum realistic effective length of its designated yielding members (buckling restrained braces). This length has an inverse relationship to the optimized stiffness as shown by the classical axial stiffness relationship:

$$K_{axial} = \frac{AE}{L} \qquad \text{Eq. 5-1}$$

where A is the cross sectional area of the yielding core, E is the elastic modulus and L is the length of the yielding core. While the length (L) is not a parameter that can be readily altered in an effort to enable targeted stiffness properties, cross sectional area (A) can be directly assigned to target a specific stiffness for the NRTMDF. However, yield strength of the designated yielding member (Py) is also a function of A as shown by another classical relationship:

$$Py = FyA \qquad \text{Eq. 5-2}$$

where Fy represents the material yield strength. Therefore, determination of effective stiffness parameters for the NRTMDF must be compared against the spatial and geometric constraints of the proposed rooftop frame. Combination of these equations also provides a convenient form for representing the behavior of the buckling restrained braces:

$$K_{axial} = \frac{\left(Py / Fy\right)E}{L} \qquad \text{Eq. 5-3}$$

For the analyses herein presented, the geometry available for the rooftop frame predicated a change to the near optimized stiffness parameters of the NRTMDF. The resulting changes in performance based on observations of peak output parameters (base shear, rooftop displacement) were not significant.

Ideally, the BRB's of the NRTMDF should be developed with properties offering the greatest degree of energy dissipation in accordance with the performance objective. To achieve this, each iteration directed toward selection of effective BRB properties

included an optimization technique to select the initial stiffness and yield strength that would yield the greatest theoretical dissipation of energy. For this process, the primary properties of the buckling restrained braces must be considered; the initial stiffness (*Ki*), yield strength (*Py*), effective stiffness (*Ke*) with the yielded stiffness (*Ky*) parameter typically taken as a fraction of the initial stiffness (approximately 3.5%). Among these parameters, initial stiffness and yield strength are most conveniently controlled as they are directly proportioned in the BRB core area and length as reflected in Equations 5-1 and 5-2. Control over *Ke* is less realistic as it is a highly transient parameter directly correlated to the nonlinear displacement of the BRB at each time instant of NRTMDF nonlinearity. As such, it is typically reported and analyzed at its minimum value which occurs at its peak deformation. Figure 3.22 depicts these parameters within the context of the typical BRB hysteretic backbone. Within each iteration of NRTMDF design for effective properties, these variables and their influence on one another must be considered. As indicated in Section 3.6, effective stiffness (*Ke*) was selected as key parameter of consideration for each iteration. To begin, an initial effective stiffness must be selected along with a target displacement. Through experimental processes, a starting *Ke* approximately equal to 5% of the average story stiffness was found to be effective. Coupled with a target displacement of approximately 200mm (roughly 3.5% of the projected BRB core length for most cases) it then becomes possible to calculate values for initial stiffness (*Ki*) and yield strength (*Py*) that will satisfy the effective stiffness following a bi-linear load displacement relationship as depicted in Figure 3.22. The key to this approach is to calculate these values in such manner as to maximize the area under the bi-linear function of the load-displacement relationship. This was accomplished

using a simple algorithm with the Visual Basic module of the Microsoft Excel application. Upon solving for the effective parameters of *Ki* and *Py,* these values could then be used as input parameters for the nonlinear model. After running the model, peak BRB deformation values were extracted and used for comparison or replacement of the values from the previous iteration. Normally, few iterations (3 or less) were required to converge upon values striking the appropriate proximity of balance between input and output performance parameters (BRB deformation). Following this, alteration of effective stiffness was utilized to determine trends toward maximum reduction in peak output parameters (e.g rooftop displacement). Several such iterations were utilized within each scenario to reach the most effective parameters of initial stiffness and yield strength for the BRB's of the NRTMDF.

Unlike the equivalent result tables for the linear elastic methods, Tables 5.1 through 5.10 do not provide simple damped and undamped periods along with modal mass information. This is due to the transient nature of these parameters introduced when nonlinear behavior occurs. As elements are subjected to hysteretic nonlinearity, the stiffness of the structure is continually changing thereby driving continual changes in fundamental periods for each instant in time while nonlinear behavior is occurring. Nevertheless, Tables 5.1 through 5.10 include the damped period reflecting the initial stiffness of the NRTMDF (prior to yielding) and the average peak damped period, reflecting the average of peak effective stiffness of the NRTMDF for each structure and load case. It should be noted here that these periods do not reflect distinctive modal behaviors as would be demonstrated with linear elastic analysis methods; rather, this represents the range of transient periods seen in the structure as it experiences hysteretic

nonlinearity. This demonstrates the concept that when nonlinear behavior occurs, structural periods and modal characteristics are not static but transient.

5.1 Discussion of Nonlinear Inelastic Analysis Results

The tabulated results for the nonlinear inelastic analyses corroborate the theory that the beneficial effects of the NRTMDF can be amplified when it can develop active, stable nonlinear hysteretic behavior. Table 5.11 demonstrates reductions in average peak output parameters for each structure and the broad based SAC ground motion suite representing hard through soft sites. Marked enhancements in reduction can be observed between this and the comparable table reflecting the linear analysis methods (Table 4.11). Table 5.12 lists the comparison of the results between the linear elastic modeling approaches and the nonlinear inelastic approaches of Table 5.11. Fundamentally the analyses demonstrate the potential for significant improvements in expected behavior when utilizing nonlinear inelastic analysis methods in lieu of linear elastic analysis

Table 5.11 Changes in Average Peak Output Parameters and Peak NRTMDF Displacement for Nonlinear Inelastic Analyses

Structure	Change in Peak Base Shear	Change in Peak Rooftop Displacement	Peak NRTMDF Displacement (mm)
BF-1	-1.7%	-10.3%	90
BF-2	-3.2%	-12.7%	120
BF-3	-2.8%	-22.5%	176
BF-4	-3.1%	-19.8%	270
BF-5	-9.7%	-22.9%	432
EBF-1	-6.0%	-20.5%	257
SW-1	-1.6%	-19.7%	139
SW-2	-4.1%	-23.8%	175
MF-1	-4.4%	-20.8%	548
MF-2	-10.9%	-22.2%	660

Table 5.12 Improvement in Reduction of Peak Output Parameters from Linear to Nonlinear Analysis Methods

Structure	Peak Base Shear*	Peak Rooftop Displacement	Peak NRTMDF Displacement (mm)
BF-1	-66.9%	535.9%	15.2%
BF-2	-12.8%	627.1%	60.9%
BF-3	-67.6%	343.2%	26.9%
BF-4	-71.0%	59.7%	28.4%
BF-5	-27.4%	98.7%	-0.5%
EBF-1	25.9%	299.9%	21.2%
SW-1	-67.6%	616.3%	74.6%
SW-2	-41.2%	396.9%	48.2%
MF-1	-72.8%	93.3%	22.5%
MF-2	-17.7%	24.8%	23.3%

* Negative value reflects minimized change in base shear for nonlinear inelastic modeling which constrains base shear forces to maximum frame nonlinear capacities.

methods. Furthermore, the nonlinear inelastic methods are more reliable inasmuch as they are a more accurate reflection of element and therefore overall structural behavior.

Figures 5.1 through 5.8 reflect the acceleration response spectra for the SAC ground motion suite on which the undamped elastic period for each structure is shown along with the period shifts driven by the NRTMDF. For this, two period shifts are presented. The first reflects the period shift accounted for with the initial elastic stiffness of the NRTMDF while the second shift reflects the extended period shift driven by its yielding and altered effective stiffness. Since the spectra reflect the peak transient acceleration developed in an equivalent elastic single degree of freedom system, it is an effective qualitative demonstration of the approximate peak acceleration attracted by the structure at the peak transient acceleration demand which is accompanied by peak performance (deformation) in the NRTMDF.

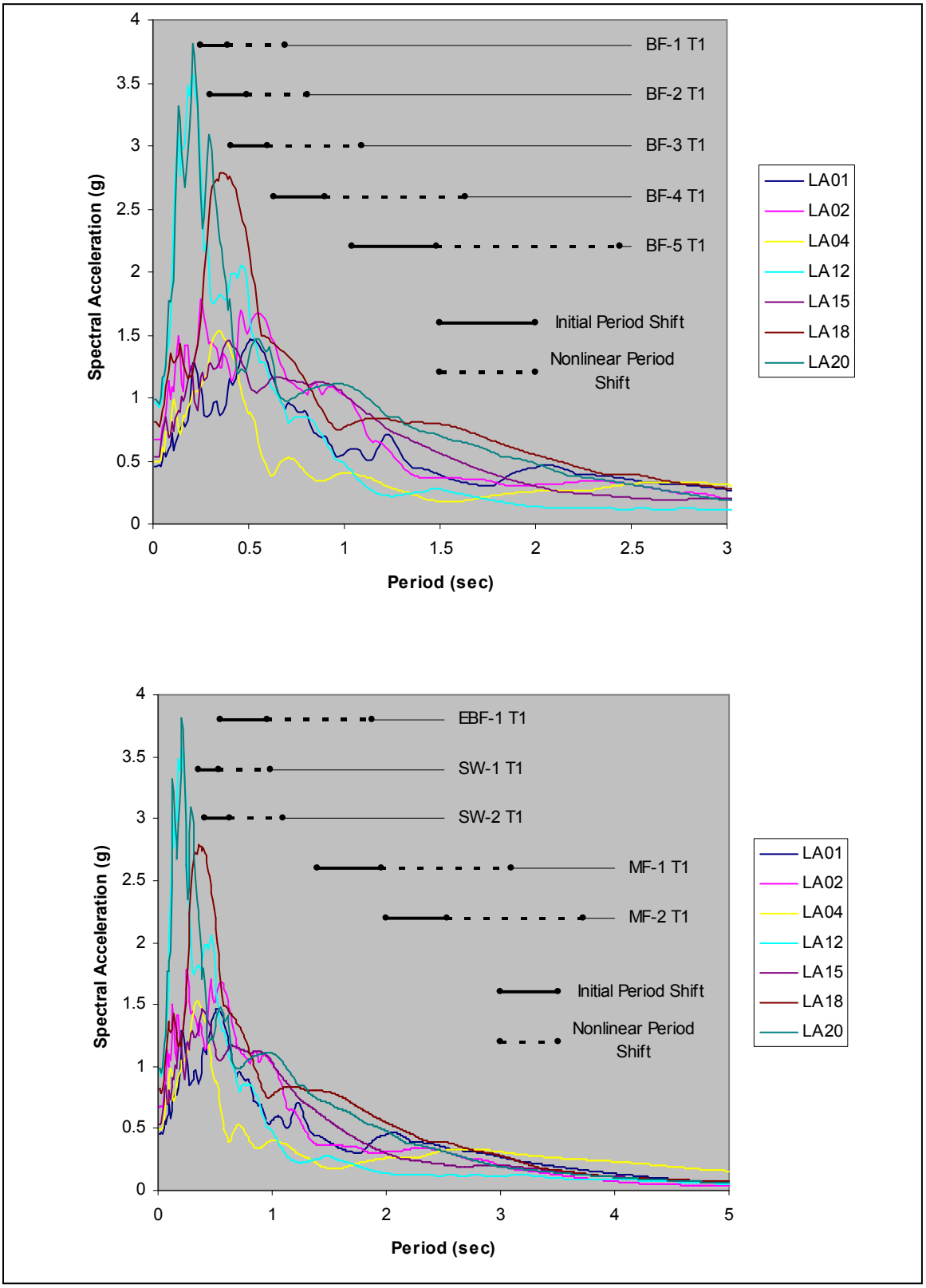

Figure 5.1 LA 10% in 50-Year Spectra with Linear and Nonlinear Period Shifts

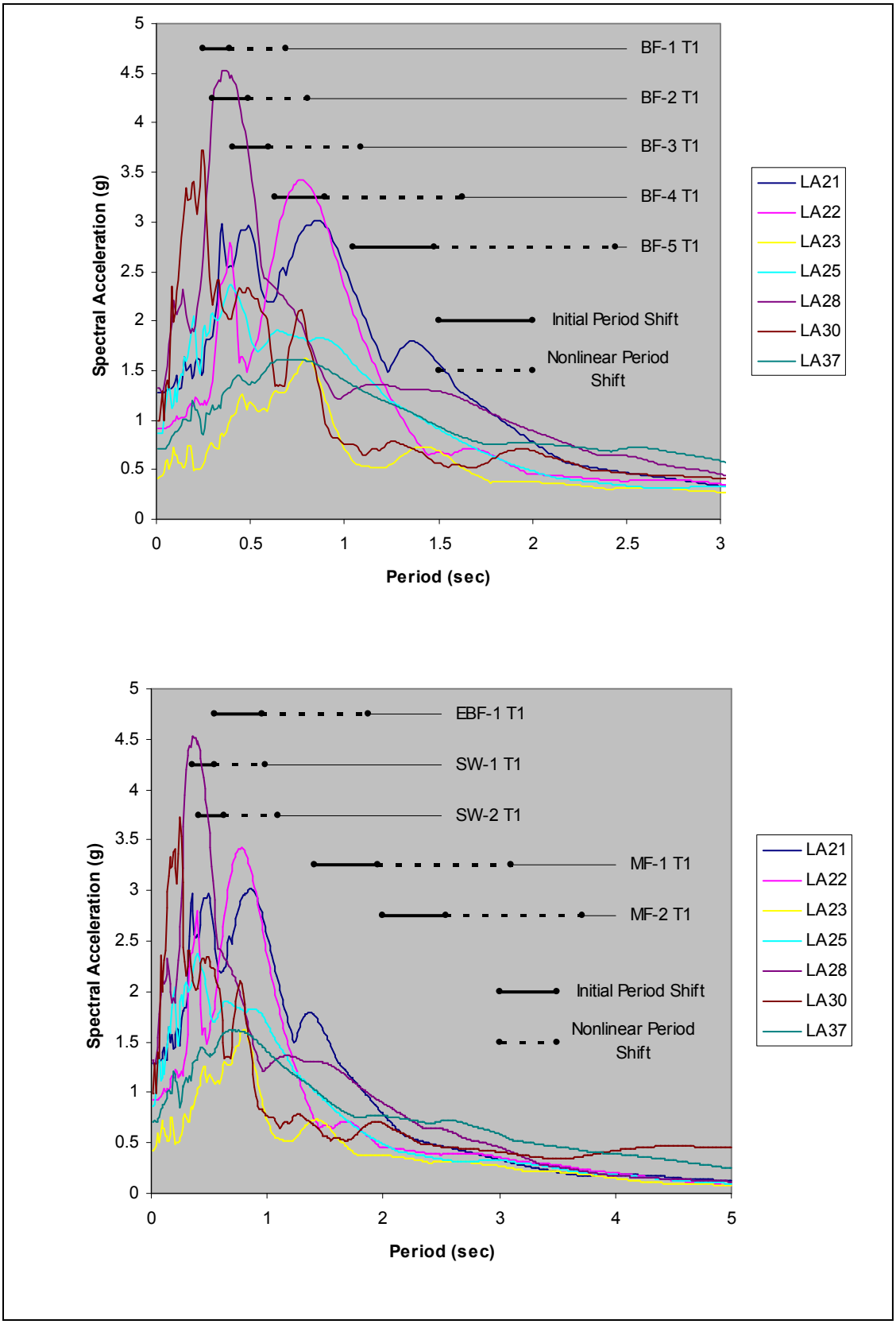

Figure 5.2 LA 2% in 50-Year Spectra with Linear and Nonlinear Period Shifts

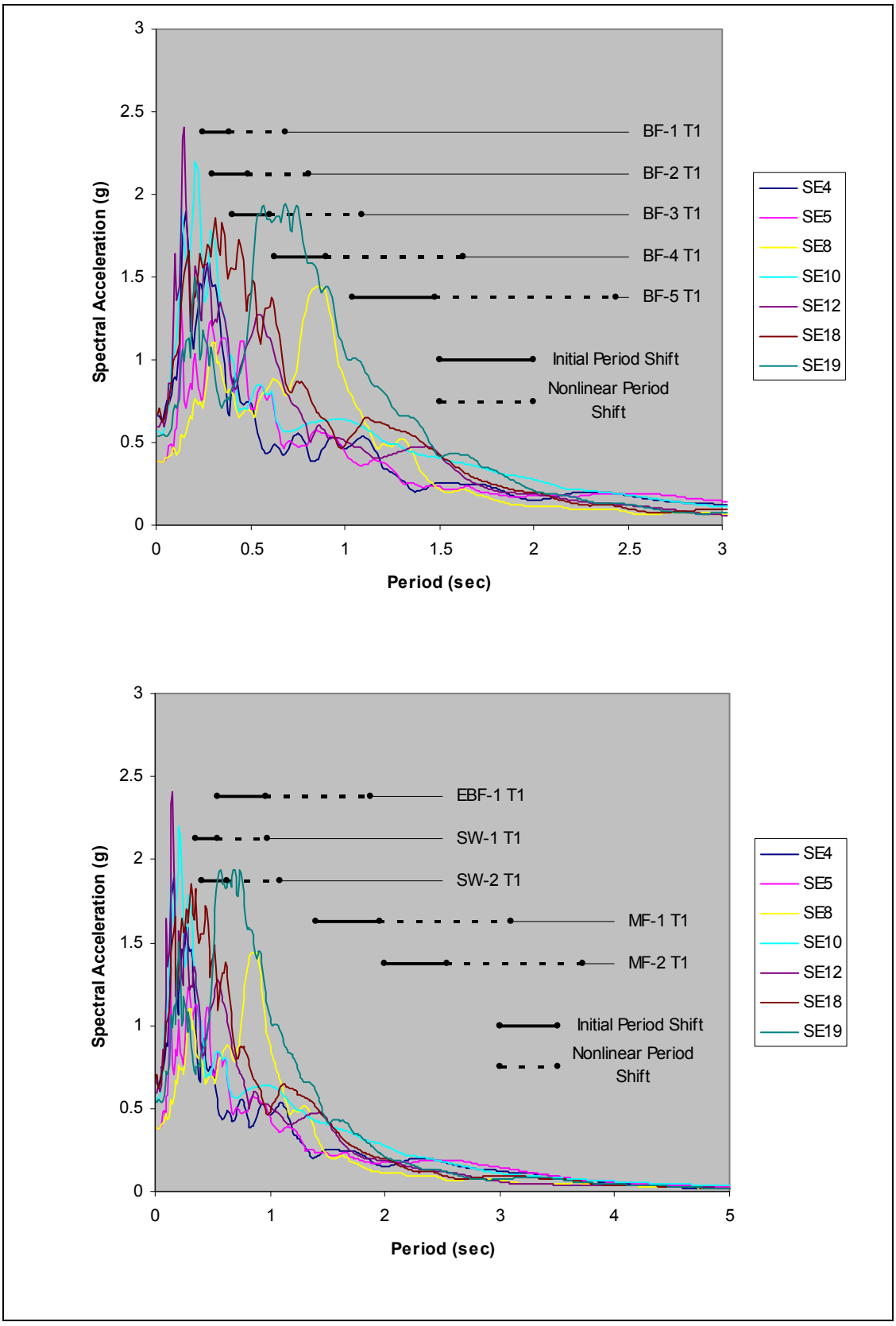

Figure 5.3 SE10% in 50-Year Spectra with Linear and Nonlinear Period Shifts

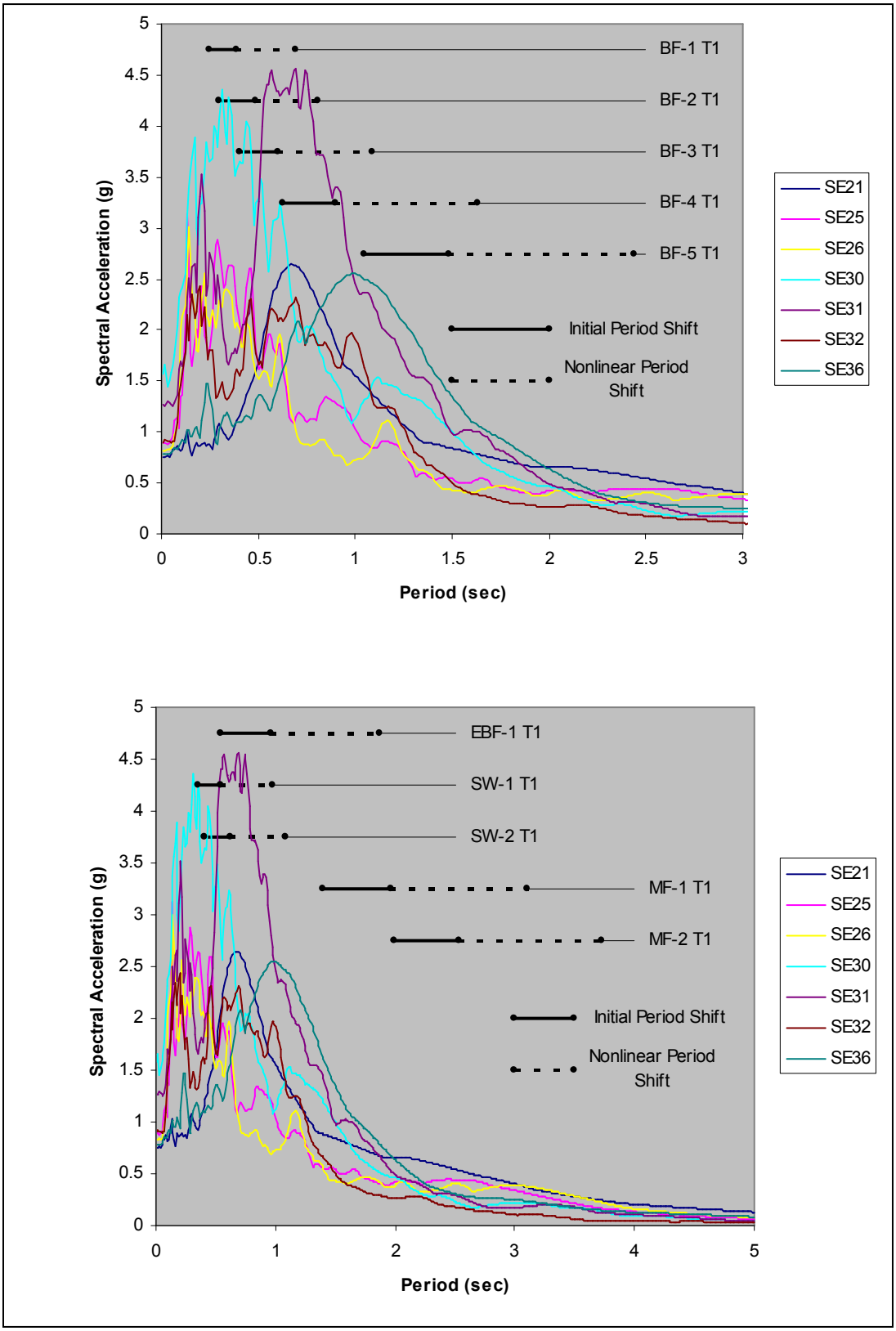

Figure 5.4 SE2% in 50-Year Spectra with Linear and Nonlinear Period Shifts

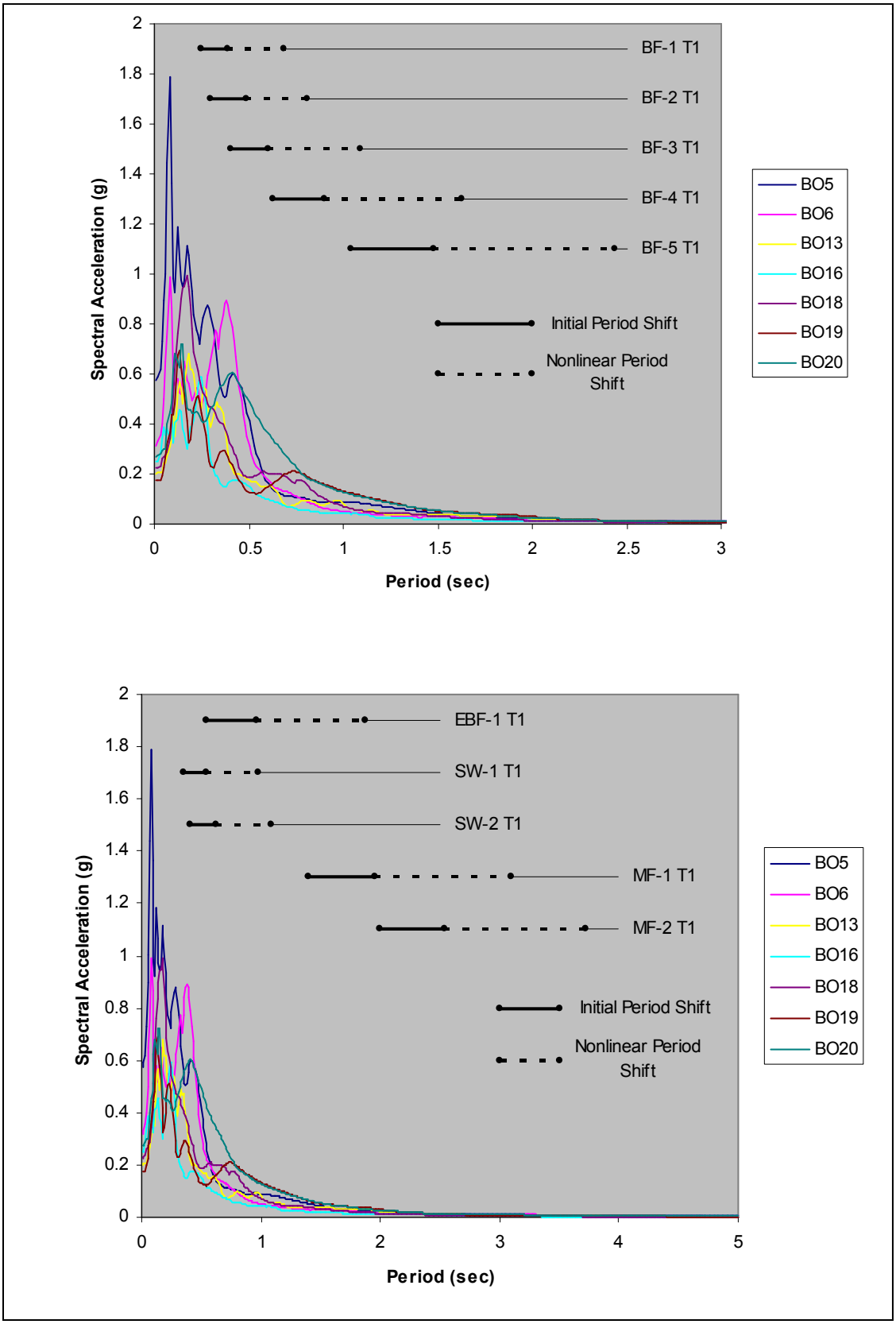

Figure 5.5 BO 10% in 50-Year Spectra with Linear and Nonlinear Period Shifts

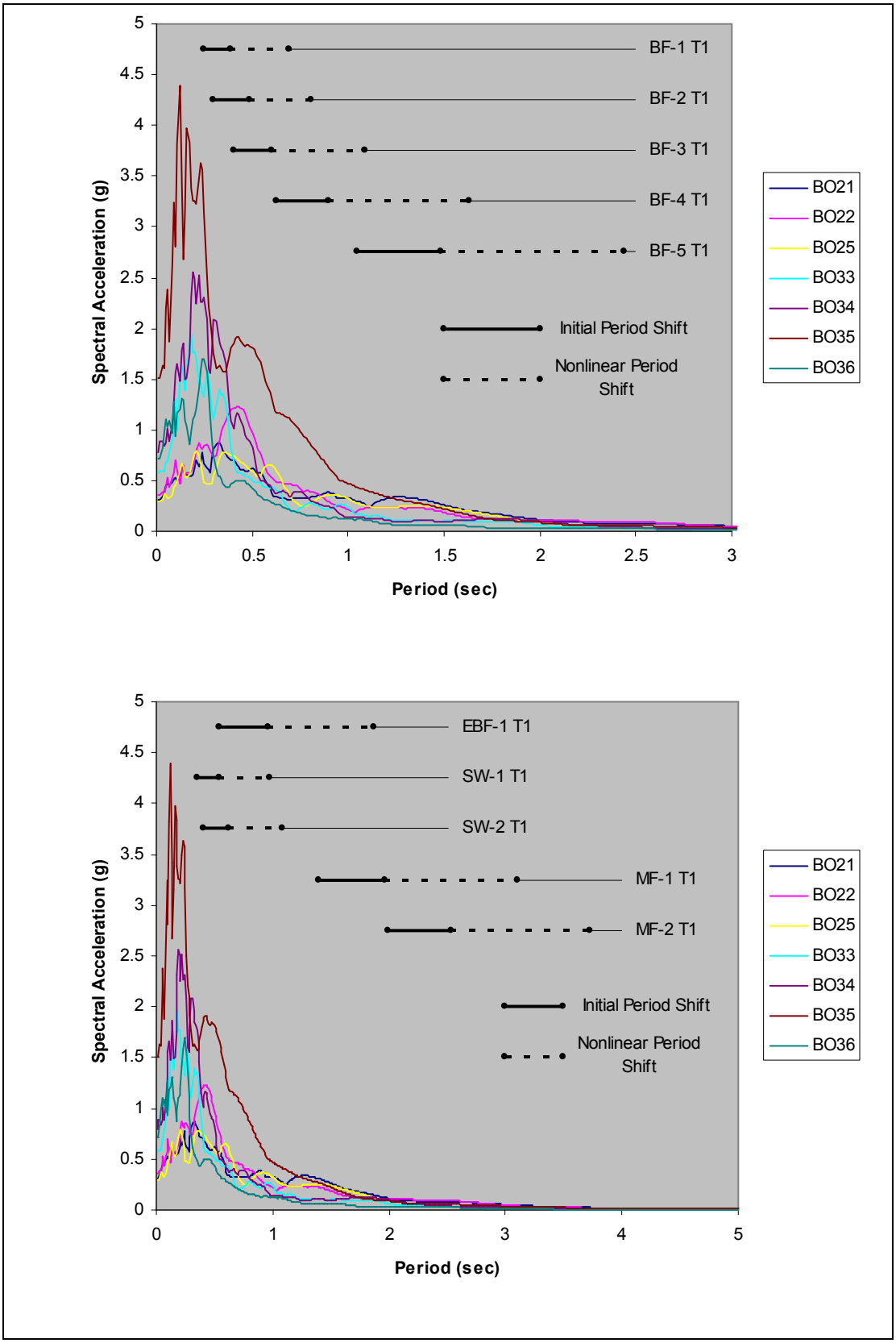

Figure 5.6 BO 2% in 50-Year Spectra with Linear and Nonlinear Period Shifts

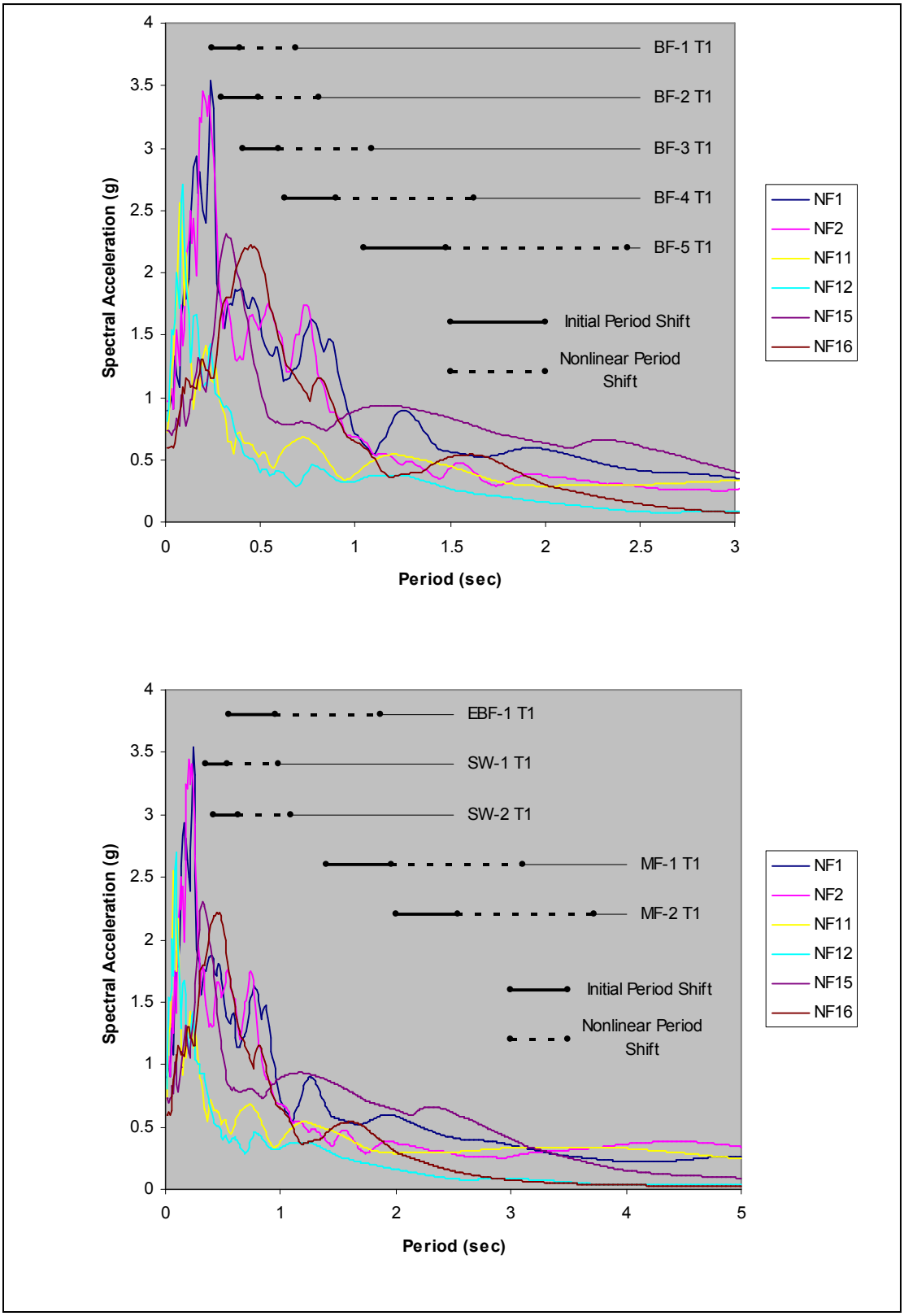

Figure 5.7 Near Field 2% in 50-Year Spectra with Linear and Nonlinear Period Shifts

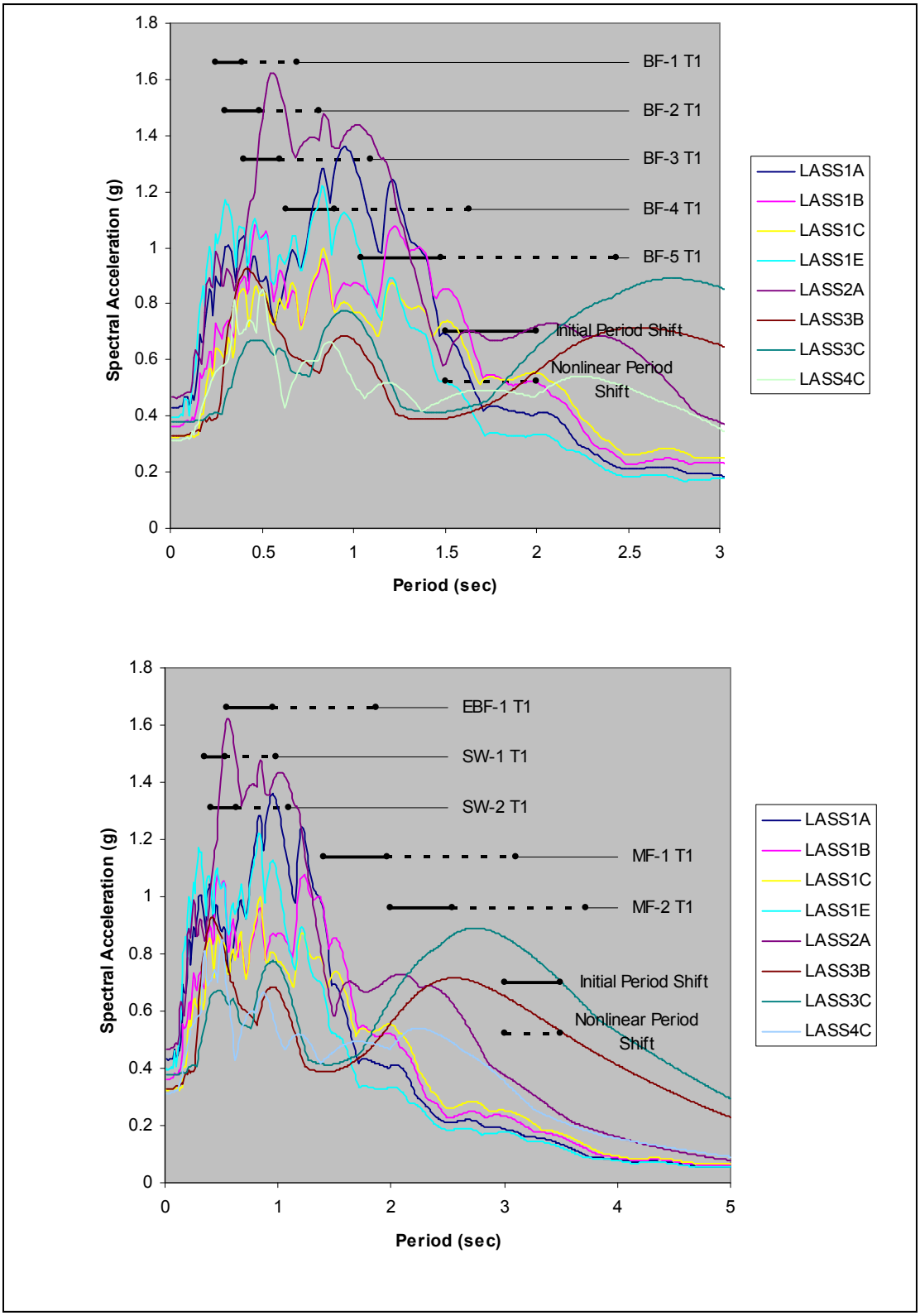

Figure 5.8 Near Field 2% in 50-Year Spectra with Linear and Nonlinear Period Shifts

Examination of test structure BF-4 and ground motion SE18 provides a demonstration of an effective NRTMDF and the beneficial effects it enables by virtue of fundamental elastic period shift which is then lengthened by its inelastic period shift (Figure 5.9). The undamped period for this structure is 0.63 seconds giving a spectral acceleration 1.30g. The period shift in the damped structure, due to the initial (linear) NRTMDF stiffness becomes 0.90 seconds with a spectral acceleration ordinate of 0.63g. As the NRTMDF yields and its stiffness is reduced, the damped period shifts transiently to 1.63 seconds correlating to a spectral acceleration of 0.32g.

Changes in spectral acceleration ordinates correlating to the linear and nonlinear period shifts for BF-4 and the SE18 motion are significant as is the targeted energy dissipation enabled by the NRTMDF. Nonlinear analyses indicate a total input energy for undamped BF-4 and the SE18 record of 17,396 kilojoules. For the damped structure, this becomes 16,794 kilojoules. Of this, 9,270 kilojoules are dissipated through hysteretic nonlinearity of the NRTMDF for a total reduction in energy demand on the undamped structure of 9,872 kilojoules (57%). Figure 5.10 demonstrates the hysteretic behavior of the NRTMDF for damped BF-4 and ground motion SE18. As demonstrated, nonlinear behavior is significant with dissipated energy reflected in the accumulated areas captured within each cycle of NRTMDF motion. Figure 5.11 depicts the accumulated energy demand throughout the time history of record SE18 for undamped BF-4 and also depicts the same information for damped BF-4. This figure also shows the accumulated hysteretic energy dissipated by the NRTMDF for this structure. Examination of the total values at the end of the time domain provides the aforementioned energy values associated with this structure. The resulting reductions in

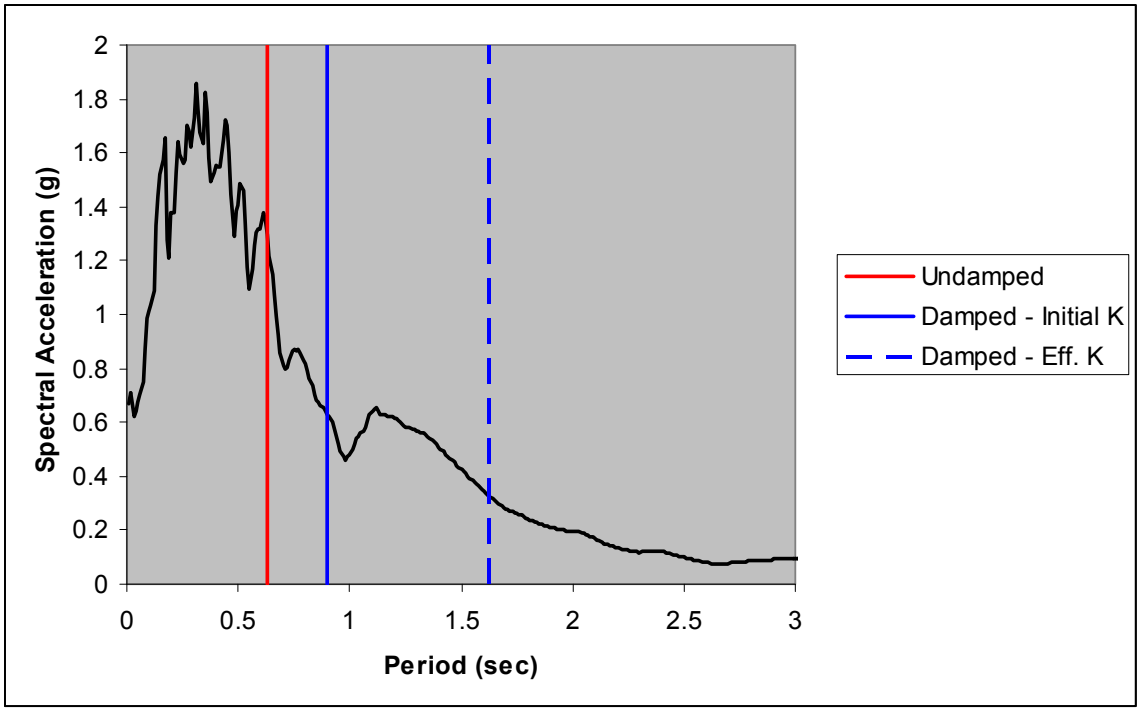

Figure 5.9 5% Damped Spectrum for SE18 Motion and BF-4 Period Shifts

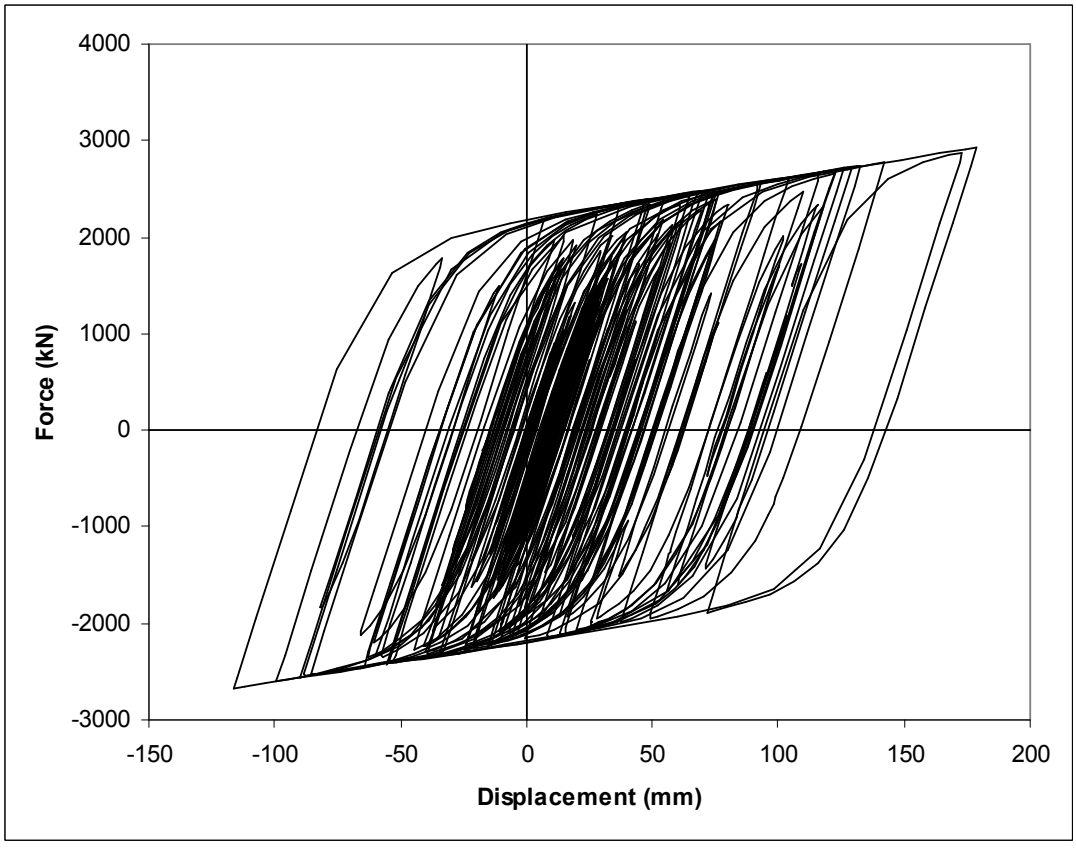

Figure 5.10 NRTMDF Hysteresis for Damped BF-4 and SE18 Ground Motion

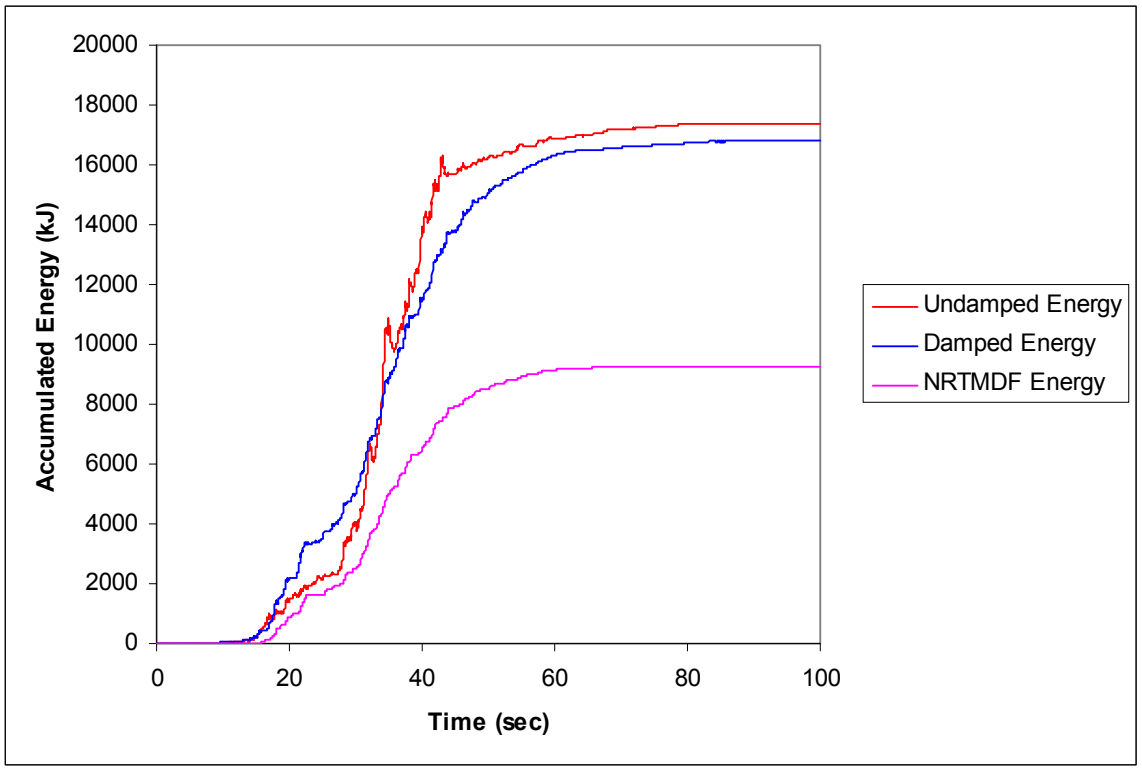

Figure 5.11 Hysteretic Energy Demands for Nonlinear Analysis of BF-4 and SE18 Motion

peak base shear and peak rooftop displacement are 5.3% and 63%, respectively (Table 5.4). The minimized reduction in base shear reflects nonlinear behavior for both the damped and undamped models and the inability of the frame to deliver higher forces to the foundation even with vastly higher lateral displacements. The available geometry for the NRTMDF allows for buckling restrained braces with yielding core lengths of approximately 16,275mm (based on lengthened BRB core as described in Section 9.5) while the maximum damper displacement is 179mm for an axial strain of 1.1%, well within the capable strain of typical BRB yielding cores of 3.5% .[35]

Histories of base shear and rooftop displacement for undamped and damped BF-4 and ground motion SE18 are shown in Figures 5.12 through 5.15, respectively. These

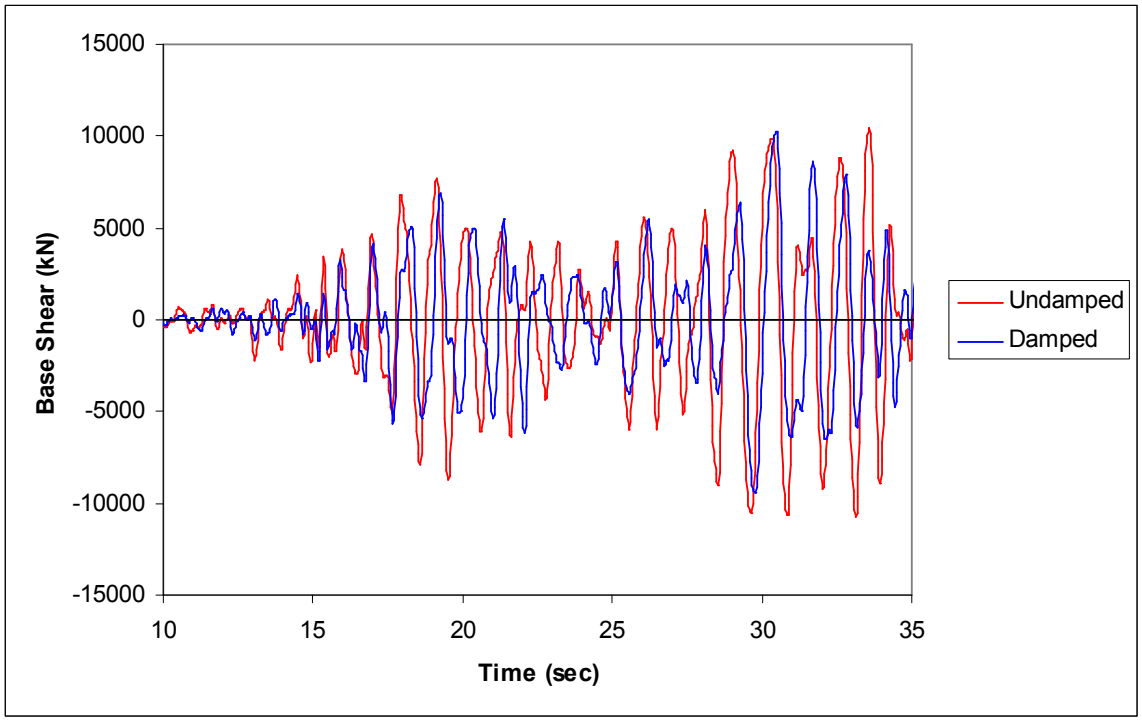

Figure 5.12 Base Shear Responses for Undamped and Damped BF-4, SE18 Motion, 10 to 35 sec

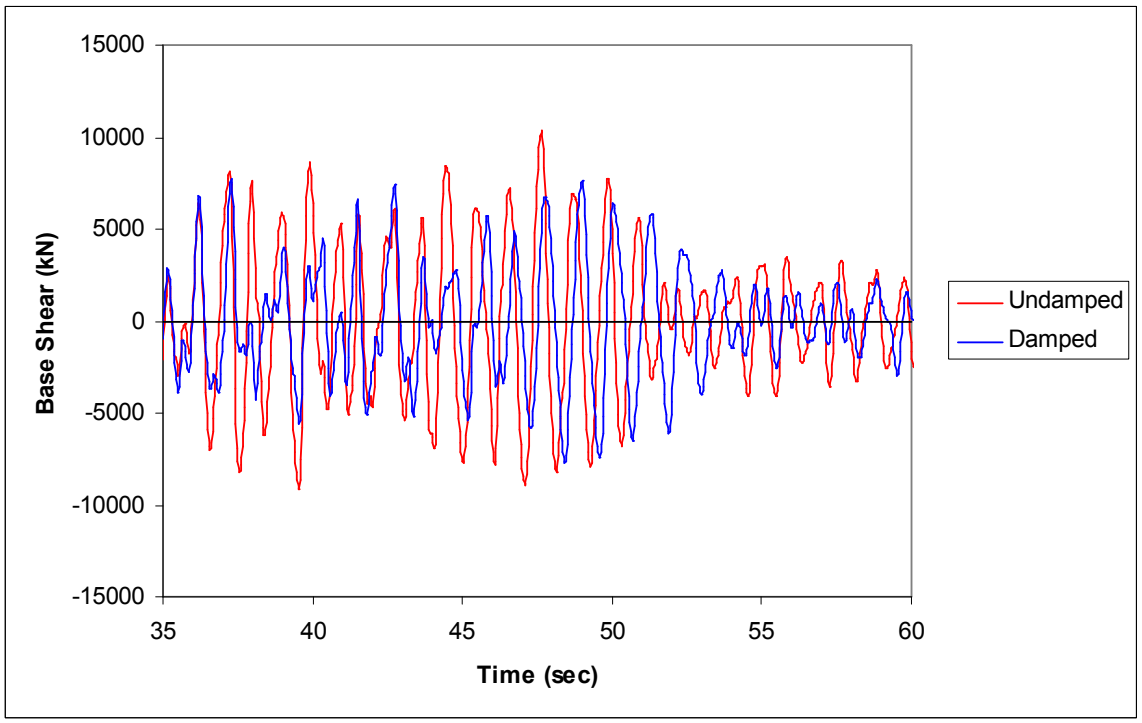

Figure 5.13 Base Shear Responses for Undamped and Damped BF-4, SE18 Motion, 35 to 60 sec

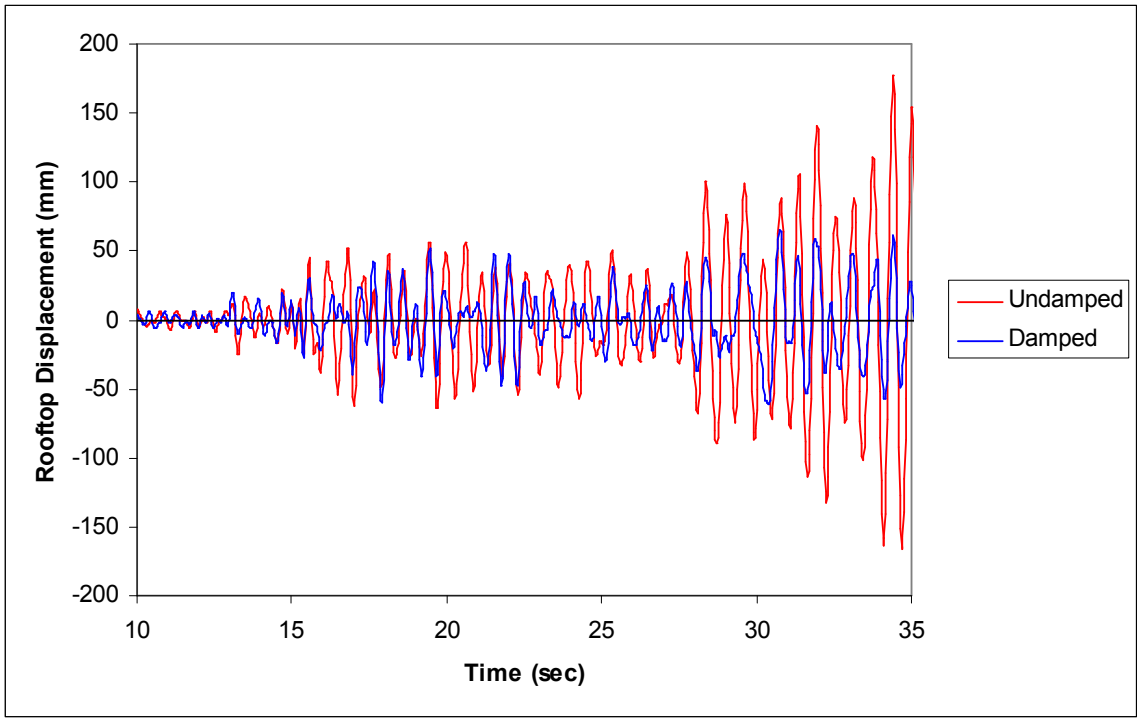

Figure 5.14 Rooftop Displacements for Undamped and Damped BF-4, SE18 Motion, 10 to 35 sec

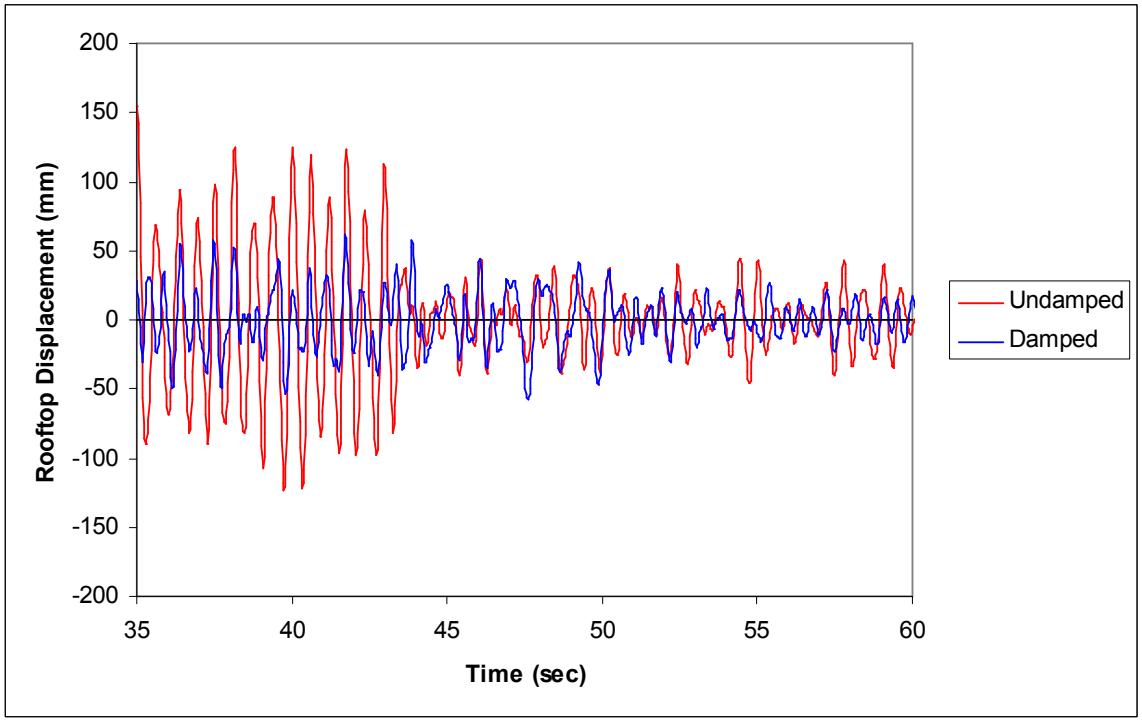

Figure 5.15 Rooftop Displacements for Undamped and Damped BF-4, SE18 Motion, 35 to 60 sec

histories, accompanied by the balanced hysteretic behavior of the NRTMDF shown in Figure 5.10, demonstrate the ideal NRTMDF performance which is realized for many of the models and the SAC ground motion suite. For cases where beneficial behavior is not enabled by the NRTMDF, the following behaviors may be observed:

- Increases in spectral acceleration due to period shifts result in increases of the spectral acceleration ordinates for the ground motion in question.
- Unbalanced hysteretic behavior of the NRTMDF driven by ground motions with frequency content that exacerbates pulses due to near-field effects.
- Unusually high NRTMDF displacements result for structures with relatively long undamped fundamental periods leading to even longer periods due to the initial elastic period shift and the longer still due to the inelastic period shift. On soft soil conditions this reflects the resonant condition.

Shifts in fundamental period corresponding to an increase in the spectral acceleration ordinates can be observed for certain ground motions for all ten of the test structures. As a specific example, consider MF-1 and ground motion LASS3C. The undamped fundamental period for this structure is 1.40 seconds corresponding to a spectral acceleration ordinate of 0.41g. As this period lengthens with the addition of the NRTMDF, the period shifts elastically to 1.96 seconds (with initial stiffness) and inelastically to 3.10 seconds (with effective stiffness) corresponding to spectral acceleration ordinates of 0.62g and 0.84g respectively as shown in Figure 5.16. The spectral acceleration increase of more than 100% results in increased response due to the NRTMDF that cannot be overcome by its inherent damping and energy dissipation. The two phenomena (elastic and inelastic period shifts) counteract rather than complement

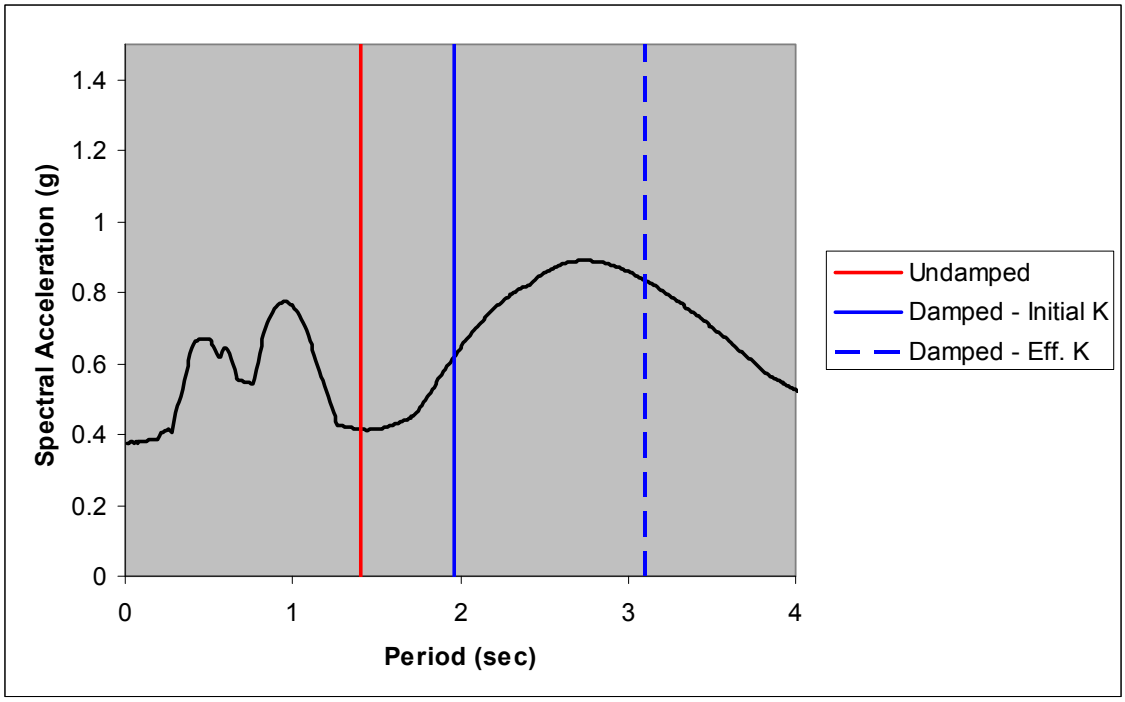

Figure 5.16 5% Damped Spectrum for LASS3C Motion and MF-1 Period Shifts

one another as is the case for many other structures and ground motions. The diminished performance capability for this scenario can also be observed by examination of the NRTMDF hysteresis (Figure 5.17) which demonstrates a calculated lateral displacement of 1512 mm, well beyond a practical axial strain of 3.5% which will be presented hereafter. Likewise, examination of energy relationships indicates the increased spectral acceleration drives an increase in energy demand that cannot be overcome by the NRTMDF. Figure 5.18 demonstrates a total undamped energy demand of 1080 kilojoules and 11005 kilojoules for the damped case with 7358 kilojoules of energy dissipation in the NRTMDF. Even with significant energy dissipation of the NRTMDF (67% of damped case total), the balance of energy on the base structure is far greater (3647 kJ) for the damped case than the undamped case (1080 kJ). The increased spectral acceleration also translates to an increase in peak transient output parameters

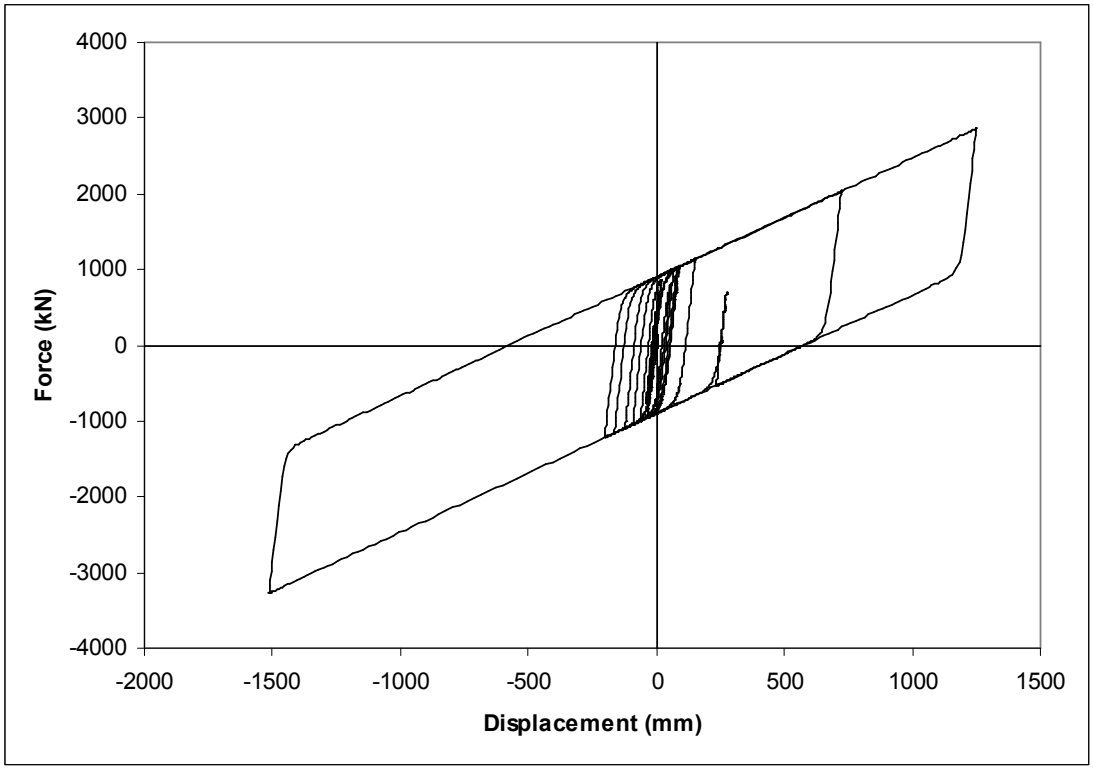

Figure 5.17 NRTMDF Hysteresis Loop for MF-1 and LASS3C Ground Motion

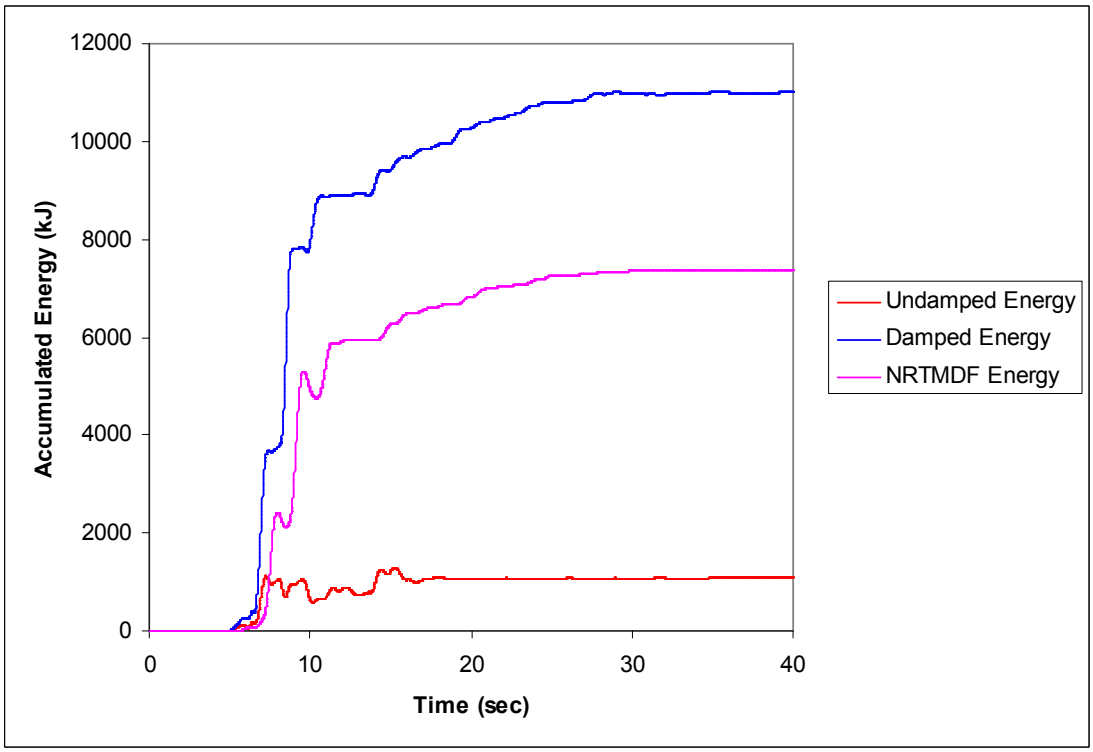

Figure 5.18 Hysteretic Energy Demands for Nonlinear Analysis of MF-1 and LASS3C Motion

with an increase in peak base shear of 34.0% and an increase in peak rooftop displacement of 41.9% as demonstrated in Figures 5.19 and 5.20, respectively. Noteworthy with respect to these results is that although the spectral acceleration ordinates for the fundamental modes are increased by more than 100%, the peak transient response parameters increase by only 18.7% (base shear) and 41.9% (rooftop displacement) thereby reflecting the capability for response reduction due to the NRTMDF, its nonlinearity, energy dissipation and introduction of opposing inertial forces.

A noteworthy observation with the results listed in Tables 5.1 through 5.12 is the diminished reduction in base shear response for many of the analysis models and ground motions as compared to the linear analysis approach of Section 4. As indicated in Tables 5.11 and 5.12, the nonlinear analysis approach can yield a diminished reduction in peak base shear demand on the structures due to the NRTMDF as compared to peak

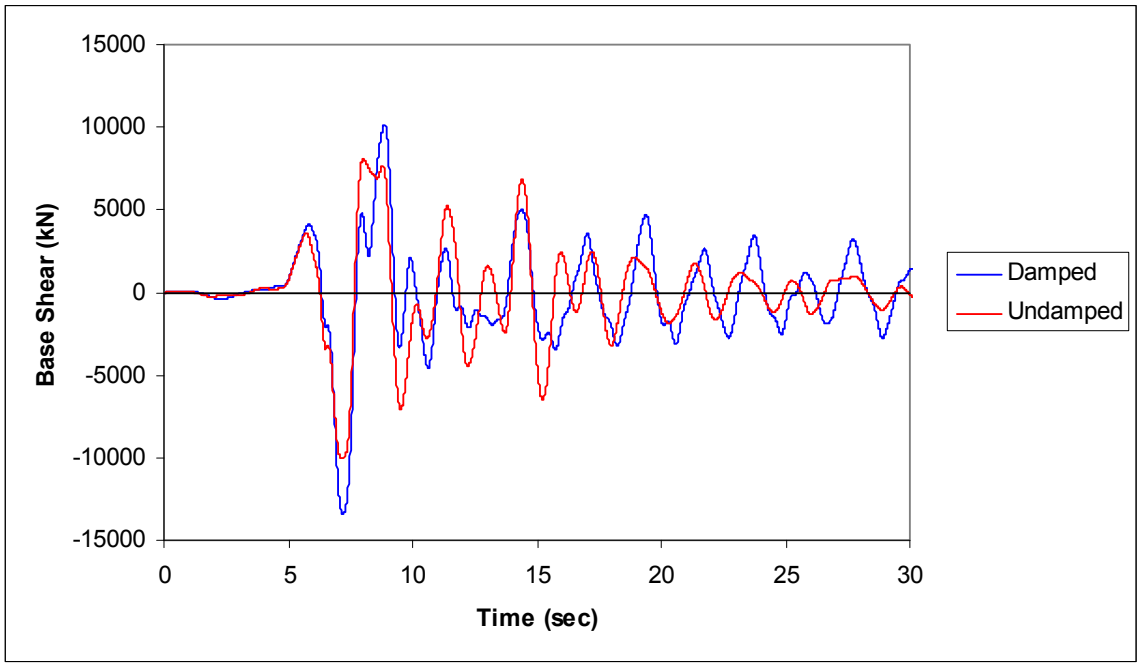

Figure 5.19 MF-1 Base Shear History for LASS3C Motion

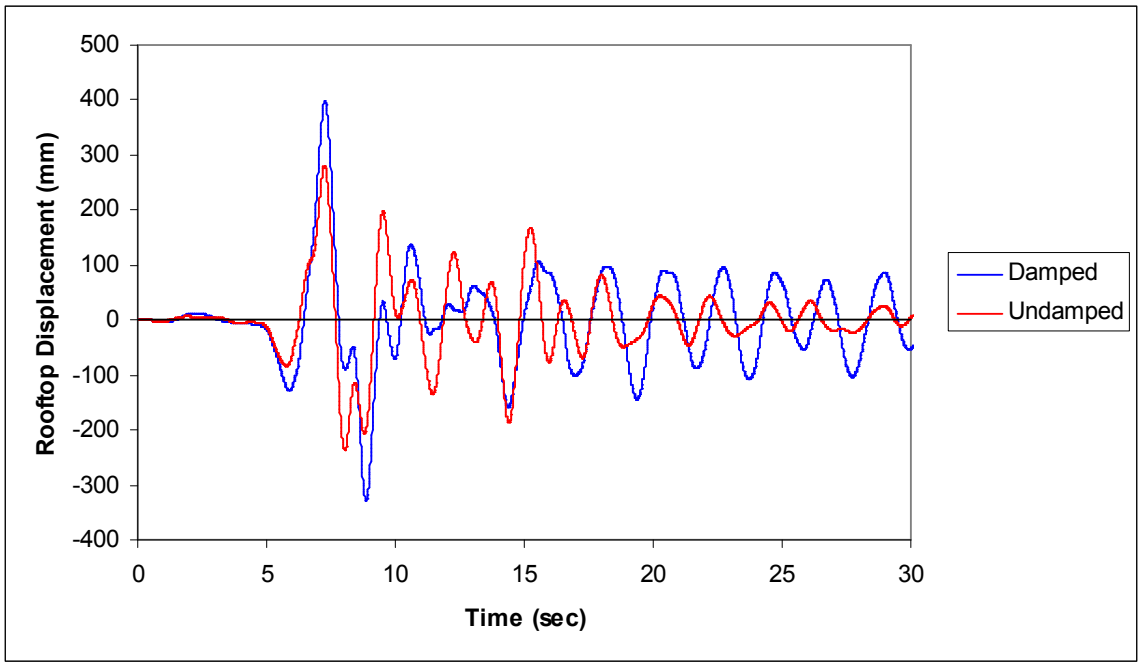

Figure 5.20 MF-1 Rooftop Displacement History for LASS3C Motion

rooftop displacement. This reflects the nonlinear strengths of the base structures and their inability to deliver forces to the foundation higher than those predicated by their maximum capable strengths. This concept is illustrated in Figure 5.21 which depicts the nonlinear pushover curve for test structure MF-2. For this, a dramatic difference in calculated base shear can be observed between the nonlinear and the linear model, which calculates base shears much higher than practical frame strengths. As demonstrated, elastic modeling methods predict a base shear of nearly 73,000 kN, nearly double the calculated nonlinear base shear of 34,000 kN at the same displacement (925mm).

5.2 Unbalanced NRTMDF Hysteretic Behavior

Unbalanced hysteretic behavior can be observed within a minority of test structures and ground motions for which the beneficial effects of the NRTMDF are not

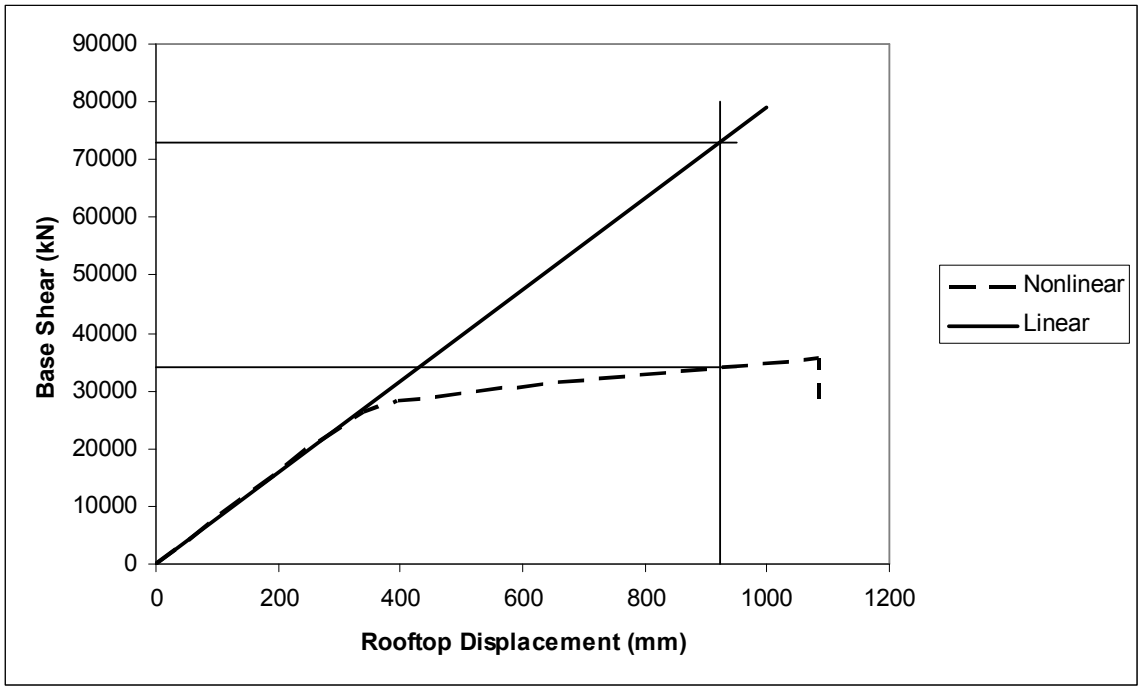

Figure 5.21 Linear vs Nonlinear Base Shear Response

realized. A specific example of this is BF-4 and ground motion LA04. For this structure, an undamped period of 0.63 seconds lengthens to 0.90 seconds due to the initial elastic shift enabled by adding the NRTMDF which lengthens again to 1.63 seconds when the NRTMDF develops active hysteretic nonlinearity. For these three periods, the spectral acceleration ordinates are 0.39g, 0.34g and 0.18g, respectively. Decreases such as this would typically result in a reduction in peak responses. However, for this case the peak base shear and rooftop displacement increase by 5.0% and 39.3% respectively (Table 5.4). Examination of the rooftop displacement histories of Figure 5.22 and the NRTMDF hysteresis loop of Figure 5.23 demonstrate unusually unbalanced behavior, particularly for the damped case which appears to resonate with unidirectional frequency content within the record. This causes a permanent nonlinear deformation in one direction. The root of this behavior is a unidirectional pulse within the original ground motion creating

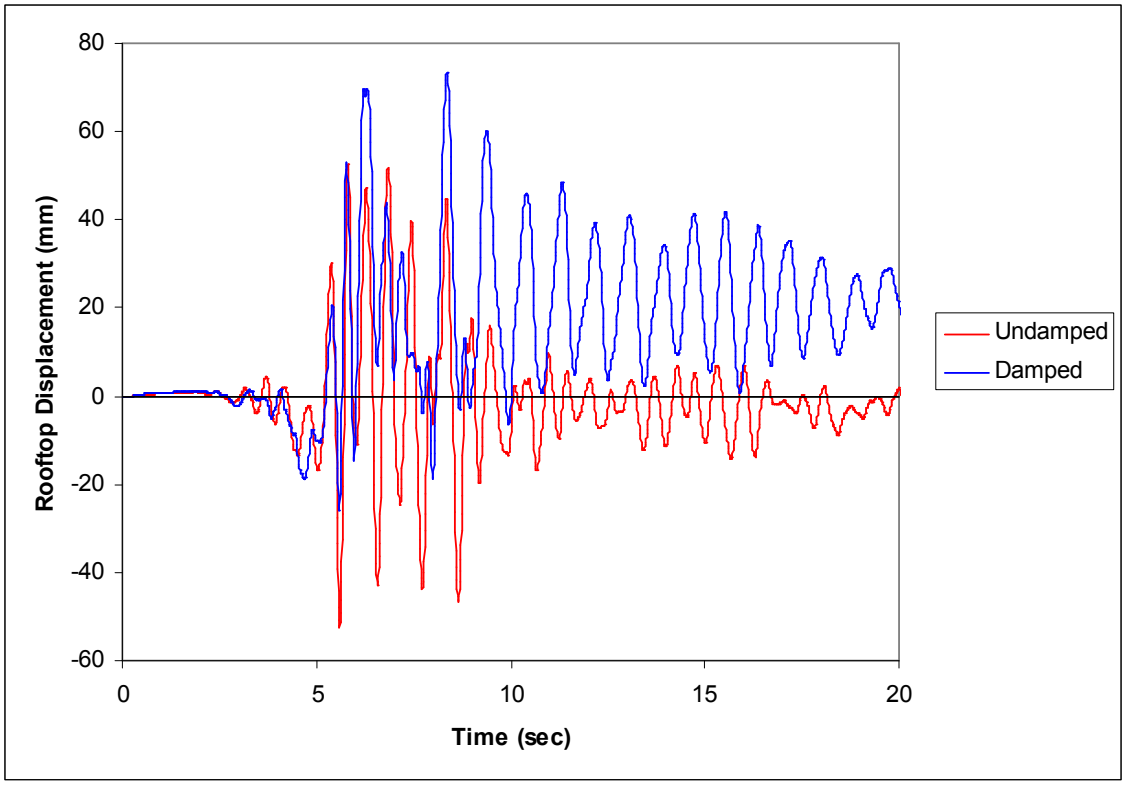

Figure 5.22 Undamped and Damped Rooftop Displacement Histories for Nonlinear Analysis of BF-4, LA04 Motion

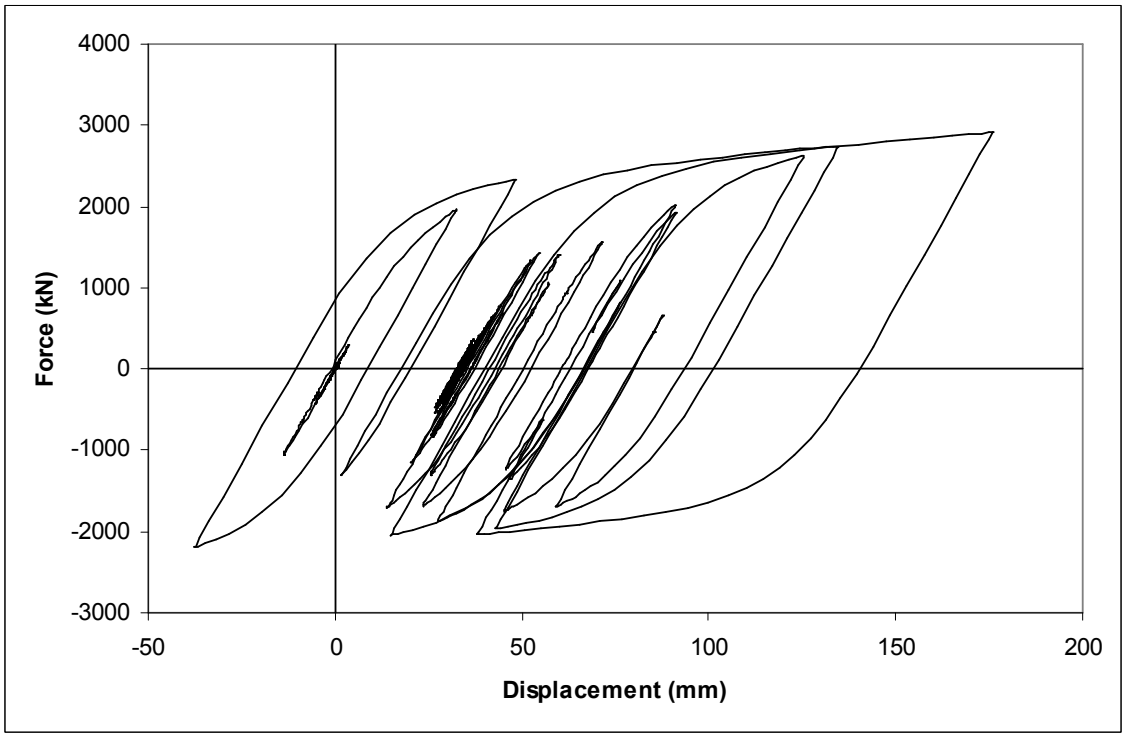

Figure 5.23 NRTMDF Hysteresis for Damped BF-4, LA04 Motion

an unbalanced response in the structure with which the structure resonates. Bray and Rodriguez-Marek indicate such motions are characterized as pulses due to near field effect which may result in permanent ground displacement accompanied by one-sided velocity pulses in the ground motion or by a pulse-like forward directivity.[36] These characteristics are most often manifest in near source ground motions such as LA04 which has a distance to source of 4.1km. These phenomena may not be readily apparent by examining the acceleration spectra alone but may be apparent as one-sided pulses in either the velocity or the displacement earthquake record. For the LA04 ground motion, the displacement record shown in Figure 5.24 indicates a one-sided pulse from approximately 5 seconds to 7 seconds in the record. This pulse is nearly two times the magnitude of the opposite direction in the adjacent time increments before and after this

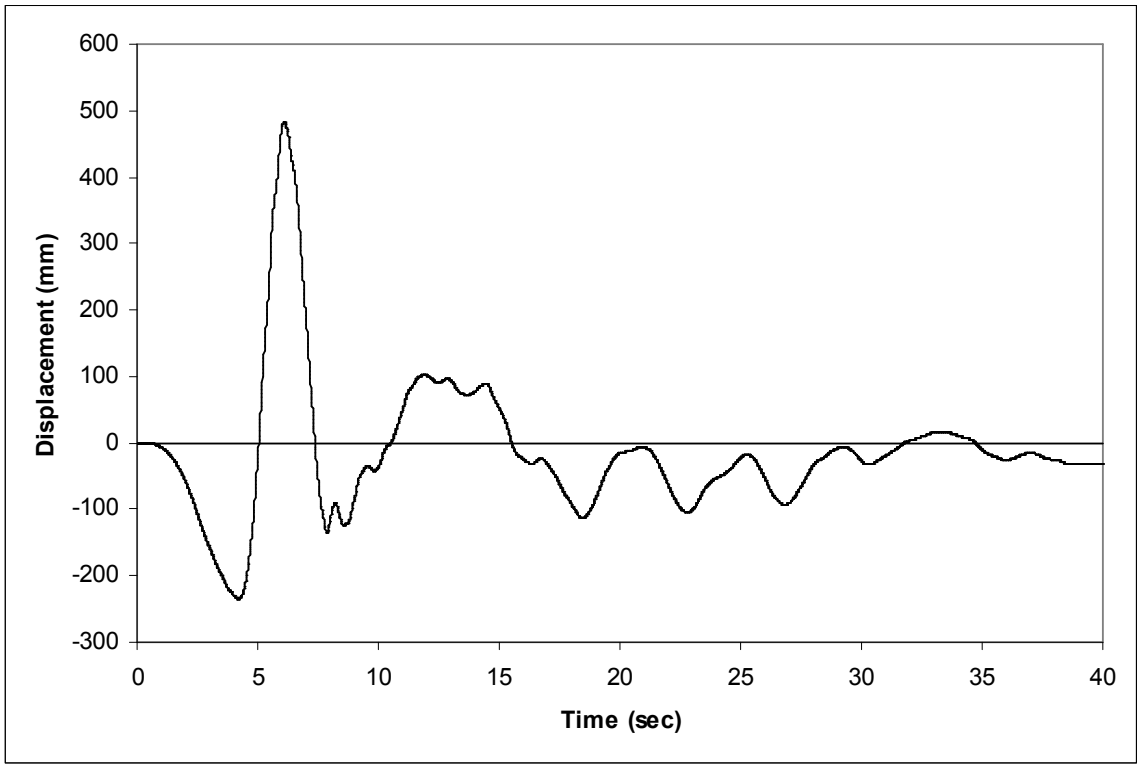

Figure 5.24 Displacement Record for LA04 Ground Motion

region in the acceleration history. Another sign of this phenomenon is peak displacements of the NRTMDF in opposing directions. When opposing displacements exhibit significantly different magnitudes, unbalanced hysteretic behavior is manifest and pulses due to near-field effects may be present in the record. The fundamental effect of this phenomenon is to develop an aggregate of inelastic NRTMDF displacements in one direction from which it cannot likely recover. This unbalanced behavior may lead to instability in the NRTMDF due to excessive displacement (strain of yielding core) and appears to compromise its ability to provide beneficial changes in overall structural dynamics. For this condition, the unbalanced behavior is not only manifest in the NRTMDF for the damped condition, but is also manifest in the rooftop displacement, primarily for the damped condition of BF-4 and the LA04 ground motion as shown in the hysteretic relationship of Figure 5.25. The stochastic nature of the force-displacement

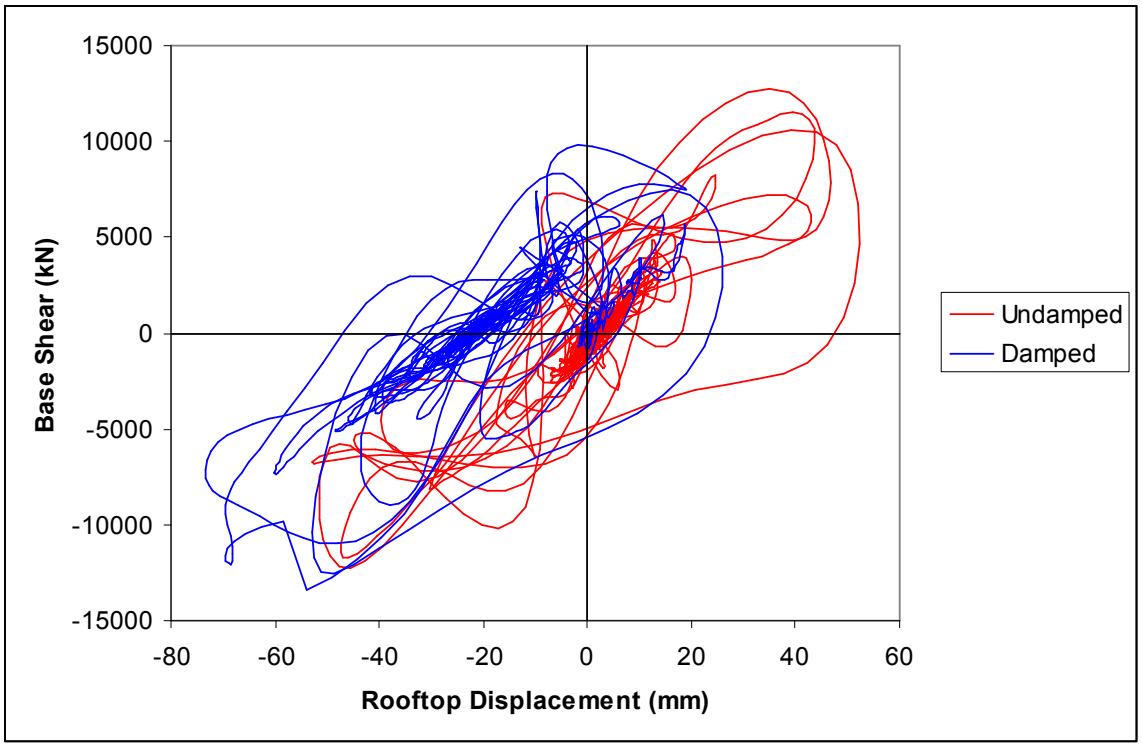

Figure 5.25 Hysteresis Loop for BF-4 and LA04 Motion

relationship shown in this figure is due to higher mode effects reflecting the indirect relationship between base shear and rooftop displacement. This notwithstanding, the general trend of the relationship can be observed to reflect the nonlinear static pushover curve for building BF-4 (see Appendix F). Most notably, the concentration of behavior at approximately -25mm rooftop displacement reflects the nonlinear action and the unbalanced behavior mentioned previously. The concentration of action at this ordinate on the load-displacement figure reflects the permanent nonlinear deflection in the roof of the structure due to uni-directional yielding of its primary members which is exacerbated by the NRTMDF for the damped case. These results support the conclusion that the NRTMDF approach may not be well suited for acceleration records exhibiting relatively high pulses due to near-field effects. In essence, the NRTMDF cannot be effectively tuned for the differing behaviors occurring in opposing directions.

The unbalanced hysteretic behavior observed with the pulse due to near-field effects is a phenomenon that can sometimes be explained by unbalanced stiffness within the structure. This can occur for structures which are not symmetric or have some other dynamic irregularity that drives the unbalanced hysteretic behavior of the NRTMDF. To assess whether such behavior is due to pulses within the motion or as a dynamic property of the structure a negative scaling factor may be used. This should be equal to the magnitude of the original scale factor and has the simple effect of shaking the structure with the inverse time history function. A mirrored hysteretic output response of the NRTMDF supports the conclusion that the unbalanced behavior is due to a pulse effect within the ground motion and not an effect of the structure's dynamics. Figure 5.26 demonstrates the NRTMDF hysteretic relationship for the original analysis and for

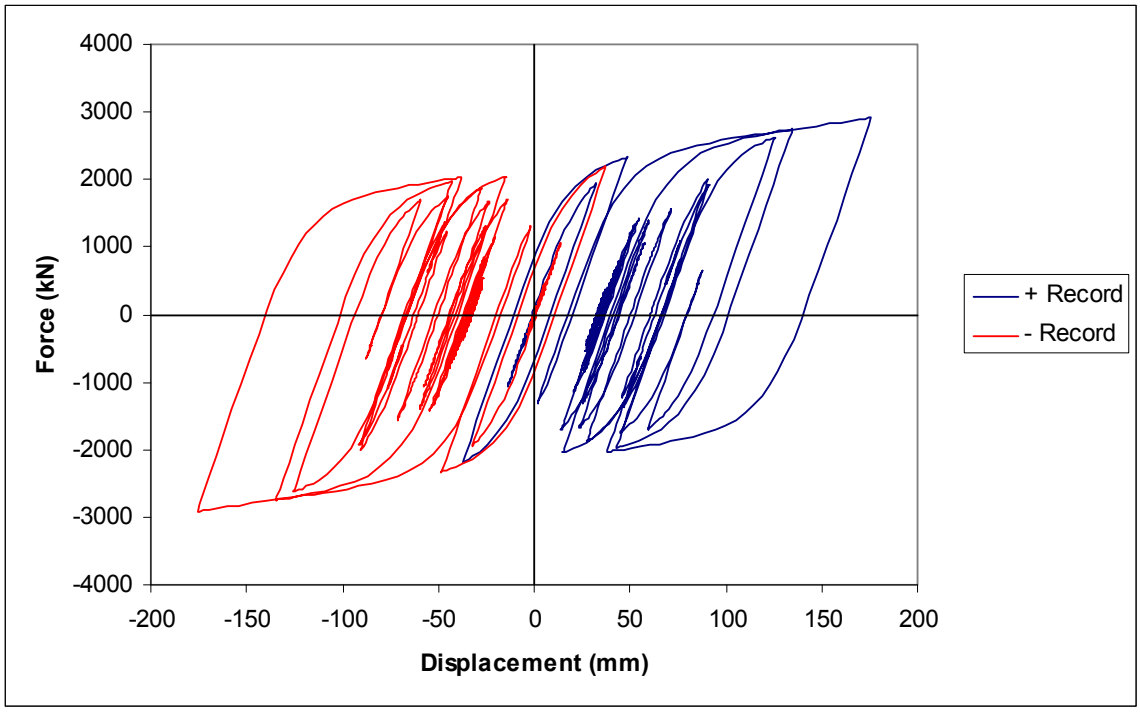

Figure 5.26 NRTMDF Hysteresis for Damped BF-4, LA04 Motion, Positive and Negative Input Motions

the analysis with the equal magnitude but opposite direction scaling factor. The mirrored behavior reflects the conclusion that the unbalanced hysteretic behavior of the NRTMDF is driven by the input motion as opposed to a dynamic property of the structure.

5.3 Maximum Recommended NRTMDF Displacement

Relatively high NRTMDF displacements occur when shifted fundamental periods become relatively long. This can be qualitatively observed by examining the displacement spectra for most records in question along with the models with longer fundamental periods (9 story BF-5, 5 story MF-1 and 8 story MF-2). For these buildings the analyses demonstrate high magnitudes of NRTMDF drift potentially beyond the range of capable performance (breach of maximum capable tensile strain). Full scale hysteretic testing of buckling restrained braces has indicated capable strains of yielding

cores as high as 3.5%. Such strains predicate maximum capable NRTMDF drifts based on practical geometries and brace arrangements. Table 5.13 lists the approximate maximum capable frame displacements based on this criterion. Based on this information, the NRTMDF displacement becomes problematic for the longer period models and higher magnitude ground motions plus motions containing pulses due to near-field effects. As a specific example, consider model MF-2. Maximum capable NRTMDF strains are surpassed for most of the higher magnitude acceleration records. Though the analysis indicates beneficial effects of the NRTMDF for such structures, lack of ability of the NRTMDF for such large displacements makes its use impractical unless the NRTMDF geometry can be altered to accommodate buckling restrained braces with longer yielding cores. Comparison of Table 5.13 results to the results listed in Tables 5.1 through 5.10 also demonstrates a breach in maximum capable NRTMDF drifts for several of the ground motions when applied to shorter period structures. While the geometries considered in this analysis reflect drifts surpassing peak capabilities, altered geometries (longer yielding cores) may enable higher BRB strains thereby

Table 5.13 Maximum Recommended Capable NRTMDF Displacements

Structure	3.5% Core Strain (mm)	Max Recommended Capable Story Drift (mm)
BF-1	391	414
BF-2	637	655
BF-3	487	505
BF-4	570	585
BF-5	493	507
EBF-1	574	594
SW-1	333	359
SW-2	221	269
MF-1	614	630
MF-2	362	383

accommodating larger NRTMDF drift. Also noteworthy is the magnitude of accelerations for which maximum capable NRTMDF drift is surpassed. The LA 2% in 50-Year motions as well as the SE 2% in 50-Year motions contain unusually high acceleration magnitudes as reflected in the spectra shown in Figure 4.2 and Figure 4.4. In fact, these magnitudes may represent extreme motions that may be beyond practical performance objectives (Immediate Occupancy and Life Safety) for many design scenarios. Likewise, for performance objectives where the NRTMDF displacements are less than the capable NRTMDF drift, lesser objectives will readily be satisfied.

The analyses typically demonstrate breach in maximum recommended capable displacement in the NRTMDF for ground motions with high spectral accelerations usually accompanied by longer fundamental periods of interest. Generally, the high displacements occur for soft sites with high spectral accelerations correlating to longer periods. The higher displacements are primarily manifested as excessive strains in the yielding core of the buckling restrained braces (axial strains beyond 3.5%). While excessive displacements are a function of the specific inherent dynamics of each structure, the subject ground motion is also a significant factor for driving NRTMDF displacements beyond maximum capable BRB strains. The predominant ground motions from the SAC inventory for which excessive displacements in NRTMDF's occur include LA21, LA25, LA28, LA30, LA37, SE21, SE31, SE36, NF01, NF15, LASS2A and LASS3C. Figure 5.27 displays the acceleration spectra for these motions. Observations of the spectra demonstrate a correlation when short period spectral accelerations (at periods of approximately 0.2 to 0.8 seconds) are approximately 2.0g or greater and when long period spectral accelerations (at periods of approximately 1.0 seconds) are

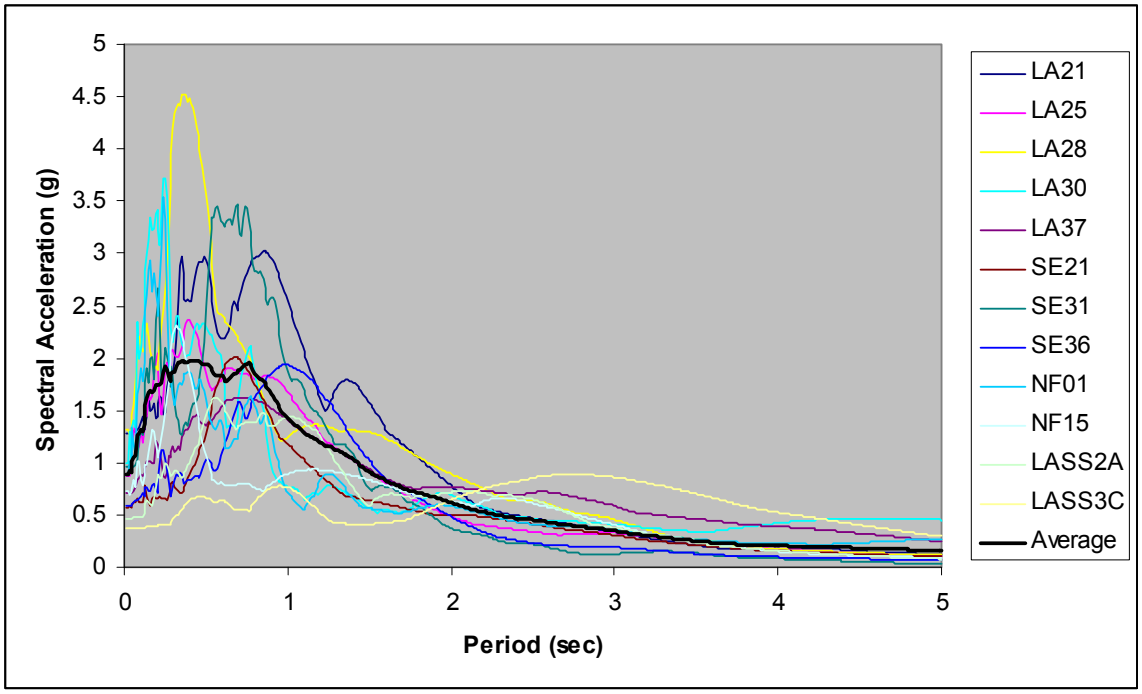

Figure 5.27 Spectra for Ground Motions with NRTMDF BRB Strains Exceeding 3.5%

approximately 1.5g or greater. Contemporary codes prescribe design accelerations of this magnitude for some areas in the most densely populated regions of the United States.[2] This notwithstanding, it should be noted that these regions are geographically very small as shown in Figures 5.28 and 5.29 (e.g Los Angeles Basin, San Francisco Bay Area, New Madrid). As such, the areas and sites for which this approach may be ineffective on the basis of high magnitude spectral acceleration leading to excessive NRTMDF displacements are relatively few. An additional consideration is the performance objective for the specific project located on such a site and whether it includes ground motions reflecting a large, rare seismic event which would produce the higher magnitude accelerations. If the performance objective is directed toward limited damage rather than collapse prevention, the considered motions would be of lesser magnitude thereby precluding relatively high magnitude accelerations causing excessive NRTMDF

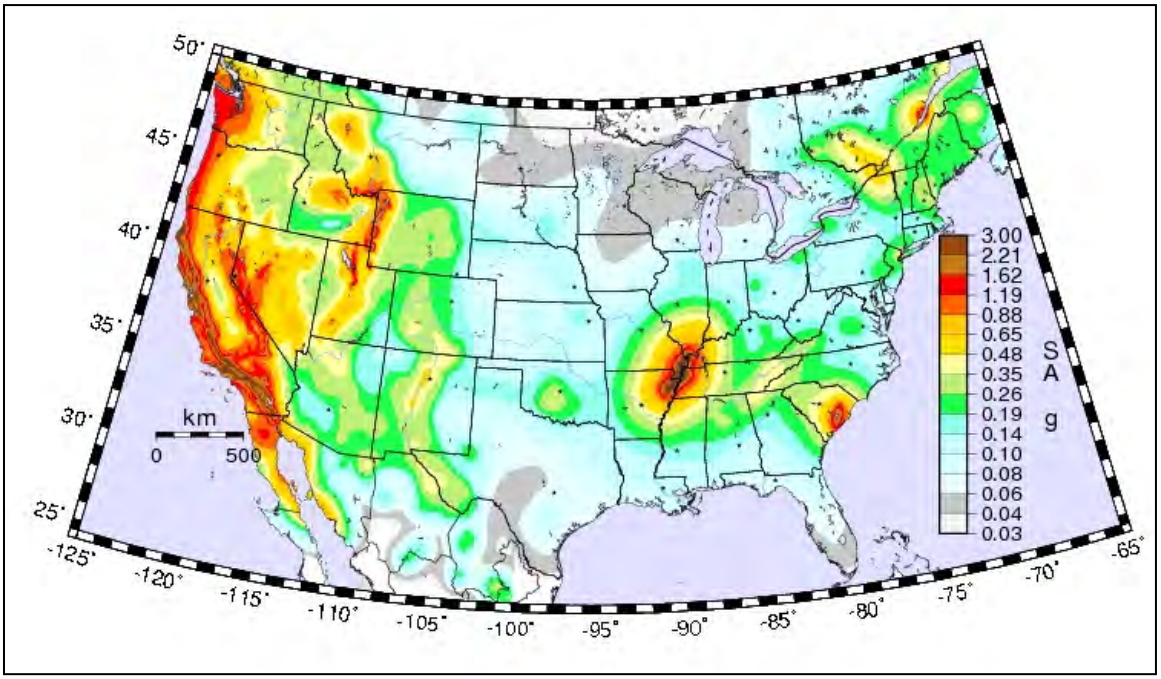

Figure 5.28 Mapped Spectral Accelerations for 0.2 Second Period, 2% in 50-Year Event

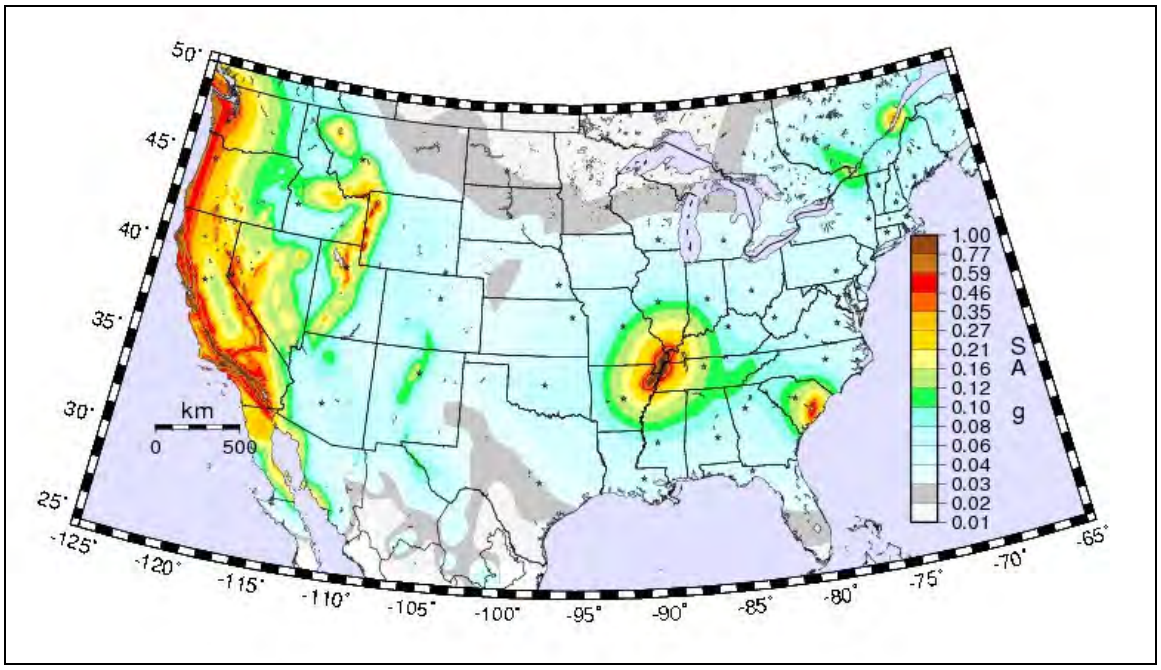

Figure 5.29 Mapped Spectral Accelerations for 1.0 Second Period, 2% in 50-Year Event

displacements. Ordinarily, the design of buckling restrained braces may account for the relatively high magnitude accelerations in question and in fact may often be the optimal primary lateral force resisting system for such scenarios. However, ultimate brace capacity is not a governing parameter for the approach embodied in this research. The research targets NRTMDF stiffness and yield strength as the primary variables for enabling the near optimal reduction in response of the system. While brace strength could be adjusted to accommodate relatively high spectral accelerations and corresponding forces, this may compromise the effectiveness of the NRTMDF rendering it less capable of meeting the specific performance objective.

While the results indicate the potential for a breach of maximum capable BRB strain, options exist which may yet enable a stable NRTMDF. Such an approach is to use dual braces in the same line acting in the same direction but with one brace in tension while the other is in compression. This is enabled by incorporating dual braces in a 'V' or inverted 'V' configuration spanning over two bays of structure. For more information regarding this concept, see Section 9.7.

The potential for enhanced drifts notwithstanding, realization of relatively high strains in BRB cores is an issue requiring further research and investigation. Contemporary standards for seismic design of buckling restrained braces (AISC Seismic Design Manual) prescribe a testing protocol with peak BRB strains correlating to design story drifts.[37] This approach is directed toward long-held guidelines reflecting pragmatic performance of structural frames in consideration of many issues outside of the structural system (nonstructural elements and components). While many framing systems (moment frames, buckling restrained braced frames) are capable of much higher drifts, this

limitation translates to an inventory of BRB test results that do not sufficiently reflect maximum capable BRB strains. Ongoing research efforts and future testing will likely expand the data reflecting extreme strain behaviors in buckling restrained braces but current data in this regard is somewhat limited.

5.4 Nonlinear Static Pushover and NRTMDF Mobilization

The primary benefit of the NRTMDF approach is theorized to be the reduction in demand on the global structure. This is brought about by fundamentally changing the structure's inherent dynamic properties with an effective mass and varying stiffness of the NRTMDF. The analyses demonstrate that the shift in dynamic properties is one of the beneficial effects due to the NRTMDF while added beneficial effects are driven by its targeted nonlinearity. Ideally, the active nonlinearity of the NRTMDF reduces the demand for nonlinearity on the base structure thus reducing base shear, drift and stress. Assurance of this benefit is found in ensuring active nonlinearity in the NRTMDF is achieved prior to yielding of the global structure. Whether this is achieved for an NRTMDF design may be determined within the context of the nonlinear response history analysis. However, this is a very calculation intensive and time consuming process. Other more straightforward nonlinear methods hold the potential for assessing whether active nonlinearity of the NRTMDF is likely before significant nonlinearity of the base structure occurs.

Nonlinear pushover analyses of the ten test models, each with optimized NRTMDF structures may demonstrate active nonlinearity in the NRTMDF prior to development of nonlinear mechanisms in the original structure. Figures 5.30 and 5.31 show building cross-sections for BF-4 and BF-5 and demonstrate the point of

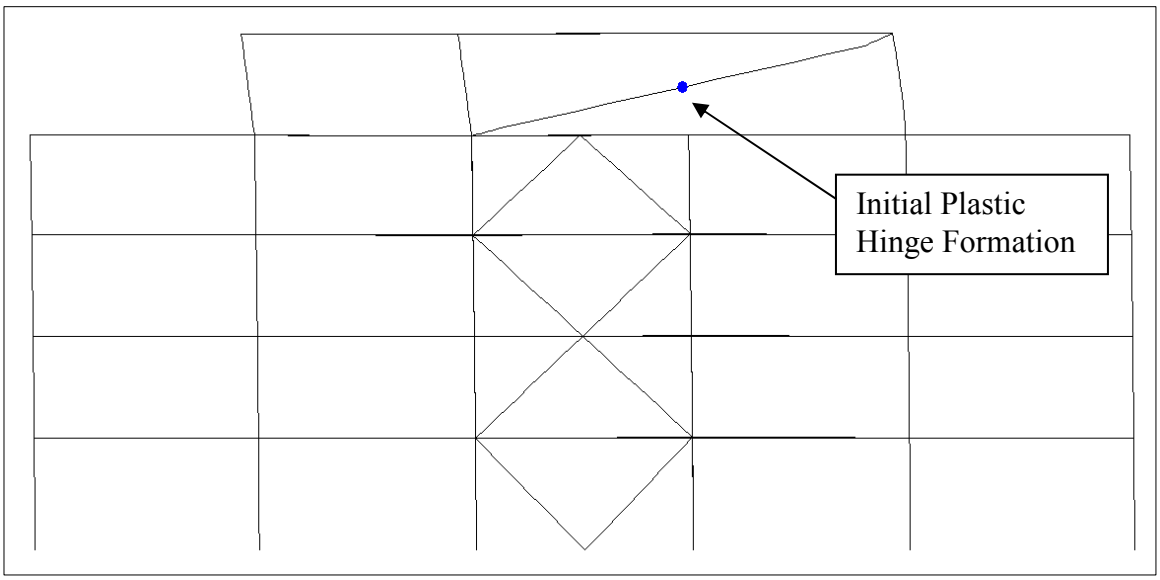

Figure 5.30 BF-4 Pushover Analysis with Initial Nonlinear Mechanisms

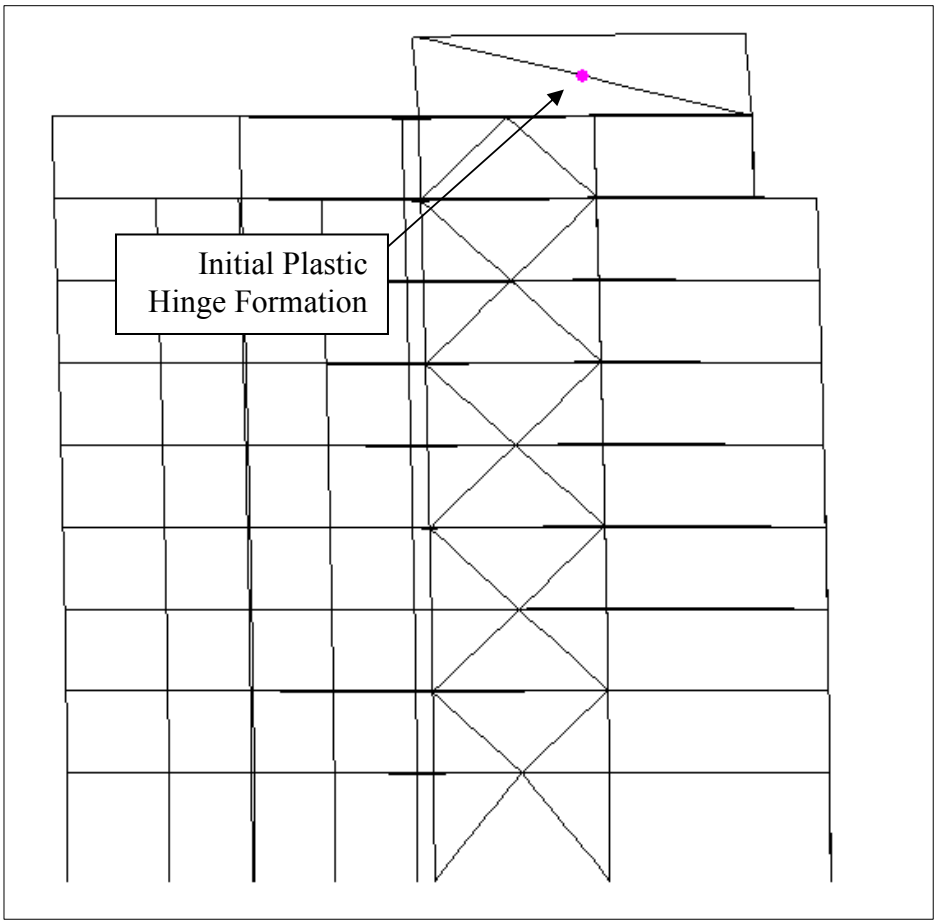

Figure 5.31 BF-5 Pushover Analysis with Initial Nonlinear Mechanism

initialization of nonlinear mechanisms. For all ten model buildings the nonlinear pushover analysis shows that the BRB of the NRTMDF yields prior to the development of yielding, buckling or significant nonlinear behaviors in the base structure. This demonstrates that an appropriately designed NRTMDF, which enables at least a moderate shift in fundamental period, will most likely have nonlinear properties with a propensity to mobilize prior to plastic hinge formation of primary seismic force resisting elements in the base structure.

A caveat with respect to the nonlinear pushover analysis is its fundamental premise of a targeted displacement pattern. Pushover analysis, as a matter of methodology, incorporates the piecewise monotonic displacement of a structure, accounting for nonlinear behaviors in individual elements while calculating the reaction at its base. The piecewise displacement most often follows a load pattern consistent with the fundamental mode or the code prescribe pseudo-static lateral load pattern. The fundamental mode is appropriate for this in most structures since this is the mode where the majority of mass becomes mobilized. However, for the approach embodied in this research the analyses have demonstrated significant higher mode response. In fact, mode 2 may account for mass in similar proportions or higher than mass accounted for in mode 1. Hence, the mode 1 pattern alone may not be accurate for an appropriate displacement pattern for the nonlinear pushover analysis. A consideration in this regard is the fact that fundamental dynamics become altered by virtue of the NRTMDF. As originally postulated, the mode 2 contributions mentioned previously do not theoretically become active until yielding of the NRTMDF has occurred. However the results of the analyses for damped models indicate that higher mode (mode 2) effects are significant both before

and after the yielding of the BRB's of the NRTMDF. Table 5.14 lists the differences in activated modal mass for modes 1 and 2 for each damped structure. As indicated, significant proportions of modal mass are active for modes 1 and 2 prior to and following yielding of the NRTMDF. Also, Figures 5.32 through 5.41 demonstrate the mode shapes for the damped buildings prior to yielding of the NRTMDF and at its peak performance point (displacement). The modal component in these figures reflects the relative shape of modal deformations for the damped cases of each model. Current methods of nonlinear pushover analysis do not include a prescribed protocol for modal combinations in the pushover displacement pattern. This is, in fact, and area of active research and many researchers are developing rational protocols for modal combinations for nonlinear static pushover analysis. This notwithstanding, the utilization of mode 1 as the sole displacement pattern is not without value. Following this approach, if the pushover analysis demonstrates yielding of the base structure prior to NRTMDF yielding, a rational conclusion is that active mobilization of the NRTMDF does not occur for the model under study before yielding of the structural elements of the primary structure.

Table 5.14 Percent Modal Mass Participation Before and After NRTMDF Mobilization

	Pre-Mobilization		Post Mobilization (Transient)	
Structure	Mode 1	Mode 2	Mode 1	Mode 2
BF-1	47.9%	49.6%	19.7%	76.9%
BF-2	43.2%	56.1%	20.7%	78.4%
BF-3	55.7%	31.9%	23.0%	62.6%
BF-4	60.8%	26.1%	27.1%	57.8%
BF-5	58.8%	20.6%	33.2%	41.9%
EBF-1	60.9%	31.4%	25.7%	65.6%
SW-1	49.8%	24.6%	21.2%	50.3%
SW-2	50.9%	23.4%	21.4%	48.6%
MF-1	72.3%	15.7%	42.5%	42.3%
MF-2	74.4%	13.5%	45.8%	37.7%

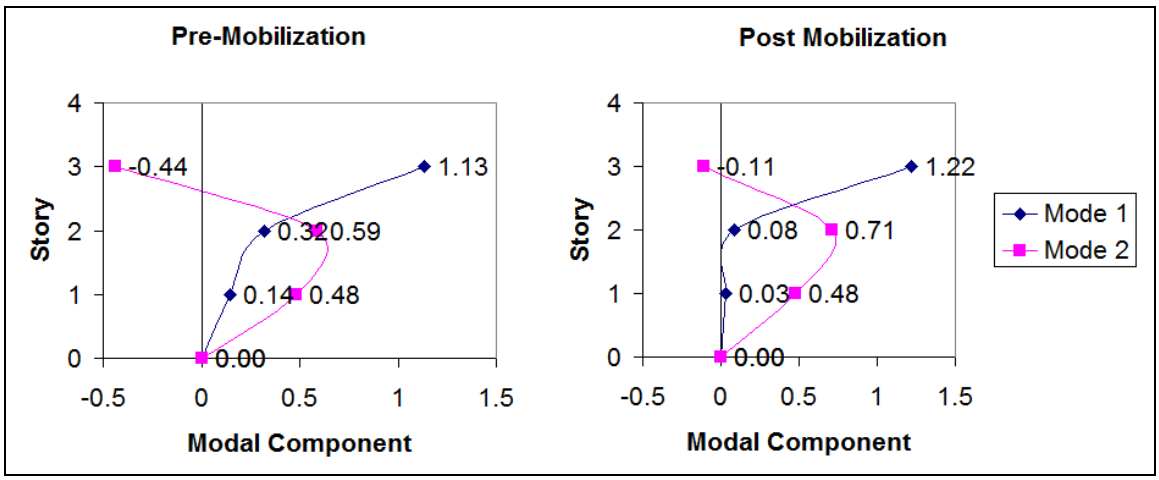

Figure 5.32 Damped 2 Story BF-1 Mode Shapes for Initial and Yielded NRTMDF Stiffness

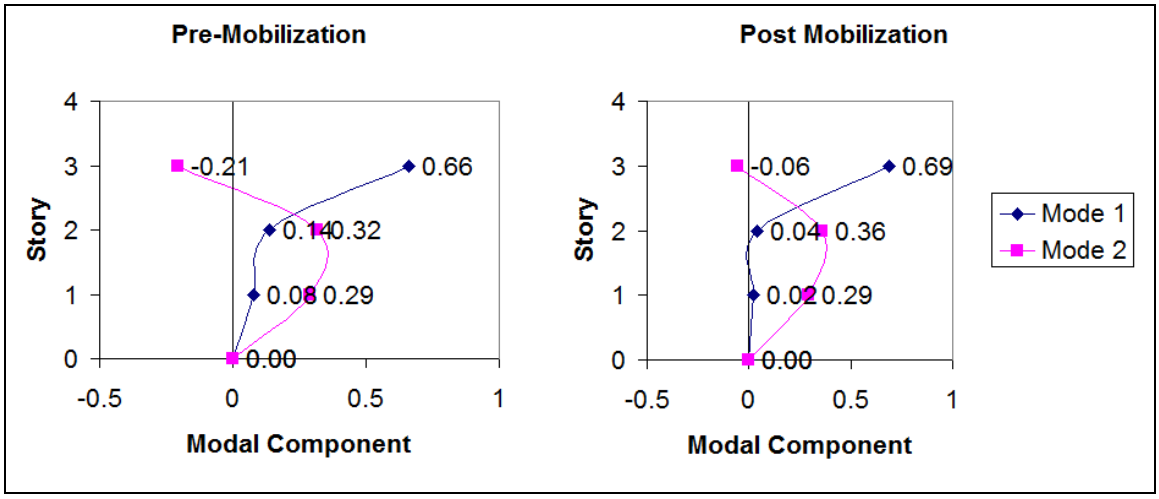

Figure 5.33 Damped 2 Story BF-2 Mode Shapes for Initial and Yielded NRTMDF Stiffness

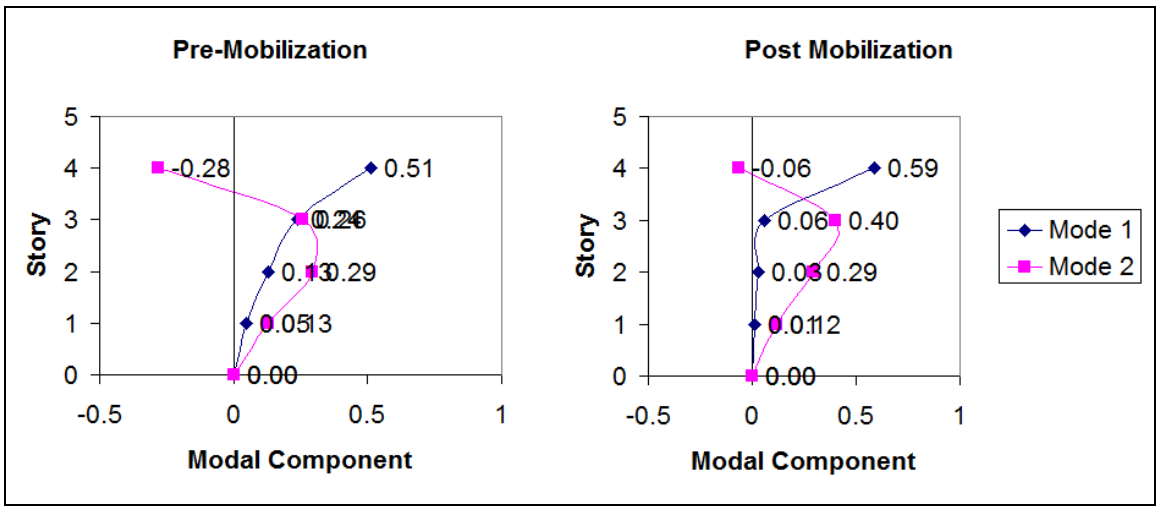

Figure 5.34 Damped 3 Story BF-3 Mode Shapes for Initial and Yielded NRTMDF Stiffness

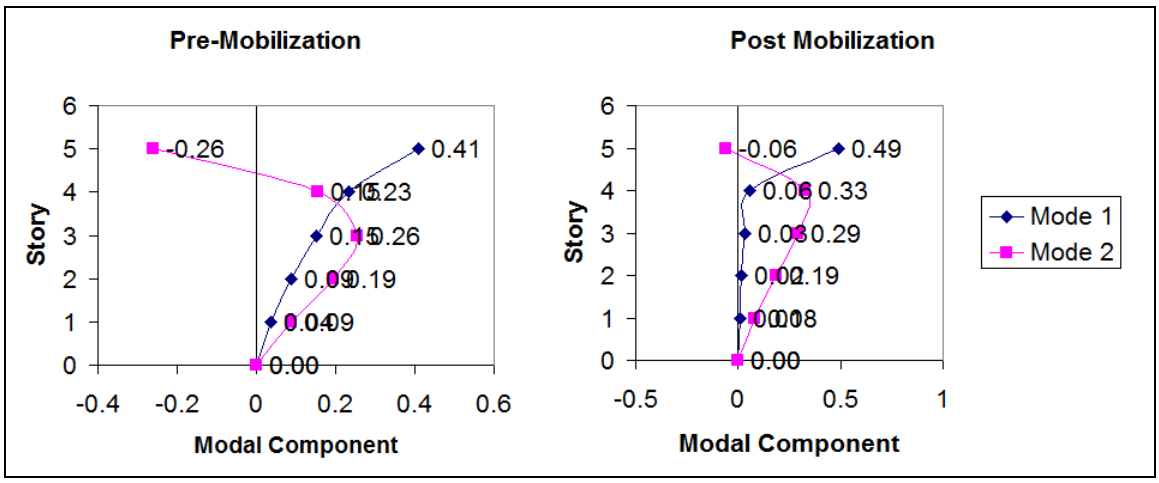

Figure 5.35 Damped 4 Story BF-4 Mode Shapes for Initial and Yielded NRTMDF Stiffness

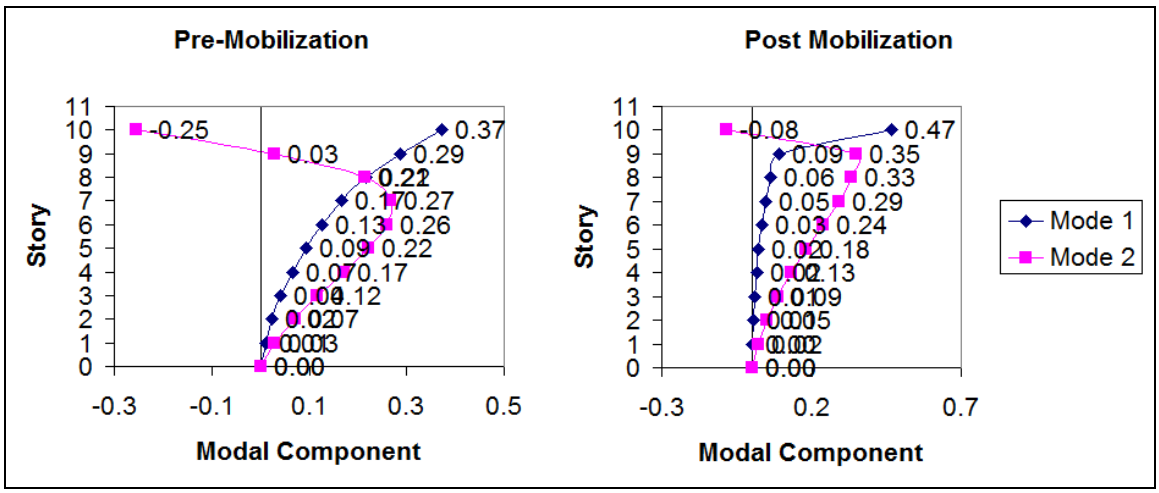

Figure 5.36 Damped 4 Story BF-4 Mode Shapes for Initial and Yielded NRTMDF Stiffness

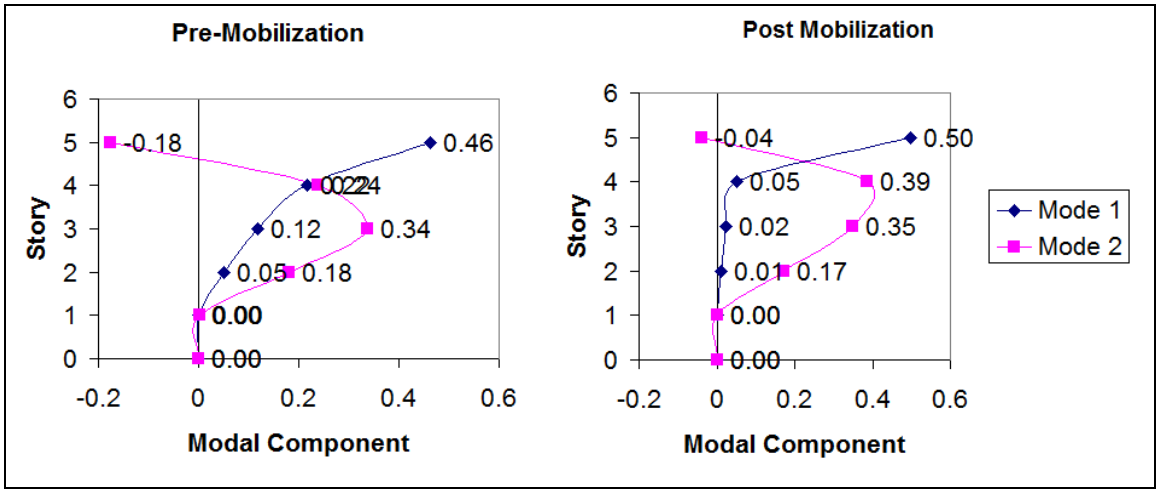

Figure 5.37 Damped 5 Story EBF-1 Mode Shapes for Initial and Yielded NRTMDF Stiffness

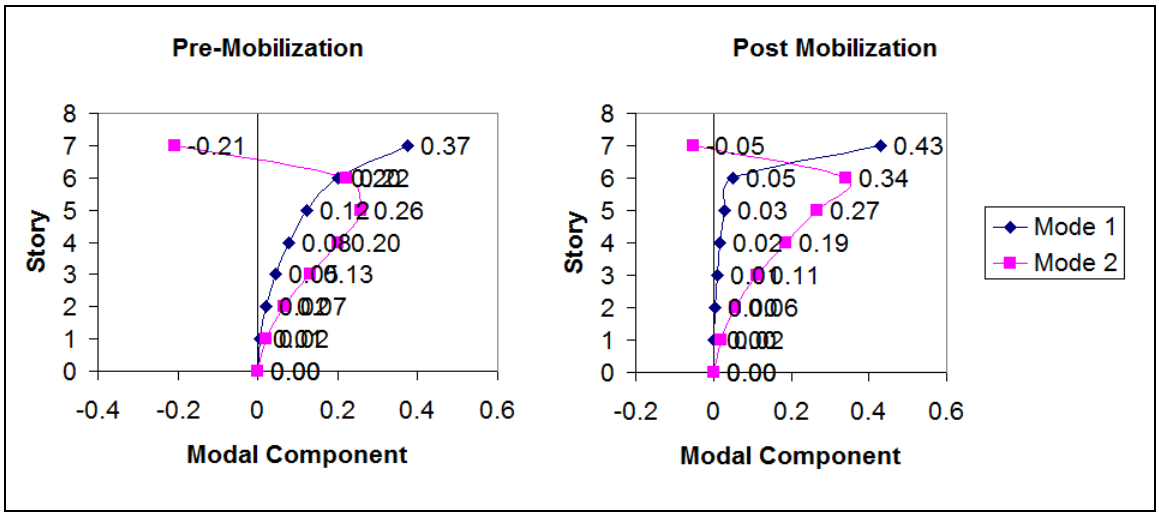

Figure 5.38 Damped 6 Story SW-1 Mode Shapes for Initial and Yielded NRTMDF Stiffness

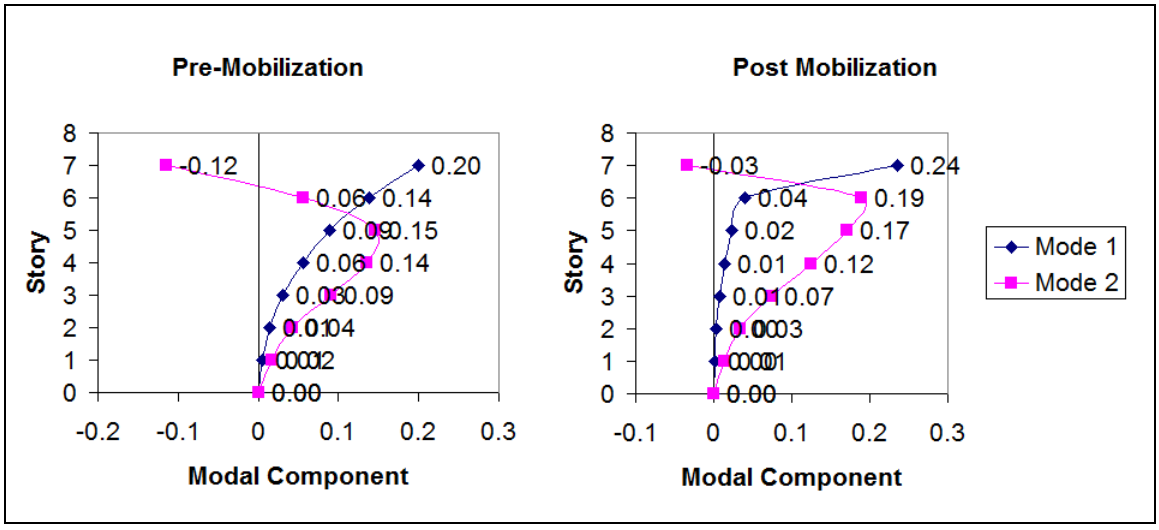

Figure 5.39 Damped 6 Story SW-2 Mode Shapes for Initial and Yielded NRTMDF Stiffness

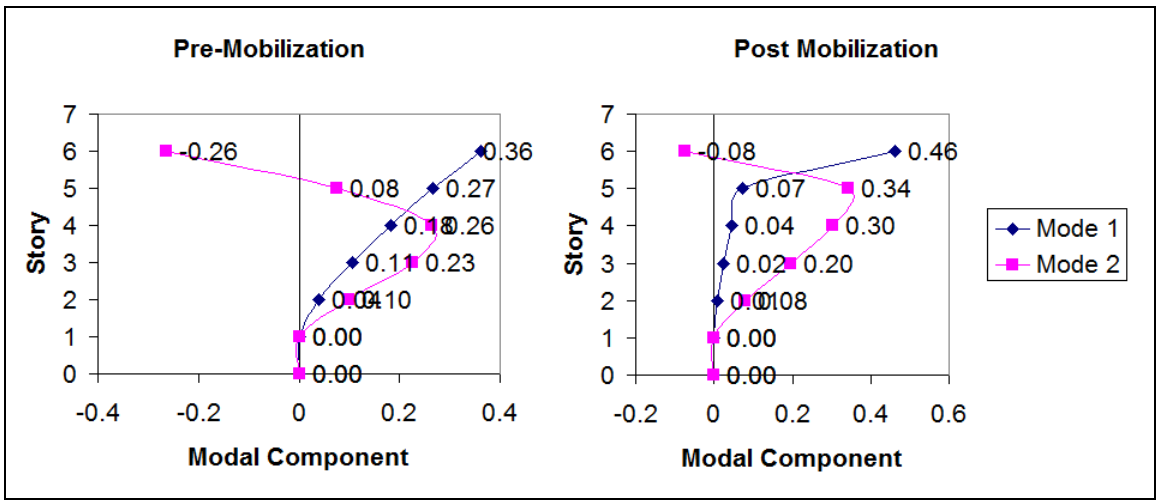

Figure 5.40 Damped 5 Story MF-1 Mode Shapes for Initial and Yielded NRTMDF Stiffness

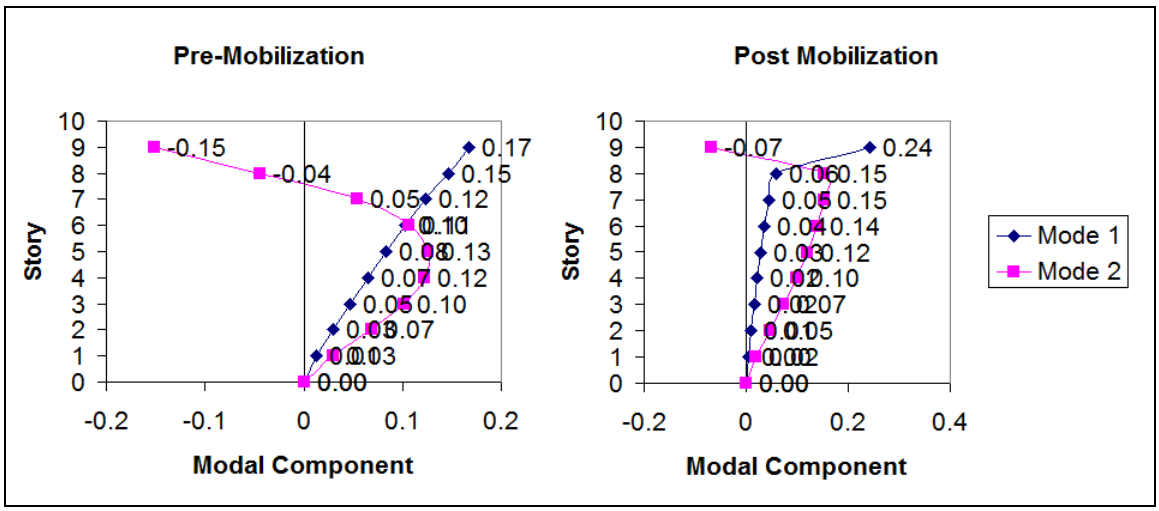

Figure 5.41 Damped 8 Story MF-2 Mode Shapes for Initial and Yielded NRTMDF Stiffness

When this occurs, the design of the NRTMDF is fundamentally flawed or the approach embodied within this research is simply not effective for the model. In fact, this outcome should be identified as criteria reflecting a flawed design when it occurs. If included in the analysis for such cases, the mode 2 displacement pattern will only exacerbate the analytically predicted first evident yielding of the base structure thereby reinforcing this

conclusion. This conclusion is a slight departure from the concept postulated in Section 3.6. Whereas the original postulate was to verify active nonlinearity of the NRTMDF prior to yielding of the base structure, the research demonstrates the nonlinear pushover analysis serves better to identify, to a certainty, whether yielding of the base structure will occur before yielding of the NRTMDF. For cases where the base structure does not yield before the NRTMDF, active nonlinearity of the NRTMDF should be deemed likely, but cannot be verified without further pushover analyses incorporating higher mode shapes or more sophisticated analyses such as nonlinear response history analyses with appropriately selected ground motions.

In addition to nonlinear pushover analyses of the optimized test models utilizing a mode 1 displacement pattern, pushover analyses using mode 2 as the displacement pattern were executed. For these, 8 of the 10 test structures demonstrate yielding of the NRTMDF prior to buckling, yielding or nonlinearity of the base structure. The two exceptions are BF-1 and BF-2. Observation of these structures demonstrates that with optimized NRTMDF's, the mode 2 response becomes the predominant response mode and thereby indicating the potential for yielding of the base structure before yielding of the NRTMDF. This is corroborated by the results summarized in Table 5.14 where more than 75% of structural mass is mobilized in mode 2 for each structure. Figures 5.42 and 5.43 demonstrate the initial formation of nonlinear mechanisms for BF-2 using a mode 1 and mode 2 displacement shapes respectively. As shown, mode 1 demonstrates active nonlinearity in the NRTMDF before yielding of base structure and for a mode 2

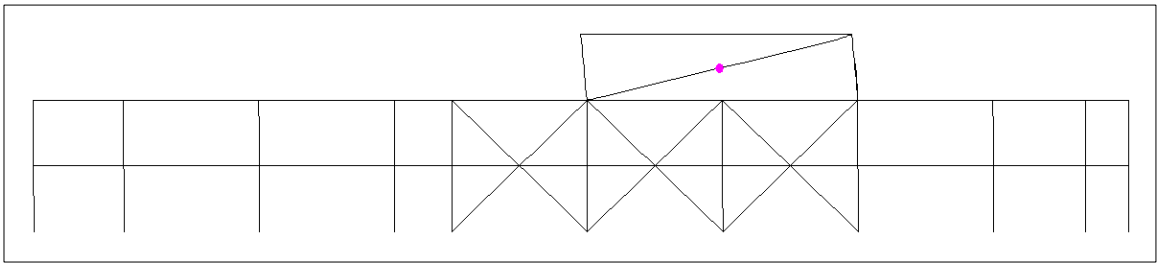

Figure 5.42 BF-2 with Initial Hinge Formation, Mode 1 Displacement Shape

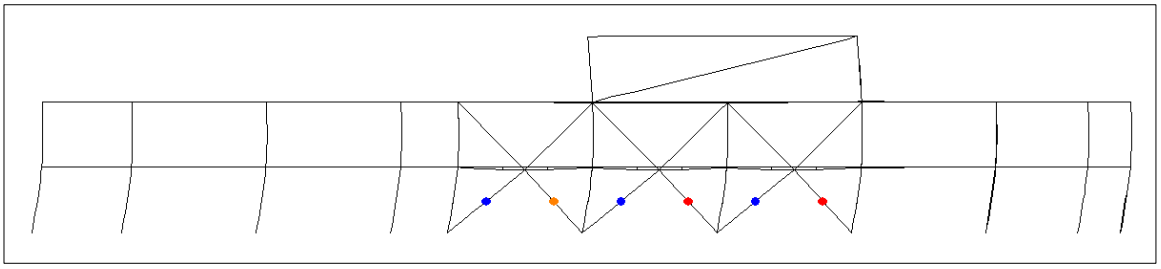

Figure 5.43 BF-2 with Initial Hinge Formation, Mode 2 Displacement Shape

displacement pattern, the opposite is true. A conclusion is that nonlinear pushover analysis may reliably predict whether active nonlinearity in the NRTMDF is achieved prior to yielding of the base structure when the activated modal mass for mode 2 is less than 60 percent of total mass for the transient case using modal analyses with effective NRTMDF stiffness parameters.

While current methods for pushover analysis do not include a protocol for modal combinations within the pushover pattern, a rational approach for this research is to use modes 1 and 2 simultaneously with an equal weighting for each. This reflects the roughly equal weighting of post mobilized modal mass percentages reflected in modes 1 and 2 for the results shown in Table 5.14. For this table, modal mass participation factors between modes 1 and 2 reflect an approximate 50% weighting when considering the balance between the pre mobilized and post mobilized cases. While this weighting is a very rough approximation, it should be noted that transient behavior due to nonlinearity

creates modal participation factors and mode shapes that are as transient as the motion under consideration. This notwithstanding, the 50% weighting approach for modes 1 and 2 in the pushover pattern reflects an accounting for the simultaneous behaviors of the two modes. This is deemed a rational approach for verifying the likelihood of active nonlinearity in the NRTMDF before yielding of the base structure thereby corroborating the previous conclusions. The pushover analyses results following this approach demonstrate a likelihood of yielding of the original structure's lateral resisting force elements before yielding of the NRTMDF for BF-1 and BF-2. While this does not necessarily signify that this will be the nature of behavior, it cannot preclude this as a possibility. For the remaining test models, the pushover analyses following this approach demonstrate yielding of NRTMDF and its active hysteretic nonlinearity will most likely be achieved before yielding of the primary lateral force resisting members of the base structure. As this occurs the NRTMDF becomes an active mechanism for targeted energy dissipation. This energy is dissipated from the system and is no longer available to cause damage elsewhere in the structure.

5.5 NRTMDF Mass Discussion

As mentioned in Chapter 4 and earlier in this chapter, selection of effective mass requires consideration practical magnitudes of NRTMDF mass with respect to the overall structure. In addition, the mass must be sufficient to develop beneficial inertial effects of the NRTMDF that counteract the motion of the primary of the structure while driving nonlinear and energy dissipating behavior of the BRB's which brace the NRTMDF. Chapters 4 and 5 of this research target a combination of NRTMDF mass and stiffness to enable an effective reduction in peak transient response parameters in consideration of

the broad-based SAC ground motion suite. Differences between linear and nonlinear analysis methods resulted in significant differences in NRTMDF mass and stiffness for each structure which were targeted toward the apparent greatest reduction in peak transient response parameters.

While rough corollaries can be drawn between linear and nonlinear methods, the analyses demonstrate that only indirect correlations of mass and stiffness between the two methods can be drawn. This is due to several factors. Chief among these is the fact that linear analysis methods offer virtually no limit to the inertial reaction force between the NRTMDF and the structure below. For this, the reaction is simply calculated as the NRTMDF displacement multiplied by its stiffness. For nonlinear analysis methods, the BRB's of the NRTMDF serve as a fuse to limit the maximum lateral force that can develop between the NRTMDF and the structure below. As a result, the nonlinear analysis methods resulted in a higher NRTMDF mass than linear analysis methods when the analysis was directed toward the maximum reduction in peak transient response parameters (base shear, rooftop displacement). Table 5.15 lists the summary results of NRTMDF mass and peak reactions using the linear analysis methods of Chapter 4. Table 5.16 lists the same information but for the nonlinear analysis methods of Chapter 5. As indicated the average NRTMDF mass for linear analysis methods is 12.0% of the mass of the structure below. For nonlinear analysis methods the average NRTMDF mass is 18.4%.

Table 5.15 NRTMDF Mass Summary for Linear Methods

Structure	NRTMDF Mass (kg)	NRTMDF Mass vs. Total Str. Mass	Average Peak NRTMDF Reaction (kN)
BF-1	58826	10%	1089
BF-2	201642	11%	2654
BF-3	324723	13%	5379
BF-4	359591	10%	6380
BF-5	426337	11%	6215
EBF-1	458861	13%	4054
SW-1	465902	10%	5091
SW-2	1545298	10%	18688
MF-1	559420	14%	3292
MF-2	2498806	18%	8553
	Average	12.0%	

Table 5.16 NRTMDF Mass Summary for Nonlinear Methods

Structure	NRTMDF Mass (kg)	NRTMDF Mass vs. Total Str. Mass	Average Peak NRTMDF Reaction (kN)
BF-1	88239	15%	702
BF-2	366622	20%	1998
BF-3	374680	15%	2386
BF-4	719183	20%	2480
BF-5	775159	20%	2702
EBF-1	705940	20%	1153
SW-1	931804	20%	2999
SW-2	2163417	14%	13298
MF-1	799172	20%	906
MF-2	2776452	20%	3787
	Average	18.4%	

The reaction between the NRTMDF and the structure below for linear and nonlinear analysis methods can be observed in its force-displacement relationship. Observation of this relationship reflects the reaction between the NRTMDF and the structure below. For each of the test models, the linear analysis methods of Chapter 4 yielded an elastic stiffness falling between the initial stiffness and the peak effective stiffness (developed from peak NRTMDF displacements) of the NRTMDF developed using the nonlinear analysis methods of Chapter 5. For an illustration of this concept, consider test model BF-5. For this structure, linear analysis methods yielded an effective NRTMDF mass equal to approximately 11% of the total structural mass. For nonlinear methods, the analyses yielded an effective NRTMDF mass equal to approximately 20% of the total structural mass. The added mass for nonlinear methods reflects the need to overcome the limitation in forces transmitted through the BRB's which reduce forces by virtue of yielding behavior. While the linear methods yield a reaction of 6215 kN, the nonlinear methods yield a reaction of 2702 kN. Figure 5.44 displays the NRTMDF force-displacement for this structure for both the linear analysis methods of Chapter 4 and nonlinear analysis methods of Chapter 5.

The addition of NRTMDF masses for their application with new structures is a trivial matter not covered herein. The NRTMDF mass on existing structures as indicated in Tables 5.15 and 5.16 can be accommodated by retrofitting and strengthening the structures as needed to support the added load (see Chapter 9). However, such retrofitting may not be economically pragmatic within the context of a seismic retrofit. While the masses reflect the objective of enabling the maximum reduction of peak transient response parameters, this does not mean for the NRTMDF approach to be

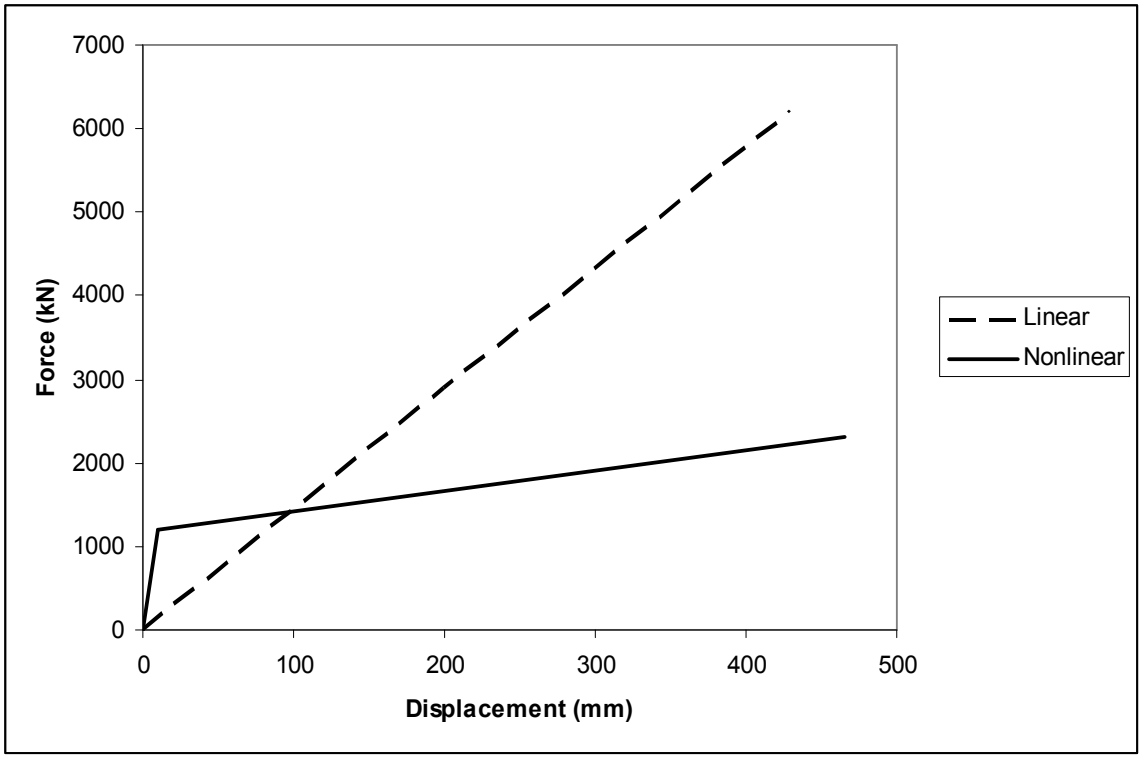

Figure 5.44 Model BF-5 NRTMDF Force-Displacement Behaviors for Linear and Nonlinear Analysis Methods

effective it must use this magnitude of mass. Analyses show that reduced masses may still enable favorable performance. For instance, the analyses for EBF-1 using linear analysis methods yielded an NRTMDF mass equal to approximately 13% of the base structure. For this, the average reduction in peak rooftop displacement is 8.7% between the undamped and damped cases. Upon reducing the NRTMDF mass to 10% of the total structural mass, the average reduction in peak rooftop displacement is 7.9%. Similar results can be observed for nonlinear analysis methods where an effective NRTMDF mass of 20% of the total structural mass yielded a reduction in peak rooftop displacement of 20.6%. Upon reducing the NRTMDF mass to 10% of the building mass, the reduction in peak rooftop displacement becomes 15.5%. Hence, while the most effective

NRTMDF mass may not be pragmatically incorporated in the structure reductions in this mass still reflect beneficial performance enabled by the NRTMDF approach.

Additional issues reflect the NRTMDF mass and its practical addition to an existing structure. For some structures, adding NRTMDF mass as high as 20% of the total structural mass may be accomplished within pragmatic limits. For others, adding 20% mass may simply not be practical. As an example, consider model BF-1. For this model a practical NRTMDF (penthouse) occupying a footprint equal to approximately 25% of the total building footprint area would require concrete deck thickness of approximately 180mm to enable the NRTMDF mass to reach 20% of the total structural mass. For BF-3, the same scenario would yield a concrete deck thickness of 260mm. For BF-4, the approach would yield a thickness of approximately 400mm which is still deemed practical. However, model BF-5 has a relatively small footprint and has 9 stories of total height. For this model, using 25% of the building footprint for adding an NRTMDF with mass equal to 20% of the total structural mass equates to a concrete deck thickness in excess of 1,000mm which is not likely practical. This thickness may be reduced to 250mm while keeping the same total mass provided the area of the NRTMDF is broadened to occupy the entire building footprint, essentially making this structure 10 stories in lieu of 9 stories with the top story comprising the NRTMDF. Test model SW-2 represents the most extreme case in this regard. This cast-in-place concrete building is unusually heavy and with an NRTMDF area occupying 25% of the building footprint would need a concrete deck thickness of approximately 2787mm which is impractical. If the NRTMDF mass is reduced to 10% of the building mass and expanded to the full building footprint, the concrete deck thickness would be approximately 348mm which is

considered far more practical. These concepts demonstrate the addition of the NRTMDF mass and whether it can be added to an existing structure in a practical matter is an issue which would require investigation within the context of any structure for which the NRTMDF approach is undertaken.

5.6 Nonlinear Inelastic vs. Nonlinear Elastic Distinction

The NRTMDF behavior herein characterized follows a nonlinear inelastic mode of behavior. The object of this by design is to introduce a method of targeted energy dissipation which is measured as the area encompassed within the force-displacement hysteretic relationship of the buckling restrained braces as demonstrated conceptually in Figure 1.7 and by example in Figure 5.10. This behavior is characterized through the development of a bilinear hysteretic pattern which traces the projected BRB behavior until a reversal occurs. At this point the hysteretic pattern ideally becomes inverted reflecting the concept that a similar bi-linear force-displacement pattern is followed from the point of reversal as the BRB acts in the opposite direction. This is the designed and targeted behavior of BRB's as reflected in tested assemblies.[3,4] A comparable mode of behavior which can be captured within many analysis applications is the nonlinear elastic hysteretic model which essentially means the force-displacement hysteretic relationship traces the same pattern without respect to direction of loading and without departing from the originally defined bilinear force-displacement relationship. Lack of an enveloped hysteretic area for this elastic approach reflects lack of energy dissipation and therefore a failure to develop a targeted approach for energy dissipation.

This research targets the nonlinear inelastic approach for the NRTMDF as opposed to a nonlinear elastic approach. As an example, consider test model BF-4.

Parallel analyses of nonlinear inelastic and nonlinear elastic versions of the damped model using the SE18 ground motion demonstrate important differences in the overall behavior between the two models. Figure 5.45 demonstrates the superimposed hysteretic behavior of the braces of the NRTMDF, the first demonstrating nonlinear inelastic behavior and the second demonstrating nonlinear elastic behavior. Note the lack of hysteretic envelope for the nonlinear elastic model. Failure to introduce targeted energy dissipation for the this model is manifest not only as an increase in elastic strain energy resulting in increased peak displacement of the NRTMDF but as a diminished capability for response reduction in the primary structure below. Figures 5.46 and 5.47 reflect this concept and demonstrate a greater potential for reduction of rooftop displacement in the nonlinear inelastic model than the equivalent nonlinear elastic model. In short, capturing the inelastic behavior of the buckling restrained braces is an important concept that not only reflects the BRB behavior in a more realistic manner; it demonstrates better capabilities for accounting for the reduction in seismic response.

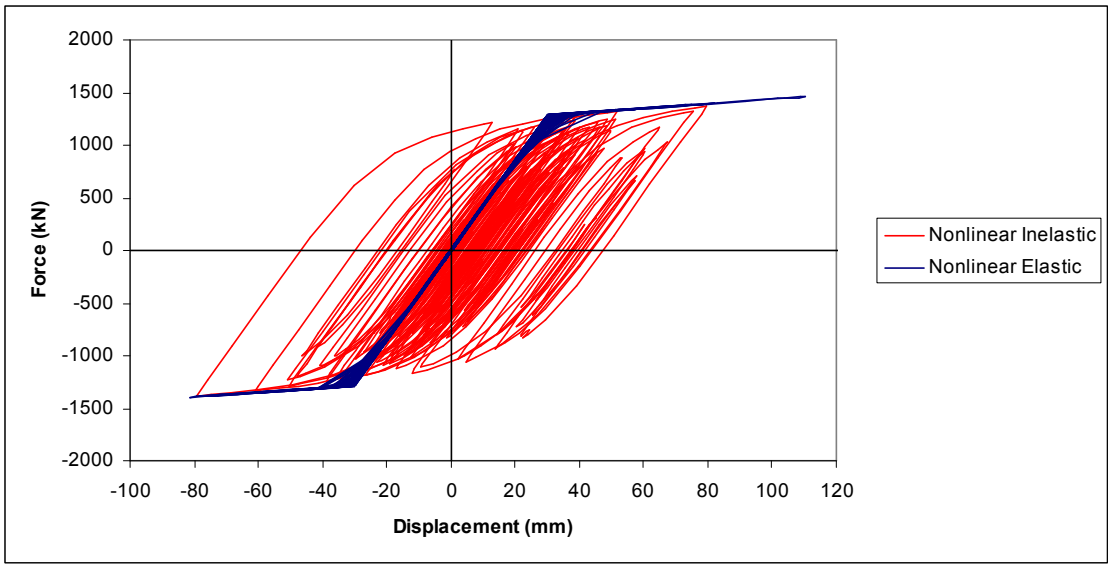

Figure 5.45 Nonlinear Inelastic vs. Nonlinear Elastic Behavior of NRTMDF Braces

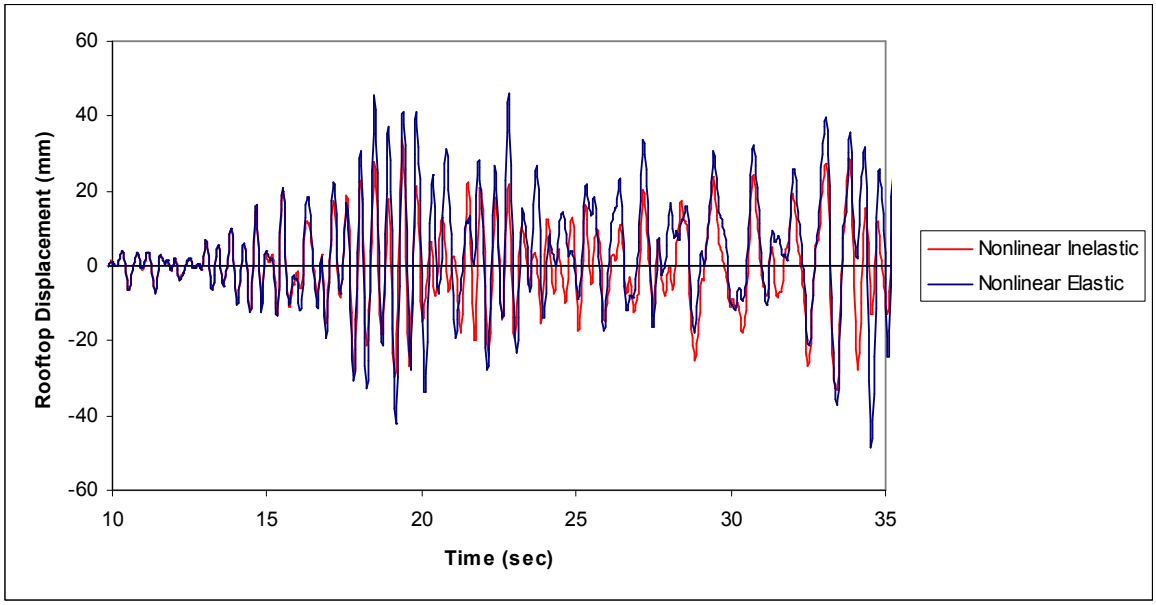

Figure 5.46 BF-4 Rooftop Displacement History for SE18 Nonlinear Inelastic vs. Nonlinear Elastic model, 10 to 35 seconds

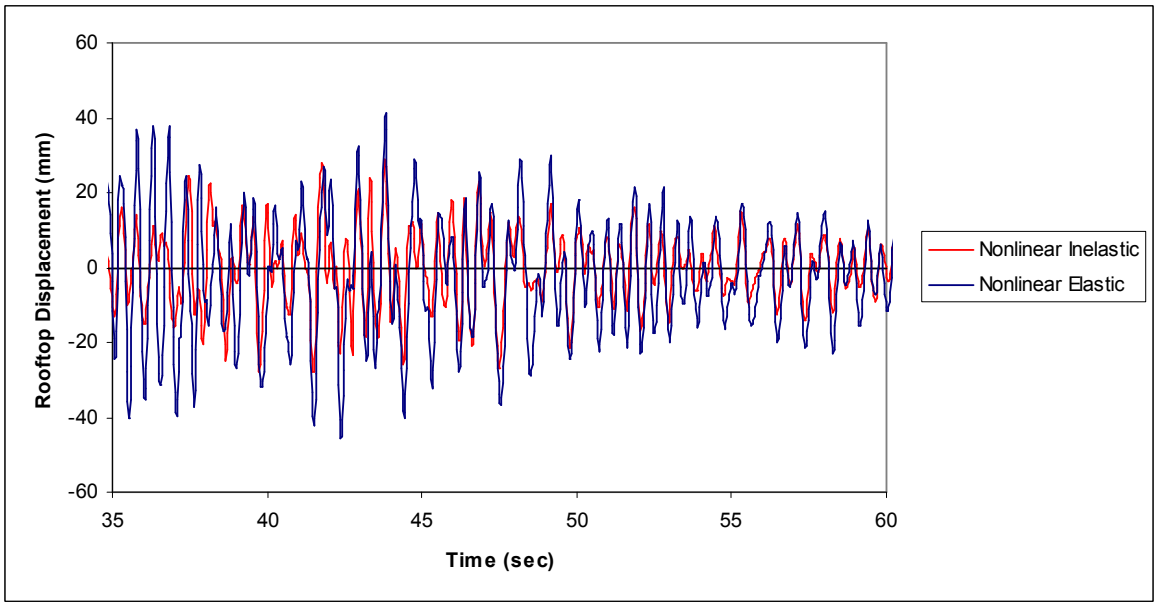

Figure 5.47 BF-4 Rooftop Displacement History for SE18 Nonlinear Inelastic vs. Nonlinear Elastic model, 35 to 60 seconds

6 RESULTS OF NONLINEAR INELASTIC ANALYSES FOR THE BASIC SAFETY OBJECTIVE (BSO)

Prior analyses using the broad array of acceleration records (Chapters 4 and 5) serve the purpose of identifying the nature of structures and ground motions for which the NRTMDF approach for reducing seismic response is effective. However, the diverse array of ground motions utilized does not represent a reasonable scenario in which ground motions would be selected, developed or scaled to represent the expected accelerations for a specific performance objective for a specific building at a given site. The Basic Safety Objective (BSO) included in ASCE 41 represents a reasonable scenario for the selection and utilization of ground motions.[28] Following this methodology, suites of motions reflecting an event with a 10% probability of being exceeded in 50-years at a specific site are utilized and are designated Basic Safety Earthquake 1 (BSE-1). For these motions, Life Safety Performance as outlined in ASCE 41 is the common performance objective. Also, this methodology prescribes analyses for motions having a 2% probability of being exceeded in 50-years, designated Basic Safety Earthquake 2 (BSE-2) for which Collapse Prevention Performance is the performance objective. For response history analyses, ASCE 41 prescribes a minimum of three acceleration records for analysis and indicates that when seven or more records are utilized, the average peak response parameters may be utilized to measure performance rather than the maximum peak response parameters.

In the interest of diversity within the group of considered ground motions, suites representing the Basic Safety Objective have been utilized reflecting hard, medium and soft soil conditions. While medium stiffness sites reflect the majority of conditions, hard sites and soft sites were included to address the upper and lower boundaries of potential soil conditions. Tables 3.3 through 3.5 summarize the ground motions and Figures 3.23 through 3.34 depict the spectra for the motions.

The analysis and optimization of the NRTMDF for this scenario for each suite of ground motions followed an iterative approach with mass targeted at approximately 20% of the total building mass. As outlined previously, the iterative approach enables the determination of parameters based primarily on trial and error directed to convergence upon a near optimal solution based on key output parameters (peak rooftop displacement and base shear). After determining the near optimal NRTMDF properties (mass, stiffness) the properties were altered (initial stiffness, yielding strength, effective stiffness) in accordance with the existing geometry of the rooftop and its constraints regarding a practical NRTMDF configuration. As found in the analyses of Chapter 5, these adjustments in NRTMDF properties did not typically create significant differences in peak output parameters.

Tables 6.1 through 6.30 summarize the structural properties, and the changes in key output parameters enabled by the incorporation of an optimized NRTMDF for each structure for the hard, medium and soft soil conditions. Tables 6.31 through 6.33 outline the average changes in peak output parameters for analyses reflecting hard, medium and soft sites for each of the ten models for the Basic Safety Objective. Results reflecting the magnitudes of displacement and base shear can be found in Appendix C. While the

Table 6.1 Change in Peak Output Parameters for BF-1, Hard Sites

NRTMDF Properties

Mass = 94123 kg
Initial Stiffness = 35.09 kN/mm
Damper Yield Strength = 807.7 kN
Initial Damped Period = 0.38 sec
BSE-1 Avg. Eff. Stiffness = 29.05 kN/mm
BSE-1 Avg. Peak Damped Period = 0.4 sec
BSE-2 Avg. Eff. Stiffness = 14.55 kN/mm
BSE-2 Avg. Peak Damped Period = 0.53 sec

Ground Motions	Base Shear	Rooftop Displacement	NRTMDF Displacement
BSE-1	(% Change)	(% Change)	(mm)
LA20	-17.7%	-20.7%	27
BO7	-27.4%	7.1%	25
SE04	-23.3%	-35.8%	28
LA12	-13.7%	-15.8%	44
SE05	-10.1%	9.2%	28
SE06	-8.5%	-3.9%	36
SE12	-1.1%	-17.9%	26
Average	-14.5%	-11.1%	31
BSE-2			
LA28	-0.1%	-11.3%	60
LA30	-1.8%	-37.2%	79
LA39	0.0%	-3.3%	51
LA33	-1.2%	-24.6%	75
SE39	-1.6%	-36.9%	59
SE25	-1.0%	-15.8%	104
SE30	-1.3%	-30.0%	85
Average	-1.0%	-22.7%	73

Table 6.2 Change in Peak Output Parameters for BF-1, Medium Sites

NRTMDF Properties

Mass = 117646 kg
Initial Stiffness = 24.34 kN/mm
Damper Yield Strength = 468.8 kN
Initial Damped Period = 0.48 sec
BSE-1 Avg. Eff. Stiffness = 13.24 kN/mm
BSE-1 Avg. Peak Damped Period = 0.62 sec
BSE-2 Avg. Eff. Stiffness = 5.63 kN/mm
BSE-2 Avg. Peak Damped Period = 0.92 sec

Ground Motions	Base Shear	Rooftop Displacement	NRTMDF Displacement
BSE-1	(% Change)	(% Change)	(mm)
LA13	-0.1%	-17.3%	49
LA14	-28.8%	-35.9%	38
LA18	-11.9%	-11.9%	42
LA02	-6.5%	-21.8%	53
SE03	-8.4%	-14.0%	53
SE15	-0.1%	-13.2%	34
SE18	0.0%	-3.3%	60
Average	-8.0%	-16.8%	47
BSE-2			
LA23	0.6%	4.1%	125
LA24	4.3%	4.3%	88
SE23	-0.3%	-9.8%	219
LA31	-0.3%	-8.1%	119
LA32	-0.7%	-19.1%	145
SE28	-0.7%	-15.7%	146
SE32	-0.3%	-10.1%	158
Average	0.4%	-7.8%	143

Table 6.3 Change in Peak Output Parameters for BF-1, Soft Sites

NRTMDF Properties

Mass = 94123 kg
Initial Stiffness = 27.8 kN/mm
Damper Yield Strength = 535.5 kN
Initial Damped Period = 0.41 sec
BSE-1 Avg. Eff. Stiffness = 14.47 kN/mm
BSE-1 Avg. Peak Damped Period = 0.53 sec
BSE-2 Avg. Eff. Stiffness = 6.45 kN/mm
BSE-2 Avg. Peak Damped Period = 0.77 sec

Ground Motions	Base Shear	Rooftop Displacement	NRTMDF Displacement
BSE-1	(% Change)	(% Change)	(mm)
SE01	-0.2%	-21.3%	33
LA03	4.7%	10.3%	45
LA15	-0.1%	-8.0%	83
LA09	-4.5%	-24.1%	52
LA10	-0.5%	-20.3%	58
LA07	0.0%	-8.1%	40
SE07	-0.3%	-30.5%	67
Average	-0.1%	-14.6%	54
BSE-2			
LA38	0.9%	25.6%	269
LA40	0.4%	12.8%	151
SE24	0.3%	8.4%	242
LA35	-1.0%	-22.5%	202
LA36	-1.0%	-26.5%	137
SE33	-5.8%	-26.8%	113
SE36	0.1%	5.4%	167
Average	-0.9%	-3.4%	183

Table 6.4 Change in Peak Output Parameters for BF-2, Hard Sites

NRTMDF Properties

Mass = 403278 kg
Initial Stiffness = 104.13 kN/mm
Damper Yield Strength = 3265.8 kN
Initial Damped Period = 0.46 sec
BSE-1 Avg. Eff. Stiffness = 87.37 kN/mm
BSE-1 Avg. Peak Damped Period = 0.49 sec
BSE-2 Avg. Eff. Stiffness = 48.95 kN/mm
BSE-2 Avg. Peak Damped Period = 0.61 sec

Ground Motions	Base Shear	Rooftop Displacement	NRTMDF Displacement
BSE-1	(% Change)	(% Change)	(mm)
LA20	-14.8%	-37.9%	24
BO7	-12.3%	-38.3%	24
SE04	-13.4%	-31.6%	45
LA12	3.4%	8.8%	67
SE05	-11.5%	-31.1%	33
SE06	-5.2%	-15.6%	42
SE12	-6.5%	-19.3%	37
Average	-8.6%	-23.6%	39
BSE-2			
LA28	-6.9%	-36.0%	86
LA30	-1.7%	-13.7%	114
LA39	-11.3%	-27.2%	88
LA33	-9.4%	-34.8%	60
SE39	-13.0%	-45.1%	90
SE25	-4.9%	-38.3%	96
SE30	-3.2%	-28.1%	102
Average	-7.2%	-31.9%	91

Table 6.5 Change in Peak Output Parameters for BF-2, Medium Sites

NRTMDF Properties

Mass = 293298 kg
Initial Stiffness = 104.13 kN/mm
Damper Yield Strength = 3265.8 kN
Initial Damped Period = 0.4 sec
BSE-1 Avg. Eff. Stiffness = 81.25 kN/mm
BSE-1 Avg. Peak Damped Period = 0.43 sec
BSE-2 Avg. Eff. Stiffness = 51.62 kN/mm
BSE-2 Avg. Peak Damped Period = 0.51 sec

Ground Motions	Base Shear	Rooftop Displacement	NRTMDF Displacement
BSE-1	(% Change)	(% Change)	(mm)
LA13	-13.6%	-31.1%	39
LA14	-18.1%	-43.2%	32
LA18	-9.3%	-22.2%	51
LA02	-3.3%	-9.1%	31
SE03	-9.6%	-23.9%	32
SE15	-8.2%	-21.1%	29
SE18	-12.0%	-27.1%	43
Average	-10.6%	-25.4%	37
BSE-2			
LA23	-1.6%	-3.4%	79
LA24	4.4%	11.3%	46
SE23	-4.9%	-38.2%	116
LA31	-7.6%	-49.3%	91
LA32	-3.9%	-27.7%	115
SE28	-4.5%	-32.3%	85
SE32	3.3%	30.3%	104
Average	-2.1%	-15.6%	91

Table 6.6 Change in Peak Output Parameters for BF-2, Soft Sites

NRTMDF Properties

Mass = 348291 kg
Initial Stiffness = 69.14 kN/mm
Damper Yield Strength = 2168.4 kN
Initial Damped Period = 0.5 sec
BSE-1 Avg. Eff. Stiffness = 43.4 kN/mm
BSE-1 Avg. Peak Damped Period = 0.6 sec
BSE-2 Avg. Eff. Stiffness = 19.97 kN/mm
BSE-2 Avg. Peak Damped Period = 0.85 sec

Ground Motions	Base Shear	Rooftop Displacement	NRTMDF Displacement
BSE-1	(% Change)	(% Change)	(mm)
SE01	5.5%	15.0%	52
LA03	-11.2%	-26.6%	59
LA15	-13.6%	-29.6%	88
LA09	12.3%	34.7%	76
LA10	-6.1%	-12.5%	85
LA07	-0.5%	-1.2%	105
SE07	-15.4%	-31.1%	60
Average	-4.1%	-7.3%	75
BSE-2			
LA38	7.9%	20.1%	279
LA40	2.2%	4.4%	159
SE24	-0.5%	-4.3%	285
LA35	-1.5%	-15.6%	303
LA36	-1.2%	-13.8%	207
SE33	-3.9%	-21.0%	207
SE36	10.9%	24.3%	215
Average	2.0%	-0.8%	236

Table 6.7 Change in Peak Output Parameters for BF-3, Hard Sites

NRTMDF Properties

Mass = 624467 kg
Initial Stiffness = 124.79 kN/mm
Damper Yield Strength = 2993.6 kN
Initial Damped Period = 0.63 sec
BSE-1 Avg. Eff. Stiffness = 89.9 kN/mm
BSE-1 Avg. Peak Damped Period = 0.68 sec
BSE-2 Avg. Eff. Stiffness = 32.1 kN/mm
BSE-2 Avg. Peak Damped Period = 0.96 sec

Ground Motions	Base Shear	Rooftop Displacement	NRTMDF Displacement
BSE-1	(% Change)	(% Change)	(mm)
LA20	6.7%	-19.3%	25
BO7	17.3%	2.3%	33
SE04	-26.5%	-30.7%	34
LA12	-20.5%	-48.2%	44
SE05	-15.3%	-17.0%	60
SE06	5.2%	-18.4%	78
SE12	-36.1%	4.4%	42
Average	-9.9%	-18.1%	45
BSE-2			
LA28	-0.3%	-34.0%	236
LA30	-2.4%	-39.4%	130
LA39	-2.2%	-27.9%	131
LA33	-1.0%	-28.3%	117
SE39	-0.1%	-6.8%	102
SE25	-1.5%	-28.1%	225
SE30	-2.5%	-45.7%	160
Average	-1.4%	-30.0%	157

Table 6.8 Change in Peak Output Parameters for BF-3, Medium Sites

NRTMDF Properties

Mass = 524555 kg
Initial Stiffness = 67.7 kN/mm
Damper Yield Strength = 1624.1 kN
Initial Damped Period = 0.68 sec
BSE-1 Avg. Eff. Stiffness = 27.2 kN/mm
BSE-1 Avg. Peak Damped Period = 0.94 sec
BSE-2 Avg. Eff. Stiffness = 11.67 kN/mm
BSE-2 Avg. Peak Damped Period = 1.37 sec

Ground Motions	Base Shear	Rooftop Displacement	NRTMDF Displacement
BSE-1	(% Change)	(% Change)	(mm)
LA13	0.0%	2.3%	117
LA14	14.1%	14.1%	85
LA18	-0.3%	-35.8%	121
LA02	-17.5%	-21.6%	70
SE03	-16.2%	-16.2%	94
SE15	0.2%	5.8%	92
SE18	-0.7%	-37.3%	90
Average	-2.9%	-12.7%	96
BSE-2			
LA23	-2.3%	-34.2%	170
LA24	-0.2%	-24.4%	203
SE23	-0.7%	-11.3%	302
LA31	-0.4%	-35.7%	188
LA32	0.1%	14.9%	256
SE28	0.1%	5.0%	350
SE32	-1.5%	-27.6%	231
Average	-0.7%	-16.2%	243

Table 6.9 Change in Peak Output Parameters for BF-3, Soft Sites

NRTMDF Properties

Mass = 499577 kg
Initial Stiffness = 56.35 kN/mm
Damper Yield Strength = 1352 kN
Initial Damped Period = 0.7 sec
BSE-1 Avg. Eff. Stiffness = 15.41 kN/mm
BSE-1 Avg. Peak Damped Period = 1.18 sec
BSE-2 Avg. Eff. Stiffness = 5.66 kN/mm
BSE-2 Avg. Peak Damped Period = 1.89 sec

Ground Motions	Base Shear	Rooftop Displacement	NRTMDF Displacement
BSE-1	(% Change)	(% Change)	(mm)
SE01	-0.4%	-24.1%	154
LA03	0.1%	13.4%	179
LA15	-1.2%	-24.8%	210
LA09	0.0%	3.1%	219
LA10	-1.0%	-30.5%	133
LA07	-7.0%	-29.7%	108
SE07	-0.8%	-30.2%	155
Average	-1.5%	-17.5%	165
BSE-2			
LA38	1.7%	17.9%	958
LA40	-2.4%	-32.5%	1000
SE24	-0.1%	-9.7%	712
LA35	-0.2%	-21.4%	805
LA36	-0.1%	-13.4%	631
SE33	-18.0%	-23.3%	455
SE36	-0.6%	-8.4%	489
Average	-2.8%	-13.0%	721

Table 6.10 Change in Peak Output Parameters for BF-4, Hard Sites

NRTMDF Properties

Mass = 898979 kg	BSE-1 Avg. Eff. Stiffness = 33.12 kN/mm
Initial Stiffness = 61.31 kN/mm	BSE-1 Avg. Peak Damped Period = 1.22 sec
Damper Yield Strength = 1764.6 kN	BSE-2 Avg. Eff. Stiffness = 10.81 kN/mm
Initial Damped Period = 1.03 sec	BSE-2 Avg. Peak Damped Period = 1.91 sec

Ground Motions	Base Shear	Rooftop Displacement	NRTMDF Displacement
BSE-1	(% Change)	(% Change)	(mm)
LA20	-16.6%	-16.7%	82
BO7	-37.5%	-41.3%	45
SE04	2.1%	-11.7%	62
LA12	-14.0%	-42.9%	52
SE05	-37.7%	-40.0%	66
SE06	-36.7%	-37.4%	65
SE12	-30.1%	-51.5%	75
Average	-24.4%	-34.5%	64
BSE-2			
LA28	-0.6%	-23.0%	261
LA30	-0.4%	-13.8%	414
LA39	-0.8%	-28.1%	263
LA33	-1.0%	-39.2%	263
SE39	-0.9%	-37.9%	192
SE25	-1.1%	-35.0%	280
SE30	-8.5%	-15.8%	181
Average	-1.9%	-27.6%	265

Table 6.11 Change in Peak Output Parameters for BF-4, Medium Sites

NRTMDF Properties

Mass = 719186 kg
Initial Stiffness = 71.8 kN/mm
Damper Yield Strength = 2440.5 kN
Initial Damped Period = 0.92 sec
BSE-1 Avg. Eff. Stiffness = 34.56 kN/mm
BSE-1 Avg. Peak Damped Period = 1.09 sec
BSE-2 Avg. Eff. Stiffness = 11.42 kN/mm
BSE-2 Avg. Peak Damped Period = 1.67 sec

Ground Motions	Base Shear	Rooftop Displacement	NRTMDF Displacement
BSE-1	(% Change)	(% Change)	(mm)
LA13	-7.0%	-31.0%	166
LA14	-23.9%	-51.2%	107
LA18	-25.1%	-32.2%	105
LA02	-19.7%	-46.8%	91
SE03	-24.4%	-57.0%	119
SE15	-10.6%	-26.0%	91
SE18	-28.6%	-60.9%	79
Average	-19.9%	-43.6%	108
BSE-2			
LA23	-4.2%	-44.3%	283
LA24	7.6%	-47.4%	270
SE23	-1.9%	-23.3%	538
LA31	-4.8%	-47.8%	301
LA32	-5.4%	-46.5%	402
SE28	-3.5%	-30.7%	414
SE32	-4.9%	-46.1%	361
Average	-2.5%	-40.9%	367

Table 6.12 Change in Peak Output Parameters for BF-4, Soft Sites

NRTMDF Properties

Mass = 898979 kg
Initial Stiffness = 48.18 kN/mm
Damper Yield Strength = 1352 kN
Initial Damped Period = 1.1 sec
BSE-1 Avg. Eff. Stiffness = 8.51 kN/mm
BSE-1 Avg. Peak Damped Period = 2.13 sec
BSE-2 Avg. Eff. Stiffness = 4.22 kN/mm
BSE-2 Avg. Peak Damped Period = 2.96 sec

Ground Motions	Base Shear	Rooftop Displacement	NRTMDF Displacement
BSE-1	(% Change)	(% Change)	(mm)
SE01	-0.5%	-6.5%	542
LA03	-0.5%	-9.1%	292
LA15	-1.0%	-20.3%	329
LA09	-1.3%	-23.6%	283
LA10	-1.1%	-22.4%	158
LA07	-1.9%	-29.4%	212
SE07	-1.6%	-15.2%	192
Average	-1.1%	-18.1%	287
BSE-2			
LA38	-0.5%	-2.8%	1259
LA40	1.5%	19.3%	1254
SE24	-2.5%	-13.9%	963
LA35	-19.3%	-19.9%	1129
LA36	0.1%	12.0%	912
SE33	-1.6%	-15.4%	458
SE36	-5.1%	-27.3%	510
Average	-3.9%	-6.9%	926

Table 6.13 Change in Peak Output Parameters for BF-5, Hard Sites

NRTMDF Properties

Mass = 930184 kg
Initial Stiffness = 27.86 kN/mm
Damper Yield Strength = 676 kN
Initial Damped Period = 1.73 sec
BSE-1 Avg. Eff. Stiffness = 9.73 kN/mm
BSE-1 Avg. Peak Damped Period = 2.28 sec
BSE-2 Avg. Eff. Stiffness = 3.19 kN/mm
BSE-2 Avg. Peak Damped Period = 3.57 sec

Ground Motions	Base Shear	Rooftop Displacement	NRTMDF Displacement
BSE-1	(% Change)	(% Change)	(mm)
LA20	-29.4%	-40.1%	116
BO7	8.2%	-6.6%	65
SE04	-24.9%	-57.6%	128
LA12	-32.0%	-28.8%	119
SE05	-37.8%	-30.6%	93
SE06	-38.6%	-44.9%	90
SE12	-37.2%	-52.8%	80
Average	-27.4%	-37.3%	99
BSE-2			
LA28	-3.5%	-17.6%	475
LA30	0.5%	3.4%	759
LA39	-2.1%	-14.0%	614
LA33	-8.1%	-29.5%	528
SE39	-12.0%	-38.5%	345
SE25	-7.1%	-19.5%	310
SE30	-20.2%	-39.5%	254
Average	-7.5%	-22.2%	469

Table 6.14 Change in Peak Output Parameters for BF-5, Medium Sites

NRTMDF Properties

Mass = 1162738 kg
Initial Stiffness = 44.51 kN/mm
Damper Yield Strength = 1079.8 kN
Initial Damped Period = 1.76 sec
BSE-1 Avg. Eff. Stiffness = 18.3 kN/mm
BSE-1 Avg. Peak Damped Period = 2.09 sec
BSE-2 Avg. Eff. Stiffness = 6.47 kN/mm
BSE-2 Avg. Peak Damped Period = 2.95 sec

Ground Motions	Base Shear	Rooftop Displacement	NRTMDF Displacement
BSE-1	(% Change)	(% Change)	(mm)
LA13	-36.7%	-49.5%	105
LA14	-39.0%	-42.2%	174
LA18	-31.8%	-8.9%	120
LA02	-41.3%	-57.0%	117
SE03	-28.0%	-36.2%	118
SE15	-2.5%	-16.0%	157
SE18	-35.9%	-41.8%	116
Average	-30.7%	-36.0%	130
BSE-2			
LA23	-0.6%	-1.9%	516
LA24	-5.9%	-19.9%	564
SE23	-6.6%	-23.4%	599
LA31	-11.5%	-41.5%	402
LA32	-4.7%	-22.5%	508
SE28	-10.7%	-38.0%	312
SE32	-6.0%	-40.5%	470
Average	-6.6%	-26.8%	481

Table 6.15 Change in Peak Output Parameters for BF-5, Soft Sites

NRTMDF Properties

Mass = 775159 kg
Initial Stiffness = 72.73 kN/mm
Damper Yield Strength = 1624.1 kN
Initial Damped Period = 1.47 sec
BSE-1 Avg. Eff. Stiffness = 10.22 kN/mm
BSE-1 Avg. Peak Damped Period = 2.06 sec
BSE-2 Avg. Eff. Stiffness = 5.12 kN/mm
BSE-2 Avg. Peak Damped Period = 2.66 sec

Ground Motions	Base Shear	Rooftop Displacement	NRTMDF Displacement
BSE-1	(% Change)	(% Change)	(mm)
SE01	-1.3%	-3.9%	406
LA03	-5.9%	-24.4%	373
LA15	-5.9%	-24.6%	469
LA09	-2.5%	-6.9%	444
LA10	-20.1%	-47.4%	212
LA07	-9.7%	-37.1%	243
SE07	-26.6%	-58.5%	208
Average	-10.3%	-29.0%	336
BSE-2			
LA38	-0.7%	-3.2%	1944
LA40	-3.6%	-13.3%	1894
SE24	-3.6%	-18.3%	1493
LA35	-6.5%	-8.5%	1407
LA36	-2.2%	-11.6%	1318
SE33	-8.0%	-29.8%	999
SE36	-8.2%	-30.4%	1203
Average	-4.7%	-16.4%	1466

Table 6.16 Change in Peak Output Parameters for EBF-1, Hard Sites

NRTMDF Properties

Mass = 882420 kg
Initial Stiffness = 47.81 kN/mm
Damper Yield Strength = 1352 kN
Initial Damped Period = 1.11 sec
BSE-1 Avg. Eff. Stiffness = 28.18 kN/mm
BSE-1 Avg. Peak Damped Period = 1.3 sec
BSE-2 Avg. Eff. Stiffness = 9.14 kN/mm
BSE-2 Avg. Peak Damped Period = 2.06 sec

Ground Motions	Base Shear	Rooftop Displacement	NRTMDF Displacement
BSE-1	(% Change)	(% Change)	(mm)
LA20	-25.4%	-24.4%	55
BO7	-21.0%	-43.9%	36
SE04	4.7%	-23.4%	106
LA12	-10.0%	-30.0%	63
SE05	-21.0%	-30.2%	89
SE06	-31.8%	-36.1%	58
SE12	-39.3%	-56.7%	72
Average	-20.6%	-35.0%	68
BSE-2			
LA28	-3.5%	-16.4%	255
LA30	-8.2%	-32.6%	389
LA39	-9.7%	-40.1%	277
LA33	-2.4%	-16.5%	231
SE39	-4.2%	-24.9%	170
SE25	-8.8%	-35.8%	228
SE30	-7.3%	-33.1%	163
Average	-6.3%	-28.5%	245

Table 6.17 Change in Peak Output Parameters for EBF-1, Medium Sites

NRTMDF Properties

Mass = 564758 kg
Initial Stiffness = 62.4 kN/mm
Damper Yield Strength = 1764.6 kN
Initial Damped Period = 0.86 sec
BSE-1 Avg. Eff. Stiffness = 28.99 kN/mm
BSE-1 Avg. Peak Damped Period = 1.05 sec
BSE-2 Avg. Eff. Stiffness = 10.49 kN/mm
BSE-2 Avg. Peak Damped Period = 1.55 sec

Ground Motions	Base Shear	Rooftop Displacement	NRTMDF Displacement
BSE-1	(% Change)	(% Change)	(mm)
LA13	-5.6%	-37.8%	122
LA14	-2.3%	-19.4%	79
LA18	-3.6%	-28.3%	106
LA02	-6.2%	-41.8%	88
SE03	-12.2%	-52.7%	98
SE15	12.6%	18.9%	66
SE18	-18.7%	-44.1%	67
Average	-5.1%	-29.3%	89
BSE-2			
LA23	-9.5%	-38.9%	250
LA24	-8.7%	-41.9%	281
SE23	-3.9%	-16.0%	432
LA31	-3.3%	-14.6%	228
LA32	-5.1%	-21.3%	379
SE28	-15.0%	-41.5%	326
SE32	-11.5%	-38.5%	302
Average	-8.1%	-30.4%	314

Table 6.18 Change in Peak Output Parameters for EBF-1, Soft Sites

NRTMDF Properties

Mass = 1058915 kg
Initial Stiffness = 43.15 kN/mm
Damper Yield Strength = 1220.3 kN
Initial Damped Period = 1.24 sec
BSE-1 Avg. Eff. Stiffness = 7.7 kN/mm
BSE-1 Avg. Peak Damped Period = 2.44 sec
BSE-2 Avg. Eff. Stiffness = 3.94 kN/mm
BSE-2 Avg. Peak Damped Period = 3.33 sec

Ground Motions	Base Shear	Rooftop Displacement	NRTMDF Displacement
BSE-1	(% Change)	(% Change)	(mm)
SE01	-0.7%	-4.3%	562
LA03	1.2%	8.9%	387
LA15	-2.3%	-14.7%	200
LA09	-2.7%	-18.0%	344
LA10	-3.0%	-20.3%	278
LA07	-6.7%	-35.7%	218
SE07	-3.6%	-24.8%	199
Average	-2.6%	-15.6%	313
BSE-2			
LA38	0.8%	3.6%	1271
LA40	0.6%	3.2%	1156
SE24	-5.7%	-23.8%	816
LA35	-9.7%	-31.1%	1165
LA36	-7.4%	-28.2%	980
SE33	-2.3%	-10.6%	410
SE36	-0.7%	-3.5%	519
Average	-3.5%	-12.9%	902

Table 6.19 Change in Peak Output Parameters for SW-1, Hard Sites

NRTMDF Properties

Mass = 1024991 kg
Initial Stiffness = 248.72 kN/mm
Damper Yield Strength = 4082.2 kN
Initial Damped Period = 0.57 sec
BSE-1 Avg. Eff. Stiffness = 151.01 kN/mm
BSE-1 Avg. Peak Damped Period = 0.64 sec
BSE-2 Avg. Eff. Stiffness = 56.56 kN/mm
BSE-2 Avg. Peak Damped Period = 0.92 sec

Ground Motions	Base Shear	Rooftop Displacement	NRTMDF Displacement
BSE-1	(% Change)	(% Change)	(mm)
LA20	-20.2%	-25.1%	30
BO7	-6.6%	5.9%	26
SE04	-23.5%	-55.1%	25
LA12	-34.3%	-30.4%	41
SE05	-35.1%	-30.1%	63
SE06	-28.4%	-28.5%	47
SE12	-18.3%	-15.9%	42
Average	-23.8%	-25.6%	39
BSE-2			
LA28	-25.1%	-27.4%	207
LA30	-21.0%	-34.4%	98
LA39	-26.1%	-44.0%	119
LA33	-28.8%	-47.6%	118
SE39	-27.8%	-45.0%	78
SE25	-21.5%	-36.0%	117
SE30	-8.2%	-52.5%	134
Average	-22.6%	-41.0%	125

Table 6.20 Change in Peak Output Parameters for SW-1, Medium Sites

NRTMDF Properties

Mass = 885209 kg
Initial Stiffness = 140.94 kN/mm
Damper Yield Strength = 4626.5 kN
Initial Damped Period = 0.62 sec
BSE-1 Avg. Eff. Stiffness = 125.49 kN/mm
BSE-1 Avg. Peak Damped Period = 0.64 sec
BSE-2 Avg. Eff. Stiffness = 43.15 kN/mm
BSE-2 Avg. Peak Damped Period = 0.96 sec

Ground Motions	Base Shear	Rooftop Displacement	NRTMDF Displacement
BSE-1	(% Change)	(% Change)	(mm)
LA13	-27.1%	-29.4%	60
LA14	-8.7%	7.6%	35
LA18	-36.2%	-36.9%	65
LA02	0.7%	14.6%	56
SE03	0.2%	6.0%	52
SE15	-1.3%	-19.6%	35
SE18	-2.9%	-35.4%	56
Average	-10.8%	-13.3%	51
BSE-2			
LA23	-17.4%	-8.1%	162
LA24	14.4%	5.7%	111
SE23	-19.8%	-27.9%	214
LA31	-18.4%	-22.2%	184
LA32	4.4%	7.3%	210
SE28	-10.6%	-31.7%	171
SE32	-14.5%	3.4%	180
Average	-8.8%	-10.5%	176

Table 6.21 Change in Peak Output Parameters for SW-1, Soft Sites

NRTMDF Properties

Mass = 978403 kg
Initial Stiffness = 148.69 kN/mm
Damper Yield Strength = 2440.5 kN
Initial Damped Period = 0.63 sec
BSE-1 Avg. Eff. Stiffness = 99.07 kN/mm
BSE-1 Avg. Peak Damped Period = 0.72 sec
BSE-2 Avg. Eff. Stiffness = 37.42 kN/mm
BSE-2 Avg. Peak Damped Period = 1.07 sec

Ground Motions	Base Shear	Rooftop Displacement	NRTMDF Displacement
BSE-1	(% Change)	(% Change)	(mm)
SE01	2.9%	7.8%	68
LA03	-22.2%	-17.6%	86
LA15	-30.2%	-19.5%	120
LA09	19.8%	14.9%	76
LA10	-7.9%	-19.4%	79
LA07	1.2%	-4.0%	91
SE07	-20.2%	-23.2%	78
Average	-8.1%	-8.7%	85
BSE-2			
LA38	1.7%	18.6%	395
LA40	-0.4%	-3.9%	286
SE24	-1.9%	-13.4%	366
LA35	-3.2%	-20.2%	337
LA36	0.0%	-0.2%	289
SE33	-2.0%	-10.3%	432
SE36	-0.2%	-2.7%	296
Average	-0.9%	-4.6%	343

Table 6.22 Change in Peak Output Parameters for SW-2, Hard Sites

NRTMDF Properties

Mass = 2936068 kg	BSE-1 Avg. Eff. Stiffness = 392.81 kN/mm
Initial Stiffness = 459.01 kN/mm	BSE-1 Avg. Peak Damped Period = 0.72 sec
Damper Yield Strength = 14985.7 kN	BSE-2 Avg. Eff. Stiffness = 140.54 kN/mm
Initial Damped Period = 0.7 sec	BSE-2 Avg. Peak Damped Period = 1.01 sec

Ground Motions	Base Shear	Rooftop Displacement	NRTMDF Displacement
BSE-1	(% Change)	(% Change)	(mm)
LA20	-0.6%	-14.0%	34
BO7	0.5%	16.0%	45
SE04	-2.2%	-41.6%	38
LA12	-3.4%	-49.4%	47
SE05	-1.0%	-25.2%	46
SE06	-1.4%	-28.7%	52
SE12	-0.4%	-12.0%	44
Average	-1.2%	-22.1%	44
BSE-2			
LA28	-5.8%	-38.7%	273
LA30	-4.2%	-33.1%	125
LA39	-3.0%	-29.3%	152
LA33	-2.4%	-26.3%	122
SE39	0.1%	1.4%	131
SE25	-3.9%	-33.0%	198
SE30	-8.0%	-54.5%	159
Average	-3.9%	-30.5%	166

Table 6.23 Change in Peak Output Parameters for SW-2, Medium Sites

NRTMDF Properties

Mass = 2936068 kg
Initial Stiffness = 250.35 kN/mm
Damper Yield Strength = 8173.2 kN
Initial Damped Period = 0.82 sec
BSE-1 Avg. Eff. Stiffness = 126.17 kN/mm
BSE-1 Avg. Peak Damped Period = 1.05 sec
BSE-2 Avg. Eff. Stiffness = 52.49 kN/mm
BSE-2 Avg. Peak Damped Period = 1.54 sec

Ground Motions	Base Shear	Rooftop Displacement	NRTMDF Displacement
BSE-1	(% Change)	(% Change)	(mm)
LA13	-0.5%	-10.1%	132
LA14	0.9%	24.5%	73
LA18	-2.1%	-27.7%	134
LA02	-0.9%	-17.2%	81
SE03	-1.4%	-30.0%	72
SE15	0.3%	6.1%	116
SE18	-3.0%	-39.0%	57
Average	-1.0%	-13.3%	95
BSE-2			
LA23	-4.8%	-10.1%	178
LA24	-2.0%	24.5%	257
SE23	-1.0%	-27.7%	333
LA31	-5.8%	-17.2%	186
LA32	0.2%	-30.0%	263
SE28	0.2%	6.1%	375
SE32	-5.0%	-39.0%	220
Average	-2.6%	-13.3%	259

Table 6.24 Change in Peak Output Parameters for SW-2, Soft Sites

NRTMDF Properties

Mass = 2936068 kg
Initial Stiffness = 208.4 kN/mm
Damper Yield Strength = 6803.7 kN
Initial Damped Period = 0.87 sec
BSE-1 Avg. Eff. Stiffness = 82.8 kN/mm
BSE-1 Avg. Peak Damped Period = 1.26 sec
BSE-2 Avg. Eff. Stiffness = 29.51 kN/mm
BSE-2 Avg. Peak Damped Period = 2.02 sec

Ground Motions	Base Shear	Rooftop Displacement	NRTMDF Displacement
BSE-1	(% Change)	(% Change)	(mm)
SE01	-0.9%	-14.0%	180
LA03	1.1%	15.3%	179
LA15	-2.5%	-26.2%	224
LA09	-0.5%	-7.2%	185
LA10	-2.2%	-25.0%	150
LA07	-1.3%	-20.3%	140
SE07	-2.5%	-28.4%	176
Average	-1.3%	-15.1%	176
BSE-2			
LA38	1.9%	21.8%	1032
LA40	-5.4%	-35.0%	1058
SE24	-2.2%	-16.3%	730
LA35	-2.7%	-21.7%	779
LA36	-1.5%	-12.0%	628
SE33	-5.8%	-30.3%	468
SE36	0.1%	1.7%	485
Average	-2.2%	-13.1%	740

Table 6.25 Change in Peak Output Parameters for MF-1, Hard Sites

NRTMDF Properties

Mass = 799172 kg
Initial Stiffness = 31.37 kN/mm
Damper Yield Strength = 948.1 kN
Initial Damped Period = 1.96 sec
BSE-1 Avg. Eff. Stiffness = 18.33 kN/mm
BSE-1 Avg. Peak Damped Period = 2.07 sec
BSE-2 Avg. Eff. Stiffness = 4.27 kN/mm
BSE-2 Avg. Peak Damped Period = 3.04 sec

Ground Motions	Base Shear	Rooftop Displacement	NRTMDF Displacement
BSE-1	(% Change)	(% Change)	(mm)
LA20	-30.5%	-27.8%	108
BO7	-10.6%	-13.0%	61
SE04	-14.2%	4.1%	118
LA12	-9.8%	-27.5%	55
SE05	-7.3%	-3.8%	66
SE06	-20.4%	-17.5%	89
SE12	-19.3%	-39.1%	62
Average	-18.9%	-17.8%	80
BSE-2			
LA28	-7.2%	-14.7%	435
LA30	-6.8%	-12.9%	678
LA39	-15.3%	-26.8%	549
LA33	-15.1%	-25.1%	684
SE39	-13.9%	-26.8%	346
SE25	-26.6%	-34.5%	237
SE30	-31.1%	-47.1%	274
Average	-16.6%	-26.8%	457

Table 6.26 Change in Peak Output Parameters for MF-1 Medium Sites

NRTMDF Properties

Mass = 998961 kg
Initial Stiffness = 26.72 kN/mm
Damper Yield Strength = 807.7 kN
Initial Damped Period = 2.14 sec
BSE-1 Avg. Eff. Stiffness = 7.49 kN/mm
BSE-1 Avg. Peak Damped Period = 2.78 sec
BSE-2 Avg. Eff. Stiffness = 2.73 kN/mm
BSE-2 Avg. Peak Damped Period = 4.07 sec

Ground Motions	Base Shear	Rooftop Displacement	NRTMDF Displacement
BSE-1	(% Change)	(% Change)	(mm)
LA13	-50.7%	-52.7%	110
LA14	-42.4%	-47.1%	173
LA18	-12.2%	-13.4%	171
LA02	14.0%	14.0%	183
SE03	-14.6%	-14.6%	267
SE15	-18.3%	-19.8%	272
SE18	-54.6%	-57.6%	146
Average	-25.5%	-27.3%	189
BSE-2			
LA23	-18.3%	-25.6%	729
LA24	-23.4%	-35.9%	1258
SE23	-12.2%	-19.9%	853
LA31	-25.2%	-38.8%	701
LA32	-12.9%	-20.1%	507
SE28	-29.1%	-45.2%	440
SE32	-18.7%	-33.5%	450
Average	-20.0%	-31.3%	705

Table 6.27 Change in Peak Output Parameters for MF-1, Soft Sites

NRTMDF Properties

Mass = 799172 kg
Initial Stiffness = 31.37 kN/mm
Damper Yield Strength = 948.1 kN
Initial Damped Period = 1.96 sec
BSE-1 Avg. Eff. Stiffness = 4.11 kN/mm
BSE-1 Avg. Peak Damped Period = 3.09 sec
BSE-2 Avg. Eff. Stiffness = 2.23 kN/mm
BSE-2 Avg. Peak Damped Period = 3.98 sec

Ground Motions	Base Shear	Rooftop Displacement	NRTMDF Displacement
BSE-1	(% Change)	(% Change)	(mm)
SE01	-6.6%	-13.3%	1036
LA03	4.0%	9.1%	743
LA15	-13.3%	-25.6%	346
LA09	-27.2%	-43.0%	451
LA10	-31.9%	-51.0%	521
LA07	-23.2%	-30.1%	367
SE07	-35.0%	-47.0%	186
Average	-19.0%	-28.7%	521
BSE-2			
LA38	-1.7%	-8.9%	2618
LA40	-1.2%	-19.0%	2425
SE24	-0.5%	-10.5%	1890
LA35	-12.8%	-25.7%	1057
LA36	-5.2%	-22.6%	1729
SE33	-19.4%	-32.3%	1031
SE36	-5.8%	-17.3%	1233
Average	-6.7%	-19.5%	1712

Table 6.28 Change in Peak Output Parameters for MF-2, Hard Sites

NRTMDF Properties

Mass = 2915283 kg
Initial Stiffness = 75.88 kN/mm
Damper Yield Strength = 1352 kN
Initial Damped Period = 2.63 sec
BSE-1 Avg. Eff. Stiffness = 18.34 kN/mm
BSE-1 Avg. Peak Damped Period = 3.2 sec
BSE-2 Avg. Eff. Stiffness = 6.25 kN/mm
BSE-2 Avg. Peak Damped Period = 4.64 sec

Ground Motions	Base Shear	Rooftop Displacement	NRTMDF Displacement
BSE-1	(% Change)	(% Change)	(mm)
LA20	-21.0%	-36.1%	139
BO7	-43.5%	-22.0%	89
SE04	-18.8%	2.3%	158
LA12	-12.9%	16.0%	85
SE05	-43.8%	-34.1%	140
SE06	-18.6%	-23.9%	138
SE12	-30.1%	-35.5%	94
Average	-27.0%	-19.1%	120
BSE-2			
LA28	-4.6%	-20.3%	634
LA30	-2.2%	-8.9%	1701
LA39	-5.1%	-21.6%	804
LA33	-3.9%	-15.3%	919
SE39	-14.8%	-31.7%	390
SE25	-13.0%	-24.8%	580
SE30	-26.3%	-28.3%	271
Average	-10.0%	-21.5%	757

Table 6.29 Change in Peak Output Parameters for MF-2, Medium Sites

NRTMDF Properties

Mass = 4164672 kg
Initial Stiffness = 136.99 kN/mm
Damper Yield Strength = 2440.5 kN
Initial Damped Period = 2.82 sec
BSE-1 Avg. Eff. Stiffness = 27.76 kN/mm
BSE-1 Avg. Peak Damped Period = 3.36 sec
BSE-2 Avg. Eff. Stiffness = 11.15 kN/mm
BSE-2 Avg. Peak Damped Period = 4.39 sec

Ground Motions	Base Shear	Rooftop Displacement	NRTMDF Displacement
BSE-1	(% Change)	(% Change)	(mm)
LA13	-29.3%	-31.2%	127
LA14	-39.0%	-12.2%	180
LA18	-34.2%	-25.1%	192
LA02	-32.2%	-14.1%	238
SE03	-53.7%	-57.7%	177
SE15	-40.7%	-20.6%	277
SE18	-31.2%	-50.8%	93
Average	-37.2%	-30.2%	184
BSE-2			
LA23	-8.0%	-29.9%	1091
LA24	-12.3%	-41.5%	1452
SE23	-9.4%	-34.2%	1253
LA31	-3.4%	-15.0%	559
LA32	-2.2%	-9.9%	530
SE28	-9.7%	-31.1%	393
SE32	-13.7%	-21.0%	344
Average	-8.4%	-26.1%	803

Table 6.30 Change in Peak Output Parameters for MF-2, Soft Sites

NRTMDF Properties

Mass = 2776448 kg	BSE-1 Avg. Eff. Stiffness = 12.71 kN/mm
Initial Stiffness = 136.99 kN/mm	BSE-1 Avg. Peak Damped Period = 3.48 sec
Damper Yield Strength = 2440.5 kN	BSE-2 Avg. Eff. Stiffness = 8.28 kN/mm
Initial Damped Period = 2.54 sec	BSE-2 Avg. Peak Damped Period = 4.05 sec

Ground Motions	Base Shear	Rooftop Displacement	NRTMDF Displacement
BSE-1	(% Change)	(% Change)	(mm)
SE01	-4.2%	-16.6%	1544
LA03	-2.8%	-12.2%	1098
LA15	-16.7%	-24.5%	364
LA09	-6.1%	-16.8%	419
LA10	-8.8%	-11.0%	431
LA07	-16.4%	-28.4%	634
SE07	-36.5%	-36.5%	185
Average	-13.1%	-20.8%	668
BSE-2			
LA38	-4.8%	-11.9%	3191
LA40	-8.9%	-20.1%	3627
SE24	-15.0%	-36.5%	2514
LA35	-8.6%	-21.4%	3007
LA36	-16.9%	-39.7%	3011
SE33	-10.5%	-29.0%	1438
SE36	-7.6%	-27.1%	939
Average	-10.3%	-26.5%	2532

Table 6.31 Summary of Avg. Changes in Peak Output Parameters for BSO, Hard Sites

Model	Base Shear (% Change)	Rooftop Displacement (% Change)	NRTMDF Displacement (mm)
		BSE-1	
BF-1	-14.5%	-11.1%	31
BF-2	-8.6%	-23.6%	39
BF-3	-9.9%	-18.1%	45
BF-4	-25.2%	-37.0%	65
BF-5	-27.4%	-37.3%	99
EBF-1	-20.6%	-35.0%	68
SW-1	-1.3%	-24.1%	40
SW-2	-1.2%	-22.1%	44
MF-1	-20.3%	-20.3%	78
MF-2	-19.1%	-19.1%	120
		BSE-2	
BF-1	-1.0%	-22.7%	73
BF-2	-7.2%	-31.9%	91
BF-3	-1.4%	-30.0%	157
BF-4	-0.9%	-31.6%	268
BF-5	-7.5%	-22.2%	469
EBF-1	-6.3%	-28.5%	245
SW-1	-5.7%	-42.7%	126
SW-2	-3.9%	-30.5%	166
MF-1	-20.0%	-31.0%	452
MF-2	-10.0%	-21.5%	757

Table 6.32 Summary of Avg. Changes in Peak Output Parameters for BSO, Med. Sites

Model	Base Shear (% Change)	Rooftop Displacement (% Change)	NRTMDF Displacement (mm)
		BSE-1	
BF-1	-8.0%	-16.8%	47
BF-2	-10.6%	-25.4%	37
BF-3	-2.9%	-12.7%	96
BF-4	-21.5%	-43.5%	107
BF-5	-30.7%	-36.0%	130
EBF-1	-5.1%	-29.3%	89
SW-1	-1.1%	-13.3%	49
SW-2	-1.0%	-13.3%	95
MF-1	-26.7%	-28.8%	190
MF-2	-30.2%	-30.2%	184
		BSE-2	
BF-1	0.4%	-7.8%	143
BF-2	-2.1%	-15.6%	91
BF-3	-0.7%	-16.2%	243
BF-4	-4.2%	-41.4%	382
BF-5	-6.6%	-26.8%	481
EBF-1	-8.1%	-30.4%	314
SW-1	-1.9%	-11.6%	175
SW-2	-2.6%	-13.3%	259
MF-1	-20.9%	-33.2%	716
MF-2	-8.4%	-26.1%	803

Table 6.33 Summary of Avg. Changes in Peak Output Parameters for BSO, Soft Sites

Model	Base Shear (% Change)	Rooftop Displacement (% Change)	NRTMDF Displacement (mm)
		BSE-1	
BF-1	-0.1%	-14.6%	54
BF-2	-4.1%	-7.3%	75
BF-3	-1.5%	-17.5%	165
BF-4	-1.2%	-21.2%	287
BF-5	-10.3%	-29.0%	336
EBF-1	-2.6%	-15.6%	313
SW-1	-0.9%	-10.2%	84
SW-2	-1.3%	-15.1%	176
MF-1	-19.1%	-29.2%	534
MF-2	-13.1%	-20.8%	668
		BSE-2	
BF-1	-0.9%	-3.4%	183
BF-2	2.0%	-0.8%	236
BF-3	-2.8%	-13.0%	721
BF-4	-7.7%	-12.5%	936
BF-5	-4.7%	-16.4%	1466
EBF-1	-3.5%	-12.9%	902
SW-1	-1.3%	-6.4%	319
SW-2	-2.2%	-13.1%	740
MF-1	-6.0%	-19.8%	1824
MF-2	-10.3%	-26.5%	2532

results listed are quantitatively different than those of the prior broad based nonlinear analysis approach (Chapter 5), the results are qualitatively the same. Namely, reductions in peak base shear and peak rooftop displacement can be achieved by virtue of the NRTMDF and its ability to alter fundamental dynamic properties and by enabling targeted nonlinearity and energy dissipation at the NRTMDF itself. However, in some cases response parameters are increased by virtue of the NRTMDF when the altered properties drive the structure toward resonance with the site rather than away from site resonance. An example of this is reflected in the results listed in Table 6.3 for Model BF-1 and motion LA38 reflecting a soft site condition. For this case, the undamped fundamental period is 0.25 seconds correlating to a spectral acceleration of 1.03g (Figure 3.34). For the damped case, the fundamental period (using initial NRTMDF elastic stiffness) is 0.41 seconds correlating to a spectral acceleration of 1.03g. As the NRTMDF softens due to nonlinear behavior, a peak transient period of 0.77 seconds is reached correlating to a spectral acceleration ordinate of 1.49g. Hence, the NRTMDF drives the structure closer to resonance yielding an increased spectral acceleration response and producing calculated increases in peak transient rooftop displacement increase of 25.6%.

Alteration of the fundamental dynamics of the system is demonstrated by a shift in mode 1 and mode 2 periods which typically result in favorable changes in acceleration ordinates corresponding to the spectra reflecting the ground motions of the Basic Safety Objective. Figures 6.1 through 6.6 demonstrate the average of spectra for the BSO and the mode 1 period shifts enabled by the NRTMDF. These figures demonstrate the concept of transient dynamic properties addressed in Chapter 5. These are reflected in

the period shifts which are first driven by elastic behavior in the NRTMDF (initial elastic period shift). Once the NRTMDF yields, effective stiffness properties can be determined based on peak ordinates of hysteresis loops of the NRTMDF for each ground motion. For this, each ground motion drives the NRTMDF to a displacement and force which define effective stiffness properties which can be utilized to assess transient dynamic modal properties reflecting primary mode period shifts. Upon comparing the altered periods to the spectra, the qualitative changes in performance may be observed as reflected in changes of the spectral acceleration ordinates. For the Basic Safety Objective, the BSE-1 (10% in 50-year event) records are lower magnitude and therefore do not create NRTMDF displacements as high as those of BSE-2 (2% in 50-year event). As such, the effective stiffness properties corresponding to BSE-1 are higher than those of BSE-2 resulting in lower nonlinear period shifts as reflected in Figures 6.1 through 6.6.

Observation of the spectra shown in Figures 6.1 through 6.6 demonstrates that the BSE-2 motions are significantly higher than those of BSE-1. If the ratio of ordinates between BSE-2 and BSE-1 are compared, a value greater than 2.0 will result. This is true for the ground motions considered in this research as well as the prescribed BSE motions for most sites across the United States. In this context an effective design approach for most areas is to establish NRTMDF properties that assure yielding of the NRTMDF for the BSE-1 motions. With appropriately proportioned properties, the NRTMDF may be designed such that BSE-1 motions are sufficient to just yield the buckling restrained braces but not result in significant nonlinear behavior (e.g., behaviors yielding plastic strains of 2.0% to 3.5%). When this is satisfied, an assurance of NRTMDF yielding for

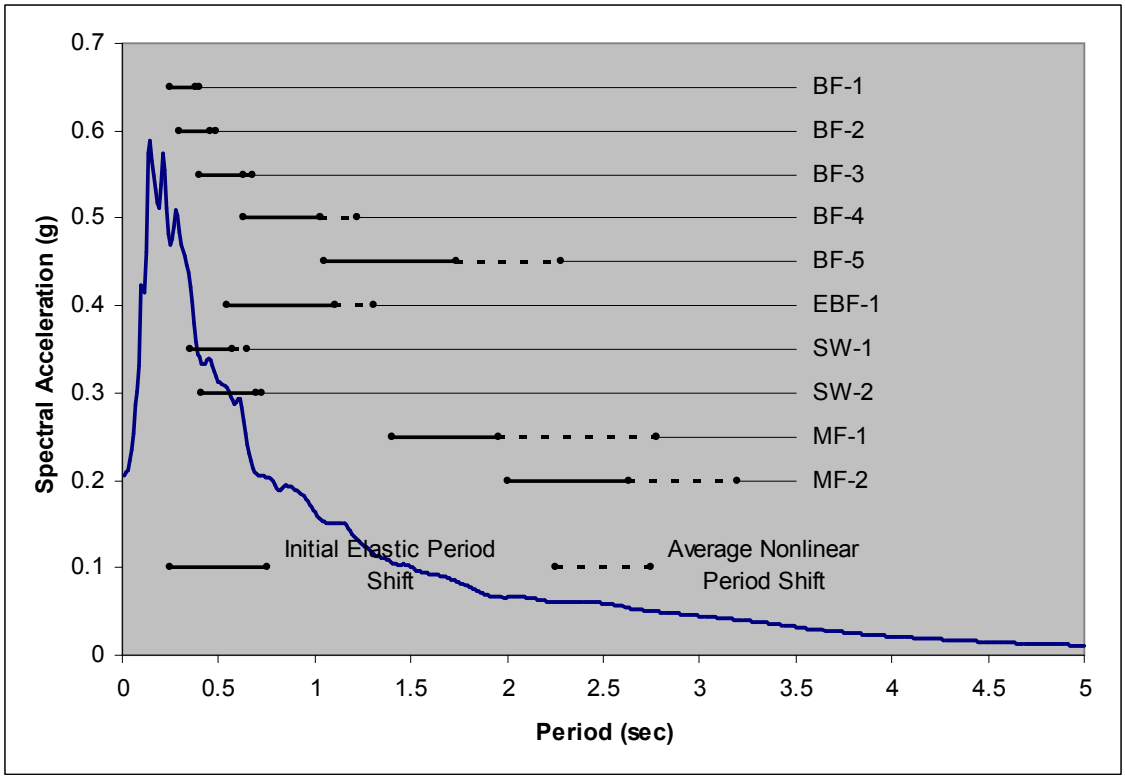

Figure 6.1 Modal Period Shifts of Building Models for BSE-1, Hard Sites

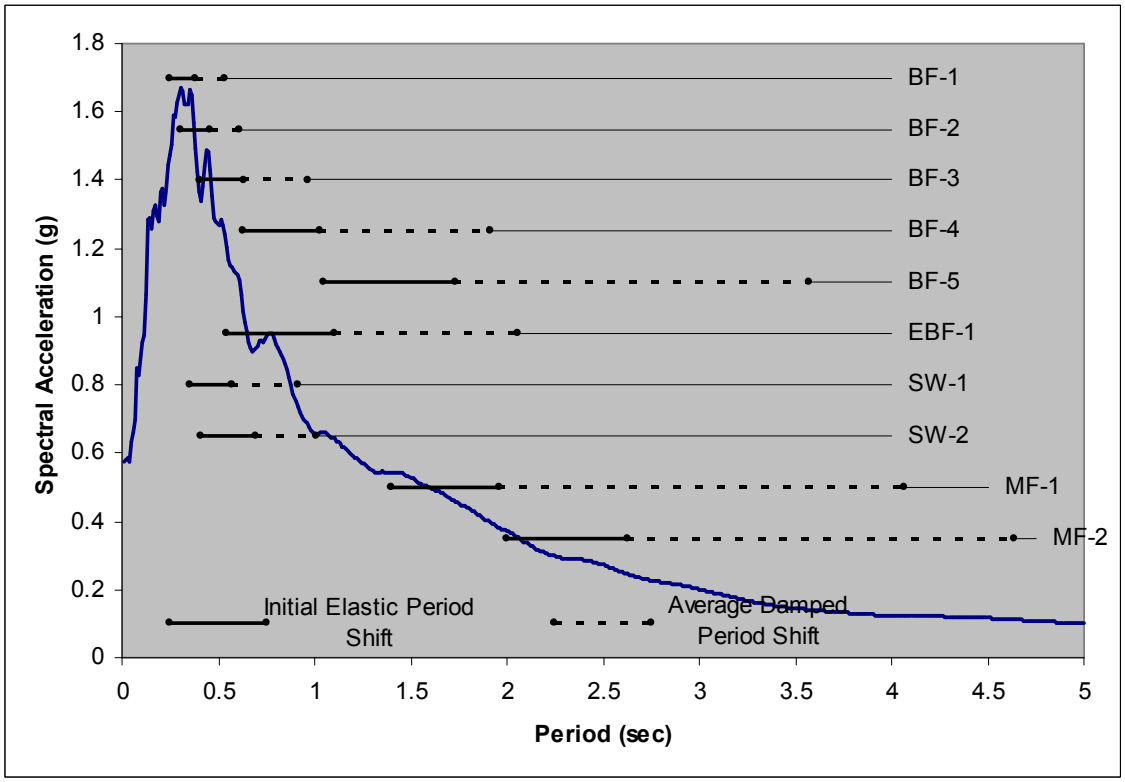

Figure 6.2 Modal Period Shifts of Building Models for BSE-2, Hard Sites

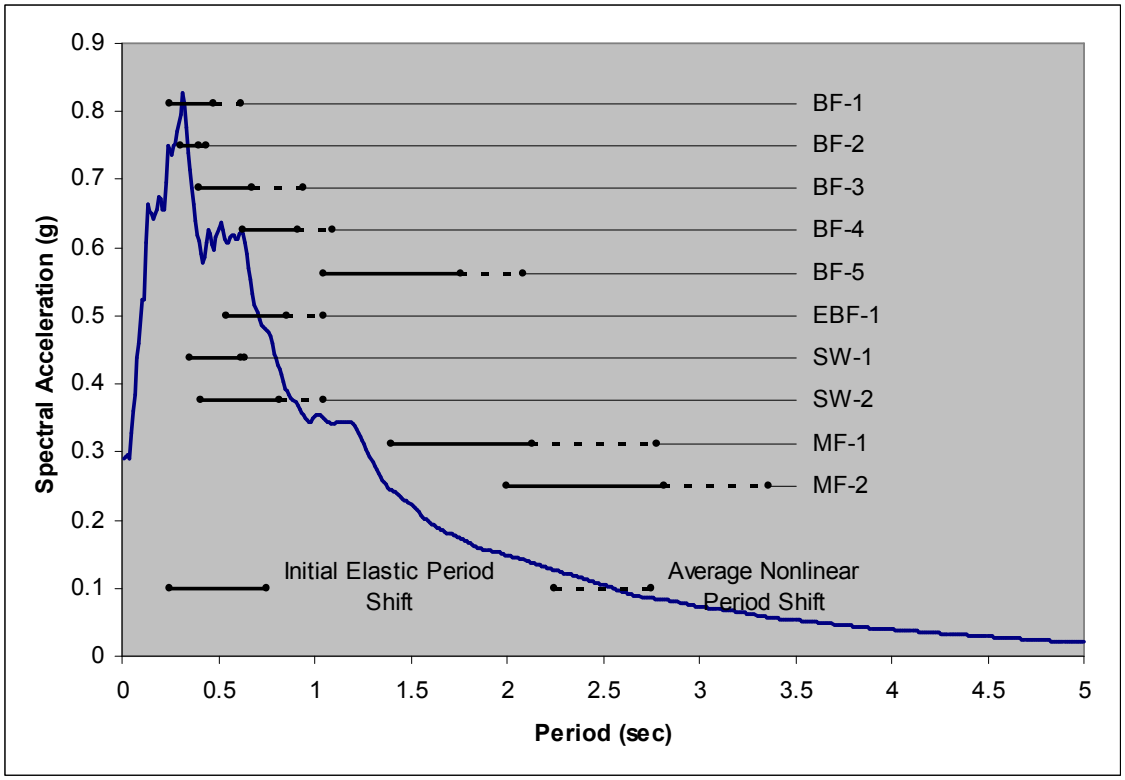

Figure 6.3 Modal Period Shifts of Building Models for BSE-1, Medium Sites

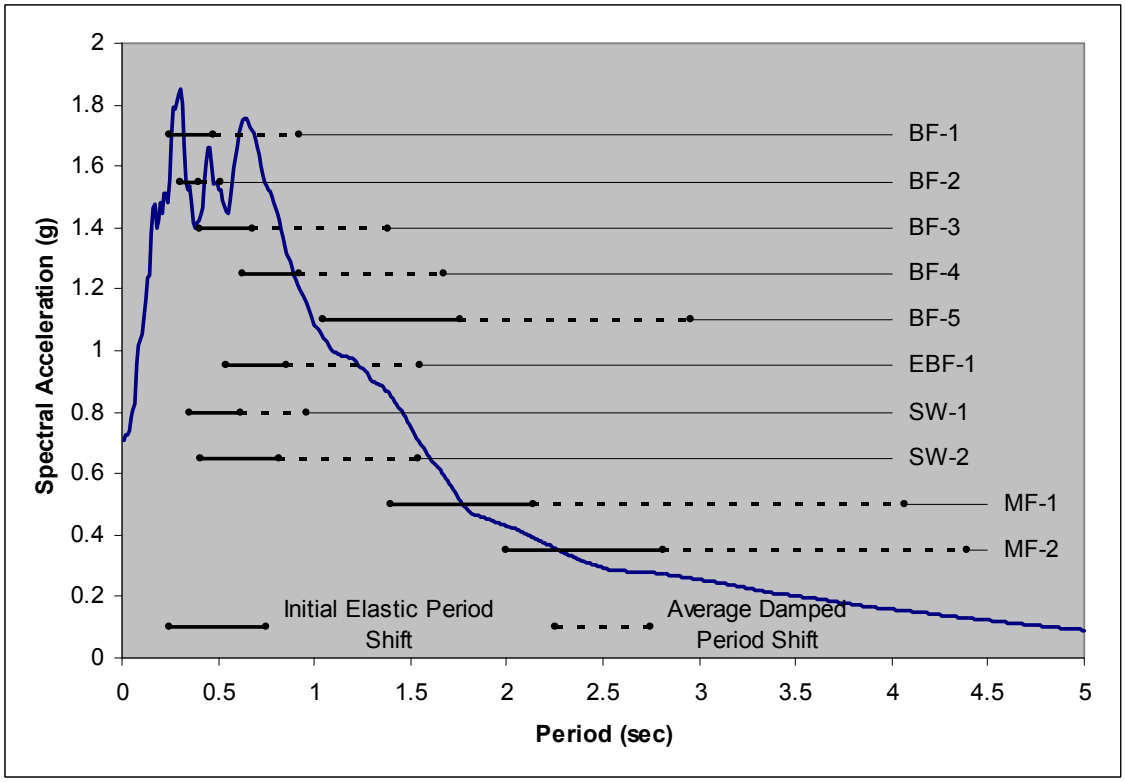

Figure 6.4 Modal Period Shifts of Building Models for BSE-2, Medium Sites

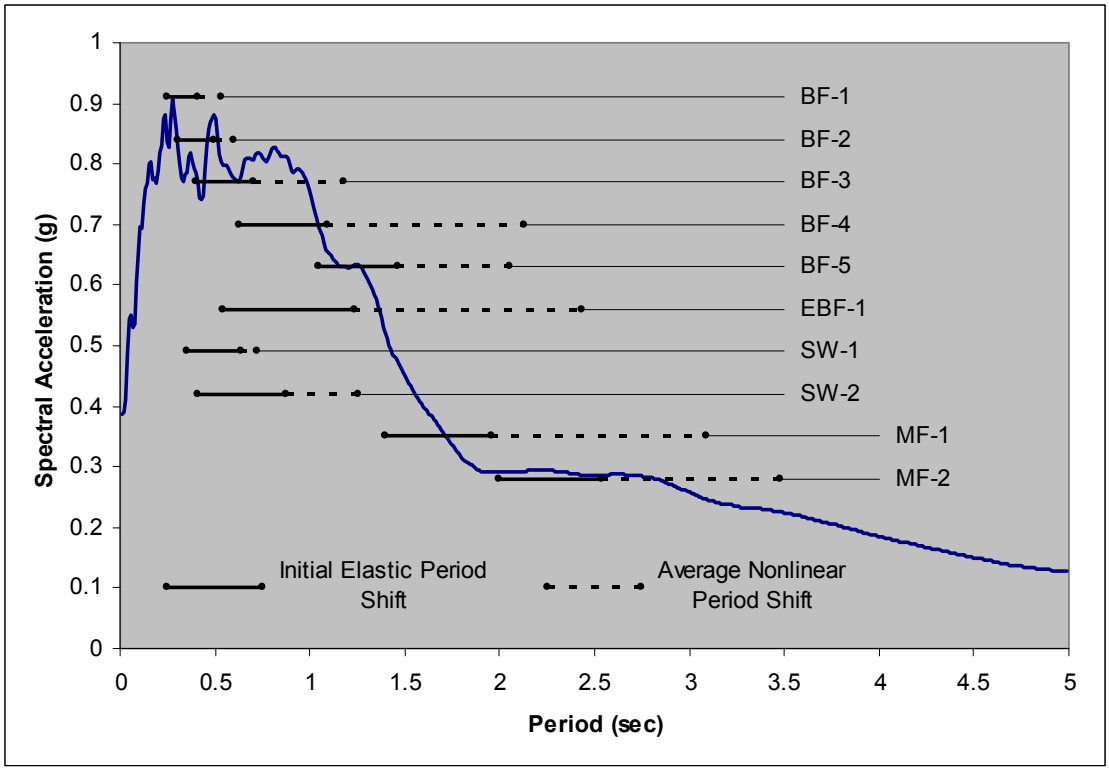

Figure 6.5 Modal Period Shifts of Building Models for BSE-1, Soft Sites

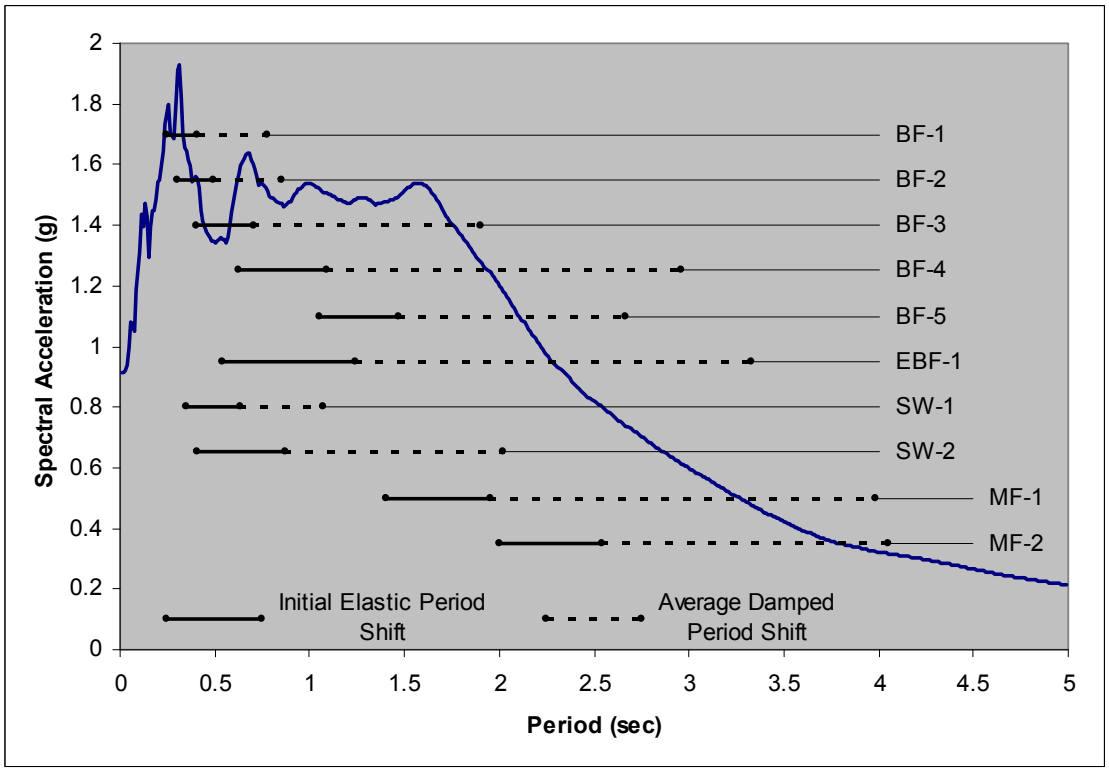

Figure 6.6 Modal Period Shifts of Building Models for BSE-2, Soft Sites

BSE-2 is reached and the design scenario reflects a condition of active nonlinearity of the NRTMDF for a moderate to major event that will most likely enable the buckling restrained braces of the NRTMDF to remain within reasonable limits of maximum tensile strain. This concept will be presented within the context of the hysteretic output examples which follow (Section 6.1). The results will demonstrate that effective reductions in peak transient parameters will be achieved for both BSE-1 and BSE-2 ground motion suites. With these, hysteretic behaviors of the NRTMDF for both ground motion suites will demonstrate that for BSE-1, the NRTMDF just yields whereas for BSE-2, significant yielding and nonlinearity are observed.

The hysteretic output examples of Section 6.1 will demonstrate that peak output parameter reductions are realized for BSE-1 with primarily the elastic period shift of the NRTMDF with some benefits due to small degrees of nonlinearity. For BSE-2, the same benefits are realized by both the elastic period shift and the inelastic period shift which accompanies significant NRTMDF nonlinearity and energy dissipation. Along with this is a shifting of fundamental period further from site resonance for the hard and medium site conditions and to a lesser degree, the soft site condition.

6.1 Nonlinear Hysteretic Output Examples

The tabulated output of Tables 6.1 through 6.33 demonstrate the overall effects of the NRTMDF for the damped and undamped models subjected to the ground motions of the Basic Safety Objective. Beyond this, hysteretic output for specific parameters and ground motions demonstrates the changes and the enhanced performance enabled by the NRTMDF. Also, the alteration in nonlinear demand of the base structures can be observed when considering the hystereses loops of the undamped and damped structures.

6.1.1 BF-4 Time History Output Examples

For model BF-4, ground motions SE06 and SE30 reflect representative accelerations of BSE-1 and BSE-2 for hard sites respectively. Figures 6.7 and 6.8 depict the hystereses loops for this structure and these motions showing the base shear vs. rooftop displacement. For comparative purposes, the axes for each figure match to readily demonstrate the changes in behavior apparent between the BSE-1 and BSE-2 motions. Consistent with the discussion of Section 5.2, stochastic behavior can be observed in the hystereses loops due to the less direct relationship between peak rooftop displacement and base shear. Nonetheless, the general trend can be observed reflecting the base shear and rooftop displacement characterized by pushover analyses (Appendix F). Figures 6.9 and 6.10 demonstrate the rooftop displacement histories for these same cases. Nonlinear behavior for these is apparent and is manifest as permanent nonlinear

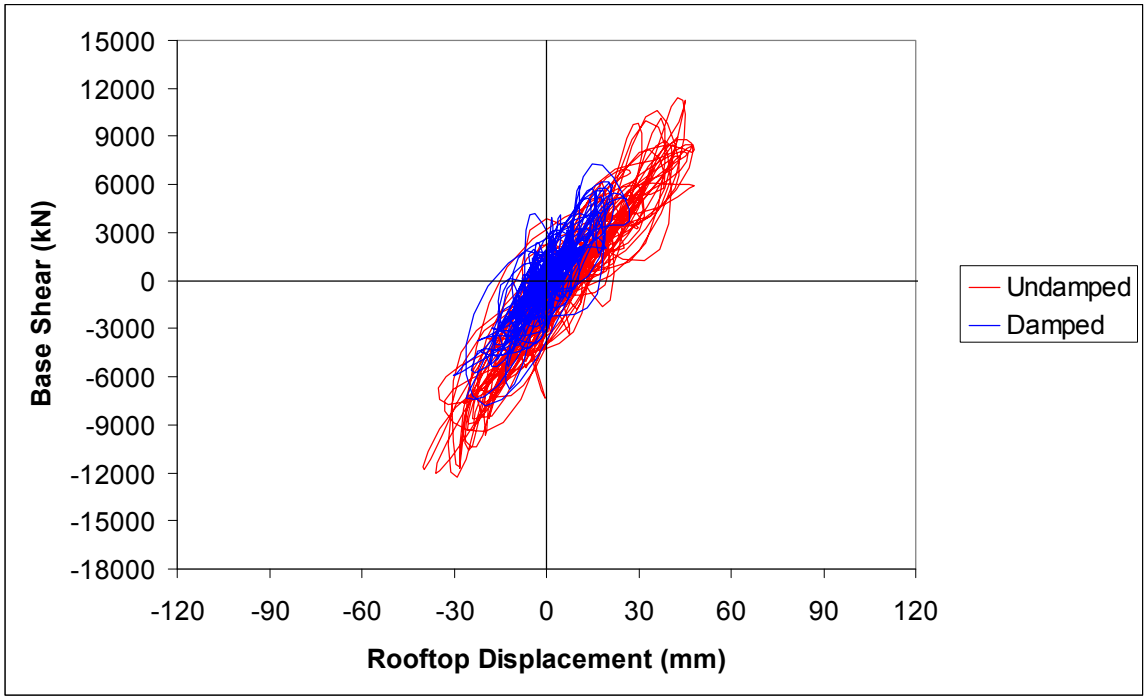

Figure 6.7 BF-4 Hysteresis Loop for Hard Site, BSE-1, SE06 Motion

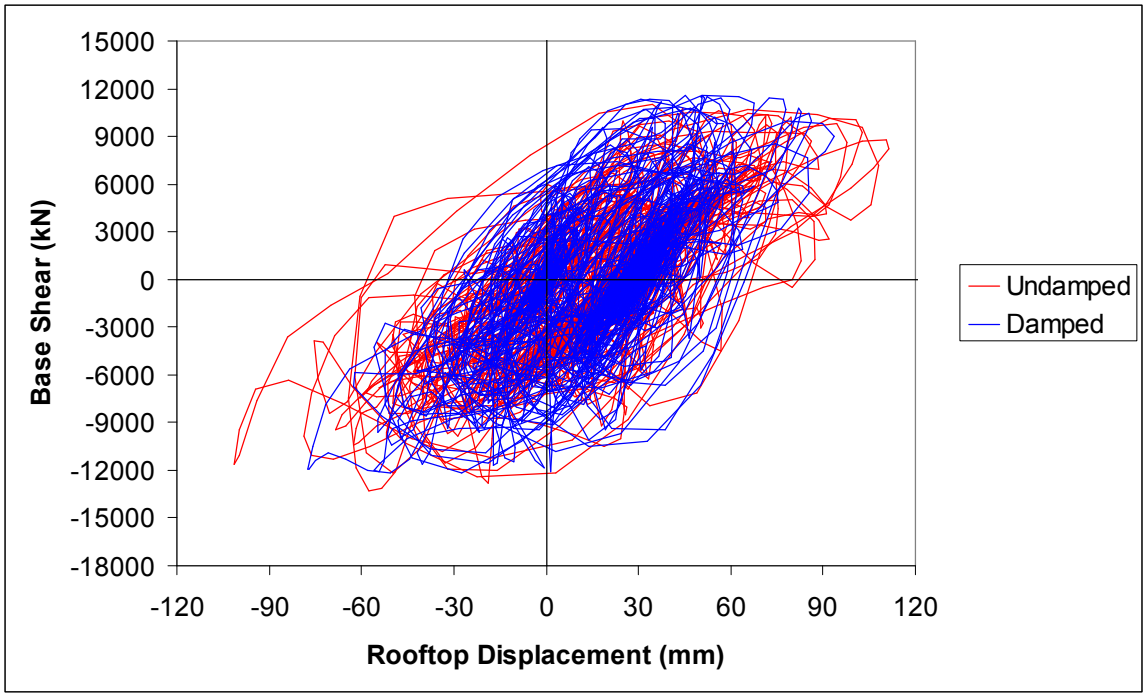

Figure 6.8 BF-4 Hysteresis Loop for Hard Site, BSE-2, SE30 Motion

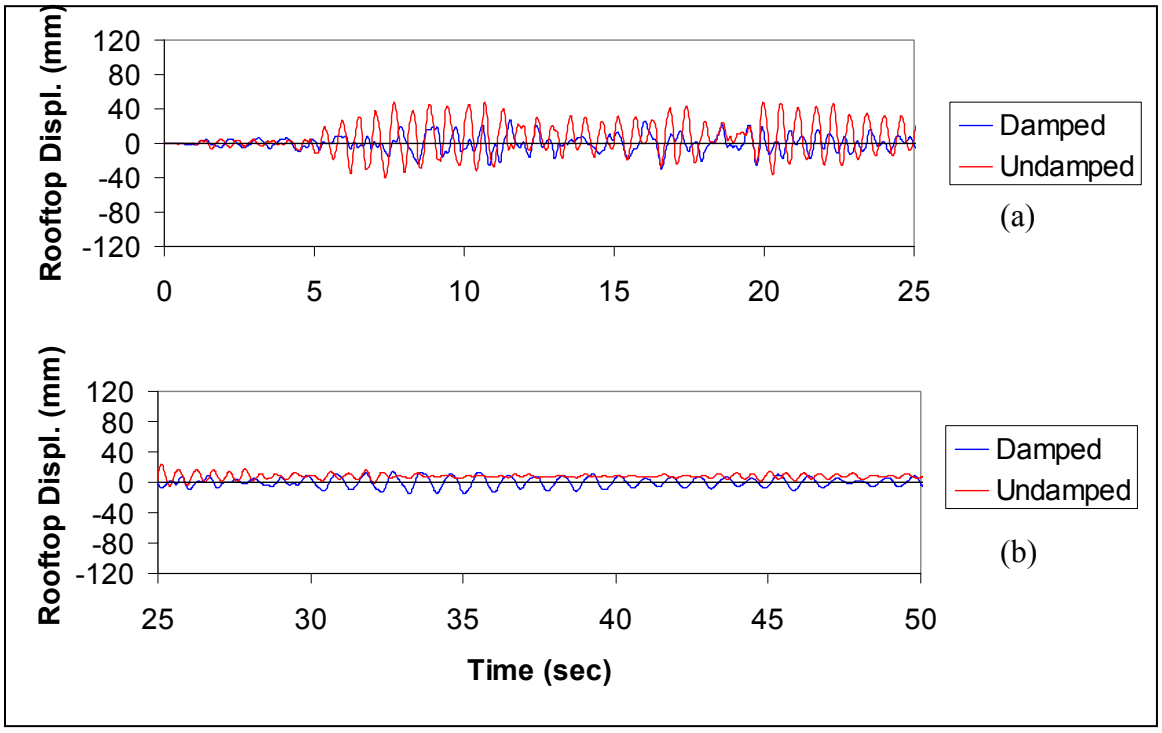

Figure 6.9 BF-4 Rooftop Displacement History for Hard Site, BSE-1 SE06 Motion

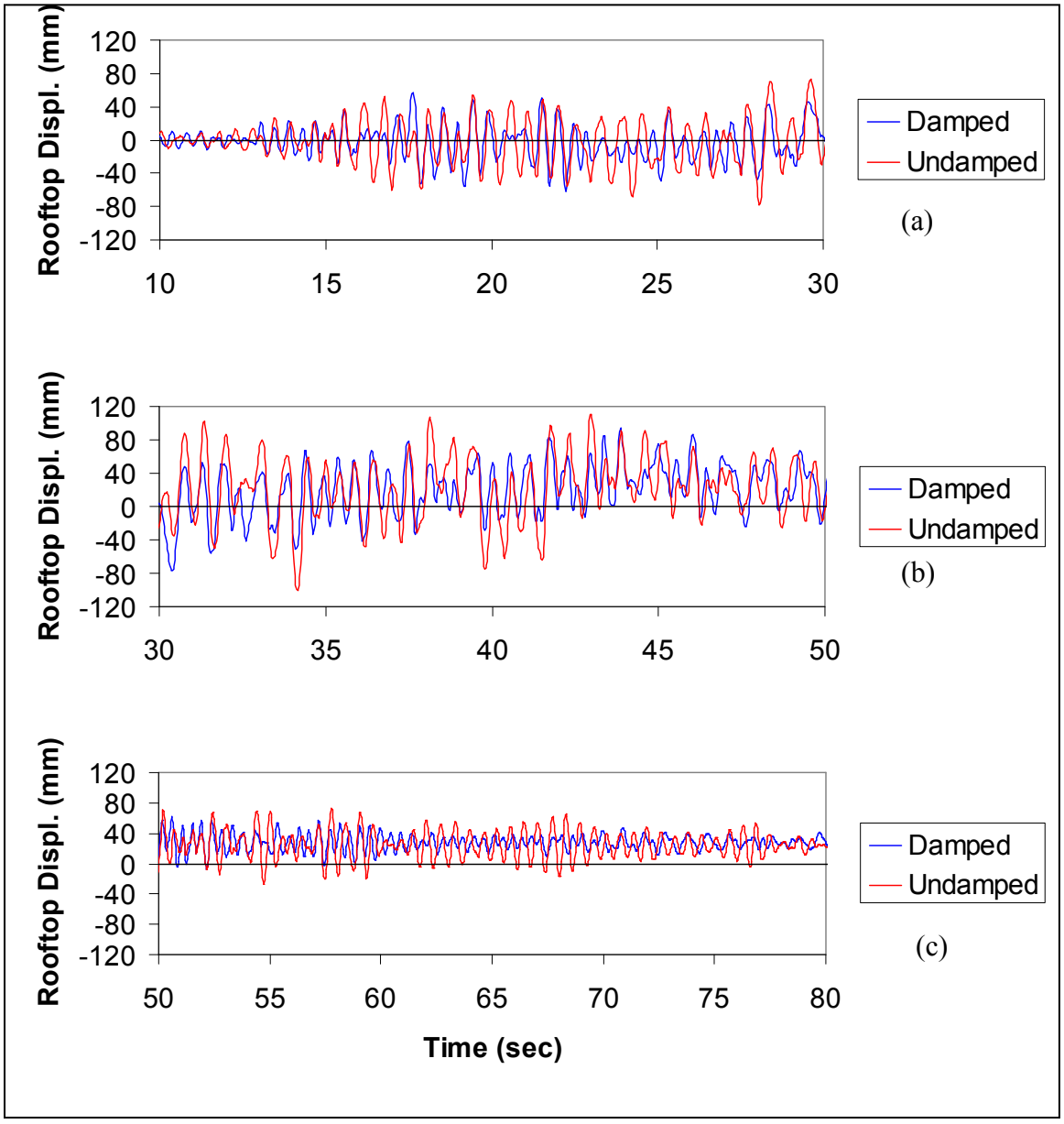

Figure 6.10 BF-4 Rooftop Displacement History for Hard Site, BSE-2, SE30 Motion

rooftop displacement, indicating yielding of elements in the lateral force resisting system within the base structure. Figures 6.11 and 6.12 depict the hysteretic behavior of one of two buckling restrained braces within the NRTMDF. Here too, hysteretic nonlinearity may be observed, with a much larger envelope of nonlinear behavior for the BSE-2 motion than the BSE-1 counterpart owing to the higher magnitude motion and the

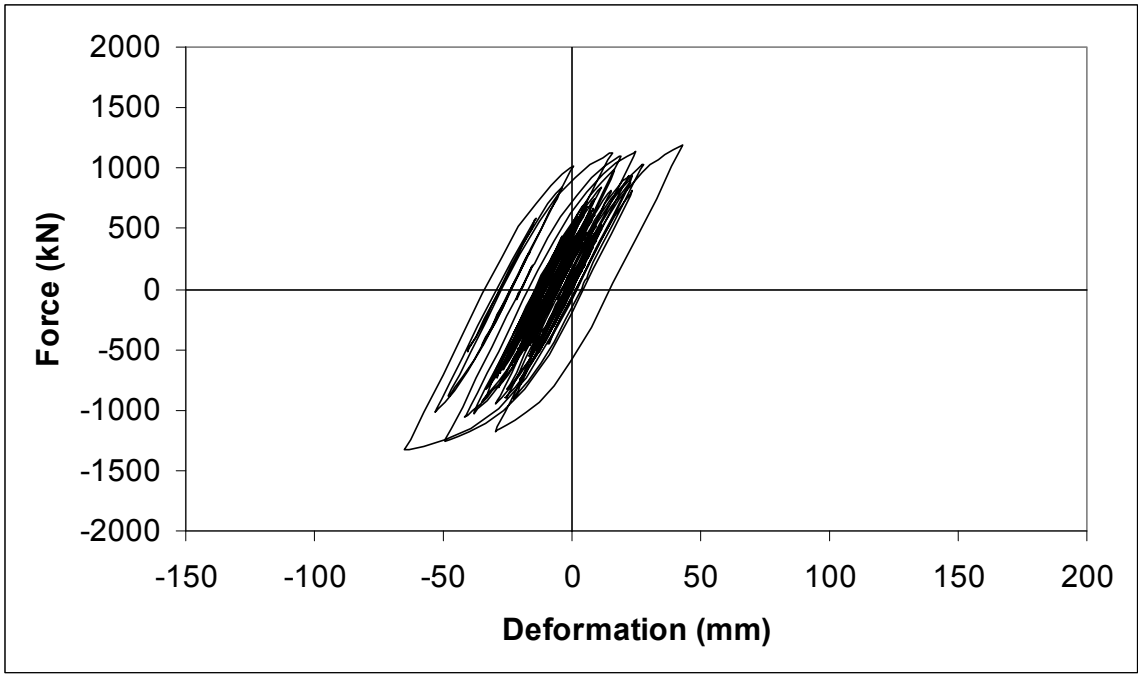

Figure 6.11 BF-4 NRTMDF Buckling Restrained Brace Hysteresis Loop for Hard Site, BSE-1, SE06 Motion

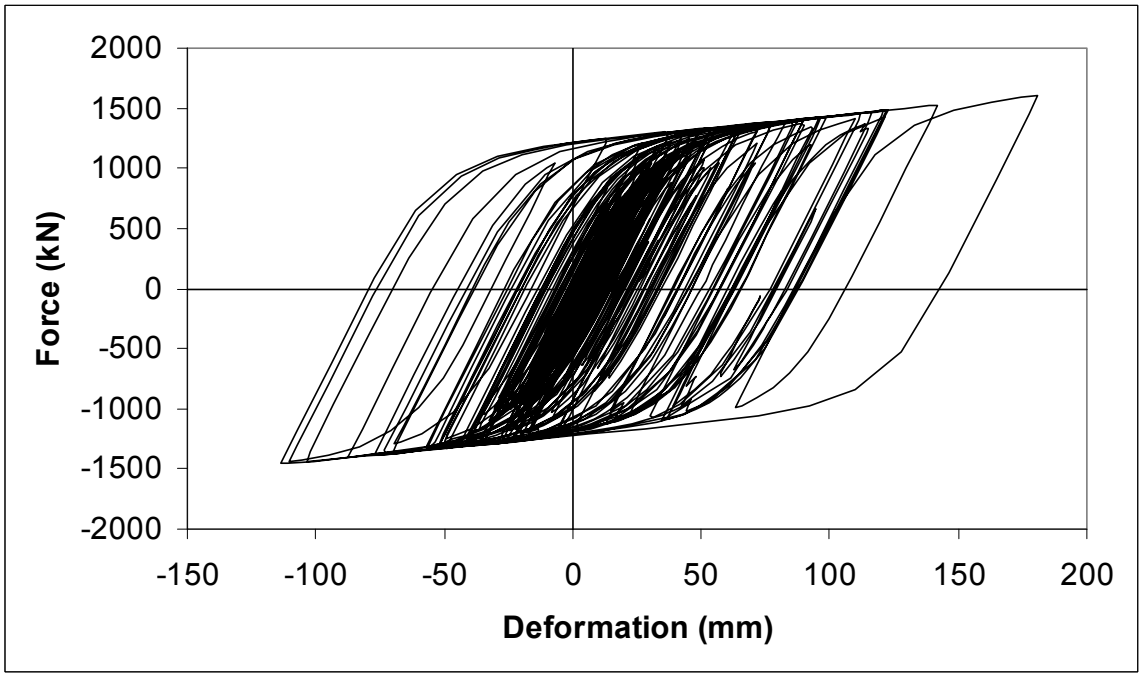

Figure 6.12 BF-4 NRTMDF Buckling Restrained Brace Hysteresis Loop for Hard Site BSE-2, SE30 Motion

condition where the NRTMDF just yields for BSE-1 but exhibits significant nonlinear behavior for BSE-2.

Comparison of the buckling restrained brace hystereses of Figures 6.11 and 6.12 demonstrates significant differences in behavior reflecting the duality of performance between BSE-1 and BSE-2 of the Basic Safety Objective. Effective performance of the system predicates that maximum energy dissipation of the NRTMDF be achieved. This occurs when the maximum capable displacements of the NRTMDF are reached while remaining with stable performance parameters (recommended 3.5% maximum axial strain). For this case, a significant difference occurs between the analyses for BSE-1 and BSE-2 with little nonlinearity occurring in the NRTMDF for the BSE-1 case and significant nonlinearity for BSE-2. Such performance characteristics suggest that the targeted performance objective (Life Safety for a moderate event such as BSE-1 and/or Collapse Prevention for a larger event such as BSE-2) for most areas be weighted toward the earthquake which best represents the scenario for which most effective performance is sought.

Additional output parameters which demonstrate the effectiveness of the NRTMDF include peak story displacements, drift indices and story shears. Figures 6.13 through 6.15 depict these values for the undamped and damped conditions for BSE-1 (SE06) and BSE-2 (SE30). While these figures demonstrate a general trend of reduction for the models damped with the NRTMDF, the top story of the structure does not typically reflect reductions in drift and shear. This is due to the reactions of immediately adjacent NRTMDF at the roof.

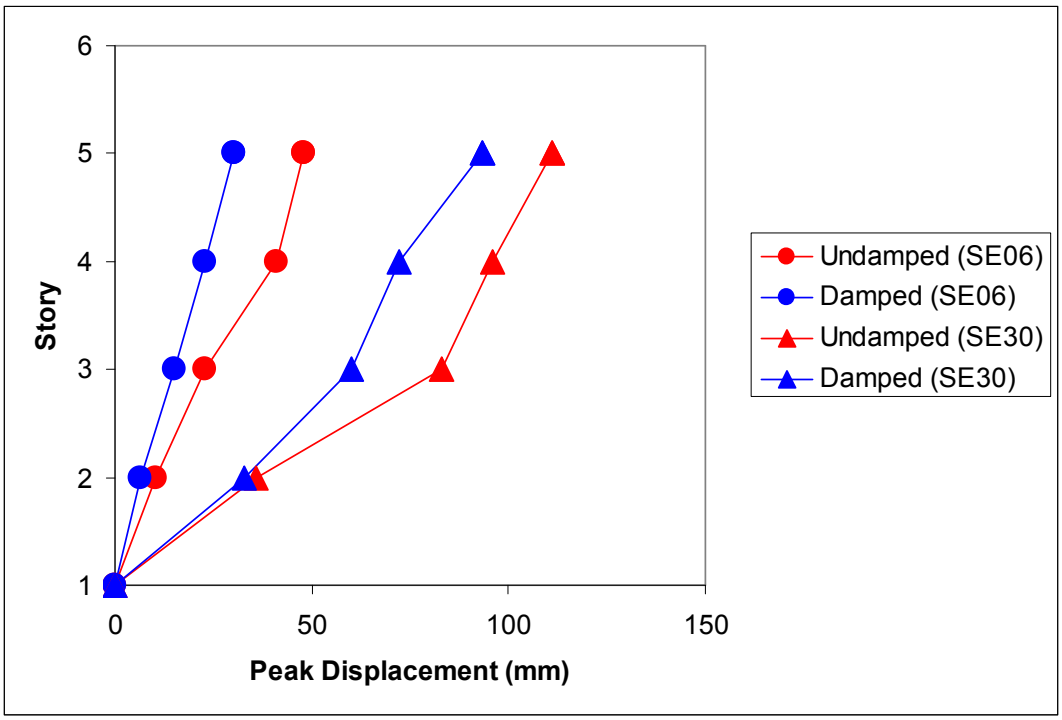

Figure 6.13 Peak Displacements for BF-4, BSE-1 (SE06) and BSE-2 (SE30) Motions

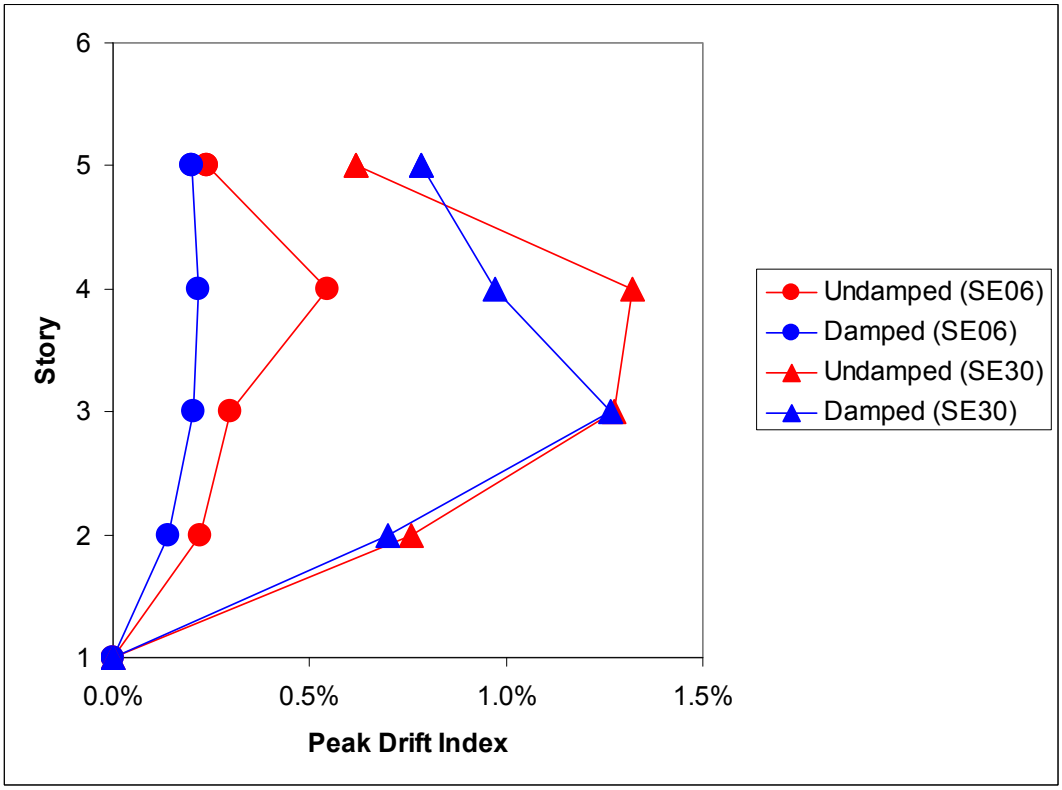

Figure 6.14 Peak Drift Indices for BF-4, BSE-1 (SE06) and BSE-2 (SE30) Motions

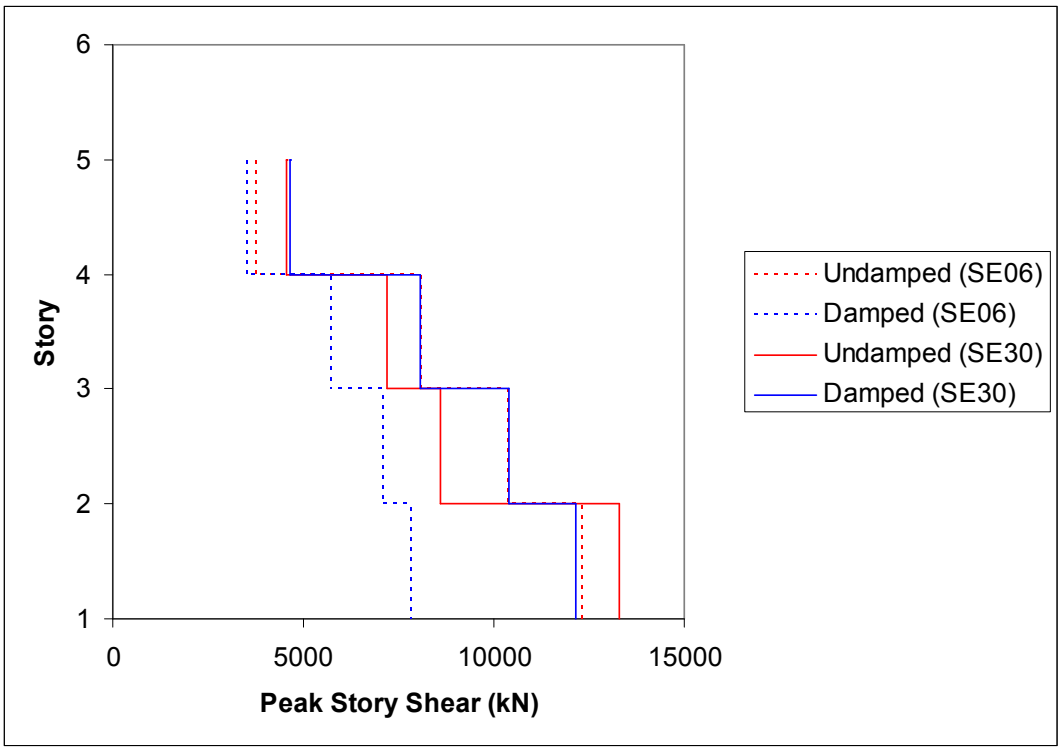

Figure 6.15 Peak Story Shears for BF-4, BSE-1 (SE06) and BSE-2 (SE30) Motions

The story drift indices shown in Figure 6.14 for BSE-1 (SE06) reflect a dramatic reduction and seemingly unbalanced change in story drift as compared to adjacent stories for the fourth level. This result occurs in the model due to brace buckling which occurs for the undamped case but is prevented in the damped case due to the action of the NRTMDF.

Figure 6.16 depicts the formation of nonlinear mechanisms in the braces for the fourth level for the BSE-1 motion (SE06) for the undamped case. This behavior is manifest as tensile yielding of the brace but even more as compression buckling which drives a far greater alteration in behavior which is characterized as a sudden and abrupt change in stiffness that could exacerbate soft story or extreme plan torsional conditions. Such phenomena could be catastrophic and their potential prevention enabled by the NRTMDF highlights the beneficial effects of the NRTMDF and damped condition for

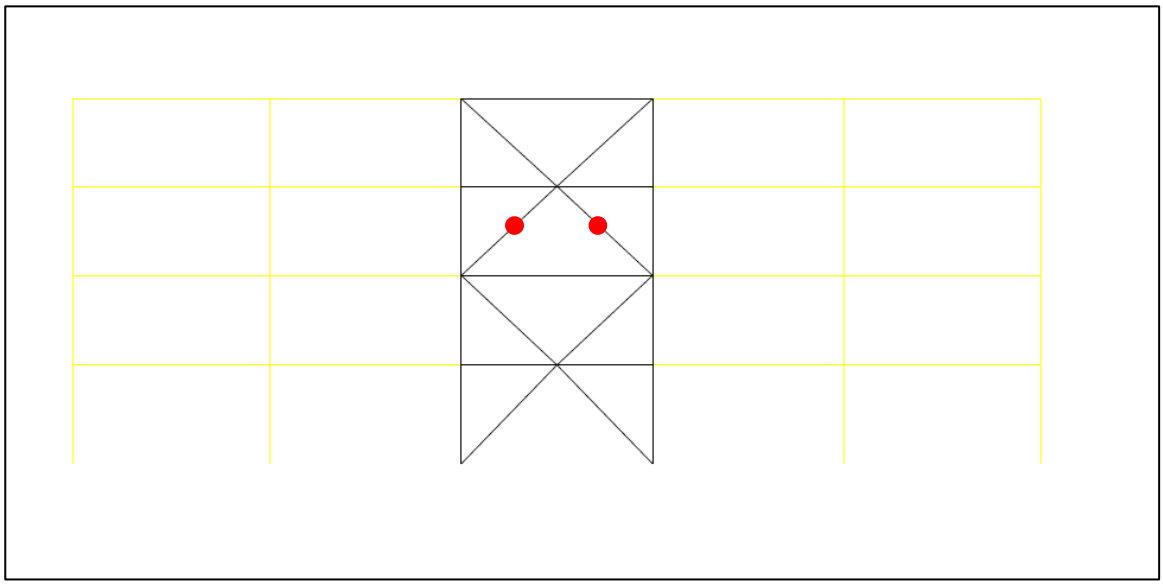

Figure 6.16 Plastic Hinge Formations for Undamped BF-4, Hard Site and BSE-1 (SE06)

motion which the modeling predicts that nonlinearity of the brace, in tension and compression, does not occur. For the BSE-2 condition, the modeling predicts a reduction in response as demonstrated in previous figures. However, the reduction is not sufficient to prevent nonlinearity of the bracing members. Figure 6.17 depicts the predicted hinge formations for the BSE-2 condition of BF-4 and the hard site (SE30 motion). As shown, tensile yielding and compression buckling of braces is expected for both the undamped and damped cases. However, the nonlinear (ductility) demand of these braces is reduced as reflected in the performance measures shown in Figures 6.13 through 6.15. As nonlinearity of braces occurs, particularly in the form of compression buckling, the modeled behavior of the braces becomes extremely numerically sensitive. This creates an irregular and perhaps unrealistic result in the story shears indicated in Figure 6.15 which shows predicted story shears higher for the damped case than the undamped case for all but the bottom story. For this, it is thought that the diminished hysteretic axial demand on the brace for the damped case yields a more numerically stable condition

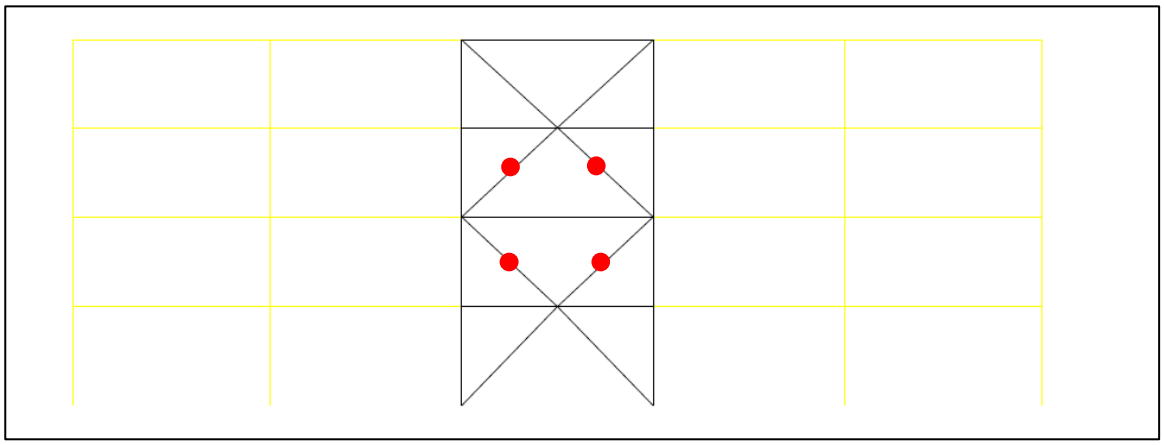

Figure 6.17 Plastic Hinge Formations for Damped and Undamped BF-4, Hard Site and BSE-2 (SE30) Motion

which is less sensitive numerically, does not skip the peak hysteretic compression limiting capacity and thus yields higher values for shear since the peak compressive capacity of the brace is more likely to be accounted for.

For medium stiffness site conditions and model BF-4, similar hysteretic trends can be observed for the BSE-1 and BSE-2 motions which for Figures 6.18 and 6.19 are represented by the SE18 and the LA24 motions respectively. Similar to the hard site condition, the BSE-1 hysteresis in Figure 6.18 demonstrates primarily linear behavior observed as a relatively narrow hysteresis loop concentrated at a theoretical elastic stiffness value indicating little (if any) nonlinear behavior in the base structure. Conversely, the BSE-2 hysteresis in Figure 6.19 demonstrates a broad envelop in the force-displacement relationship indicating significant nonlinear demand, which as demonstrated is far greater for the undamped case than the damped case. Also noteworthy on the hysteresis loops is the magnitude of base shear for the BSE-1 and BSE-2 motions. While significant difference is observed in the motions themselves, the resulting structural response demonstrates peak base shears of similar magnitude thereby reflecting yielding of the system and its incapacity for delivering higher inertial forces to

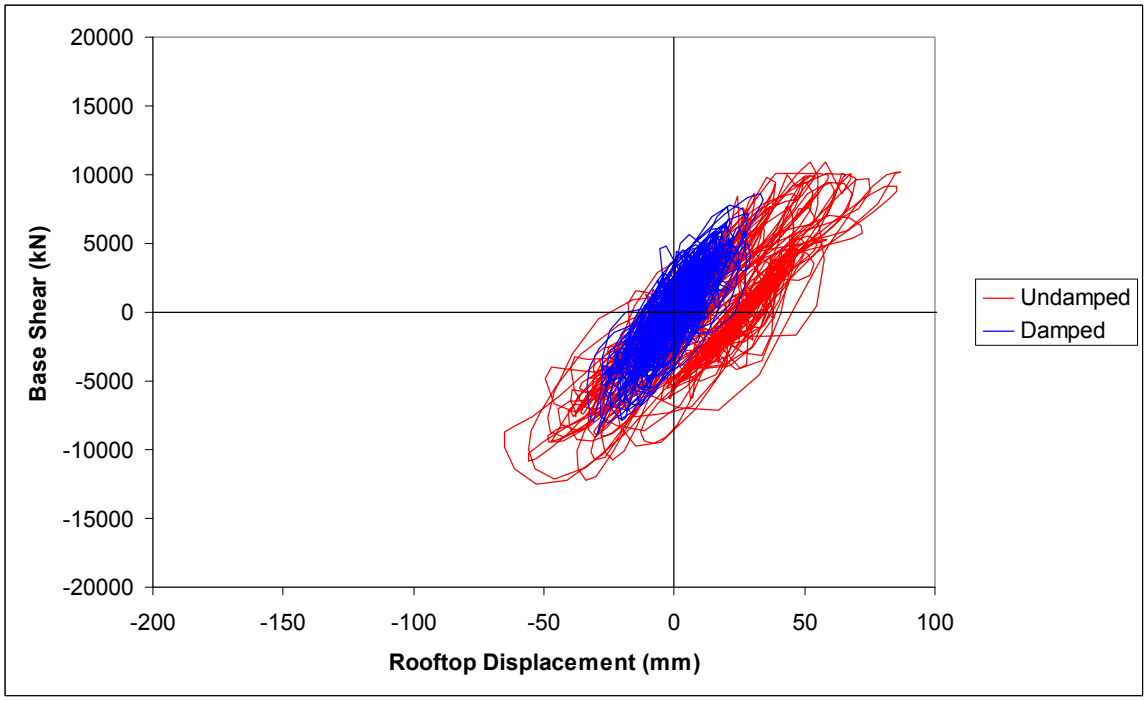

Figure 6.18 BF-4 Hysteresis Loop for Medium Site, BSE-1, SE18 Motion

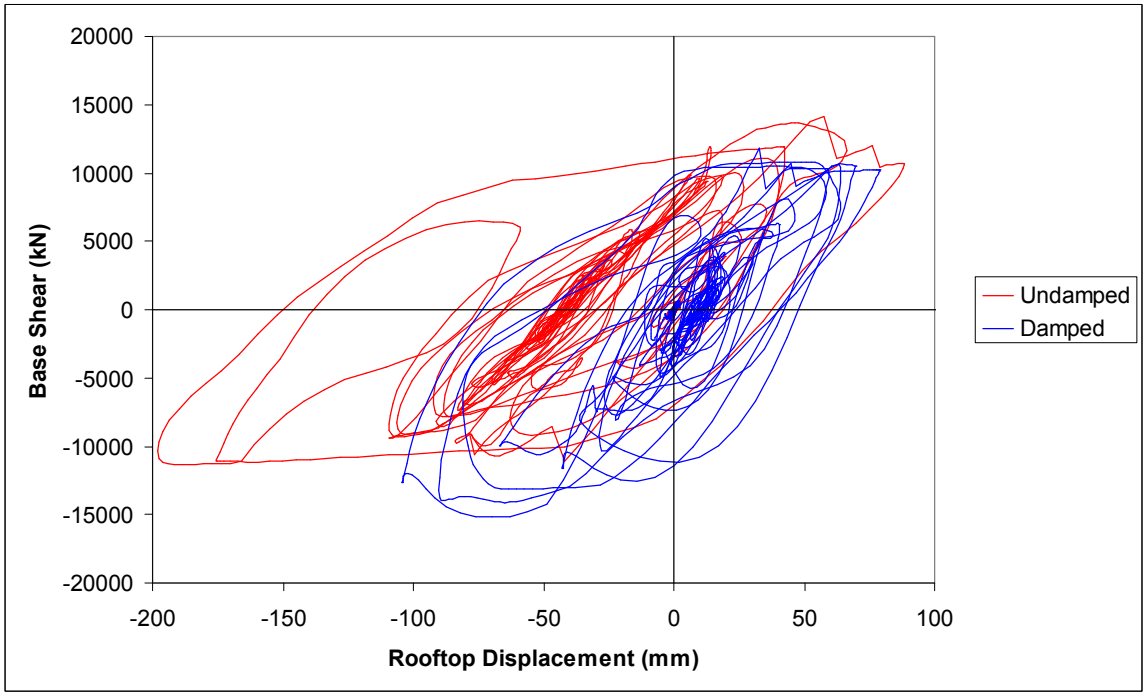

Figure 6.19 BF-4 Hysteresis Loop for Medium Site, BSE-2, LA24 Motion

the base of the structure. Figures 6.20 and 6.21 demonstrate the rooftop displacement histories and show the corroboration of the BRB hystereses loops of Figure 6.22 and 6.23. Namely, for the BSE-1 motion, the building hysteresis loop of Figure 6.18 shows primarily linear behavior for the damped structure with clear signs of nonlinearity occurring for the undamped structure. This is corroborated in the rooftop displacement of Figure 6.20 which shows permanent nonlinear displacement at the roof level of the undamped structure while the rooftop of the damped structure returns to its origin. Likewise, Figure 6.19 demonstrates the building hysteresis loop for BSE-2 for the damped and undamped models with a far larger envelope of nonlinearity for the undamped structure. Figure 6.21 corroborates this nonlinearity as it demonstrates not only a larger peak rooftop displacement but a permanent nonlinear rooftop displacement of the undamped structure (198mm) nearly double that of the damped structure (104mm). The heightened demand for nonlinear performance is further illustrated with Figures 6.22

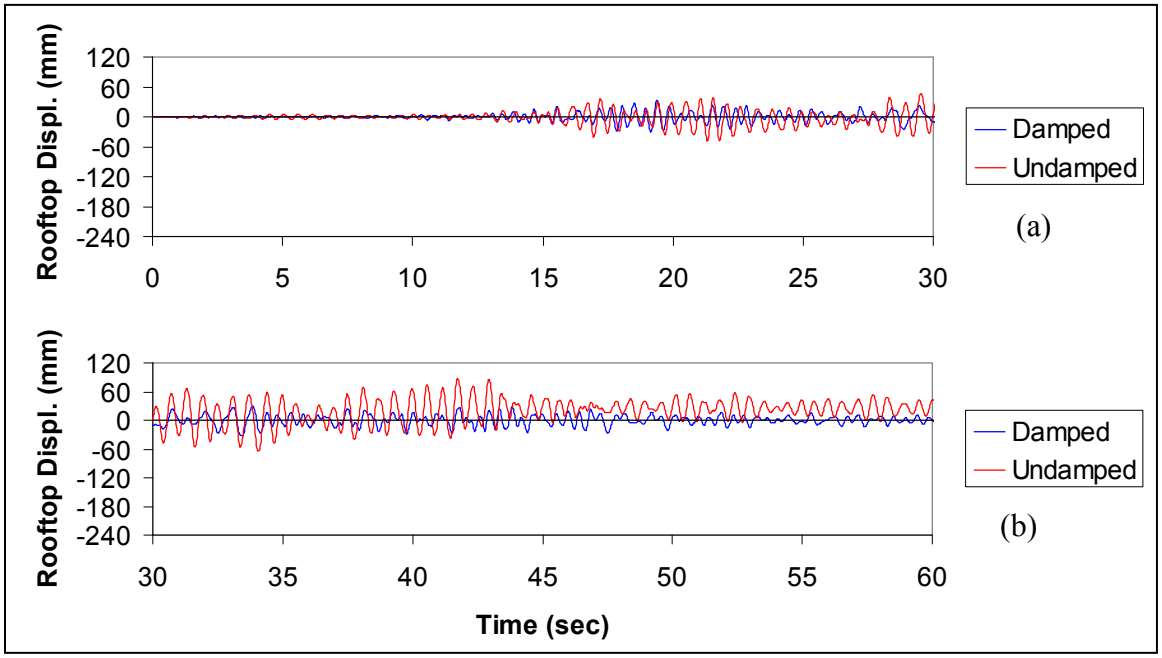

Figure 6.20 BF-4 Rooftop Displacement History for Medium Site, BSE-1, SE18 Motion

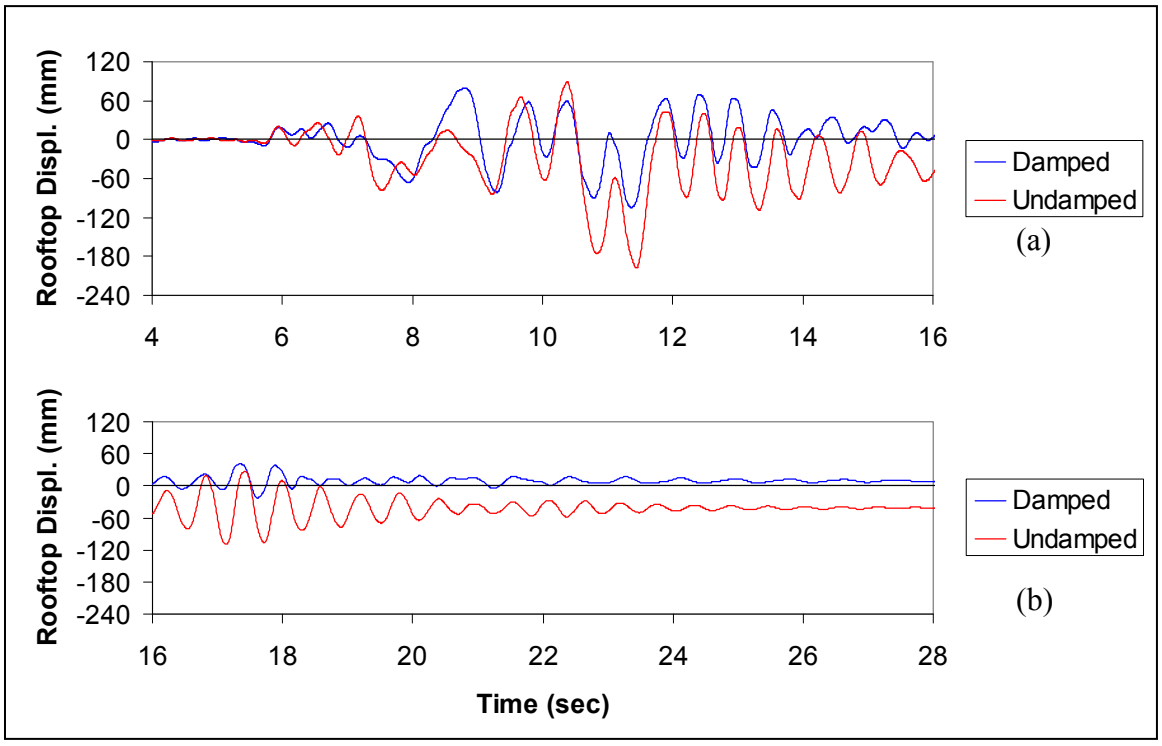

Figure 6.21 BF-4 Rooftop Displacement History for Medium Site, BSE-2, LA24 Motion

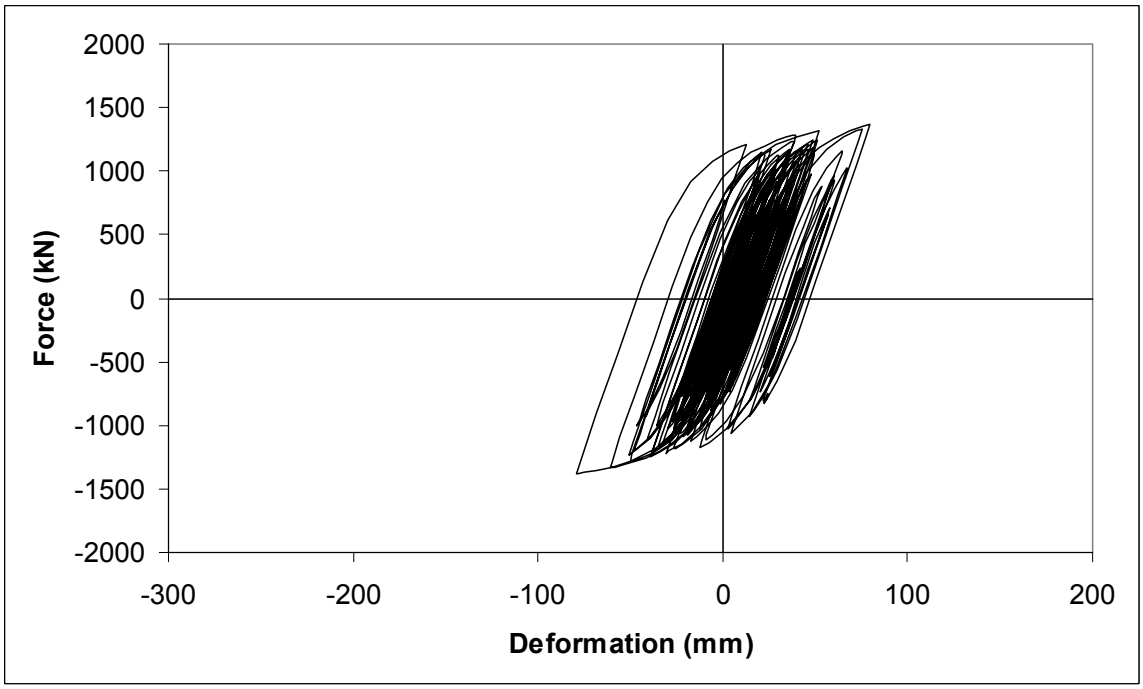

Figure 6.22 BF-4 NRTMDF Buckling Restrained Brace Hysteresis Loop for Medium Site, BSE-1, SE18 Motion

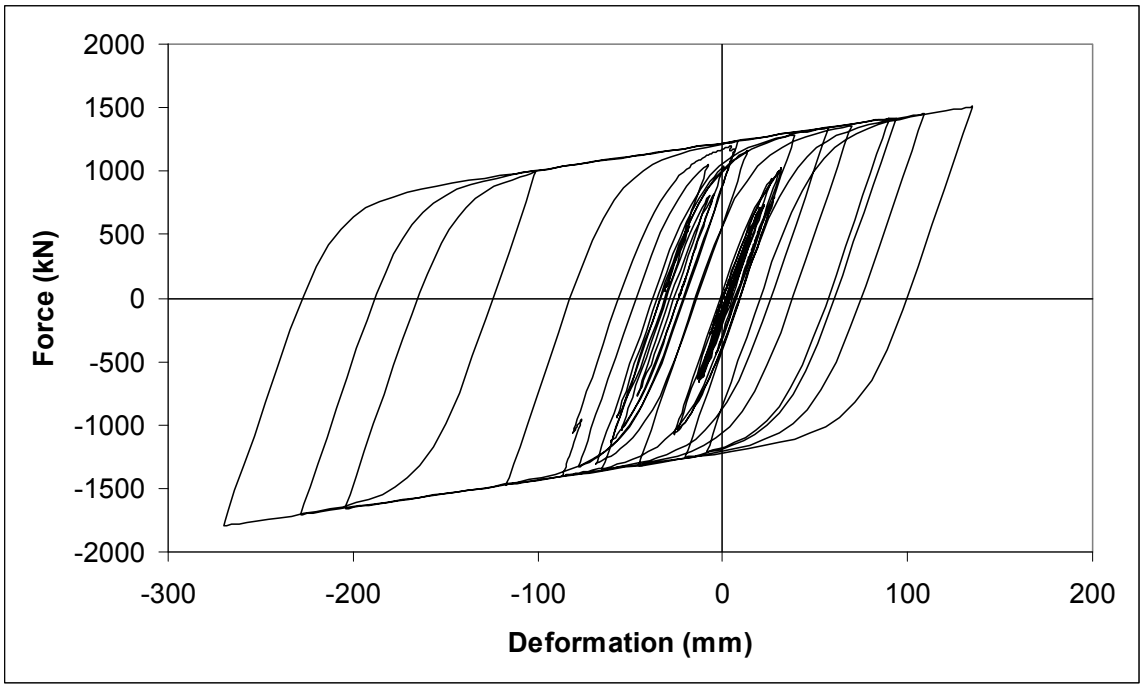

Figure 6.23 BF-4 NRTMDF Buckling Restrained Brace Hysteresis Loop for Medium Site BSE-2, LA24 Motion.

and 6.23 showing the hysteresis loops of buckling restrained braces for the NRTMDF of the structure for both BSE-1 and BSE-2 which also demonstrates significant energy dissipation correlating to the nonlinear demand, particularly for the BSE-2 record (SE30). Figures 6.24 through 6.26 depict the peak story displacements, story drift indices and story shears for the undamped and damped conditions of model BF-4 and the medium site condition. Much like the analyses for the hard site condition, these results reflect the reduction in response enabled by the NRTMDF. In particular, the ability of the NRTMDF to reduce response to the degree that brace buckling is prevented in the base structure is demonstrated to be a major benefit. Specifically, the story drift indices are dramatically reduced for the BSE-(SE18) motion as shown in Figure 6.25 reflecting braces that do not buckle. This reflects the prevention of soft story behavior that often accompanies brace buckling and exacerbates seismic story drift.

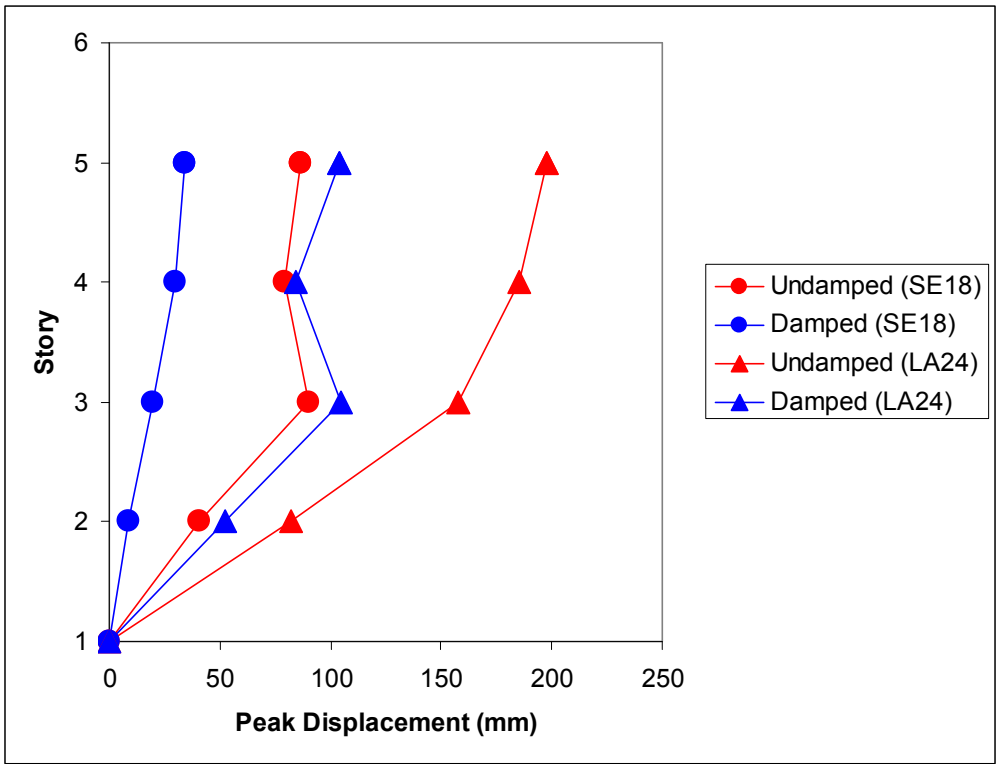

Figure 6.24 Peak Story Displacements for BF-4, BSE-1 (SE18) and BSE-2 (LA24) Motions

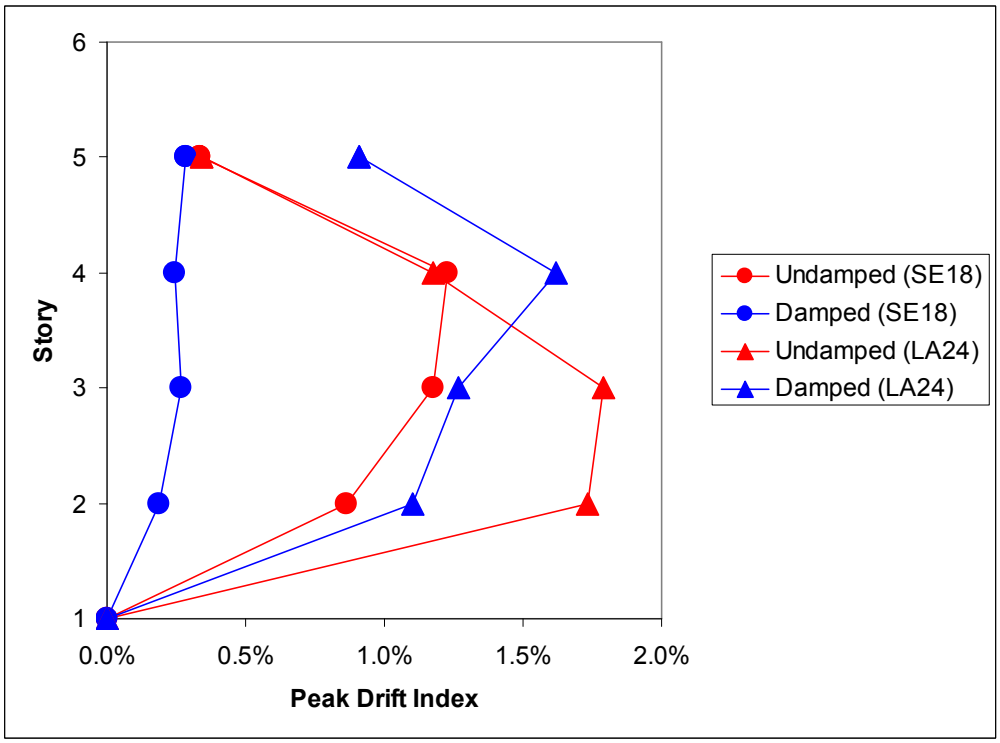

Figure 6.25 Peak Story Drift Indices for BF-4, BSE-1 (SE18) and BSE-2 (LA24) Motions

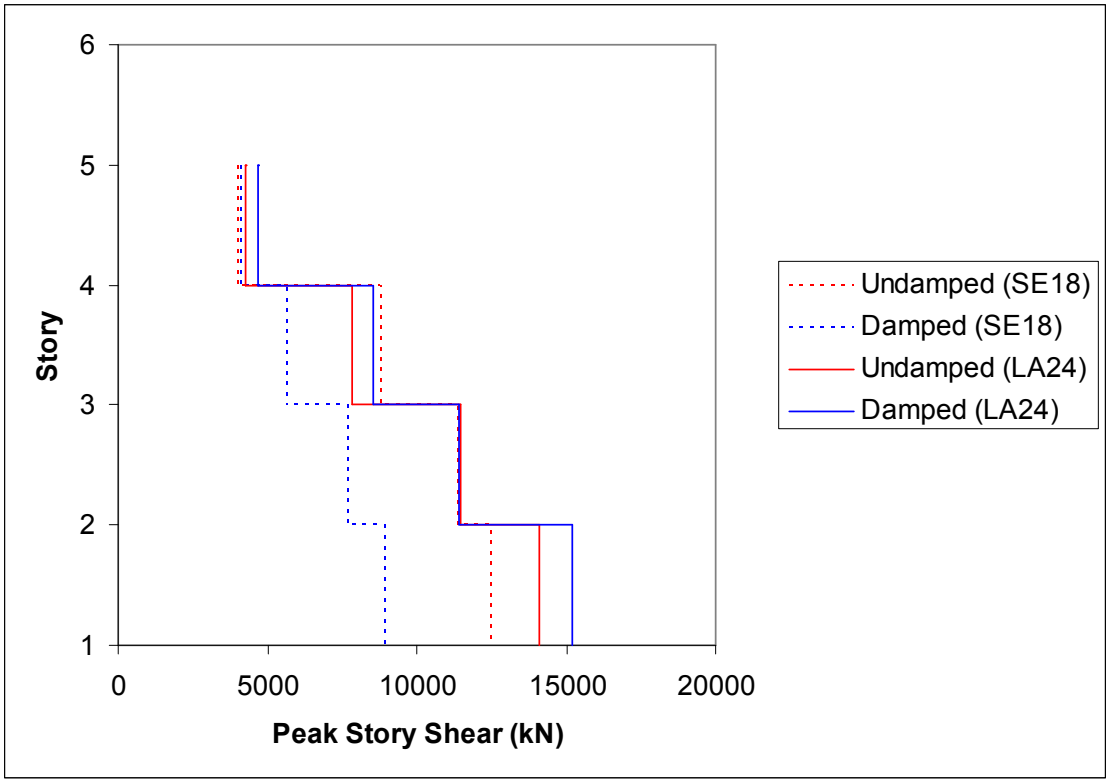

Figure 6.26 Peak Story Shears for BF-4, BSE-1 (SE18) and BSE-2 (LA24) Motions

The story shears demonstrated in Figure 6.26 again reflect the numerical instabilities introduced as braces buckle in compression. Due to the relatively small time interval over which buckling occurs, the peak brace compressive load becomes inherently omitted from the numerical analysis as the hysteresis loop skips the peak capable buckling load and proceeds immediately to a post-buckled capacity with lower reaction and high displacement as demonstrated in Figures 6.24, 6.25 and 6.26. While the modeling predicts that buckling of braces does not occur for the damped case of the BSE-1 ground motion (SE18) Figure 6.27 depicts brace nonlinearity (buckling) for the undamped case. This figure is also an accurate reflection of the brace nonlinearity for the damped case of the BSE-2 (LA24) ground motion. This is consistent with peak story displacements shown in Figure 6.24 which shows a similarity of the peak story

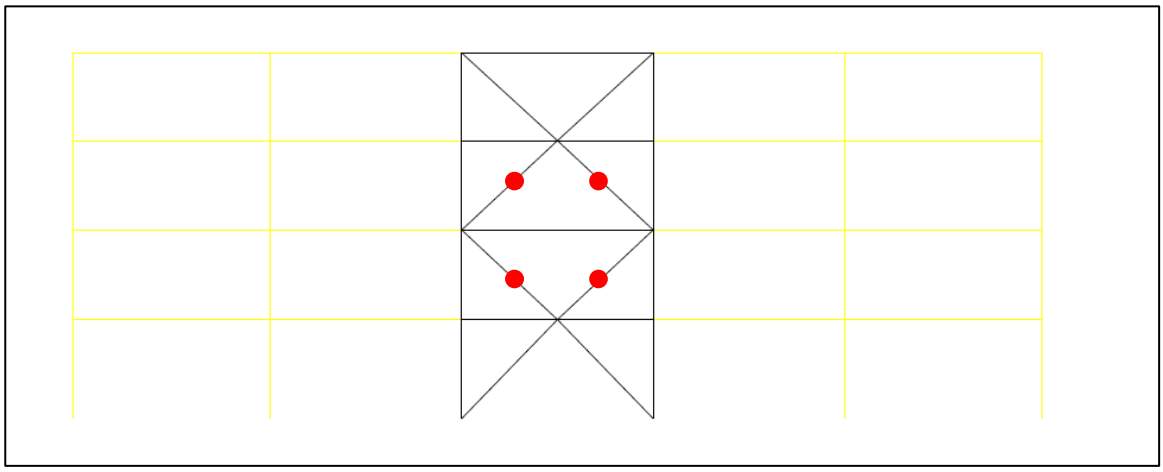

Figure 6.27 Plastic Hinge Formations for Undamped BF-4, Medium Site and BSE-1 (SE18) Motion and Damped BF-4, Medium Site BSE-2 (LA24)

displacements between the undamped case of BSE-1 and the damped case for BSE-2. Figure 6.28 depicts the brace nonlinearity (buckling) for the undamped model for BF-4, the BSE-2 (LA24) motion and the medium site condition. As shown, the degree of nonlinearity for this case is markedly greater than the damped case demonstrating the beneficial effects of the NRTMDF.

For the soft site condition for BF-4, motions SE07 and LA36 represent BSE-1 and BSE-2 respectively. Figures 6.29 and 6.30 illustrate the building hystereses loops for each motion. Similar to the hard and medium site conditions, the BSE-1 record demonstrates primarily linear behavior with roughly similar demands for nonlinearity between the damped and undamped cases. For the BSE-2 motion, Figure 6.30 demonstrates significant nonlinear demands for both the damped and undamped cases. As demonstrated previously (Table 6.12 and Figure 6.6) the nonlinear period shift for this case does not serve to decrease the spectral acceleration ordinate until significant yielding and soft behavior of the NRTMDF has occurred. In fact, the shift produced by initial elastic behavior of the NRTMDF results in no decrease of the spectral acceleration but a

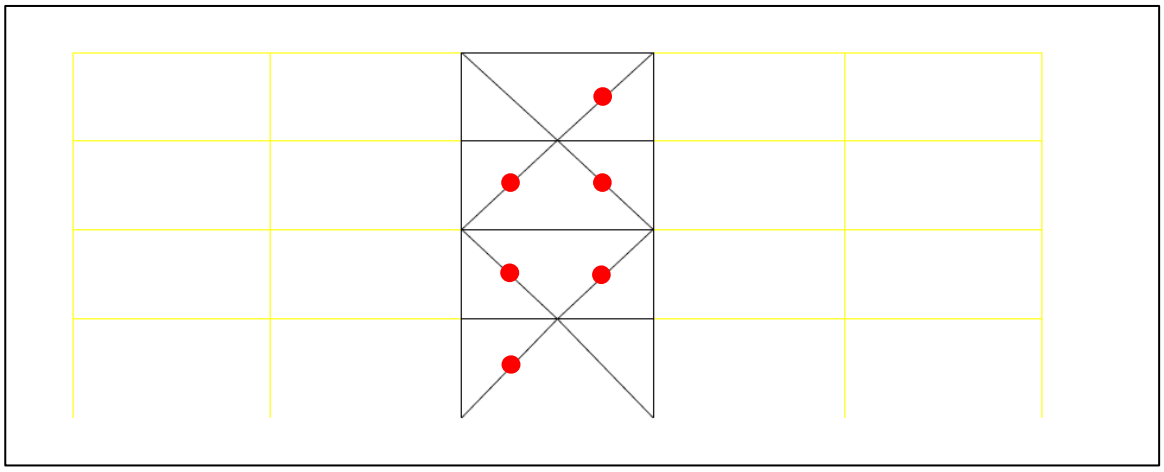

Figure 6.28 Plastic Hinge Formations for Undamped BF-4, Medium Site and BSE-2 (LA24) Motion

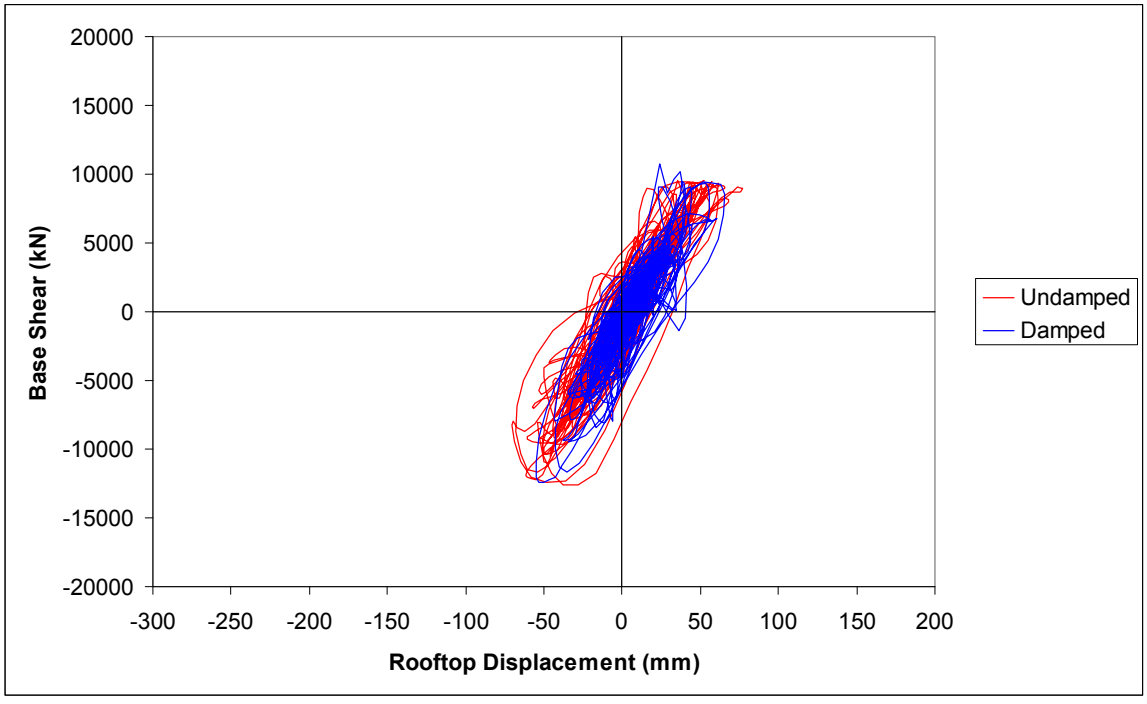

Figure 6.29 BF-4 Hysteresis Loop for Soft Site, BSE-1, SE07 Motion

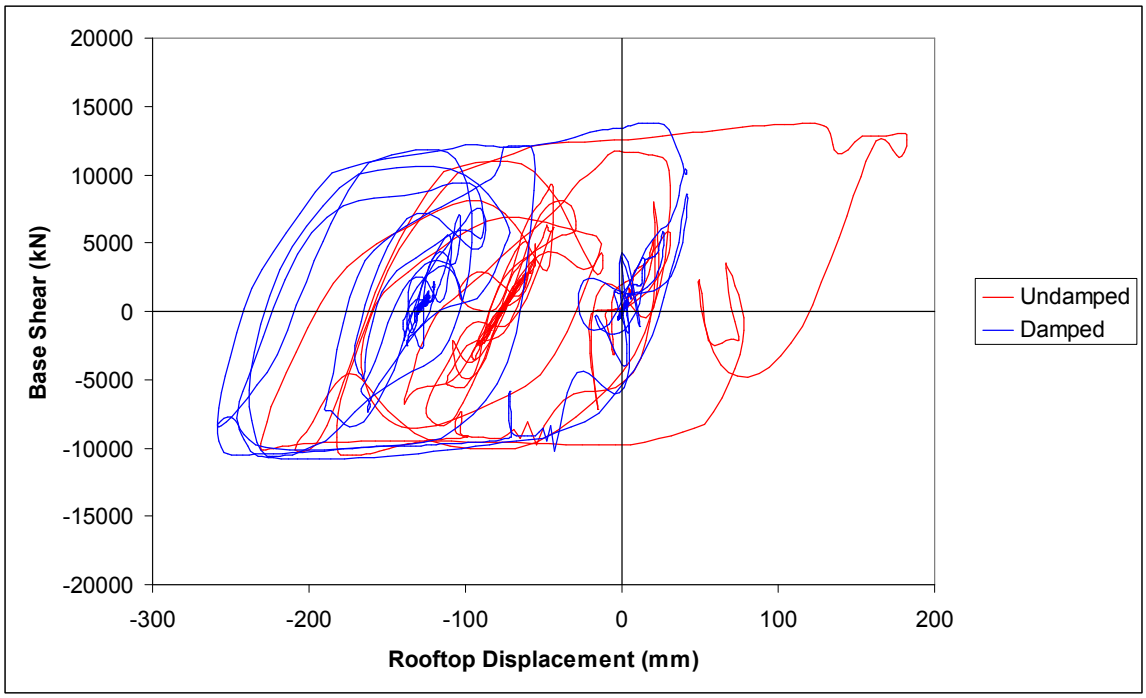

Figure 6.30 BF-4 Hysteresis Loop for Soft Site, BSE-2, LA36 Motion

small increase in the ordinate. The increased mass due to the NRTMDF then simply translates to larger overall demand with no appreciable reduction discernible in any output parameter. This is reflected in the rooftop displacement histories of Figure 6.31 and 6.32. For BSE-1, a difference is observed between the damped and undamped cases which can be corroborated by observing the change in spectral acceleration ordinate of Figure 6.5 enabled by the NRTMDF. For BSE-2, the rooftop displacement history demonstrates nonlinearity for both damped and undamped cases, with higher permanent nonlinear rooftop displacement for the damped case (128mm) as opposed to the undamped case (75mm). Hystereses loops for the buckling restrained braces of the NRTMDF also reflect an unfavorable response for the soft soil condition for the model. Figures 6.33 and 6.34 depict the hystereses loops and demonstrate a relatively small envelope of nonlinear demand for the BSE-1 condition while the BSE-2 condition

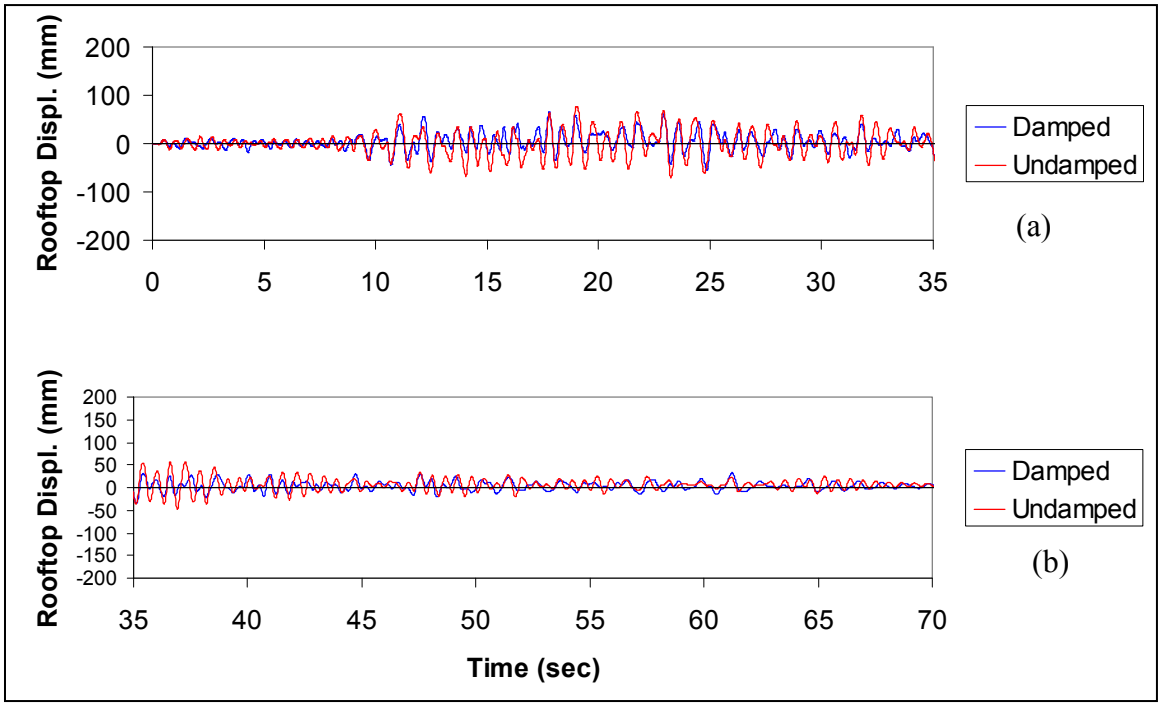

Figure 6.31 BF-4 Rooftop Displacement History for Soft Site, BSE-1, SE07 Motion

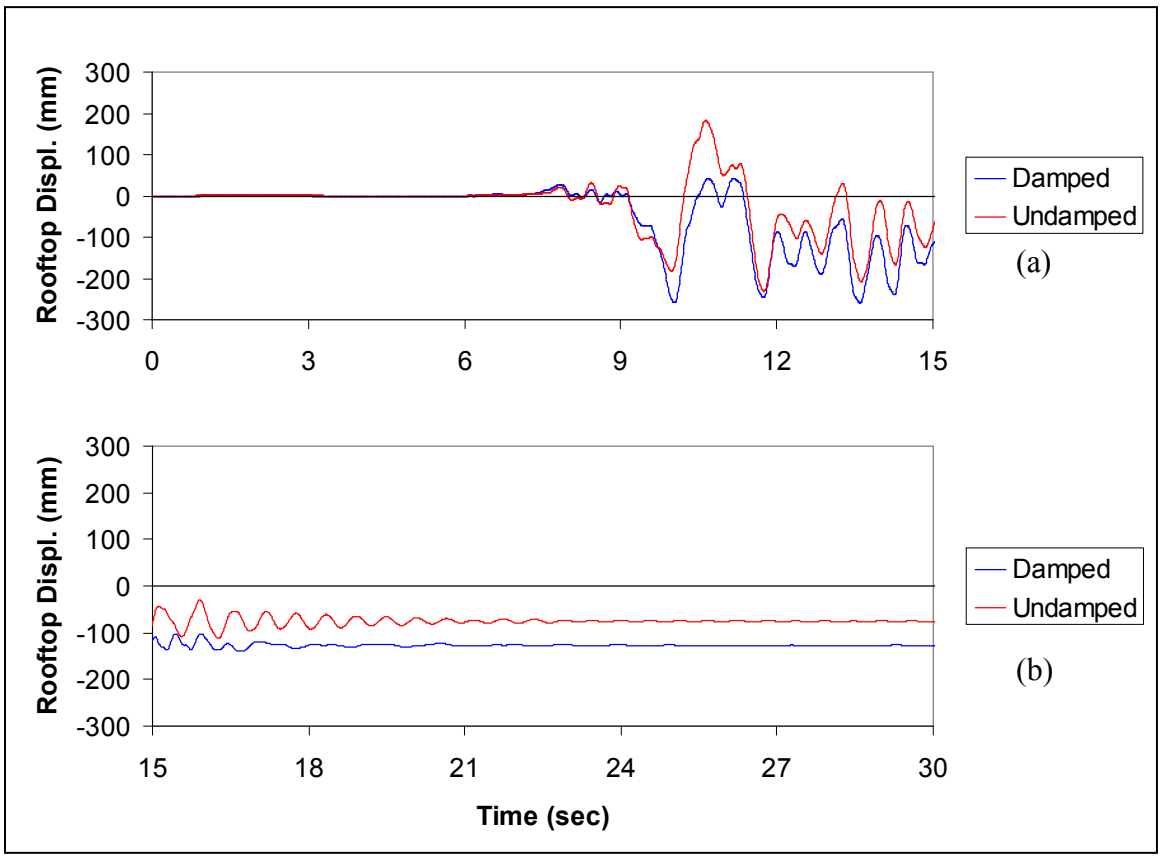

Figure 6.32 BF-4 Rooftop Displacement History for Soft Site, BSE-2, LA36 Motion

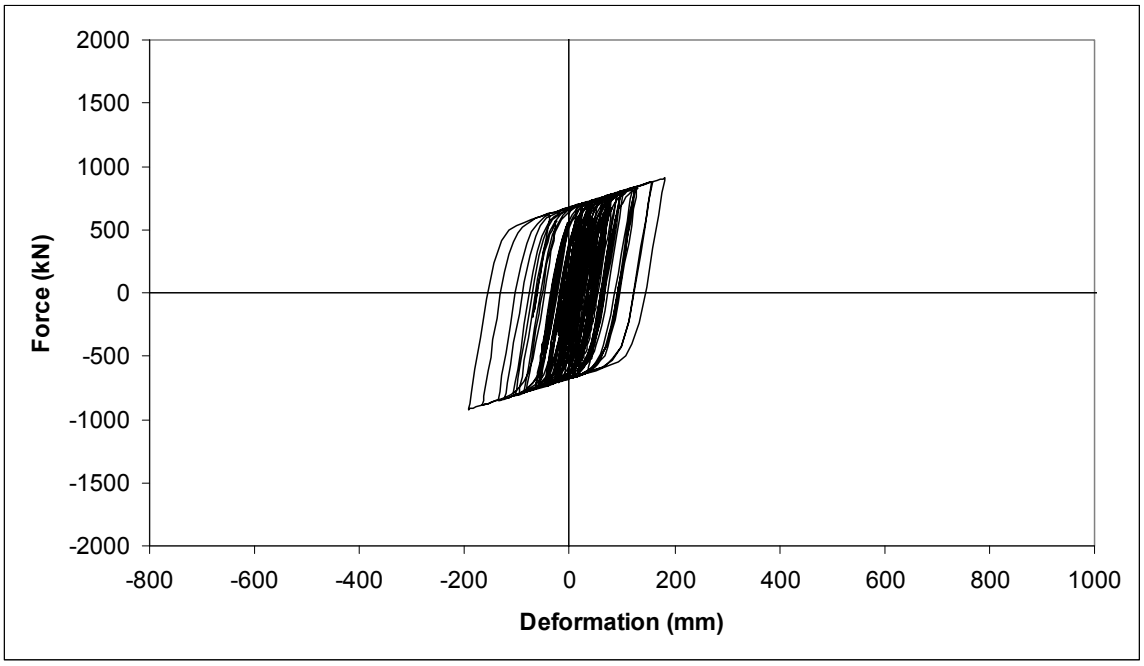

Figure 6.33 BF-4 NRTMDF Buckling Restrained Brace Hysteresis Loop for Soft Site, BSE-1, SE18 Motion

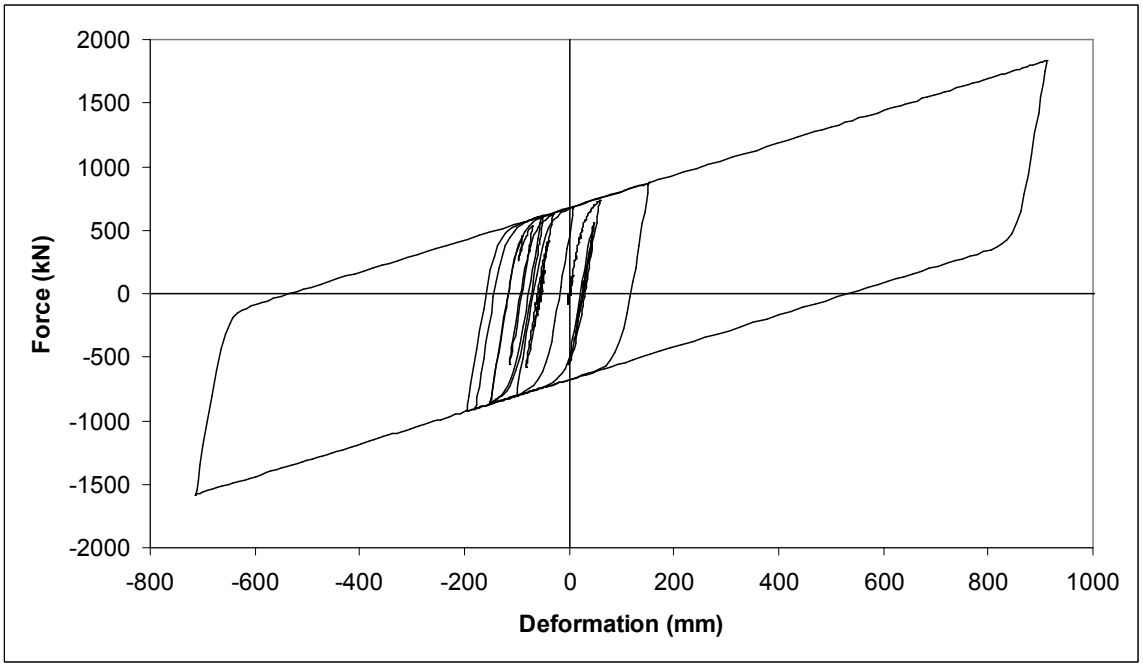

Figure 6.34 BF-4 NRTMDF Buckling Restrained Brace Hysteresis Loop for Soft Site, BSE-2, LA36 Motion

demonstrates significant nonlinear demand with deformations likely beyond the deformational capacity of the buckling restrained brace yielding cores. Such deformations reflect the overall motion of the NRTMDF and the inability to tune the system for effective performance for BSE-1 and BSE-2 while maintaining an NRTMDF with displacements within a practical range. For BSE-1, performance enhancements should be realized. However, the BSE-2 motion and soft site ground condition reflect a reduced ability for enhanced performance. Attempts to tune for optimal performance for BSE-2 may come at the expense of effective performance for BSE-1 thereby reflecting an incompatibility in the performance objectives for this condition. This reflects the concept of competing performance objectives and supports the concept of weighting the performance toward the magnitude of event correlating to the preferred objective. For instance, BSE-2 may represent an earthquake of such destructive capacity yet so rare for a particular site that it may be beyond pragmatic purposes to design the system for its eventuality. For such a case, BSE-1 may more appropriately represent the targeted event and performance of the system may be tuned for its magnitude and characteristics.

Figures 6.35 through 6.37 depict the peak story displacements, drift indices and story shears for BF-4 and the soft site conditions for BSE-1 (SE07) and BSE-2 (LA36) motions. While these parameters in general reflect a reduction in response enabled by the NRTMDF the reductions are not as great as those of the hard and medium site conditions. Furthermore, the output parameters are of larger magnitude thereby reflecting amplified behavior expected of a soft site condition. The modeling predicts this increase in response and demonstrates the formation of mechanisms, specifically, braces buckling in

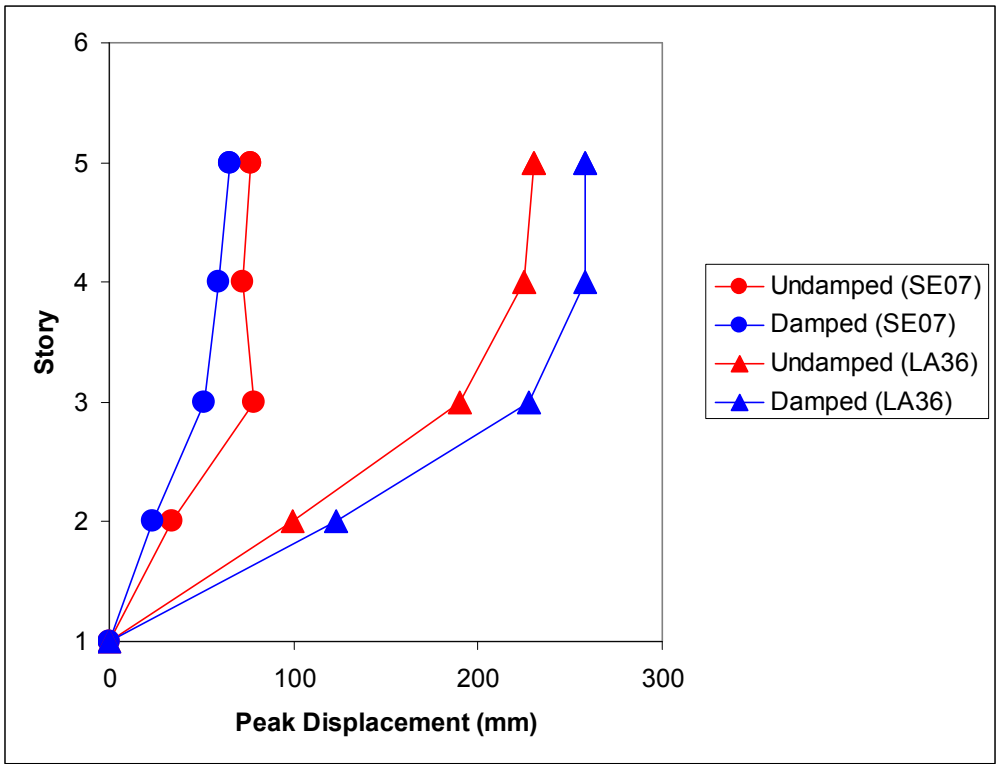

Figure 6.35 Peak Story Displacements for BF-4, BSE-1 (SE07) and BSE-2 (LA36) Motions

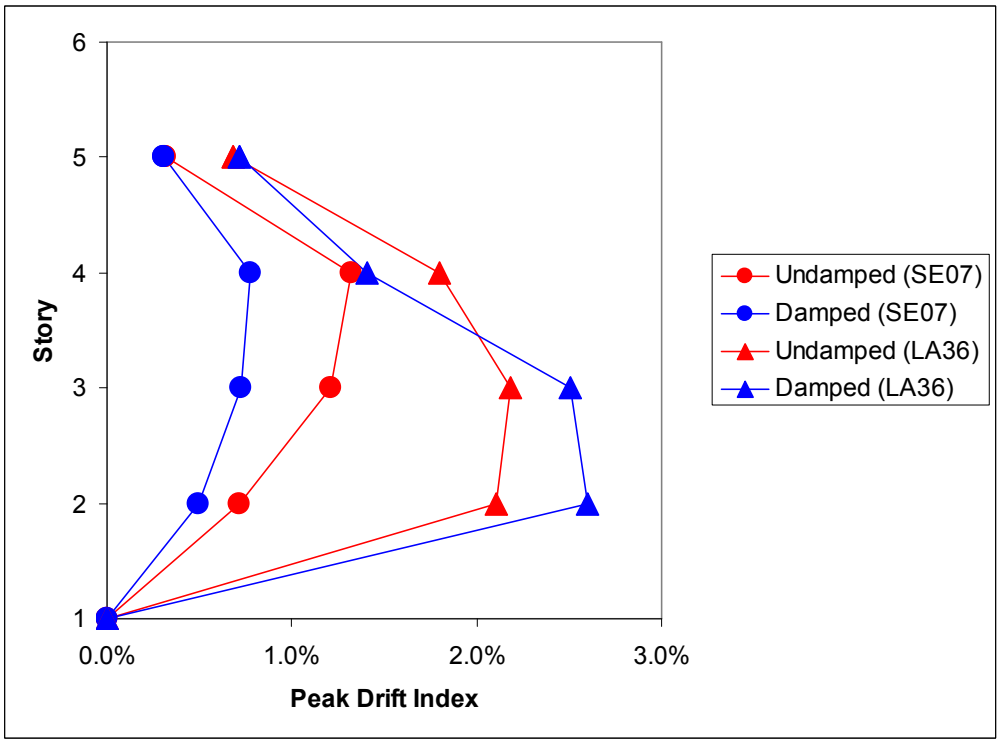

Figure 6.36 Peak Drift Indices for BF-4, BSE-1 (SE07) and BSE-2 (LA36) Motions

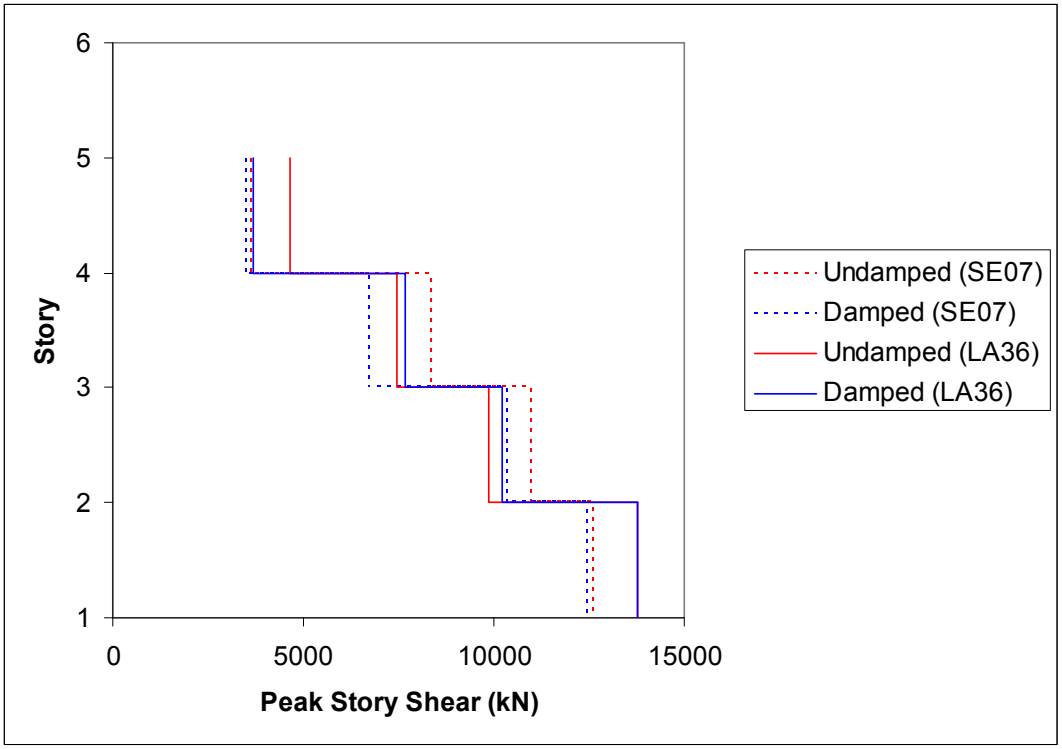

Figure 6.37 Peak Story Shears for BF-4, BSE-1 (SE07) and BSE-2 (LA36) Motions

compression. For these cases, Figures 6.38 and 6.39 depict the buckling of braces for the undamped and damped cases respectively for BSE-1 (SE07 motion). Likewise, Figure 6.40 depicts the buckling of braces for the undamped and damped conditions of BSE-2 (LA36) with little difference between the two cases, reflecting the relatively small change in peak displacements shown in Figure 6.35. These results reflect the concept of diminished capability of performance for the NRTMDF for the soft site soil conditions.

6.1.2 SW-1 Time History Output Examples

Hysteretic output for model SW-1 demonstrates similar trends to those shown for BF-4 with deviations reflecting different dynamic properties of this relatively stiff shear wall building. Figures 6.41 and 6.42 demonstrate the building hysteresis of the damped and undamped structures for the hard site condition using representative ground motions

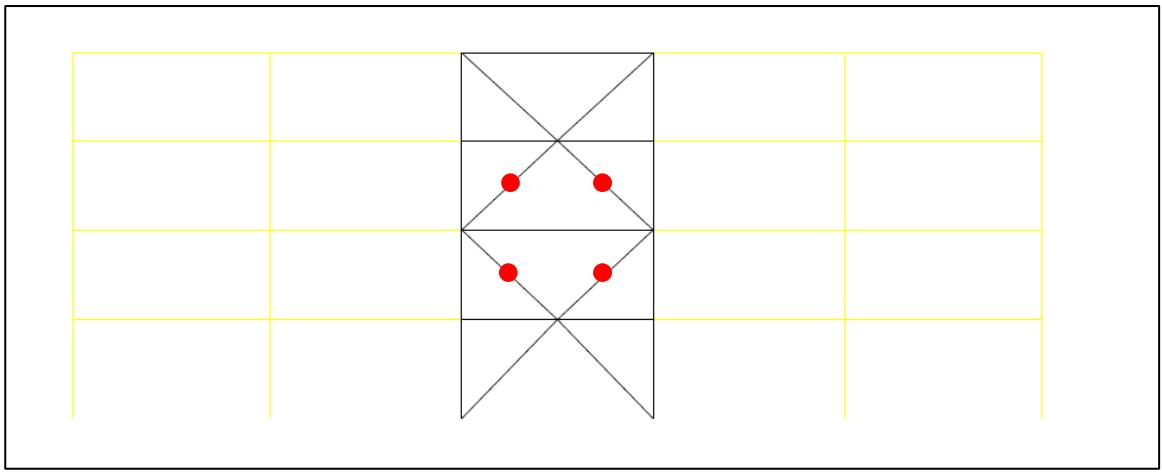

Figure 6.38 Plastic Hinge Formations for Undamped BF-4, Soft Site and BSE-1 (SE07) Motion

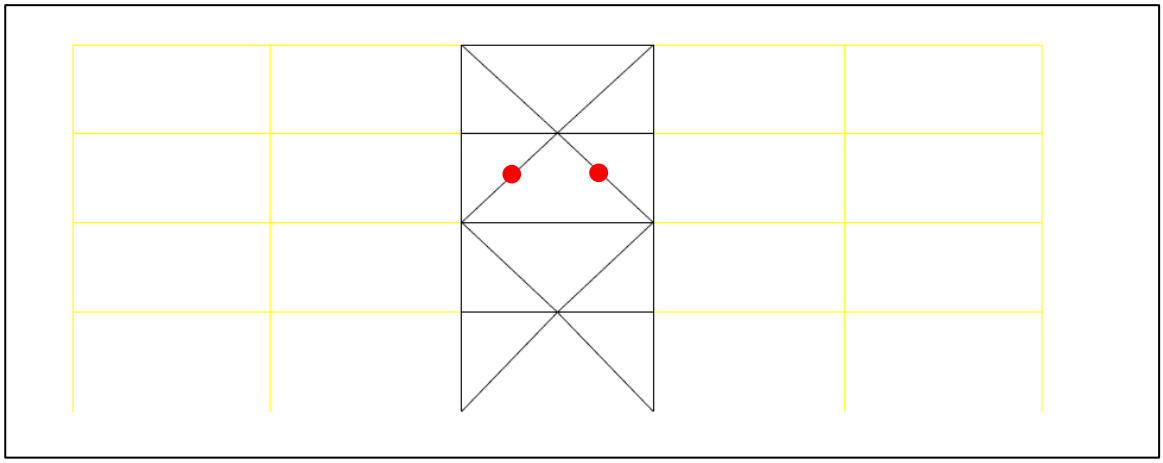

Figure 6.39 Plastic Hinge Formations for Damped BF-4, Soft Site and BSE-1 (SE07) Motion

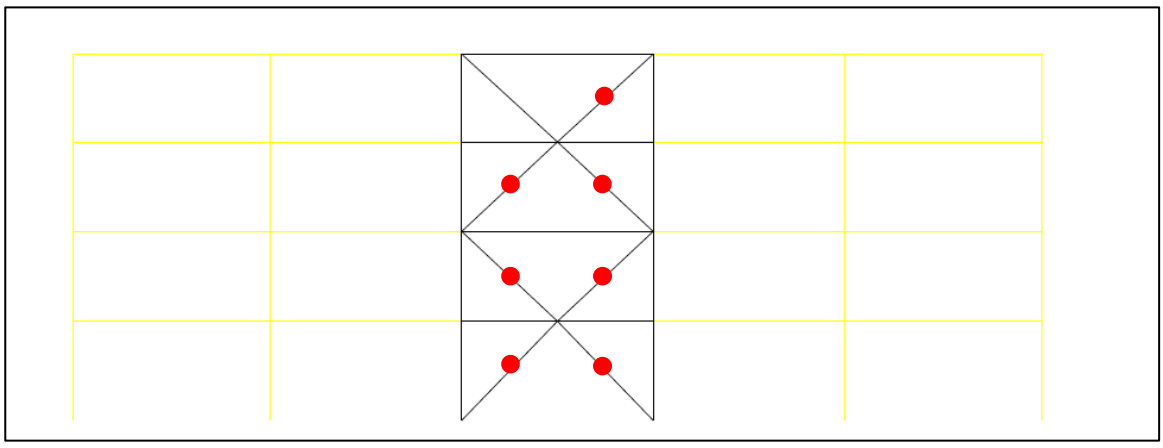

Figure 6.40 Plastic Hinge Formations for Undamped and Damped BF-4, Soft Site and BSE-2 (LA36) Motion

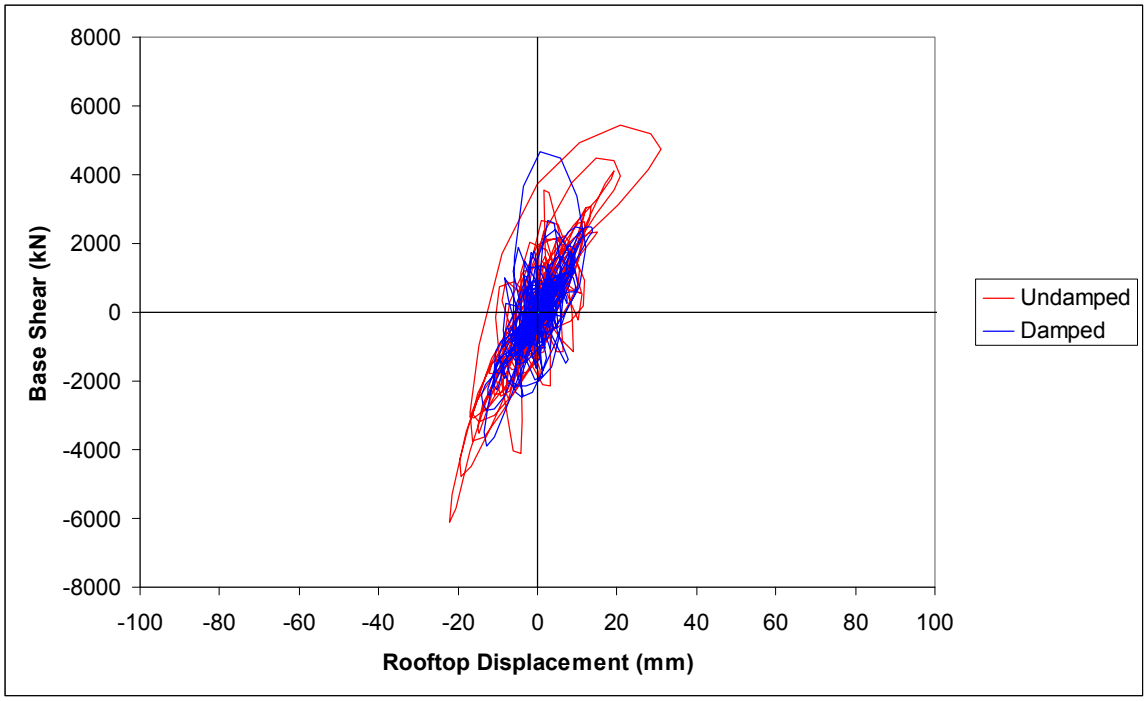

Figure 6.41 SW-1 Hysteresis Loop for Hard Site, BSE-1, SE04 Motion

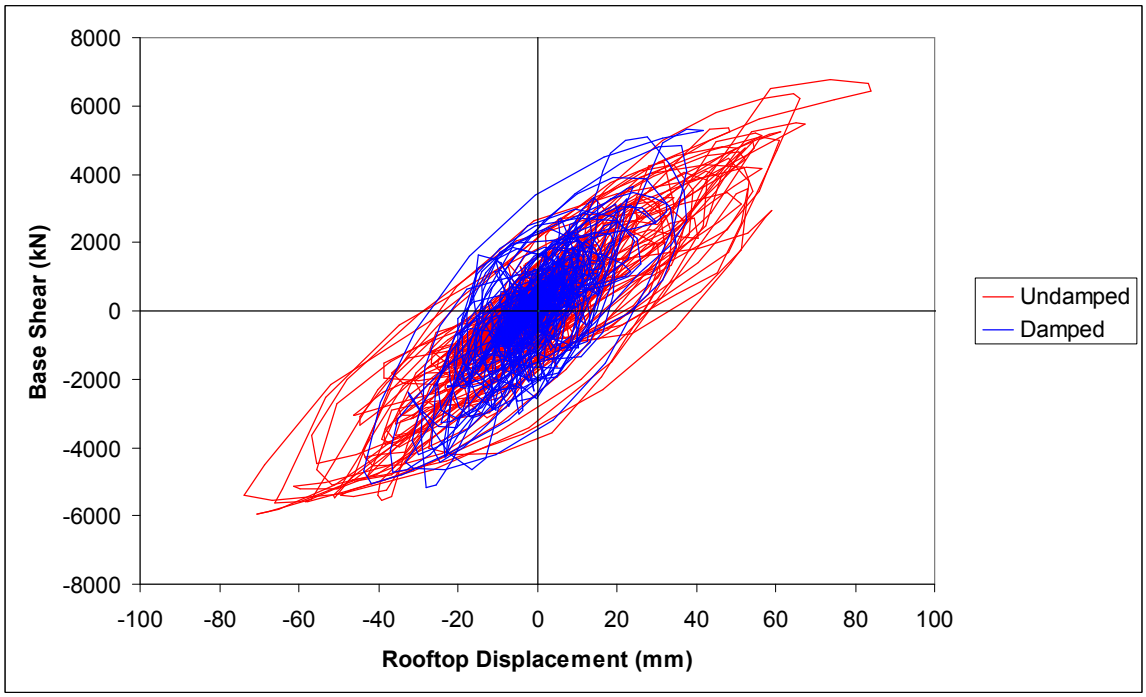

Figure 6.42 SW-1 Hysteresis Loop for Hard Site, BSE-2, SE25 Motion

SE04 and SE25 taken from the BSE-1 and BSE-2 suites, respectively. As demonstrated by the somewhat narrow hysteresis of Figure 6.41, the lesser BSE-1 motion drives minor nonlinear behavior of the system for both the damped and undamped cases. The NRTMDF enables reduced response for this structure primarily due to its mass, elastic action and the accompanying fundamental period shift. This can be observed in the hysteresis diagram as well as the rooftop displacement history of Figure 6.43. For the BSE-2 motion nonlinear action of the structure is increased as demonstrated by the hystereses of Figure 6.42. This figure also demonstrates the reduction in hysteretic demand for the damped case, while Figure 6.44 reflects this reduction in diminished peak rooftop displacement. Likewise, the hystereses loops of the NRTMDF shown in Figures

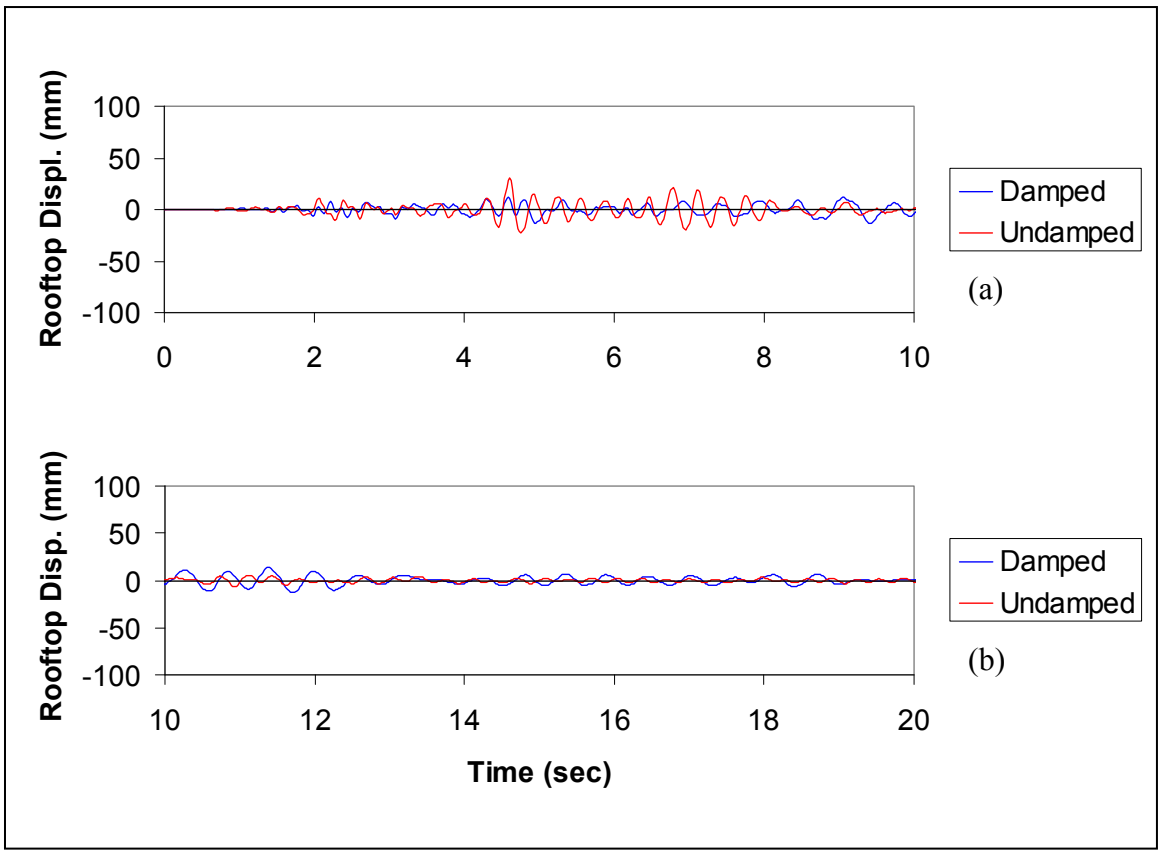

Figure 6.43 SW-1 Rooftop Displacement History for Hard Site, BSE-1, SE04 Motion

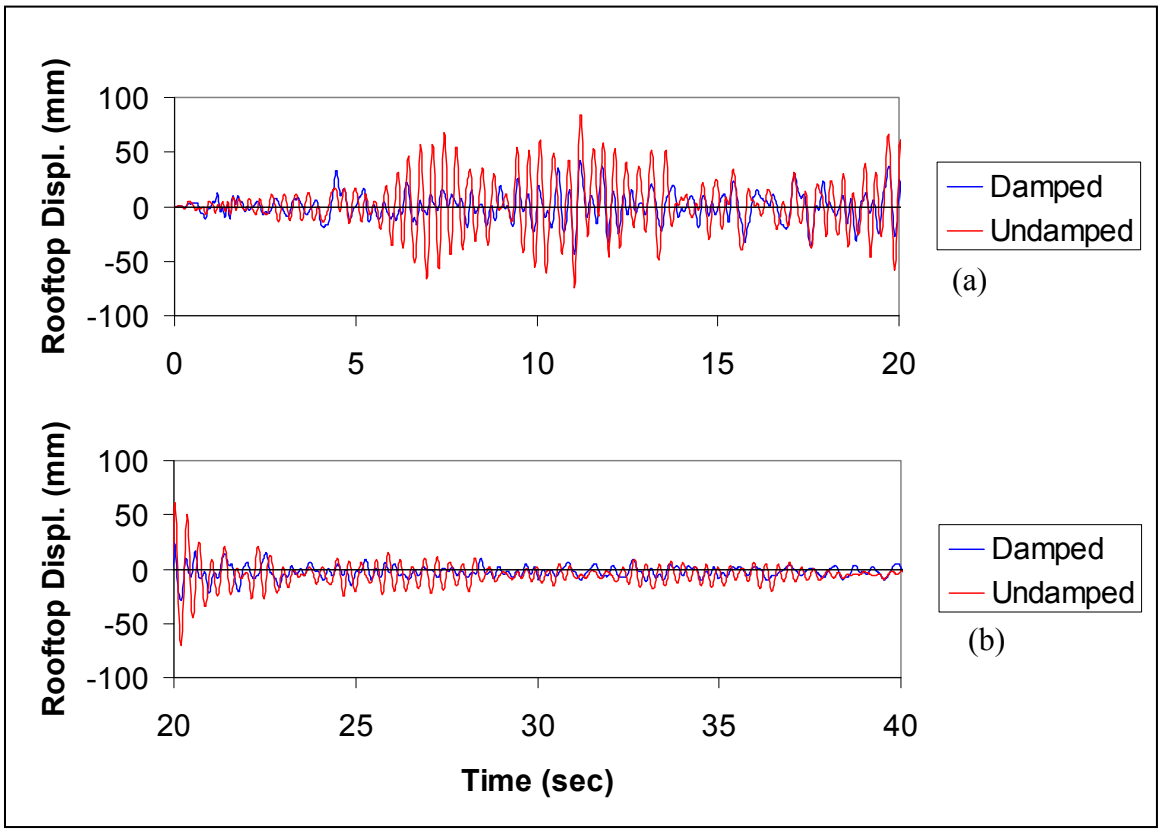

Figure 6.44 SW-1 Rooftop Displacement History for Hard Site, BSE-2, SE25 Motion

6.45 and 6.46 reflect minor nonlinearity for BSE-1 and significant nonlinearity for BSE-2. Figure 6.44 demonstrates permanent nonlinear deformation in undamped and damped rooftop motion histories for BSE 2 and the hard site condition with the damped permanent deformation being slightly less than the undamped permanent deformation.

Peak story displacements, story drifts and story shears are depicted in Figures 6.47, 6.48 and 6.49 respectively for SW-1 for BSE-1 (SE04), BSE-2 (SE25) and the hard site condition. These figures depict primarily elastic behavior with no plastic hinge formation occurring except for the undamped case of BSE-2. Likewise Figure 6.50 displays the hinge formation at the bottom stories only for this case which is also apparent in the drift index at the bottom floor, which is nearly 4 times greater for the

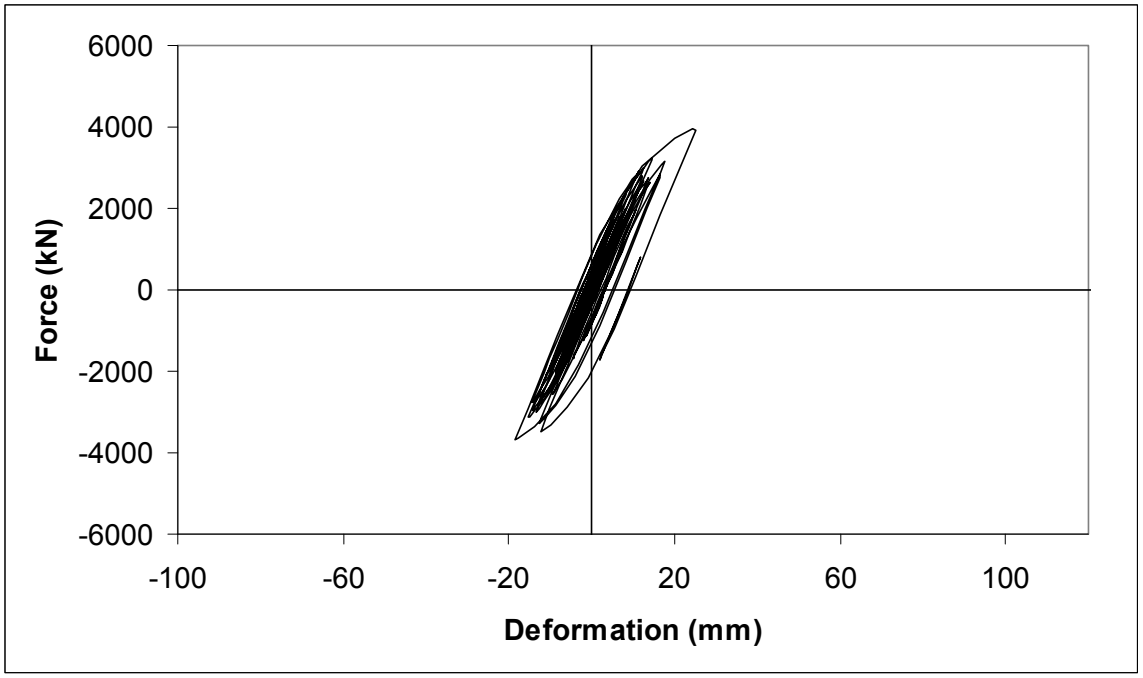

Figure 6.45 SW-1 NRTMDF Buckling Restrained Brace Hysteresis Loop for Hard Site, BSE-1, SE04 Motion

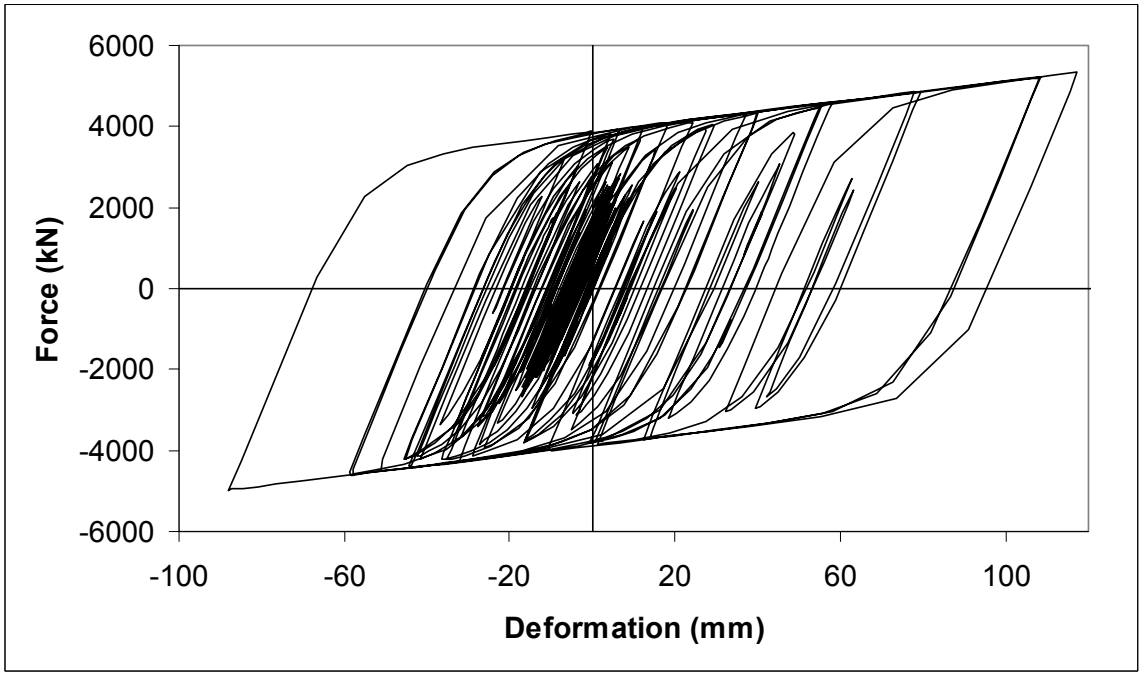

Figure 6.46 SW-1 NRTMDF Buckling Restrained Brace Hysteresis Loop for Hard Site, BSE-2, SE25 Motion

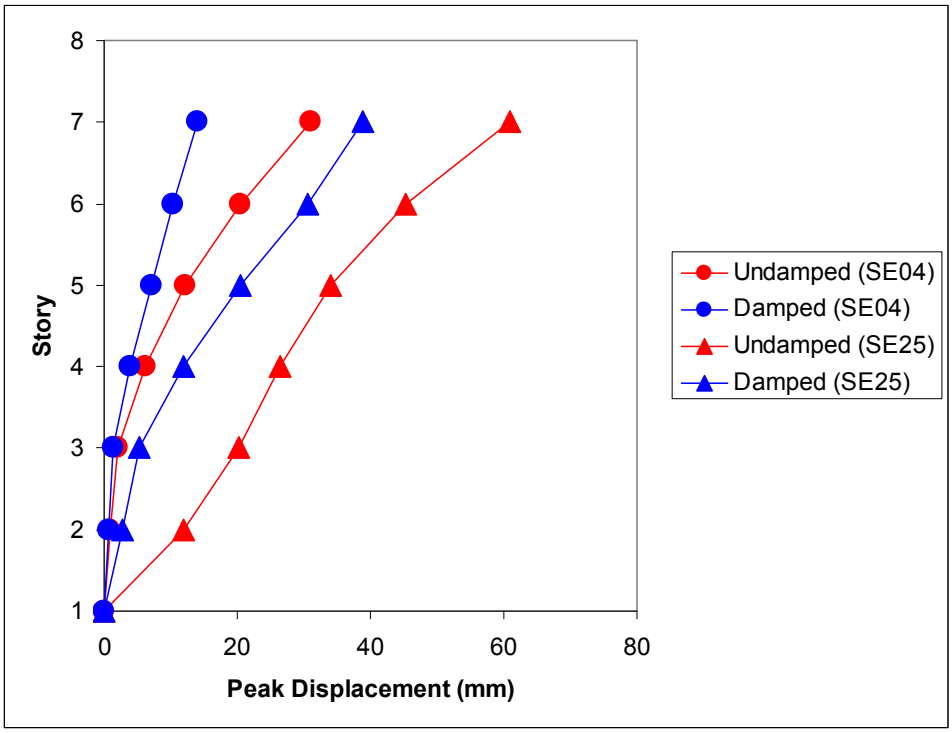

Figure 6.47 Peak Story Displacements for SW-1, BSE-1 (SE04) and BSE-2 (SE25) Motions

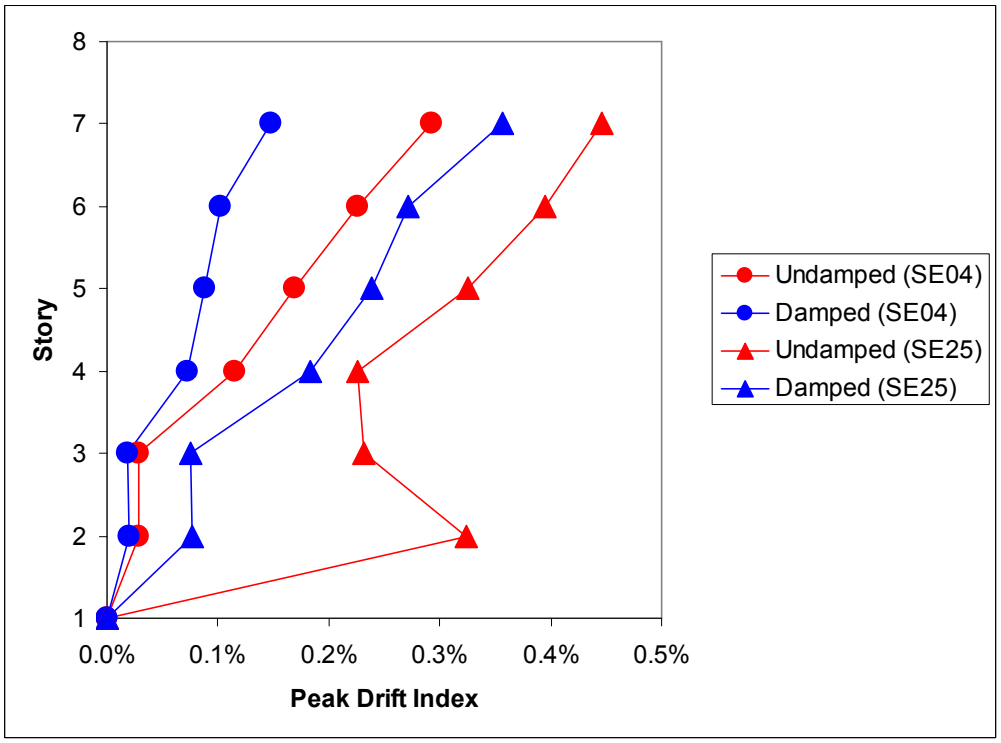

Figure 6.48 Peak Story Drift Indices for SW-1, BSE-1 (SE04) and BSE-2 (SE25) Motions

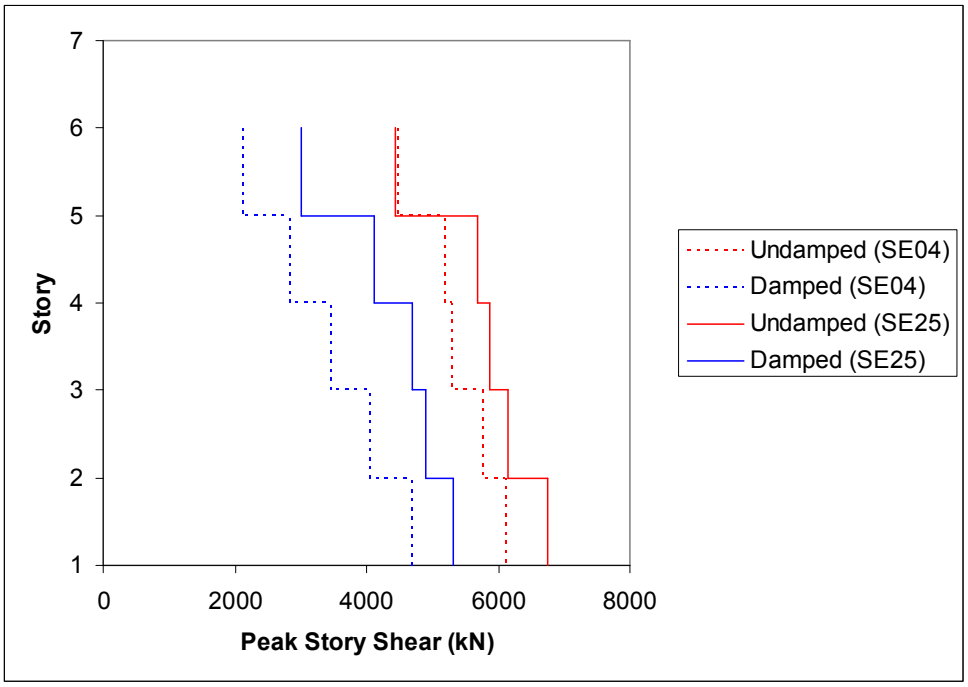

Figure 6.49 Peak Story Drift Indices for SW-1, BSE-1 (SE04) and BSE-2 (SE25) Motions

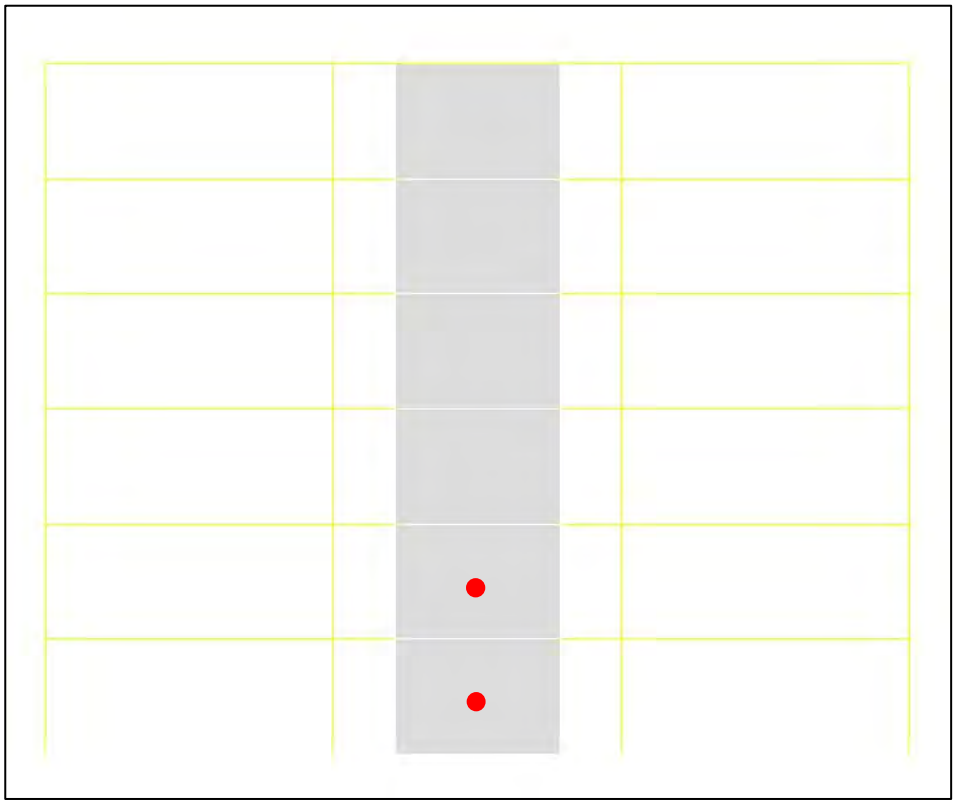

Figure 6.50 Plastic Hinge Formations for Damped SW-1, Soft Site and BSE-2 (LA36) Motion

undamped case than the damped case. Figures 6.51 and 6.52 depict the pier rotation and the curvature vs. yield curvature ratio for the piers at each story.

As reflected in the figures, the NRTMDF enables a significant reduction in response for this structure and the motions indicated. Perhaps the greatest benefit for this case is the predicted ability of the NRTMDF to mitigate nonlinearity of the shear walls of the building's lateral force resisting system for the BSE-2 motion.

The medium site condition for model SW-1 demonstrates behavior consistent with the hard site behavior and the similar condition for BF-4. Motions LA18 and SE28 represent BSE-1 and BSE-2 respectively for this case. Figures 6.53 and 6.54 demonstrate the undamped and damped building hystereses loops for this building and these motions where primarily linear behavior is observed for the BSE-1 motion and significant

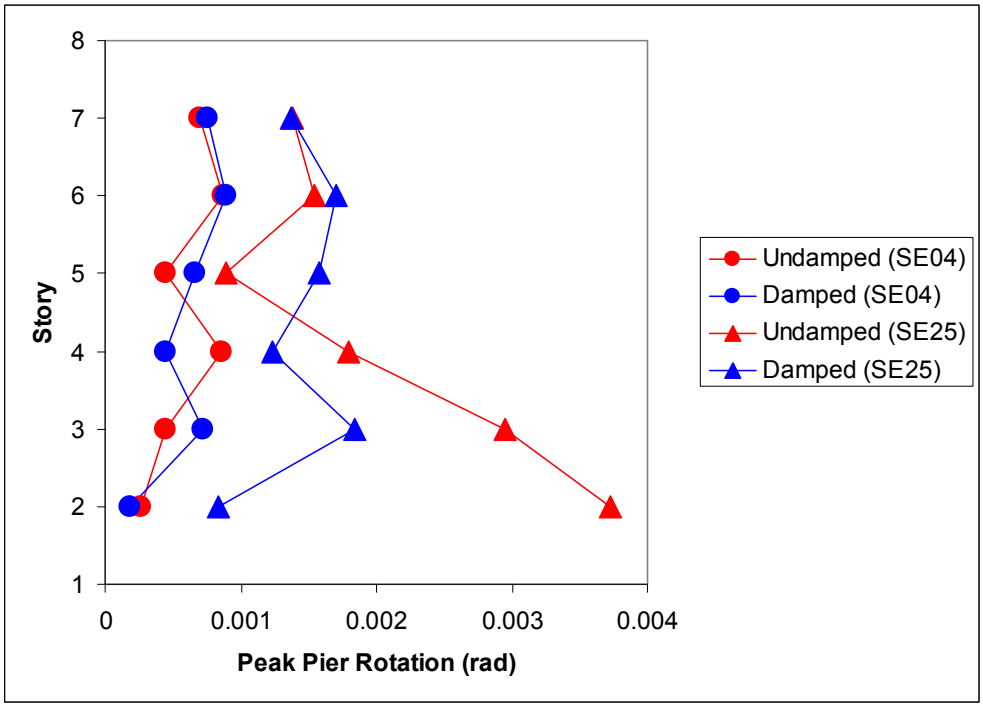

Figure 6.51 Peak Story Pier Rotations for SW-1, BSE-1 (SE04) and BSE-2 (SE25) Motions

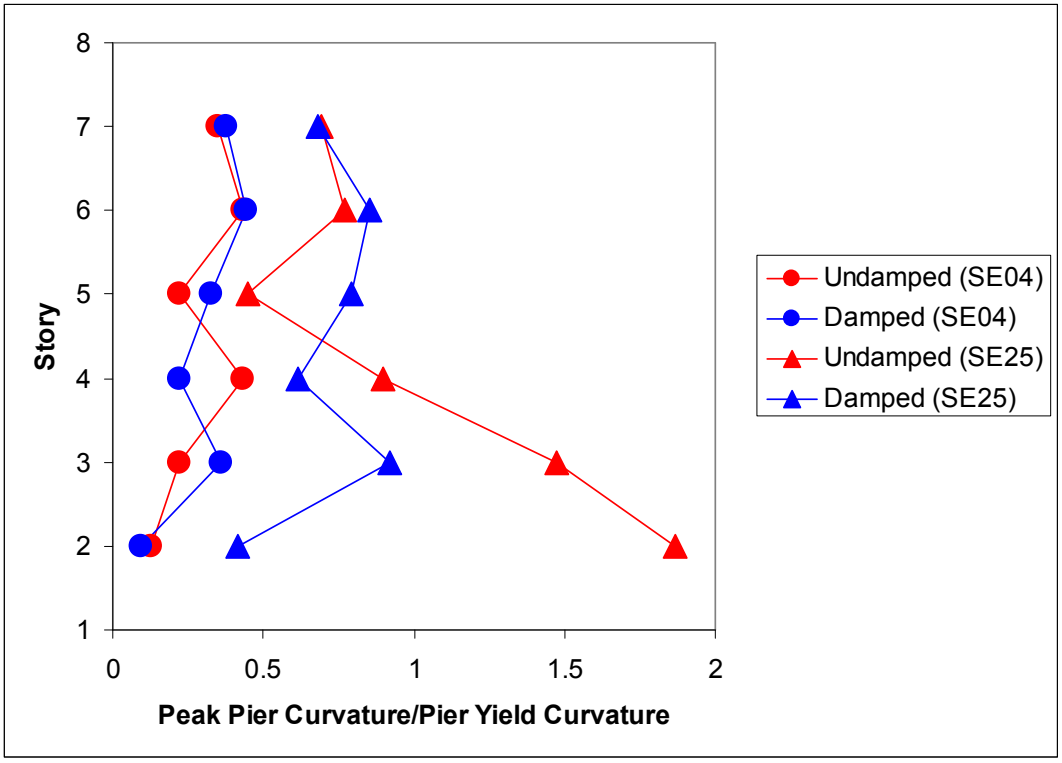

Figure 6.52 Peak Story Curvature Ratios for SW-1, BSE-1 (SE04) and BSE-2 (SE25) Motions

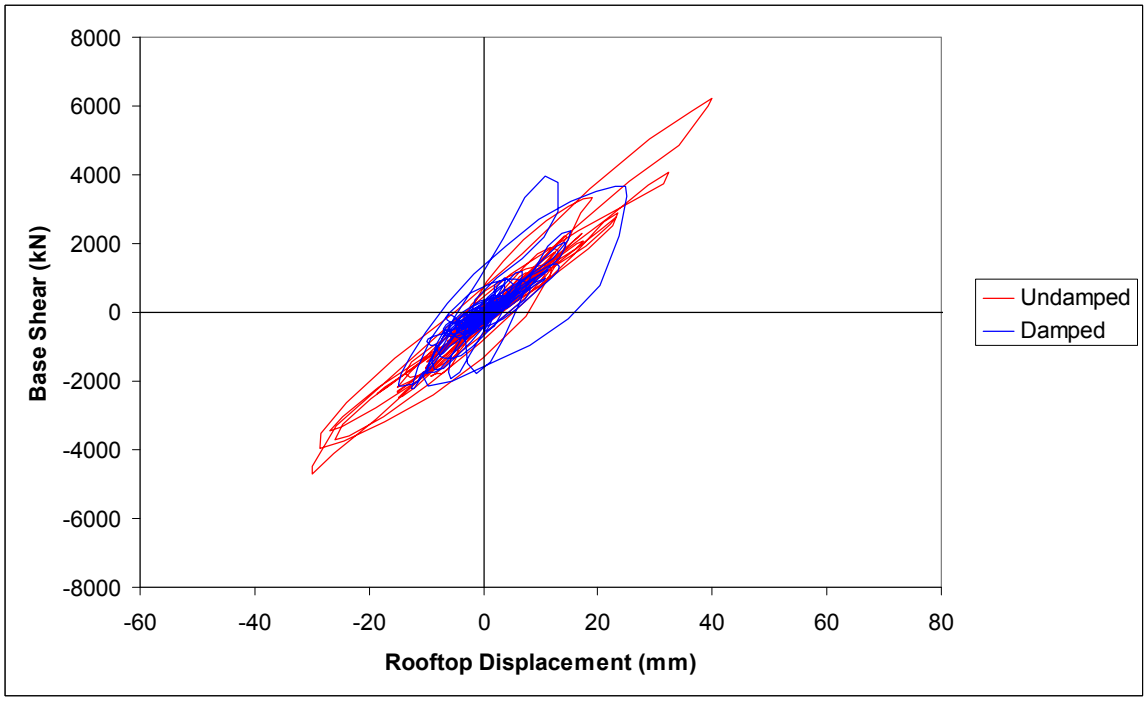

Figure 6.53 Hysteresis Loop for SW-1, Medium Site, BSE-1, LA18 Motion.

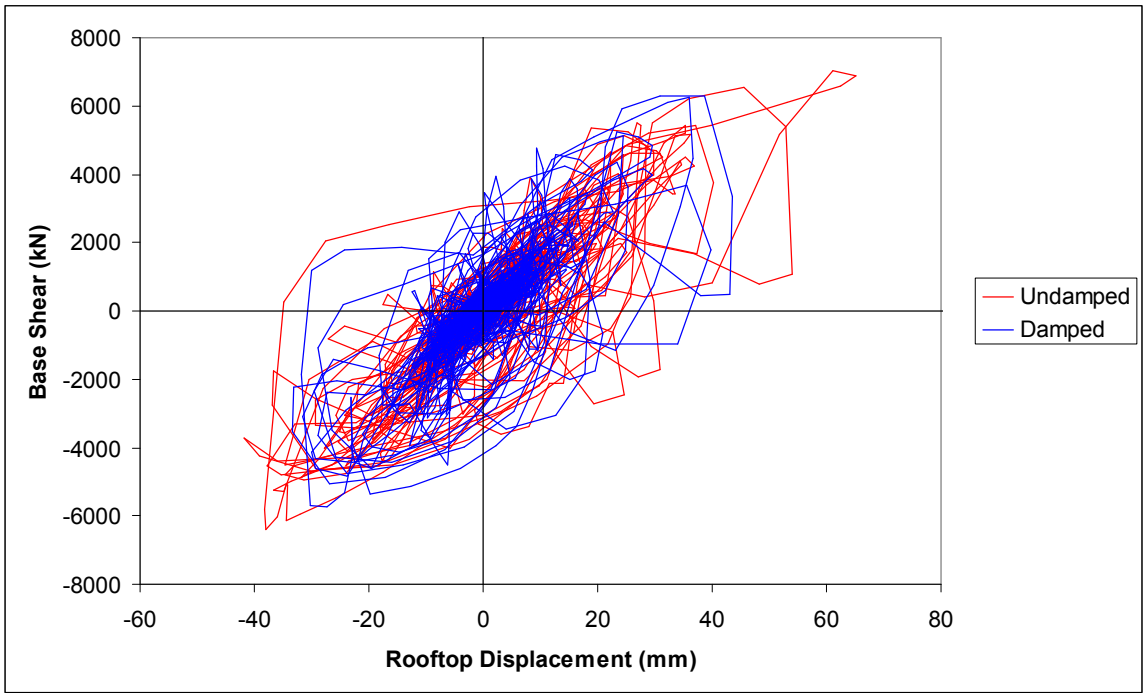

Figure 6.54 Hysteresis Loop for SW-1, Medium Site, BSE-2, SE28 Motion

nonlinear behavior can be observed for higher magnitude BSE-2 motion. Figures 6.55 and 6.56 depict the rooftop displacement histories which also reflect primarily linear behavior for BSE-1 and significant nonlinear demand for BSE-2. For each, the damped case reflects diminished demand with a reduced permanent nonlinear deformation for the damped case of BSE-2. Figures 6.57 and 6.58 depict the NRTMDF hysteresis loops and also reflect primarily linear behavior for BSE-1 and significant nonlinear behavior for BSE-2.

Figure 6.59, 6.60 and 6.61 depict the peak story displacements, story drift indices and story shears for SW-1 and the undamped and damped cases for BSE-1 (LA18) and BSE-2 (SE28). The figures demonstrate primarily elastic behavior for the BSE-1 motion

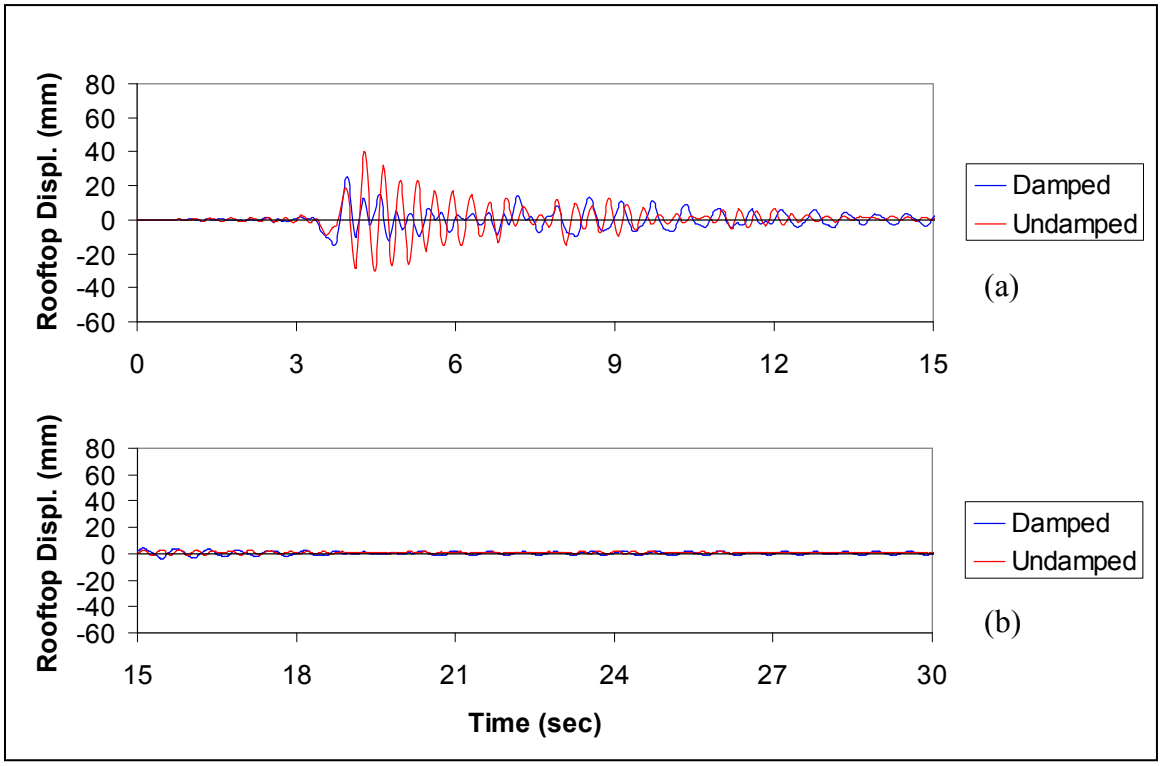

Figure 6.55 Rooftop Displacement History for SW-1, Medium Site, BSE-1, LA18 Motion

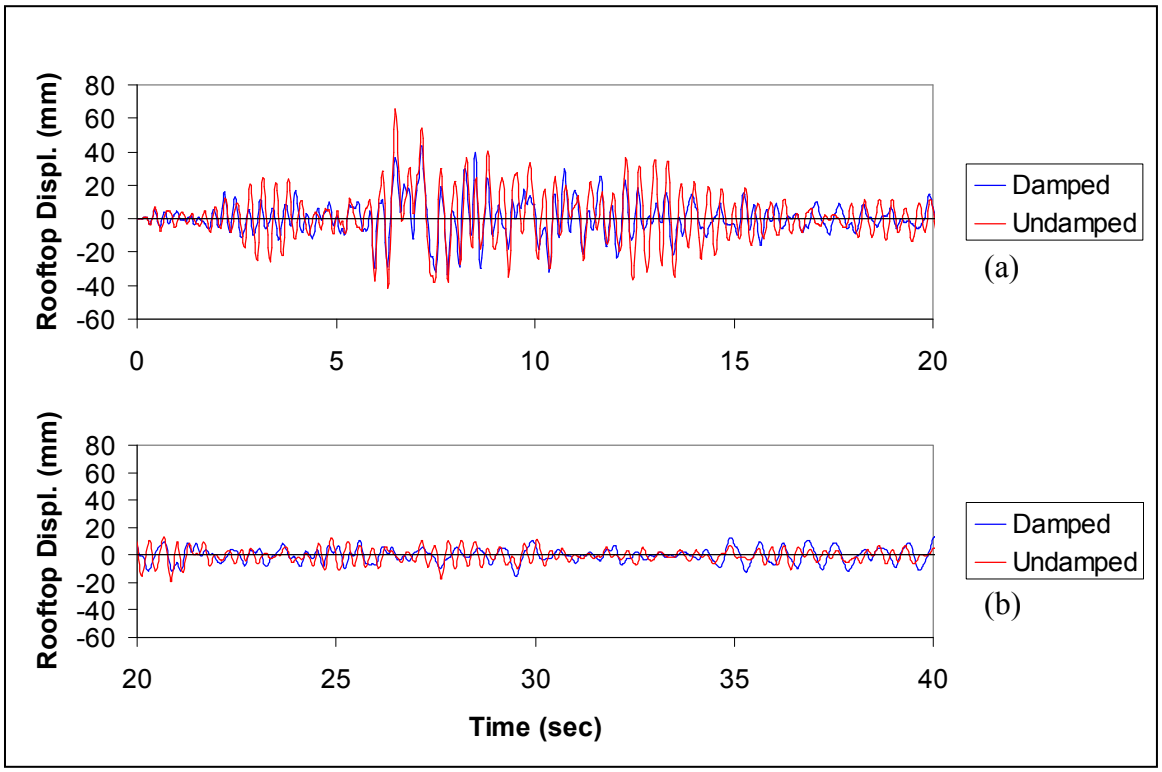

Figure 6.56 Rooftop Displacement History for SW-1, Medium Site, BSE-2, SE28 Motion

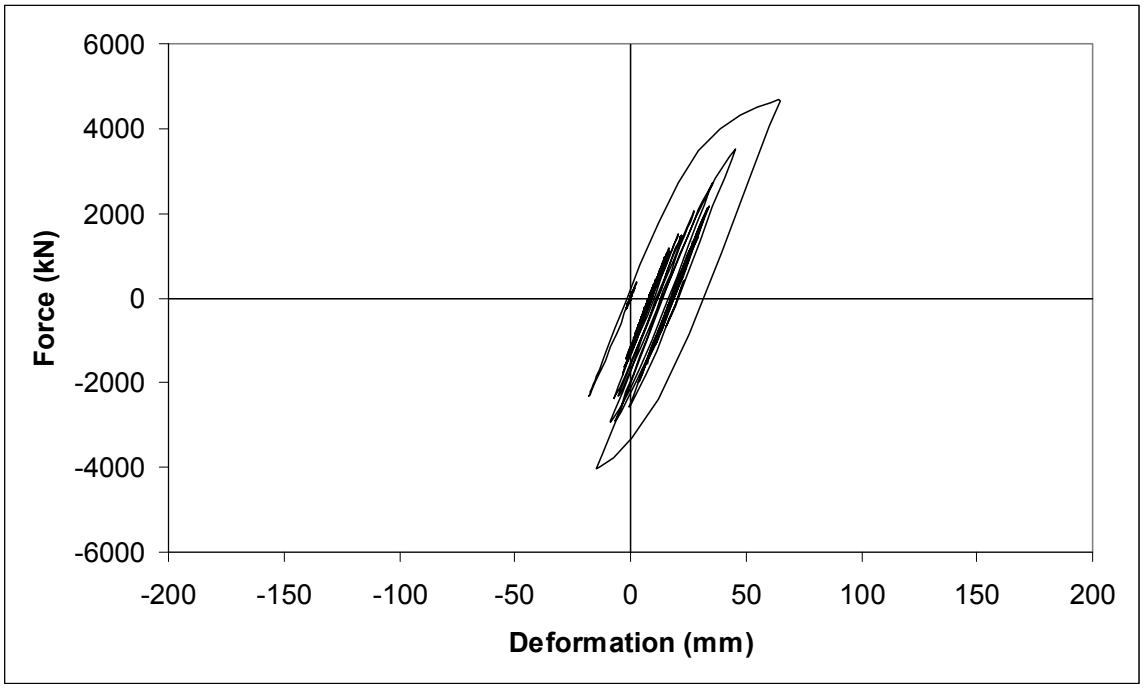

Figure 6.57 NRTMDF Buckling Restrained Brace Hysteresis Loop for SW-1, Medium Site, BSE-1, LA18 Motion

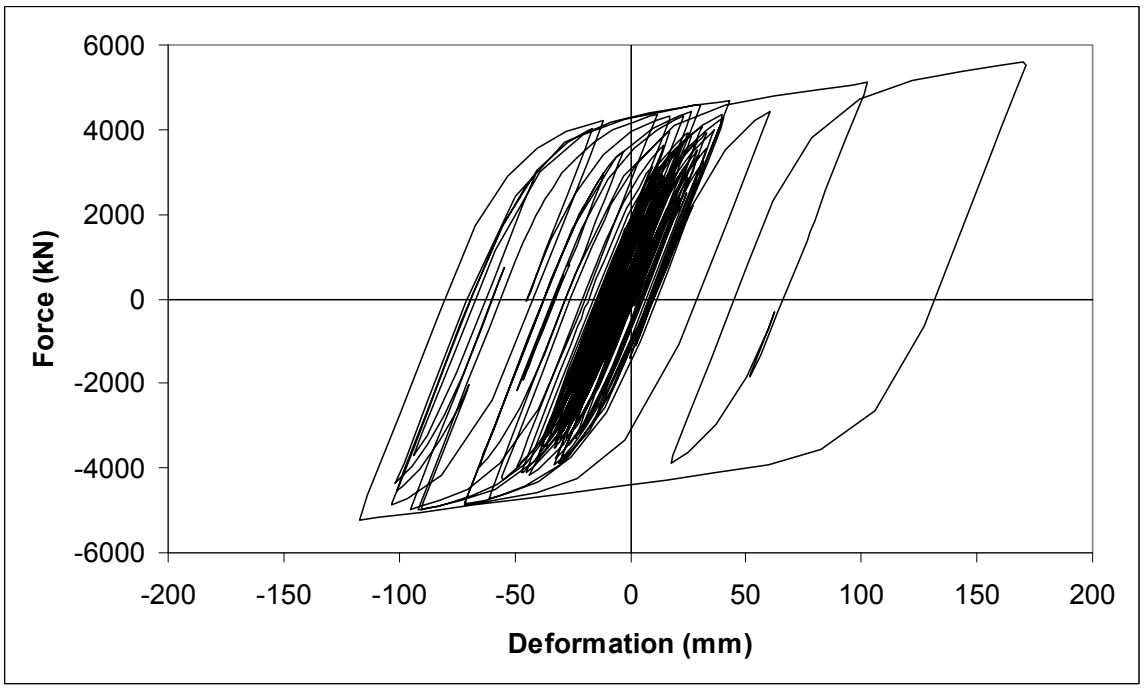

Figure 6.58 NRTMDF Buckling Restrained Brace Hysteresis Loop for SW-1, Medium Site, BSE-2, SE28 Motion

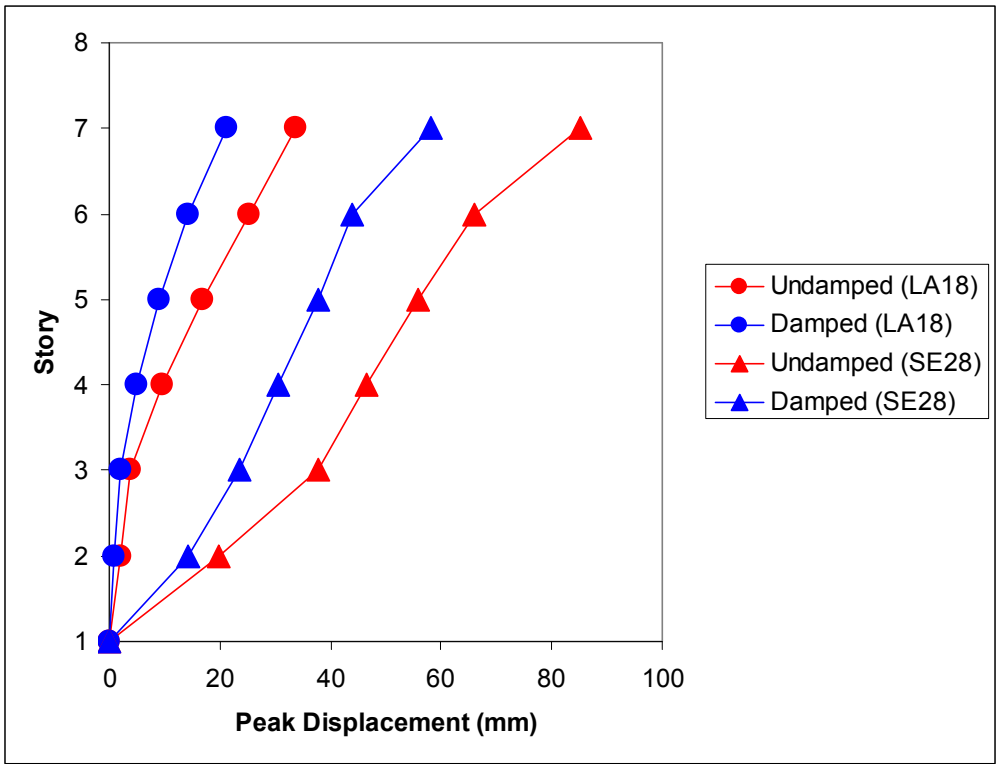

Figure 6.59 Peak Story Displacements for SW-1, BSE-1 (LA18) and BSE-2 (SE28) Motions

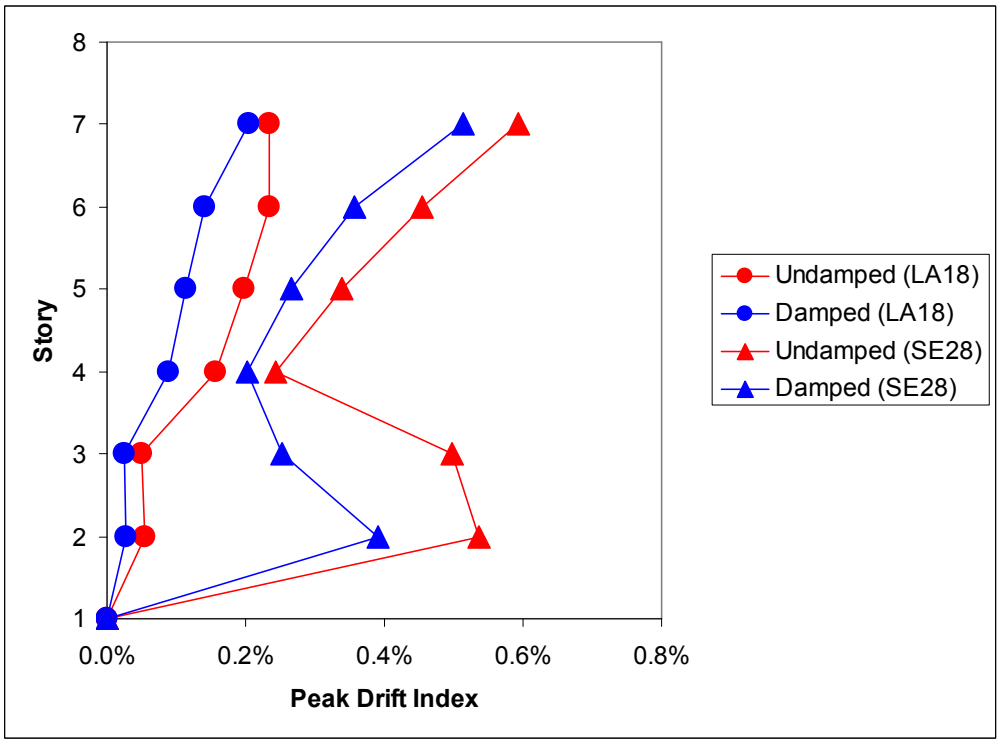

Figure 6.60 Peak Drift Indices for SW-1, BSE-1 (LA18) and BSE-2 (SE28) Motions

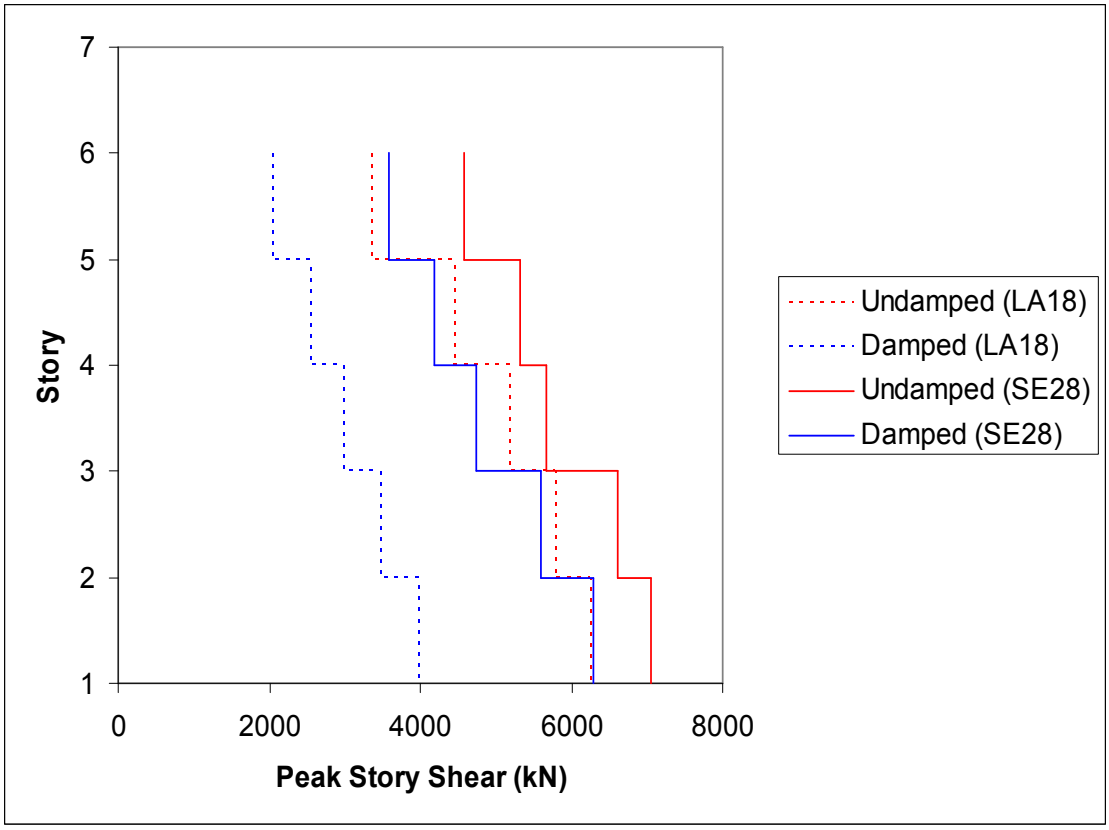

Figure 6.61 Peak Story Shears for SW-1, BSE-1 (LA18) and BSE-2 (SE28) Motions

and formation of plastic hinges for the BSE-2 motion. Figure 6.62 reflects the BSE-2 hinge formations which are also apparent upon examining pier rotations and pier curvature ratios of Figures 6.63 and 6.64. While general trends indicate a reduction in response enabled by the NRTMDF for this case, higher mode effects drive peak pier rotations and curvatures for BSE-1 which are higher for the damped case than the undamped case for this model. However, as demonstrated in Figure 6.63 and Figure 6.64 the rotations and curvatures for BSE-1 are far below the yield value for both the damped and undamped cases.

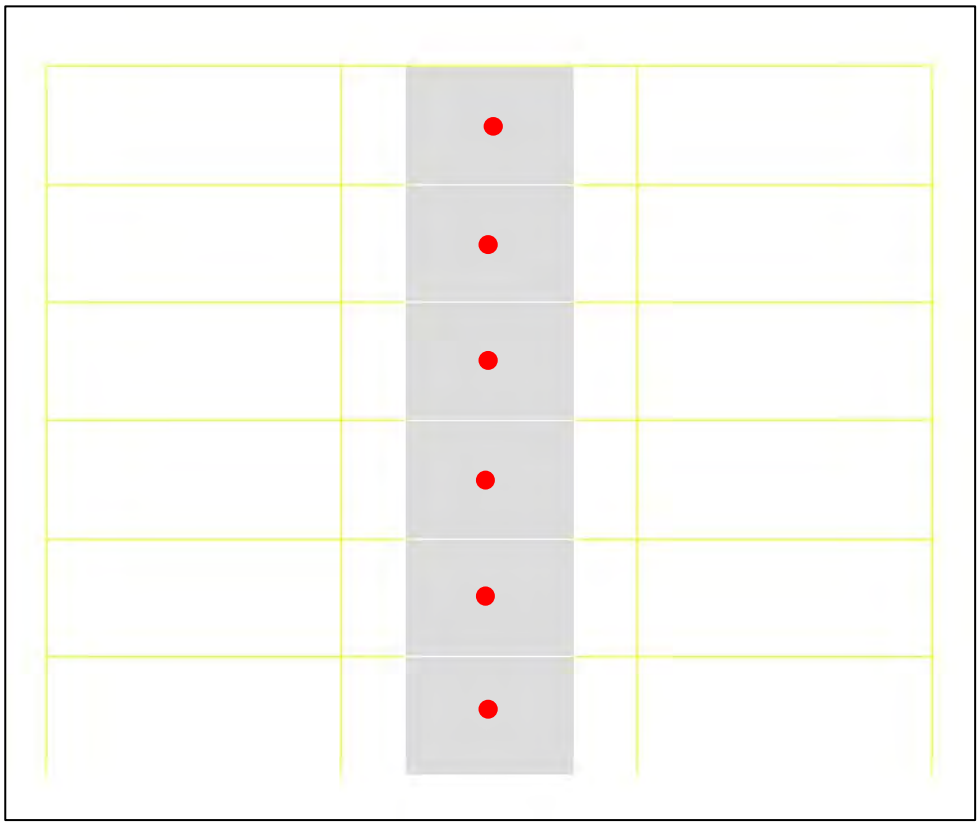

Figure 6.62 Plastic Hinge Formation for SW-1, Medium Site and BSE-2 (SE28) Motion

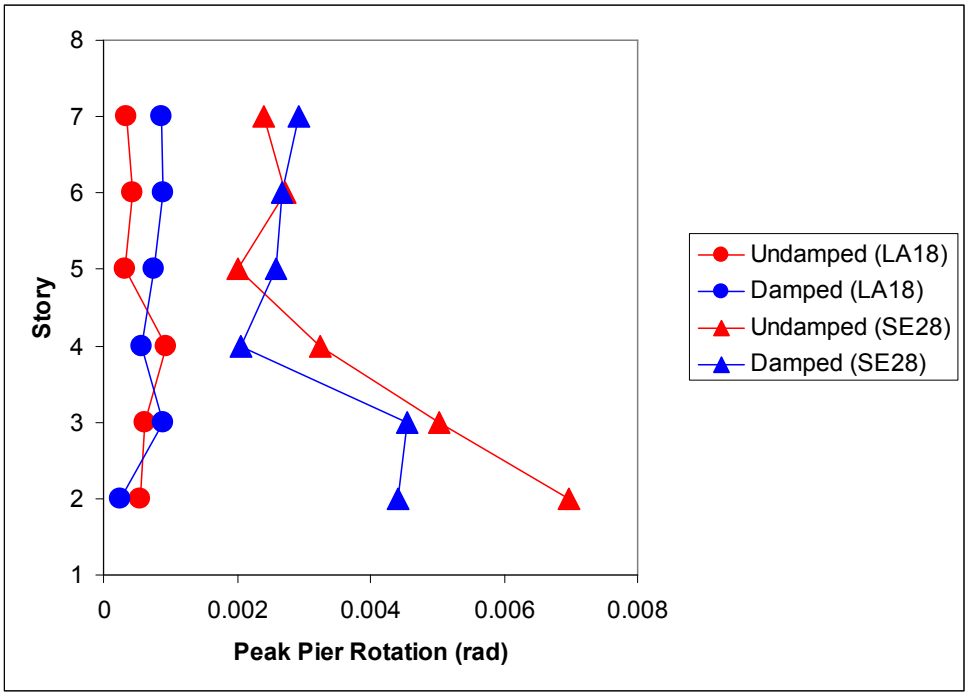

Figure 6.63 Peak Pier Rotations for SW-1, BSE-1 (LA18) and BSE-2 (SE28) Motions

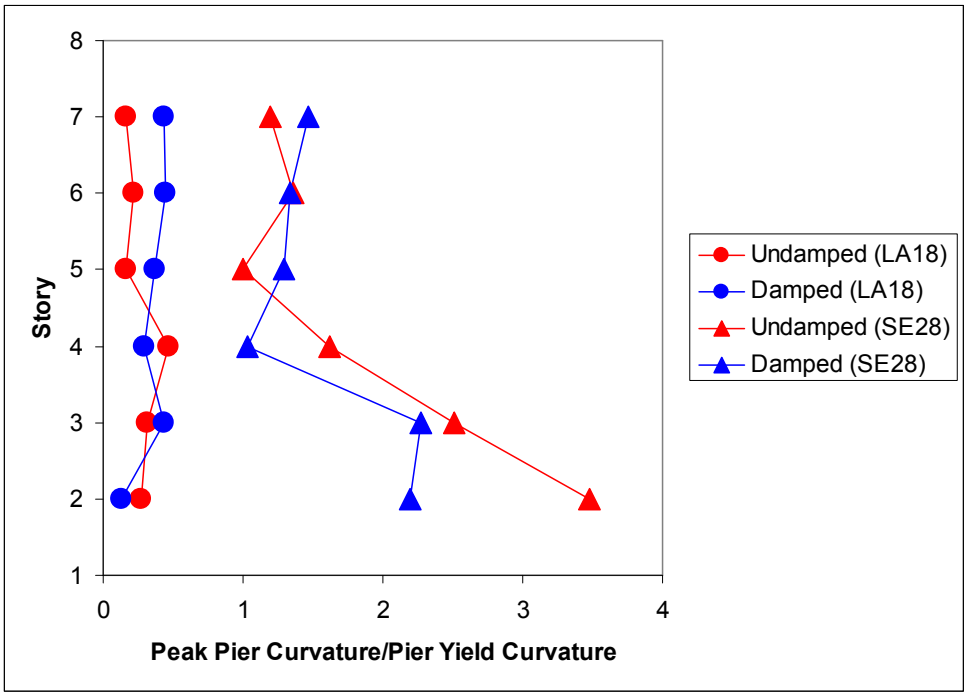

Figure 6.64 Peak Pier Curvature Ratios for SW-1, BSE-1 (LA18) and BSE-2 (SE28) Motions

For model SW-1, motions LA10 and SE33 represent motions in the SAC suite for BSE-1 and BSE-2 respectively for the soft site condition. Figures 6.65 and 6.66 depict the hysteresis loops for these in the undamped and damped conditions. As observed in the hystereses loops, peak performance parameters (displacements and base shears) do not reflect major differences between the damped and undamped cases. This is also discernible from the spectra and period shifts for SW-1 shown in Figures 6.5 and 6.6. This notwithstanding, the NRTMDF enables a reduction for the LA10 motion which can be observed for the damped case in the building hysteresis loop of Figure 6.65 and the rooftop history of Figure 6.67. Similarly the BSE-2 rooftop displacement history of Figure 6.68 demonstrates permanent nonlinear displacement for both the undamped and damped cases with marginal reduction in this parameter for the damped case enabled by the NRTMDF.

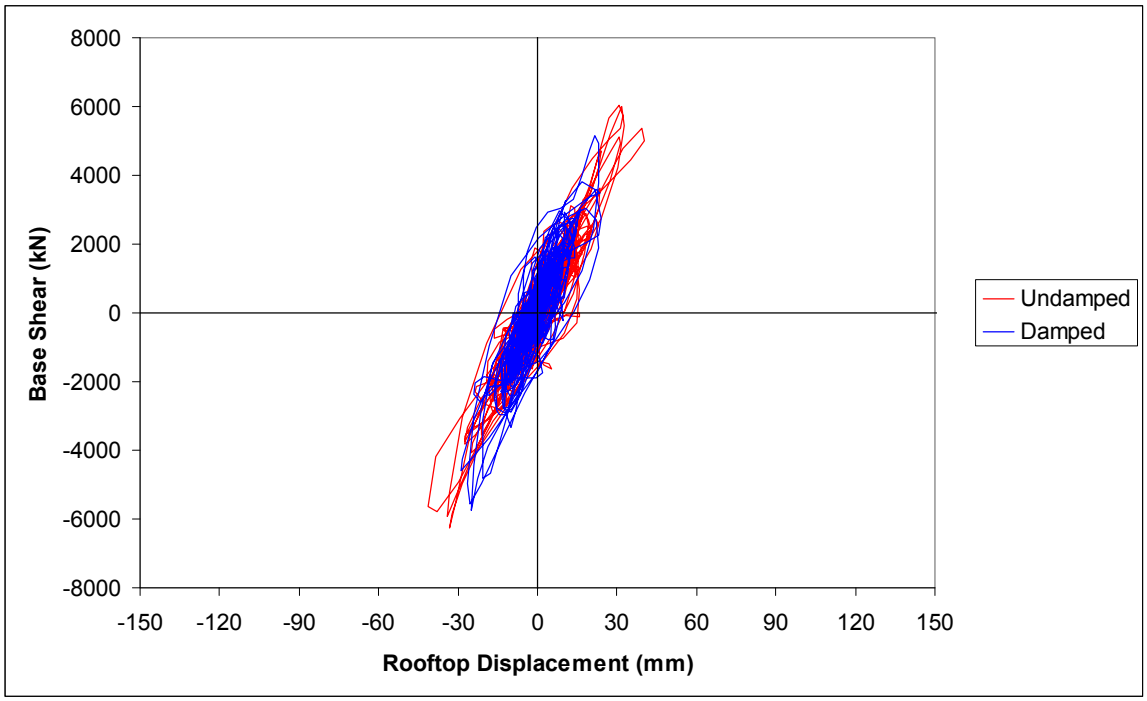

Figure 6.65 Hysteresis Loop for SW-1, Soft Site, BSE-1, LA10 Motion

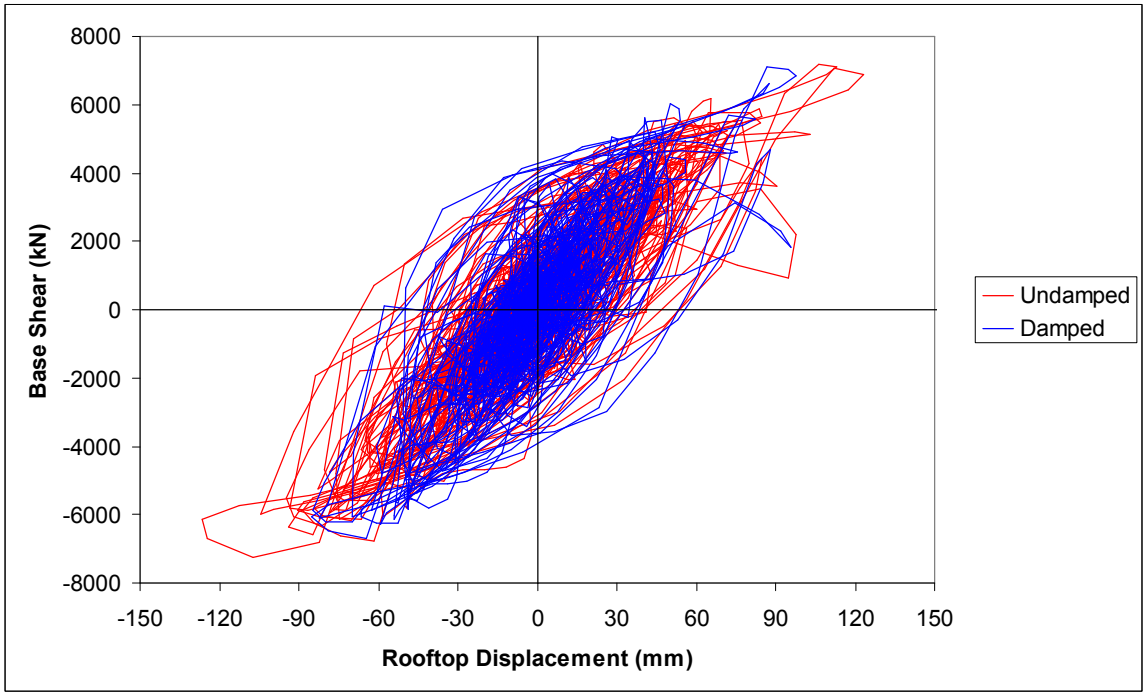

Figure 6.66 Hysteresis Loop for SW-1, Soft Site, BSE-2, SE33 Motion

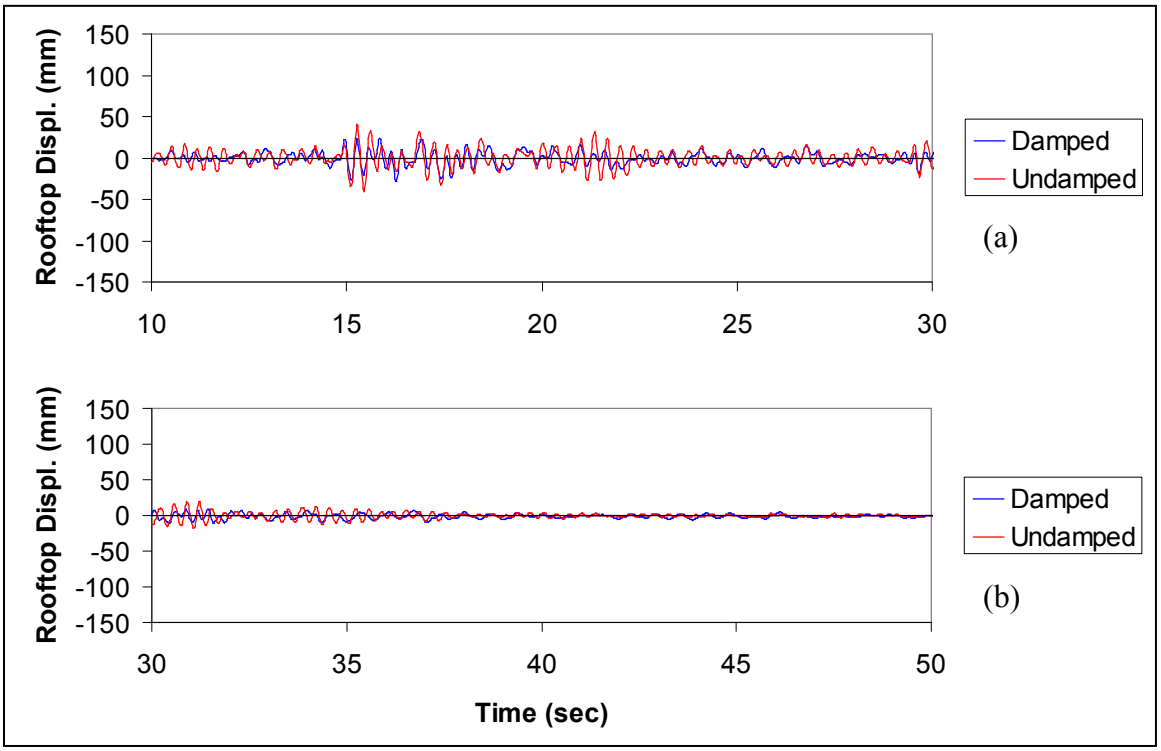

Figure 6.67 Rooftop Displacement History for SW-1, Soft Site, BSE-1, LA10 Motion

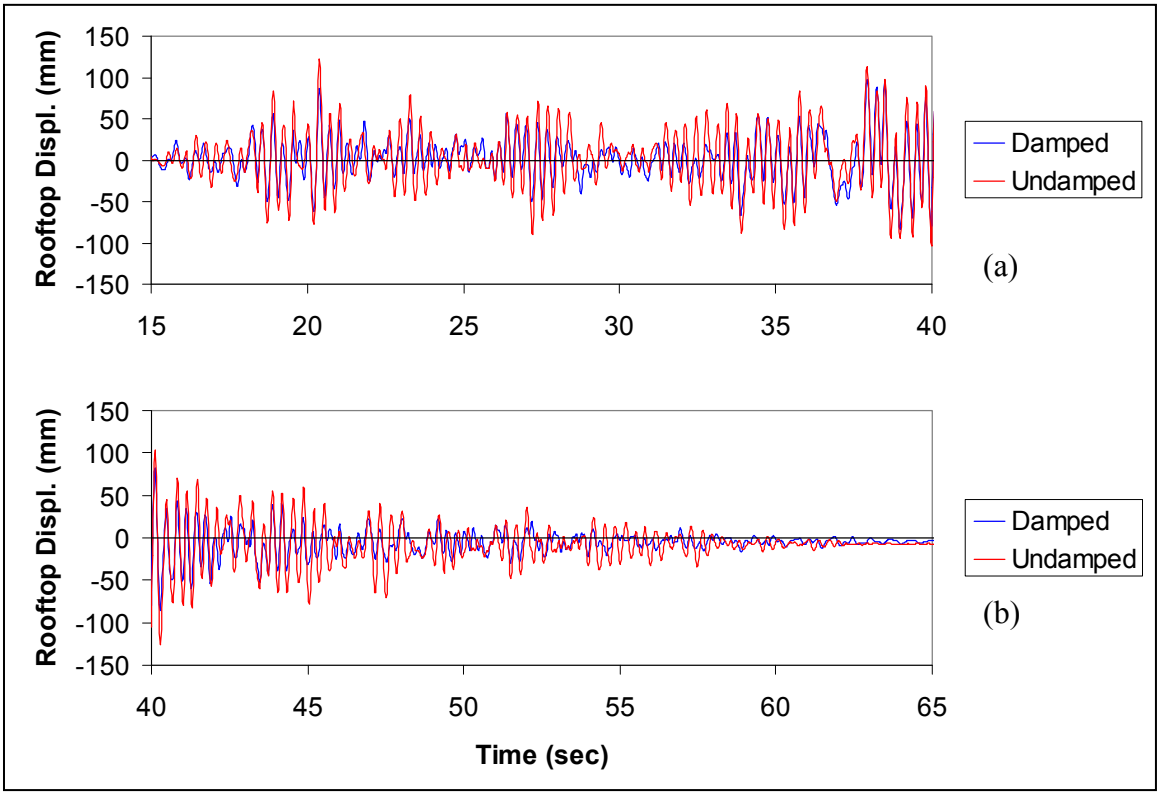

Figure 6.68 Rooftop Displacement History for SW-1, Soft Site, BSE-2, SE33 Motion

Figures 6.69 and 6.70 depict the hystereses loops for the NRTMDF for the BSE-1 and BSE-2 representative soft soil motions for SW-1. Similar to the hard and medium motions, these figures demonstrate primarily linear behavior for the lesser ground motion of BSE-1 and significant nonlinear behavior for the motion of BSE-2. For this case, Figure 6.70 demonstrates a dramatically increased NRTMDF displacement for the soft site condition of BSE-2 as compared to the hard and medium site conditions. For the soft condition, the NRTMDF displacement is approximately 430mm, more than double the peak displacement of the medium condition (188mm) and the hard condition (154mm). This is consistent with qualitative observations of Figure 6.6 which reflect a much higher spectral acceleration for this case and a correlating spectral displacement.

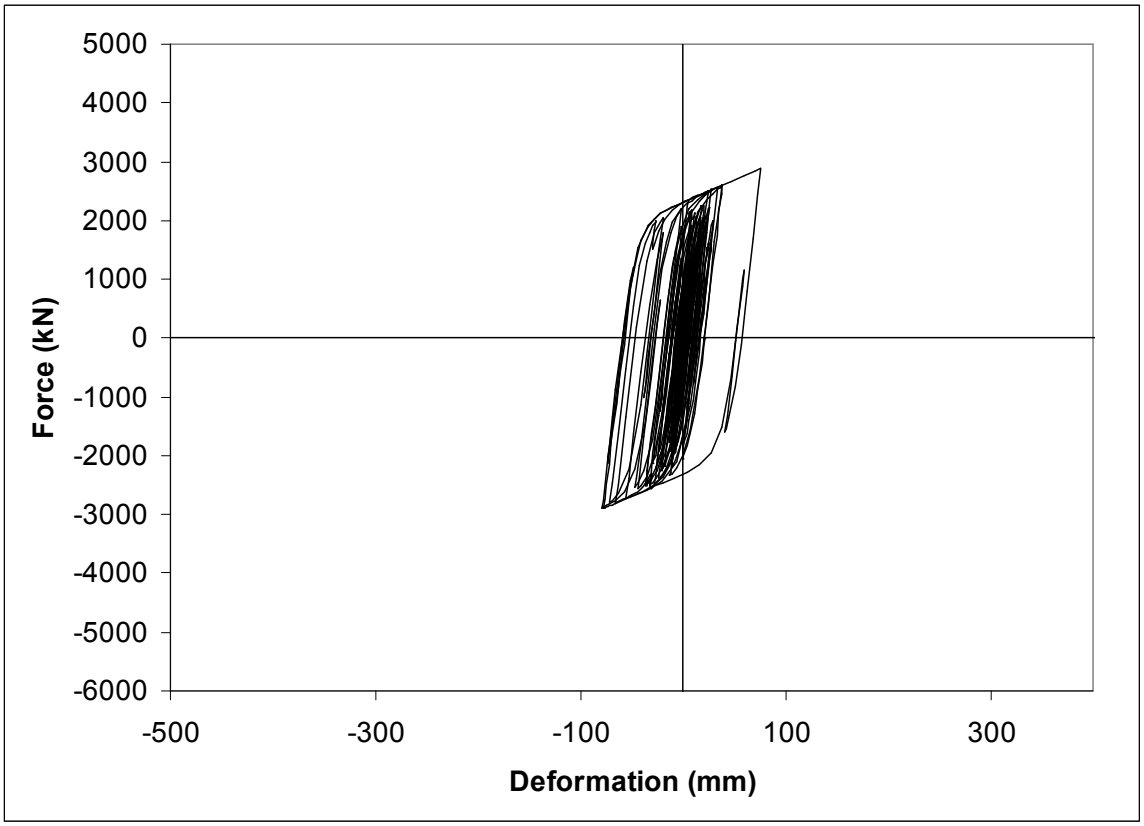

Figure 6.69 NRTMDF Buckling Restrained Brace Hysteresis Loop for SW-1, Soft Site, BSE-1, LA10 Motion

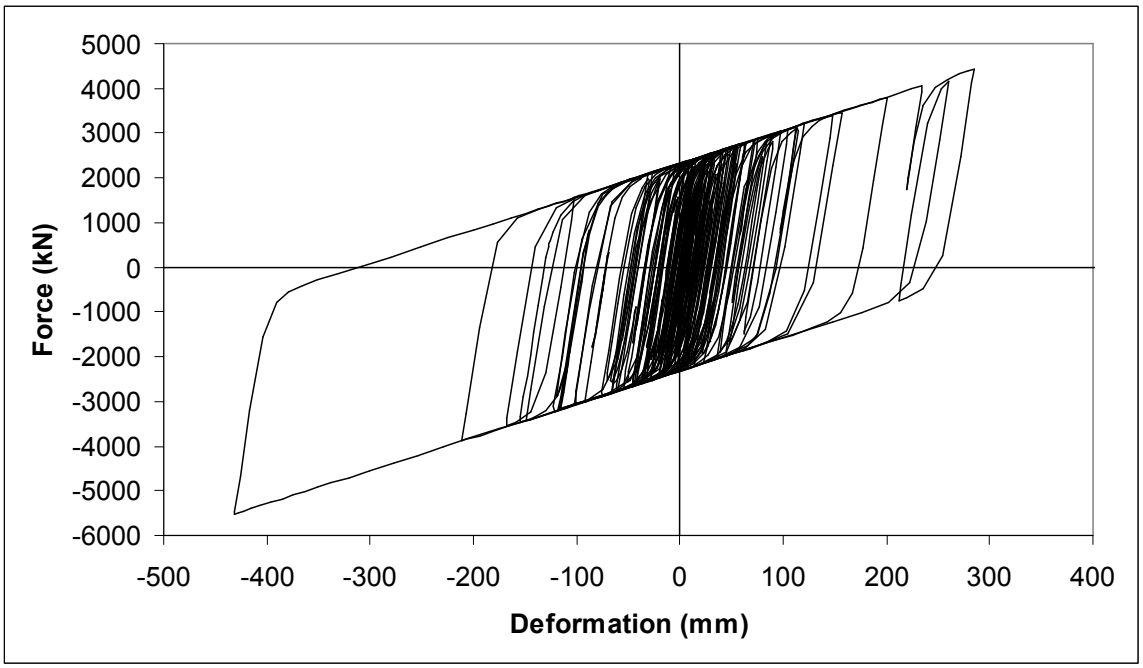

Figure 6.70 NRTMDF Buckling Restrained Brace Hysteresis Loop for SW-1, Soft Site, BSE-2, SE33 Motion

Figures 6.71, 6.72 and 6.73 reflect the peak story displacements, drift indices and story shears for undamped and damped cases of the soft site conditions represented by BSE-1 (LA10) and BSE-2 (SE33). As shown, the NRTMDF enables only a slight reduction of these peak output parameters for this case. This is reflected upon examining the pier hinge formations for BSE-1 and BSE-2 as shown in Figures 6.74 and 6.75 which are approximately the same for the undamped and damped conditions with slight reductions in magnitude as demonstrated in Figures 6.76 and 6.77. These results support similar results found throughout this research showing a diminished capacity of the NRTMDF for enhanced performance for the soft site condition.

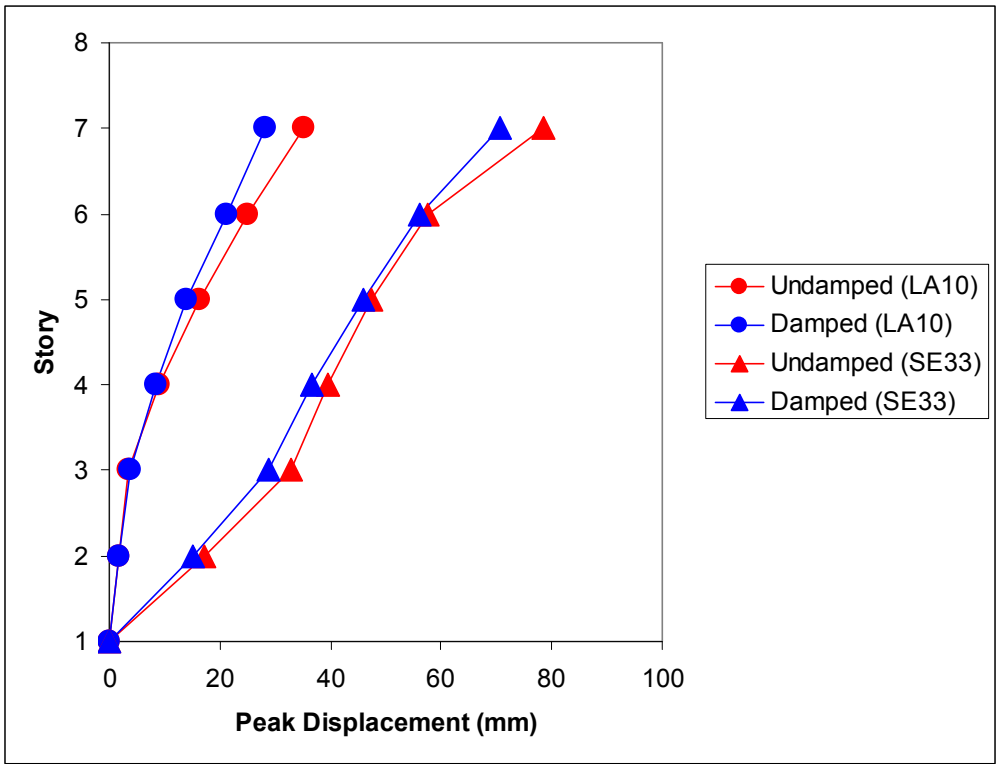

Figure 6.71 Peak Story Displacements for SW-1, BSE-1 (LA10) and BSE-2 (SE33) Motions

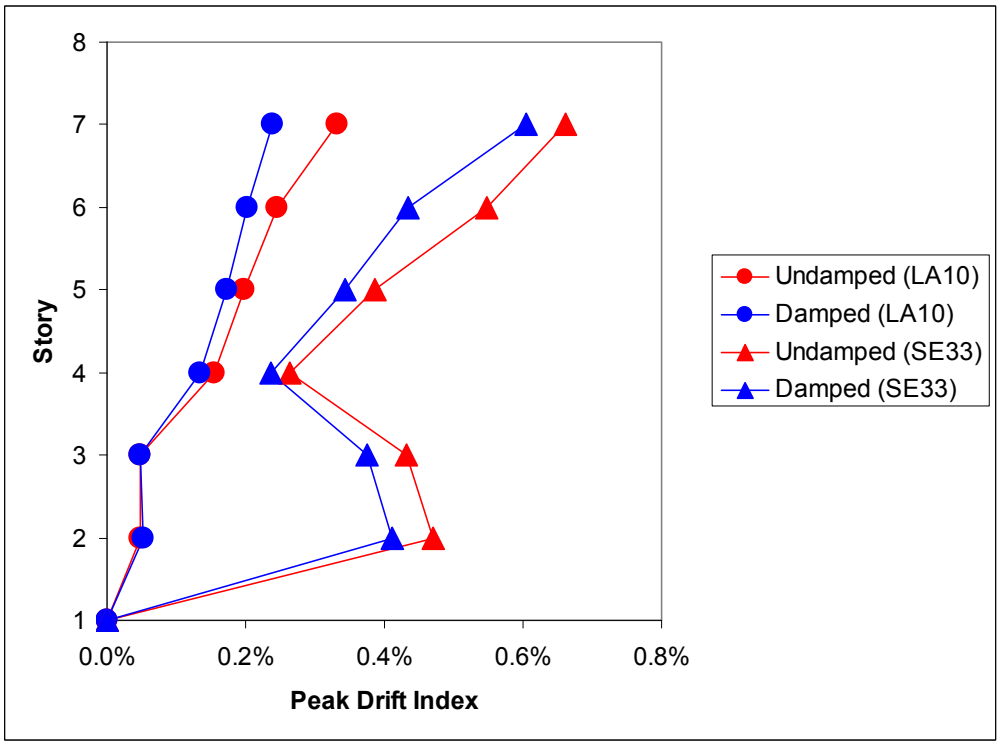

Figure 6.72 Peak Drift Indices for SW-1, BSE-1 (LA10) and BSE-2 (SE33) Motions

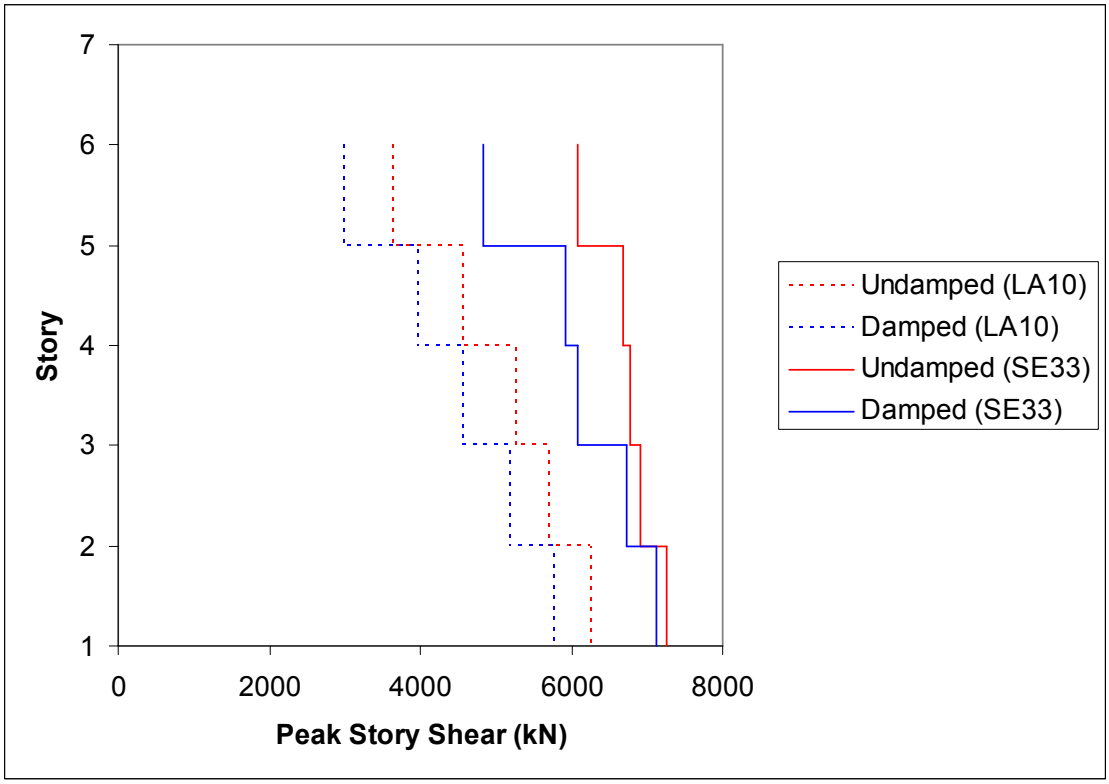

Figure 6.73 Peak Story Shears for SW-1, BSE-1 (LA10) and BSE-2 (SE33) Motions

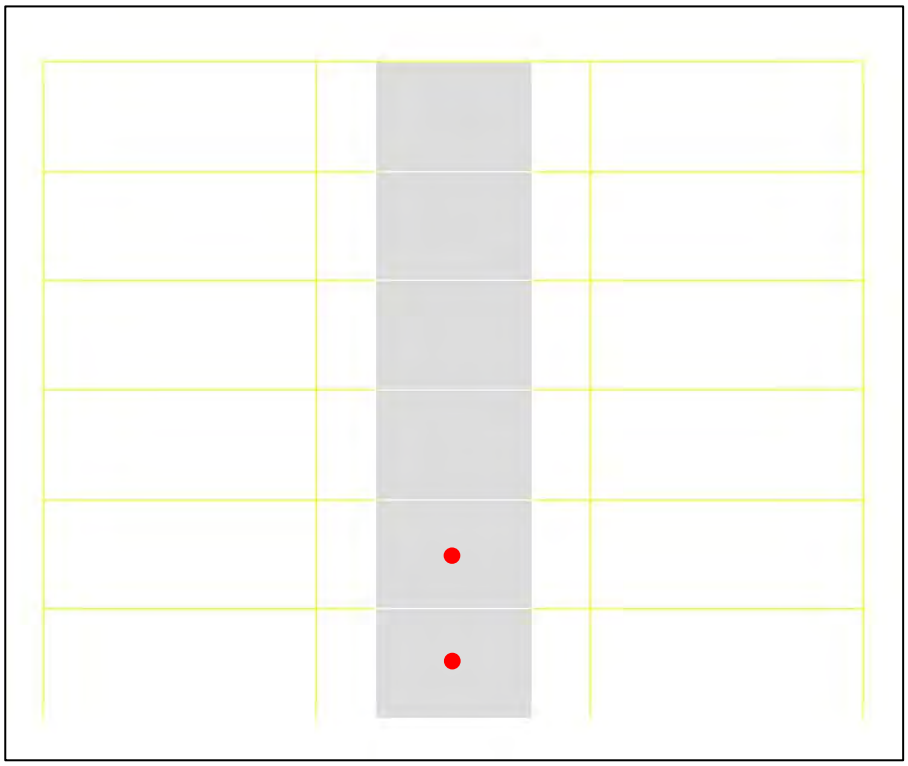

Figure 6.74 Plastic Hinge Formation for SW-1, Soft Site and BSE-1 (LA10) Motion

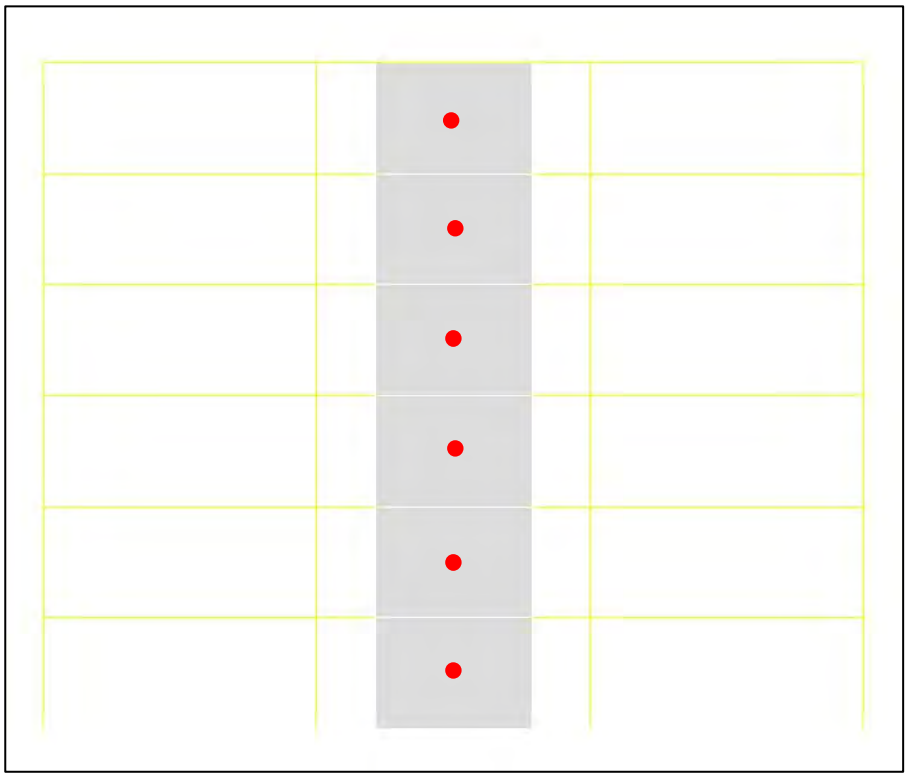

Figure 6.75 Plastic Hinge Formation for SW-1, Soft Site and BSE-1 (SE33) Motion

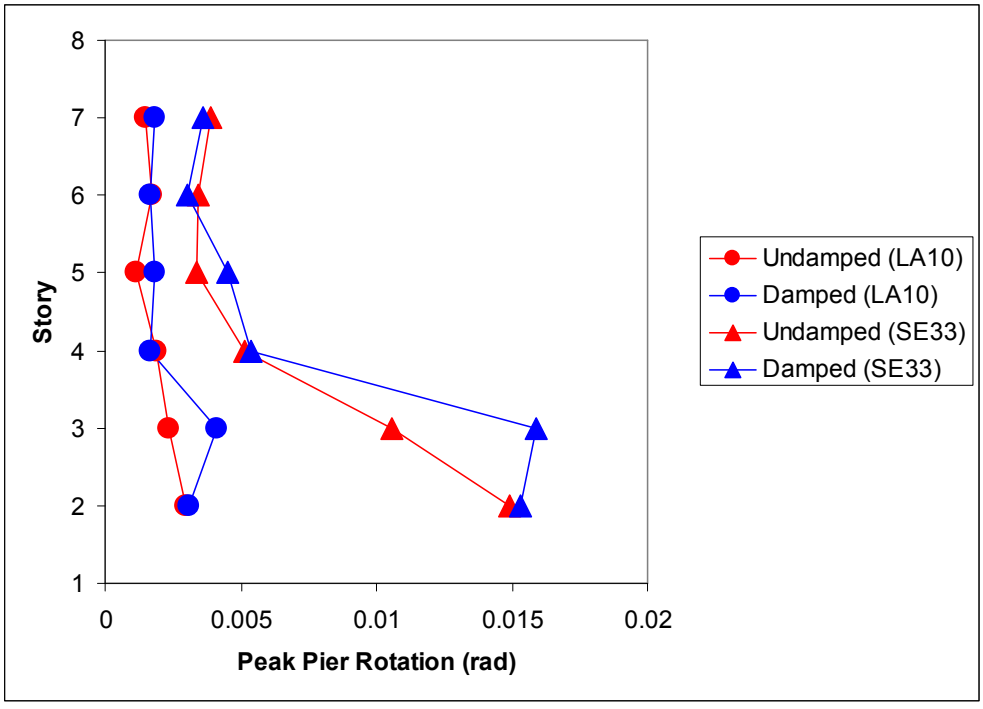

Figure 6.76 Peak Pier Rotations for SW-1, BSE-1 (LA10) and BSE-2 (SE33) Motions

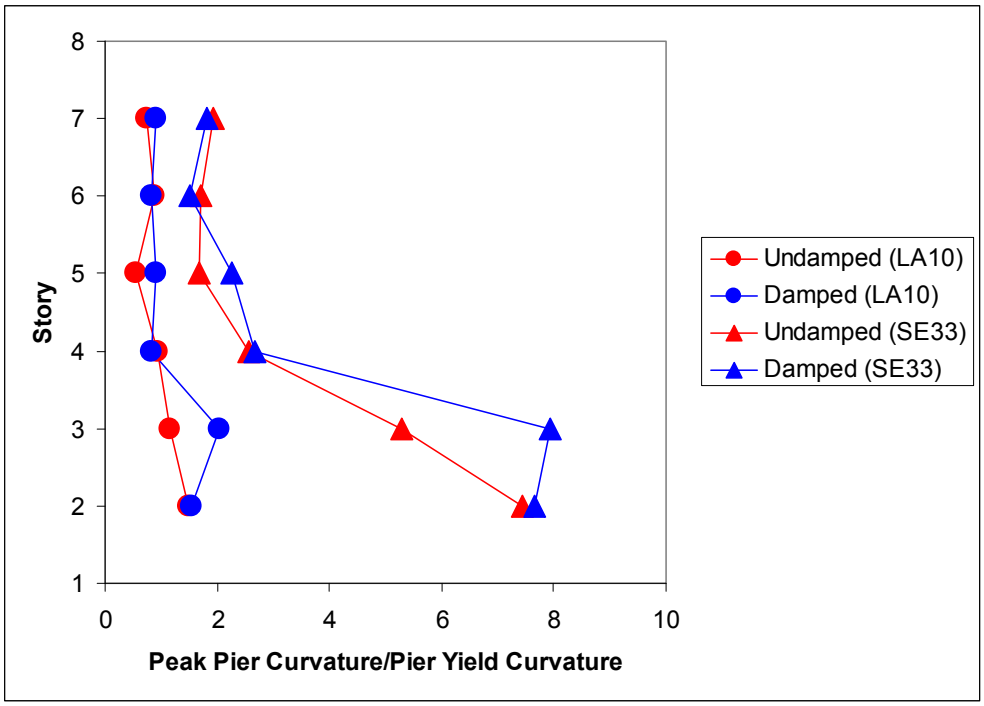

Figure 6.77 Peak Pier Curvature Ratios for SW-1, BSE-1 (LA10) and BSE-2 (SE33) Motions

6.1.3 MF-1 Time History Output Examples

Building hystereses loops for model MF-1 demonstrate a marked difference for this structure as compared to those of BF-4 and SW-1 reflecting the more limber moment frame system which can sustain dramatically higher displacements within its elastic limit state. For the hard site condition, motions SE12 and SE39 represent BSE-1 motions and BSE-2 motions respectively. Figures 6.78 and 6.79 depict the building hystereses loops for MF-1 and the undamped and damped cases for these motions. These figures reflect markedly narrower hysteresis loops, particularly for the BSE-2 motion, thereby reflecting primarily linear behavior of the moment frame system. This behavior is further demonstrated in the rooftop displacement histories of Figures 6.80 and 6.81, which, like the hysteresis loop demonstrate the rooftop displacement reductions enabled by the NRTMDF with virtually no evidence of permanent rooftop displacement thus reflecting

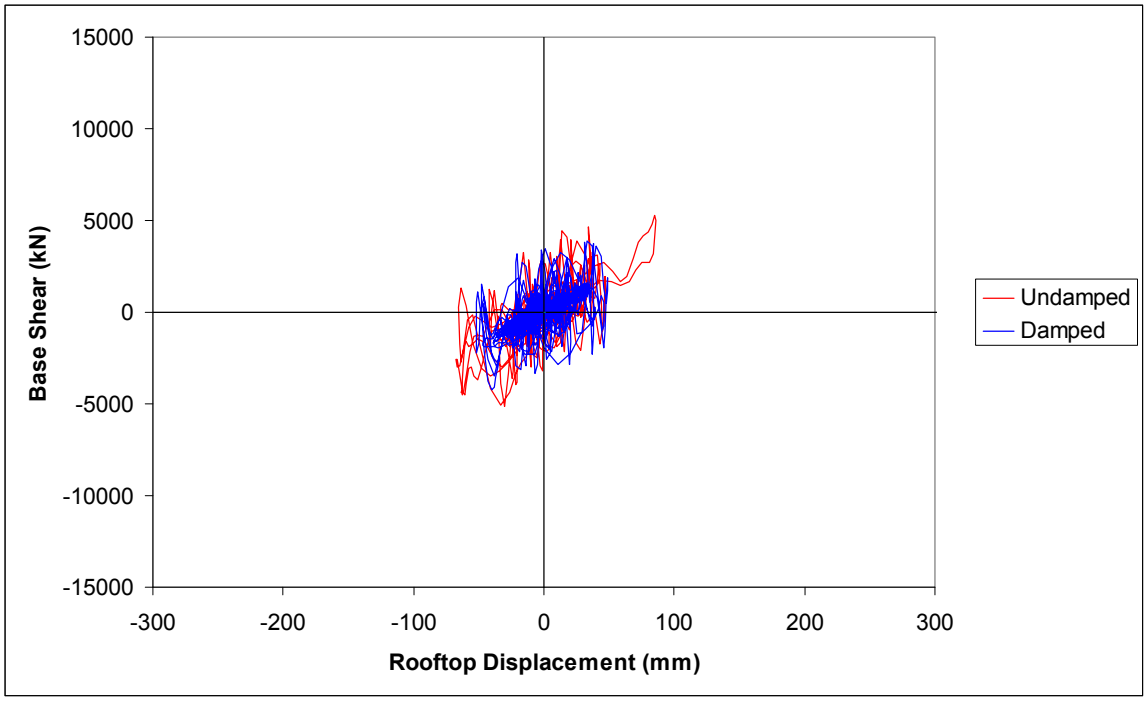

Figure 6.78 Hysteresis Loop for MF-1, Hard Site, BSE-1, SE12 Motion

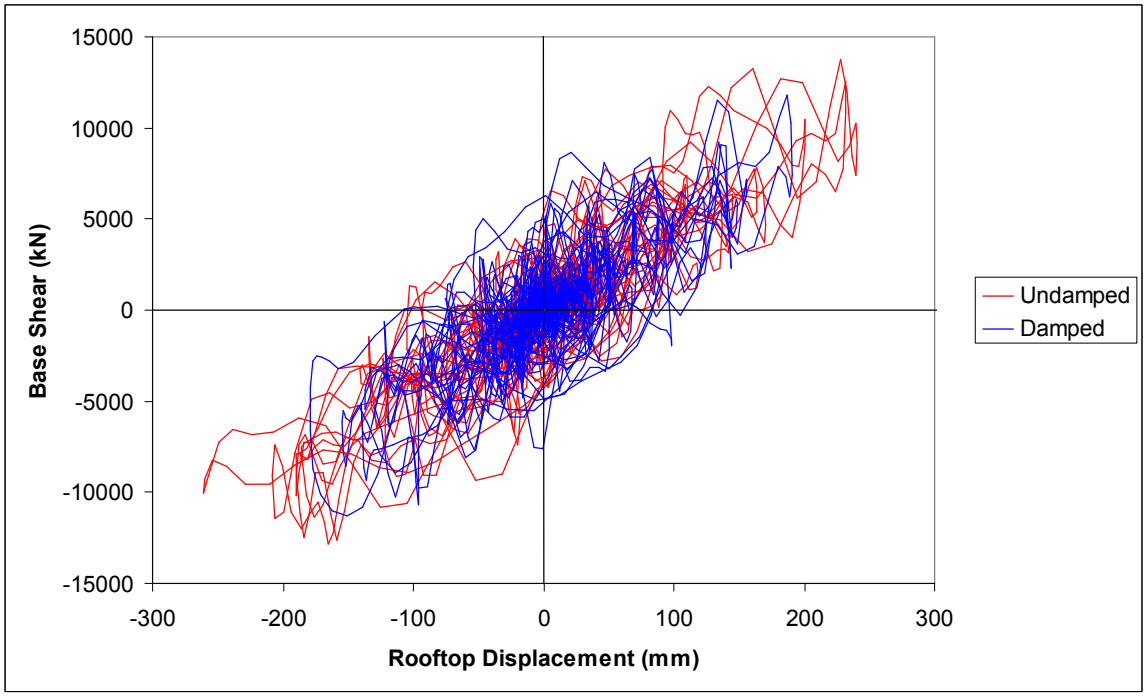

Figure 6.79 Hysteresis Loop for MF-1, Hard Site, BSE-2, SE39 Motion

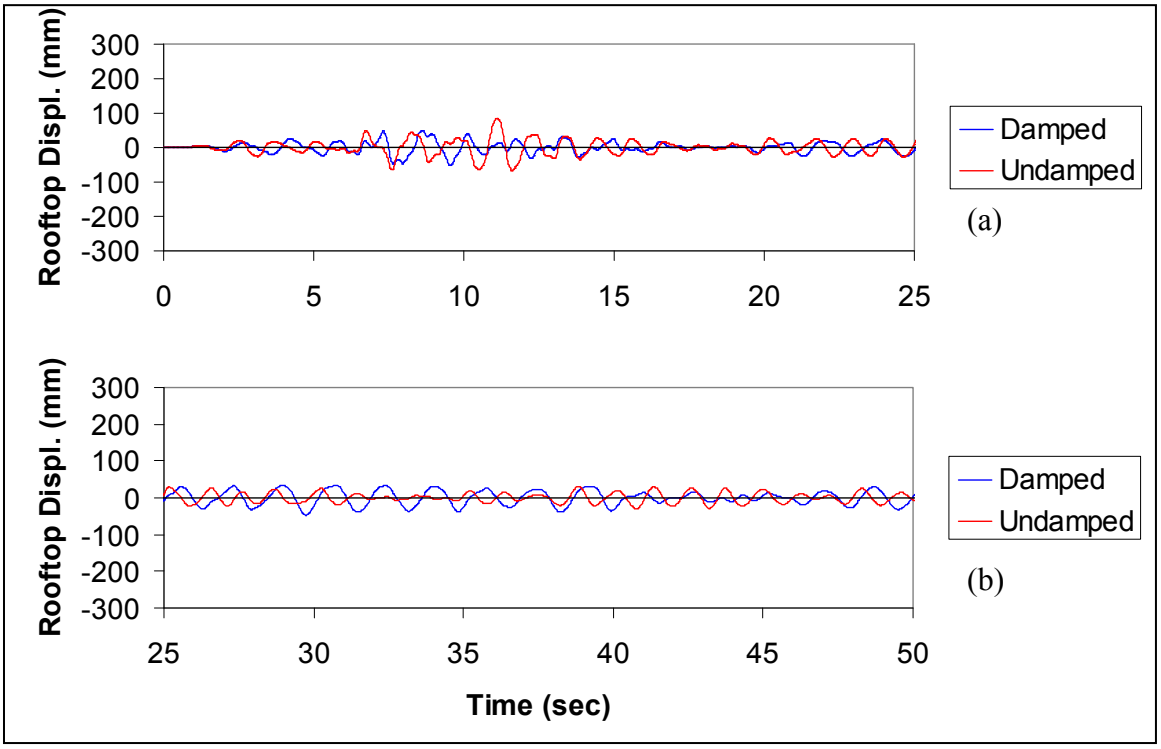

Figure 6.80 Rooftop Displacement History for MF-1, Hard Site, BSE-1, SE12 Motion

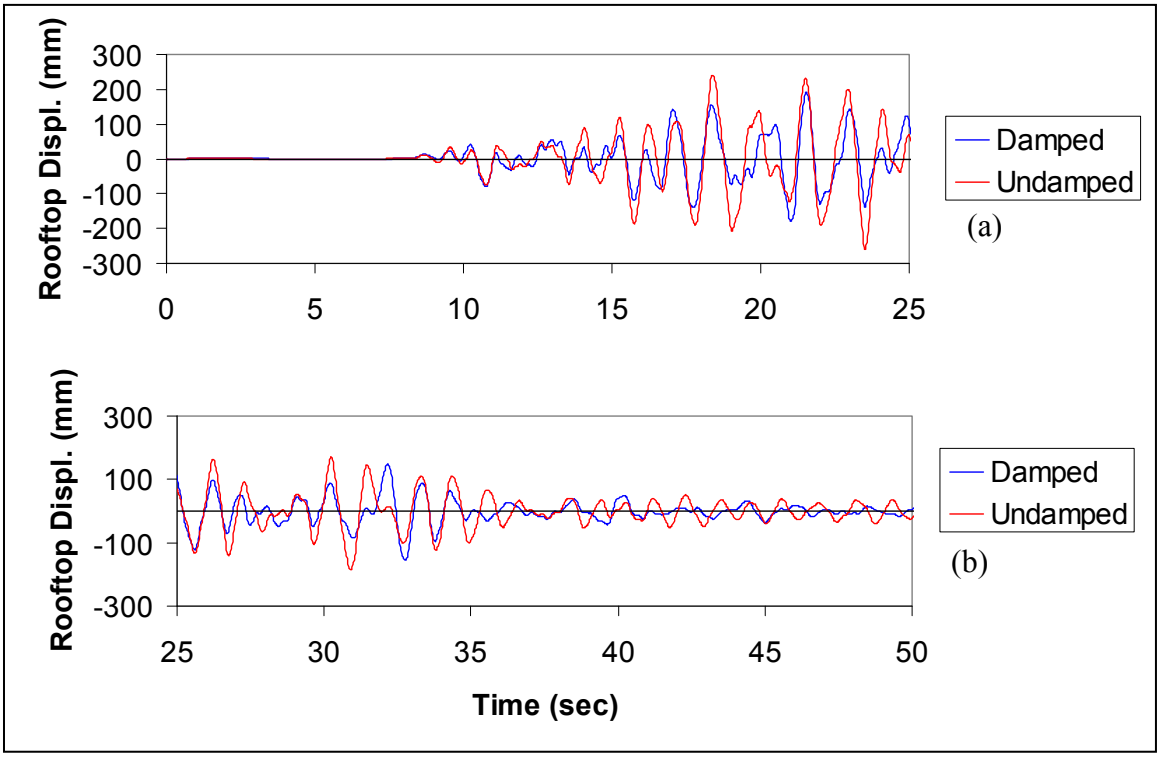

Figure 6.81 Rooftop Displacement History for MF-1, Hard Site, BSE-2, SE39 Motion

the elastic behavior. Examination of the hystereses loops of the NRTMDF for each ground motion in Figures 6.82 and 6.83 demonstrate primarily linear elastic behavior of the NRTMDF for the BSE-1 motion and significant nonlinear behavior for BSE-2. Noteworthy as well with the NRTMDF is the peak displacement of the NRTMDF for BSE-2 condition. At 345mm this is a magnitude considerably higher than similar cases of the structures with higher stiffness. This reflects the generally long period nature of this structure and the likewise long period of the NRTMDF, characteristically so to enable effective reduction in seismic response.

Additional output parameters for MF-1 and the hard site condition are demonstrated in Figures 6.84, 6.85 and 6.86 which depict peak story displacements, story drift indices and story shears for BSE-1 (SE12 motion) and BSE-2 (SE39 motion). The general trends demonstrated in these figures show reduced demand for the damped

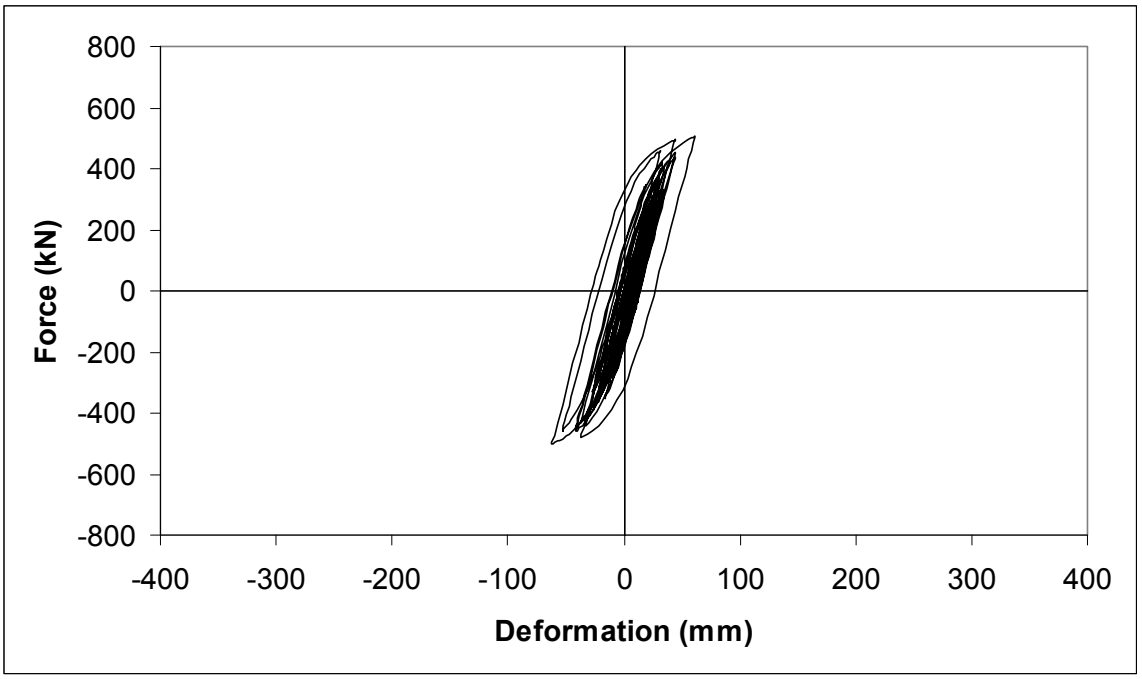

Figure 6.82 NRTMDF Buckling Restrained Brace Hysteresis Loop for MF-1, Hard Site, BSE-1, SE12 Motion

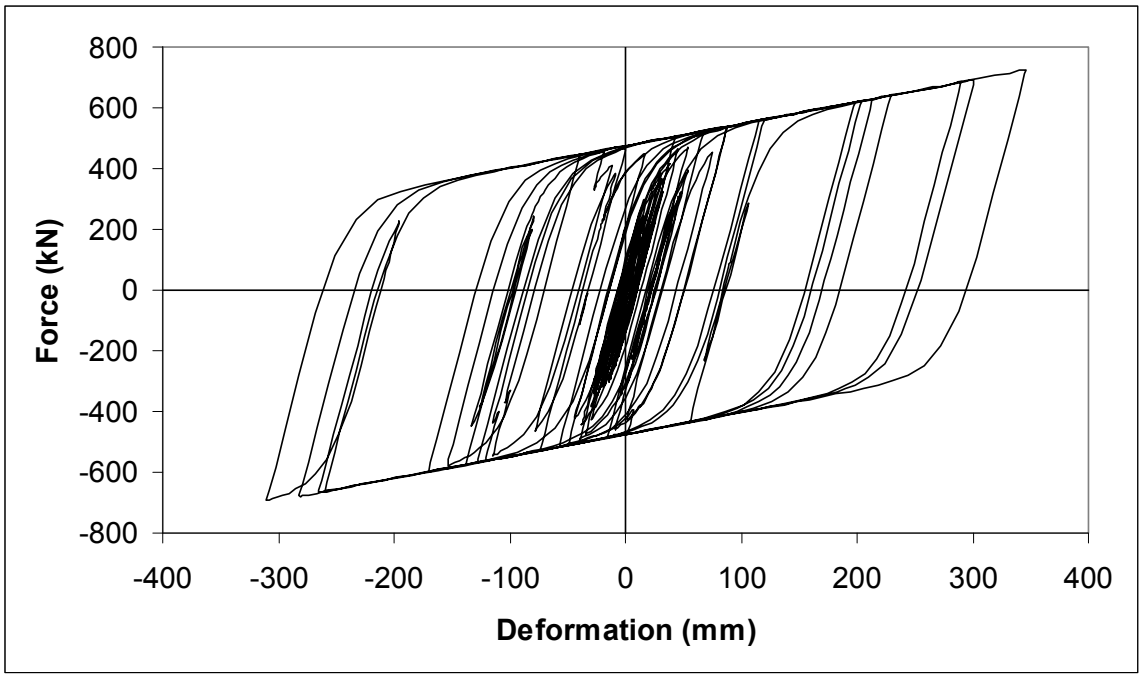

Figure 6.83 NRTMDF Buckling Restrained Brace Hysteresis Loop for MF-1, Hard Site, BSE-2, SE39 Motion

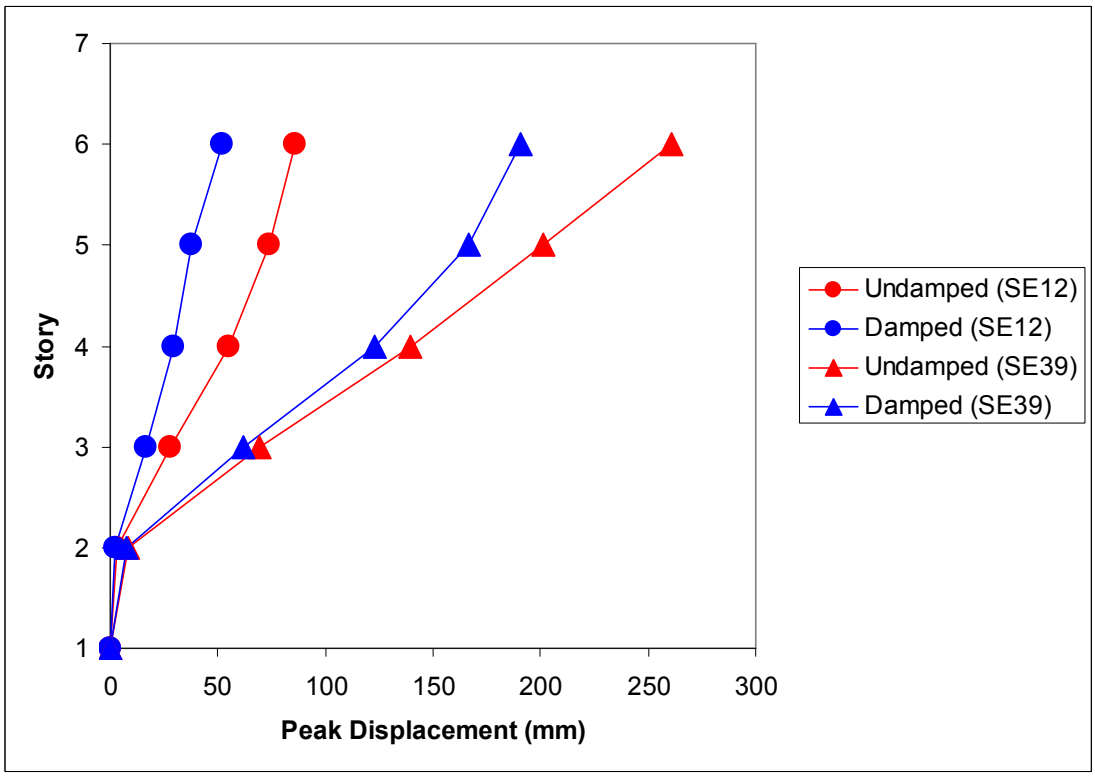

Figure 6.84 Peak Story Displacements for MF-1 Hard Site, BSE-1 (SE12) and BSE-2 (SE39)

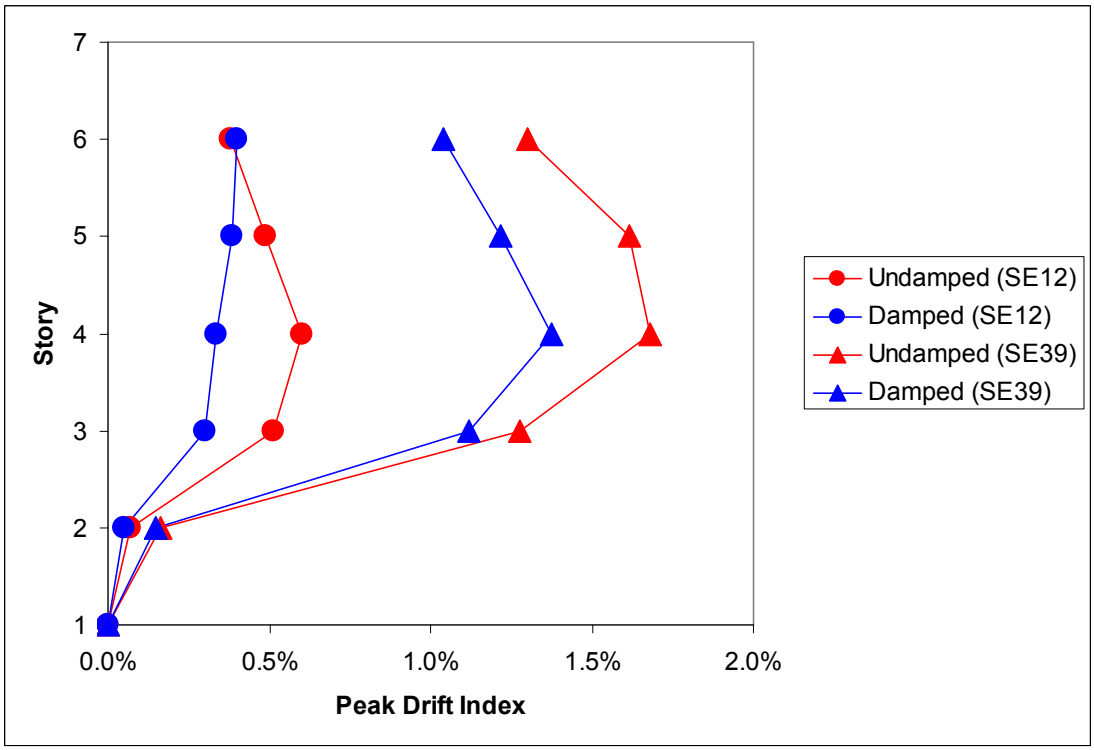

Figure 6.85 Peak Story Drift Index MF-1 Hard Site, BSE-1 (SE12) and BSE-2 (SE39)

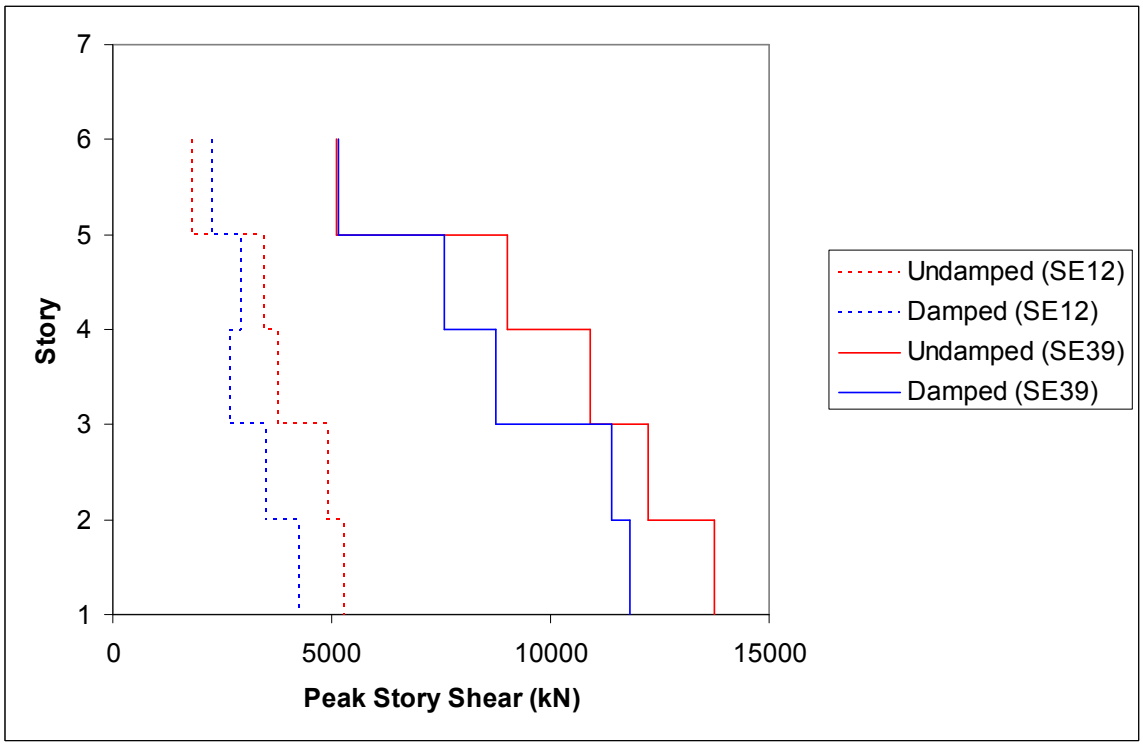

Figure 6.86 Peak Story Shears MF-1 Hard Site, BSE-1 (SE12) and BSE-2 (SE39)

condition except for drift indices of the BSE-1 case shown in Figure 6.85 and shears of the top story shown in Figure 6.86. This is due to the reactions of the NRTMDF at this story. Such behavior is expected and is thought to be acceptable since drifts and shear demands at the top story of multi-story buildings are typically well below maximum acceptable limits. Additional output parameters for this case may be considered on an elemental basis such as moment frame beam rotations and curvatures. Figure 6.87 depicts a typical frame elevation for MF-1 and marks beams for which Figures 6.88 and 6.89 demonstrate rotations and curvature ratios for the undamped and damped conditions for the motions from the BSE-1 and BSE-2 ground motion suites. Reductions in demand for these cases are manifest as reduced beam rotations from the undamped to damped cases. For the damped case of BSE-1, Figure 6.89 demonstrates no reduction in the rooftop beam rotation, once again due to the reactions of the NRTMDF immediately above this beam. The curvature ratios shown in Figure 6.90 reflect the calculated curvature divided by the yield curvature of the beam thus indicating the formation of plastic hinge mechanisms for ratios beyond unity. As shown in this figure, the only case

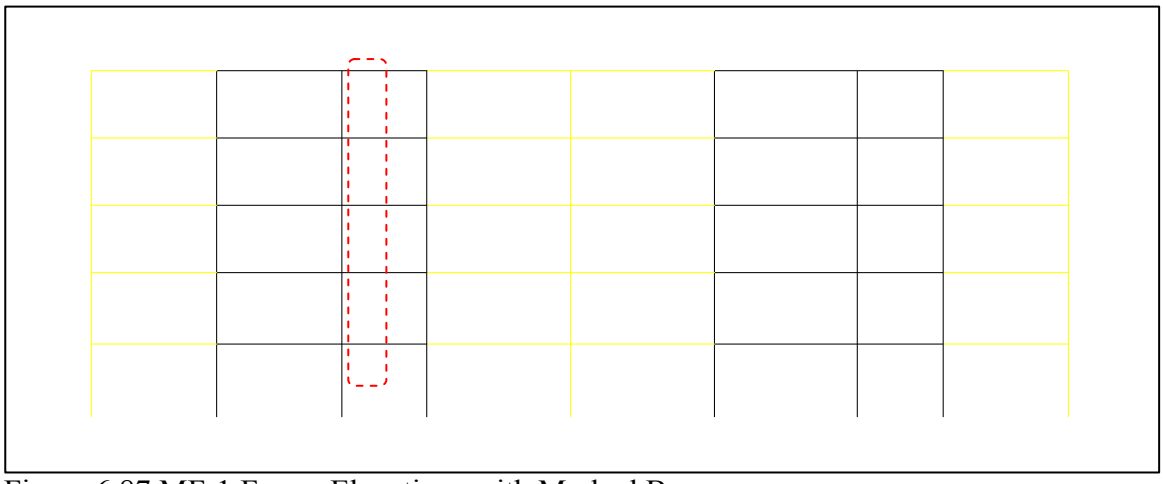

Figure 6.87 MF-1 Frame Elevations with Marked Beams

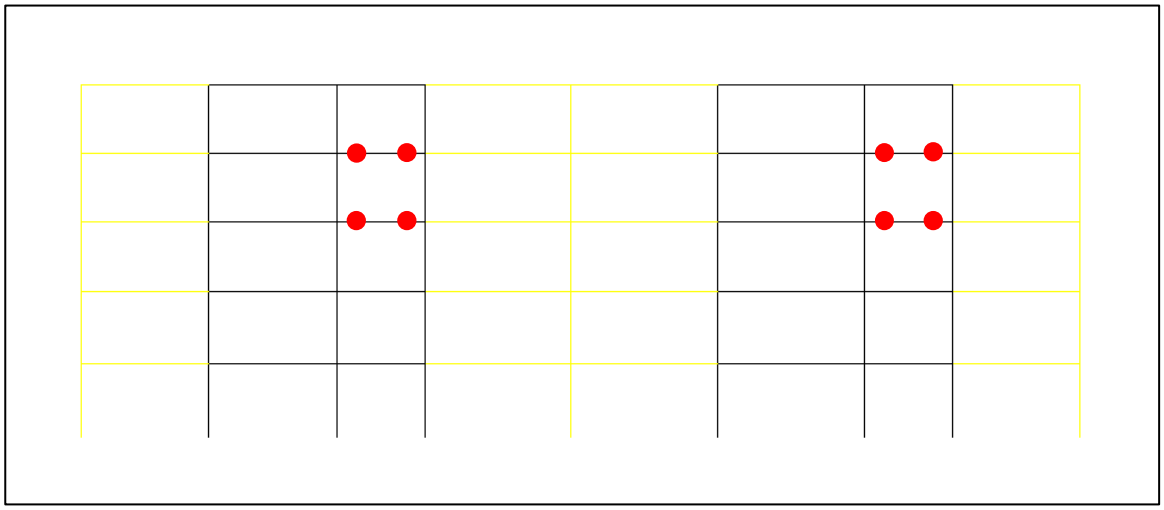

Figure 6.88 Plastic Hinge Formations for Undamped MF-1, BSE-2 (SE39) Motion

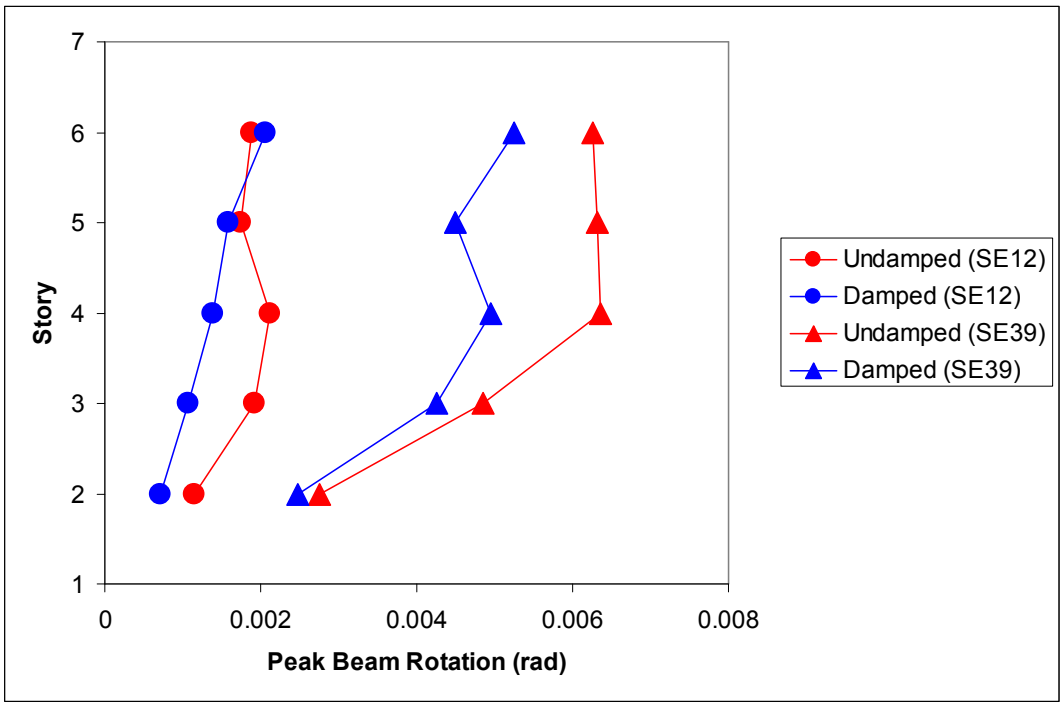

Figure 6.89 Peak Beam Rotations for MF-1 Hard Site, BSE-1 (SE12) and BSE-2 (SE39)

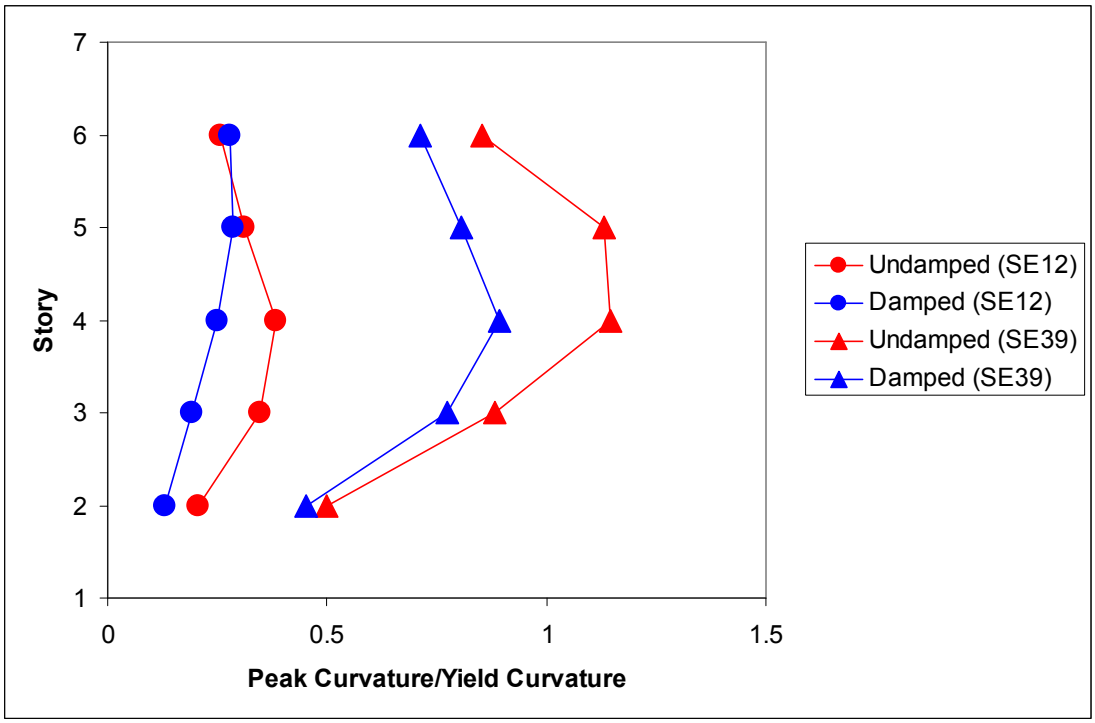

Figure 6.90 Peak Beam Curvature Ratios for MF-1 Hard Site, BSE-1 (SE12) and BSE-2 (SE39)

for which the ratios are greater than unity is the undamped condition for BSE-2 (SE39 motion). Figure 6.88 depicts the frame elevation with the projected plastic hinge formations of the moment frame elements for this case. These results reflect the concept of a reduced overall response because the fundamental period of the structure (approximately 1.4 seconds for the undamped structure as indicated in Table 3.1) is significantly displaced from the fundamental period of the site (approximately 0.1 to 0.5 seconds as shown in Figure 3.25). While the spectrum of Figures 6.1 and 6.2 demonstrates a relatively low spectral acceleration for the undamped case at a fundamental period of 1.4 seconds, the spectral accelerations are reduced even more for the damped case as shown in these figures.

Medium site conditions for MF-1 and BSE-1 and BSE-2 motions are represented by LA13 and LA23 respectively. The hysteresis loops for this building and these soils

for undamped and damped conditions are demonstrated in Figures 6.91 and 6.92. Like the hard site condition, the hysteresis loops demonstrate primarily linear elastic behavior which is also evident in the rooftop displacement histories of Figures 6.93 and 6.94. These figures reflect a reduction in the rooftop displacement response due to the NRTMDF while also demonstrating a return of the roof to the initial condition (location) thereby reflecting the primarily linear elastic behavior for this building and these motions. Examination of the hysteresis loops for the NRTMDF for BSE-1 and BSE-2 for this building and the medium site condition again reflects primarily linear behavior for the lesser motion of BSE-1 and significant nonlinearity in the NRTMDF for the BSE-2 condition as demonstrated in Figures 6.95 and 6.96. For Figure 6.96, the significant displacement of the NRTMDF (727mm) reflects the long period nature of the building

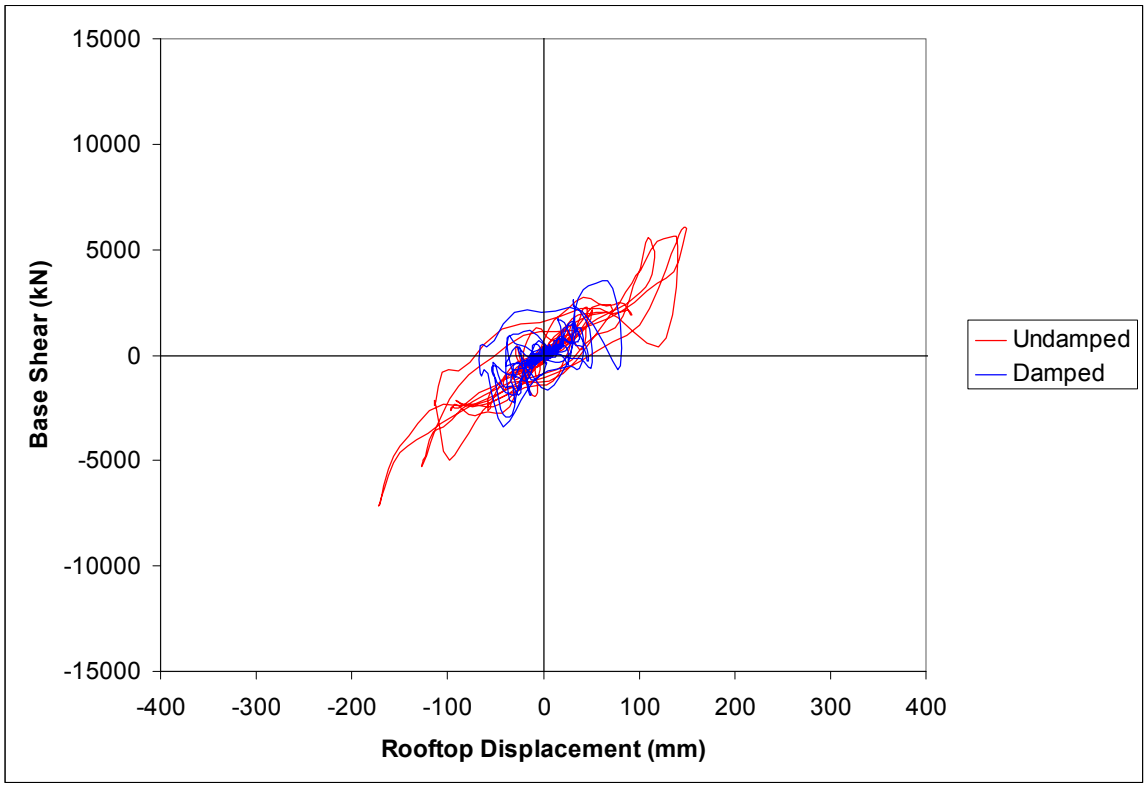

Figure 6.91 Hysteresis Loop for MF-1, Medium Site, BSE-1, LA13 Motion

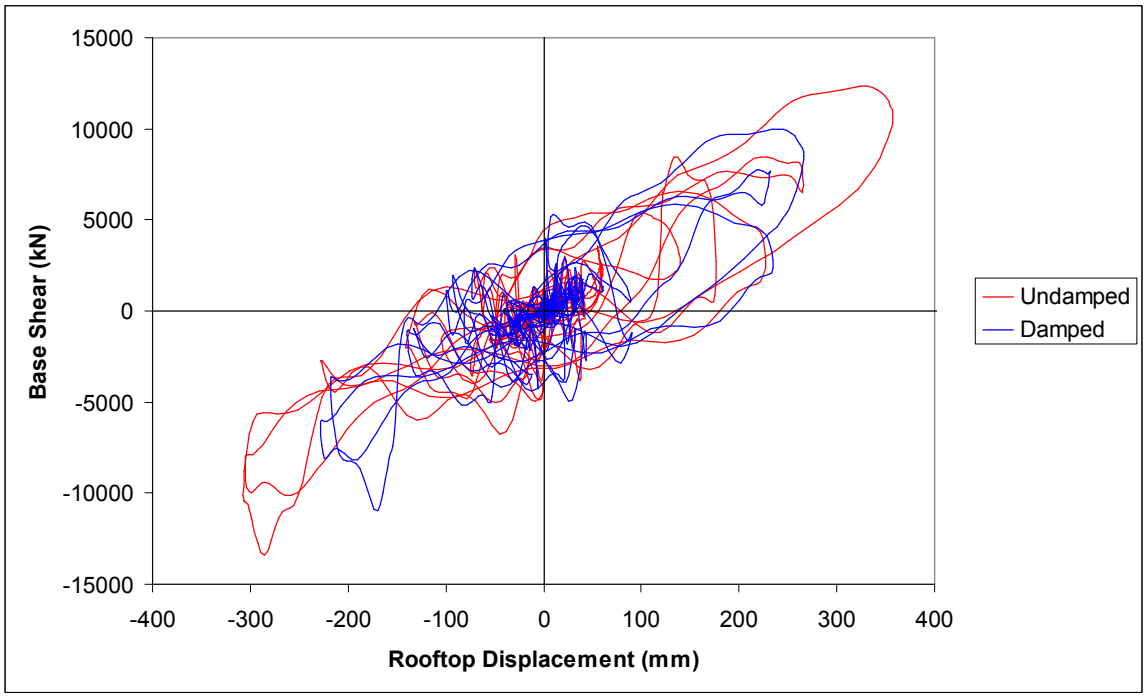

Figure 6.92 Hysteresis Loop for MF-1, Medium Site, BSE-2, LA23 Motion

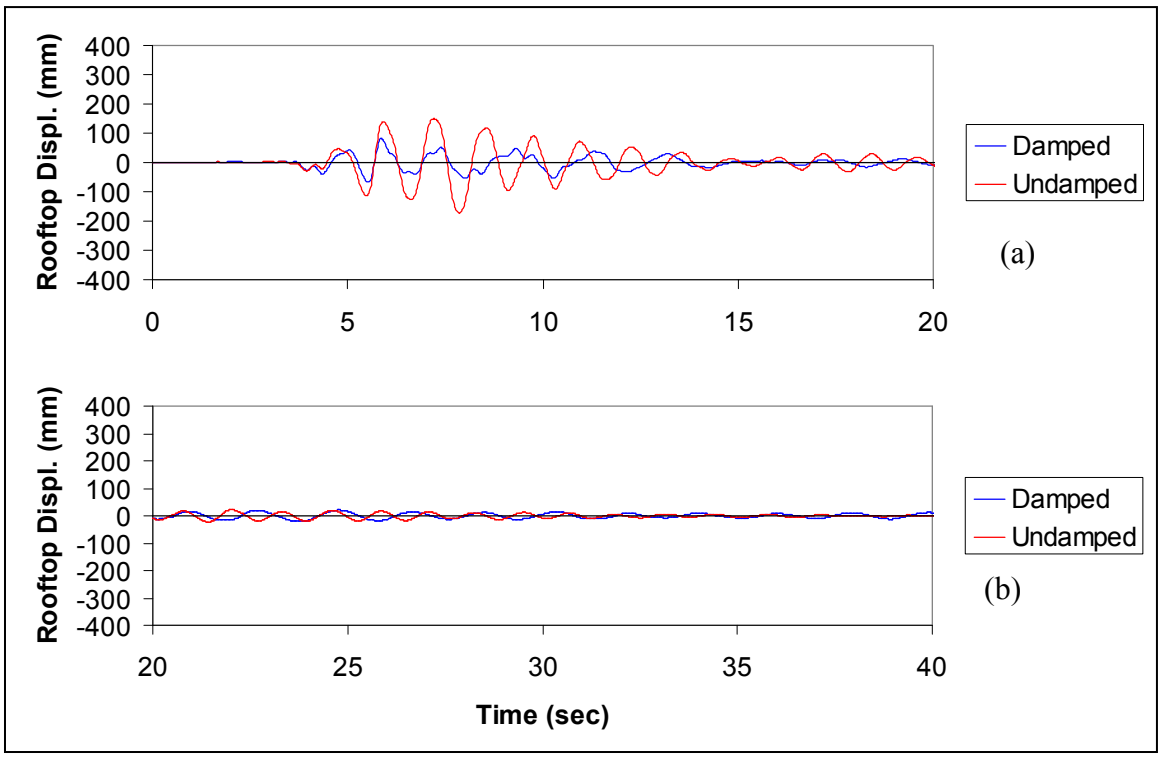

Figure 6.93 Rooftop Displacement History for MF-1, Medium Site, BSE-1, LA13 Motion

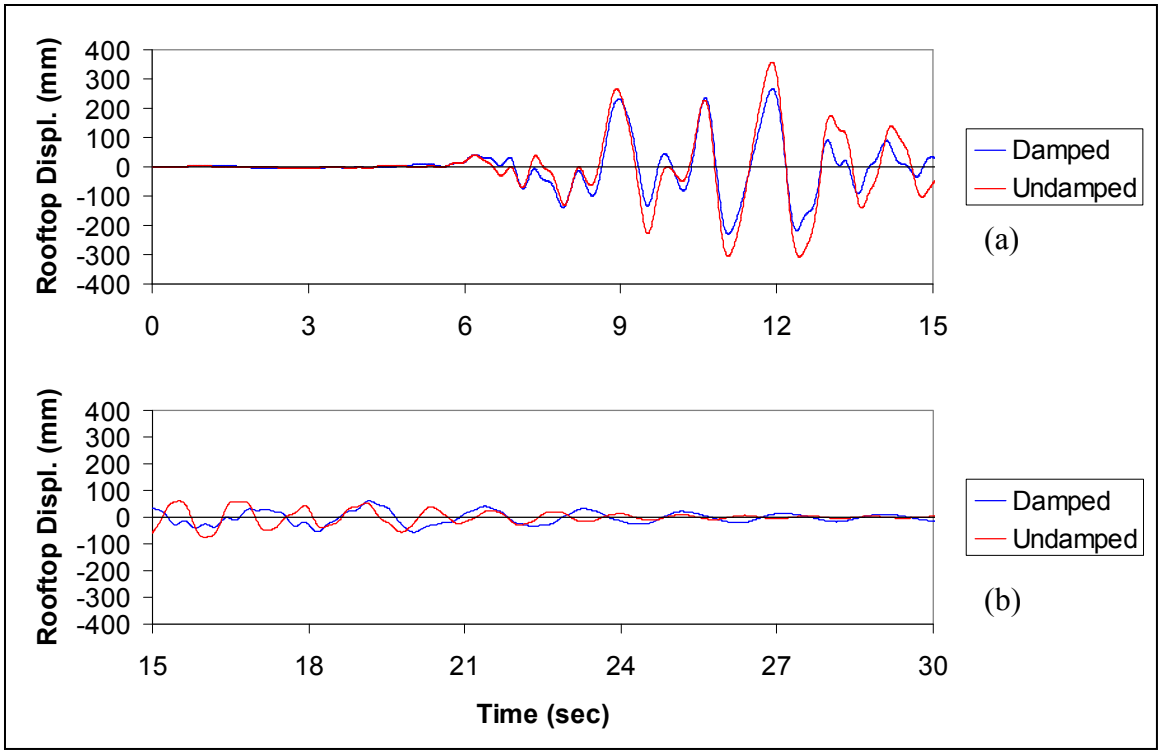

Figure 6.94 Rooftop Displacement History for MF-1, Medium Site, BSE-2, LA23 Motion

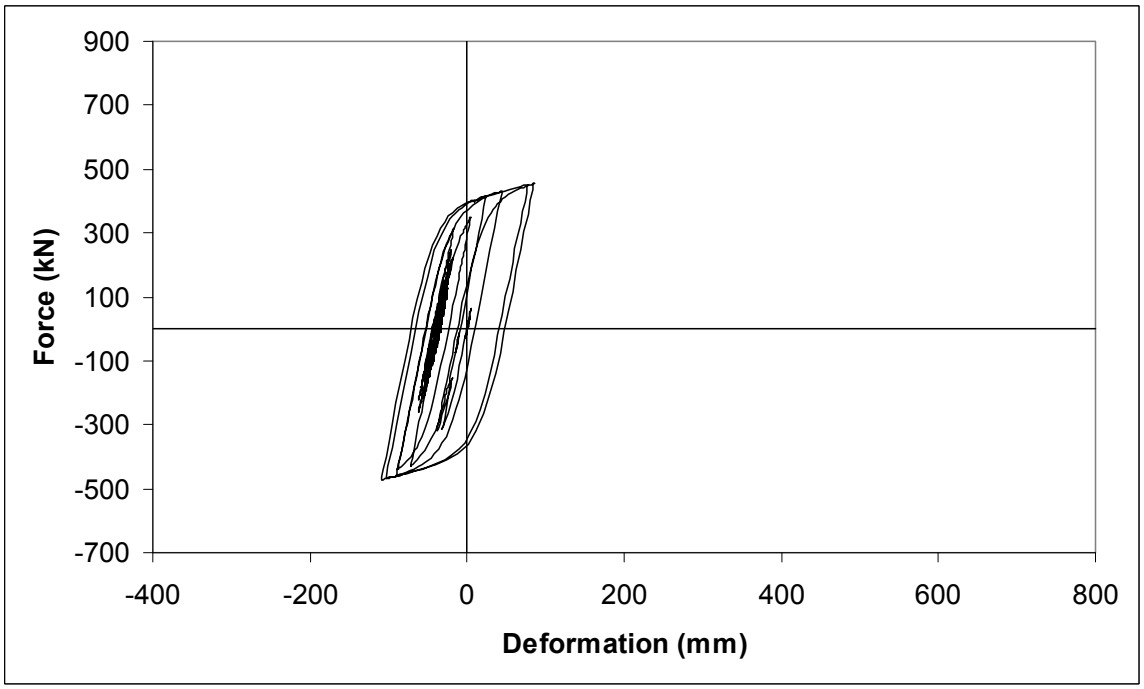

Figure 6.95 NRTMDF Buckling Restrained Brace Hysteresis Loop for MF-1, Medium Site, BSE-1, LA13 Motion

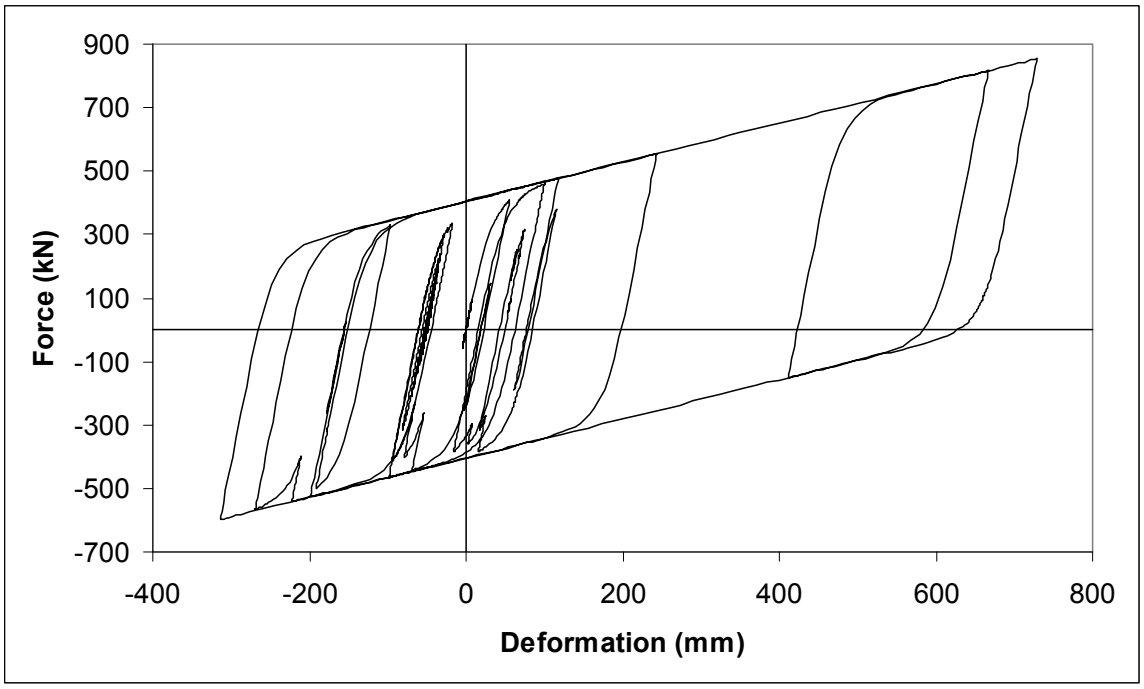

Figure 6.96 NRTMDF Buckling Restrained Brace Hysteresis Loop for MF-1, Medium Site, BSE-2, LA23 Motion

and the similarly limber NRTMDF tuned for effective performance which predicates its limber characteristics.

Figures 6.97, 6.98 and 6.99 depict the peak story displacements, drift indices and story shears for the MF-1 model, BSE-1 (LA13) and BSE-2 (LA23) ground motions. For the lesser motion (BSE-1) the model predicts elastic behavior for the moment frame with a moderate reduction in output parameters enabled by the NRTMDF. For the greater motion (BSE-2), moment frame beams are driven beyond their flexural elastic capacity and plastic hinging develops. Figures 6.100 and 6.101 depict the predicted formation of plastic hinges for the undamped and damped cases respectively. As reflected in this (along with other output parameters), the NRTMDF reduces the quantity of plastic hinge formations and likewise reduces the degree of plastic hinge rotation and curvature as depicted in Figures 6.102 and 6.103.

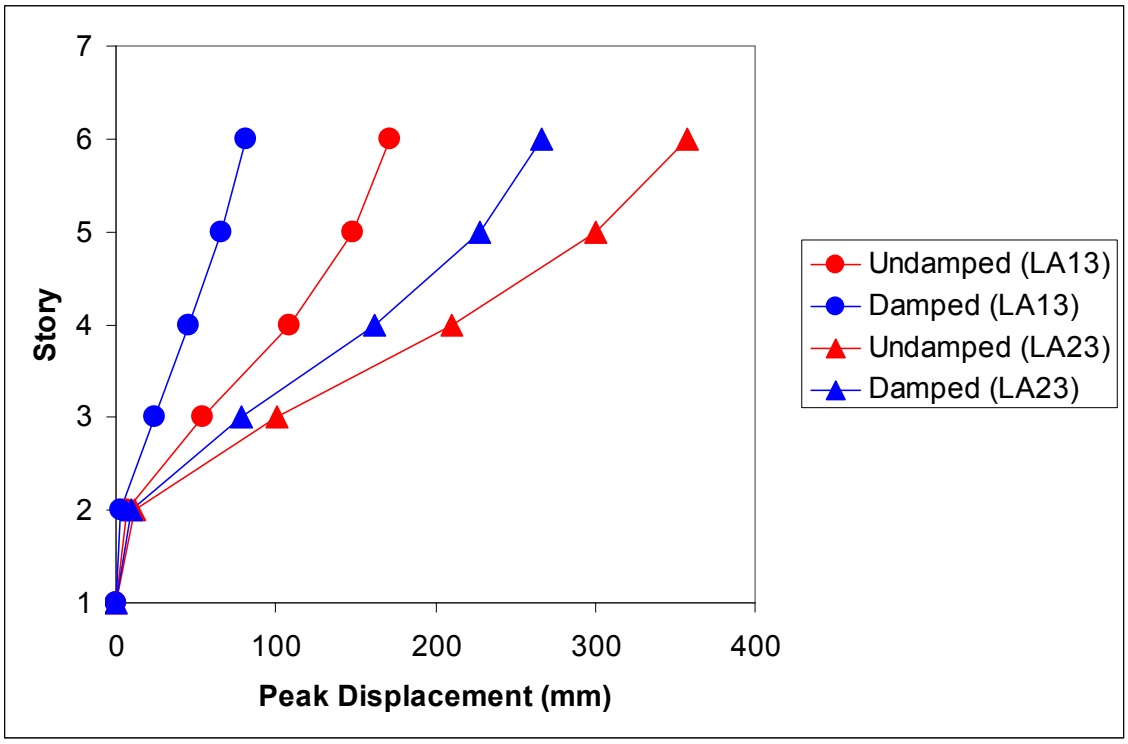

Figure 6.97 Peak Story Displacements for MF-1 Medium Site, BSE-1 (LA13) and BSE-2 (LA23)

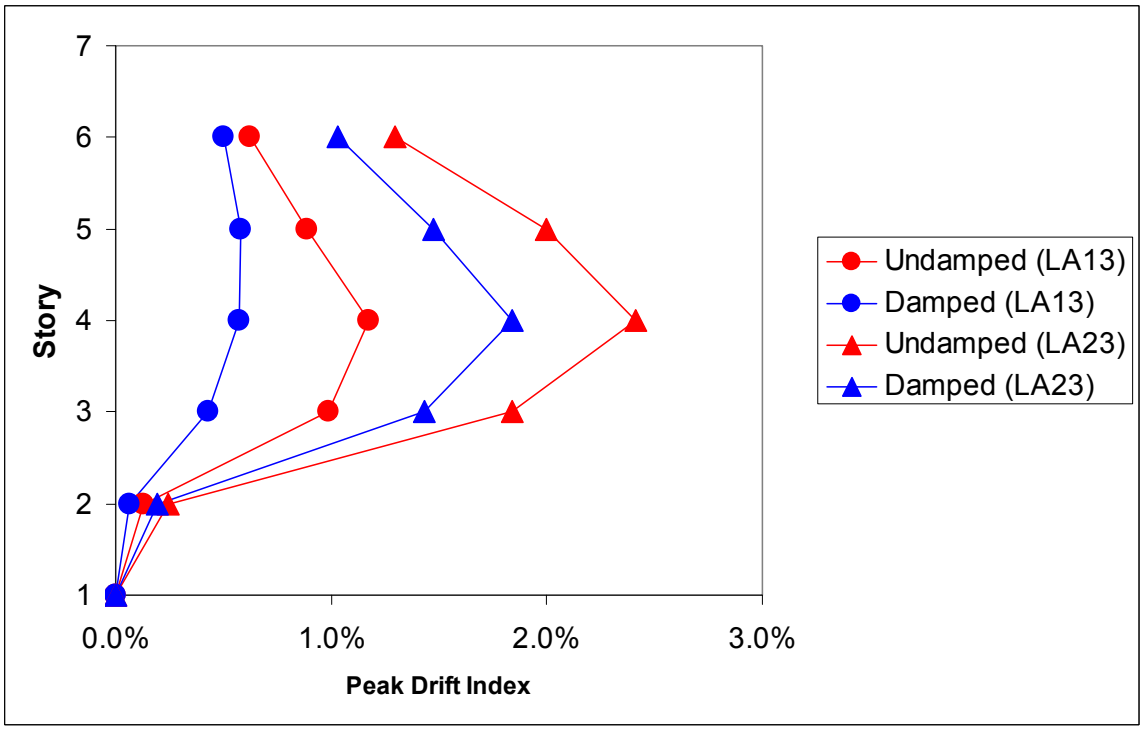

Figure 6.98 Peak Drift Indices for MF-1 Medium Site, BSE-1 (LA13) and BSE-2 (LA23)

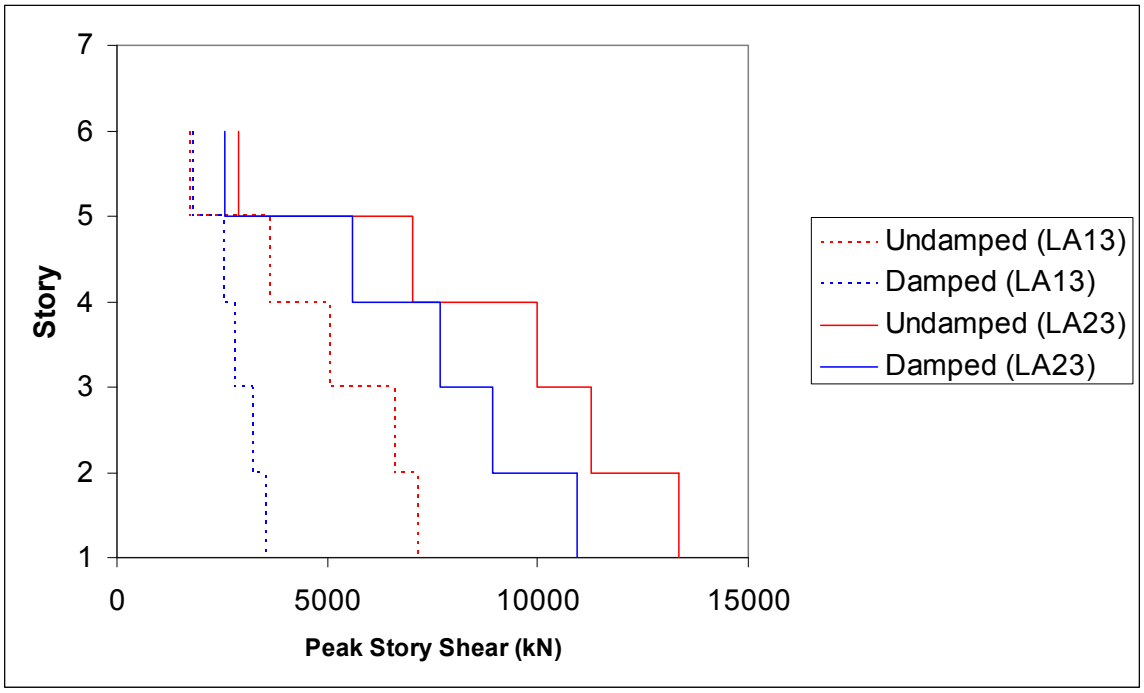

Figure 6.99 Peak Story Shears for MF-1 Medium Site, BSE-1 (LA13) and BSE-2 (LA23)

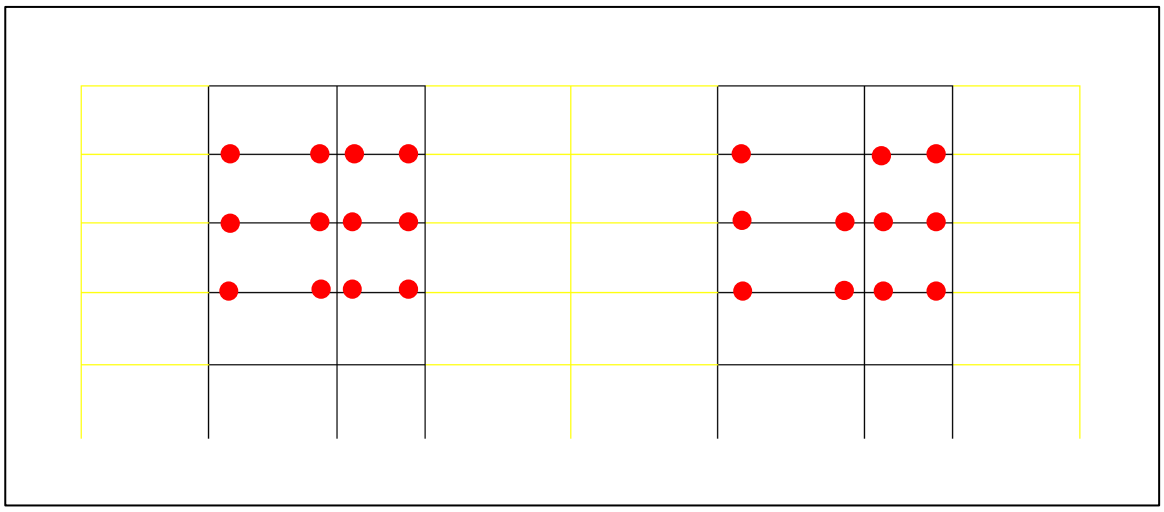

Figure 6.100 Plastic Hinge Formations for Undamped MF-1 and Medium Site, BSE-2 (LA23) Motion

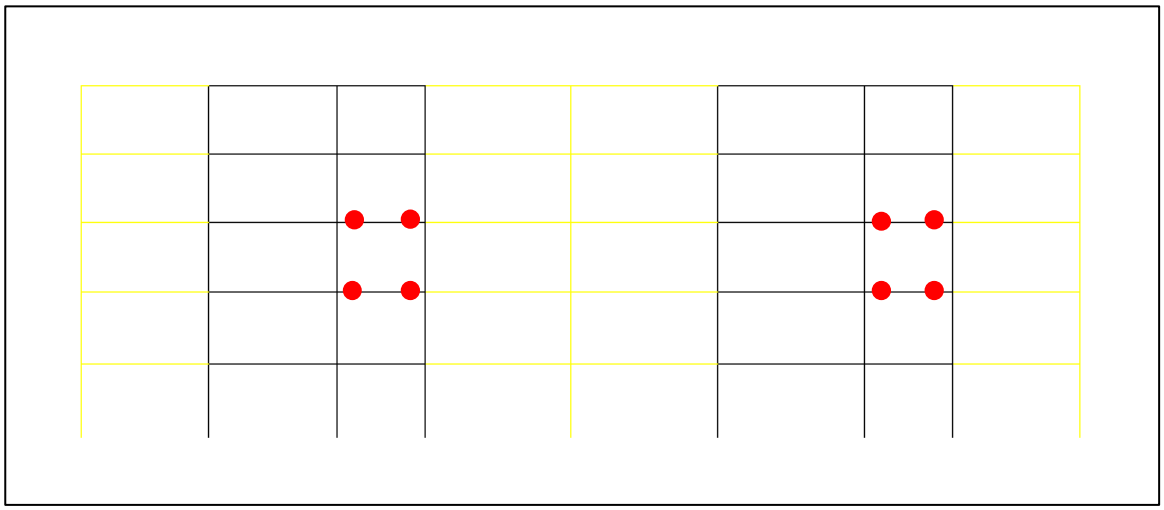

Figure 6.101 Plastic Hinge Formations for Damped MF-1 and Medium Site, BSE-2 (LA23) Motion

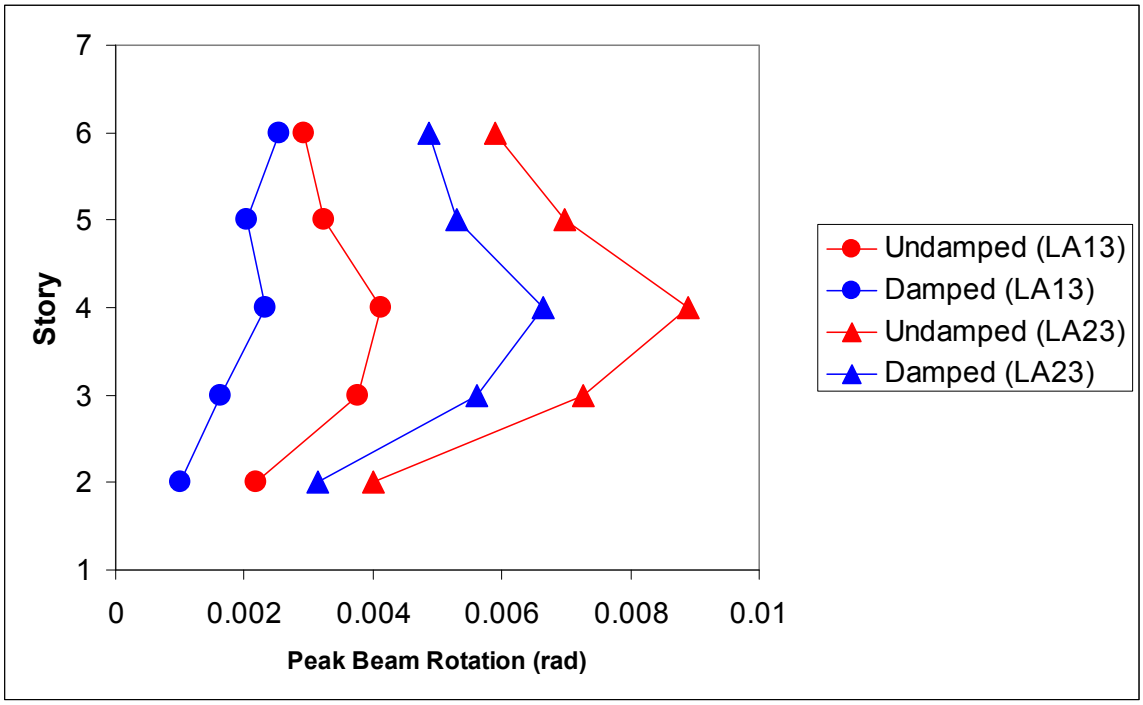

Figure 6.102 Peak Beam Rotations for MF-1 Medium Site, BSE-1 (LA13) and BSE-2 (LA23)

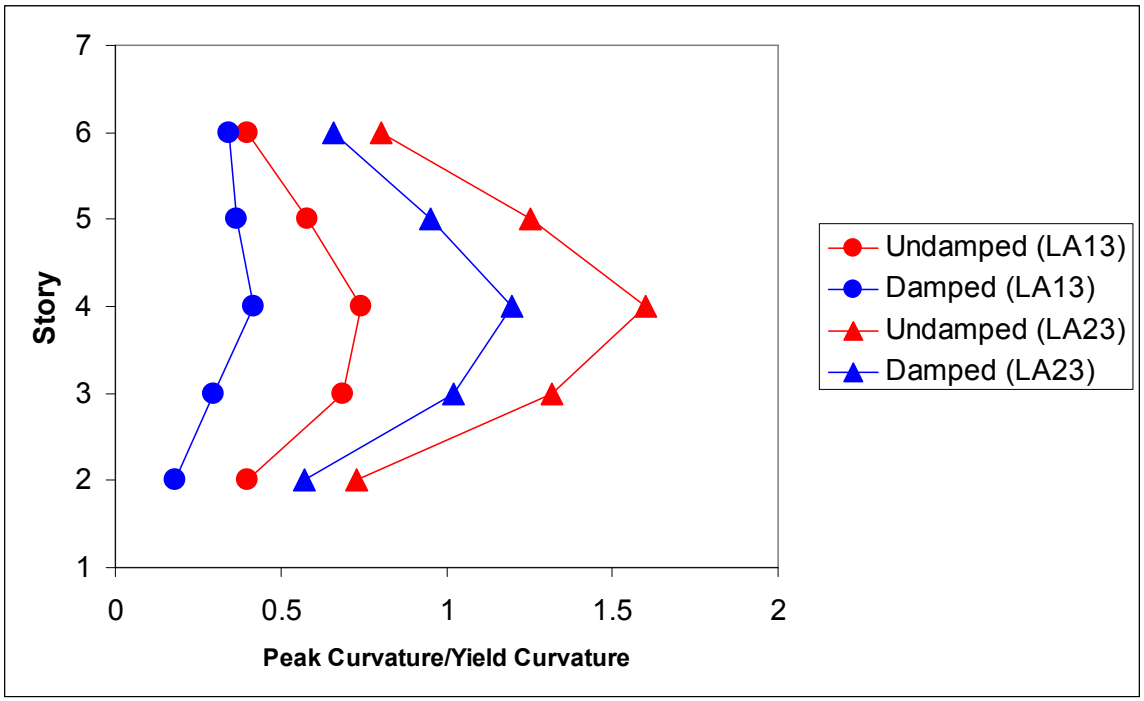

Figure 6.103 Peak Beam Curvature Ratios for MF-1 Medium Site, BSE-1 (LA13) and BSE-2 (LA23)

The combination soft sites and long period for MF-1 represents one of the more extreme cases for the analyses embodied in this research. For this, motions LA09 and LA35 reflect BSE-1 and BSE-2 respectively. The hysteresis loops of Figures 6.104 and 6.105 and the rooftop displacement histories of Figures 6.106 and 6.107 demonstrate primarily linear elastic behavior with a marginal reduction in response enabled by the NRTMDF. The hysteresis of the NRTMDF demonstrated in Figures 6.108 and 6.109 reflect significant nonlinearity of the NRTMDF, with high lateral displacement of the NRTMDF (1056mm) reflecting a soft soil condition, a limber building, and a relatively limber NRTMDF. For this, the NRTMDF is effectively tuned for the motions which drive its limber nature which, as will be shown hereafter, is likely beyond the pragmatic limit for the frame. This reflects the conclusion that the approach embodied in this research may not be effective for long period buildings and soft soil conditions.

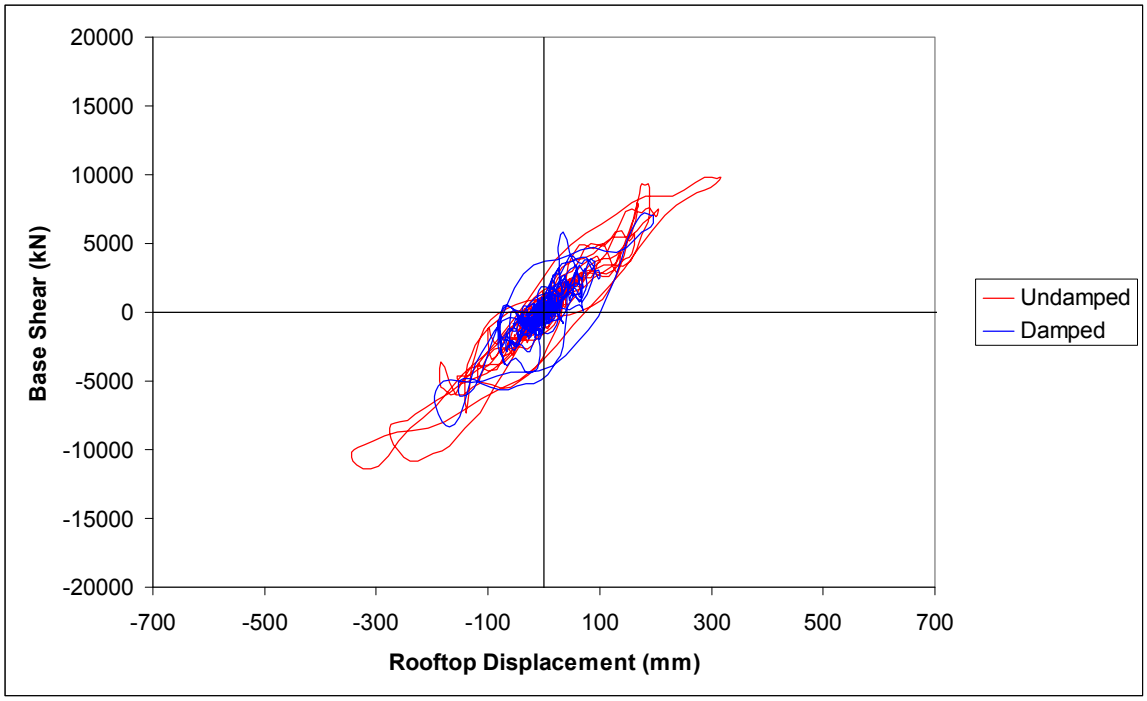

Figure 6.104 Hysteresis Loop for MF-1, Soft Site, BSE-1, LA09 Motion

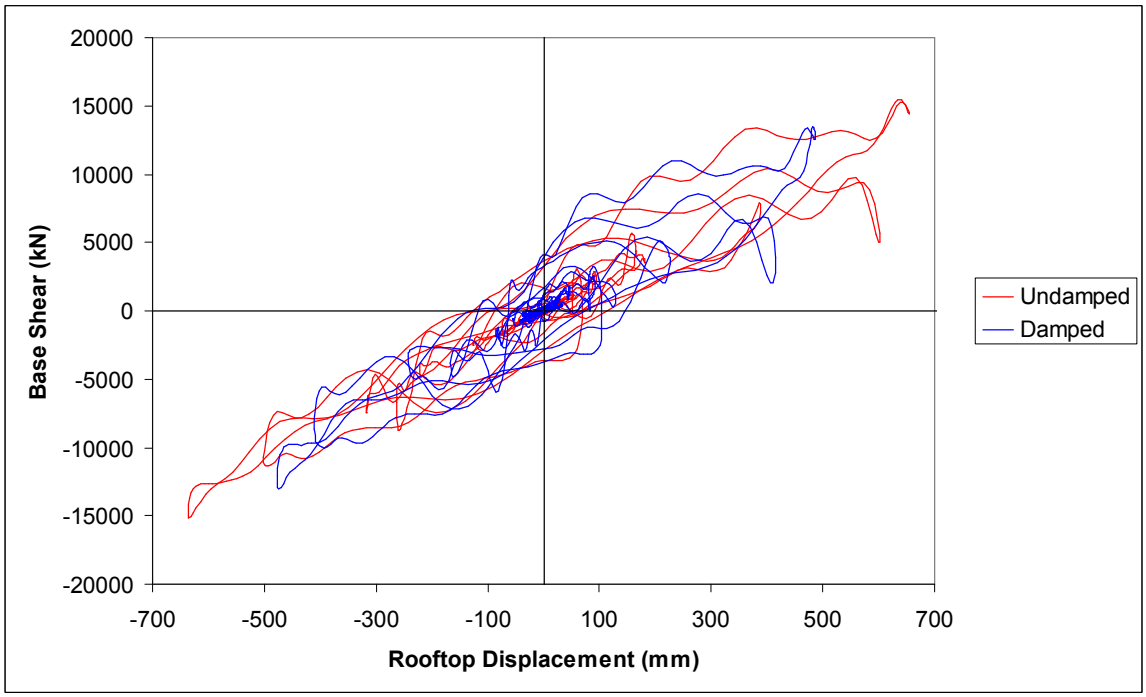

Figure 6.105 Hysteresis Loop for MF-1, Soft Site, BSE-2, LA35 Motion

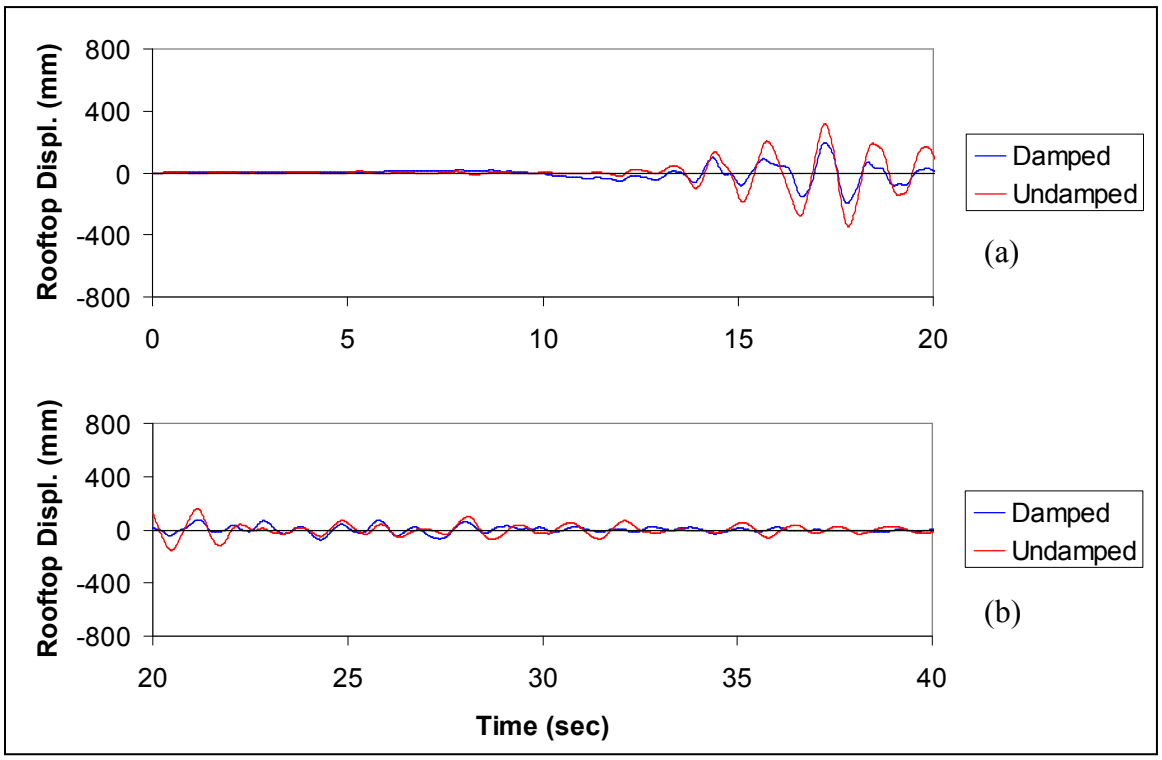

Figure 6.106 Rooftop Displacement History for MF-1, Soft Site, BSE-1, LA09 Motion

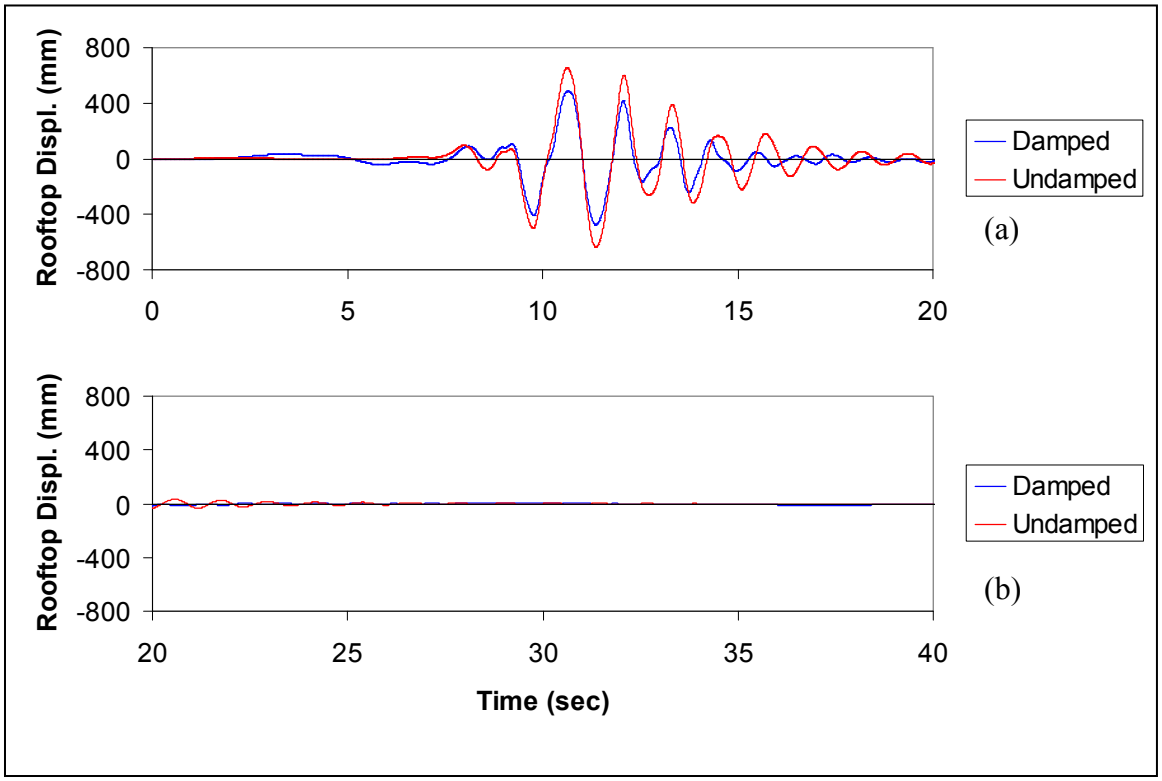

Figure 6.107 Rooftop Displacement History for MF-1, Soft Site, BSE-2, LA35 Motion

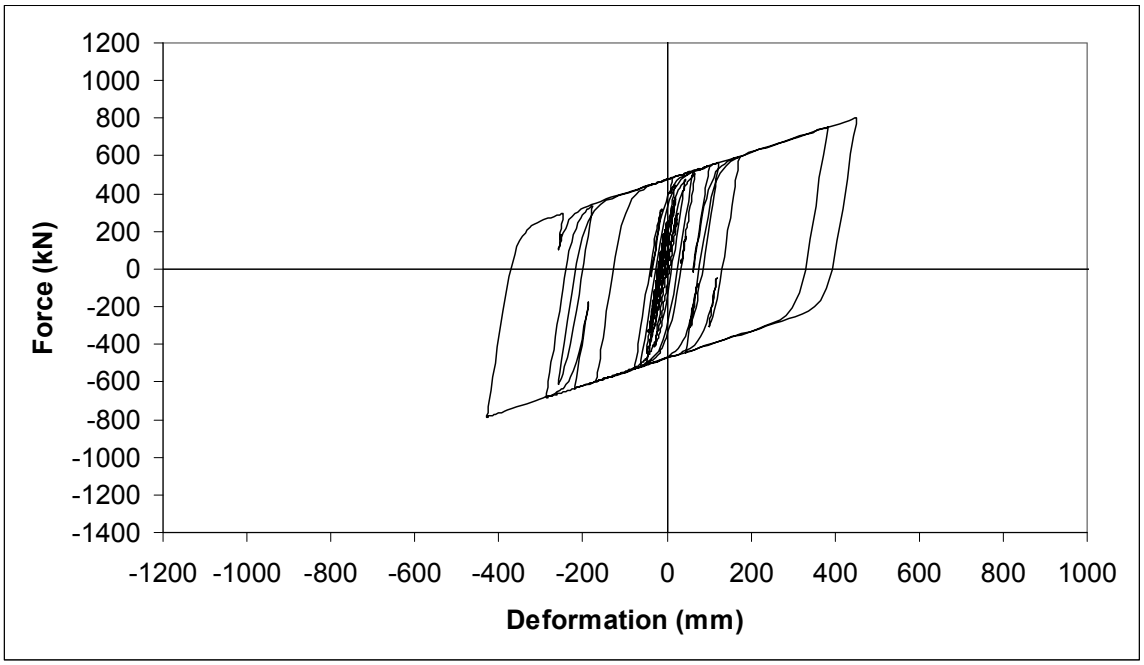

Figure 6.108 NRTMDF Buckling Restrained Brace Hysteresis Loop for MF-1, Soft Site, BSE-1, LA09 Motion

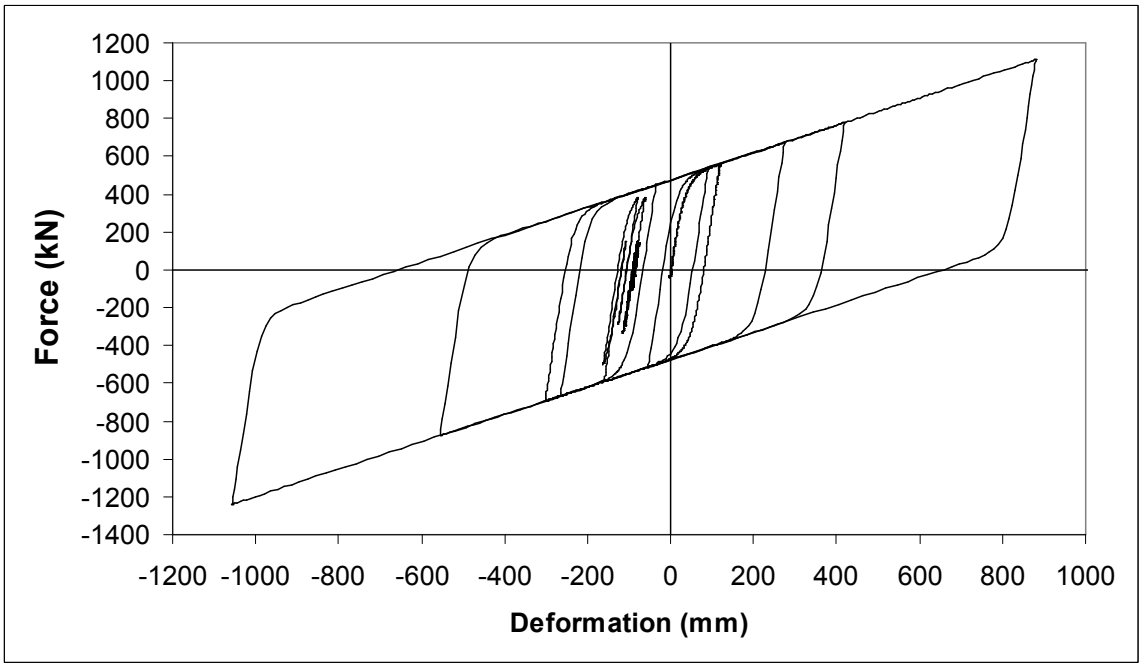

Figure 6.109 NRTMDF Buckling Restrained Brace Hysteresis Loop for MF-1, Soft Site, BSE-2, LA35 Motion

This scenario is not unlike conditions observed for the Mexico City 1985 earthquake along with the Kobe 1995 earthquake. For these events, significant ground motions occurred on sites with extremely soft characteristics. While the softness of Mexico City soils occurs naturally, many of the soft Kobe soils are the result of recently deposited alluvium, recently constructed near-shore islands and other soft materials that tend to amplify propagating waves of earthquakes. For soils of this nature, moderately tall and limber structures have a greater tendency toward site resonance. As a result, many strategies commonly undertaken to mitigate earthquake damage are not effective for this case. For instance, base isolation has the fundamental objective of lengthening a building's fundamental period thereby reducing the spectral acceleration response. However, on extremely soft sites base isolation is not effective since it drives the structural behavior toward, rather than away from site resonance. As a result, a base isolated structure on a soft soil condition may respond with higher acceleration than its fixed base counterpart. For test model MF-1 and the soft site condition, this research demonstrates a potential for reduction of peak transient responses (rooftop displacement and base shear). While examination of the spectra for the LA09 (Figure 3.31) and LA35 (Figure 3.33) motions demonstrates a potential for reduction of the spectral acceleration, this is only after the fundamental period is lengthened well beyond the undamped period which is already relatively high at 1.4 seconds. To enable such lengthening (to nearly 4.0 seconds as indicated in Table 6.27) the NRTMDF must be inordinately limber. As a result, the NRTMDF displacements are extremely high as shown in Figure 6.109 and are likely beyond a practical limit. Rectifying this would require an NRTMDF with greater stiffness, but this would come at the expense of performance. Hence, a scenario of

diminishing returned is encountered. Fundamentally, this demonstrates that the NRTMDF approach is not effective for long period structures (1.0 seconds or more) and soft soil conditions.

While the buckling restrained brace inelastic deformations may be beyond a pragmatic limit for MF-1 and the soft site conditions, the modeling indicates that a reduction in response is attainable as represented in Figures 6.104 through 6.107. Additional output parameters likewise reflect this behavior. Figures 6.110 through 6.112 depict the peak story displacements, drift indices and story shears respectively. Since this structure is closer to resonance with the site, peak performance measures are amplified beyond those of the hard and medium site conditions. The result is an increased displacement and ductility demand for the structure. The modeling predicts elastic behavior for the damped case of BSE-1 (LA09 motion) but nonlinearity is predicted for

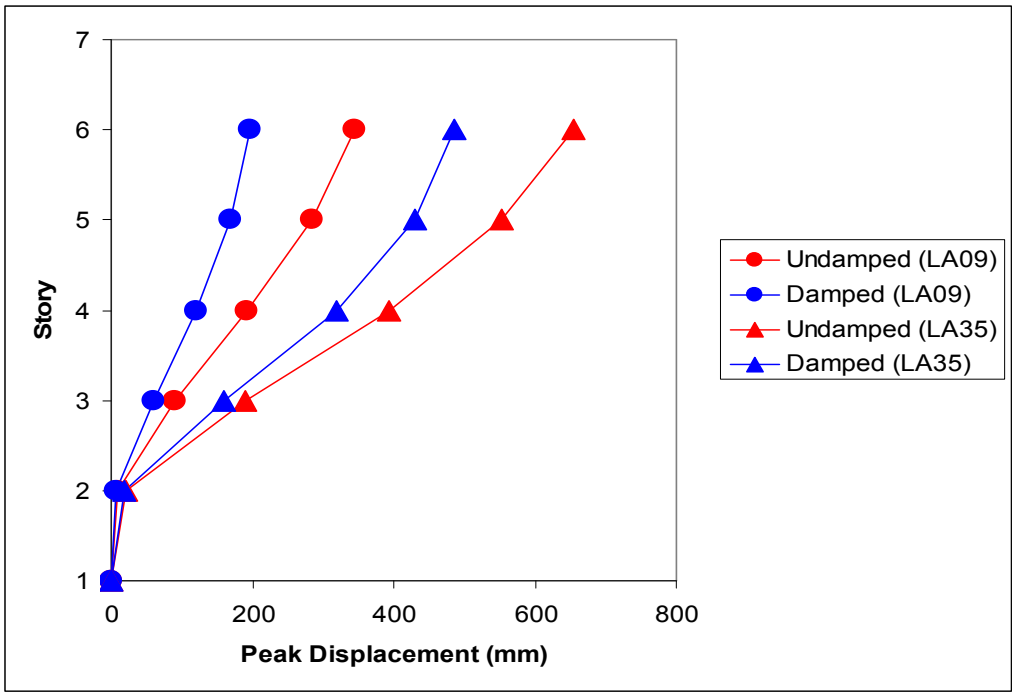

Figure 6.110 Peak Story Displacements for MF-1 Soft Site, BSE-1 (LA09) and BSE-2 (LA35)

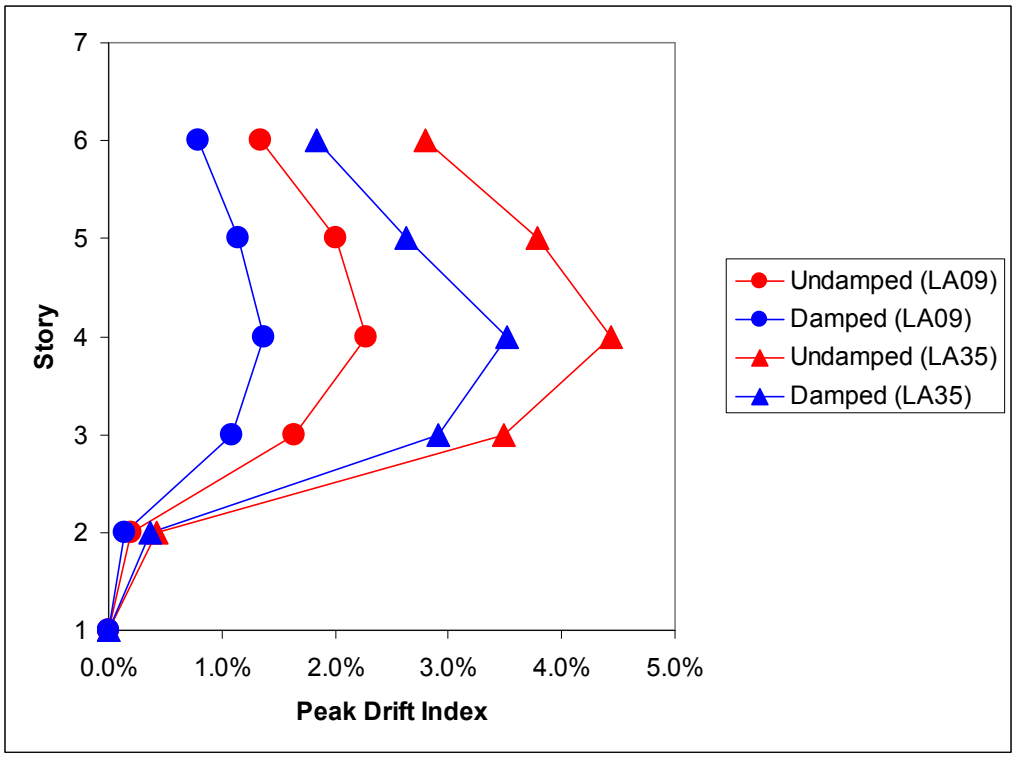

Figure 6.111 Peak Story Drift Indices for MF-1 Soft Site, BSE-1 (LA09) and BSE-2 (LA35)

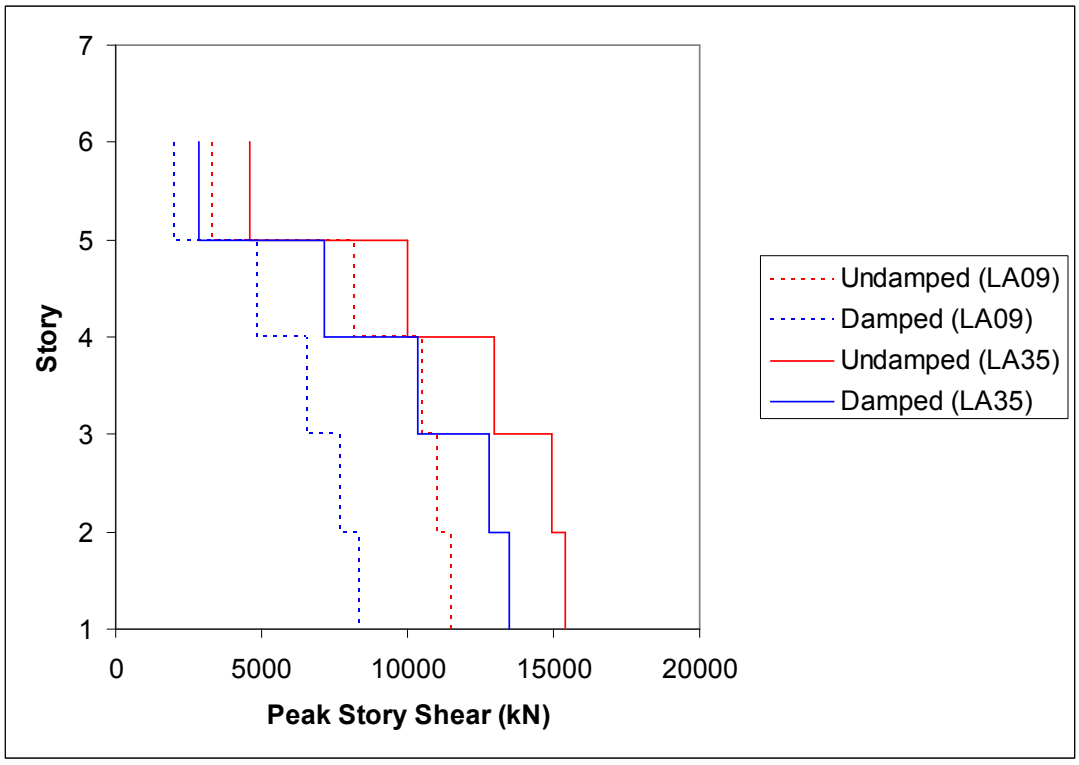

Figure 6.112 Peak Story Shears for MF-1 Soft Site, BSE-1 (LA09) and BSE-2 (LA35)

the undamped case with plastic hinge formations as indicated in Figure 6.113. For the BSE-2 case (LA35 motion) plastic hinging occurs for the undamped case and for the damped case to a lesser degree as shown in Figures 6.114 and 6.115 respectively. This behavior is also demonstrated in the beam rotations and beam curvature ratios shown in Figures 6.116 and 6.117.

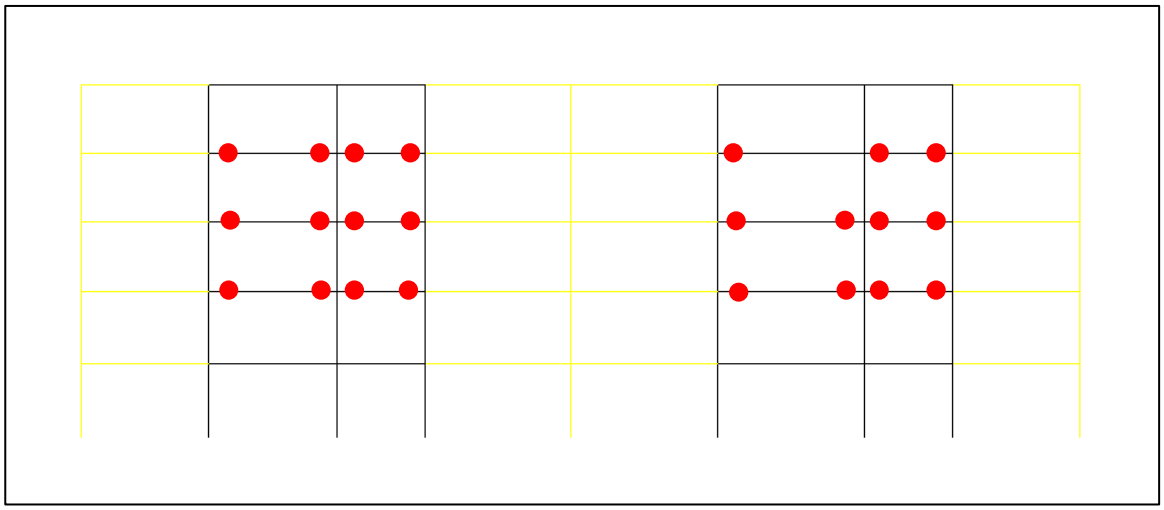

Figure 6.113 Plastic Hinge Formations for Undamped MF-1 Soft Site, BSE-1 (LA09) Motion

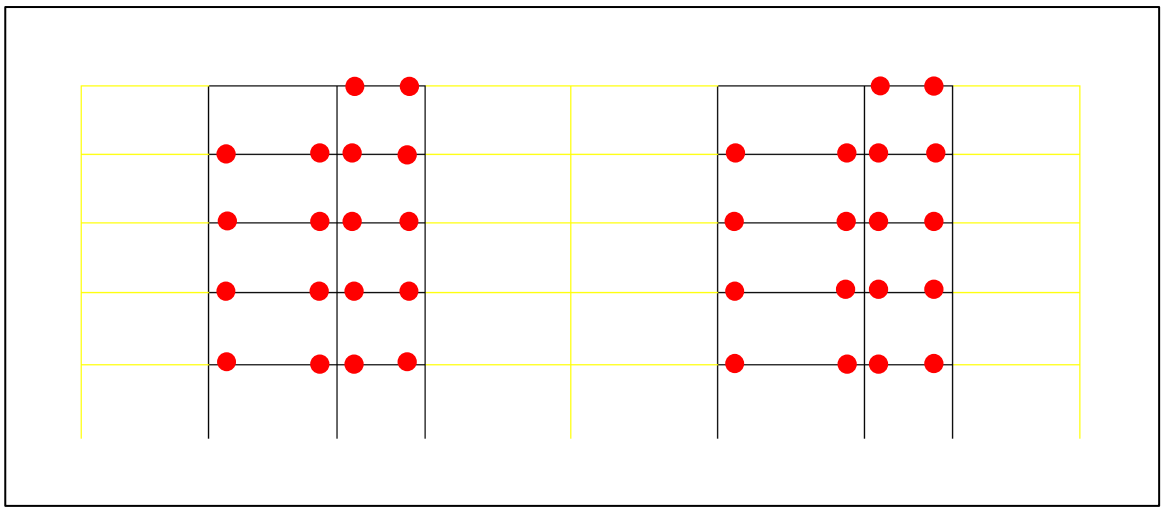

Figure 6.114 Plastic Hinge Formations for Undamped MF-1 Soft Site, BSE-2 (LA35) Motion

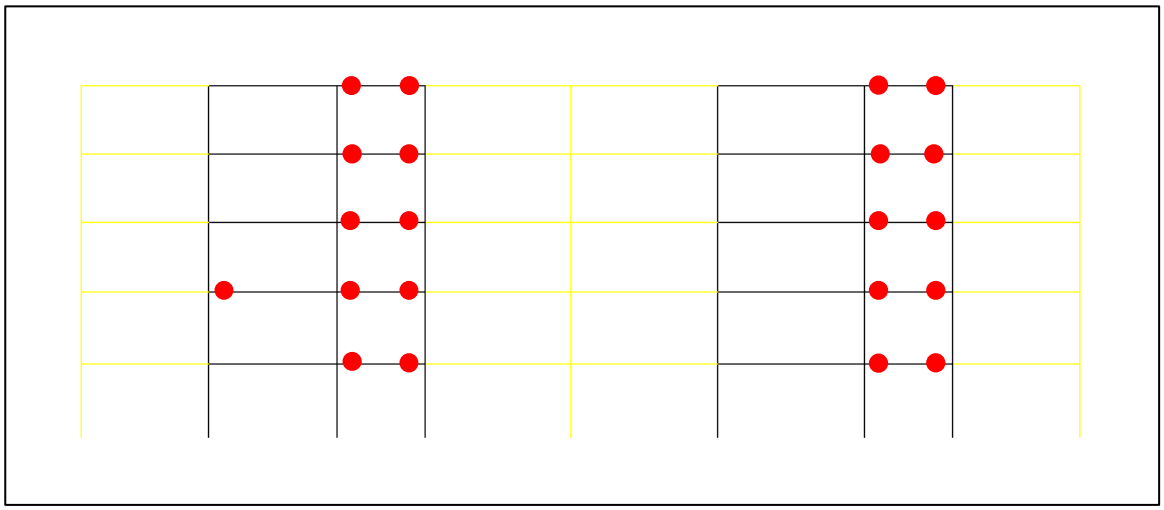

Figure 6.115 Plastic Hinge Formations for Damped MF-1 Soft Site, BSE-2 (LA35) Motion.

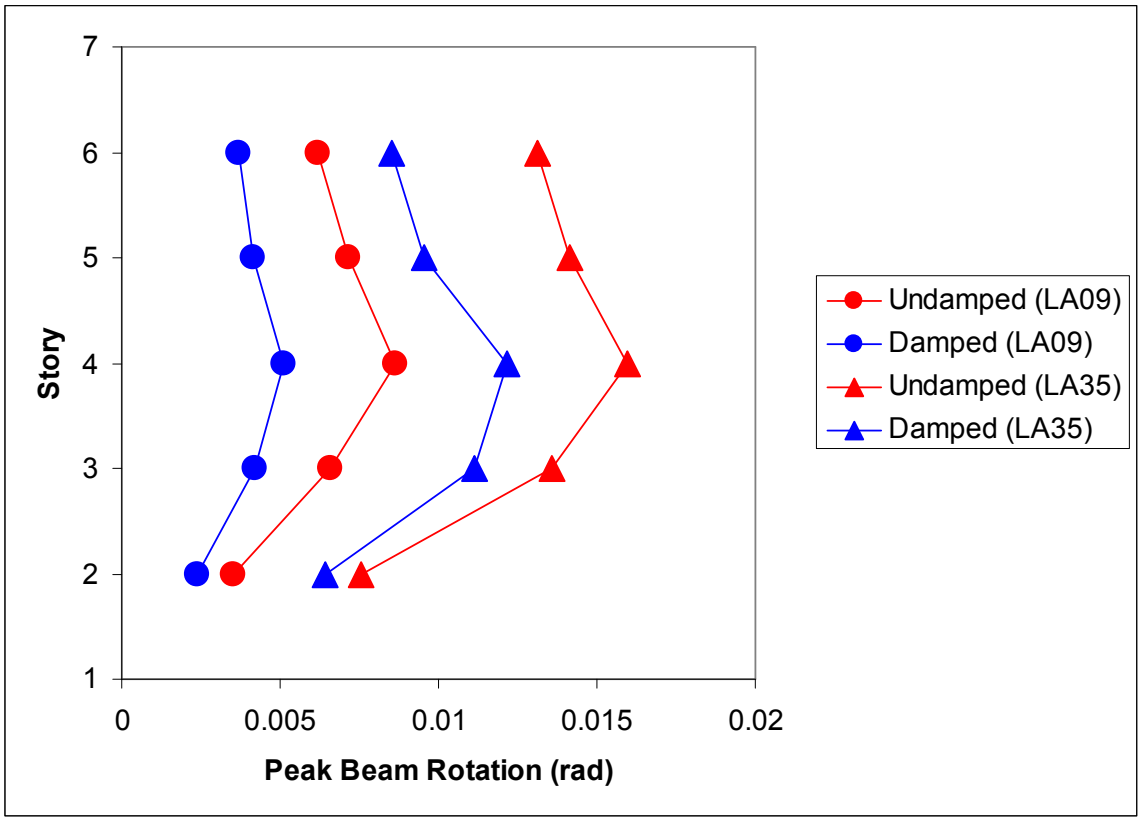

Figure 6.116 Beam Rotations for MF-1 Soft Site, BSE-1 (LA09) and BSE-2 (LA35)

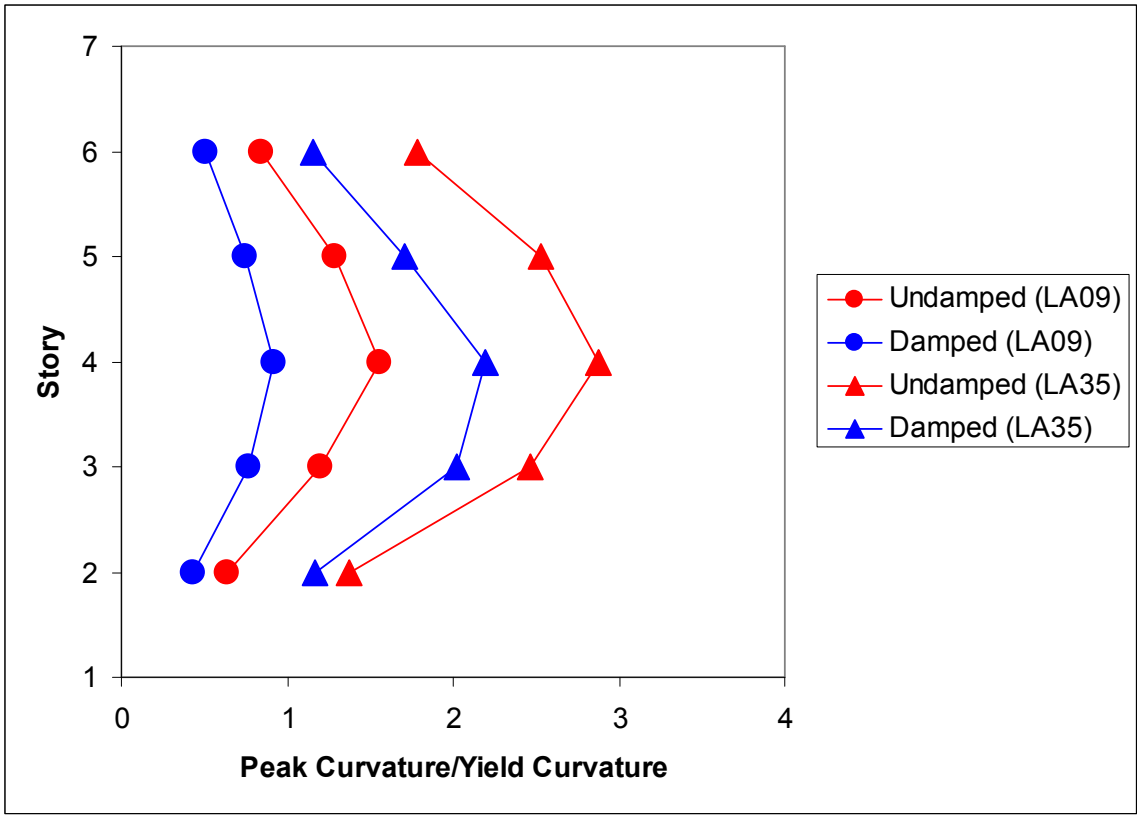

Figure 6.117 Beam Curvature Ratios for MF-1 Soft Site, BSE-1 (LA09) and BSE-2 (LA35)

6.2 NRTMDF Displacements and the Basic Safety Objective

Prior analyses outlined in Section 5.3 address the maximum displacement of the NRTMDF based on the maximum recommended strain of the buckling restrained braces. While secondary issues such as geometric nonlinearity and rotation at connections can ultimately influence NRTMDF stiffness and behavior, a primary controlling parameter of NRTMDF behavior is the yielding core of the BRB and whether it has surpassed its recommended capable strain. Full scale testing and other research has demonstrated maximum capable strains of approximately 3.5% for the yielding core.[35] This value is far less than maximum capable strains that can be achieved by mild steel (7% or more) when

loaded monotonically to failure and reflects a reduced value found in full scale testing which reflects a more realistic hysteretic loading scenario.

Table 5.13 demonstrates a usable strain range of the NRTMDF for each structure. Comparison of these values to the NRTMDF lateral displacements of Tables 6.1 through 6.30 shows the structures, soil types and ground motions for which NRTMDF stability may be problematic for the realistic design scenario (Basic Safety Objective) under consideration due to higher potential for BRB tensile rupture. Table 6.34 lists the summary of results for which likelihood of BRB tensile rupture is increased.

The results and maximum practical BRB strain reflect a tensile mode of failure which is the expected controlling mechanism. While a strain of 3.5% may be established

Table 6.34 Summary of NRTMDF Instabilities for BSO

Structure	NRTMDF Displacement (mm)	% of NRTMDF Capable Displacement	Earthquake
		Hard Sites	
MF-2	757	197.6%	BSE-2
		Medium Sites	
MF-1	716	113.7%	BSE-2
MF-2	803	209.5%	BSE-2
		Soft Sites	
MF-2	668	174.3%	BSE-1
BF-3	721	142.8%	BSE-2
BF-4	936	160.1%	BSE-2
BF-5	1466	288.9%	BSE-2
EBF-1	902	151.9%	BSE-2
SW-2	740	275.0%	BSE-2
MF-1	1824	289.4%	BSE-2
MF-2	2532	660.8%	BSE-2

as the maximum pragmatic limit for the BRB's of the NRTMDF, this value could increase significantly for behavior in compression. Furthermore, if strategic geometrical placement of redundant BRB's is utilized, it may be possible to create a scenario where two braces along the same line are simultaneously working in tension and compression. In so doing, the redundant compression mechanism could prevent significant failure of the NRTMDF due to tensile failure in the adjoining brace. This compression mechanism can even be effective for a brace that has already suffered tensile rupture. See Section 9.7 for further discussion regarding this issue.

Another consideration with respect to the buckling restrained brace performance is the aforementioned peak strain issue and the number of cycles to which a brace would be driven to the peak inelastic strain. Clearly, the ability of a buckling restrained brace to perform as designed would be reflected in the maximum strain to which it is driven. Furthermore, repeated demands to this level of strain may exacerbate the induced fatigue resulting in failure at strains less than the peak capable strain. Testing of steel coupons representing cores of buckling restrained braces shows the potential for 8% strain when loaded in tension monotonically to failure. For a more realistic cyclic loading, this value reduces to approximately 3.5% thereby demonstrating the diminished capacity for inelastic strain based on cyclic action. Observation of nonlinear analyses within this study demonstrates that for most cases, the NRTMDF is driven to only one cycle of peak displacement as demonstrated for the MF-2 test model and the soft site LA38 ground motion shown in Figure 6.118. For other cases such as the soft site SE33 ground motion for MF-2, analyses demonstrate two cycles reaching a peak displacement range as shown in Figure 6.119. Based on the analyses embodied within this research, three or more

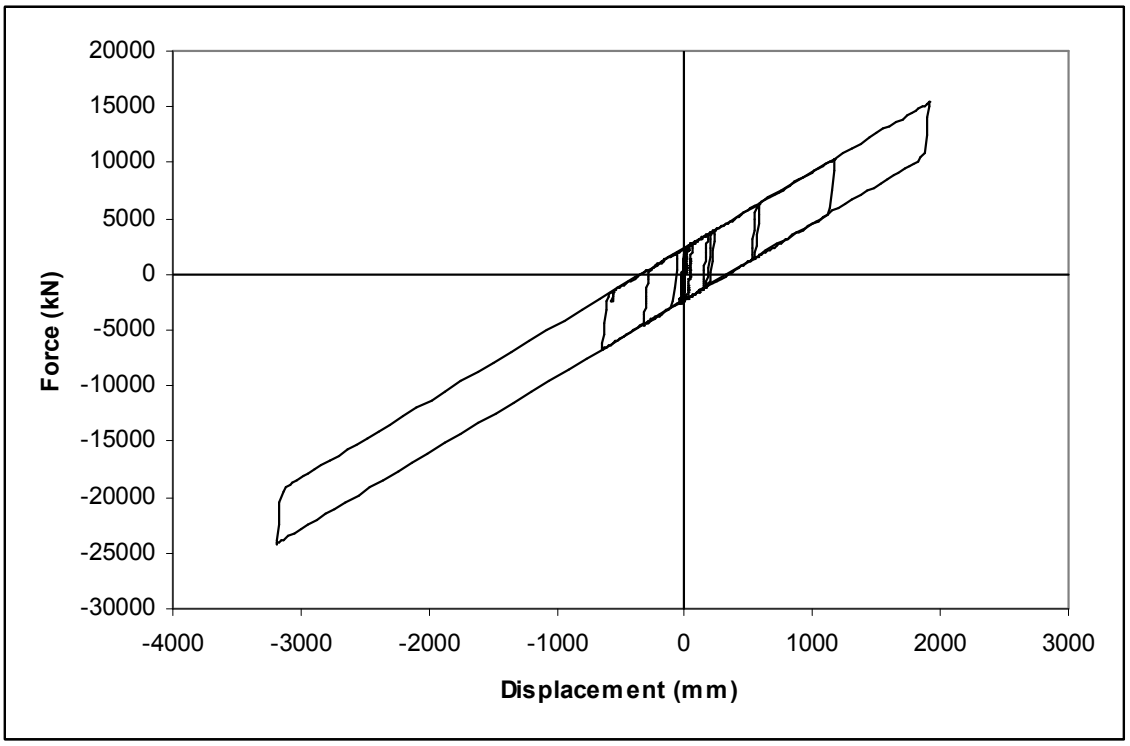

Figure 6.118 NRTMDF Hysteresis for MF-2, LA 38 Motion

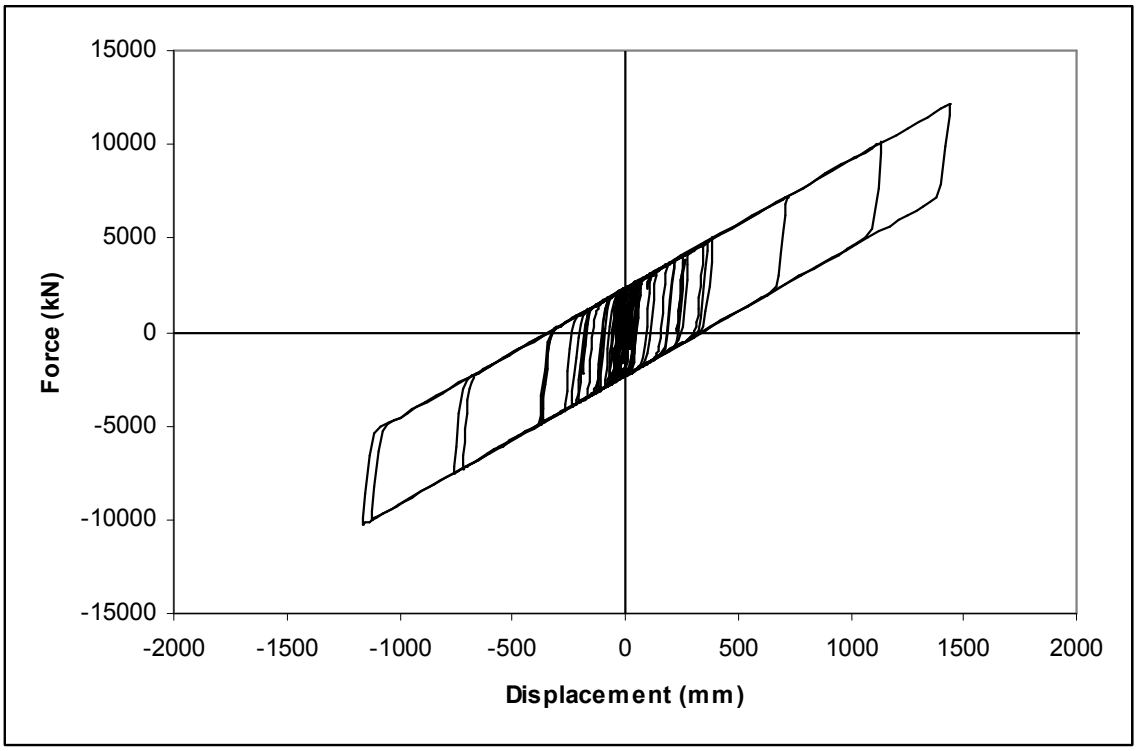

Figure 6.119 NRTMDF Hysteresis for MF-2, LA SE33 Motion

displacement cycles reaching the range of peak NRTMDF displacements were relatively rare, demonstrating that the common testing protocol of three cycles within each tested displacement magnitude is an appropriate quantity to represent a major portion of realistic performance scenarios. This concept notwithstanding, the concept of performance as related to repeated cycles peak inelasticity and measured as a cumulative inelastic ductility is a matter of further research.

6.3 Soft Soil and Long Period Structure Preliminary Conclusions

A noteworthy trend observable within these results is that extreme NRTMDF drifts and correlating instabilities predominantly occur with structures with relatively long periods when considered in their undamped condition. Specifically, MF-1 and MF-2 have undamped fundamental periods of 1.40 and 2.00 seconds, respectively. For these, the effective performance of the NRTMDF requires properties that drive its displacement beyond practical limits for many cases. While the NRTMDF could clearly be stiffened for these cases, doing so would compromise the effective dynamic properties that provide beneficial behavior in terms of reduction of peak transient parameters and energy demand. A second noteworthy trend is that NRTMDF displacements become exacerbated for the soft soil condition. Consistent with previously identified trends, when the NRTMDF does not create a period shift well displaced from the resonant site condition, accelerations, displacements and forces will be high for both the NRTMDF and the base structure. A third trend observable in Table 6.34 is that NRTMDF instabilities occur for the BSE-2 records for all but one case. A reasonable conclusion with respect to these issues is that corollaries may be drawn between period, soil type,

expected acceleration magnitude and the potential for NRTMDF instability. Specifically, NRTMDF instabilities due to BRB fracture become more likely for the following cases:

- Buildings with undamped fundamental periods greater than 1.5 seconds.
- Sites with relatively high accelerations, such as those associated with near field effects, as observed in the acceleration response spectra.
- Soft sites.

6.4 Higher Mode Effects and Story Drifts

Prior analyses demonstrate the significant influence of higher mode effects for the approach embodied within this research. Mode 2 behavior provides a counteractive inertial effect which diminishes the peak rooftop displacement response. However, an increase in mode 2 behavior drives increased story drifts for the stories adjacent to the NRTMDF. This can be observed in Tables 6.35 through 6.37 which summarize the average changes in peak story drift for each structure and each grouping of site conditions for the Basic Safety Objective. This effect notwithstanding, the analyses in general demonstrate reductions in peak story drifts enabled by the NRTMDF, in some cases as high as 45% with typical story drift reductions of approximately 15% to 30%. For this research, cases of increased story drift occurred exclusively at the top story below the NRTMDF and were driven by the higher mode (mode 2) response. While such drifts might be detrimental, for this case they are considered less consequential since they occur at the top story of the structures, which is typically where governing (peak) story drifts are not realized and the structure may have sufficient reserve capacity to perform satisfactorily even with the increased drift demand. For most structures, including models reflected in this research, roofs are comprised of significantly less mass than the

Table 6.35 Average Change in Story Drifts for BSO, Hard Sites

Structure	Story	BSE-1	BSE-2	Structure	Story	BSE-1	BSE-2
BF-1	Roof	-3.7%	-10.1%	SW-1	Roof	-3.1%	-29.9%
	2	-10.0%	-22.8%		6	-24.4%	-39.7%
BF-2	Roof	10.4%	-8.2%		5	-26.1%	-43.5%
	2	-27.5%	-30.9%		4	-24.2%	-43.4%
BF-3	Roof	15.7%	-10.7%		3	-23.7%	-42.3%
	3	-10.5%	-31.3%		2	-22.9%	-40.6%
	2	-15.0%	-29.2%	SW-2	Roof	18.7%	3.9%
BF-4	Roof	-13.5%	-23.3%		6	-23.5%	-26.9%
	4	-28.9%	-28.0%		5	-15.7%	-28.7%
	3	-33.3%	-27.5%		4	-11.1%	-28.0%
	2	-25.2%	-21.6%		3	-13.4%	-24.1%
BF-5	Roof	-6.4%	-17.4%		2	-15.7%	-22.1%
	9	-21.1%	-23.3%	MF-1	Roof	0.9%	-25.2%
	8	-27.5%	-20.1%		5	-17.4%	-28.3%
	7	-32.2%	-18.9%		4	-24.4%	-29.0%
	6	-30.2%	-22.5%		3	-21.7%	-28.6%
	5	-26.8%	-23.7%		2	0.0%	0.0%
	4	-31.0%	-22.3%	MF-2	Roof	-7.1%	-14.2%
	3	-29.7%	-18.7%		8	-12.8%	-18.0%
	2	-27.4%	-17.6%		7	-18.2%	-19.9%
EBF-1	Roof	18.3%	8.3%		6	-22.5%	-16.5%
	4	-26.4%	-26.3%		5	-25.7%	-16.2%
	3	-27.0%	-25.8%		4	-25.4%	-15.4%
	2	-16.9%	-22.0%		3	-25.1%	-20.3%
					2	-27.0%	-21.8%

Table 6.36 Average Change in Story Drifts for BSO, Medium Sites

Structure	Story	BSE-1	BSE-2	Structure	Story	BSE-1	BSE-2
BF-1	Roof	-13.3%	-4.5%	SW-1	Roof	9.8%	5.5%
	2	-14.6%	-9.3%		6	-14.9%	-11.9%
BF-2	Roof	12.7%	11.9%		5	-17.3%	-13.7%
	2	-31.2%	-19.5%		4	-14.9%	-13.1%
BF-3	Roof	-6.8%	-16.7%		3	-12.7%	-11.8%
	3	-8.1%	-13.7%		2	-10.4%	-11.6%
	2	-9.9%	-12.7%	SW-2	Roof	2.1%	-11.8%
BF-4	Roof	7.2%	-26.3%		6	-17.4%	-23.4%
	4	-43.3%	-41.8%		5	-11.4%	-19.5%
	3	-45.8%	-38.1%		4	-7.1%	-15.3%
	2	-44.1%	-34.5%		3	-8.5%	-11.0%
BF-5	Roof	3.0%	-21.0%		2	-9.3%	-9.7%
	9	-20.2%	-23.8%	MF-1	Roof	-10.8%	-26.8%
	8	-32.8%	-22.4%		5	-29.1%	-27.3%
	7	-38.5%	-20.5%		4	-33.5%	-28.3%
	6	-40.8%	-18.7%		3	-39.7%	-27.4%
	5	-40.0%	-19.2%		2	0.0%	0.0%
	4	-39.3%	-20.6%	MF-2	Roof	10.6%	-15.7%
	3	-37.3%	-19.8%		8	-19.7%	-19.5%
	2	-35.5%	-18.5%		7	-22.2%	-16.4%
EBF-1	Roof	43.6%	19.6%		6	-29.8%	-20.4%
	4	-36.5%	-27.1%		5	-32.1%	-23.8%
	3	-39.3%	-29.9%		4	-35.8%	-22.8%
	2	-35.9%	-24.9%		3	-37.1%	-22.4%
					2	-37.2%	-22.7%

Table 6.37 Average Change in Story Drifts for BSO, Soft Sites

Structure	Story	BSE-1	BSE-2	Structure	Story	BSE-1	BSE-2
BF-1	Roof	-11.2%	2.6%	SW-1	Roof	0.1%	-1.0%
	2	-15.6%	-6.8%		6	-10.1%	-6.9%
BF-2	Roof	18.8%	25.0%		5	-11.8%	-6.7%
	2	-9.6%	-5.1%		4	-13.1%	-8.0%
BF-3	Roof	-13.4%	-8.3%		3	-12.0%	-7.4%
	3	-17.2%	-13.2%		2	-10.7%	-7.3%
	2	-15.3%	-12.9%	SW-2	Roof	7.2%	9.4%
BF-4	Roof	-7.9%	-10.3%		6	-16.6%	-10.7%
	4	-21.2%	-11.6%		5	-17.4%	-13.2%
	3	-20.3%	-12.6%		4	-15.8%	-16.0%
	2	-17.6%	-8.3%		3	-14.8%	-13.4%
BF-5	Roof	18.9%	-2.5%		2	-13.4%	-10.8%
	9	-16.0%	-18.2%	MF-1	Roof	-12.7%	-19.6%
	8	-27.1%	-17.4%		5	-28.5%	-17.8%
	7	-32.2%	-16.1%		4	-28.9%	-16.5%
	6	-36.9%	-14.3%		3	-26.7%	-15.9%
	5	-38.0%	-14.1%		2	0.0%	0.0%
	4	-38.2%	-13.5%	MF-2	Roof	-5.7%	-27.0%
	3	-36.6%	-13.2%		8	-20.2%	-27.5%
	2	-34.0%	-12.0%		7	-22.7%	-24.4%
EBF-1	Roof	24.5%	21.1%		6	-18.8%	-23.3%
	4	-15.1%	-7.1%		5	-15.3%	-21.4%
	3	-12.7%	-7.3%		4	-14.0%	-19.8%
	2	-12.6%	-3.9%		3	-16.8%	-19.4%
					2	-17.1%	-19.2%

floors below. As a result, the top story of many multi-story structures has calculated story shears far less than the stories below (see Tables A.1, A.2, A.3). This notwithstanding, prescriptive code requirements along with pragmatic structural configurations often result in top story stiffness which is not significantly different than the stories below. The resulting condition is a top story shear which may have a disproportionate shear demand, and a reduced story drift. The application of the NRTMDF and a resulting increase in higher mode effect may result in an increase in drift of the top story as demonstrated for BF-4, BF-5, EBF-1, SW-1, SW-2 and MF-2. However, this increase is thought to be reasonable with respect to the potential reserve capacity often present at the top story of structures, particularly in consideration of the potential reductions in story drift for more critically loaded stories below.

6.5 Discussion of Results for BSO

The analysis results following a rational design approach prescribed by contemporary codes corroborate the earlier broad-based analysis procedures. Specifically, the results demonstrate that potential reductions in peak transient response parameters may be qualitatively assessed by comparing modal periods of the undamped structure with the spectral acceleration ordinates developed from the ground motions in question. Consider model BF-4, the medium site condition and the summary results of Table 6.11. This structure has a fundamental undamped period of 0.63 seconds (Table 3.1). When observed within the context of the spectra representing the BSE-1 and BSE-2 ground motions, a shift in fundamental period correlates to a reduction in the spectral acceleration ordinates (Figures 6.3 and 6.4). With the optimized damper, the initial mode 1 elastic period shift is to 0.92 seconds with a shift to 1.09 seconds for BSE-1 and a shift

to 1.67 seconds for BSE-2 when considering nonlinearity and the average effective stiffness parameters corresponding to the records under consideration. For these periods, the spectral acceleration ordinates indicate a dramatic change in the acceleration response. Examination of the specific results summarized in Table 6.11 indicates this to be the case with average reductions in peak base shear and rooftop displacement of 19.9% and 43.6% respectively for BSE-1. For BSE-2 the average peak reductions in base shear and rooftop displacement are 2.5% and 40.9% respectively. Such results are also apparent upon examining reduced story drifts in Table 6.36 which reflects reductions of similar magnitude except for the top story which suffers the consequences of increased mode 2 response.

Figure 6.120 demonstrates the deflected shape and drifts for damped BF-4 and the LA18 ground motion at the instant of peak story drift of Level 4. This case represents the condition where the NRTMDF does not reduce the peak response due the amplified mode 2 response acting concurrently with mode 1, resulting in the increase in drift of the top floor indicated in Table 6.36. An important consideration with this issue is that for undamped structures, the top floor typically experiences less story drift than do the stories below. As a result, this floor may typically have reserve capacity for drift thereby enabling the overall performance of the NRTMDF and its beneficial effects while not seriously compromising overall performance, based only on the peak story drift issue. Specifically, for this structure and ground motion, the peak story drift at the fourth floor increases by 30% between the undamped and damped models. However, the magnitude of the drift is very low at only 0.48% for the undamped structure and 0.37% for the damped structure, well below allowable story drifts prescribed by contemporary codes

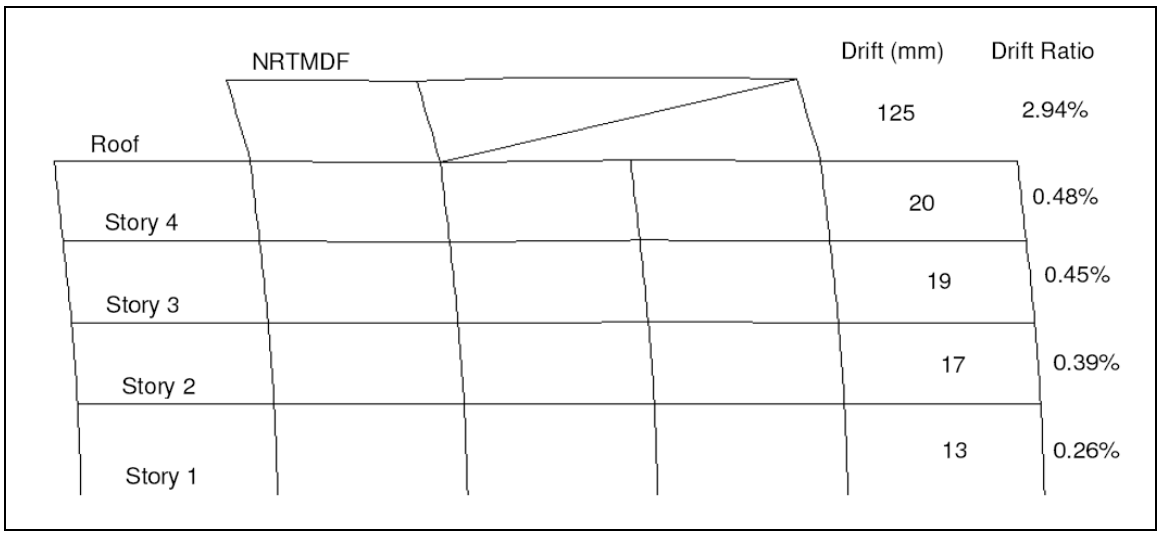

Figure 6.120 Peak Story Drifts for BF-4, LA18 Motion

which can be as high as 2.5%. Hence, the exacerbated drifts at the top story caused by the NRTMDF are not considered problematic.

Consider also model SW-1 which has a fundamental period of 0.35 seconds. When compared against the soft site ground motion spectra for BSE-1 and BSE-2 (Figures 6.5 and 6.6), it can be observed that periods must shift to at least 1.0 seconds and 2.0 seconds respectively before a reduction in the spectral acceleration response parameters can be observed. Design of an effective NRTMDF for this scenario precludes the use of mass and stiffness values that can achieve modal shifts of this magnitude since its motion would be beyond practical limitations. Hence, the NRTMDF for this study has mass and stiffness magnitude reflecting these practical limitations. For this case, the initial elastic period shift is to 0.63 seconds and the shift is to 0.72 and 1.07 seconds for BSE-1 and BSE-2 respectively considering NRTMDF nonlinearity (Table 6.21). Qualitative observation of these periods on the spectra (Figures 6.5 and 6.6) demonstrates no appreciable change in the spectral acceleration ordinates. Hence, significant

reductions in response should not be expected. Table 6.21 lists the reduction in average peak base shear and rooftop displacement responses as 8.1% and 8.7 % respectively for BSE-1. For BSE-2, the reductions in average peak base shear and rooftop displacement are 0.9% and 4.6% respectively. While the spectral acceleration ordinates demonstrate a reduced likelihood for reducing the seismic response for this scenario, a reduction is realized due to the targeted nonlinearity and energy reduction enabled by the NRTMDF. However, the reduction in response enabled by the NRTMDF is counteracted by the addition of mass due to the NRTMDF. This mass becomes active in modes 1 and 2 and creates an increase in the response simply because more mass, with no appreciable reduction in acceleration, translates to higher forces, displacements and other response parameters. Fundamentally, these results support the conclusion that a particular threshold of fundamental period may be established with respect to the spectrum for which a building may be characterized as potentially effective candidate for the NRTMDF Approach. This concept is qualitatively demonstrated in Figure 6.121 which indicates a building at the threshold of diminishing spectral acceleration response (0.4 seconds) which can be enabled by a moderate increase in period. For buildings with smaller fundamental periods (less than 0.4 seconds), a much larger and potentially impractical shift may be required to qualify the building as an effective candidate for the NRTMDF Approach. Likewise, the results for long period structures establish that a threshold value for longer periods may be established for which the approach becomes ineffective because the potential for spectral acceleration reduction due to period shift becomes diminished and the NRTMDF displacements become impractical. Figure 6.121 represents the qualitative concept of establishing the range of effectiveness for the

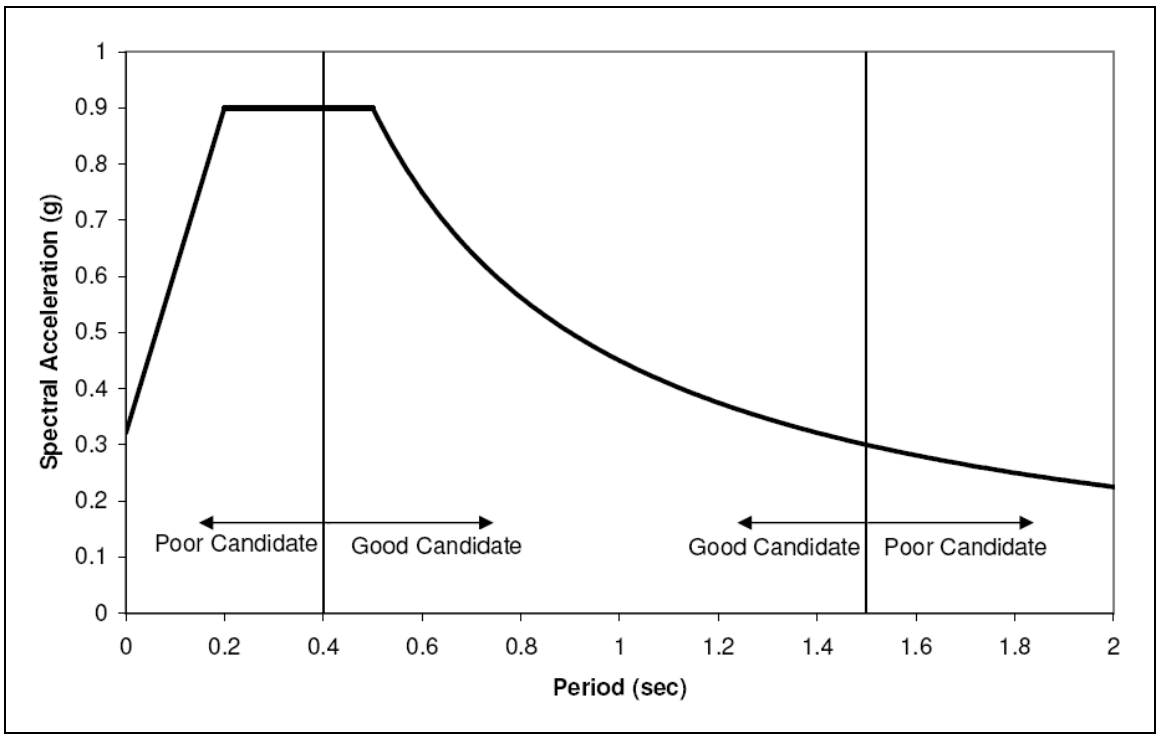

Figure 6.121 Threshold Undamped Periods of NRTMDF Approach Effectiveness

NRTMDF approach. Similar thresholds could be established for any site and correlating spectrum subject to the judgment of the engineer or design professional.

6.6 Exceptions to General Trends

The analyses support the conclusion of medium period structures on the characterized medium site condition as the combination of structures and sites most amenable to the NRTMDF approach. This notwithstanding, it must be recognized that this conclusion is not inclusive of all such sites and structures. Conditions exist within the characterized medium site condition where the attenuation of shear waves can in-fact lead to the amplification of longer periods. Consider the motion represented by the spectrum of Figure 6.122. This motion was recorded on a Type D soil at a distance of 31 km from the nearest rupture plane and is the Palo Alto 1900 Embarcadero acceleration

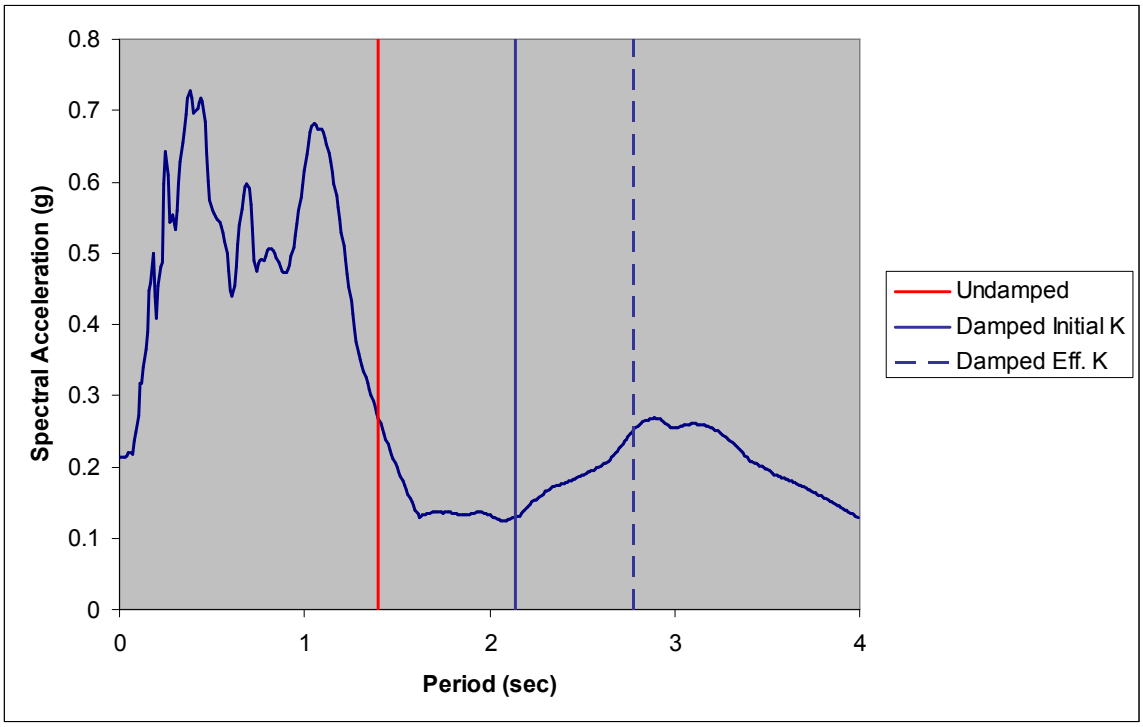

Figure 6.122 1989 Loma Prieta Palo Alto Embarcadero Ground Motion Spectrum

history of the 1989 Loma Prieta Earthquake at a direction of 55 degrees. Despite the firm soil condition, the spectrum demonstrates characteristics not unlike a soft site. Namely, accelerations become increased for structural periods in the range of 3 seconds.

Theoretically, undamped structures having periods of 1.5 to 2 seconds can be qualitatively identified as inappropriate candidates in consideration of this ground motion. Shifting of fundamental periods for this record will likely increase the seismic response and create a damped condition with less favorable performance than the undamped condition. Consider test model MF-1. This structure has an undamped period of 1.4 seconds and an initial damped period of 2.14 seconds which extends to approximately 2.78 seconds when the NRTMDF behaves inelastically. These periods correlate to spectral accelerations of 0.27g, 0.13g and 0.23g respectively. This qualitatively demonstrates the ineffectiveness of the NRTMDF for this condition as the

ordinate of spectral acceleration increases as nonlinearity of the rooftop frame occurs. The nonlinear time history analyses of the undamped and damped test models corroborate this conclusion, yielding an undamped peak rooftop displacement of 74mm and a damped rooftop displacement of 108mm, an increase of approximately 46 percent. The potential for this condition notwithstanding, it should be noted that such motions may reflect a relatively small likelihood within suite of motions included within the selected performance and analysis objective. The likelihood of occurrence of such a condition should be considered within the context of the design scenario and may not preclude the NRTMDF approach as an option for improved performance.

6.7 Comprehensive Nonlinear Modeling

A common deficiency with many structures predating contemporary standards is the lack of detailing and design of structural assemblies to enable ductile performance. In particular, connections for braced frame assemblies often lack the strength commensurate with the yield strength of the brace. Current codes prescribe the design of connections to resist forces based on the expected yield strength of the braces. Without such design, likelihood of satisfactory performance becomes diminished.

Based on the notion of brace connection deficiencies which may be encountered in a rehabilitation scenario, the ideal performance for the NRTMDF would be to reduce the demand on the base structure to such a degree that it does not yield thereby minimizing the ductility demand and enabling a reduction of overall damage. Whether the base structure yields is dependent on many factors, chiefly the magnitude of the ground motion. For many of the models and ground motions considered in this research, the NRTMDF enables a reduction in forces on the base structure to the degree that

nonlinear demand on the base structure is minimal. For others, the NRTMDF may not mitigate nonlinear demand on the base structure, but holds the potential for a significant reduction in the degree of nonlinear demand.

Consider model BF-4 and the medium site class condition for the Basic Safety Objective. The comparison of the nonlinear behavior of the base structure and that of the linear counterpart is noteworthy. In particular, for the BSE-1 suite of records, little difference is noted between a linear elastic model of the base structure and model reflecting nonlinear inelastic modeling of the primary lateral force resisting elements (braces). In fact, examination of hysteresis loops for these elements demonstrates primarily elastic behavior for the braces of the damped structure. For the undamped structure, minor to moderate element nonlinearity is observed with compression buckling of braces being the primary mode of nonlinearity with limited cases of tensile yielding. Figure 6.123 marks a key bracing element for this structure at its base level. Figure 6.124 demonstrates the hysteretic behavior of this brace for a representative record of BSE-1 (SE18) for the undamped and damped models. Note the lack of nonlinear demand on the brace for the damped model as opposed to the undamped model which experiences significant compression buckling as the primary mode of nonlinear response. This demonstrates the beneficial effect of the NRTMDF for this structure and this suite of motions. In essence, nonlinear demand has been mitigated enabling an elastic response of the base structure and an expectation for significant damage reduction. Perhaps the biggest benefit for this case is that the nonlinear demand is reduced to the degree that the brace does not buckle in compression. For BSE-2, the magnitude of forces is greater thereby driving an increase in nonlinear demand on the base structure for both the

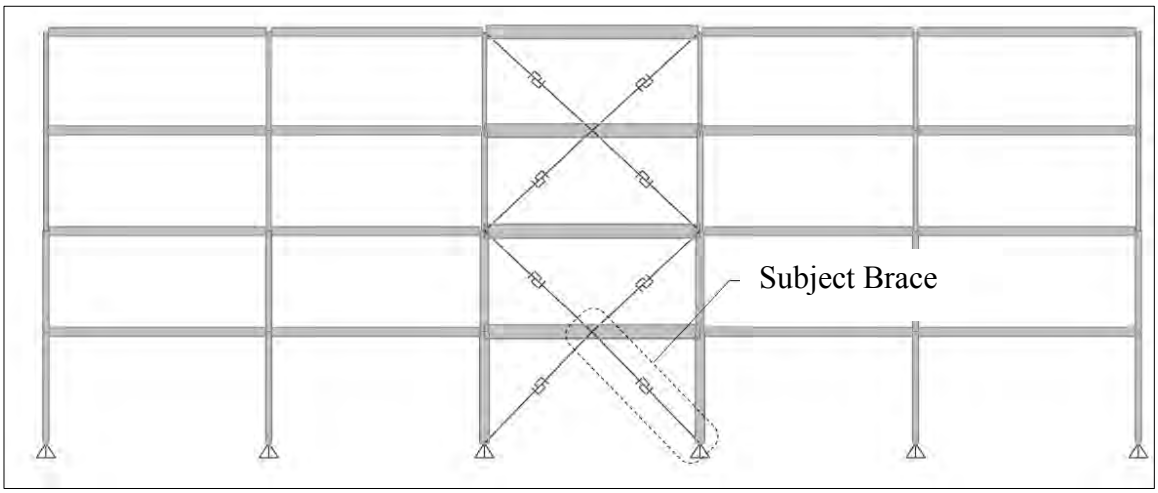

Figure 6.123 Model BF-4 and Nonlinear Brace Modeling

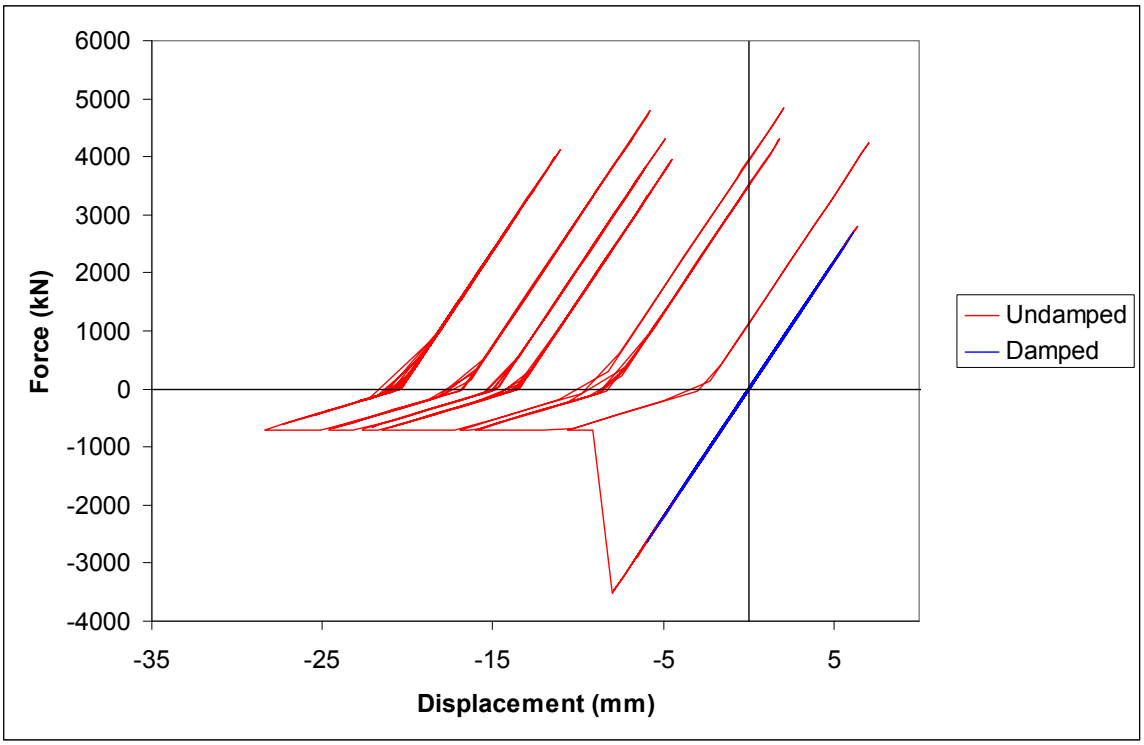

Figure 6.124 Hysteretic Brace Behavior for BF-4, BSE-1, SE18 Ground Motion

undamped and damped cases. However, the degree of nonlinear demand between the two cases is markedly different. Observe Figure 6.125 which demonstrates the hysteretic behavior of the brace for the undamped and damped conditions for the SE23 ground motion. For this, the hysteretic behavior is based on the idealized elasto-plastic behavior as prescribed in the ASCE 41 standard for nonlinear analysis.[28] While the brace demonstrates a similar compression buckling failure for the undamped and damped cases as shown in Figures 6.124 and 6.125, the degree of nonlinear demand between the two is different with relatively little nonlinear tension demand on the brace of the damped model.

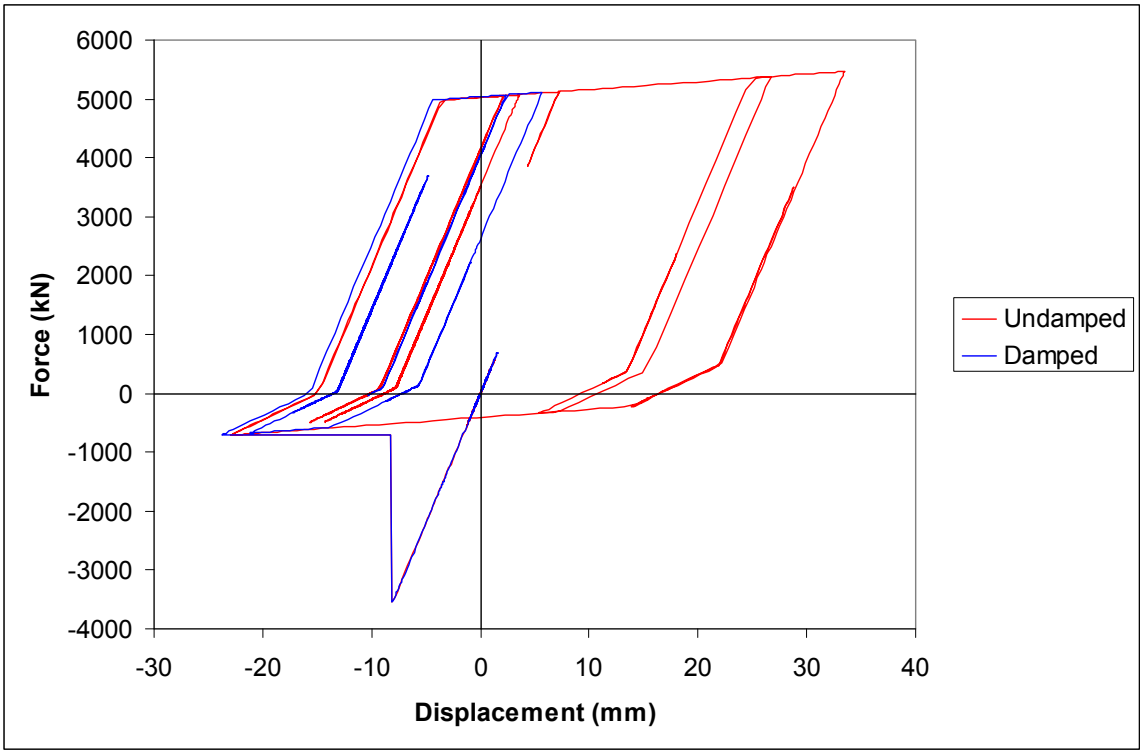

Figure 6.125 Hysteretic Brace Behavior for BF-4, BSE-2, SE23 Ground Motion

These results reflect the concept of nonlinear modeling to predict behavior of braces buckling in compression. While the modeling herein represented is thought to accurately predict whether nonlinear buckling occurs, the actual force and displacement magnitudes following buckling are believed to be highly numerically sensitive. Davaran and Adelzadeh explored this concept and indicate that cyclic behavior of brace elements in compression is not well understood particularly with respect to factors such as buckling and post buckling behavior.[39] Appendix H reflects further study regarding buckling behavior and the numerically sensitive nature of nonlinear analyses which incorporate buckling behavior of braces in compression.

In a fundamental sense, these results demonstrate that full nonlinear modeling of the entire structure may not necessarily be required. The fundamental premise of the approaches demonstrated in this research require the nonlinear modeling of the NRTMDF but modeling of the base structure is theoretically only required when the threshold of linear behavior is breached for the elements within the lateral force resisting systems of the structures.

6.8 Nonlinear Inelastic Analysis Results for PEER Ground Motion

Recent innovations developed by the Pacific Earthquake Engineer Research Center have enabled the automatic selection of ground motions based on a target acceleration response spectrum along with other parameters such as soil type, source distance and rupture mechanisms.[29] To demonstrate the utilization of this tool, the NRTMDF design and optimization procedure of this study has been utilized for one representative model, BF-4 which represents a common size, geometry and lateral force resisting system. For this building, ground motions for BSE-1 and BSE-2 were selected

based on a medium soil condition which is the predominant condition for most sites. Ground motions were also selected based on distances to source capturing a 0 to 10km range, a 10km to 30km range and a 30km to 50km+ range (see Table 3.6). Utilizing the PEER website, motions were selected and corresponding spectra were scaled to match the ASCE 7 prescribed spectra for this building. The resulting spectra are shown in Figures 3.35 through 3.38.

Analysis of an effective NRTMDF designed for the previous condition utilizing the SAC ground motions yielded a NRTMDF with properties outlined in Table 6.11. The same properties were utilized for the same condition with the PEER ground motion suite to demonstrate compatibility between both ground motion suites which were targeted to the same soil conditions and design spectrum of Table 6.38. This table also lists the results of the nonlinear response history analyses and the changes in peak response parameters utilizing the PEER motions. As indicated, the average of peak base shears are reduced by 16.8% and 8.2%, respectively, for BSE-1 and BSE-2 while the average peak rooftop displacements are reduced by 31.6% and 38.3%, respectively. In consideration of these output parameters, rooftop displacement is believed the more critical parameter as it more closely mirrors the degree of nonlinear demand on the structure as a whole. Average NRTMDF displacements are 106mm and 291mm for BSE-1 and BSE-2 respectively which are well below the maximum recommended displacement limit of the NRTMDF (585mm) as indicated in Table 5.13. The diminished reduction in base shear reflects the concept of base structure nonlinearity addressed in Chapter 5 (Figure 5.21). Other transient parameters, such as inter-story drift, and floor spectra based on peak story accelerations are also vital in assessing the effectiveness of the NRTMDF approach.

Table 6.38 Change in Peak Output Parameters for BF-4 PEER Motions

NRTMDF Properties

Mass = 719183 kg	BSE-1 Avg Eff. Stiffness = 45.87 kN/mm
Initial Stiffness = 71.8 kN/mm	BSE-1 Avg. Peak Damped Period = 1.01 sec
Damper Yield Strength = 2440.5 kN	BSE-2 Avg. Eff. Stiffness = 13.01 kN/mm
Initial Damped Period = 0.92 sec	BSE-2 Avg. Peak Damped Period = 1.58 sec

Ground Motions	Base Shear	Rooftop Displ.	NRTMDF Displ.
BSE-1	(% Change)	(% Change)	(mm)
NGA_158IMPVALL.H-AEP_FP	-14.0%	-31.1%	144
NGA_184IMPVALL.H-EDA_FN	-14.1%	-32.0%	79
NGA_184IMPVALL.H-EDA_FP	-22.9%	-37.7%	64
NGA_719SUPERST.B-BRA_FN	-3.8%	-17.6%	124
NGA_730SPITAK.GUK_FP	-19.1%	-27.1%	91
NGA_947NORTHR.ARC_FP	-16.7%	-23.4%	117
NGA_1094NORTHR.SOR_FP	-26.7%	-52.5%	122
Average	-16.8%	-31.6%	106
BSE-2			
NGA_1605DUZCE.DZC_FP	-6.5%	-33.9%	214
NGA_1615DUZCE.1062_FN	-5.2%	-27.7%	292
NGA_850LANDERS.DSP_FP	-8.7%	-42.4%	243
NGA_881LANDERS.MVH_FN	-11.6%	-43.2%	345
NGA_1602DUZCE.BOL_FN	-8.3%	-38.0%	419
NGA_838LANDERS.BRS_FP	-8.0%	-37.6%	286
NGA_1776HECTOR.12149_FP	-9.1%	-45.1%	242
Average	-8.2%	-38.3%	291

These items are addressed within the context of the SAC motions selected for the Basic Safety Objective analyses and are summarized in Section 6.4 and Chapter 7. The utilization of motions derived from the PEER website shown here serve the purpose of demonstrating parallel and closely similar results when selecting motions from different sources which are appropriately selected and scaled to address the same performance objective.

Utilization of the PEER ground motion database produces results consistent the previously outlined theory. Namely, the successful reduction in seismic response is realized by two phenomena. First is the reduced accelerations enabled by virtue of shifts in fundamental periods driven by the NRTMDF as shown in Figures 6.126 and 6.127. Second is the reduction due to targeted energy dissipation of the NRTMDF.

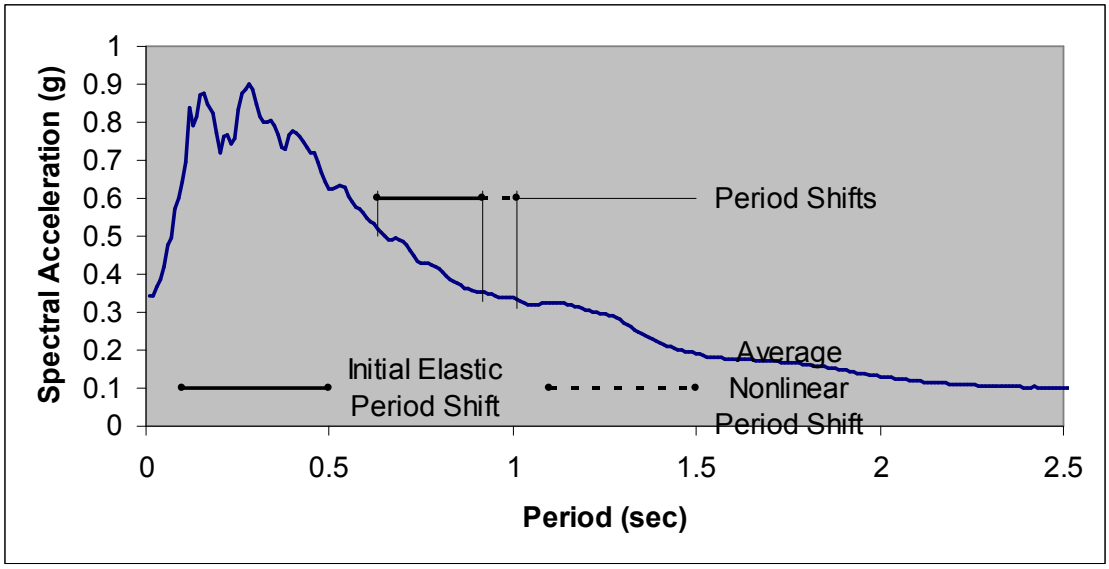

Figure 6.126 Period Shifts for BF-4, BSE-1 Average Spectrum, PEER Ground Motions

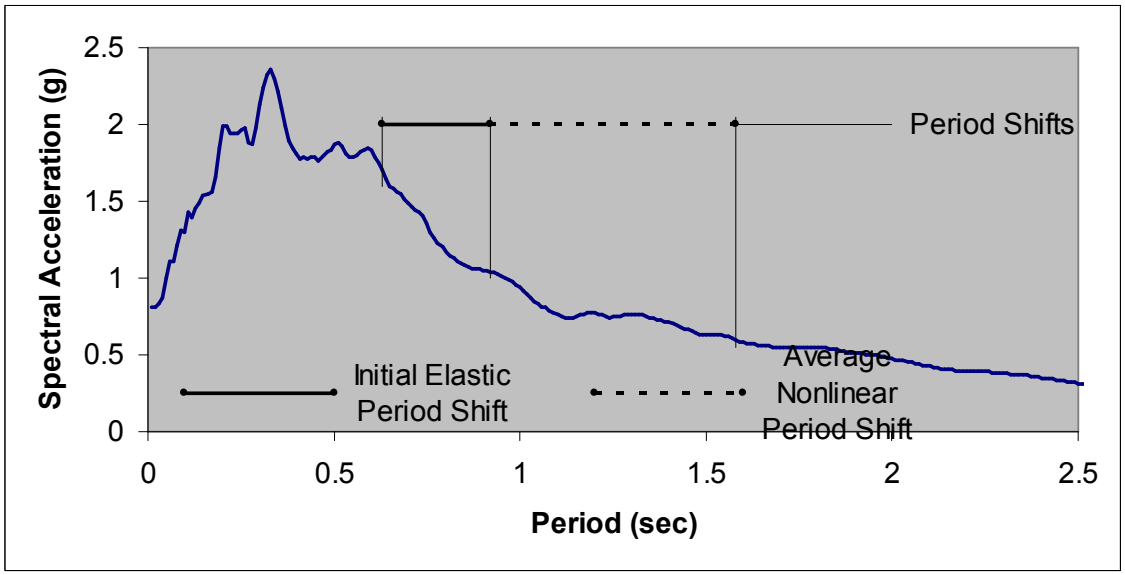

Figure 6.127 BF-4 Period Shifts for BSE-2 Average Spectrum, PEER Ground Motions

7 RESULTS OF ENERGY METHODS

Chapters 5 and 6 introduced the potential for reduction of energy demand due to altered dynamic properties and hysteretic energy dissipation enabled by the NRTMDF. Results demonstrated thus far in this research address reductions in peak transient response using parameters established by methods outlined in contemporary building codes. Primarily, these parameters include displacements, base shears and story drifts. This chapter uses energy based approaches to address total hysteretic demand as well as peak transient parameters. Such approaches are gaining favor, particularly in light of recent earthquakes such as March 11, 2011 Sendai Japan for which significant sustained accelerations were recorded with unusually long time duration. Clearly, the duration of a quake has a direct influence on total energy demand on a structure and can also be an important factor in the development of progressive failure mechanism. Current opinions (e.g. Mahony) reflect the need for duration as a consideration within the context of code driven design for new buildings.[38] Two energy approaches, the first developed by Park and Ang and the second developed by Fardis addressed herein provide rational approaches which consider the complete response time history for each record along with peak transient responses which include drift and peak energy demand.

7.1 Park and Ang Energy Method

Specific results of the Park and Ang energy approach for each structure and each ground motion of the BSO can be found in Appendix I. The pushover analyses utilized in the damage index calculations are found in Appendix F. Tables 7.1 and 7.2 list the average results of the damage index calculation (D) using Equation 3-3 following the Park and Ang approach for the undamped and damped structures as well as the percent change between the two. The listed damage indices follow a demand/capacity approach where values of D less than unity reflect scenarios where the threshold of structural failure is not surpassed and values greater than unity reflect scenarios where failure is considered likely.

Several important considerations having significant influences on the damage index calculations are apparent upon qualitatively examining the results of the energy methods. First, duration of record and duration of significant accelerations within each record was not a parameter of interest considered for record selection. Second, selection of record held no basis with respect to the number of significant acceleration pulses or spikes within the record. Record selections were made following contemporary code protocols which are devoid of requirements considering duration of record or the number of significant acceleration pulses within the record. These factors create a noteworthy result observable in the damage index calculations listed in Tables 7.1 and7.2. Namely, the calculated values for damage index (D) can exhibit extreme variations for records of similar magnitude. As an example, consider test structure SW-1 for the soft soil condition of BSE-2. Two of the records included within this analysis suite for this structure are LA38 and SE33. The calculated damage indices (D) for SW-1 and these

Table 7.1 Park and Ang Damage Index Calculations (D)

Structure	Site	Earthquake	Undamped Average D	Damped Average D	% Change
BF-1	Hard	BSE-1	0.82	0.71	-13.7%
		BSE-2	4.08	2.64	-35.4%
	Medium	BSE-1	1.19	1.02	-14.3%
		BSE-2	4.27	3.52	-17.5%
	Soft	BSE-1	1.43	1.12	-21.7%
		BSE-2	3.98	2.91	-26.9%
BF-2	Hard	BSE-1	0.14	0.11	-22.5%
		BSE-2	0.83	0.50	-39.9%
	Medium	BSE-1	0.20	0.18	-10.0%
		BSE-2	0.79	0.74	-5.7%
	Soft	BSE-1	0.24	0.20	-16.3%
		BSE-2	0.86	0.61	-28.6%
BF-3	Hard	BSE-1	0.52	0.47	-9.8%
		BSE-2	3.94	2.09	-46.9%
	Medium	BSE-1	1.02	0.70	-31.7%
		BSE-2	4.00	2.64	-34.0%
	Soft	BSE-1	1.33	0.99	-25.3%
		BSE-2	3.61	3.09	-14.6%
BF-4	Hard	BSE-1	1.00	0.58	-42.5%
		BSE-2	6.08	3.55	-46.9%
	Medium	BSE-1	2.19	1.15	-31.7%
		BSE-2	16.75	6.04	-34.0%
	Soft	BSE-1	2.63	1.80	-25.3%
		BSE-2	8.68	6.85	-14.6%
BF-5	Hard	BSE-1	0.25	0.15	-42.5%
		BSE-2	1.51	0.92	-41.7%
	Medium	BSE-1	0.51	0.29	-47.5%
		BSE-2	2.52	1.55	-64.0%
	Soft	BSE-1	1.15	0.70	-31.4%
		BSE-2	3.92	2.48	-14.6%

Table 7.2 Park and Ang Damage Index Calculations (*D*) (Continued)

Structure	Site	Earthquake	Undamped Average *D*	Damped Average *D*	% Change
EBF-1	Hard	BSE-1	0.03	0.02	-33.5%
		BSE-2	0.18	0.11	-36.8%
	Medium	BSE-1	0.07	0.04	-39.5%
		BSE-2	0.25	0.15	-42.3%
	Soft	BSE-1	0.08	0.07	-12.6%
		BSE-2	0.16	0.16	-1.0%
SW-1	Hard	BSE-1	0.43	0.34	-19.9%
		BSE-2	3.47	1.59	-54.2%
	Medium	BSE-1	0.76	0.68	-10.2%
		BSE-2	2.86	2.42	-15.6%
	Soft	BSE-1	0.92	0.66	-28.1%
		BSE-2	3.93	3.22	-18.2%
SW-2	Hard	BSE-1	0.20	0.15	-24.1%
		BSE-2	0.81	0.49	-39.0%
	Medium	BSE-1	0.29	0.23	-21.1%
		BSE-2	0.82	0.59	-28.1%
	Soft	BSE-1	0.38	0.32	-17.4%
		BSE-2	0.82	0.70	-14.0%
MF-1	Hard	BSE-1	0.10	0.08	-25.0%
		BSE-2	0.54	0.32	-41.1%
	Medium	BSE-1	0.20	0.12	-40.0%
		BSE-2	0.92	0.56	-39.0%
	Soft	BSE-1	0.52	0.29	-44.6%
		BSE-2	1.73	1.27	-26.8%
MF-2	Hard	BSE-1	0.14	0.11	-25.2%
		BSE-2	0.93	0.69	-26.1%
	Medium	BSE-1	0.29	0.18	-38.2%
		BSE-2	1.17	0.82	-29.4%
	Soft	BSE-1	0.65	0.49	-24.2%
		BSE-2	3.94	2.76	-29.9%

records are 1.40 and 10.47 respectively. This extreme variation is attributable to differences in the duration of each record (60 seconds vs 80 seconds) and differences in the domain of significant accelerations within each record (14 seconds vs 30 seconds). Also, the number of acceleration cycles reaching the range of peak accelerations are vastly different for each record with the LA38 record having only one pulse reaching the range of 0.6g to 0.8g and the SE33 record having no less than 6 pulses reaching the range of 0.6g to 0.8g as demonstrated in Figures 7.1 and 7.2. These pulse characteristics reflect many conditions for each unique event, not the least of which is distance to source. The LA38 record has a reported distance to source of only 1.5km whereas the SE33 record has a reported distance to source of 65km. In this sense, the aforementioned disparity of pulses between each record is rational. The LA38 record demonstrates a single large unidirectional pulse which is an effect commonly observed in near-field records

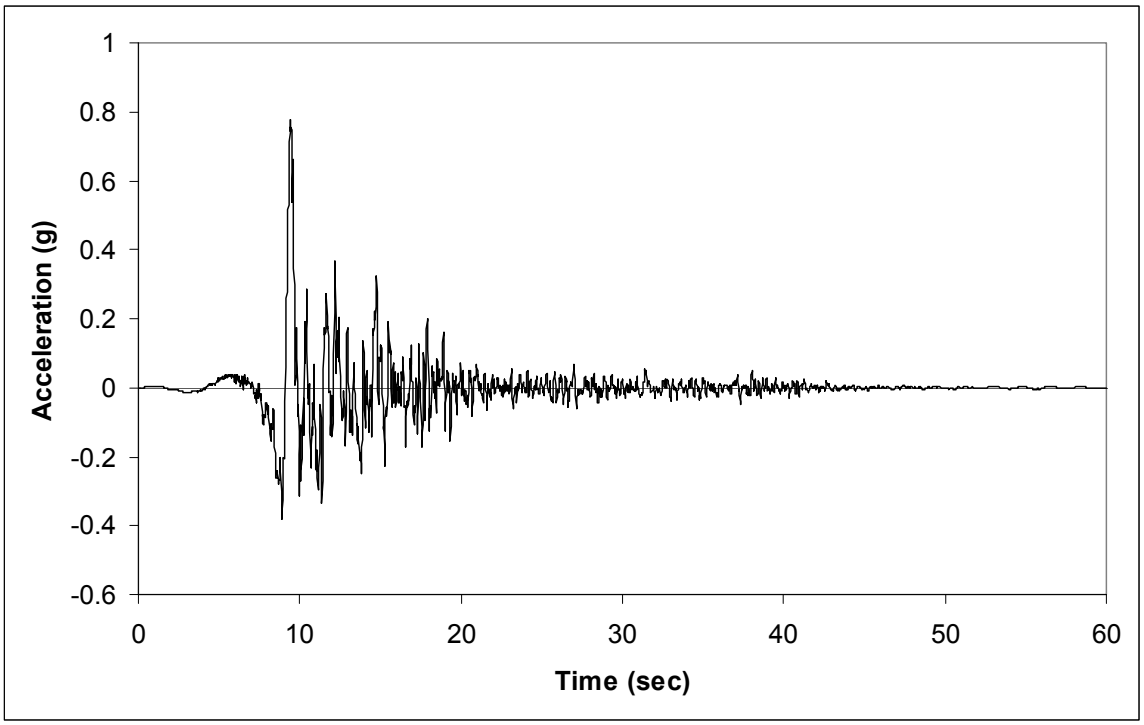

Figure 7.1 LA38 Acceleration Record

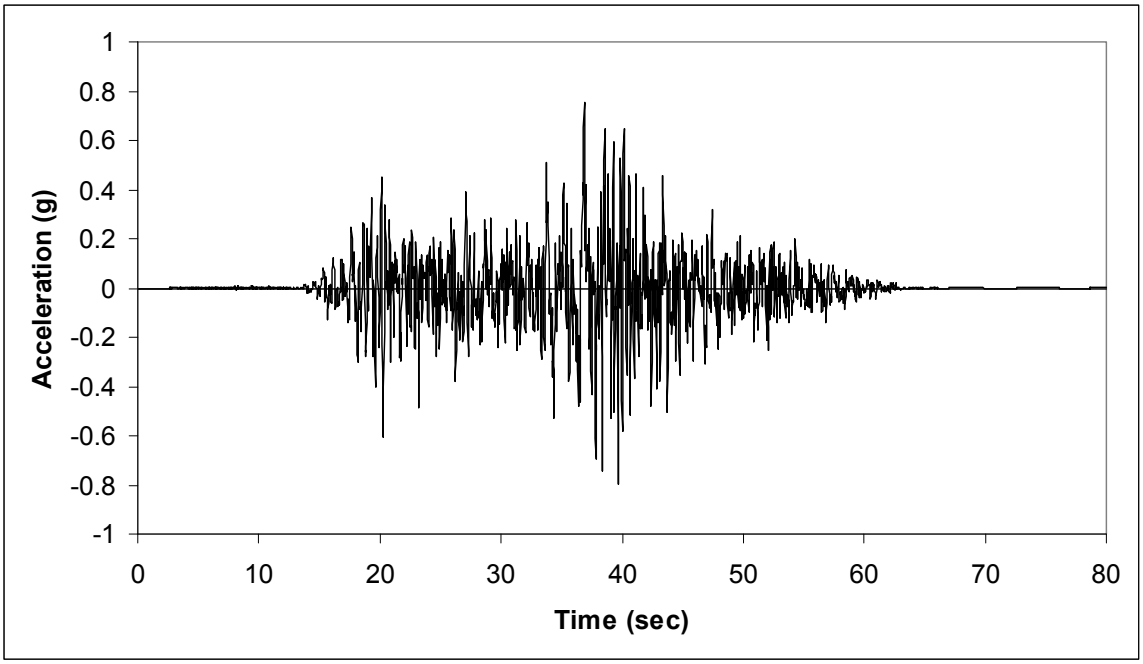

Figure 7.2 SE33 Acceleration Record

whereas the SE33 record contains many large pulses which are more characteristic of records capturing the attenuation of seismic shear waves through an expanse of soil. These results reflect the concept that consideration of the entire earthquake record may be an important assessment tool for gauging a structure's ability for seismic performance. This is a concept not addressed within the context of contemporary standards for seismic design. These results also demonstrate the criticality of accounting for distances to source and capturing the phenomena associated with near field effects. A major challenge in this regard is that no geographic region contains only one source from which seismic motions may develop. Some have a far greater propensity to exhibit near field effect, which is an issue that should be considered within the context of any design ground motion adjacent to a known and active seismic source. However, prudence dictates the rational selection of ground motions reflecting all known and active seismic sources which might affect a particular sight. The selected ground motions for this

research reflect this concept with selected motions at 0 to 10km from source, 10km to 30km from source and acceleration histories recorded at more than 30km from source.

7.2 Fardis Energy Methods

Unlike the Park and Ang method for calculating damage indices, the approach proposed by Fardis incorporates a peak energy demand in lieu of peak displacement response. The approach is reportedly less liberal in damage prediction than the Park and Ang method and enables a more accurate prediction of damage. Tables 7.3 and 7.4 list the average results for the calculation of damage indices (D_E) for this method utilizing Equation 3-4. While correlations can be observed in the damage index calculations between the two methods, the Fardis method typically yields a lower value for the damage index calculation. This notwithstanding, consistencies may be observed in behavioral trends demonstrated between the two methods. As an example, consider again model SW-1 mentioned previously and the LA38 and SE33 ground motions. For these, the Fardis damage indices (D_E) are 1.03 and 7.76 respectively, roughly correlating to the values 1.40 and 10.47 for damage indices (D) using the Park and Ang method. Likewise, the same phenomena apparent in the Park and Ang method may be observed in the Fardis method. Namely, record duration and number of pulses or spikes in the acceleration record are accounted for. While the results are quantitatively different to a modest degree, the results are qualitatively the same. The differences in results reflect the fundamental difference in the calculation between the two methods. Whereas the Park and Ang method utilizes the ratio of peak displacement over maximum capable displacement within the damage index calculation, the Fardis method uses peak transient deformational energy over total energy up to failure.

Table 7.3 Fardis Damage Index Calculations (D_E)

Structure	Site	Earthquake	Undamped Average D_E	Damped Average D_E	% Change
BF-1	Hard	BSE-1	1.39	1.31	-5.7%
		BSE-2	9.39	5.87	-37.5%
	Medium	BSE-1	2.27	2.05	-9.7%
		BSE-2	9.76	7.89	-19.2%
	Soft	BSE-1	2.67	2.07	-22.4%
		BSE-2	8.54	5.66	-33.8%
BF-2	Hard	BSE-1	0.08	0.06	-24.0%
		BSE-2	0.64	0.37	-42.4%
	Medium	BSE-1	0.13	0.11	-14.0%
		BSE-2	0.61	0.55	-10.2%
	Soft	BSE-1	0.16	0.13	-19.1%
		BSE-2	0.66	0.46	-30.4%
BF-3	Hard	BSE-1	0.51	0.46	-10.3%
		BSE-2	5.03	2.57	-48.9%
	Medium	BSE-1	1.16	0.74	-36.2%
		BSE-2	5.11	3.29	-35.6%
	Soft	BSE-1	1.54	1.11	-27.9%
		BSE-2	4.52	3.88	-14.1%
BF-4	Hard	BSE-1	0.37	0.18	-50.3%
		BSE-2	2.76	1.59	-42.5%
	Medium	BSE-1	0.93	0.45	-52.0%
		BSE-2	7.93	2.75	-65.3%
	Soft	BSE-1	1.11	0.74	-33.9%
		BSE-2	0.13	0.06	-52.2%
BF-5	Hard	BSE-1	0.13	0.06	-52.2%
		BSE-2	1.39	0.77	-44.4%
	Medium	BSE-1	0.36	0.17	-54.4%
		BSE-2	2.51	1.45	-42.3%
	Soft	BSE-1	1.03	0.55	-46.6%
		BSE-2	4.13	2.51	-39.3%

Table 7.4 Fardis Damage Index Calculations (D_E) (Continued)

Structure	Site	Earthquake	Undamped Average D_E	Damped Average D_E	% Change
EBF-1	Hard	BSE-1	0.01	0.00	-44.6%
		BSE-2	0.06	0.03	-40.0%
	Medium	BSE-1	0.02	0.01	-48.3%
		BSE-2	0.08	0.05	-45.2%
	Soft	BSE-1	0.02	0.02	-15.5%
		BSE-2	0.05	0.05	-2.8%
SW-1	Hard	BSE-1	0.30	0.24	-21.3%
		BSE-2	2.56	1.16	-54.8%
	Medium	BSE-1	0.54	0.49	-10.7%
		BSE-2	2.11	1.78	-16.0%
	Soft	BSE-1	0.66	0.47	-28.9%
		BSE-2	2.91	2.38	-18.3%
SW-2	Hard	BSE-1	0.13	0.10	-28.5%
		BSE-2	0.63	0.37	-41.1%
	Medium	BSE-1	0.20	0.16	-23.7%
		BSE-2	0.64	0.45	-29.5%
	Soft	BSE-1	0.28	0.23	-18.2%
		BSE-2	0.64	0.54	-16.4%
MF-1	Hard	BSE-1	0.03	0.02	-36.4%
		BSE-2	0.33	0.16	-51.0%
	Medium	BSE-1	0.08	0.04	-55.2%
		BSE-2	0.67	0.35	-47.4%
	Soft	BSE-1	0.32	0.14	-55.8%
		BSE-2	1.44	1.01	-30.1%
MF-2	Hard	BSE-1	0.05	0.03	-37.5%
		BSE-2	0.80	0.55	-31.5%
	Medium	BSE-1	0.16	0.08	-52.2%
		BSE-2	1.06	0.68	-35.3%
	Soft	BSE-1	0.50	0.35	-31.1%
		BSE-2	3.36	2.55	-24.1%

7.3 Energy Method Conclusions

Although the two approaches utilizing energy methods do not demonstrate exactness in comparable damage index calculation results, both predict that a significant reduction in energy demand can be achieved in the base structure by virtue of the NRTMDF. In some cases calculated demands, based on damage index calculations are reduced by as much as 70%. Such high magnitudes of reduction can be attributed to both the targeted energy dissipation of the NRTMDF as well as the reduced demand on the structure throughout the entire time history of the record in question. Consider model BF-4 and the LA24 ground motion. For this, the Park and Ang damage index and the Fardis damage index calculations show 69.8% and a 71.1% reductions respectively. Such high reductions are reflected in significant reductions in the peak rooftop displacement as well as significant reductions in the rooftop displacement throughout the complete time domain of the record including a reduction of permanent nonlinear displacement as shown in Figure 7.3.

An important phenomenon encountered through use of the Park and Ang energy method as well as the Fardis energy method is the accounting of increased hysteretic demand on the structure even though peak transient parameters are reduced. All acceleration records reflecting realistic conditions have variations in frequency content. The frequencies of lesser magnitudes with an acceleration history do not become manifest in response spectrum or time history analysis methods which consider only peak transient response. Traditional methods account for variations in frequency content and activated structural modes through use of response spectra analyses which theoretically account for the mobilization of primary structural frequencies then mathematically

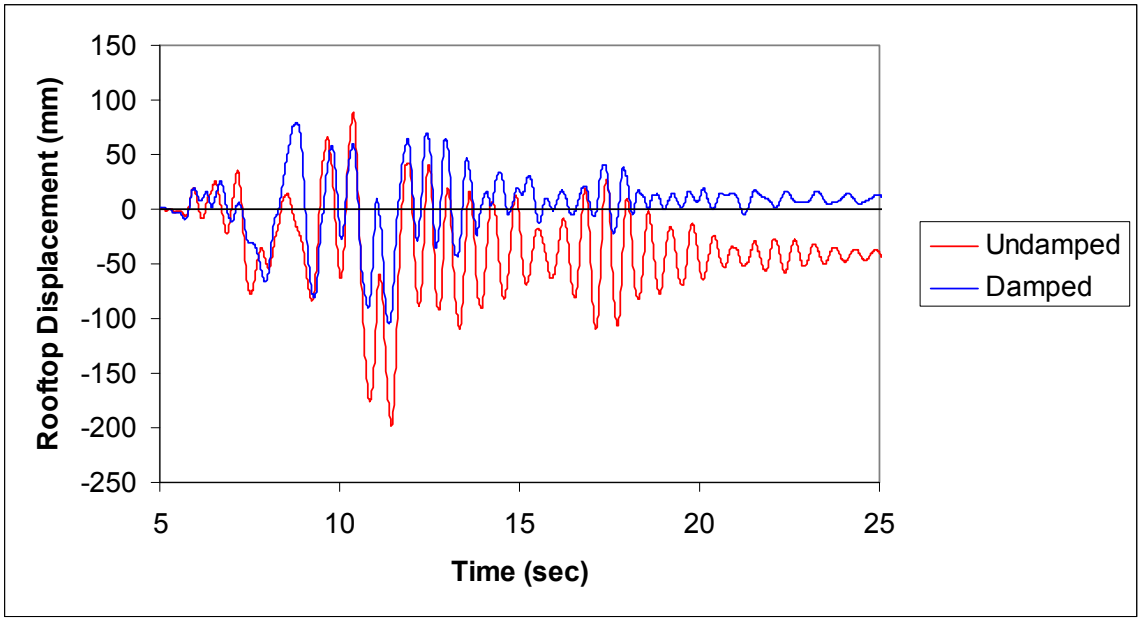

Figure 7.3 Rooftop Displacement for Undamped and Damped BF-4, Medium Site, LA24 Ground Motion

combining the results of peak transient behaviors. However, the energy methods reveal that for some cases, displacements and base shears are increased within various and significant regions of the time domain even though peak transient response parameters are reduced. As an example, consider BF-4 and the SE04 ground motion. For this, the peak rooftop displacement is reduced by 11.7% and the energy dissipation of the NRTMDF is significant at 49.8% of the total input energy. This notwithstanding, the damage index calculations demonstrate an increase damage index on the structure of 0.2% using the Park and Ang method and 4.4% using the Fardis method. The increase is caused by frequency content within the record that drives an increase in structural response outside of the time domain where the peak transient responses can be observed. Figure 7.4 depicts the rooftop displacement response history for this condition from 0 to 20 seconds and Figure 7.5 depicts the rooftop displacement response history for this condition from 20 to 40 seconds. Note the reduction in peak response at about time step

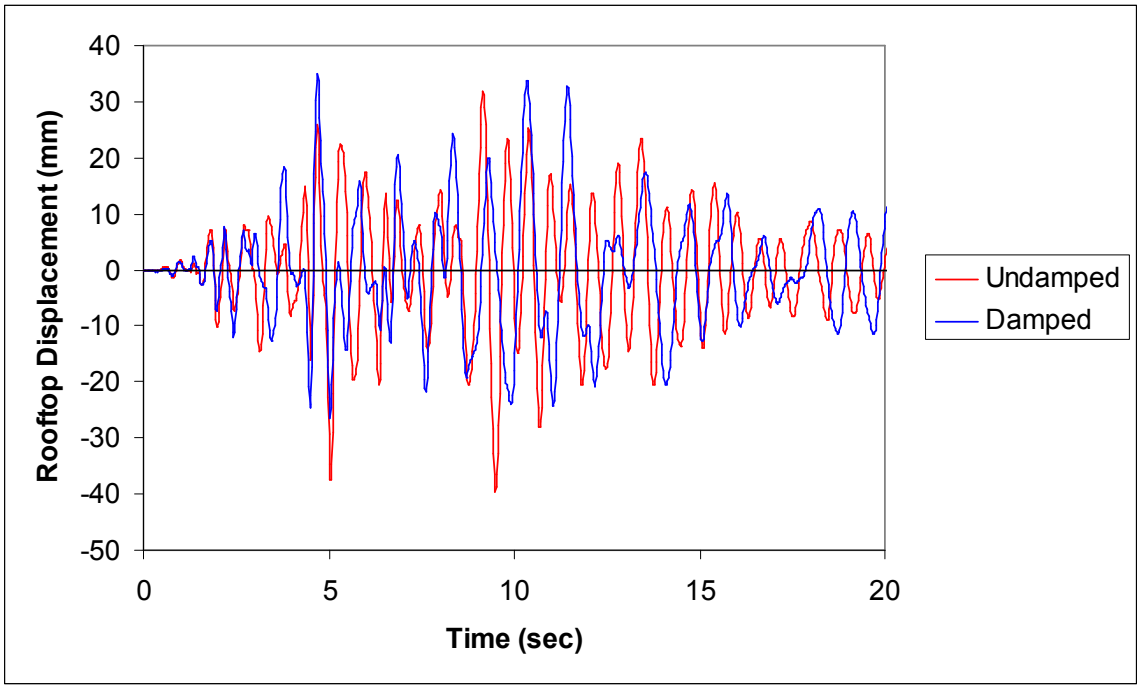

Figure 7.4 Rooftop Displacement for BF-4, Hard Site, SE04 Ground Motion, 0 to 20 Seconds

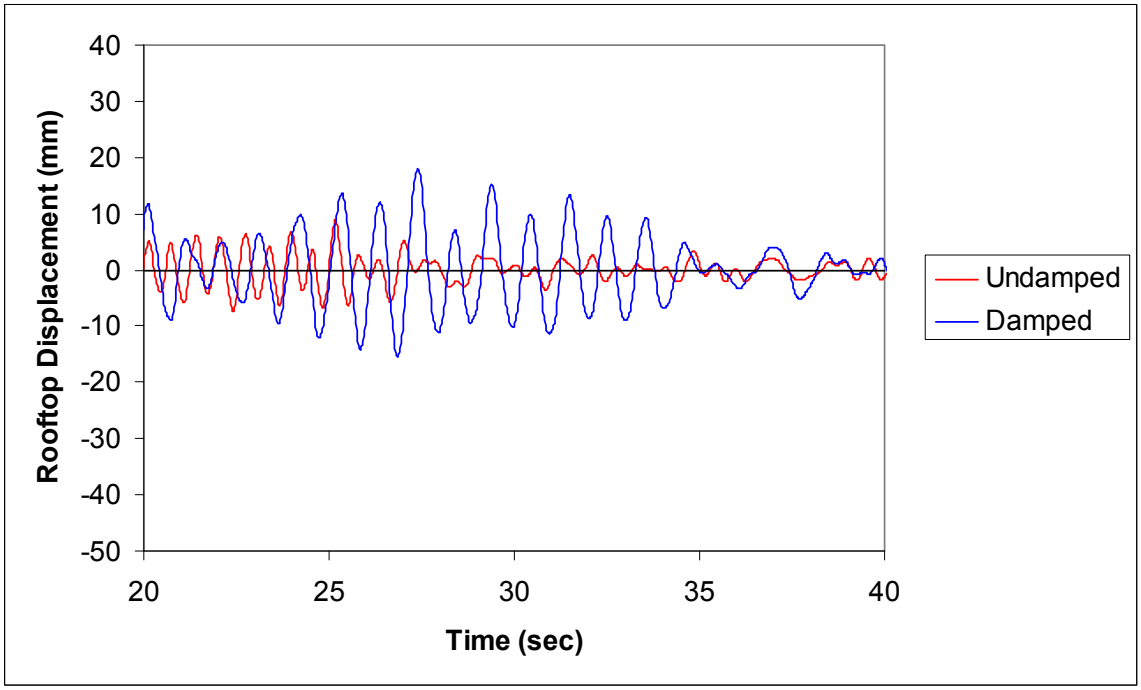

Figure 7.5 Rooftop Displacement for BF-4, Hard Site SE04 Ground Motion, 20 to 40 Seconds

9.5 seconds (enabled by the NTMDF) within the domain which has a magnitude of approximately 39.5mm for the undamped structure. For the damped structure the peak is33.9mm at about time step 4.7 seconds. Further in the record, the rooftop displacement response from 20 to 40 seconds for the damped model is significantly higher than that of the undamped structure, indicating the mobilization of frequency content at this region in the record closer to resonance with the input motion. This result demonstrates the benefits of the energy approaches enabled with time history analysis methods which reflect the entire time domain of the record in question and are not limited to the narrow measures for performance predicated by conventional methods which consider only peak transient response. The difference as herein demonstrated is that the conventional methods predict a reduction in response while the energy methods predict an increase in response.

7.4 Equivalent Damping

The adapted procedure for the hysteretically based equivalent damping calculation (outlined in Section 3.10) reveals results consistent with the energy based analysis methods of Section 7.2. Fundamentally, this procedure utilizes the nonlinear load-displacement relationship to assess the energy dissipated by the system through yielding of materials. While this approach was developed for relatively simple structures, it can be effectively adapted to multi story structures using nonlinear pushover techniques of current codes.[28] Section 3.10 establishes the basis for this approach and the adaptation of nonlinear static pushover methods as a convenient approach for measuring hysteretic energy release per cycle and comparing this to the equivalent elastic energy reflected in the effective stiffness calculation of the pushover curve. This enables the development of

an overall hysteretic relationship reflecting the predominant mode of response for the structure in question. For this research, the hysteretic relationship for each undamped structure was developed using the pushover methodology and the first mode shape as the load pattern. The nonlinear load-displacement relationships for each structure are found in the Appendix F. The resulting load-displacement relationship becomes the basis for calculating the hysteretic energy release (A_H) and the effective elastic strain energy (A_e) which can be utilized in the effective damping calculation of Equation 3-5.

The equivalent damping calculations shown in Tables 7.5 and 7.6 yield results reflecting the observed behavior of the undamped and damped structures. Primarily, when nonlinear hysteretic demand is high, the equivalent damping calculation yields a relatively high result. Likewise, when nonlinear hysteretic demand is low, the equivalent damping calculation yields a low result. In fact, this procedure yields an equivalent damping ratio of zero when yielding of the structure does not occur which equates to the absence of hysteretic nonlinearity (a value of A_H=0 in Figure 3.41). This phenomenon can be observed for 6 of the 10 test structures for BSE-1 and the hard site condition. For these cases, the equivalent damping result is zero due to the absence of hysteretic nonlinearity. Essentially, the ground motions are of a diminished magnitude coupled with a reduced amplification of motion in the structure (due to the hard site condition) such that yielding does not occur. For the correlating damped structures, the equivalent damping calculation yields a result due to hysteretic energy dissipation within the NRTMDF itself while overall motion of the base structure is diminished resulting in a reduction in elastic strain demand. For cases where equivalent damping yields a zero

Table 7.5 Equivalent Damping Ratios

Structure	Site	Earthquake	Undamped	Damped
BF-1	Hard	BSE-1	0.0%	0.7%
		BSE-2	*	19.6%
	Medium	BSE-1	10.0%	3.9%
		BSE-2	*	23.4%
	Soft	BSE-1	9.6%	13.9%
		BSE-2	*	*
BF-2	Hard	BSE-1	13.7%	7.2%
		BSE-2	11.3%	17.2%
	Medium	BSE-1	12.4%	9.3%
		BSE-2	11.4%	16.2%
	Soft	BSE-1	11.8%	16.4%
		BSE-2	10.4%	24.6%
BF-3	Hard	BSE-1	0.0%	3.0%
		BSE-2	12.6%	24.3%
	Medium	BSE-1	7.0%	5.0%
		BSE-2	12.7%	20.7%
	Soft	BSE-1	12.1%	20.0%
		BSE-2	12.3%	39.4%**
BF-4	Hard	BSE-1	0.0%	4.2%
		BSE-2	18.3%	19.3%
	Medium	BSE-1	12.4%	4.4%
		BSE-2	13.8%	33.5%
	Soft	BSE-1	13.5%	21.3%
		BSE-2	15.5%	34.4%
BF-5	Hard	BSE-1	0.0%	4.4%
		BSE-2	9.6%	11.5%
	Medium	BSE-1	0.0%	3.3%
		BSE-2	11.1%	12.2%**
	Soft	BSE-1	10.5%	4.0%
		BSE-2	*	14.1%**

*Calculated of structure displacements are beyond nonlinear capability.

**Calculated displacements of NRTMDF are beyond nonlinear capability.

Note: Values of zero reflect no yielding for no hysteretic damping.

Table 7.6 Equivalent Damping Ratios (Continued)

Structure	Site	Earthquake	Undamped	Damped
EBF-1	Hard	BSE-1	8.0%	4.3%
		BSE-2	13.5%	20.1%
	Medium	BSE-1	11.4%	4.7%
		BSE-2	13.5%	22.8%
	Soft	BSE-1	12.7%	23.4%
		BSE-2	13.6%	32.8%**
SW-1	Hard	BSE-1	13.1%	16.3%
		BSE-2	14.1%	35.0%
	Medium	BSE-1	13.5%	16.7%
		BSE-2	14.1%	39.3%
	Soft	BSE-1	13.6%	30.7%
		BSE-2	14.1%	63.3%**
SW-2	Hard	BSE-1	14.1%	12.5%
		BSE-2	15.1%	17.4%
	Medium	BSE-1	14.7%	14.8%
		BSE-2	15.1%	17.2%
	Soft	BSE-1	15.1%	16.4%
		BSE-2	15.0%	18.7%**
MF-1	Hard	BSE-1	0.0%	2.4%
		BSE-2	10.1%	4.3%
	Medium	BSE-1	0.0%	4.6%
		BSE-2	10.0%	13.3%**
	Soft	BSE-1	10.1%	5.5%
		BSE-2	10.8%	11.5%**
MF-2	Hard	BSE-1	0.0%	3.4%
		BSE-2	10.1%	9.9%**
	Medium	BSE-1	0.0%	4.1%
		BSE-2	10.4%	10.7%**
	Soft	BSE-1	8.7%	2.7%
		BSE-2	*	*

*Calculated structure displacements of model are beyond nonlinear capability.

**Calculated displacement of NRTMDF are beyond nonlinear capability.

Note: Values of zero reflect no yielding for no hysteretic damping.

result, natural damping between 2% and 5% would typically be assumed as prescribed by current codes. In some cases, the calculations show the NRTMDF entirely mitigates nonlinear demand on the base structure (structure remains elastic) and any hysteretic energy dissipation is provided entirely by the NRTMDF. This occurs for BF-1 and BF-3 for the medium site condition of BSE-1 shown in Table 7.5. For each of these, the damped case demonstrates a lower value for equivalent damping than does the undamped case. While this is a seemingly irrational outcome, it reflects an overall decrease in nonlinear hysteretic demand for the base structure due to the period shift enabled by the NRTMDF. In other words, equivalent damping is reduced because of a reduction in overall hysteretic nonlinearity (reduced lateral displacement).

Tables 7.5 and 7.6 demonstrate the most significant values for equivalent damping occur for damped structures and the BSE-2 ground motion suite. For these cases, energy dissipation can be observed in both the base structures and the NRTMDF's for the damped cases. Consider BF-4 and the medium site condition. Equivalent damping calculated following the procedure yields an average result of 33.5%. For this, the average hysteretic energy contribution of the NRTMDF is approximately 47% of the total dissipated hysteretic energy while the balance is dissipated within the base structure. As an example within the BSE-2, medium site ground motion suite, consider model BF-4 and the SE28 record. Figure 7.6 depicts the total energy input into the system along with the energy dissipated by the NRTMDF. As shown the energy dissipated by the NRTMDF is approximately 52% of the total input energy for this specific case.

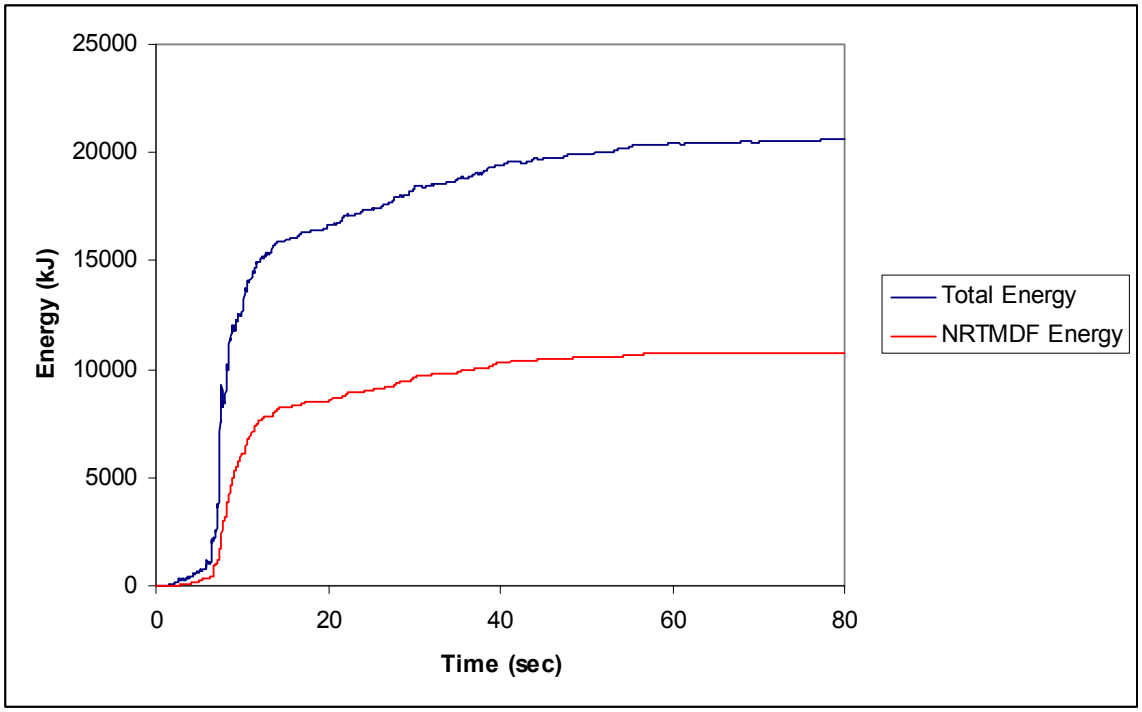

Figure 7.6 Total Energy and NRTMDF Dissipated Energy for BF-4, SE28 Motion

The results of the effective damping calculations corroborate the damage index calculations summarized in sections 7.1 and 7.2. Tables 7.5 and 7.6 identify the cases for which equivalent damping calculations produced an irrational result. Consider the undamped model BF-5 and the soft site condition for BSE-2. The average peak rooftop displacement for this case is 578mm (Appendix D) and the maximum capable displacement on the nonlinear pushover curve is 510mm (Appendix F) thereby yielding the irrational result (elastic strain A_e in the denominator of Eq. 3-5 becomes zero). For this same case, the damped rooftop displacement is 457mm thus enabling a rational calculation for effective damping. The irrational result is due to projected displacements which surpassed the maximum capable nonlinear displacement of the base structure. Upon comparing the indicated irrational results from Tables 7.5 and 7.6 to the damage index calculations of Tables 7.1 to 7.4, it can be observed that the correlating damage

index calculations yielded results far in excess of unity thus demonstrating a high likelihood for structural system failure. For other cases, unanticipated high values for equivalent damping occur when NRTMDF displacements are far beyond their reliable capable values. When this occurs, the calculations incorporate a value for hysteretic energy (A_h), comprised mostly of NRTMDF hysteretic energy which cannot be realized due to excessive NRTMDF displacement demand. For such cases, the equivalent damping calculation should be deemed unreliable since the NRTMDF may not be able to reliably develop the energy dissipation capacity commensurate with the demand predicted by the modeling and reflected in the equivalent damping calculation.

Equivalent damping calculations using the PEER ground motions for BF-4 and the medium site condition yield a result consistent with Table 7.5. For BSE-1, average equivalent damping ratios are 13.0% and 3.4% for the undamped and damped cases respectively. For BSE-2, these values become 14.0% and 30.4% respectively. These results demonstrate a strong corroboration between the scaled motions of the SAC database and those of the PEER resource thus supporting the potential for use of either for a realistic design scenario. The vastly increased equivalent damping ratio for the damped case of BSE-2 for this building (30.4%) reflects significant nonlinear hysteretic demand driven by the relatively high ground motion along with significant nonlinear performance of the NRTMDF.

8 NONSTRUCTURAL ELEMENTS AND COMPONENTS

The methods for measuring performance demonstrated within this research are aimed toward the quantification of structural demand and the reduction thereof by utilizing the Nonlinear/Inelastic Rooftop Tuned Mass Damper Frame. Certainly, these approaches may ultimately be utilized in the development of probable loss scenarios and the calculation of costs required for repairing damage caused by seismic events. However, the structural damage thus far addressed is only one aspect of building systems affected by lateral forces. Nonstructural components as well as building contents in general can have an accumulated financial value far surpassing that of the structural system. In this sense, it is appropriate to address the potential the NRTMDF has for affecting the seismic demand on nonstructural building elements and components.

A common challenge engineers face with respect to nonstructural elements and components is that they rarely have the same degree of control over mass, stiffness, location, fragility or attachment methods of such assemblies as they do for the structural system. As a result, it can be difficult to gauge the damage that might occur to a particular nonstructural element within the system. To address this, contemporary codes prescribe seismic forces on nonstructural elements and components in a manner that reflects not only the anticipated acceleration response characteristics of the nonstructural element in question, but the geometrical relationship of the element within the global structural system. It is commonly agreed that lateral accelerations within a structure

increase with respect to the building height. The ground level of a structure experiences the same acceleration motion of the ground in general but the rooftop is often subject to accelerations which are far greater. This can generally be observed in the output of any time history analysis. As an example, consider model BF-4 and the LA32 motion as a representative of the medium site condition for BSE-2. Figures 8.1 through 8.3 demonstrate accelerations at the base, third story and the roof level accelerations respectively. The accelerations in the figures demonstrate not only the reduced story accelerations enabled by the NRTMDF but the increase in acceleration which increases with story elevation within the structure. The SW-1 model demonstrates this concept also. Consider this structure and the LA33 motion representing the hard site condition for BSE-2. Figures 8.4 through 8.6 demonstrate the accelerations at the base, fourth floor and roof levels, respectively.

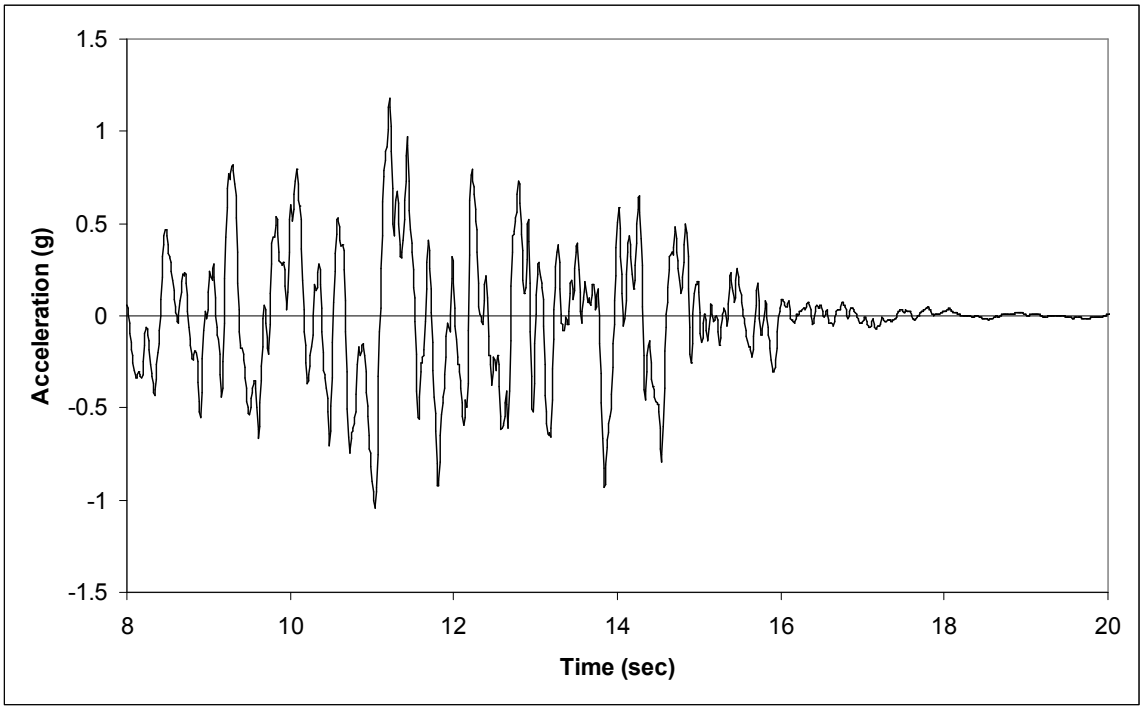

Figure 8.1 LA32 Ground Motion

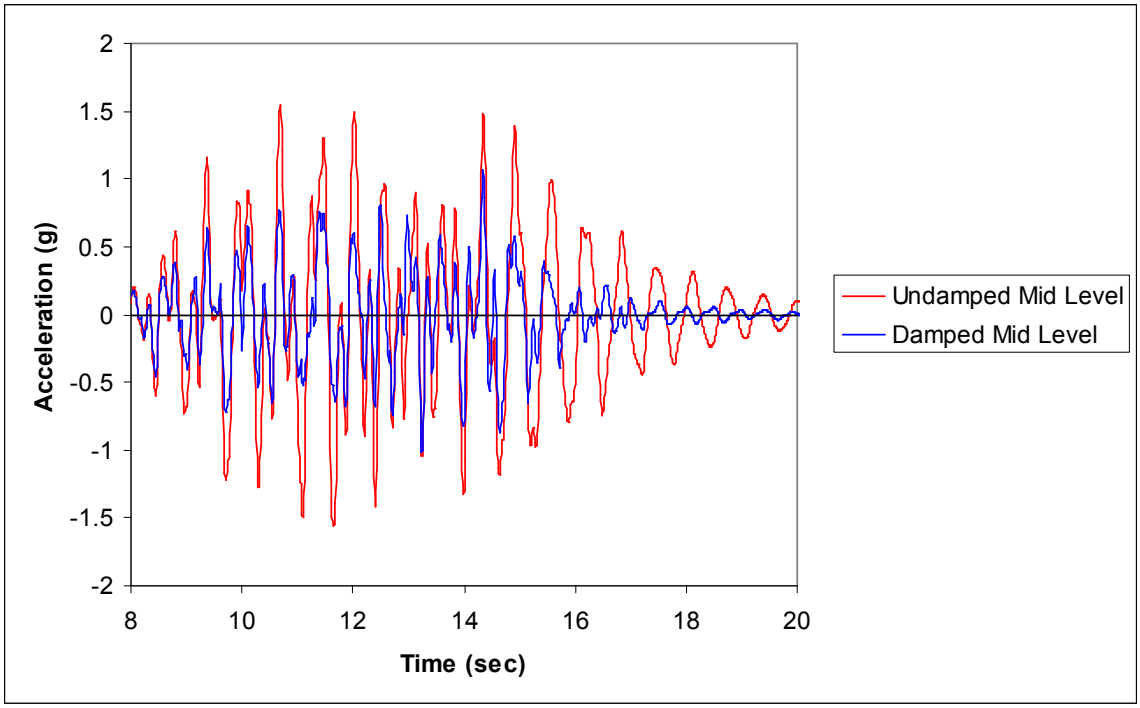

Figure 8.2 Third Floor Accelerations for BF-4, LA32 Motion.

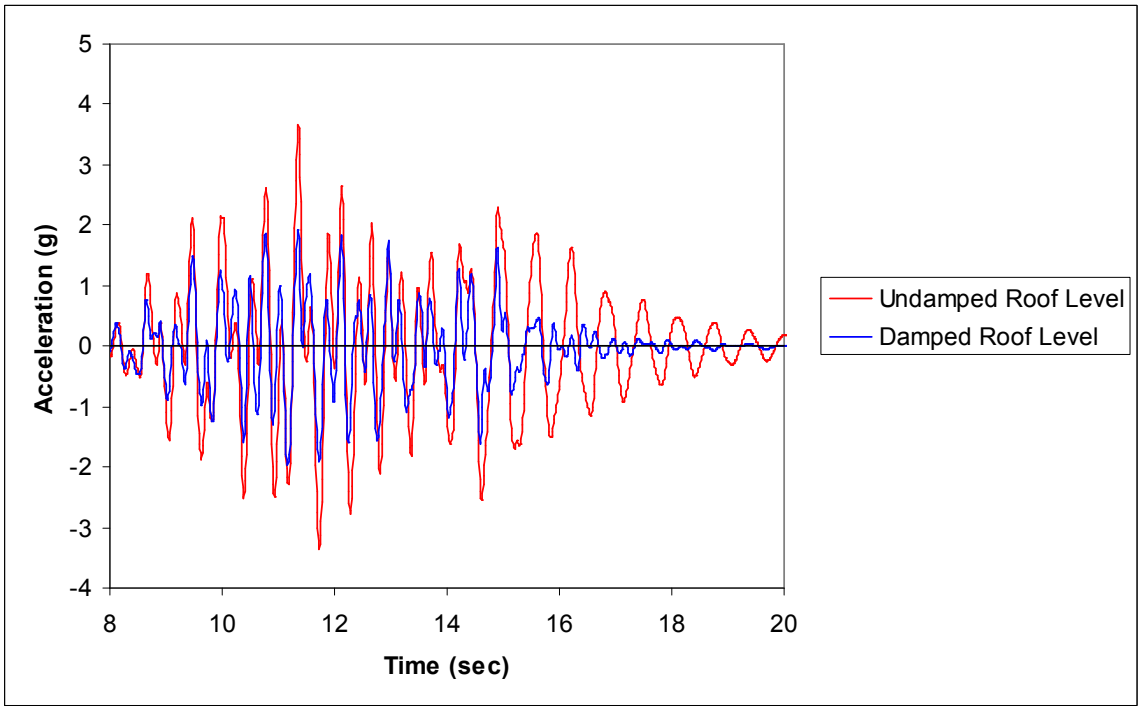

Figure 8.3 Roof Accelerations for BF-4, LA32 Motion.

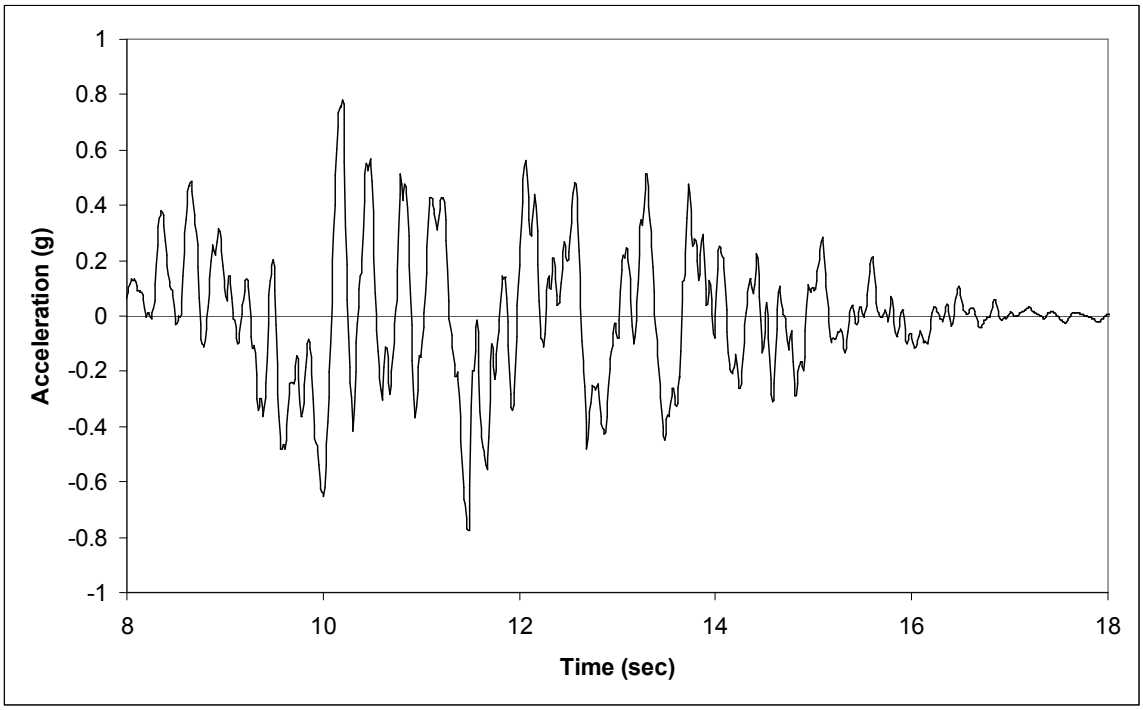

Figure 8.4 LA33 Ground Motion

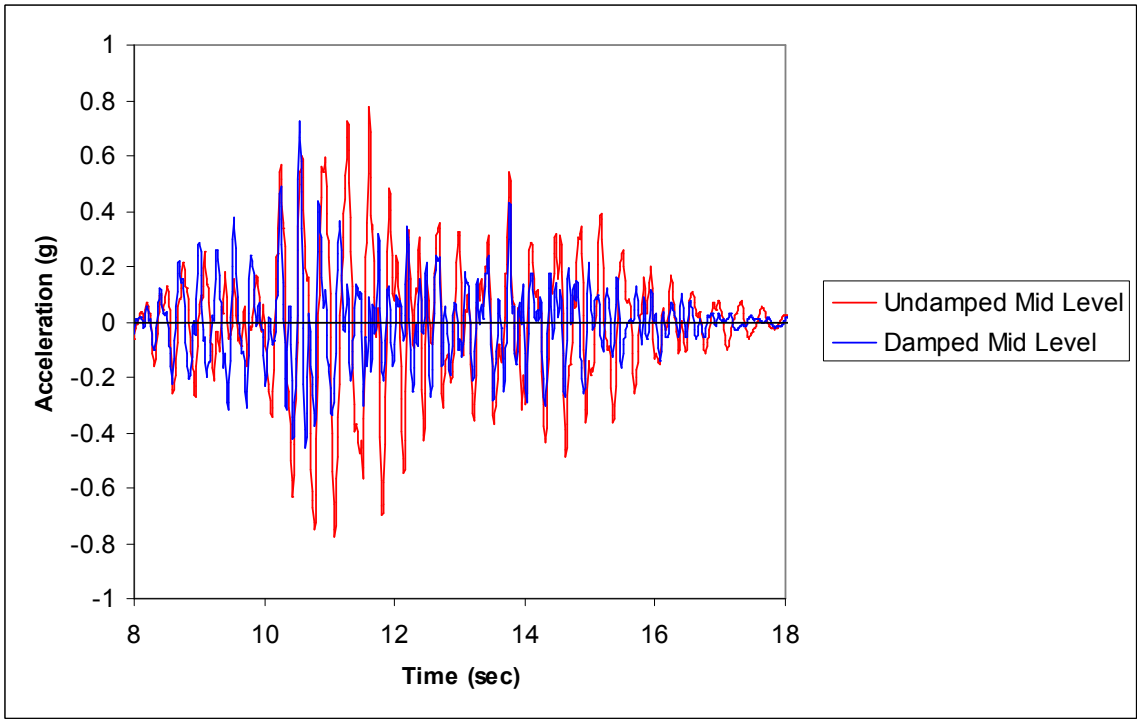

Figure 8.5 Fourth Floor Accelerations for SW-1, LA33 Motion

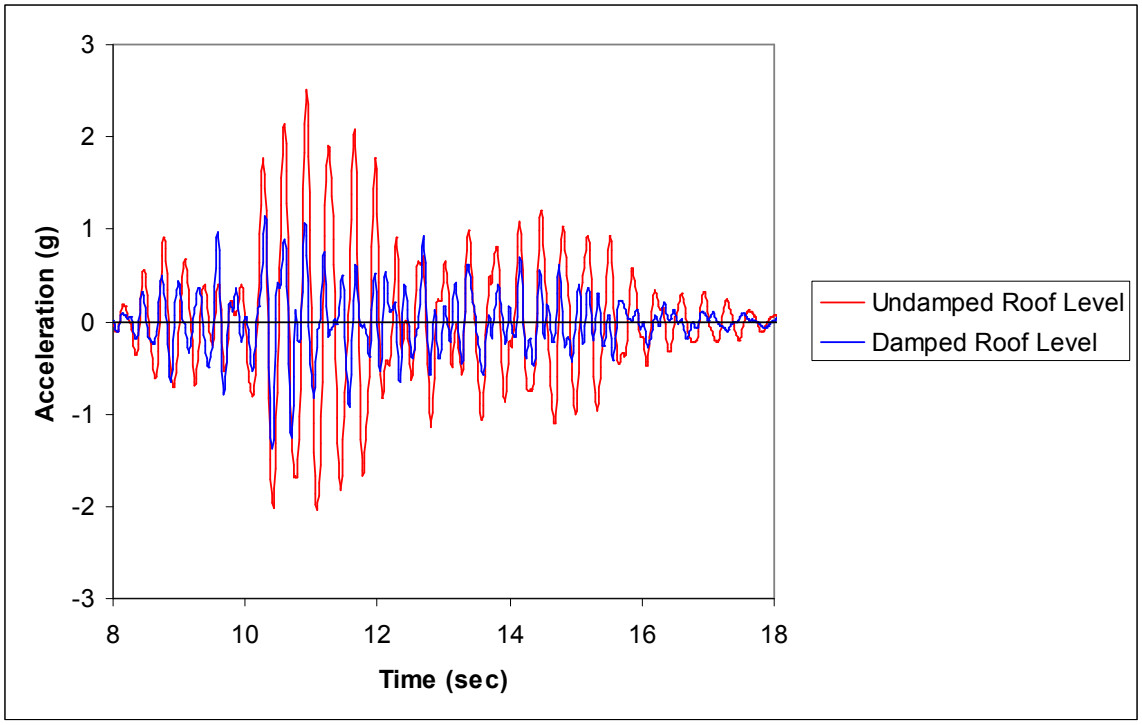

Figure 8.6 Roof Accelerations for SW-1, LA33 Motion

A rational approach for qualitatively gauging the demand on nonstructural elements and components within the context of a time history analysis is to develop floor spectra at each level within the structure. This is done by extracting the acceleration record produced at the floor level and then developing a response spectrum for that record. The spectra between undamped and damped structures can then be observed to gauge the benefits and effectiveness of damping enabled, in this case, by the NRTMDF.

The potential reductions in nonstructural demand can be qualitatively assessed by observing the floor spectra shown in Figures 8.7 through 8.14 which demonstrate the average floor spectra for several of the test structures and site conditions. For a quantitative result, Tables 8.1 and 8.2 provide a summary of the reductions of the floor

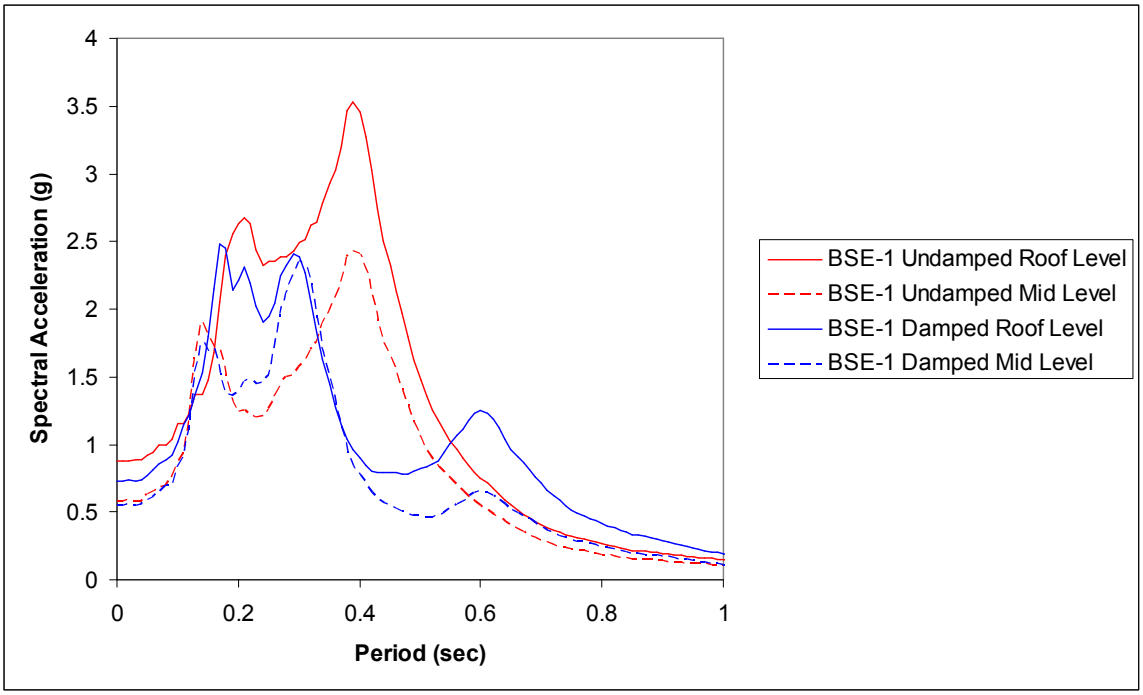

Figure 8.7 Average Floor Spectra for BF-3, BSE-1 Ground Motions, Hard Site

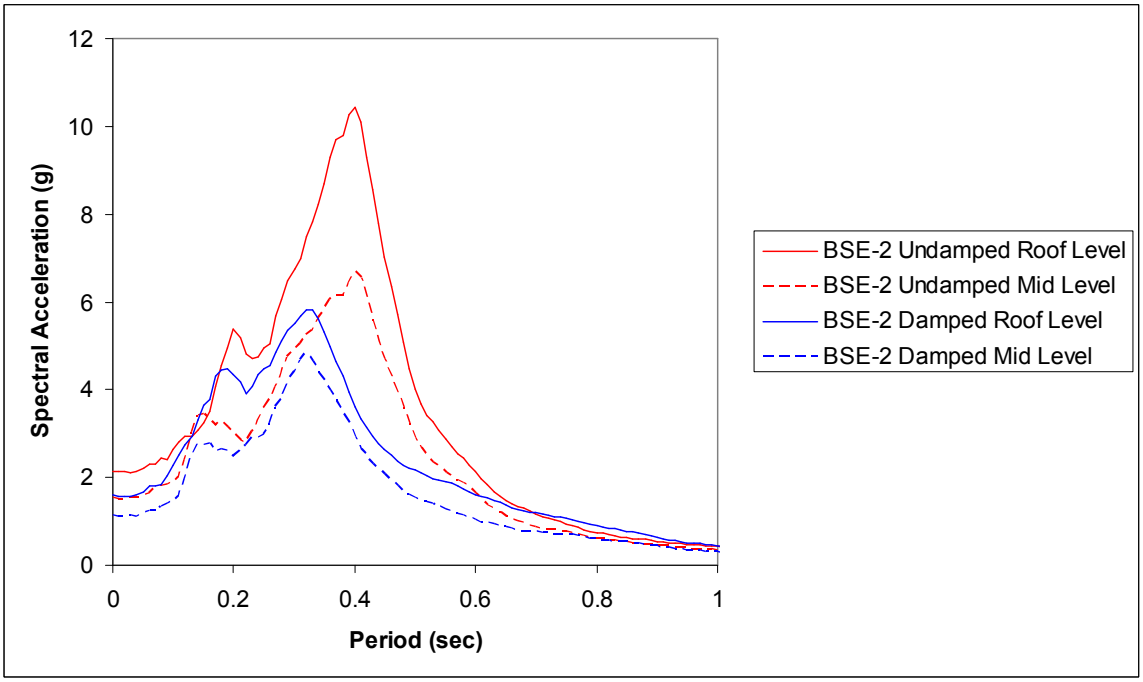

Figure 8.8 Average Floor Spectra for BF-3, BSE-2 Ground Motions, Hard Site

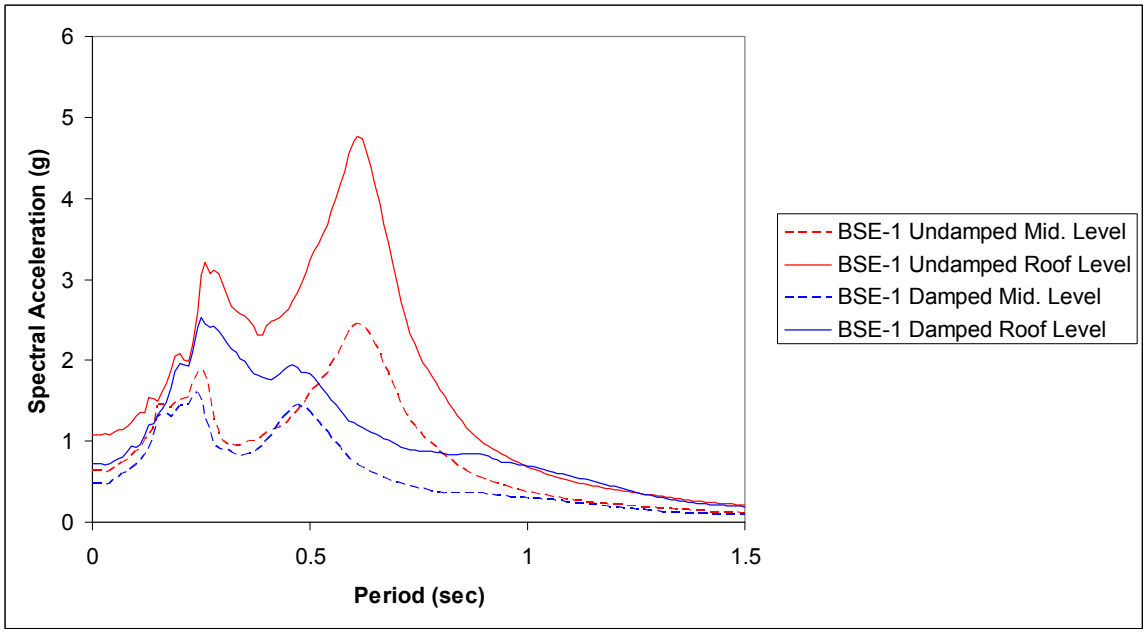

Figure 8.9 Average Floor Spectra for BF-4, BSE-1 Ground Motions, Medium Site

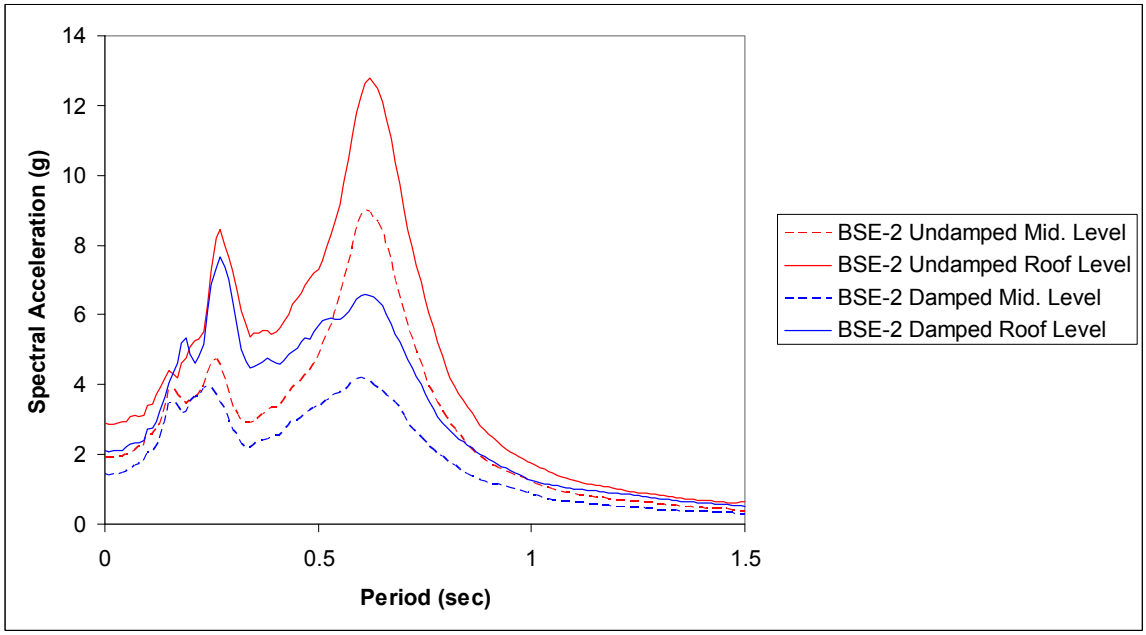

Figure 8.10 Average Floor Spectra for BF-4, BSE-2 Ground Motions, Medium Site

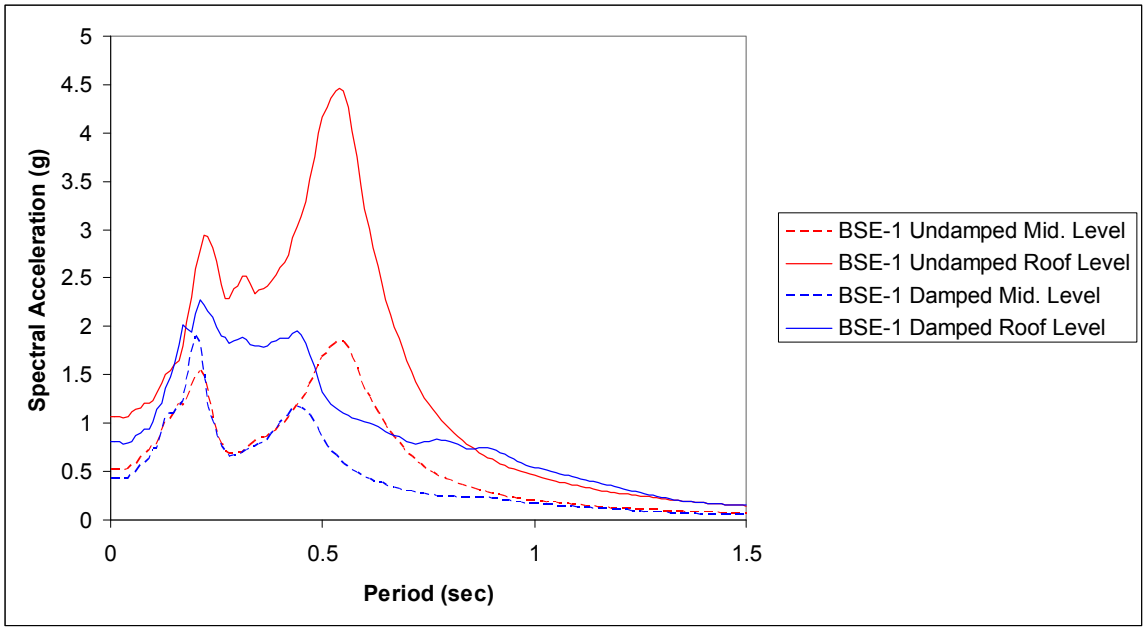

Figure 8.11 Average Floor Spectra for EBF-1, BSE-1 Ground Motions, Medium Site

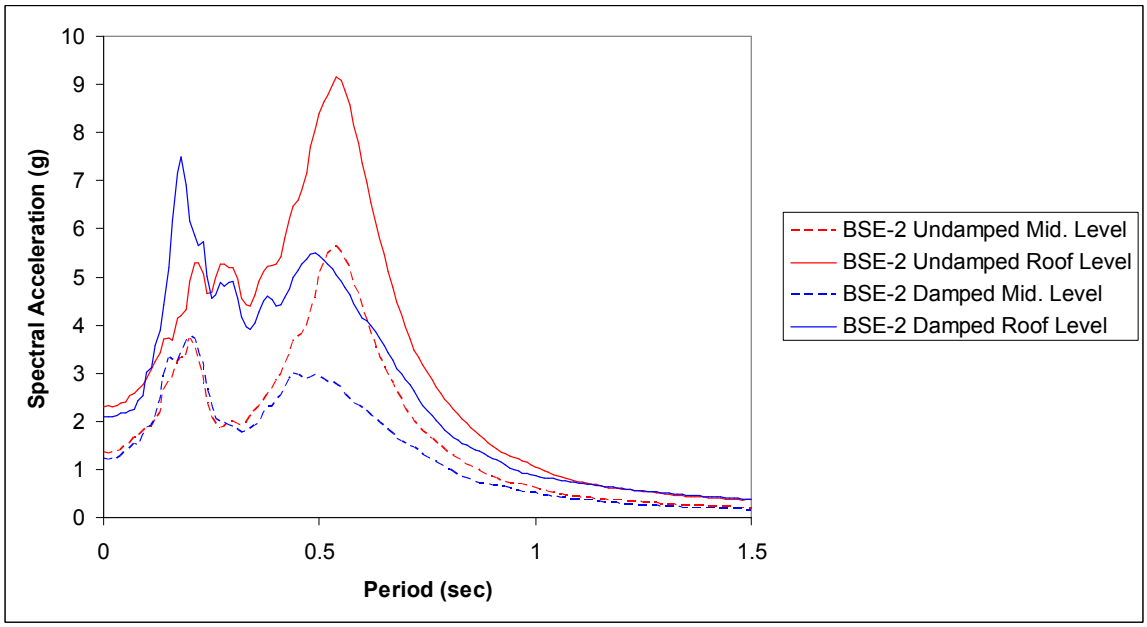

Figure 8.12 Average Floor Spectra for EBF-1, BSE-2 Ground Motions, Medium Site

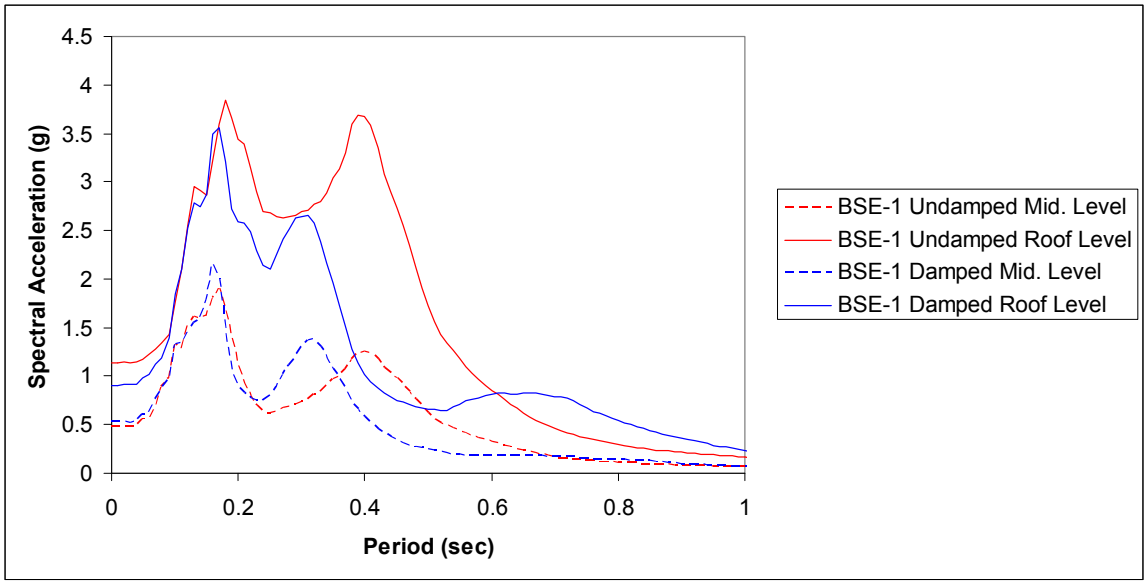

Figure 8.13 Average Floor Spectra for SW-2, BSE-1 Ground Motions, Hard Site

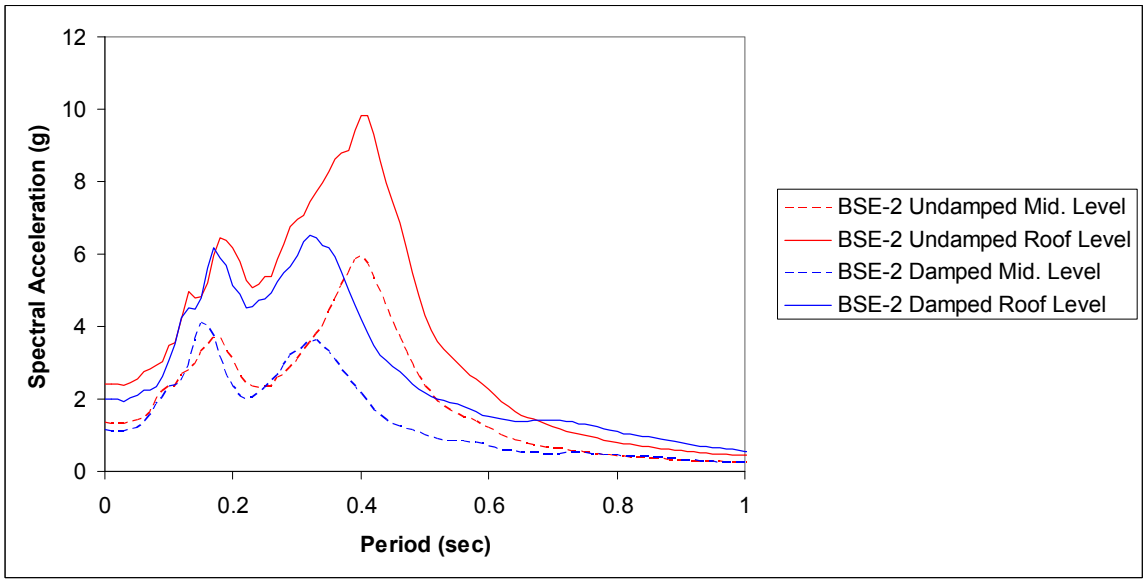

Figure 8.14 Average Floor Spectra for SW-2, BSE-2 Ground Motions, Hard Site

Table 8.1 Changes in Average Floor Spectra

Structure	Site	Earthquake	Mid. Level Spectra	Roof Spectra
BF-1	Hard	BSE-1	-10.9%	-17.2%
		BSE-2	-18.7%	-15.6%
	Medium	BSE-1	-13.0%	-17.7%
		BSE-2	-9.7%	-8.7%
	Soft	BSE-1	-15.5%	-18.7%
		BSE-2	-16.6%	-9.7%
BF-2	Hard	BSE-1	-23.6%	-25.2%
		BSE-2	-28.7%	-27.1%
	Medium	BSE-1	-25.9%	-25.0%
		BSE-2	-25.6%	-23.3%
	Soft	BSE-1	-12.3%	-14.9%
		BSE-2	-13.8%	-6.2%
BF-3	Hard	BSE-1	-20.2%	-14.1%
		BSE-2	-30.7%	-29.7%
	Medium	BSE-1	-22.9%	-17.1%
		BSE-2	-17.7%	-17.7%
	Soft	BSE-1	-22.7%	-19.3%
		BSE-2	-15.1%	-9.8%
BF-4	Hard	BSE-1	-23.6%	-35.8%
		BSE-2	-20.8%	-17.9%
	Medium	BSE-1	-35.2%	-41.6%
		BSE-2	-34.4%	-29.1%
	Soft	BSE-1	-16.9%	-23.1%
		BSE-2	-16.3%	-8.3%
BF-5	Hard	BSE-1	-10.3%	-21.5%
		BSE-2	-23.9%	-18.6%
	Medium	BSE-1	-12.3%	-20.3%
		BSE-2	-29.5%	-16.7%
	Soft	BSE-1	-16.4%	-27.3%
		BSE-2	-29.6%	-23.2%

Table 8.2 Changes in Average Floor Spectra (Continued)

Structure	Site	Earthquake	Mid. Level Spectra	Roof Spectra
EBF-1	Hard	BSE-1	-15.7%	-35.5%
		BSE-2	-20.5%	-16.3%
	Medium	BSE-1	-27.5%	-38.5%
		BSE-2	-23.1%	-18.5%
	Soft	BSE-1	-9.1%	-17.2%
		BSE-2	-8.9%	-4.4%
SW-1	Hard	BSE-1	-15.3%	-22.4%
		BSE-2	-31.6%	-27.5%
	Medium	BSE-1	-11.8%	-20.5%
		BSE-2	-11.5%	-10.4%
	Soft	BSE-1	-16.0%	-23.6%
		BSE-2	-13.1%	-5.4%
SW-2	Hard	BSE-1	-9.5%	-23.5%
		BSE-2	-27.9%	-24.9%
	Medium	BSE-1	-11.7%	-23.0%
		BSE-2	-16.4%	-9.6%
	Soft	BSE-1	-14.1%	-22.7%
		BSE-2	-12.1%	-7.7%
MF-1	Hard	BSE-1	-1.2%	-21.5%
		BSE-2	-7.8%	-11.0%
	Medium	BSE-1	-9.6%	-16.0%
		BSE-2	-9.6%	-6.0%
	Soft	BSE-1	-5.3%	-16.5%
		BSE-2	-6.5%	-4.7%
MF-2	Hard	BSE-1	-13.9%	-2.2%
		BSE-2	-8.0%	-9.3%
	Medium	BSE-1	-14.6%	-4.1%
		BSE-2	-8.9%	-8.8%
	Soft	BSE-1	-15.4%	-8.4%
		BSE-2	-9.7%	-10.7%

spectra developed for each structure and each grouping of ground motions utilized for the rational design approach of Chapter 6. The averages reflected in this table are calculated over a range of periods from 0 to 1 second, thus capturing the fundamental dynamics of plausible nonstructural elements, components, or assemblies. In the interest of capturing characteristic output, the floor spectra accounted for do not reflect every floor within every structure as this would produce an exhaustive result with little added benefit. Rather, the spectra developed represent the roof level and a mid level floor within each structure. While every potential case for the models in this research is not represented with the results shown herein, the trend of diminished acceleration response enabled by the NRTMF is clear. This approach is considered sufficient for capturing the behavior of shorter structures and is also sufficient for capturing the behavior of taller structures and higher mode effects that develop.

8.1 Conclusions for Results of Floor Spectra Analyses

Corollaries between the reduction in floor spectra of Tables 8.1 and 8.2 and peak transient parameters can be observed. Fundamentally, where reductions in peak transient response parameters are observed, reductions of similar magnitude can be observed in the floor spectra. Consider model BF-4 and medium site parameters. For BSE-1, peak base shear and peak rooftop displacements are reduced by 19.9% and 43.6% respectively. For BSE 2, these values become 2.5% and 40.9% respectively. Similarly, the floor spectra for BSE-1 are reduced by 35.2% at a mid-level floor and 41.6 % at the roof level. For BSE-2 these values become 34.4% and 29.1% thereby demonstrating that when peak transient parameters are reduced, similar reductions in the floor spectra for periods ranging from 0 to 1 second may be realized.

The floor spectra analyses demonstrate a reduction in spectral acceleration response for the damped case for most conditions. However, rare cases exist where higher mode effects become amplified for the damped case. As an example of this consider model EBF-1 and the floor spectra demonstrated in Figure 8.12. Modal analysis of the damped case using effective stiffness properties for the NTMDF indicates a period of approximately 0.18 seconds for the fourth mode. At this ordinate, the spectrum representing the average spectral acceleration increases by nearly 80 percent above the undamped case. Figure 8.15 shows the mode shape for this with modal components. As shown the modal component of the roof level is significantly larger than all other levels thereby driving increased accelerations at the roof resonating at a period of 0.18 seconds and producing the spike at this ordinate of the spectrum of Figure 8.12. This higher mode effect notwithstanding, the overall spectrum from 0 to 1 seconds has an average reduction in spectral acceleration magnitude of 18.5% as indicated in Table 8.2 which is also observed in Figure 8.12.

Another noteworthy result observable with the floor spectra is the significant reduction in spectral acceleration correlating to the ordinates of the undamped fundamental period. For instance, Figure 8.9 demonstrates an average spectral acceleration at the roof level of BF-4 of 4.73g at a period of approximately 0.63 seconds (the fundamental period of the undamped structure for BSE-1 motions and the medium site condition). For the damped structure, the spectral acceleration at this ordinate becomes 1.15g, for a reduction spectral acceleration from the undamped to damped

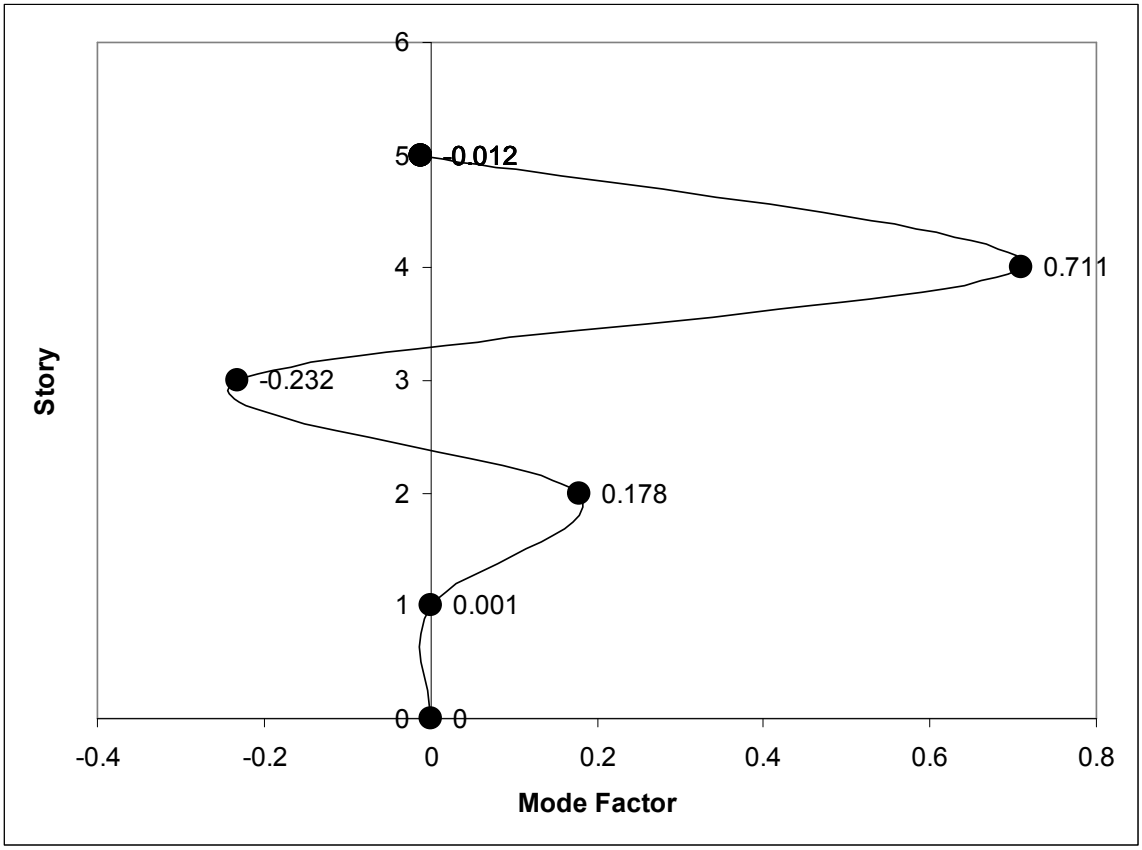

Figure 8.15 EBF-1 Damped Case Higher Mode Effect

model by a factor of 4. The reduction at this ordinate on the floor spectra is enabled primarily because the mode 1 period for the structure is shifted far beyond the original ordinate of 0.63 seconds resulting in this significant reduction of the spectral acceleration magnitude at this ordinate for the damped case.

Fundamentally, the floor spectra analyses demonstrate the potential for significant reduction of accelerations on nonstructural elements and components affixed to the structure. The benefits associated with this reduction reflect two aspects of nonstructural element and component bracing. First is the case for rehabilitation where the NRTMDF produces a softened response, reducing the lateral seismic demand on elements and components. This translates to a reduced potential for damage and a greater likelihood

for capable function and service following a seismic event. Second is the case for new construction where the NRTMDF offers the rationale for a less aggressive approach for the seismic bracing of nonstructural elements and components which can add significant expense to these assemblies. If standard prescriptive requirements are followed for bracing the nonstructural elements and components the NRTMDF approach may translate to enhanced performance by virtue of reduced accelerations and forces on the nonstructural elements and components themselves.

8.2 Floor Spectra for PEER Ground Motions

Floor spectra developed from the PEER ground motion suite demonstrate a similar result to the prior spectra developed from the SAC ground motions. Figures 8.16 and 8.17 depict the average of floor spectra developed for test structure BF-4 subject to the BSE-1 and BSE-2 acceleration records derived from the PEER ground motion suite. The spectra developed reflect the acceleration time histories taken at the roof level and at the mid-height of the structure. Utilizing the same approach developed previously for determining the average acceleration response for each spectrum, comparisons may be drawn between the undamped and damped structures at each considered story. The calculations demonstrate a reduction in average rooftop spectral acceleration for BSE-1 of 36.1%. For BSE-2 this value becomes 22.0%. At the mid-height the reduction in average spectral acceleration is 24.3% for BSE-1 and 29.1% for BSE-2.

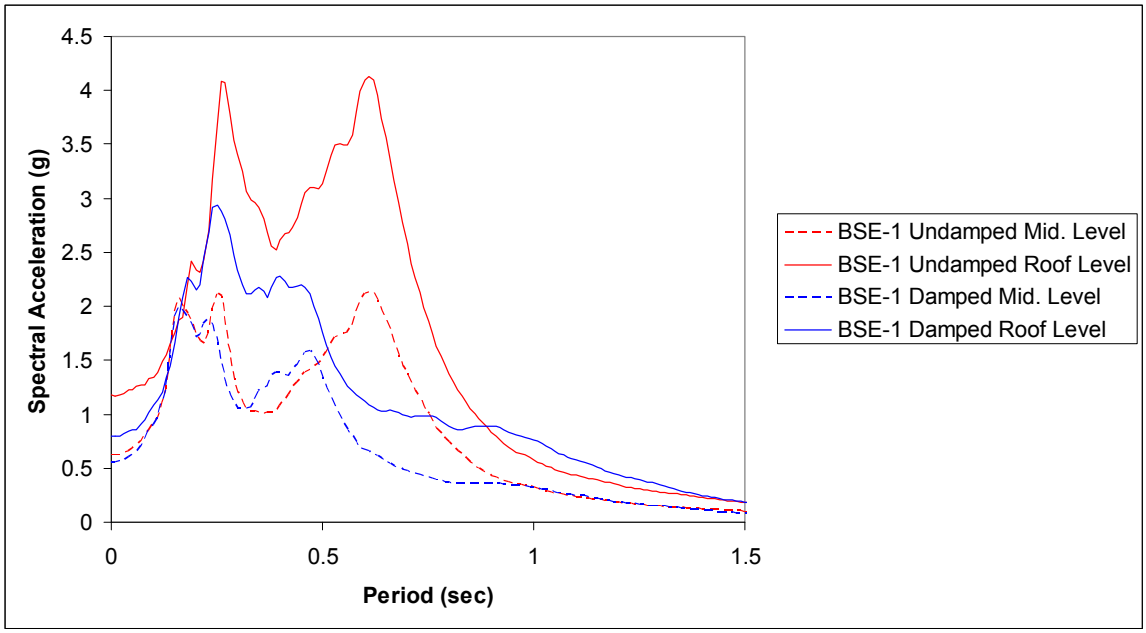

Figure 8.16 Average Floor Spectra for BF-4, BSE-1 PEER Ground Motion

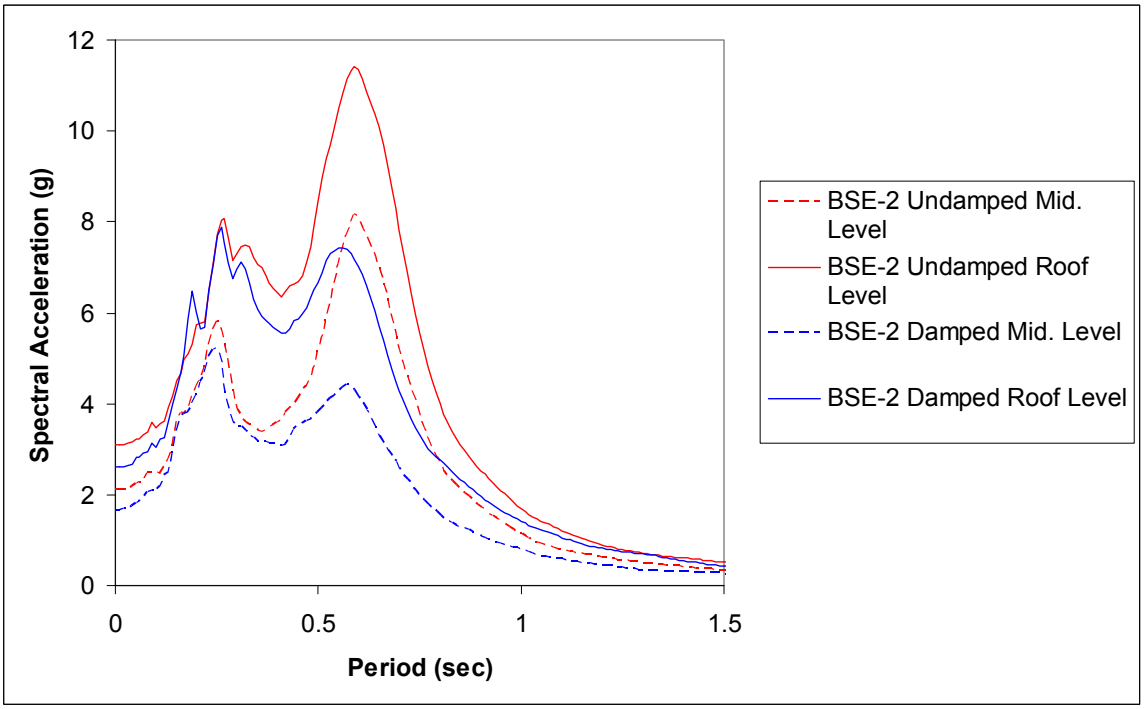

Figure 8.17 Average Floor Spectra for BF-4, BSE-2 PEER Ground Motion

Notable similarities can be observed between the floor spectra developed from the SAC ground motions (Figures 8.9 and 8.10) and those developed utilizing the PEER resource shown in Figures 8.16 and 8.17. The magnitude of spectral accelerations bear similarities since the motions were selected and scaled using the same code driven scaling procedure for both the SAC record suite and the PEER record suite. Another noteworthy observation is that the peaks in the spectra demonstrate consistencies between the spectra. This is rational inasmuch as the peaks correlate to the modal periods for both the damped and undamped versions of the test models. The correlation reflects a condition of resonance for nonstructural assemblies with periods matching the modal periods of the overall structures.

9 DETAILING AND DESIGN CONSIDERATIONS

While the emphasis of this research is to identify the structures, ground motions and other parameters for which the NRTMDF approach is most effective, there are many issues associated with the practical utilization of this approach. The ability of the NRTMDF to perform in a manner consistent with the design intent requires particular attention to the details and specific design configurations that will enable its mobilization and nonlinear behavior. Issues associated with the pragmatic design of the NRTMDF include, but are not limited to:

- Ensuring that the fundamental dynamics of the original structure are sufficiently understood to enable the design of an effective NRTMDF.
- The development of a sufficient understanding of the site, soils, and potential ground motions reflecting the specific performance objective.
- Reinforcing the original structure or otherwise ensuring it has the capacity to support the added mass of the NRTMDF. For new construction, the base structure would need to include, as part of is design, the support of the NRTMDF and the transfer of its inertial forces to the lateral force system of the structure below.
- Ensuring that the forces at the interface of the NRTMDF and the base structure are adequately transmitted.

- Ensuring that the stiffness of connections of the NRTMDF are appropriately accounted for in the frame behavior or development of details configured to minimize their influence of the connections on frame behavior.
- Ensuring the appropriate design and detailing for NRTMDF cladding to prevent its contribution to NRTMDF stiffness.
- Development of an NRTMDF geometry that will maintain marginal stability should the BRB element(s) suffer tensile failure.
- BRB orientation and directionality effects.
- Attention to nonstructural elements and assemblies fastened to the NRTMDF.

9.1 Verification of Building Fundamental Dynamics

The effective tuning of the NRTMDF to enable maximum capable reductions for the expected ground motions requires the development of a sound understanding of fundamental dynamics of the base structure. While many computer applications enable the development of analytical models to assess a structure's inherent dynamic properties, the actual properties cannot be known to a certainty without physical testing. Furthermore, most analytical approaches underestimate structural stiffness due to the presence of many nonstructural members which may contribute to structural stiffness. Cohen indicates that cladding can significantly influence overall stiffness fundamental dynamic behavior.[39] Also, the presence of nonstructural partitions, many of which span the full distance between floors, can also contribute to global stiffness and structural dynamics. Even within the structural frame itself configurations may contribute to frame stiffness that might not be appropriately accounted for in an analytical model. These include rigid end offsets for connections between beams, columns and braces. Other

factors include the composite behavior of structural assemblies such as concrete decks providing a stiffening effect for beams. Whether these factors are accounted for in the analytical model is a matter of judgment for the design engineer. When considering the NRTMDF for rehabilitation for some cases, prudence may dictate a forced vibration test for the structure in question. For this, an oscillating mass is affixed to the structure and operated at varying frequencies. Accelerometers placed throughout the structure are then utilized to identify the primary mode shapes and their periods of vibration for the structure. Whether such testing is prudent for any particular project is also a matter of judgment for the design engineer.

9.2 Site Specific Ground Motions

The research demonstrates that the specific nature of ground motions is the single most influential variable for determining the effectiveness (or lack thereof) of the NRTMDF. Therefore, the effective design and tuning of the NRTMDF requires that a sound understanding of potential ground motions be developed. Ideally this would include the development of site specific acceleration histories reflecting ground motions for the site consistent with the performance objective. While the development of acceleration records has not traditionally been an undertaking for most design scenarios, recent research and tools such as the PEER website are enabling the selection and utilization of ground motions meant to represent the specific site.[29] These tools notwithstanding, any ground motion developed with the intent of incorporating an NRTMDF must be developed using sound geoseismic design principles.

The research demonstrates that the more traditional methods (e.g. response spectrum) may be utilized for an NRTMDF design. However, these approaches have

significant limitations when assessing the effectiveness of the NRTMDF. As such, they should only be used on a preliminary basis. The pragmatic realization of an effective NRTMDF will most likely require advanced nonlinear response history analysis methods. These approaches inherently require the utilization of records reflecting the seismic event of interest.

9.3 Supporting the NRTMDF

The research demonstrates that an NRTMDF mass reflecting approximately 15-20% of the total structural mass is required to develop the effective inertial forces necessary for mobilization and for offsetting the inertia of the base structure (see Section 5.5). While this added mass can easily be accounted for if the NRTMDF is used for new construction, its incorporation in an existing structure will require attention to the columns, footings and soils that will be required to support the added mass.

For columns of the existing building, many options may be considered if the column capacity is insufficient. Cover plating is a retrofit measure commonly undertaken for columns with insufficient capacity. Likewise, carbon fiber and fiber reinforced polymers are options for increasing the capacity of existing structural elements. Also, columns are often comprised of hollow structural shapes. Filling the shapes with grout offers the opportunity for a significant increase in structural capacity. For instance, a 4.6 meter long steel column designated HSS8x8x1/4 has an axial capacity of 1050 kN in accordance with current AISC provisions.[40] Upon filling this column with grout ($f'c$=34.5MPa), the axial capacity improves to 1446 kN. Beyond these approaches, it would also be prudent to perform a careful inventory of actual dead loads and live loads. Dead loads are almost always overestimated by design engineers. Also, live loads above

and beyond prescriptive standards are regularly utilized in an effort to enable enhanced structural performance or more versatility with respect to tenant improvements and alterations. Careful examination of these issues may yield sufficient reserve capacity for the NRTMDF mass.

Footings and soils ultimately supporting the added NRTMDF mass may also prove insufficient with respect to the original design approach. For the cases where footings are deemed insufficient, several alternatives exist. First, design of simple spot footings is typically undertaken conservatively considering only one-way bending action of the footing. Accounting for two-way action in the footing design will likely yield added capacity beyond the original design. Should bearing pressures of footings on soils surpass original design provisions, soil remediation measures may be undertaken. However, in the same manner structural dead loads are typically overestimated, soil bearing capacities are typically underestimated. Supplemental soils investigations may yield allowable bearing capacities sufficient to support the added mass of the NRTMDF.

9.4 NRTMDF and Base Building Interface

The effective performance of the NRTMDF is contingent upon its ability to transmit its inertial forces through the designated yielding members (buckling restrained braces) to the base structure. Fundamentally, the braces serve as a ductile fuse limiting the maximum forces that can be transmitted to the structure below. Despite the ability of the braces to limit the forces transmitted to the base structure, these forces are still significant and must be developed into the structure in a manner that will not result in load concentrations beyond the capacity of the system. For many cases, this will require the incorporation of drag struts at the roof level to distribute seismic loads to diaphragms

in a satisfactory manner. The drag struts should be of sufficient length to not surpass unit shear capacities of the roof deck and the connection of the drag strut to the NRTMDF should sufficiently develop the forces of the corresponding buckling restrained braces (see Figure 9.1).

9.5 NRTMDF Stiffness

Ideally, the effective stiffness of the NRTMDF should be predicated by the buckling restrained braces alone as these elements provide the greatest degree of control over stiffness. However, the pragmatic design of most braced frames requires the incorporation gusset plates to which the braces connect. The gussets are connected to adjoining beams and columns as shown in Figure 9.1. For such connections, the gusset invariably provides a restraint between the beam and column thereby contributing to the total frame stiffness. Potential options for minimizing the restraining effect include

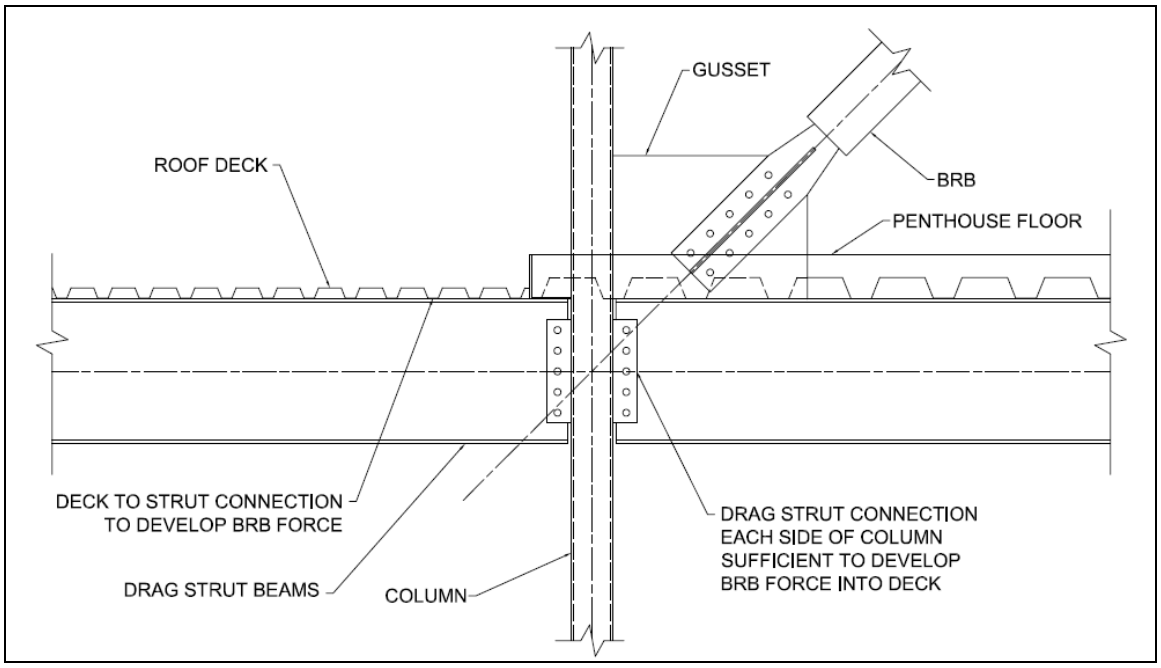

Figure 9.1 Interface of NRTMDF and Building

providing slotted bolt connections at the gusset to column interface at both ends of the brace as shown in Figures 9.2 and 9.3. Use of a pinned brace connection could also serve to alleviate the added stiffness due to the BRB connection since it offers the potential for a flexural release of the brace along with a smaller gusset as shown for the connections at both ends of the brace in Figures 9.4 and 9.5. Other approaches may include the development of flexural hinges in the beam of the frame just beyond the region of the gusset as shown in Figure 9.6 though this approach may compromise drag strut performance. Other options include the deliberate incorporation of the stiffness provided by the gusset and accounting for this stiffness in the total frame behavior. Since the drifts of the NRTMDF are expected to be unusually large with respect to common systems, the gusset should be designed in anticipation of extreme story drift and the potential yielding

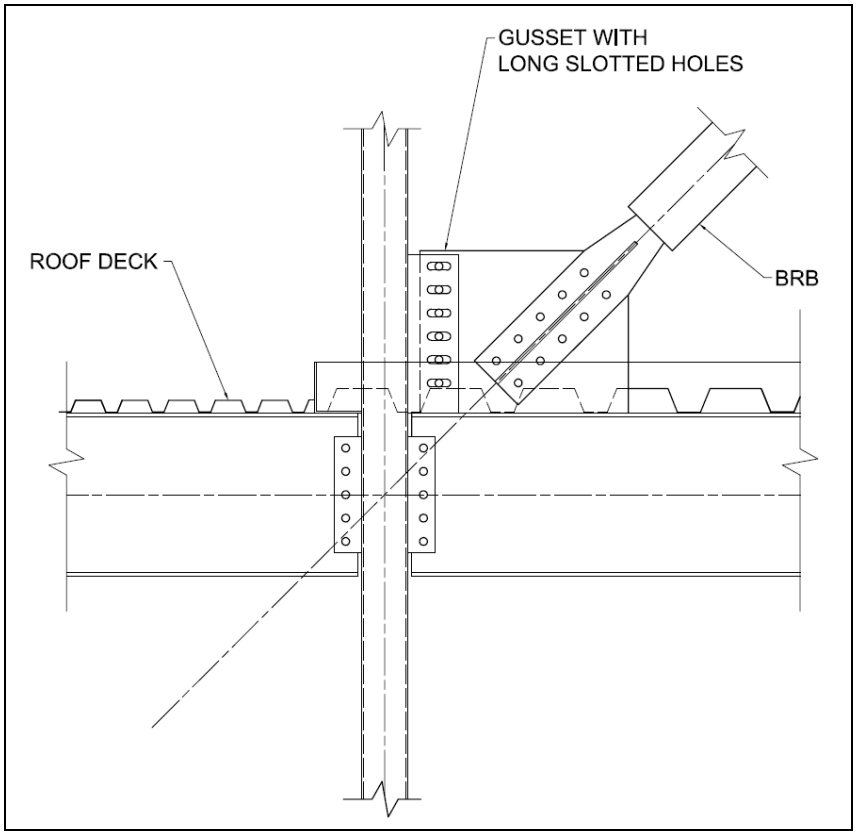

Figure 9.2 Slotted Gusset Connection at Brace Bottom End

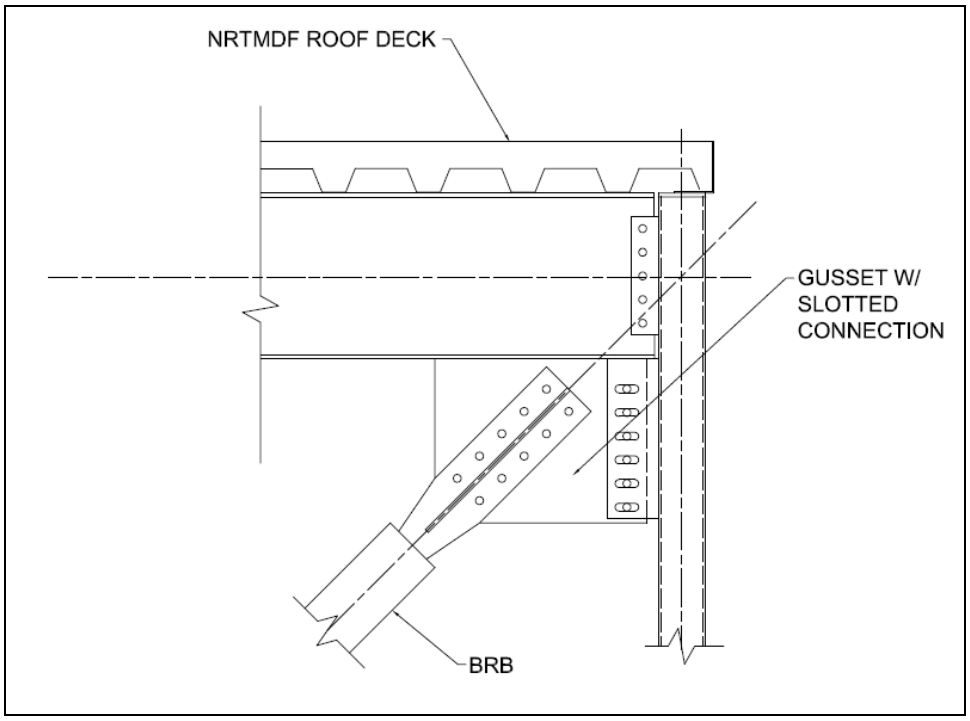

Figure 9.3 Slotted Gusset Connection at Brace Top End

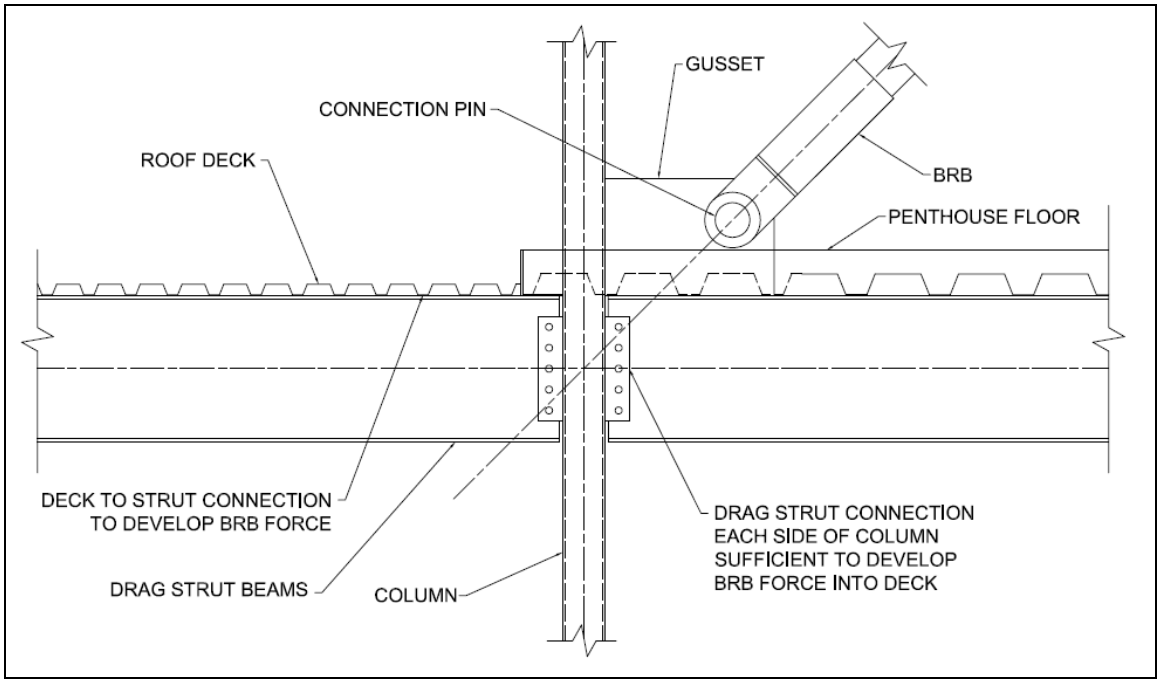

Figure 9.4 Pinned BRB Connection at Brace Bottom End

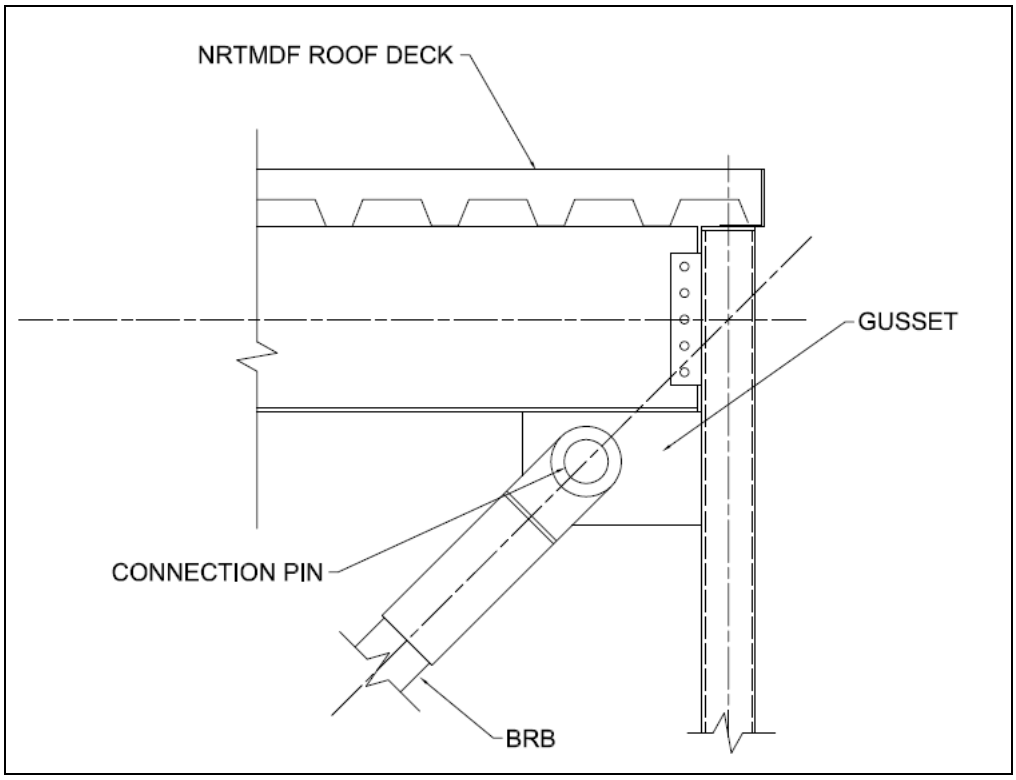

Figure 9.5 Pinned BRB Connection at Brace Top End

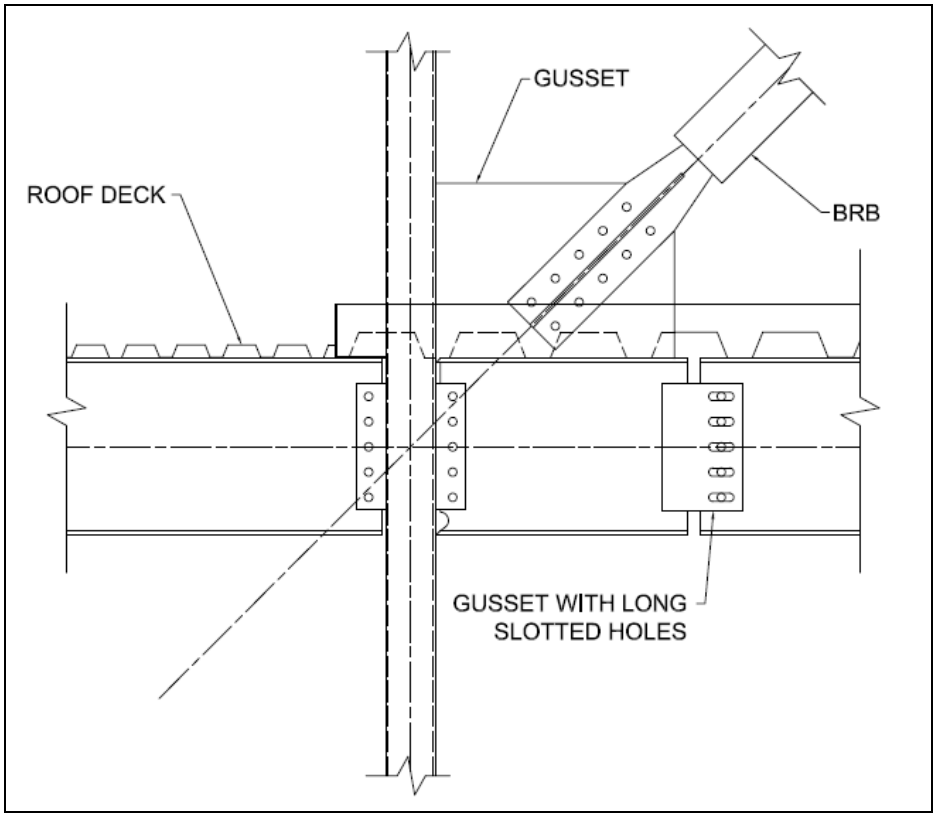

Figure 9.6 Beam Rotational Release Beyond Gusset

and/or pinching of the gusset. Similar detailing issues apply to the opposite end of the BRB at the NRTMDF roof and the gusset and beam/column interface.

Another issue dealing with NRTMDF geometry is the development of effective parameters to enable adequate ductility and stability. Table 5.13 lists the maximum capable NRTMDF displacements based on the available BRB core length. To enable displacements commensurate with effective properties core lengths were required to be longer than the available geometry within the typical structural bay. As shown in many figures within this research (e.g. Figures 5.29 and 5.30) the BRB may need to span multiple structural bays in order to enable effective core lengths and stiffness properties. Doing this may require larger beams to span the bays or adaptive detailing to enable a brace-column interface that can develop the column and brace load paths independently as shown in Figures 9.7 and 9.8.

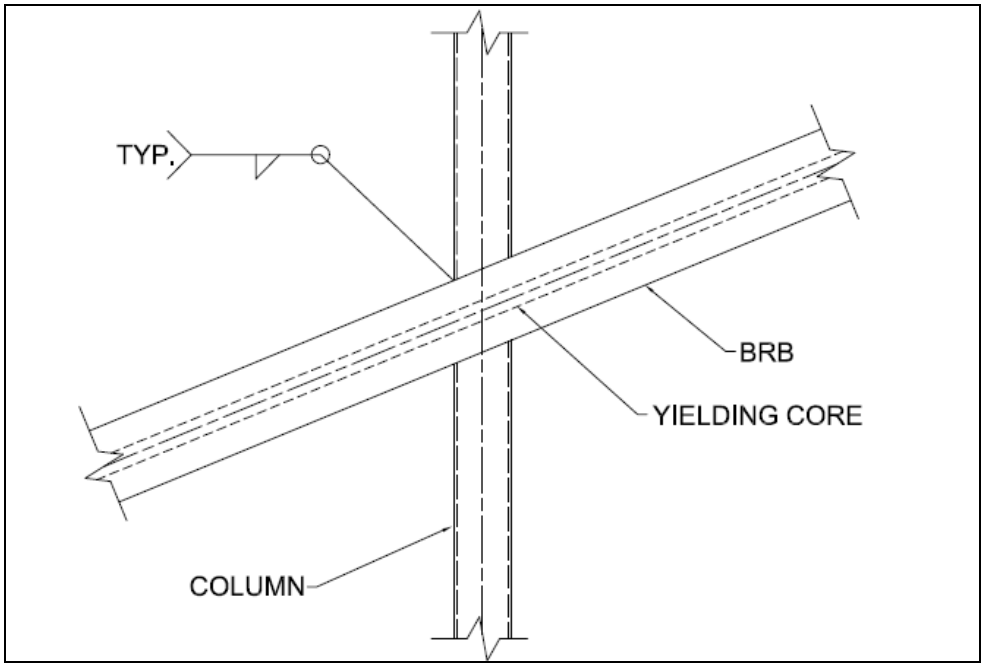

Figure 9.7 Column and BRB interface with Welded Connection

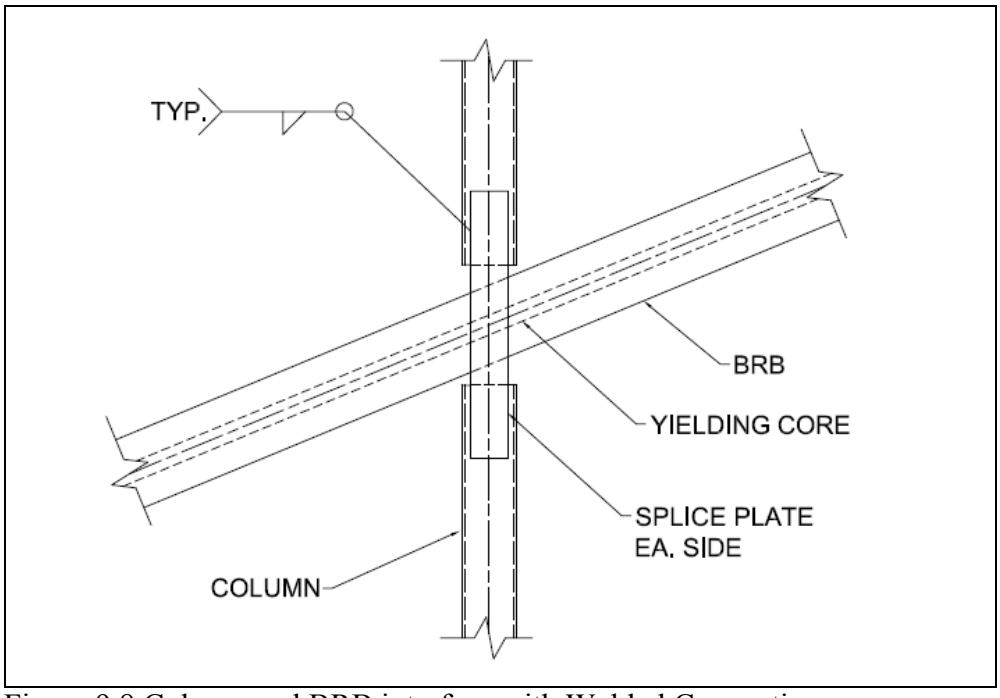

Figure 9.8 Column and BRB interface with Welded Connection

9.6 NRTMDF Cladding Issues

As indicated previously, cladding can have an unexpected influence on frame stiffness.[39] For this approach, failure to deliberately account for the effect of cladding could render the NRTMDF entirely ineffective or may even yield performance worse than the undamped case. Furthermore, the NRTMDF would often be the mechanical penthouse enclosure. Such features are often totally opaque with enveloping walls that may have considerable in-plane stiffness. To mitigate the unintended stiffness effects created by cladding, the cladding of the NRTMDF should ideally be designed to have little, if any influence on stiffness. While conventional approaches may predicate the use of connections that enable an in-plane horizontal slip where the cladding interfaces with the roof deck, such detailing may not be practical due to the magnitude of expected NRTMDF displacements. Other approaches may predicate the use of a cladding system totally suspended from the NRTMDF which is not directly attached to the structure

below. A deviation from this might include cladding with a horizontal joint with the cladding below the joint cantilevering upward to meet, but not be directly attached to the break. The most pragmatic approach for minimizing the impact of cladding on NRTMDF stiffness may be to design the cladding as a sacrificial element specifically designed to come apart and fall away from the structure at the moment of NRTMDF mobilization.

9.7 NRTMDF Fail-Safe Geometry

Full scale testing of BRB elements demonstrates primary failures in the form of tensile rupture of the BRB core. Though ultimate compression failure mechanisms are not entirely understood, it is clear that BRB compression failures likely occur at compression strains far beyond the 3.5% limitation discussed in Section 5.3. With this as a consideration, development of redundant NRTMDF geometries may enable a fail-safe approach for promoting NRTMDF stability even though BRB cores may suffer tensile rupture. Figure 9.9 demonstrates a potential geometry for the NRTMDF which drives simultaneous tensile and compressive action in adjacent braces. For this arrangement of braces, one brace must always act in compression as the other acts in tension. Should a

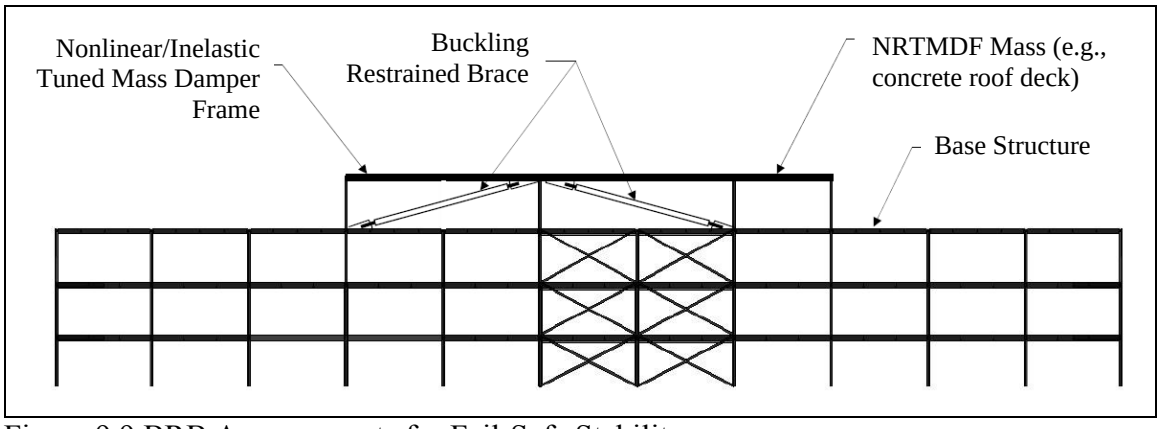

Figure 9.9 BRB Arrangements for Fail-Safe Stability

brace fail in tension, the adjacent brace may still act in compression thereby preventing a complete loss of lateral stiffness. Likewise, if both braces fail in tension, they will still have compressive capacity, but in opposing directions thereby providing a fail-safe stability mechanism for the NRTMDF.

9.8 BRB Orientation and Directionality Effects

Full scale hysteretic testing of buckling restrained braces demonstrates compression behavior and tensile behaviors that are roughly equal but with higher compression stiffness and yield strengths than those in tension.[3,4] This is rational behavior in consideration of Poisson effects, higher mode buckling and other behaviors of the BRB core. The ratio between peak compression and tension hysteretic properties is assigned the variable β and may have values as high as 10%. In consideration of this disparity and disparities such as unidirectional pulses due to near-field effects (Section 5.2) associated with some ground motions, orienting the BRB to act in compression when resisting the primary pulses of NRTMDF acceleration for such motions may enable a preferred and more stable behavior scenario for the NRTMDF. Likewise, when acting in compression to resist such pulses, the BRB may behave favorably to strains far beyond the 3.5% BRB strain limit discussed in Sections 5.3 and 6.2.

9.9 Nonstructural Systems Attached to the NRTMDF

A fundamental premise of the NRTMDF is that it may become the penthouse enclosure for rooftop mechanical equipment. Such systems often include the connection of many suspended elements (units and conduits) to the roof above (NRTMDF roof). Since the NRTMDF is expected to experience significant drift, these elements may be

subject to extreme distortion or may even rupture when the NRTMDF mobilizes. To address this, it may be prudent to re-configure the systems to preclude the attachment of the nonstructural elements to the roof above (bottom of the NTRMDF deck). Otherwise, it may be prudent to incorporate a significant number of flexible connections that will sufficiently address the potential for NRTMDF drifts associated with its nonlinear inelastic behavior.

10 CONCLUSIONS

The analyses undertaken within this research demonstrate that the Nonlinear/Inelastic Rooftop Tuned Mass Damper Frame (NRTMDF) can be an effective approach for reducing seismic response. However, like most advanced technologies, it does not provide a comprehensive solution enabling enhanced performance for any structure and any potential earthquake. For this reason, the research focused on the identification of the structure types and nature of ground motions for which the solution is most appropriate. Furthermore, the research explored and demonstrated many different methods of analysis for this approach and has served to identify effective analysis, design methods and strategies. In addition, the research has served to clearly highlight the limitations of conventional prescriptive analysis and design methods found in contemporary codes. The research described within the body of this dissertation leads to the conclusions that follow.

10.1 Seismic Response Reduction

The NRTMDF can be an effective strategy for reducing a structure's response to seismic motion. It is most effective when it can enable a fundamental period shift from a region of high spectral acceleration response to a region of lower spectral acceleration response in the context of the response spectrum representing the anticipated ground motion.

The nonlinear behavior of the NRTMDF enhances the performance of the system by further shifting the period and by serving as a designated yielding frame that enables an approach for targeted energy dissipation within the structure. The NRTMDF draws a significant amount of energy from the system and dissipates it in a safe, controlled and deliberate manner through the buckling restrained braces of the NRTMDF.

10.2 Linear Analysis Methods

Conventional linear analysis methods serve effectively to identify whether a structure may be a viable candidate for this approach. However, linear analysis methods do not adequately characterize the behavior of the NRTMDF and may not sufficiently characterize the behavior of the base structure, depending on the magnitude of the input ground motion. As such, the linear methods serve as an effective screening test for the NRTMDF. Also, linear analysis methods may demonstrate an effective NRTMDF but will not adequately characterize its behavior, particularly with respect to peak transient motions. Linear analysis methods are likely to overestimate the drift of the NRTMDF resulting in a conclusion of likely instability where it may in fact remain stable. Qualitative observations of the response spectra representing the ground motion may serve as a precursor to the linear analysis methods. For the NRTMDF approach to be effective there must be an observable and significant reduction of the spectral acceleration ordinate when considering the fundamental period shift that the NRTMDF may enable.

10.3 Nonlinear Analysis Methods

Analysis methods which incorporate nonlinearity of NRTMDF and structural systems provide the most realistic assessment of behavior. This is particularly true for the nonlinear time history analysis methods which make use of actual ground motions and model nonlinear behavior of seismic force resisting elements in a manner consistent with tested behavior and behavior observed in prior seismic events. Furthermore, the nonlinear analysis methods enable the accounting of the hysteretic damping effect as well as the assessment of damage indices, both of which require the rational nonlinear modeling of system elements which provide primary resistance to lateral forces.

A fundamental premise behind this research is the concept of targeted nonlinearity in designated yielding members. As a specialized approach for seismic response reduction, the approach of this research utilizes the buckling restrained braces of the NRTMDF as the primary designated members for targeted nonlinearity. When effectively designed, the NRTMDF may mobilize and yield before other members of the base structure. This active nonlinearity is deemed the most favored outcome since it may preclude nonlinear demand in the base structure. The research demonstrates that this can be the outcome and in fact is the predicted outcome for many of the design scenarios that were considered.

Nonlinear modeling enables two key phenomena that cannot be accounted for in linear modeling alone. First is the period shift occurring as a result of NRTMDF yielding. Linear elastic behavior of the NRTMDF enables a period shift that can drive a reduction in seismic response. As yielding of the NRTMDF occurs, it softens and enables a further period shift that can enable an even greater response reduction. Second

is the hysteretic damping which effectively reduces the building response by diverting both elastic and plastic seismic strain energy from the base structure into plastic deformation seismic energy dissipated by the NTRMDF. The net effect of these results as presented in Chapter 5 is a reduction in calculated peak rooftop displacement between linear and nonlinear methods ranging from 10.3% to 23.8% beyond the linear methods as summarized in Table 5.12. Such results not only demonstrate the ability of the NRTMDF to reduce the seismic response, but reflect the need for nonlinear modeling to accurately predict the behavior of the system.

Unlike linear elastic modeling methods, nonlinear analysis methods provide a rational approach to account for effects of unidirectional pulses and other phenomena which accompany near-field motions. Large unidirectional pulses within the acceleration record may cause unbalanced hysteretic behavior and can result in significant permanent lateral displacements. Such phenomena may reflect a diminished NRTMDF capacity or instability of the NRTMDF due to large unidirectional displacements.

10.4 Simplified Modeling

Simplified stick frame modeling (inverted pendulum) serves to adequately characterize the behavior of the global structure with the NRTMDF for many cases. For linear analysis approaches, the simplified stick framed models yield a result with near exactness to the full model. For nonlinear analysis approaches, simplified stick frame modeling is accurate insofar as the nonlinear hysteretic properties of each floor are adequately represented. As the complexity of nonlinear behavior increases, the accuracy of the stick frame modeling approach decreases. Since the NRTMDF has well defined and well balanced hysteretic properties, it can accurately be represented by a single

simple nonlinear element within the simplified stick frame model. The nonlinear behavior of the base structure can be represented with single simple nonlinear elements representing each floor within the simplified stick frame model depending on the complexity of nonlinear behavior of the base model. Nonlinear pushover analysis on a story by story basis may reveal the complexity of the nonlinear behavior and may enable qualitative judgments on whether simplified stick frame modeling of the base structure is appropriate. Also worthy of consideration is the potential for nonlinear demand on the base structure. The research demonstrates that for many cases, the NRTMDF enables reductions to such a degree that nonlinearity of the base structure does not occur. For such cases, simplified stick framed modeling is appropriate as linear behavior between stick frame models and fully developed models can match with precision, barring significant plan or vertical irregularities causing other phenomenon (e.g. torsion).

10.5 Nonlinear Static Pushover Methods

Nonlinear static pushover analysis methods serve to verify whether active nonlinearity in the NRTMDF is achieved prior to yielding of the base structure. As a fundamental benefit, the NRTMDF may reduce or totally eliminate nonlinear demand on the base structure. Key to this is to ensure yielding (active nonlinearity of NRTMDF) occurs before yielding of the base structure. Since nonlinear pushover methods serve to identify the order in which nonlinear mechanisms form within a structure, it is useful to demonstrate whether the NRTMDF is likely to yield before the base structure. A caveat here is that one of the tenets of NRTMDF effectiveness is its ability to enable a mode 2 response (see Section 5.4) which enables a counteracting inertial effect which diminishes peak transient response. Nonlinear pushover methods inherently consider only one

vibration mode at a time thereby negating the higher mode effects. Methods to address this include rationally combining the first two modes of vibration for one pushover analysis load pattern or other rational modal combinations of displacement pattern within the pushover analysis. Such rational approaches may include a bounded approach that captures the maximum limits for primary mode shapes. These may include the consideration of modes 1 and 2 independently and then the numerical aggregate of the two for combinations considering both positive and negative loading directions of the loading pattern represented by each mode as presented in Section 5.4. Following this approach, the research demonstrates that utilization of a mode 1 displacement pattern can accurately predict whether yielding of the NRTMDF occurs prior to yielding of the base structure when it can be demonstrated that the mode 2 response accounts for approximately 60% (or less) of total mobilized mass within the system. Observation of results from the current research in general indicates this is true for the test structures with three or more stories.

10.6 Cost vs. Benefit Discussion

There is no advanced technology within the inventory of seismic resistant design that provides a comprehensive solution for seismic response reduction for all buildings and all possible earthquakes. Some approaches are better than others and some can actually create a negative effect if used improperly. An example of this would be the use of base isolation technology on extremely soft soil conditions as this may lead to a condition of structure resonance with the site that amplifies the seismic response. Likewise, the approach embodied within this research can be detrimental when the shift in fundamental period places the building at a higher acceleration ordinate on the

acceleration response spectrum representing the seismic event. However, when used appropriately base isolation reduces the seismic response. Likewise, this research demonstrates the effectiveness of the NRTMDF when used appropriately. The nonlinear rooftop tuned mass damper frame may not be as effective as seismic base isolation for a certain class of structures such as low to mid-rise buildings. However, base isolation is not as effective for mid-rise to tall structure due to concerns with overturning instability; the NRTMDF may be advantageous in this case. In addition, consideration of a cost vs. benefit scenario establishes the NRTMDF as a worthy alternative. Seismic isolation of existing structures is very costly, often requiring the complete removal and replacement of foundations. This must invariably be accompanied by sophisticated load transfer systems and temporary shoring. Such measures are not only costly, but carry risks associated with structural stability. For new construction, many of these items may be mitigated but at the very least, base isolation requires deeper foundations along with the addition of a suspended level of construction, both of which are more costly than the slab at grade and shallower foundations of an equivalent fixed base system.

For the NRTMDF approach as a retrofit strategy, the penthouse shell must be added or removed and replaced. Existing columns may require retrofit. Footings may require reinforcement and reinforcing of existing roof structures may be required to effectively transmit lateral forces between the original structure and the NRTMDF. While detailed studies and development of cost models may be required to assess the financial ramifications of this approach, it is deemed far less costly than the measures associated with base isolation. For new construction, the NRTMDF is also expected to come at a lower premium than the base isolated counterpart. Unlike base

isolation, it does not require an added level of suspended structure (tying the isolation system together). It requires more materials (concrete and steel) at the penthouse along with the addition of buckling restrained braces but overall is deemed a less costly approach than base isolation.

In the overall consideration of cost vs benefit the NRTMDF approach is deemed a viable candidate for reducing a building's seismic response. It is not as effective as base isolation for a certain class of buildings, but it is not as costly. The NRTMDF may have advantages over base isolation in consideration of structures where large overturning loads may cause isolator instabilities. The NRTMDF will likely enable an improved margin of performance over the base condition and might well enable a project to achieve the owner's, and other stakeholders' performance expectations and do so within the context of available budget.

10.7 Energy Methods

Energy methods utilized for calculating damage indices are not found within the prescriptive requirements of current building codes. Nonetheless, their utilization is deemed of significant benefit for characterizing the benefits of the approach embodied within this research. Rather that assessing performance based on peak transient parameters, the energy methods consider the complete time domain for the applicable acceleration records representing seismic ground motion. Furthermore, they account for the quantity of peaks within the record and their effect on structural demand. These approaches identified situations of higher structural demand that were not possible to identify using more traditional methods. Energy methods address the earthquake duration issue which is not addressed within the context of contemporary codes for new

design and codes for seismic rehabilitation. Peak transient demands can only account for peak transient energy. Total accumulated energy is deemed an appropriate reflection of the demand placed on the structure and the NRTMDF approach demonstrates a clear and analytically measurable method for measuring the reduction of this demand.

Two energy methods were utilized within this research and yielded consistent results. The Fardis method yielded damage index values slightly less than those of Park and Ang method. Both methods show a potential decreased structural demand for the NRTMDF approach from the energy perspective. This reduction is primarily manifested as a diminished nonlinear hysteretic demand on the base structure when the NRTMDF is utilized. In essence, the NRTMDF creates two phenomena that enable the reduction in structural demand. First is the fundamental period shift which means the structure may attract less acceleration and less energy simply because it is further from resonance with the site. Second is the targeted energy dissipation of the buckling restrained braces of the NRTMDF. Energy dissipated here is not free to propagate elsewhere in the structure. For the base structure, this translates to less stress, less fatigue and less overall damage (lower damage index).

10.8 Equivalent Damping

Damping due to hysteretic nonlinear behavior of lateral force resisting elements represents an important approach for seismic energy dissipation of high performance systems. Utilization of rational methods for hysteretic energy measurement and its application to equivalent damping demonstrates the beneficial effects of the NRTMDF. Results of equivalent damping calculations listed in Chapter 7 generally demonstrate higher equivalent damping for buildings damped with the NRTMDF than undamped

buildings. For these cases, the NRTMDF dissipates a major portion of seismic energy attracted by the system. When accounted for, this energy drives the equivalent damping calculation upward. The results demonstrate that in a minority of cases, equivalent damping is higher in undamped structures than in damped structures. For these, the NRTMDF behaves linearly and causes a period shift that enables a reduction in seismic response sufficient to diminish nonlinear demand for the base structure. The result is that the undamped structure experiences higher overall nonlinearity than the damped structure and therefore yields a higher equivalent damping.

10.9 Nonstructural Elements and Components – Floor Spectra

Nonstructural elements and components often represent a major portion of a building's value. Development and comparison of floor spectra between undamped and damped structures demonstrates the potential for the NRTMDF approach to reduce seismic demand on nonstructural elements and components. While this may translate to a diminished need for seismic bracing of these components, a more important contribution is the damage reduction enabled by the NRTMDF. Such performance can preclude significant rehabilitation costs following a major seismic event. The research demonstrates that the NRTMDF enables a reduction in the average floor spectra for every case considered, with reductions of the average floor spectra between the undamped and damped cases as high as 30 to 40 percent.

10.10 NRTMDF Subassembly Detailing

The targeted behavior of the NRTMDF reflected in this research is the most important issue with respect to its performance and ability to reduce seismic response.

For this reason, careful attention to detailing should be considered to ensure the targeted mass and stiffness of the NRTMDF is achieved in a practical sense.

Under normal circumstances, structures may be stiffer than reflected in their initial design. Items such as connection gusset plates, panel zones, shorter effective brace lengths and fixity of gravity connections all contribute to frame stiffness but are rarely accounted for in actual design. The result may be a structure with a lower fundamental period than anticipated in design. Normally this does not bear serious consequences and may even be beneficial. However, for the NRTMDF, the specific structural dynamics are important to consider for the system to be effective in targeting energy to the NRTMDF. To address this, careful attention may be required for items such as beam to column connections with bracing gussets as well as other beam to column connections in general. As deemed prudent, forced vibration testing of the base structure is prudent for rehabilitation purposes. The NRTMDF can also be considered and accommodated accordingly within the context of new construction. In addition, prudent analysis measures should include attention to cladding and its contribution to stiffness and mitigation of its effects.

10.11 Future research

This research presents a broad-based approach for assessing whether the NRTMDF is a rational and valid approach for reducing seismic response. While the research has demonstrated the effectiveness of the NRTMDF, it has not addressed a simplified modeling approach. Even advanced seismic systems such as base isolation have simplified methods which are codified to such an extent that significant nonlinear analyses are not required. The NRTMDF approach reflected in this research follows

sophisticated nonlinear modeling techniques for both the NRTMDF and the base structure. Future research may focus on the development of simplified and reliable methods for developing the NRTMDF properties that will enable significant reduction in seismic response. In addition, implementation of the NRTMDF developed in the research in an actual structure would be a worthwhile research endeavor and would illuminate several aspects and conclusions obtained in the present study and would likely identify more issues requiring study.

Other avenues for future research include the utilization of alternate framing systems for the NRTMDF as outlined in Section 10.12. Future research may include analysis of structural irregularities (plan, vertical and torsional) and the potential for reduction in their effects on the system enabled by the NRTMDF. Other options for additional research include the development of multiple tuned mass dampers which may be located not only at the roof level, but at other stories within the structure. Wong and Johnson investigated such approaches with traditional dampers.[19] The approach embodied within this research focuses inertial damping resistance at the roof level. For taller structures, effective performance may be realized with dampers not only at the roof, but at multiple levels within the structure. Such mechanisms could be realized within dedicated structural bays and may be called a Nonlinear/Inelastic Tuned Mass Damper Frame (NTMDF).

The research encountered unusual response conditions when records included motions with large pulses due to near-field effects. The observed result is diminished performance of the NRTMDF and for the system as a whole due to the unidirectional pulses that controlled peak transient responses. Buckling restrained braces exhibit a

behavior which could be exploited with respect to such phenomena. Due to poisson and other such effects that accompany buckling restrained braces under compression, compression stiffness and compression yielding forces are typically higher than these same parameters in tension. For most analyses, including those addressed in this research, average parameters between compression and tension are typically utilized. However, when considering unidirectional pulses, it may be beneficial to orient the BRB's to act in compression when resisting forces arising from such phenomena. This is true for the NRTMDF approach addressed in this research and for lateral force systems comprised of braces in general. If unidirectional pulses are characterized as likely in accordance with the geoseismic study, orienting the braces for their most capable performance, be it compression (buckling restrained braces) or tension (conventional braces), may be a prudent measure to deliberately consider within the context of the lateral force resisting system design. Whether such measures are truly an effective approach for improving performance is a matter of further research. When considered, the analyses require added complexity when modeling the elements. Whereas many nonlinear elements can be modeled with simple symmetric bilinear load-displacement patterns, this approach would require an asymmetric and perhaps multi linear load displacement pattern. Very few modeling applications are capable of such sophistication.

10.12 Other Technologies

Buckling restrained braces were selected as the designated yielding members of the Nonlinear Rooftop Tuned Mass Damper Frame because they provide superior hysteretic inelastic performance with a larger degree of control over design parameters (stiffness, yield strength, etc.) than other systems. This notwithstanding, other

technologies hold the potential for similar performance though with a diminished capacity for control of design parameters. Such technologies include the eccentric braced frame, special moment frame, special steel plate shear wall, perforated plate dampers and even viscous fluid dampers. Any such systems capable of developing frame hysteretic behavior akin to that of buckling restrained braced frames should be considered as viable candidates for serving the same function as the buckling restrained braces of the NRTMDF assemblies embodied in this research.

Codes for new construction and codes for seismic rehabilitation prescribe design criteria for eccentric braced frames and special moment frames reflecting ductility akin to that of buckling restrained braces.[2,25] Of the two, eccentric braced frames hold the potential as the most effective substitute for the buckling restrained braces incorporated in this research. This is primarily due to the ability of eccentric braced frames to develop hysteretic performance characteristics which are very similar to those of the buckling restrained braced frame. Also, the stiffness of the eccentric braced frame can be controlled to a large degree through the length of the shear link. Special moment frames can also develop well balanced hysteretic properties with the potential for high ductility and energy dissipation. In fact, the hysteretic behavior of moment frames is not unlike that of buckling restrained braced frames and eccentric braced frames, which makes such frames amenable to the NRTMDF approach. The special moment frame was the system developed in past research by Johnson, Pantelides and Reaveley investigating rooftop yielding frames for seismic response reduction.[10,11] A drawback of the special moment frame is the limitation with respect to its stiffness control. Rolled steel shapes have finite dimensions and engineers do not often have the latitude (development of

specific penthouse dimensions) in developing a system geometry that would enable the targeting of a specific stiffness of this system when developed as an NRTMDF. Special moment frames are a viable option for the NRTMDF but they do not offer the same control over performance as the buckling restrained braces investigated in this research.

Special steel plate shear walls and perforated plate dampers are uniquely detailed framing assemblies capable of developing hysteretic properties that may enable their effective use for a nonlinear rooftop frame. Whether these are effective substitutes for the buckling restrained braces is a matter of further research though each is believed to be appropriate. In consideration of perforated plate dampers as an alternate, Ross developed a unique detailing method for augmenting the capability for nonlinear performance by placing a curved reinforcing plate over the perforated plate fuse.[5] This approach is a particularly attractive alternate to the buckling restrained brace system in this research, especially for cases where the NRTMDF is driven to excessive displacements that might be beyond practical limits. In essence, the curved reinforcing plate acts as a fail-safe mechanism that only becomes active when a specific and targeted threshold of strain in the perforated plate is breached. When this occurs, the curved plate has already been pulled straight and begins to act in tension, eventually developing nonlinear performance characteristics well beyond the displacements of the original perforated plate. This behavior enables a complex tri-linear load-displacement relationship that may enable favorable behavior for extreme conditions. Like the special steel plate shear wall, the perforated plate damper's effectiveness as part of the NRTMDF is a matter of further research.

Viscous fluid dampers and visco-elastic dampers hold the potential as alternate approaches for the Nonlinear/Inelastic Rooftop Tuned Mass Damper Frame though the approach would require renaming the system as a Fluid Damped Rooftop Tuned Mass Damper Frame or a Viso-elastically Damped Rooftop Tuned Mass Damper Frame. For the viscous fluid damper, the energy dissipating characteristics would be driven primarily by velocity of the damper mass and its inertial effects in forcing fluid through orifices of the damping apparatus. Visco-elastic dampers operate in a similar fashion only with a visco-elastic material acting as the primary energy fuse. With such behavior, these approaches differ from the method of this research which drives energy dissipation through inelastic behavior of solid materials. Like the other approaches mentioned previously, the effectiveness of a viscous fluid or visco-elastic dampers in lieu of buckling restrained braces is a matter of further research.

10.13 Fundamental Conclusion

The present research demonstrates that the NRTMDF is an effective approach for providing a significant reduction of a building's seismic response for the appropriate structure and site. Fundamentally, the approach is sound when the NRTMDF enables a shift in fundamental period reflected as a reduction in the acceleration ordinate of the site design spectrum. For this reason, determining whether a structure is a viable candidate for this approach should begin by examining the response spectra representing ground motions of the seismic performance objective. The spectra may even be those from prescribe building codes (e.g., ASCE 7). Where a reduction in the spectral acceleration ordinate is clear, the NRTMDF will most likely yield a reduction in the seismic response.

Beyond the qualitative comparison of the building period and spectrum, analyses using linear methods with simplified damper tuning serves to further qualify whether a structure is a viable candidate for this approach. Once this has been demonstrated, full nonlinear analysis can enable the development of near optimal NRTMDF parameters (mass, stiffness, yield strength). The full nonlinear analysis also includes the most accurate assessment of peak transient response parameters such as base shear and peak rooftop displacement. Energy methods further serve to verify the effectiveness of the approach and enable the calculation of damage indices and equivalent damping measures. Development of floor spectra also serves to demonstrate the effectiveness of the approach. Comparison of the floor spectra between undamped and damped cases demonstrates the effectiveness of the approach with respect to nonstructural elements and components while also predicting the magnitude of lateral forces on the nonstructural elements and components of the system damped with the NRTMDF.

The research demonstrates that viable building candidates and sites for which the NRTMDF can be identified. It also demonstrates the negative effects of a building and site which may not be suited to the approach. Primarily, the analyses demonstrate that soft buildings and/or soft sites are not well suited to the approach. For these, NRTMDF deflections may be excessive and may be beyond stable limits. Likewise, fundamental period shifts for such cases may not enable a reduction in response in consideration of the ground motion spectrum and in fact may create an increase in response. In addition, the NRTMDF approach does not appear to be particularly well suited to extremely high ground accelerations. Such conditions result in NRTMDF stiffness properties that are not amenable to the development of a suitable period shift. Otherwise, a suitable period shift

may be enabled, but may result in NRTMDF displacements which are beyond a stable limit. The approach is less effective for short period structures (less than 3 stories typically). This is because the necessary period shifts become too large, requiring a NRTMDF with limber properties that might suffer excessive displacements.

In a fundamental sense, this research introduces and demonstrates another method for reducing a structure's response to seismic motion. While not as effective as other advanced approaches such as base isolation for certain classes of structures such as low to mid-rise buildings, the costs for its implementation are far less. However, the NRTMDF is well suited for structures in the mid-rise to high-rise category which are relatively stiff. Hence, the NRTMDF offers the opportunity for improvements of performance but at a cost far less than other advanced systems. It represents improved seismic performance for less cost. This is applicable to retrofit scenarios and for new construction. The improved performance is reflected as less damage, diminished threat to life and lower construction cost when utilized as either a rehabilitation measure or as a strategy to improve performance for new construction.

APPENDIX A

MODEL DATA

Analytical models represented in this research were developed as full mathematical models representing the spatial geometry of each building. Also, simplified inverted pendulum models were developed for preliminary analysis runs which yielded results sufficiently matching those of the full mathematical models. Tables A.1 through A.3 list the story mass and story stiffness for each of the test models and Figures A.1 through A.10 depict the frame member sizes of the lateral force resisting systems in the direction of interest for each model.

Table A.1 Test Model Masses and Stiffness at Each Floor

	BF-1		BF-2		BF-3	
	Mass	Stiffness	Mass	Stiffness	Mass	Stiffness
Floor	kg	kN/mm	kg	kN/mm	kg	kN/mm
2	444865	435	1457143	869	1014346	1239
3	142931	260	374513	803	1056638	665
4					424902	345

Table A.2 Test Model Masses and Stiffness at Each Floor (Continued)

	BF-4		BF-5		EBF-1	
Floor	Mass kg	Stiffness kN/mm	Mass kg	Stiffness kN/mm	Mass kg	Stiffness kN/mm
2	1084558	907	479656	1258	1403581	67357
3	1071676	608	466984	843	962905	453
4	1049715	408	455644	706	978626	309
5	387114	230	452104	493	181788	157
6			447056	411		
7			443218	309		
8			435804	241		
9			424446	166		
10			267809	91		

Table A.3 Test Model Masses and Stiffness at Each Floor (Continued)

	SW-1		SW-2	
Floor	Mass kg	Stiffness kN/mm	Mass kg	Stiffness kN/mm
2	801676	13489	3141783	23935
3	800133	6166	3278019	15678
4	800133	3866	2811386	6892
5	800133	2598	2609968	4524
6	800133	1669	2482057	3000
7	653118	839	1117508	1572

Table A.4 Test Model Masses and Stiffness at Each Floor (Continued)

	MF-1		MF-2	
Floor	Mass kg	Stiffness kN/mm	Mass kg	Stiffness kN/mm
2	911183	1751	1835055	726
3	871695	177	1826292	527
4	898476	103	1822033	477
5	896846	77	1815443	443
6	414491	48	1808064	393
7			1793903	337
8			1778672	253
9			1191787	168

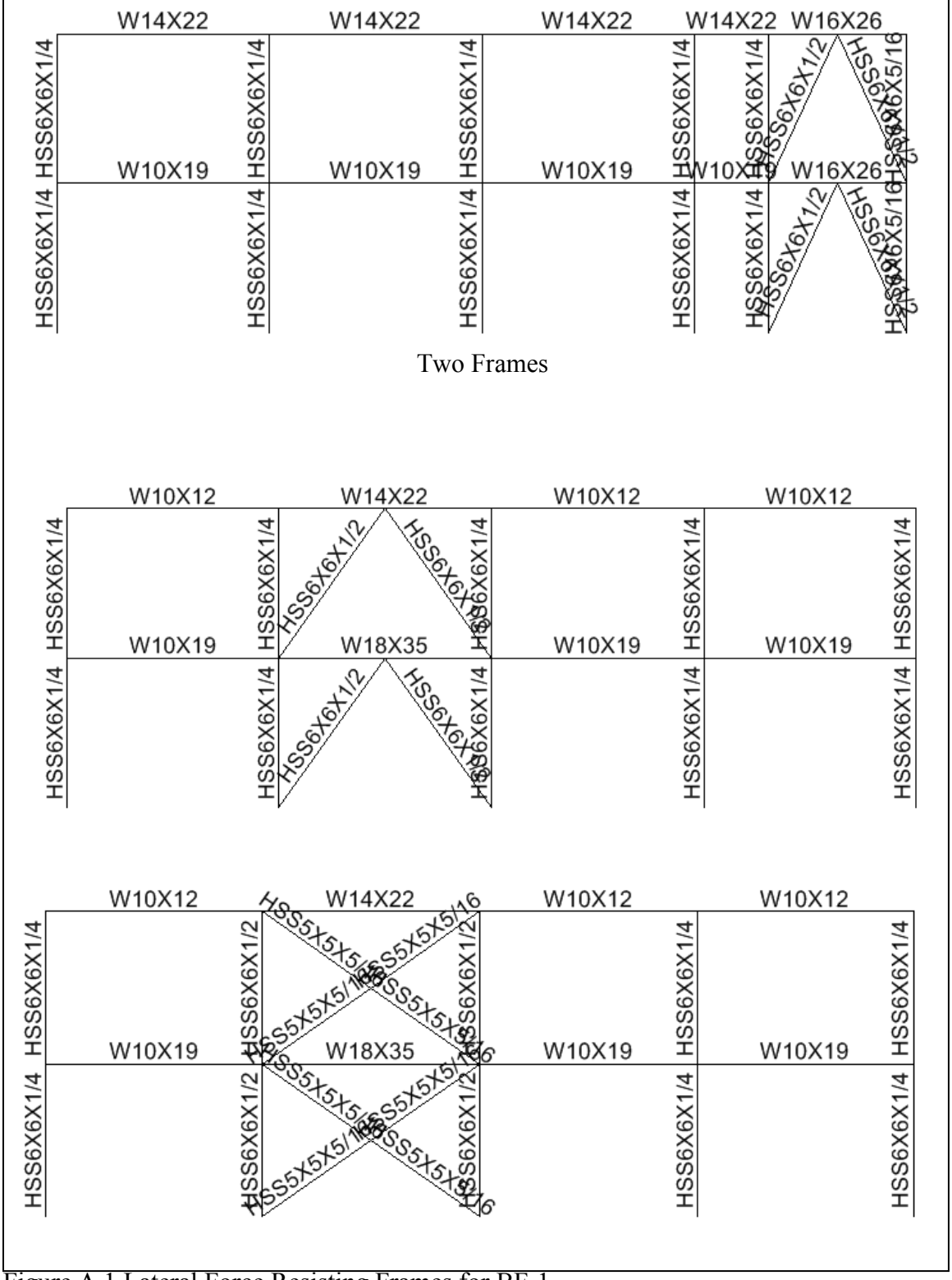

Two Frames

Figure A.1 Lateral Force Resisting Frames for BF-1

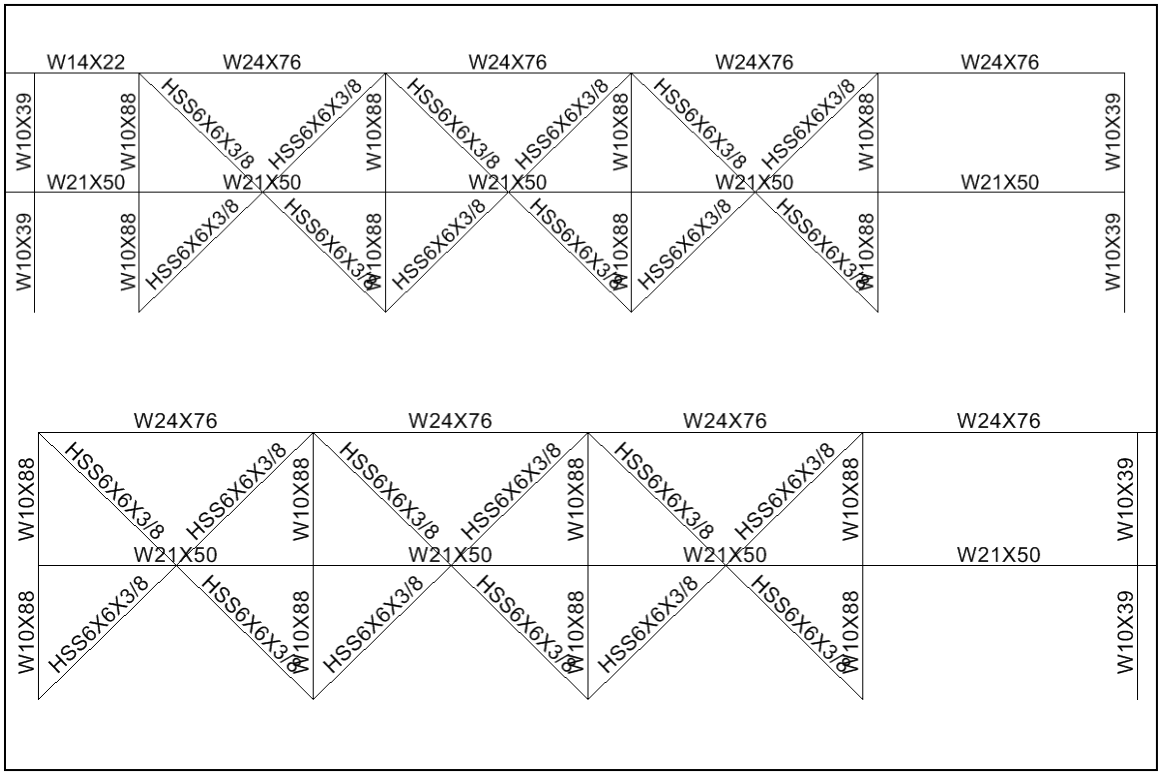

Figure A.2 Lateral Force Resisting Frames for BF-2

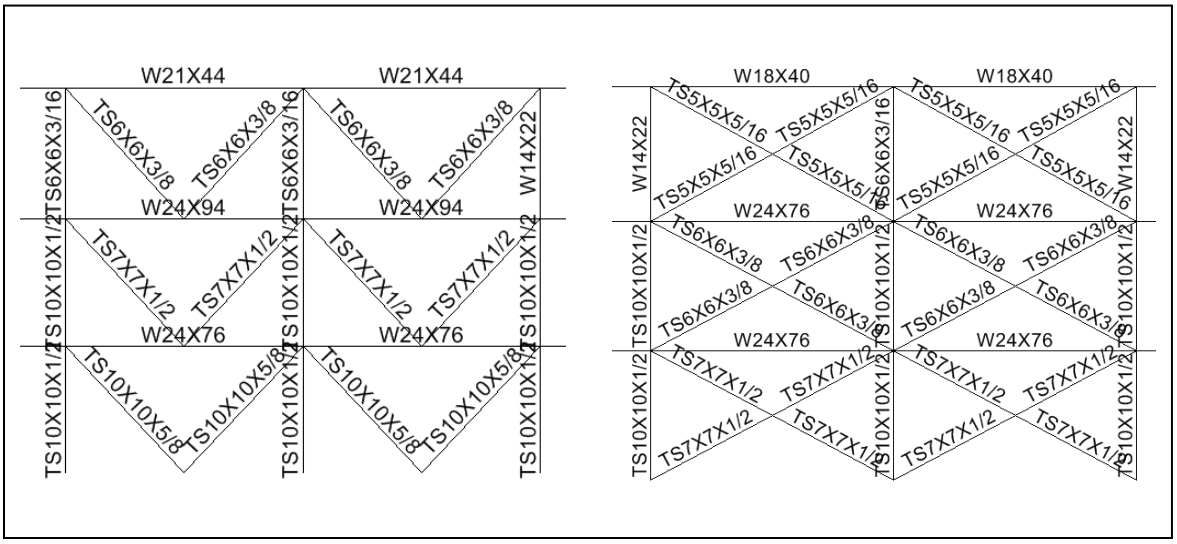

Figure A.3 Lateral Force Resisting Frames for BF-3

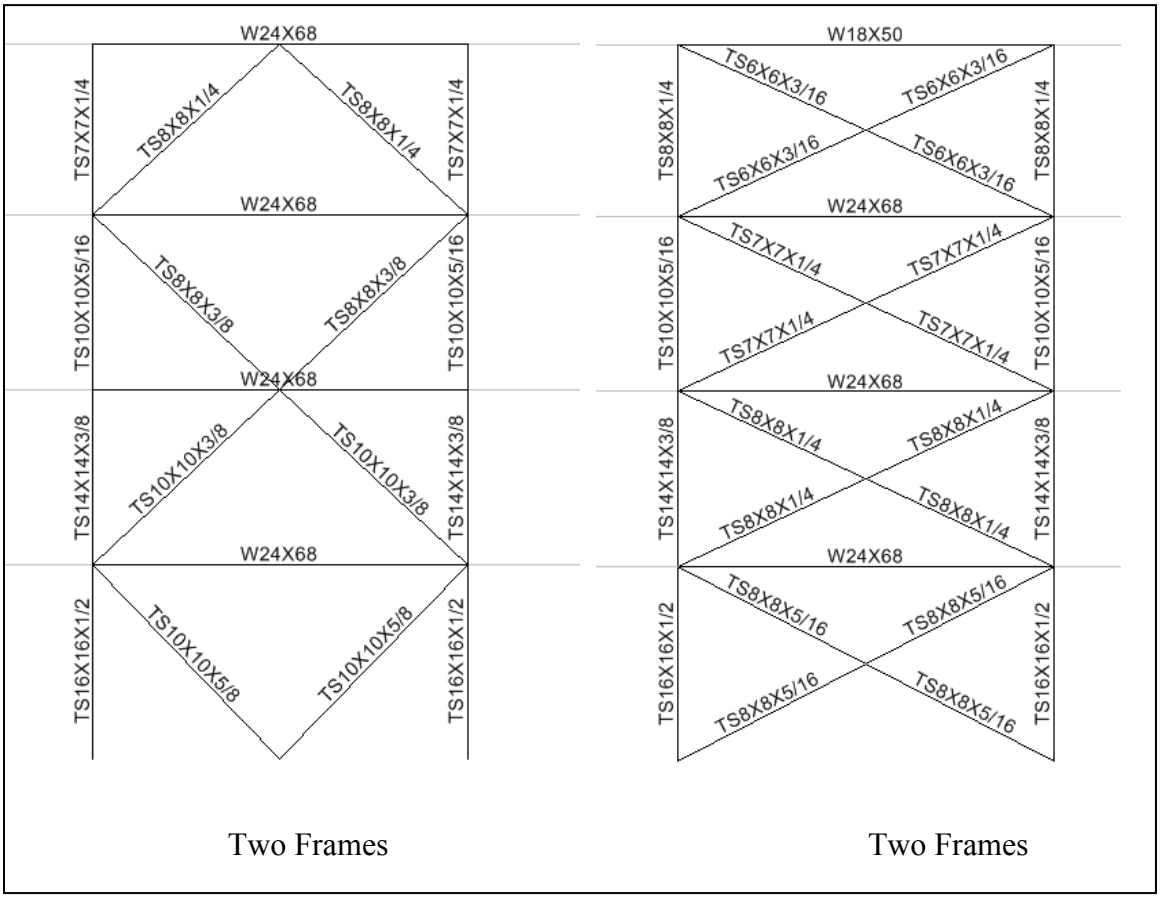

Figure A.4 Lateral Force Resisting Frames for BF-4

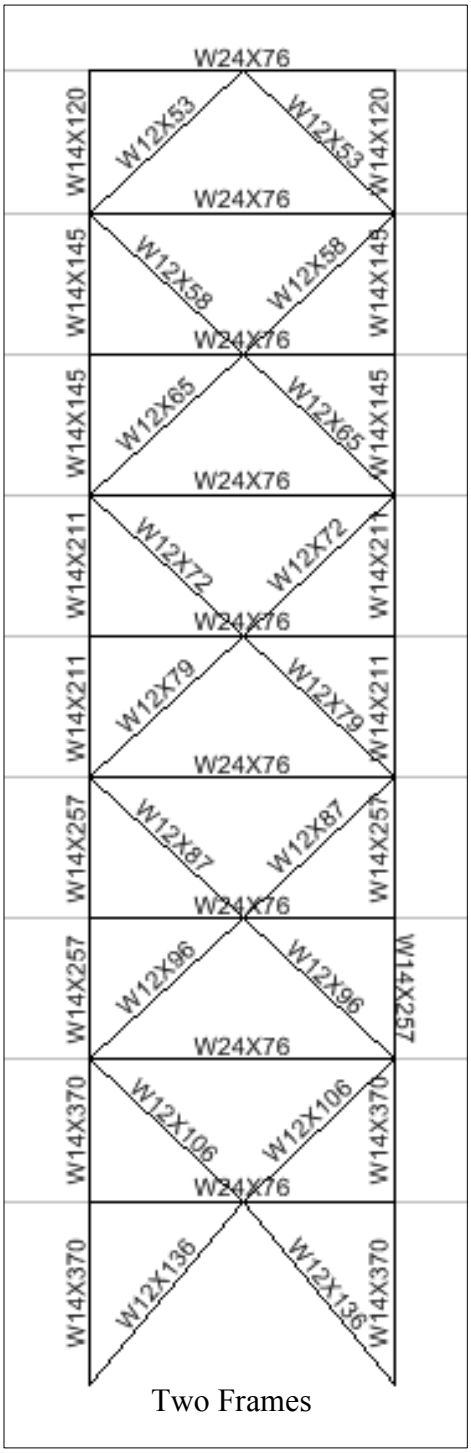

Figure A.5 Lateral Force Resisting Frames for BF-5

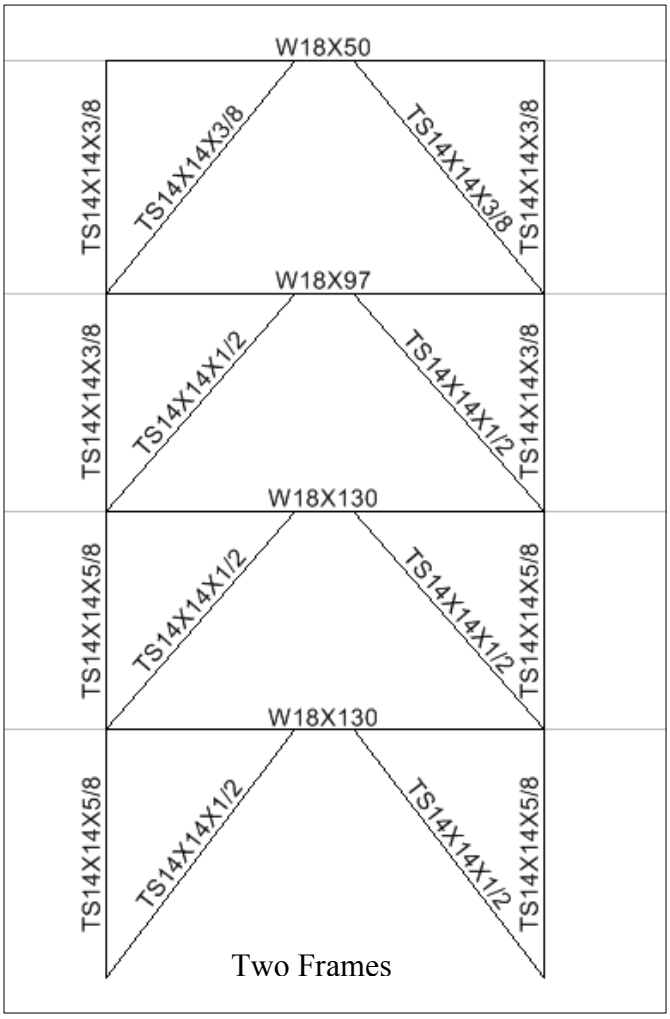

Figure A.6 Lateral Force Resisting Frames for EBF-1

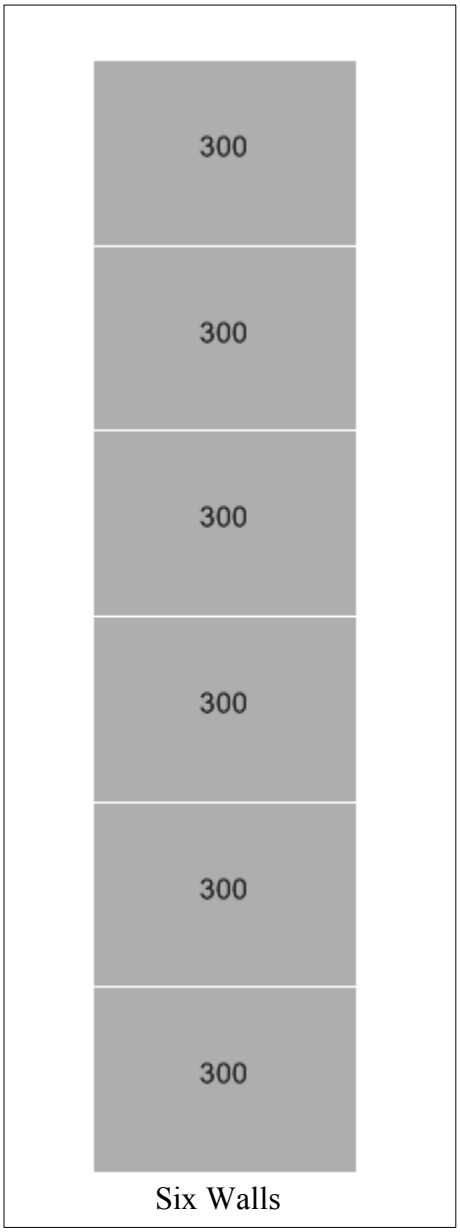

Figure A.7 Lateral Force Resisting Walls for SW-1 (thickness in mm as shown)

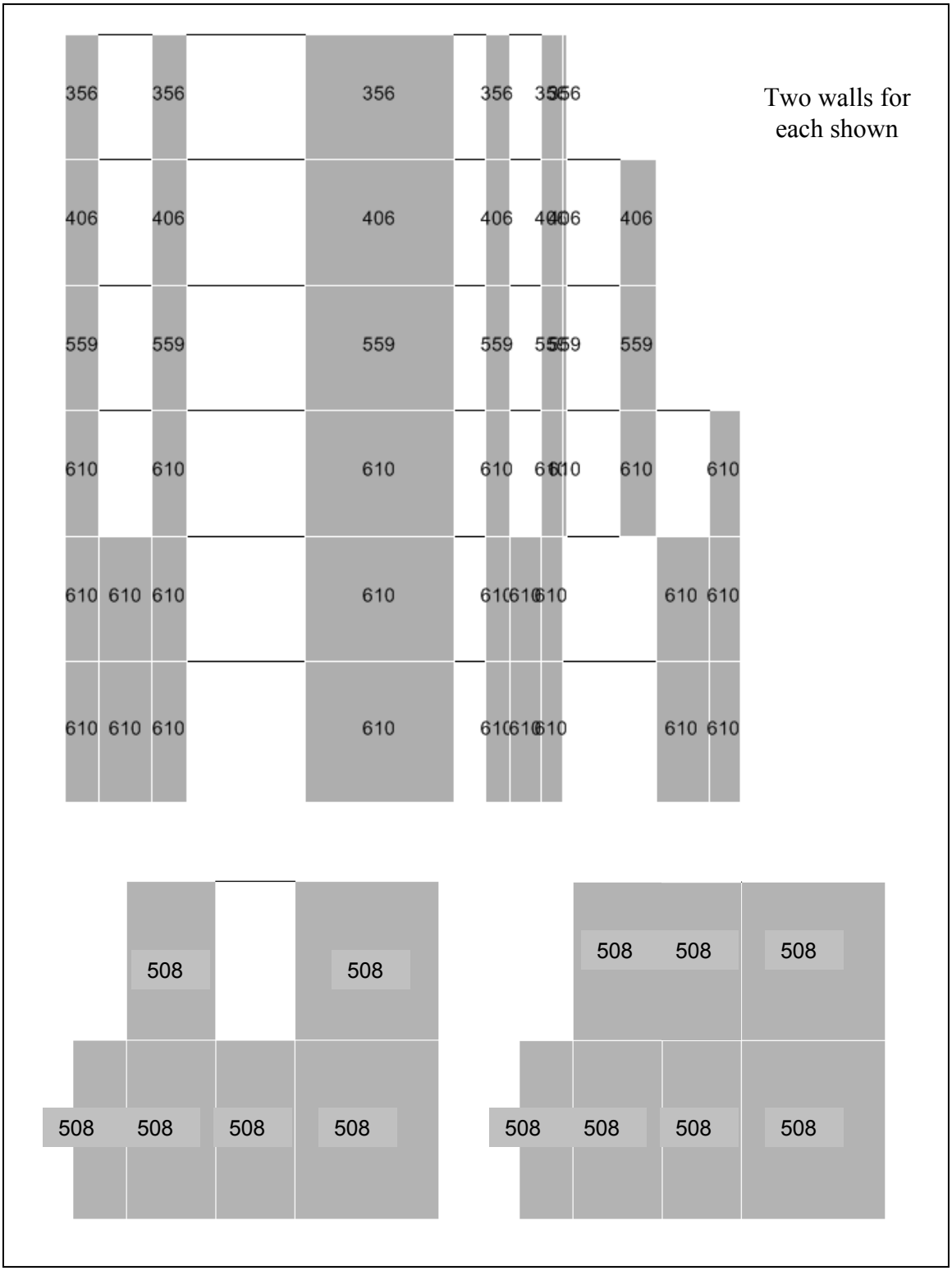

Figure A.8 Lateral Force Resisting Shear Walls for SW-2 (thickness in mm as shown)

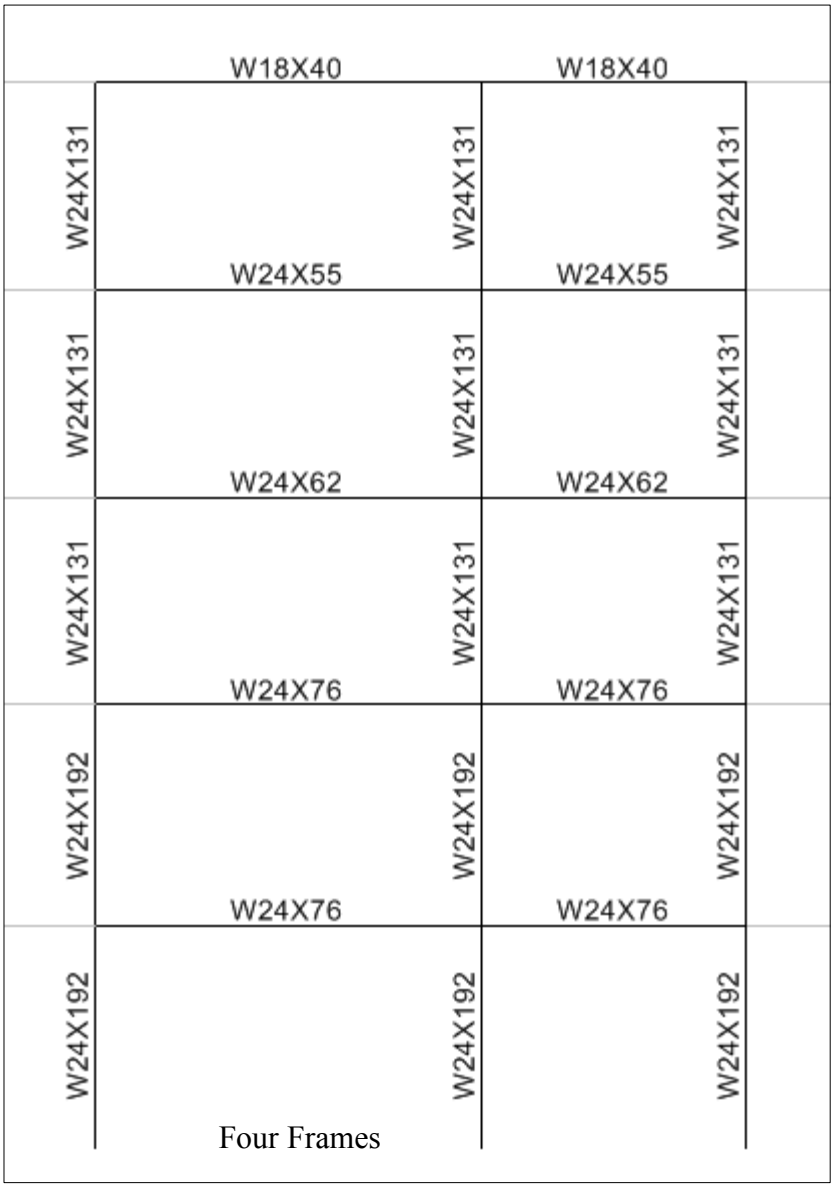

Figure A.9 Lateral Force Resisting Frames for MF-1

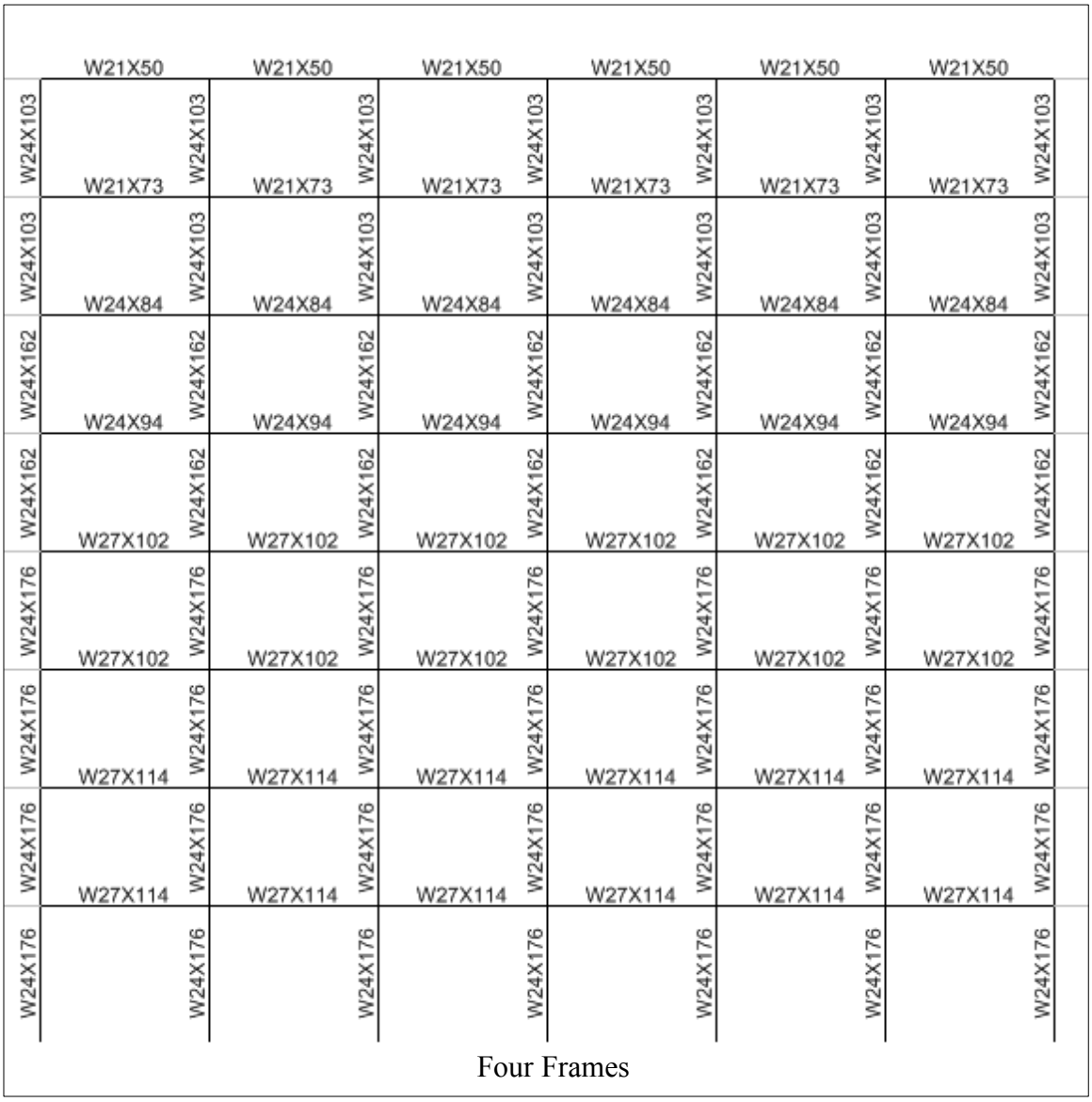

Figure A.10 Lateral Force Resisting Frames for MF-2

APPENDIX B

LINEAR ANALYSES OUTPUT

Tables B.1 through B.20 list the output values of peak output parameters results listed in Chapter 4. Values shown reflect the peak rooftop displacements and the peak base shears for the undamped and damped cases. Also shown are the percent changes from the undamped to damped cases along with the peak drift of the NRTMDF for each damped case.

Table B.1 Peak Base Shear for BF-1, Linear Analysis Methods.

Acc. History	U kN	D kN	% Change	Acc. History	U kN	D kN	% Change
LA01	6118	5834	-4.6%	BO05	4171	3902	-6.4%
LA02	9343	7807	-16.4%	BO06	2629	2147	-18.3%
LA04	6066	5160	-14.9%	BO13	2454	2394	-2.4%
LA12	16794	15120	-10.0%	BO16	3296	2930	-11.1%
LA15	6315	5076	-19.6%	BO18	3061	2783	-9.1%
LA18	8961	6700	-25.2%	BO19	2519	2476	-1.7%
LA20	14819	15072	1.7%	BO20	2355	2213	-6.1%
LA21	7714	10546	36.7%	BO21	4075	3708	-9.0%
LA22	6438	6907	7.3%	BO22	4613	4156	-9.9%
LA23	3082	3258	5.7%	BO25	2846	3012	5.8%
LA25	10278	8260	-19.6%	BO33	7024	6853	-2.4%
LA28	14583	10900	-25.3%	BO34	12952	10968	-15.3%
LA30	20582	17330	-15.8%	BO35	18203	19074	4.8%
LA37	4760	5096	7.1%	BO36	9472	8421	-11.1%
SE04	7908	7467	-5.6%	NF01	19225	18057	-6.1%
SE05	4261	3972	-6.8%	NF02	16931	15406	-9.0%
SE08	3986	4269	7.1%	NF11	5910	5999	1.5%
SE10	8550	8696	1.7%	NF12	7203	7226	0.3%
SE12	7563	5850	-22.6%	NF15	8145	6077	-25.4%
SE18	8369	8574	2.5%	NF16	6285	6327	0.7%
SE19	6100	6116	0.3%	LASS1A	4967	4172	-16.0%
SE21	4997	5952	19.1%	LASS1B	3958	3375	-14.7%
SE25	9953	9276	-6.8%	LASS1C	3537	2931	-17.1%
SE26	11107	10851	-2.3%	LASS1E	5800	4700	-19.0%
SE30	19611	20090	2.4%	LASS2A	5315	5121	-3.7%
SE31	14314	14366	0.4%	LASS3B	2221	2660	19.8%
SE32	9998	8776	-12.2%	LASS3C	2360	2446	3.6%
SE36	7822	8224	5.1%	LASS4C	3096	2975	-3.9%
				Averages	7768	7287	-5.2%

U- Undamped

D- Damped

Table B.2 Peak Rooftop Displacements and Damper Drift for BF-1, Linear Analysis Methods

Acc. History	U mm	D mm	% Change	DD mm	Acc. History	U mm	D mm	% Change	DD mm
LA01	21	21	-1.3%	107	BO05	16	14	-10.3%	40
LA02	35	27	-23.2%	142	BO06	9	7	-29.9%	37
LA04	21	18	-13.3%	77	BO13	9	8	-5.7%	19
LA12	60	51	-14.1%	190	BO16	12	10	-14.0%	21
LA15	22	18	-17.2%	93	BO18	11	9	-15.0%	19
LA18	30	25	-17.0%	174	BO19	9	9	-7.7%	18
LA20	53	53	-0.5%	129	BO20	8	8	-0.4%	42
LA21	26	43	61.3%	221	BO21	15	14	-6.7%	52
LA22	22	27	22.4%	115	BO22	16	16	-0.4%	92
LA23	10	13	31.8%	84	BO25	10	10	5.2%	51
LA25	35	29	-17.2%	151	BO33	25	24	-5.8%	56
LA28	49	40	-17.1%	283	BO34	45	37	-17.1%	85
LA30	75	62	-16.5%	206	BO35	69	68	-1.3%	199
LA37	17	21	22.3%	100	BO36	34	29	-14.0%	59
SE04	28	27	-1.4%	85	NF01	69	63	-9.1%	179
SE05	15	14	-6.0%	64	NF02	61	53	-12.7%	169
SE08	14	16	16.5%	59	NF11	21	21	-1.5%	52
SE10	31	30	-0.5%	75	NF12	26	25	-4.2%	55
SE12	27	20	-24.7%	99	NF15	28	20	-28.9%	84
SE18	30	30	1.1%	113	NF16	23	24	4.5%	171
SE19	21	23	8.0%	91	LASS1A	17	15	-14.1%	63
SE21	17	24	44.0%	109	LASS1B	14	13	-7.0%	78
SE25	35	33	-6.1%	148	LASS1C	12	11	-10.7%	63
SE26	40	38	-4.1%	147	LASS1E	20	16	-19.0%	82
SE30	70	71	1.1%	265	LASS2A	19	20	5.0%	92
SE31	50	54	8.1%	214	LASS3B	7	11	51.2%	59
SE32	36	33	-8.5%	141	LASS3C	8	10	26.9%	44
SE36	27	30	11.7%	88	LASS4C	11	12	12.5%	55
					Averages	27	26	-1.6%	104

U- Undamped
D- Damped
DD- Damper Drift

Table B.3 Peak Base Shear for BF-2, Linear Analysis Methods.

Acc. History	U kN	D kN	% Change	Acc. History	U kN	D kN	% Change
LA01	15278	13904	-9.0%	BO05	14867	14433	-2.9%
LA02	25835	26117	1.1%	BO06	11377	10462	-8.0%
LA04	24173	22391	-7.4%	BO13	6901	6831	-1.0%
LA12	33501	35052	4.6%	BO16	4937	5248	6.3%
LA15	22938	21627	-5.7%	BO18	8378	8162	-2.6%
LA18	44708	42263	-5.5%	BO19	4146	4609	11.2%
LA20	55909	54997	-1.6%	BO20	8114	7103	-12.5%
LA21	32658	30310	-7.2%	BO21	13828	12768	-7.7%
LA22	24385	22916	-6.0%	BO22	13217	11936	-9.7%
LA23	13751	13865	0.8%	BO25	9124	7951	-12.9%
LA25	37333	35198	-5.7%	BO33	19750	19550	-1.0%
LA28	72715	68756	-5.4%	BO34	35494	31057	-12.5%
LA30	38801	37232	-4.0%	BO35	32177	31603	-1.8%
LA37	20157	18431	-8.6%	BO36	14189	15083	6.3%
SE04	25791	25468	-1.3%	NF01	30951	30109	-2.7%
SE05	21783	20732	-4.8%	NF02	29228	29534	1.0%
SE08	19107	18047	-5.5%	NF11	16555	15869	-4.1%
SE10	32261	31732	-1.6%	NF12	16773	17610	5.0%
SE12	23320	23500	0.8%	NF15	38738	37043	-4.4%
SE18	29803	26978	-9.5%	NF16	30339	27046	-10.9%
SE19	18811	17919	-4.7%	LASS1A	17619	16468	-6.5%
SE21	19007	21347	12.3%	LASS1B	12806	12340	-3.6%
SE25	50847	48420	-4.8%	LASS1C	10862	11595	6.7%
SE26	38527	34969	-9.2%	LASS1E	20621	19516	-5.4%
SE30	69956	63261	-9.6%	LASS2A	15766	15903	0.9%
SE31	44174	42082	-4.7%	LASS3B	10899	10846	-0.5%
SE32	23024	23788	3.3%	LASS3C	8062	8730	8.3%
SE36	16910	19900	17.7%	LASS4C	10385	10018	-3.5%
				Averages	24314	23404	-3.7%

U- Undamped

D- Damped

Table B.4 Peak Rooftop Displacements and Damper Drift for BF-2, Linear Analysis Methods

Acc. History	U mm	D mm	% Change	DD mm	Acc. History	U mm	D mm	% Change	DD mm
LA01	22	20	-10.1%	142	BO05	22	21	-8.5%	32
LA02	37	39	6.2%	205	BO06	16	15	-9.9%	30
LA04	35	32	-7.7%	76	BO13	10	10	-1.6%	17
LA12	49	51	5.0%	180	BO16	8	8	0.0%	17
LA15	33	31	-5.7%	208	BO18	12	12	-1.4%	40
LA18	65	61	-5.8%	256	BO19	6	7	17.0%	36
LA20	82	80	-2.0%	189	BO20	11	10	-14.6%	44
LA21	47	46	-1.7%	514	BO21	20	18	-8.7%	72
LA22	35	39	12.9%	579	BO22	19	16	-13.5%	81
LA23	20	20	2.6%	275	BO25	13	11	-12.8%	52
LA25	53	50	-5.7%	338	BO33	28	28	-1.6%	50
LA28	105	99	-5.7%	416	BO34	52	44	-14.3%	71
LA30	57	52	-8.1%	360	BO35	49	45	-7.7%	170
LA37	29	26	-10.6%	269	BO36	22	22	0.0%	48
SE04	38	37	-3.1%	90	NF01	46	43	-5.8%	295
SE05	31	29	-6.1%	89	NF02	43	42	-2.0%	256
SE08	28	26	-6.1%	209	NF11	24	23	-6.4%	110
SE10	47	46	-2.0%	109	NF12	25	26	5.5%	82
SE12	34	34	-0.8%	131	NF15	56	54	-2.7%	172
SE18	44	39	-11.3%	165	NF16	44	38	-13.2%	195
SE19	27	28	1.9%	312	LASS1A	25	24	-6.9%	194
SE21	27	33	21.4%	415	LASS1B	18	18	-0.8%	145
SE25	73	69	-6.0%	207	LASS1C	16	18	13.3%	148
SE26	56	49	-12.3%	188	LASS1E	30	28	-5.2%	196
SE30	102	91	-11.4%	387	LASS2A	23	24	4.7%	237
SE31	63	65	1.8%	732	LASS3B	16	17	6.6%	96
SE32	33	35	6.6%	351	LASS3C	11	14	18.4%	87
SE36	24	33	35.5%	335	LASS4C	15	15	2.7%	103
					Averages	35	34	-1.7%	193

U- Undamped
D- Damped
DD- Damper Drift

Table B.5 Peak Base Shear for BF-3, Linear Analysis Methods

Acc. History	U kN	D kN	% Change	Acc. History	U kN	D kN	% Change
LA01	25018	17576	-29.7%	BO05	13039	10651	-18.3%
LA02	24609	26589	8.0%	BO06	16944	14885	-12.1%
LA04	29088	25371	-12.8%	BO13	5150	6104	18.5%
LA12	40023	30498	-23.8%	BO16	3977	2811	-29.3%
LA15	29757	26121	-12.2%	BO18	6897	6402	-7.2%
LA18	57628	47688	-17.2%	BO19	4465	5596	25.3%
LA20	37617	30174	-19.8%	BO20	12273	9800	-20.1%
LA21	54467	44944	-17.5%	BO21	14146	12089	-14.5%
LA22	52922	46015	-13.1%	BO22	24693	20077	-18.7%
LA23	21187	20204	-4.6%	BO25	15620	11854	-24.1%
LA25	48428	42509	-12.2%	BO33	14744	17469	18.5%
LA28	93753	77563	-17.3%	BO34	22040	20638	-6.4%
LA30	46555	34803	-25.2%	BO35	39408	30589	-22.4%
LA37	31076	25616	-17.6%	BO36	11424	8081	-29.3%
SE04	17150	12287	-28.4%	NF01	42071	35993	-14.4%
SE05	16736	19442	16.2%	NF02	31694	29696	-6.3%
SE08	16309	17341	6.3%	NF11	13913	15186	9.1%
SE10	21704	17393	-19.9%	NF12	12119	14182	17.0%
SE12	20600	20469	-0.6%	NF15	37815	36672	-3.0%
SE18	32653	24862	-23.9%	NF16	44816	36557	-18.4%
SE19	18618	16683	-10.4%	LASS1A	22690	22270	-1.9%
SE21	27060	23660	-12.6%	LASS1B	19840	19777	-0.3%
SE25	39040	45398	16.3%	LASS1C	18781	19372	3.1%
SE26	36635	31315	-14.5%	LASS1E	22948	23487	2.3%
SE30	76599	58332	-23.8%	LASS2A	22627	23763	5.0%
SE31	43662	39171	-10.3%	LASS3B	19815	15849	-20.0%
SE32	32980	35692	8.2%	LASS3C	14288	13090	-8.4%
SE36	25909	30640	18.3%	LASS4C	15271	12088	-20.8%
				Averages	27880	24703	-8.8%

U- Undamped

D- Damped

Table B.6 Peak Rooftop Displacements and Damper Drift for BF-3, Linear Analysis Methods

Acc. History	U mm	D mm	% Change	DD mm	Acc. History	U mm	D mm	% Change	DD mm
LA01	66	55	-16.8%	174	BO05	38	23	-39.2%	53
LA02	70	79	12.7%	215	BO06	49	39	-20.1%	59
LA04	79	66	-17.3%	114	BO13	14	16	15.5%	27
LA12	121	85	-30.0%	192	BO16	10	7	-29.0%	19
LA15	83	71	-14.7%	220	BO18	18	18	2.8%	43
LA18	157	123	-21.8%	306	BO19	14	16	13.6%	43
LA20	108	90	-16.1%	231	BO20	35	27	-21.1%	72
LA21	143	129	-9.9%	601	BO21	40	33	-18.4%	80
LA22	154	120	-22.3%	654	BO22	70	52	-26.4%	120
LA23	60	64	6.1%	313	BO25	42	32	-25.1%	86
LA25	136	116	-14.7%	358	BO33	40	46	15.5%	79
LA28	255	200	-21.8%	498	BO34	63	58	-8.5%	112
LA30	127	107	-15.6%	414	BO35	119	87	-26.3%	221
LA37	77	67	-12.6%	317	BO36	29	20	-29.0%	54
SE04	51	38	-25.3%	95	NF01	111	102	-8.5%	299
SE05	48	49	0.9%	122	NF02	70	68	-3.2%	283
SE08	44	54	20.6%	232	NF11	38	46	20.3%	94
SE10	62	52	-16.2%	133	NF12	38	41	9.6%	97
SE12	51	55	7.9%	170	NF15	104	99	-4.2%	208
SE18	91	66	-27.0%	208	NF16	126	98	-21.6%	237
SE19	47	57	20.4%	341	LASS1A	58	63	9.4%	210
SE21	66	83	26.6%	450	LASS1B	50	57	13.5%	165
SE25	113	114	0.9%	285	LASS1C	48	56	17.6%	168
SE26	115	89	-22.1%	228	LASS1E	59	69	16.1%	209
SE30	214	156	-27.0%	489	LASS2A	57	72	26.2%	255
SE31	110	133	20.5%	801	LASS3B	52	44	-15.3%	99
SE32	92	101	9.3%	402	LASS3C	36	38	5.1%	87
SE36	59	94	58.9%	375	LASS4C	39	37	-7.2%	117
					Averages	76	69	-5.1%	224

U- Undamped
D- Damped
DD- Damper Drift

Table B.7 Peak Base Shear for BF-4, Linear Analysis Methods

Acc. History	U kN	D kN	% Change	Acc. History	U kN	D kN	% Change
LA01	33505	30130	-10.1%	BO05	4802	5438	13.3%
LA02	43330	37048	-14.5%	BO06	3531	3602	2.0%
LA04	11430	13516	18.2%	BO13	4033	3566	-11.6%
LA12	31578	30286	-4.1%	BO16	3416	3316	-2.9%
LA15	34249	30345	-11.4%	BO18	6489	4385	-32.4%
LA18	39032	34831	-10.8%	BO19	6227	4370	-29.8%
LA20	38400	34633	-9.8%	BO20	8967	7449	-16.9%
LA21	64441	61585	-4.4%	BO21	9335	12806	37.2%
LA22	83457	43133	-48.3%	BO22	12560	16231	29.2%
LA23	38617	22441	-41.9%	BO25	17424	13902	-20.2%
LA25	55739	49392	-11.4%	BO33	11540	10204	-11.6%
LA28	63532	56659	-10.8%	BO34	11081	9907	-10.6%
LA30	39840	49350	23.9%	BO35	38944	30463	-21.8%
LA37	47317	39305	-16.9%	BO36	9819	9527	-3.0%
SE04	13663	14672	7.4%	NF01	34516	33403	-3.2%
SE05	18609	19261	3.5%	NF02	42127	39693	-5.8%
SE08	25926	16867	-34.9%	NF11	20792	15263	-26.6%
SE10	22146	19959	-9.9%	NF12	13790	11875	-13.9%
SE12	30958	26064	-15.8%	NF15	19862	23750	19.6%
SE18	38139	25591	-32.9%	NF16	36495	29862	-18.2%
SE19	53965	39072	-27.6%	LASS1A	27385	27262	-0.4%
SE21	74340	43438	-41.6%	LASS1B	25040	21994	-12.2%
SE25	43483	44957	3.4%	LASS1C	25030	19289	-22.9%
SE26	47417	34320	-27.6%	LASS1E	30317	25428	-16.1%
SE30	89540	60045	-32.9%	LASS2A	42410	36639	-13.6%
SE31	126625	91729	-27.6%	LASS3B	20215	19812	-2.0%
SE32	63543	41277	-35.0%	LASS3C	19470	19295	-0.9%
SE36	47821	43861	-8.3%	LASS4C	13891	16528	19.0%
				Averages	32860	27304	-10.9%

U- Undamped

D- Damped

Table B.8 Peak Rooftop Displacements and Damper Drift for BF-4, Linear Analysis Methods

Acc. History	U mm	D mm	% Change	DD mm	Acc. History	U mm	D mm	% Change	DD mm
LA01	157	122	-22.2%	284	BO05	24	27	14.7%	38
LA02	205	163	-20.8%	397	BO06	24	21	-11.4%	31
LA04	53	63	17.2%	159	BO13	20	16	-22.9%	34
LA12	147	136	-7.8%	324	BO16	14	13	-11.7%	23
LA15	158	138	-12.7%	426	BO18	28	19	-31.8%	48
LA18	208	158	-23.9%	436	BO19	26	21	-21.0%	64
LA20	170	169	-0.5%	433	BO20	48	35	-26.9%	83
LA21	310	342	10.4%	1047	BO21	51	67	32.8%	133
LA22	374	266	-28.7%	995	BO22	72	67	-6.4%	133
LA23	178	101	-43.1%	354	BO25	80	61	-23.5%	156
LA25	257	224	-12.7%	694	BO33	58	45	-22.9%	98
LA28	338	257	-24.0%	710	BO34	55	45	-18.6%	101
LA30	210	176	-15.9%	380	BO35	177	129	-27.2%	332
LA37	218	185	-15.4%	532	BO36	41	36	-11.7%	67
SE04	70	75	7.1%	193	NF01	161	112	-30.4%	373
SE05	96	93	-3.6%	226	NF02	187	158	-15.7%	263
SE08	122	111	-9.4%	406	NF11	74	54	-26.5%	104
SE10	98	97	-0.5%	250	NF12	48	49	1.9%	149
SE12	149	109	-27.3%	213	NF15	118	125	6.2%	281
SE18	177	106	-39.8%	279	NF16	193	133	-31.2%	347
SE19	258	153	-40.6%	479	LASS1A	125	159	26.5%	420
SE21	357	227	-36.3%	761	LASS1B	114	120	5.2%	285
SE25	225	217	-3.6%	528	LASS1C	108	105	-2.3%	255
SE26	261	148	-43.3%	320	LASS1E	128	146	14.0%	374
SE30	415	249	-39.9%	656	LASS2A	205	194	-5.3%	461
SE31	604	359	-40.5%	1125	LASS3B	90	85	-5.8%	230
SE32	286	213	-25.5%	681	LASS3C	83	93	12.4%	228
SE36	222	258	16.1%	803	LASS4C	60	80	32.0%	203
					Averages	156	127	-12.4%	346

U- Undamped
D- Damped
DD- Damper Drift

Table B.9 Peak Base Shear for BF-5, Linear Analysis Methods

Acc. History	U kN	D kN	% Change	Acc. History	U kN	D kN	% Change
LA01	19325	12952	-33.0%	BO05	4026	3614	-10.2%
LA02	27724	20110	-27.5%	BO06	3875	4243	9.5%
LA04	11811	9980	-15.5%	BO13	2194	2007	-8.6%
LA12	17716	16817	-5.1%	BO16	1945	1466	-24.6%
LA15	27994	17619	-37.1%	BO18	2617	3295	25.9%
LA18	33093	26736	-19.2%	BO19	4178	2642	-36.7%
LA20	33415	26359	-21.1%	BO20	5287	4478	-15.3%
LA21	60196	55012	-8.6%	BO21	10185	8126	-20.2%
LA22	57087	39840	-30.2%	BO22	9047	7278	-19.6%
LA23	15098	25036	65.8%	BO25	8792	7061	-19.7%
LA25	45563	28671	-37.1%	BO33	6277	5744	-8.5%
LA28	53821	43496	-19.2%	BO34	7944	9134	15.0%
LA30	27408	27015	-1.4%	BO35	19390	13073	-32.6%
LA37	34170	29254	-14.4%	BO36	5589	4213	-24.6%
SE04	12921	9961	-22.9%	NF01	20695	32847	58.7%
SE05	11253	10081	-10.4%	NF02	19825	20646	4.1%
SE08	20469	18393	-10.1%	NF11	14057	16482	17.3%
SE10	19272	15206	-21.1%	NF12	11379	9515	-16.4%
SE12	13397	15533	15.9%	NF15	29798	22965	-22.9%
SE18	15272	11166	-26.9%	NF16	17725	21095	19.0%
SE19	25618	20193	-21.2%	LASS1A	31995	20332	-36.5%
SE21	30302	34459	13.7%	LASS1B	25232	19697	-21.9%
SE25	26265	23542	-10.4%	LASS1C	22249	18623	-16.3%
SE26	25445	17414	-31.6%	LASS1E	27298	17025	-37.6%
SE30	35837	26202	-26.9%	LASS2A	36851	23728	-35.6%
SE31	60102	47393	-21.1%	LASS3B	17829	16112	-9.6%
SE32	45485	26398	-42.0%	LASS3C	20905	16305	-22.0%
SE36	67163	37250	-44.5%	LASS4C	14441	14663	1.5%
				Averages	22765	18545	-13.4%

U- Undamped

D- Damped

Table B.10 Peak Rooftop Displacements and Damper Drift for BF-5, Linear Analysis Methods

Acc. History	U mm	D mm	% Change	DD mm	Acc. History	U mm	D mm	% Change	DD mm
LA01	235	223	-5.2%	325	BO05	45	37	-16.8%	55
LA02	382	215	-43.6%	425	BO06	32	30	-6.4%	41
LA04	169	115	-31.6%	198	BO13	26	19	-28.5%	39
LA12	203	159	-21.6%	244	BO16	22	16	-25.9%	24
LA15	410	307	-25.2%	518	BO18	32	26	-20.4%	46
LA18	323	403	24.7%	458	BO19	58	35	-38.5%	77
LA20	429	407	-5.0%	544	BO20	61	48	-22.3%	76
LA21	1025	834	-18.7%	1191	BO21	137	119	-13.2%	215
LA22	875	436	-50.2%	1120	BO22	107	96	-10.8%	165
LA23	261	410	57.2%	599	BO25	111	123	10.4%	200
LA25	667	499	-25.2%	843	BO33	75	54	-28.4%	111
LA28	526	655	24.6%	746	BO34	67	87	30.4%	113
LA30	286	346	20.7%	522	BO35	218	171	-21.8%	268
LA37	571	413	-27.7%	722	BO36	62	46	-25.9%	69
SE04	205	114	-44.7%	132	NF01	274	378	38.1%	518
SE05	155	154	-0.3%	234	NF02	289	242	-16.2%	355
SE08	312	190	-39.2%	439	NF11	177	219	23.8%	268
SE10	247	235	-5.0%	314	NF12	156	154	-1.3%	200
SE12	213	212	-0.3%	359	NF15	318	400	25.8%	522
SE18	236	208	-12.0%	271	NF16	250	327	30.7%	506
SE19	404	292	-27.7%	590	LASS1A	505	341	-32.5%	686
SE21	634	453	-28.6%	894	LASS1B	341	365	6.9%	583
SE25	361	360	-0.3%	546	LASS1C	302	338	11.9%	495
SE26	326	305	-6.5%	363	LASS1E	422	261	-38.1%	584
SE30	554	487	-12.0%	636	LASS2A	587	338	-42.4%	578
SE31	947	684	-27.7%	1385	LASS3B	261	199	-23.5%	225
SE32	733	351	-52.2%	705	LASS3C	289	209	-27.7%	212
SE36	1014	677	-33.3%	1260	LASS4C	191	253	32.7%	276
					Averages	324	269	-11.5%	430

U- Undamped
D- Damped
DD- Damper Drift

Table B.11 Peak Base Shear for EBF-1, Linear Analysis Methods

Acc. History	U kN	D kN	% Change	Acc. History	U kN	D kN	% Change
LA01	27430	22509	-17.9%	BO05	4827	5316	10.1%
LA02	31957	25210	-21.1%	BO06	3925	4094	4.3%
LA04	13200	14106	6.9%	BO13	3158	2756	-12.7%
LA12	25716	25134	-2.3%	BO16	2353	2236	-5.0%
LA15	20497	19531	-4.7%	BO18	4297	3576	-16.8%
LA18	31699	38101	20.2%	BO19	2514	2261	-10.1%
LA20	28675	24539	-14.4%	BO20	7859	7081	-9.9%
LA21	46592	47818	2.6%	BO21	11224	11054	-1.5%
LA22	36650	25247	-31.1%	BO22	14822	15189	2.5%
LA23	20543	18811	-8.4%	BO25	10507	9979	-5.0%
LA25	33364	31790	-4.7%	BO33	9038	7890	-12.7%
LA28	51567	61981	20.2%	BO34	10154	9989	-1.6%
LA30	40565	38060	-6.2%	BO35	29151	28396	-2.6%
LA37	27811	23690	-14.8%	BO36	6765	6428	-5.0%
SE04	9642	10838	12.4%	NF01	25381	26360	3.9%
SE05	15968	11587	-27.4%	NF02	31793	29398	-7.5%
SE08	15289	10990	-28.1%	NF11	10930	11721	7.2%
SE10	16527	14155	-14.4%	NF12	8019	7340	-8.5%
SE12	23067	19509	-15.4%	NF15	15388	22330	45.1%
SE18	22100	22341	1.1%	NF16	32245	33200	3.0%
SE19	35876	26838	-25.2%	LASS1A	15666	16096	2.7%
SE21	41397	33498	-19.1%	LASS1B	17632	21605	22.5%
SE25	37271	27062	-27.4%	LASS1C	13995	17002	21.5%
SE26	29437	24878	-15.5%	LASS1E	17045	20044	17.6%
SE30	51823	52400	1.1%	LASS2A	30863	22284	-27.8%
SE31	84208	62982	-25.2%	LASS3B	15124	15336	1.4%
SE32	40346	26205	-35.0%	LASS3C	12587	12942	2.8%
SE36	24896	22276	-10.5%	LASS4C	13035	15588	19.6%
				Averages	22579	20885	-4.8%

U- Undamped

D- Damped

Table B.12 Peak Rooftop Displacements and Damper Drift for EBF-1, Linear Analysis Methods

Acc. History	U mm	D mm	% Change	DD mm	Acc. History	U mm	D mm	% Change	DD mm
LA01	144	99	-31.2%	316	BO05	28	31	8.5%	43
LA02	167	122	-26.7%	271	BO06	24	25	4.9%	22
LA04	69	70	1.2%	172	BO13	17	13	-20.1%	26
LA12	141	114	-18.8%	179	BO16	14	13	-6.3%	21
LA15	105	92	-12.5%	394	BO18	20	15	-25.6%	28
LA18	172	213	23.8%	371	BO19	13	11	-19.0%	46
LA20	144	134	-6.7%	418	BO20	42	32	-22.4%	64
LA21	244	259	6.1%	824	BO21	57	64	13.1%	147
LA22	181	120	-33.5%	526	BO22	78	70	-10.8%	116
LA23	108	89	-18.0%	284	BO25	59	48	-19.1%	117
LA25	171	149	-12.5%	642	BO33	47	38	-20.1%	73
LA28	280	347	23.8%	603	BO34	56	57	1.6%	83
LA30	216	169	-22.0%	380	BO35	175	129	-26.6%	231
LA37	138	165	20.2%	531	BO36	40	37	-6.3%	59
SE04	60	54	-8.7%	141	NF01	132	145	9.9%	428
SE05	82	59	-28.4%	167	NF02	177	128	-27.4%	217
SE08	72	57	-21.8%	230	NF11	46	55	19.7%	231
SE10	83	77	-6.7%	241	NF12	38	40	7.4%	161
SE12	132	94	-28.9%	213	NF15	87	138	58.0%	381
SE18	112	113	0.7%	324	NF16	180	171	-4.9%	245
SE19	185	120	-35.4%	378	LASS1A	81	105	29.3%	478
SE21	207	155	-25.3%	604	LASS1B	93	125	34.9%	420
SE25	192	138	-28.3%	389	LASS1C	74	98	33.1%	358
SE26	159	139	-12.3%	361	LASS1E	95	111	17.4%	367
SE30	262	264	0.7%	760	LASS2A	160	118	-26.4%	520
SE31	435	281	-35.4%	887	LASS3B	76	77	2.0%	194
SE32	204	138	-32.1%	494	LASS3C	62	67	8.3%	187
SE36	119	162	36.2%	881	LASS4C	68	90	32.5%	210
					Averages	118	108	-5.1%	312

U- Undamped
D- Damped
DD- Damper Drift

Table B.13 Peak Base Shear for SW-1, Linear Analysis Methods

Acc. History	U kN	D kN	% Change	Acc. History	U kN	D kN	% Change
LA01	29716	26832	-9.7%	BO05	23548	20053	-14.8%
LA02	43538	44181	1.5%	BO06	26652	23024	-13.6%
LA04	50247	46631	-7.2%	BO13	14458	13789	-4.6%
LA12	55695	52131	-6.4%	BO16	5759	5398	-6.3%
LA15	42231	37935	-10.2%	BO18	14175	13763	-2.9%
LA18	89757	89174	-0.6%	BO19	11168	10541	-5.6%
LA20	65514	58988	-10.0%	BO20	20669	18584	-10.1%
LA21	97252	96820	-0.4%	BO21	23412	25136	7.4%
LA22	78084	76095	-2.5%	BO22	34622	30988	-10.5%
LA23	29222	23163	-20.7%	BO25	23486	20215	-13.9%
LA25	68731	61744	-10.2%	BO33	41387	39467	-4.6%
LA28	146002	145033	-0.7%	BO34	54054	53259	-1.5%
LA30	64099	66709	4.1%	BO35	56378	49475	-12.2%
LA37	41707	36352	-12.8%	BO36	16529	15508	-6.2%
SE04	32422	30782	-5.1%	NF01	59845	57318	-4.2%
SE05	36716	33690	-8.2%	NF02	41192	42754	3.8%
SE08	28577	25564	-10.5%	NF11	23052	23469	1.8%
SE10	37773	34015	-10.0%	NF12	35354	34572	-2.2%
SE12	47669	47413	-0.5%	NF15	72605	74917	3.2%
SE18	57411	49840	-13.2%	NF16	59340	54102	-8.8%
SE19	25009	24444	-2.3%	LASS1A	27850	28952	4.0%
SE21	35833	38059	6.2%	LASS1B	22876	22328	-2.4%
SE25	85725	78657	-8.2%	LASS1C	23471	20339	-13.3%
SE26	70794	68351	-3.5%	LASS1E	31077	30217	-2.8%
SE30	134676	116887	-13.2%	LASS2A	31511	29803	-5.4%
SE31	58710	57362	-2.3%	LASS3B	28016	25601	-8.6%
SE32	50850	52651	3.5%	LASS3C	19861	19913	0.3%
SE36	39191	44169	12.7%	LASS4C	26818	27380	2.1%
				Averages	44863	42759	-4.9%

U- Undamped

D- Damped

Table B.14 Peak Rooftop Displacements and Damper Drift for SW-1, Linear Analysis Methods

Acc. History	U mm	D mm	% Change	DD mm	Acc. History	U mm	D mm	% Change	DD mm
LA01	38	33	-12.3%	151	BO05	28	28	-2.2%	44
LA02	54	54	0.7%	311	BO06	36	30	-17.1%	46
LA04	67	61	-8.8%	103	BO13	22	20	-10.7%	28
LA12	83	75	-10.0%	172	BO16	8	8	0.7%	19
LA15	58	51	-11.9%	311	BO18	18	17	-6.0%	40
LA18	124	122	-1.4%	273	BO19	14	10	-28.7%	51
LA20	107	96	-10.2%	296	BO20	27	26	-6.3%	56
LA21	130	135	3.7%	755	BO21	36	38	6.5%	112
LA22	107	116	7.9%	675	BO22	47	41	-13.5%	93
LA23	38	33	-14.2%	221	BO25	36	29	-18.7%	99
LA25	94	83	-11.9%	507	BO33	64	57	-10.7%	79
LA28	202	199	-1.4%	445	BO34	80	75	-6.3%	97
LA30	97	92	-5.2%	210	BO35	79	75	-6.0%	161
LA37	55	53	-3.0%	369	BO36	22	22	0.7%	54
SE04	52	53	2.0%	129	NF01	77	72	-6.5%	242
SE05	49	43	-12.2%	145	NF02	66	66	-0.3%	190
SE08	40	42	5.1%	302	NF11	28	26	-7.6%	80
SE10	62	55	-10.2%	171	NF12	33	36	8.8%	106
SE12	58	53	-8.8%	150	NF15	97	104	7.2%	258
SE18	81	66	-18.2%	167	NF16	85	77	-10.2%	188
SE19	33	36	11.3%	320	LASS1A	41	40	-1.4%	362
SE21	40	50	25.1%	452	LASS1B	30	31	3.8%	241
SE25	115	101	-12.2%	338	LASS1C	29	26	-8.1%	223
SE26	112	95	-15.4%	228	LASS1E	45	42	-5.8%	309
SE30	190	155	-18.2%	391	LASS2A	37	50	36.3%	366
SE31	77	85	11.4%	751	LASS3B	36	35	-4.0%	167
SE32	58	64	11.2%	542	LASS3C	24	27	12.8%	189
SE36	51	69	34.7%	662	LASS4C	36	40	11.6%	171
					Averages	62	59	-2.8%	243

U- Undamped
D- Damped
DD- Damper Drift

Table B.15 Peak Base Shear for SW-2, Linear Analysis Methods

Acc. History	U kN	D kN	% Change	Acc. History	U kN	D kN	% Change
LA01	120086	111771	-6.9%	BO05	79750	71678	-10.1%
LA02	116209	107976	-7.1%	BO06	77099	78235	1.5%
LA04	145581	136453	-6.3%	BO13	23831	29870	25.3%
LA12	234796	208434	-11.2%	BO16	20460	15861	-22.5%
LA15	148846	135210	-9.2%	BO18	35776	35236	-1.5%
LA18	284656	276376	-2.9%	BO19	23834	21986	-7.8%
LA20	182524	191479	4.9%	BO20	58401	54404	-6.8%
LA21	296058	259148	-12.5%	BO21	65896	69487	5.4%
LA22	231406	267865	15.8%	BO22	116411	108554	-6.7%
LA23	104517	98825	-5.4%	BO25	72532	68309	-5.8%
LA25	242237	220036	-9.2%	BO33	68219	85510	25.3%
LA28	463107	449667	-2.9%	BO34	111910	90794	-18.9%
LA30	269657	206575	-23.4%	BO35	246787	213531	-13.5%
LA37	168409	142335	-15.5%	BO36	58762	45556	-22.5%
SE04	106637	75082	-29.6%	NF01	256877	202645	-21.1%
SE05	91606	79718	-13.0%	NF02	175563	163142	-7.1%
SE08	75315	72508	-3.7%	NF11	78359	75391	-3.8%
SE10	105306	110464	4.9%	NF12	77735	68279	-12.2%
SE12	92096	92703	0.7%	NF15	189018	198899	5.2%
SE18	159897	139211	-12.9%	NF16	219196	197382	-10.0%
SE19	98861	81132	-17.9%	LASS1A	117081	106443	-9.1%
SE21	147685	120758	-18.2%	LASS1B	101353	95874	-5.4%
SE25	213970	186021	-13.1%	LASS1C	94793	90943	-4.1%
SE26	175761	179629	2.2%	LASS1E	115423	107904	-6.5%
SE30	375054	326577	-12.9%	LASS2A	120408	106760	-11.3%
SE31	231762	190356	-17.9%	LASS3B	101074	91069	-9.9%
SE32	175420	189810	8.2%	LASS3C	75528	68114	-9.8%
SE36	145631	139309	-4.3%	LASS4C	82382	79634	-3.3%
				Averages	144063	132802	-6.9%

U- Undamped

D- Damped

Table B.16 Peak Rooftop Displacements and Damper Drift for SW-2, Linear Analysis Methods

Acc. History	U mm	D mm	% Change	DD mm	Acc. History	U mm	D mm	% Change	DD mm
LA01	72	62	-14.0%	150	BO05	43	34	-20.9%	59
LA02	78	79	1.0%	352	BO06	53	48	-10.6%	68
LA04	87	77	-11.4%	136	BO13	15	17	15.9%	30
LA12	135	104	-23.1%	179	BO16	12	9	-22.2%	20
LA15	91	81	-11.4%	299	BO18	21	17	-18.9%	38
LA18	174	170	-2.2%	317	BO19	15	15	-3.6%	53
LA20	122	100	-18.1%	304	BO20	39	35	-8.0%	68
LA21	161	180	11.9%	761	BO21	43	47	7.5%	111
LA22	163	186	14.0%	712	BO22	78	66	-16.0%	124
LA23	68	65	-5.1%	241	BO25	47	38	-20.5%	108
LA25	149	132	-11.4%	486	BO33	43	50	15.9%	86
LA28	282	276	-2.2%	515	BO34	72	60	-16.9%	96
LA30	145	124	-14.2%	241	BO35	138	125	-9.4%	195
LA37	87	87	0.6%	398	BO36	34	27	-22.2%	58
SE04	66	50	-24.2%	143	NF01	119	111	-6.3%	256
SE05	52	50	-4.9%	150	NF02	80	69	-13.9%	205
SE08	49	48	-2.5%	295	NF11	45	45	-0.8%	94
SE10	71	58	-18.2%	175	NF12	41	49	16.9%	109
SE12	57	54	-5.0%	162	NF15	112	128	14.1%	235
SE18	104	85	-18.2%	167	NF16	143	119	-16.6%	228
SE19	56	56	-0.5%	328	LASS1A	62	65	3.6%	393
SE21	75	74	-1.8%	485	LASS1B	54	54	-1.3%	272
SE25	122	116	-4.9%	349	LASS1C	52	51	-0.7%	250
SE26	127	110	-13.8%	270	LASS1E	63	60	-4.1%	341
SE30	244	200	-18.2%	393	LASS2A	66	72	8.7%	408
SE31	131	130	-0.4%	770	LASS3B	58	50	-13.9%	179
SE32	109	125	14.3%	582	LASS3C	41	42	3.5%	195
SE36	65	97	49.2%	694	LASS4C	44	47	6.4%	178
					Averages	85	81	-4.8%	259

U- Undamped
D- Damped
DD- Damper Drift

Table B.17 Peak Base Shear for MF-1, Linear Analysis Methods

Acc. History	U kN	D kN	% Change	Acc. History	U kN	D kN	% Change
LA01	11380	12571	10.5%	BO05	1594	1797	12.7%
LA02	11245	11669	3.8%	BO06	1825	1265	-30.7%
LA04	6548	8020	22.5%	BO13	958	691	-27.9%
LA12	8623	6748	-21.7%	BO16	642	747	16.2%
LA15	13755	12684	-7.8%	BO18	950	768	-19.1%
LA18	22794	19562	-14.2%	BO19	1506	1405	-6.7%
LA20	19375	17409	-10.1%	BO20	2207	2061	-6.6%
LA21	43541	28605	-34.3%	BO21	7096	6020	-15.2%
LA22	18165	22096	21.6%	BO22	5823	4297	-26.2%
LA23	19023	12323	-35.2%	BO25	6888	4593	-33.3%
LA25	22387	20645	-7.8%	BO33	2739	1977	-27.8%
LA28	37072	31815	-14.2%	BO34	3881	2047	-47.3%
LA30	17061	19187	12.5%	BO35	8021	7218	-10.0%
LA37	28067	25260	-10.0%	BO36	1851	2145	15.9%
SE04	5837	5762	-1.3%	NF01	18002	19898	10.5%
SE05	6597	7255	10.0%	NF02	8769	10064	14.8%
SE08	7542	8395	11.3%	NF11	11504	11604	0.9%
SE10	11178	10041	-10.2%	NF12	7493	6410	-14.5%
SE12	11660	7794	-33.2%	NF15	22205	18361	-17.3%
SE18	14994	13097	-12.7%	NF16	12302	9685	-21.3%
SE19	13193	11715	-11.2%	LASS1A	23622	19265	-18.4%
SE21	22079	20889	-5.4%	LASS1B	23724	17712	-25.3%
SE25	15402	16946	10.0%	LASS1C	18790	13777	-26.7%
SE26	16562	17000	2.6%	LASS1E	17251	13389	-22.4%
SE30	35183	30727	-12.7%	LASS2A	20631	23546	14.1%
SE31	30931	27499	-11.1%	LASS3B	9517	15122	58.9%
SE32	15075	16227	7.6%	LASS3C	10575	18873	78.5%
SE36	38912	36214	-6.9%	LASS4C	10804	15067	39.5%
				Averages	14024	12999	-5.0%

U- Undamped

D- Damped

Table B.18 Peak Rooftop Displacements and Damper Drift for MF-1, Linear Analysis Methods

Acc. History	U mm	D mm	% Change	DD mm	Acc. History	U mm	D mm	% Change	DD mm
LA01	324	340	5.1%	749	BO05	32	27	-13.0%	48
LA02	249	356	43.1%	727	BO06	22	12	-44.1%	26
LA04	162	226	39.7%	520	BO13	25	16	-37.3%	31
LA12	201	167	-17.1%	347	BO16	16	11	-27.3%	19
LA15	471	337	-28.5%	676	BO18	29	23	-19.9%	31
LA18	495	353	-28.8%	1054	BO19	46	38	-18.5%	58
LA20	510	372	-27.0%	961	BO20	43	44	2.0%	61
LA21	1166	738	-36.7%	1466	BO21	211	146	-30.8%	291
LA22	537	624	16.4%	1078	BO22	159	130	-18.6%	252
LA23	498	339	-32.0%	691	BO25	171	94	-44.8%	177
LA25	767	549	-28.5%	1101	BO33	71	44	-37.3%	88
LA28	805	573	-28.8%	1714	BO34	70	42	-40.0%	113
LA30	448	504	12.6%	1021	BO35	180	154	-14.5%	233
LA37	691	616	-10.8%	1377	BO36	45	33	-27.4%	56
SE04	149	150	0.9%	352	NF01	479	485	1.3%	1054
SE05	159	179	12.8%	347	NF02	271	311	14.9%	663
SE08	231	194	-16.1%	349	NF11	325	323	-0.4%	599
SE10	294	215	-27.0%	554	NF12	211	155	-26.3%	341
SE12	340	201	-40.8%	384	NF15	565	460	-18.6%	1201
SE18	363	269	-26.1%	436	NF16	314	162	-48.2%	425
SE19	433	307	-29.1%	423	LASS1A	638	434	-32.0%	887
SE21	633	590	-6.8%	1200	LASS1B	643	391	-39.2%	881
SE25	371	419	12.8%	811	LASS1C	510	356	-30.1%	839
SE26	373	426	14.4%	878	LASS1E	469	313	-33.3%	667
SE30	852	630	-26.1%	1023	LASS2A	523	693	32.7%	1537
SE31	1015	720	-29.0%	995	LASS3B	269	512	90.1%	1261
SE32	486	449	-7.5%	652	LASS3C	284	624	119.8%	1429
SE36	1080	843	-22.0%	1395	LASS4C	285	422	48.4%	1049
					Averages	375	324	-10.8%	671

U- Undamped
D- Damped
DD- Damper Drift

Table B.19 Peak Base Shear for MF-2, Linear Analysis Methods.

Acc. History	U kN	D kN	% Change	Acc. History	U kN	D kN	% Change
LA01	49191	26393	-46.3%	BO05	5250	5324	1.4%
LA02	40753	27886	-31.6%	BO06	4078	4161	2.0%
LA04	32944	26259	-20.3%	BO13	3356	3230	-3.7%
LA12	20457	19163	-6.3%	BO16	2154	1545	-28.3%
LA15	35593	33905	-4.7%	BO18	4039	3288	-18.6%
LA18	63454	51768	-18.4%	BO19	3957	3529	-10.8%
LA20	63601	44465	-30.1%	BO20	6583	6356	-3.4%
LA21	96493	88878	-7.9%	BO21	12189	13146	7.9%
LA22	79354	64220	-19.1%	BO22	12364	10630	-14.0%
LA23	44563	45666	2.5%	BO25	8827	11627	31.7%
LA25	57922	55177	-4.7%	BO33	9592	9235	-3.7%
LA28	103215	84200	-18.4%	BO34	14643	14828	1.3%
LA30	78487	71440	-9.0%	BO35	20281	18653	-8.0%
LA37	82450	65175	-21.0%	BO36	6192	4442	-28.3%
SE04	19649	16144	-17.8%	NF01	76088	57253	-24.8%
SE05	22572	16223	-28.1%	NF02	49055	46461	-5.3%
SE08	19228	16349	-15.0%	NF11	31627	40953	29.5%
SE10	36676	25633	-30.1%	NF12	17269	17582	1.8%
SE12	21498	17258	-19.7%	NF15	66740	51363	-23.0%
SE18	26168	22949	-12.3%	NF16	40432	42756	5.7%
SE19	39732	39038	-1.7%	LASS1A	49432	37679	-23.8%
SE21	97473	67746	-30.5%	LASS1B	58235	43518	-25.3%
SE25	52710	37920	-28.1%	LASS1C	62111	48727	-21.5%
SE26	47095	53124	12.8%	LASS1E	42680	34454	-19.3%
SE30	61435	53930	-12.2%	LASS2A	72517	58222	-19.7%
SE31	93272	91603	-1.8%	LASS3B	70114	46516	-33.7%
SE32	41839	34450	-17.7%	LASS3C	79496	51232	-35.6%
SE36	52274	51981	-0.6%	LASS4C	52448	33333	-36.4%
				Averages	42176	35160	-13.3%

U- Undamped

D- Damped

Table B.20 Peak Rooftop Displacements and Damper Drift for MF-2, Linear Analysis Methods

Acc. History	U mm	D mm	% Change	DD mm	Acc. History	U mm	D mm	% Change	DD mm
LA01	667	350	-47.6%	888	BO05	36	33	-9.1%	44
LA02	421	308	-26.8%	624	BO06	26	26	1.9%	48
LA04	339	294	-13.4%	1052	BO13	34	29	-13.4%	47
LA12	176	245	39.3%	479	BO16	17	11	-37.2%	16
LA15	517	377	-27.1%	679	BO18	25	24	-3.6%	28
LA18	785	530	-32.5%	1273	BO19	49	42	-12.8%	44
LA20	740	437	-40.9%	1031	BO20	48	42	-11.9%	50
LA21	1051	868	-17.4%	1610	BO21	177	143	-19.3%	246
LA22	620	746	20.3%	1518	BO22	166	95	-42.6%	172
LA23	556	444	-20.2%	892	BO25	135	156	15.6%	165
LA25	841	613	-27.1%	1105	BO33	97	84	-13.3%	133
LA28	1276	861	-32.5%	2070	BO34	148	125	-15.2%	171
LA30	1035	857	-17.2%	1488	BO35	146	113	-22.5%	153
LA37	1104	918	-16.9%	2183	BO36	48	30	-37.1%	46
SE04	214	186	-12.9%	419	NF01	843	616	-26.9%	1311
SE05	244	178	-26.9%	424	NF02	569	579	1.8%	1151
SE08	230	195	-15.2%	238	NF11	429	560	30.7%	1238
SE10	427	252	-41.0%	595	NF12	245	197	-19.8%	373
SE12	271	203	-25.1%	296	NF15	876	604	-31.0%	1494
SE18	312	258	-17.5%	361	NF16	474	436	-8.0%	595
SE19	324	326	0.7%	607	LASS1A	646	435	-32.6%	724
SE21	969	801	-17.4%	1701	LASS1B	720	424	-41.0%	904
SE25	570	417	-26.9%	990	LASS1C	774	454	-41.3%	936
SE26	534	523	-2.1%	1199	LASS1E	547	387	-29.2%	635
SE30	733	605	-17.4%	847	LASS2A	1035	649	-37.3%	1243
SE31	761	767	0.8%	1426	LASS3B	734	744	1.4%	2245
SE32	422	361	-14.4%	421	LASS3C	849	808	-4.8%	2684
SE36	1014	829	-18.2%	1133	LASS4C	681	365	-46.3%	1142
					Averages	495	392	-17.8%	814

U- Undamped
D- Damped
DD- Damper Drift

APPENDIX C

NONLINEAR ANALYSES OUTPUT

Tables C.1 through C.20 list the output values of peak output parameters results listed in Chapter 5. Values shown reflect the peak rooftop displacements and the peak base shears for the undamped and damped cases. Also shown are the percent changes from the undamped to damped cases along with the peak drift of the NRTMDF for each damped case.

Table C.1 Peak Base Shear for BF-1, Nonlinear Analysis Methods.

Acc. History	U kN	D kN	% Change	Acc. History	U kN	D kN	% Change
LA01	3695	3669	-0.7%	BO05	3662	3475	-5.1%
LA02	3771	3699	-1.9%	BO06	2630	2360	-10.3%
LA04	3694	3682	-0.3%	BO13	2455	2107	-14.2%
LA12	3911	3861	-1.3%	BO16	3297	2070	-37.2%
LA15	3696	3693	-0.1%	BO18	3062	2406	-21.4%
LA18	3743	3723	-0.5%	BO19	2518	2187	-13.2%
LA20	3873	3812	-1.6%	BO20	2356	2451	4.0%
LA21	3724	3760	1.0%	BO21	3656	2887	-21.1%
LA22	3700	3726	0.7%	BO22	3667	3654	-0.3%
LA23	3089	3654	18.3%	BO25	2848	3650	28.2%
LA25	3772	3747	-0.7%	BO33	3715	3684	-0.9%
LA28	3848	3835	-0.3%	BO34	3826	3765	-1.6%
LA30	3996	3904	-2.3%	BO35	3964	3885	-2.0%
LA37	3669	3691	0.6%	BO36	3764	3687	-2.0%
SE04	3730	3690	-1.1%	NF01	3965	3839	-3.2%
SE05	3660	3735	2.1%	NF02	3917	3842	-1.9%
SE08	3652	3848	5.4%	NF11	3694	3670	-0.7%
SE10	3747	3707	-1.1%	NF12	3720	3655	-1.7%
SE12	3726	3673	-1.4%	NF15	3730	3706	-0.6%
SE18	3743	3703	-1.1%	NF16	3702	3702	0.0%
SE19	3694	3674	-0.6%	LASS1A	3671	3664	-0.2%
SE21	3669	3704	1.0%	LASS1B	3651	3217	-11.9%
SE25	3773	3732	-1.1%	LASS1C	3541	3275	-7.5%
SE26	3799	3746	-1.4%	LASS1E	3688	3660	-0.8%
SE30	3970	3926	-1.1%	LASS2A	3680	3677	-0.1%
SE31	3855	3818	-1.0%	LASS3B	2225	2683	20.6%
SE32	3777	3756	-0.6%	LASS3C	2366	2713	14.7%
SE36	3726	3725	0.0%	LASS4C	3098	2624	-15.3%
				Averages	3549	3484	-1.7%

U- Undamped

D- Damped

Table C.2 Peak Rooftop Displacements and Damper Drift for BF-1, Nonlinear Analysis Methods

Acc. History	U mm	D mm	% Change	DD mm	Acc. History	U mm	D mm	% Change	DD mm
LA01	21	17	-22.0%	56	BO05	16	13	-16.7%	33
LA02	35	22	-36.8%	98	BO06	9	10	7.3%	34
LA04	21	19	-10.3%	76	BO13	9	7	-22.3%	20
LA12	60	51	-15.1%	98	BO16	12	6	-46.4%	14
LA15	22	21	-2.2%	100	BO18	11	8	-27.4%	24
LA18	30	26	-11.6%	123	BO19	9	6	-29.8%	19
LA20	53	42	-20.5%	109	BO20	8	10	17.1%	30
LA21	26	33	24.8%	318	BO21	15	11	-24.6%	45
LA22	22	27	21.1%	236	BO22	16	14	-13.4%	73
LA23	10	14	39.9%	51	BO25	10	13	34.8%	55
LA25	35	31	-12.7%	189	BO33	25	19	-22.5%	65
LA28	49	46	-4.7%	250	BO34	45	34	-24.3%	64
LA30	75	58	-21.9%	193	BO35	69	55	-20.3%	113
LA37	17	21	22.5%	153	BO36	34	20	-40.7%	41
SE04	28	20	-26.1%	57	NF01	69	47	-32.3%	126
SE05	15	13	-16.2%	57	NF02	61	48	-21.7%	95
SE08	14	13	-4.5%	36	NF11	21	17	-20.5%	62
SE10	31	24	-23.0%	58	NF12	26	14	-44.8%	40
SE12	27	17	-35.0%	56	NF15	28	23	-15.5%	129
SE18	30	23	-24.2%	79	NF16	23	23	-0.4%	90
SE19	21	18	-17.2%	48	LASS1A	17	16	-7.3%	82
SE21	17	23	37.6%	96	LASS1B	14	12	-11.8%	55
SE25	35	28	-20.7%	117	LASS1C	12	12	3.8%	50
SE26	40	30	-23.7%	134	LASS1E	20	15	-24.6%	75
SE30	70	62	-11.2%	187	LASS2A	19	18	-3.2%	54
SE31	50	43	-13.2%	245	LASS3B	7	11	43.4%	42
SE32	36	32	-10.6%	131	LASS3C	8	10	31.2%	30
SE36	27	27	-0.5%	84	LASS4C	11	10	-4.3%	39
					Averages	27	23	-10.3%	90

U- Undamped
D- Damped
DD- Damper Drift

Table C.3 Peak Base Shear for BF-2, Nonlinear Analysis Methods.

Acc. History	U kN	D kN	% Change	Acc. History	U kN	D kN	% Change
LA01	7016	6698	-4.5%	BO05	7094	5821	-17.9%
LA02	8316	7953	-4.4%	BO06	6268	5447	-13.1%
LA04	8266	7047	-14.8%	BO13	5358	5316	-0.8%
LA12	8555	8381	-2.0%	BO16	5040	5231	3.8%
LA15	8216	7250	-11.8%	BO18	5654	5195	-8.1%
LA18	8860	8640	-2.5%	BO19	4146	5063	22.1%
LA20	9184	8676	-5.5%	BO20	5581	5516	-1.2%
LA21	8518	8505	-0.2%	BO21	6782	5616	-17.2%
LA22	8265	8383	1.4%	BO22	6615	6396	-3.3%
LA23	6735	6985	3.7%	BO25	5799	5624	-3.0%
LA25	8642	8410	-2.7%	BO33	7889	7579	-3.9%
LA28	9681	9410	-2.8%	BO34	8604	7664	-10.9%
LA30	8713	8602	-1.3%	BO35	8549	8567	0.2%
LA37	8049	8152	1.3%	BO36	6991	7413	6.0%
SE04	8353	8135	-2.6%	NF01	8489	8378	-1.3%
SE05	8175	6993	-14.5%	NF02	8435	8342	-1.1%
SE08	7809	7042	-9.8%	NF11	7358	6925	-5.9%
SE10	8520	7727	-9.3%	NF12	7393	6238	-15.6%
SE12	8245	7809	-5.3%	NF15	8686	8410	-3.2%
SE18	8452	8243	-2.5%	NF16	8458	8210	-2.9%
SE19	7718	7605	-1.5%	LASS1A	7497	6568	-12.4%
SE21	7780	8172	5.0%	LASS1B	6542	6557	0.2%
SE25	9021	8669	-3.9%	LASS1C	6159	6313	2.5%
SE26	8687	8362	-3.7%	LASS1E	8094	6955	-14.1%
SE30	9599	9071	-5.5%	LASS2A	7117	7252	1.9%
SE31	8833	8629	-2.3%	LASS3B	6149	6202	0.9%
SE32	8218	8397	2.2%	LASS3C	5575	6122	9.8%
SE36	7312	8173	11.8%	LASS4C	6062	5795	-4.4%
				Averages	7609	7336	-3.2%

U- Undamped

D- Damped

Table C.4 Peak Rooftop Displacements and Damper Drift for BF-2, Nonlinear Analysis Methods

Acc. History	U mm	D mm	% Change	DD mm	Acc. History	U mm	D mm	% Change	DD mm
LA01	22	20	-10.5%	96	BO05	22	13	-41.1%	39
LA02	37	29	-21.5%	135	BO06	16	7	-57.1%	30
LA04	35	22	-36.3%	76	BO13	10	10	-3.1%	22
LA12	49	39	-20.3%	131	BO16	8	9	18.4%	16
LA15	33	24	-28.2%	122	BO18	12	9	-27.7%	20
LA18	65	53	-17.6%	224	BO19	6	8	28.3%	16
LA20	82	55	-32.3%	146	BO20	11	11	-4.1%	44
LA21	47	46	-1.4%	461	BO21	20	12	-41.9%	42
LA22	35	39	12.7%	255	BO22	19	17	-8.4%	78
LA23	20	22	9.1%	86	BO25	13	12	-9.7%	42
LA25	53	41	-22.6%	225	BO33	28	26	-8.0%	68
LA28	105	93	-11.4%	430	BO34	52	27	-48.3%	71
LA30	57	51	-10.0%	148	BO35	49	50	2.0%	183
LA37	29	31	3.8%	202	BO36	22	25	14.1%	43
SE04	38	30	-20.6%	62	NF01	46	39	-14.6%	124
SE05	31	22	-30.7%	58	NF02	43	38	-12.0%	95
SE08	28	22	-20.1%	70	NF11	24	21	-12.9%	60
SE10	47	27	-42.6%	71	NF12	25	16	-34.0%	53
SE12	34	28	-18.6%	67	NF15	56	41	-26.9%	188
SE18	44	34	-22.2%	94	NF16	44	33	-25.7%	134
SE19	27	26	-3.0%	89	LASS1A	25	19	-26.5%	62
SE21	27	31	13.8%	172	LASS1B	18	19	0.6%	80
SE25	73	55	-25.0%	135	LASS1C	16	17	7.2%	56
SE26	56	38	-31.4%	139	LASS1E	30	21	-27.8%	78
SE30	102	76	-25.9%	248	LASS2A	23	24	4.3%	110
SE31	63	53	-16.7%	362	LASS3B	16	16	2.5%	65
SE32	33	40	20.1%	154	LASS3C	11	15	34.7%	54
SE36	24	31	30.1%	201	LASS4C	15	13	-13.0%	56
					Averages	35	29	-12.7%	118

U- Undamped
D- Damped
DD- Damper Drift

Table C.5 Peak Base Shear for BF-3, Nonlinear Analysis Methods.

Acc. History	U kN	D kN	% Change	Acc. History	U kN	D kN	% Change
LA01	10462	10422	-0.4%	BO05	10374	7333	-29.3%
LA02	10475	10417	-0.6%	BO06	10410	6702	-35.6%
LA04	10503	10400	-1.0%	BO13	5177	4855	-6.2%
LA12	10633	10499	-1.3%	BO16	3977	2915	-26.7%
LA15	10516	10451	-0.6%	BO18	6948	6931	-0.2%
LA18	10743	10666	-0.7%	BO19	4469	4770	6.7%
LA20	10592	10503	-0.8%	BO20	10366	7758	-25.2%
LA21	10700	10586	-1.1%	BO21	10382	9143	-11.9%
LA22	10735	10549	-1.7%	BO22	10475	10379	-0.9%
LA23	10445	10432	-0.1%	BO25	10389	10090	-2.9%
LA25	10677	10588	-0.8%	BO33	10383	12055	16.1%
LA28	11046	10957	-0.8%	BO34	10454	10401	-0.5%
LA30	10651	10558	-0.9%	BO35	10625	10548	-0.7%
LA37	10495	10486	-0.1%	BO36	11422	7991	-30.0%
SE04	10417	10388	-0.3%	NF01	10602	10477	-1.2%
SE05	10408	10386	-0.2%	NF02	10475	10458	-0.2%
SE08	10396	10380	-0.1%	NF11	10377	11170	7.6%
SE10	10451	10380	-0.7%	NF12	10375	11068	6.7%
SE12	10416	10406	-0.1%	NF15	10578	10519	-0.6%
SE18	10539	10415	-1.2%	NF16	10646	10567	-0.7%
SE19	10404	10410	0.1%	LASS1A	10437	10424	-0.1%
SE21	10462	10454	-0.1%	LASS1B	10414	10391	-0.2%
SE25	10607	10504	-1.0%	LASS1C	10407	10399	-0.1%
SE26	10613	10574	-0.4%	LASS1E	10441	10421	-0.2%
SE30	10917	10713	-1.9%	LASS2A	10434	10420	-0.1%
SE31	10599	10542	-0.5%	LASS3B	10419	10366	-0.5%
SE32	10543	10498	-0.4%	LASS3C	10370	10371	0.0%
SE36	10440	10459	0.2%	LASS4C	10380	9919	-4.4%
				Averages	10145	9873	-2.8%

U- Undamped

D- Damped

Table C.6 Peak Rooftop Displacements and Damper Drift for BF-3, Nonlinear Analysis Methods

Acc. History	U mm	D mm	% Change	DD mm	Acc. History	U mm	D mm	% Change	DD mm
LA01	66	53	-19.6%	183	BO05	38	16	-56.1%	40
LA02	70	51	-26.8%	135	BO06	49	14	-72.1%	34
LA04	79	46	-42.1%	119	BO13	14	14	-1.0%	26
LA12	122	78	-36.0%	135	BO16	10	7	-31.7%	15
LA15	83	63	-25.1%	257	BO18	18	18	0.4%	35
LA18	157	132	-15.9%	412	BO19	14	11	-23.3%	22
LA20	108	79	-26.6%	193	BO20	35	20	-42.0%	54
LA21	143	106	-25.7%	458	BO21	40	23	-43.3%	69
LA22	154	94	-39.1%	360	BO22	70	39	-44.4%	88
LA23	60	56	-6.8%	214	BO25	42	30	-29.7%	61
LA25	136	107	-21.4%	432	BO33	40	30	-26.0%	55
LA28	255	226	-11.3%	718	BO34	63	46	-27.1%	72
LA30	127	97	-23.6%	307	BO35	119	94	-21.1%	154
LA37	77	74	-4.1%	369	BO36	29	18	-36.5%	48
SE04	51	42	-18.7%	51	NF01	112	71	-36.5%	175
SE05	48	41	-14.9%	99	NF02	70	65	-8.0%	193
SE08	44	40	-11.1%	137	NF11	38	24	-37.9%	79
SE10	62	39	-36.8%	99	NF12	38	28	-25.3%	42
SE12	51	48	-6.2%	154	NF15	104	84	-18.6%	338
SE18	91	51	-44.2%	183	NF16	126	100	-20.4%	176
SE19	47	49	4.3%	148	LASS1A	58	54	-7.2%	107
SE21	66	63	-3.8%	238	LASS1B	50	43	-14.8%	103
SE25	113	79	-29.7%	300	LASS1C	48	46	-5.0%	104
SE26	115	102	-11.0%	280	LASS1E	59	53	-10.8%	102
SE30	214	147	-31.1%	379	LASS2A	57	52	-7.5%	175
SE31	110	92	-16.7%	523	LASS3B	52	35	-33.3%	109
SE32	92	78	-16.0%	266	LASS3C	36	36	0.7%	89
SE36	59	65	10.5%	361	LASS4C	39	26	-33.7%	83
					Averages	76	59	-22.5%	181

U- Undamped
D- Damped
DD- Damper Drift

Table C.7 Peak Base Shear for BF-4, Nonlinear Analysis Methods.

Acc. History	U kN	D kN	% Change	Acc. History	U kN	D kN	% Change
LA01	12425	12312	-0.9%	BO05	4992	7582	51.9%
LA02	12524	12376	-1.2%	BO06	3496	4830	38.1%
LA04	12784	13423	5.0%	BO13	4113	3256	-20.8%
LA12	12405	12319	-0.7%	BO16	3253	3649	12.2%
LA15	12427	12402	-0.2%	BO18	7295	3356	-54.0%
LA18	12529	12444	-0.7%	BO19	6373	4781	-25.0%
LA20	12452	12390	-0.5%	BO20	9348	6990	-25.2%
LA21	12735	12588	-1.2%	BO21	9201	10956	19.1%
LA22	12864	12723	-1.1%	BO22	12252	9945	-18.8%
LA23	12467	12311	-1.2%	BO25	12269	8763	-28.6%
LA25	12628	12558	-0.5%	BO33	11768	8196	-30.4%
LA28	12794	12684	-0.9%	BO34	11511	9014	-21.7%
LA30	12533	12480	-0.4%	BO35	12466	12359	-0.9%
LA37	12550	12515	-0.3%	BO36	9350	9509	1.7%
SE04	12248	12241	-0.1%	NF01	12433	12385	-0.4%
SE05	12302	12239	-0.5%	NF02	12487	12410	-0.6%
SE08	12354	12276	-0.6%	NF11	12256	12233	-0.2%
SE10	12306	12269	-0.3%	NF12	12782	9647	-24.5%
SE12	12410	12272	-1.1%	NF15	12346	12308	-0.3%
SE18	10775	10202	-5.3%	NF16	12499	12379	-1.0%
SE19	12629	12370	-2.0%	LASS1A	12361	12325	-0.3%
SE21	12831	12694	-1.1%	LASS1B	12337	12296	-0.3%
SE25	12562	12425	-1.1%	LASS1C	12325	12291	-0.3%
SE26	12636	12339	-2.4%	LASS1E	12366	12298	-0.5%
SE30	12949	12641	-2.4%	LASS2A	12523	12369	-1.2%
SE31	13333	13023	-2.3%	LASS3B	12288	12269	-0.2%
SE32	12686	12425	-2.1%	LASS3C	12274	12291	0.1%
SE36	12557	12426	-1.0%	LASS4C	14403	12299	-14.6%
				Averages	11501	11078	-3.1%

U- Undamped

D- Damped

Table C.8 Peak Rooftop Displacements and Damper Drift for BF-4, Nonlinear Analysis Methods

Acc. History	U mm	D mm	% Change	DD mm	Acc. History	U mm	D mm	% Change	DD mm
LA01	157	101	-35.5%	194	BO05	24	28	16.8%	37
LA02	206	133	-35.4%	254	BO06	24	20	-15.4%	26
LA04	53	74	39.3%	176	BO13	20	15	-27.3%	21
LA12	147	105	-28.8%	162	BO16	14	11	-22.1%	17
LA15	158	146	-7.7%	487	BO18	28	22	-18.6%	27
LA18	208	166	-20.1%	363	BO19	26	34	29.9%	32
LA20	170	140	-17.9%	338	BO20	48	34	-29.8%	51
LA21	310	237	-23.3%	652	BO21	51	51	0.9%	82
LA22	373	304	-18.6%	582	BO22	72	50	-30.2%	108
LA23	178	101	-43.0%	213	BO25	80	45	-43.3%	69
LA25	257	223	-13.3%	755	BO33	58	42	-27.1%	78
LA28	339	284	-16.0%	706	BO34	55	43	-22.9%	89
LA30	210	184	-12.3%	593	BO35	177	124	-29.9%	237
LA37	218	201	-7.8%	619	BO36	41	33	-19.4%	43
SE04	70	66	-4.7%	122	NF01	161	138	-14.5%	325
SE05	96	65	-32.1%	144	NF02	187	150	-20.2%	250
SE08	122	83	-31.6%	157	NF11	74	62	-15.5%	132
SE10	98	80	-18.5%	197	NF12	48	50	4.9%	73
SE12	150	82	-45.4%	213	NF15	118	99	-15.9%	342
SE18	177	66	-62.9%	179	NF16	194	134	-30.6%	253
SE19	258	130	-49.5%	355	LASS1A	125	108	-13.8%	350
SE21	357	289	-18.9%	641	LASS1B	114	93	-17.9%	254
SE25	225	157	-30.2%	383	LASS1C	108	91	-15.3%	278
SE26	261	115	-56.1%	246	LASS1E	128	95	-26.0%	250
SE30	415	263	-36.5%	404	LASS2A	205	130	-37.0%	279
SE31	604	451	-25.3%	613	LASS3B	90	80	-10.5%	256
SE32	286	157	-44.9%	356	LASS3C	83	91	10.0%	274
SE36	222	158	-29.0%	720	LASS4C	60	95	57.4%	177
					Averages	156	117	-19.8%	272

U- Undamped
D- Damped
DD- Damper Drift

Table C.9 Peak Base Shear for BF-5, Nonlinear Analysis Methods.

Acc. History	U kN	D kN	% Change	Acc. History	U kN	D kN	% Change
LA01	19086	12589	-34.0%	BO05	4231	3268	-22.8%
LA02	14292	15945	11.6%	BO06	3881	4182	7.7%
LA04	11929	9237	-22.6%	BO13	1914	2133	11.5%
LA12	16674	9950	-40.3%	BO16	2212	1417	-36.0%
LA15	14545	19456	33.8%	BO18	2776	2806	1.0%
LA18	34206	28593	-16.4%	BO19	4048	2481	-38.7%
LA20	14545	26701	83.6%	BO20	5453	4316	-20.8%
LA21	15122	15107	-0.1%	BO21	10636	6406	-39.8%
LA22	15111	15103	-0.1%	BO22	9219	4755	-48.4%
LA23	15191	13653	-10.1%	BO25	8780	6538	-25.5%
LA25	15097	15087	-0.1%	BO33	5474	5017	-8.4%
LA28	15087	14545	-3.6%	BO34	7919	7070	-10.7%
LA30	28961	28145	-2.8%	BO35	18964	13213	-30.3%
LA37	15090	14545	-3.6%	BO36	6356	4068	-36.0%
SE04	13124	7505	-42.8%	NF01	22102	24849	12.4%
SE05	11556	7113	-38.4%	NF02	20541	16861	-17.9%
SE08	20301	11273	-44.5%	NF11	14661	16185	10.4%
SE10	19865	13627	-31.4%	NF12	11281	8597	-23.8%
SE12	13529	8451	-37.5%	NF15	30740	25917	-15.7%
SE18	15978	9920	-37.9%	NF16	18298	14532	-20.6%
SE19	14545	17160	18.0%	LASS1A	14873	22342	50.2%
SE21	15094	14545	-3.6%	LASS1B	25343	16427	-35.2%
SE25	13446	17979	33.7%	LASS1C	22327	14320	-35.9%
SE26	25466	17184	-32.5%	LASS1E	14545	16993	16.8%
SE30	15088	25862	71.4%	LASS2A	15091	14545	-3.6%
SE31	15116	15107	-0.1%	LASS3B	18124	16991	-6.3%
SE32	15101	13964	-7.5%	LASS3C	21500	21484	-0.1%
SE36	15121	15103	-0.1%	LASS4C	15201	11965	-21.3%
				Averages	14728	13270	-9.7%

U- Undamped

D- Damped

Table C.10 Peak Rooftop Displacements and Damper Drift for BF-5, Nonlinear Analysis Methods

Acc. History	U mm	D mm	% Change	DD mm	Acc. History	U mm	D mm	% Change	DD mm
LA01	235	171	-27.4%	317	BO05	45	31	-31.2%	25
LA02	382	211	-44.7%	417	BO06	32	24	-25.7%	26
LA04	169	114	-32.7%	186	BO13	26	23	-11.4%	14
LA12	203	126	-37.8%	237	BO16	22	15	-29.9%	14
LA15	410	308	-24.9%	605	BO18	32	17	-48.0%	32
LA18	324	275	-15.1%	546	BO19	58	34	-41.8%	36
LA20	429	307	-28.4%	599	BO20	61	40	-33.9%	54
LA21	1024	812	-20.7%	1022	BO21	137	130	-4.8%	154
LA22	875	763	-12.8%	1068	BO22	107	93	-12.9%	77
LA23	261	241	-7.6%	379	BO25	111	110	-1.0%	206
LA25	667	529	-20.7%	900	BO33	75	65	-13.7%	48
LA28	527	441	-16.2%	999	BO34	67	61	-8.4%	76
LA30	287	306	6.4%	830	BO35	217	154	-28.8%	311
LA37	571	423	-26.0%	1097	BO36	62	43	-30.6%	40
SE04	205	109	-47.1%	120	NF01	274	276	0.9%	767
SE05	154	121	-21.6%	149	NF02	289	192	-33.6%	451
SE08	312	154	-50.6%	206	NF11	177	220	24.1%	468
SE10	247	173	-29.8%	336	NF12	156	144	-7.7%	154
SE12	213	116	-45.6%	155	NF15	318	310	-2.7%	700
SE18	236	179	-24.0%	258	NF16	250	228	-8.6%	423
SE19	404	294	-27.1%	400	LASS1A	505	298	-41.0%	553
SE21	634	463	-27.0%	1151	LASS1B	341	228	-33.2%	401
SE25	361	232	-35.7%	407	LASS1C	302	232	-23.2%	437
SE26	326	184	-43.6%	473	LASS1E	422	252	-40.3%	396
SE30	554	310	-44.1%	543	LASS2A	587	424	-27.8%	967
SE31	947	809	-14.6%	910	LASS3B	261	258	-1.0%	555
SE32	733	367	-49.9%	538	LASS3C	289	296	2.5%	807
SE36	1014	762	-24.9%	1229	LASS4C	191	236	23.6%	334
					Averages	324	245	-22.9%	439

U- Undamped
D- Damped
DD- Damper Drift

Table C.11 Peak Base Shear for EBF-1, Nonlinear Analysis Methods.

Acc. History	U kN	D kN	% Change	Acc. History	U kN	D kN	% Change
LA01	8437	7527	-10.8%	BO05	7969	6512	-18.3%
LA02	8775	7757	-11.6%	BO06	4591	5550	20.9%
LA04	7343	7186	-2.1%	BO13	3506	3261	-7.0%
LA12	8392	7857	-6.4%	BO16	4117	4171	1.3%
LA15	7867	7921	0.7%	BO18	5000	3545	-29.1%
LA18	8848	8493	-4.0%	BO19	4681	3759	-19.7%
LA20	8439	7789	-7.7%	BO20	6945	6205	-10.7%
LA21	9897	9442	-4.6%	BO21	7161	6966	-2.7%
LA22	8979	8428	-6.1%	BO22	7482	7081	-5.4%
LA23	7916	7250	-8.4%	BO25	7200	7925	10.1%
LA25	8828	8743	-1.0%	BO33	7029	9408	33.8%
LA28	10337	9963	-3.6%	BO34	7158	6943	-3.0%
LA30	9493	8646	-8.9%	BO35	8894	8146	-8.4%
LA37	8346	8325	-0.2%	BO36	11830	11946	1.0%
SE04	7207	7104	-1.4%	NF01	8267	7885	-4.6%
SE05	7536	7152	-5.1%	NF02	8915	7817	-12.3%
SE08	7393	7075	-4.3%	NF11	7012	7142	1.8%
SE10	7548	7208	-4.5%	NF12	20080	7006	-65.1%
SE12	8257	7188	-12.9%	NF15	7611	7817	2.7%
SE18	7969	7205	-9.6%	NF16	8969	8236	-8.2%
SE19	9040	7561	-16.4%	LASS1A	7523	7458	-0.9%
SE21	9365	8525	-9.0%	LASS1B	7692	7302	-5.1%
SE25	9137	8160	-10.7%	LASS1C	7416	7280	-1.8%
SE26	8654	7864	-9.1%	LASS1E	7720	7385	-4.3%
SE30	10167	9317	-8.4%	LASS2A	8669	7715	-11.0%
SE31	11332	10330	-8.8%	LASS3B	7439	7305	-1.8%
SE32	9309	8011	-13.9%	LASS3C	7235	7344	1.5%
SE36	8076	7759	-3.9%	LASS4C	7326	7410	1.1%
				Averages	8184	7541	-6.0%

U- Undamped

D- Damped

Table C.12 Peak Rooftop Displacements and Damper Drift for EBF-1, Nonlinear Analysis Methods

Acc. History	U mm	D mm	% Change	DD mm	Acc. History	U mm	D mm	% Change	DD mm
LA01	144	82	-43.3%	215	BO05	28	27	-5.0%	38
LA02	167	97	-41.7%	274	BO06	24	23	-3.7%	28
LA04	69	58	-15.6%	198	BO13	17	18	7.7%	21
LA12	141	104	-26.0%	159	BO16	14	10	-27.3%	14
LA15	105	109	3.5%	418	BO18	20	14	-30.4%	20
LA18	172	148	-14.1%	398	BO19	13	22	66.4%	35
LA20	144	100	-30.9%	308	BO20	42	27	-36.4%	51
LA21	244	213	-12.8%	696	BO21	57	43	-23.6%	79
LA22	181	143	-20.9%	454	BO22	78	51	-35.0%	74
LA23	108	63	-42.2%	208	BO25	59	40	-32.6%	90
LA25	171	165	-3.4%	526	BO33	47	35	-25.2%	60
LA28	280	248	-11.3%	747	BO34	56	42	-26.2%	86
LA30	216	158	-26.8%	580	BO35	175	124	-29.2%	236
LA37	138	136	-1.0%	665	BO36	40	21	-48.4%	38
SE04	60	53	-11.8%	147	NF01	132	106	-19.8%	388
SE05	82	56	-32.0%	140	NF02	177	101	-42.6%	316
SE08	72	51	-30.1%	190	NF11	46	55	19.2%	200
SE10	83	60	-28.1%	145	NF12	38	46	21.7%	89
SE12	132	58	-55.6%	151	NF15	87	101	16.2%	326
SE18	112	60	-46.8%	137	NF16	180	130	-27.8%	209
SE19	185	84	-54.7%	292	LASS1A	81	77	-5.5%	346
SE21	207	150	-27.7%	671	LASS1B	93	66	-28.7%	227
SE25	192	125	-34.9%	308	LASS1C	74	65	-12.6%	263
SE26	159	105	-34.1%	216	LASS1E	95	72	-24.2%	243
SE30	262	204	-22.2%	401	LASS2A	160	94	-40.9%	323
SE31	435	279	-35.9%	446	LASS3B	76	66	-12.1%	311
SE32	204	115	-43.7%	273	LASS3C	62	69	12.1%	296
SE36	119	97	-18.2%	560	LASS4C	68	74	8.5%	167
					Averages	118	88	-20.5%	259

U- Undamped
D- Damped
DD- Damper Drift

Table C.13 Peak Base Shear for SW-1, Nonlinear Analysis Methods.

Acc. History	U kN	D kN	% Change	Acc. History	U kN	D kN	% Change
LA01	6209	6221	0.2%	BO05	6096	5909	-3.1%
LA02	6396	6283	-1.8%	BO06	6192	5871	-5.2%
LA04	6555	6093	-7.0%	BO13	6024	5873	-2.5%
LA12	6750	6381	-5.5%	BO16	5607	5864	4.6%
LA15	6448	6303	-2.2%	BO18	5974	5899	-1.3%
LA18	7232	6912	-4.4%	BO19	5921	5869	-0.9%
LA20	7030	6589	-6.3%	BO20	6083	5995	-1.4%
LA21	7303	6704	-8.2%	BO21	6184	6017	-2.7%
LA22	7034	6593	-6.3%	BO22	6320	6091	-3.6%
LA23	6210	6219	0.1%	BO25	6182	6083	-1.6%
LA25	6880	6679	-2.9%	BO33	6516	6085	-6.6%
LA28	2233	2162	-3.2%	BO34	6710	6116	-8.9%
LA30	6913	6587	-4.7%	BO35	6702	6600	-1.5%
LA37	6410	6514	1.6%	BO36	6023	6045	0.4%
SE04	6373	6149	-3.5%	NF01	6678	6457	-3.3%
SE05	6344	6097	-3.9%	NF02	6546	6285	-4.0%
SE08	6233	6220	-0.2%	NF11	6090	6157	1.1%
SE10	6492	6148	-5.3%	NF12	6150	6070	-1.3%
SE12	6446	6248	-3.1%	NF15	6907	6536	-5.4%
SE18	6719	6278	-6.6%	NF16	6772	6508	-3.9%
SE19	6147	6340	3.1%	LASS1A	6242	6224	-0.3%
SE21	6230	6373	2.3%	LASS1B	6116	6133	0.3%
SE25	7123	6483	-9.0%	LASS1C	6100	6135	0.6%
SE26	7086	6534	-7.8%	LASS1E	6289	6232	-0.9%
SE30	2204	7029	218.9%	LASS2A	6198	6283	1.4%
SE31	6669	6774	1.6%	LASS3B	6192	6148	-0.7%
SE32	6446	6564	1.8%	LASS3C	6048	6162	1.9%
SE36	6367	6439	1.1%	LASS4C	6183	6074	-1.8%
				Averages	6277	6208	-1.6%

U- Undamped

D- Damped

Table C.14 Peak Rooftop Displacements and Damper Drift for SW-1, Nonlinear Analysis Methods

Acc. History	U mm	D mm	% Change	DD mm	Acc. History	U mm	D mm	% Change	DD mm
LA01	38	39	2.5%	127	BO05	28	13	-55.5%	29
LA02	54	44	-17.6%	138	BO06	36	9	-74.3%	22
LA04	67	28	-58.1%	71	BO13	22	10	-57.1%	19
LA12	83	52	-37.3%	107	BO16	8	9	13.5%	14
LA15	58	46	-21.1%	184	BO18	18	12	-34.9%	16
LA18	124	97	-21.7%	304	BO19	14	9	-32.1%	13
LA20	107	70	-34.7%	142	BO20	27	20	-27.0%	34
LA21	130	80	-38.8%	400	BO21	36	22	-39.3%	29
LA22	107	70	-34.6%	278	BO22	47	28	-40.9%	62
LA23	38	39	2.0%	138	BO25	36	27	-23.4%	42
LA25	94	77	-17.9%	321	BO33	64	27	-56.9%	57
LA28	202	171	-15.0%	572	BO34	80	30	-62.5%	53
LA30	97	70	-28.3%	164	BO35	79	71	-10.8%	166
LA37	55	64	16.0%	286	BO36	22	24	8.3%	34
SE04	52	33	-36.6%	47	NF01	77	59	-24.1%	156
SE05	49	28	-42.2%	99	NF02	66	44	-33.1%	145
SE08	40	39	-2.9%	96	NF11	28	33	20.1%	50
SE10	62	33	-47.0%	69	NF12	33	26	-20.4%	54
SE12	58	41	-28.9%	87	NF15	97	65	-32.4%	256
SE18	81	44	-46.0%	126	NF16	85	63	-26.1%	155
SE19	33	49	49.7%	126	LASS1A	41	39	-3.7%	74
SE21	40	52	30.3%	209	LASS1B	30	31	4.7%	89
SE25	115	61	-47.0%	164	LASS1C	29	32	10.2%	83
SE26	112	65	-41.6%	171	LASS1E	45	40	-10.7%	83
SE30	190	107	-43.6%	228	LASS2A	37	44	19.4%	153
SE31	77	85	11.6%	417	LASS3B	36	33	-10.1%	84
SE32	58	68	17.1%	207	LASS3C	24	34	39.7%	71
SE36	51	57	11.8%	292	LASS4C	36	26	-25.8%	44
					Averages	62	46	-19.7%	137

U- Undamped
D- Damped
DD- Damper Drift

Table C.15 Peak Base Shear for SW-2, Nonlinear Analysis Methods.

Acc. History	U kN	D kN	% Change	Acc. History	U kN	D kN	% Change
LA01	189832	186635	-1.7%	BO05	182615	176836	-3.2%
LA02	191592	186416	-2.7%	BO06	185124	174560	-5.7%
LA04	193704	183456	-5.3%	BO13	175286	174625	-0.4%
LA12	206076	192851	-6.4%	BO16	174493	14889	-91.5%
LA15	194921	189743	-2.7%	BO18	176830	175471	-0.8%
LA18	216024	209199	-3.2%	BO19	175401	174603	-0.5%
LA20	202879	195020	-3.9%	BO20	181351	178576	-1.5%
LA21	212866	201925	-5.1%	BO21	182602	177894	-2.6%
LA22	213364	197184	-7.6%	BO22	191577	182347	-4.8%
LA23	189026	186140	-1.5%	BO25	183565	180693	-1.6%
LA25	209651	201563	-3.9%	BO33	182434	178618	-2.1%
LA28	217886	217768	-0.1%	BO34	189962	183007	-3.7%
LA30	208658	198793	-4.7%	BO35	206924	200047	-3.3%
LA37	193666	191681	-1.0%	BO36	180194	176983	-1.8%
SE04	188293	182326	-3.2%	NF01	201919	194272	-3.8%
SE05	184858	182675	-1.2%	NF02	192109	188485	-1.9%
SE08	183990	183656	-0.2%	NF11	183064	179639	-1.9%
SE10	189583	182626	-3.7%	NF12	182092	179283	-1.5%
SE12	186080	185111	-0.5%	NF15	200205	196036	-2.1%
SE18	198181	186524	-5.9%	NF16	208197	199703	-4.1%
SE19	185776	185842	0.0%	LASS1A	187480	186336	-0.6%
SE21	190833	190145	-0.4%	LASS1B	185406	183519	-1.0%
SE25	202750	192806	-4.9%	LASS1C	184682	184224	-0.2%
SE26	204116	199134	-2.4%	LASS1E	187582	185385	-1.2%
SE30	217732	212588	-2.4%	LASS2A	188361	187563	-0.4%
SE31	205058	197341	-3.8%	LASS3B	186452	181010	-2.9%
SE32	199440	193682	-2.9%	LASS3C	181935	181961	0.0%
SE36	188064	188695	0.3%	LASS4C	182856	180262	-1.4%
				Averages	192600	184971	-4.1%

U- Undamped

D- Damped

Table C.16 Peak Rooftop Displacements and Damper Drift for SW-2, Nonlinear Analysis Methods

Acc. History	U mm	D mm	% Change	DD mm	Acc. History	U mm	D mm	% Change	DD mm
LA01	72	59	-17.4%	175	BO05	43	21	-51.7%	30
LA02	78	58	-25.7%	142	BO06	53	12	-77.2%	27
LA04	87	47	-46.0%	107	BO13	15	12	-17.2%	16
LA12	135	83	-38.2%	131	BO16	12	8	-32.4%	10
LA15	91	71	-22.1%	253	BO18	21	16	-25.3%	22
LA18	174	147	-15.3%	394	BO19	15	12	-20.2%	15
LA20	122	92	-25.0%	172	BO20	39	28	-28.0%	38
LA21	161	119	-26.4%	435	BO21	43	25	-42.2%	39
LA22	163	100	-38.6%	372	BO22	78	42	-45.9%	77
LA23	68	57	-16.4%	176	BO25	47	36	-23.7%	74
LA25	149	117	-21.2%	422	BO33	43	28	-34.7%	54
LA28	282	253	-10.4%	732	BO34	72	45	-37.6%	58
LA30	145	106	-26.5%	295	BO35	138	111	-19.4%	147
LA37	87	79	-8.9%	340	BO36	34	22	-36.7%	27
SE04	66	42	-35.4%	59	NF01	119	89	-25.1%	205
SE05	52	44	-16.3%	116	NF02	80	66	-17.5%	161
SE08	49	48	-2.7%	115	NF11	45	32	-29.5%	73
SE10	71	44	-38.4%	97	NF12	41	31	-26.4%	49
SE12	57	53	-6.6%	133	NF15	112	96	-14.5%	327
SE18	104	59	-43.6%	154	NF16	143	110	-23.1%	181
SE19	56	56	0.5%	171	LASS1A	62	58	-7.1%	141
SE21	75	73	-3.5%	272	LASS1B	54	47	-13.5%	109
SE25	122	83	-31.8%	240	LASS1C	52	50	-3.5%	105
SE26	127	108	-15.3%	216	LASS1E	63	54	-13.6%	121
SE30	244	160	-34.4%	278	LASS2A	66	63	-4.7%	201
SE31	131	101	-23.0%	527	LASS3B	58	37	-36.3%	120
SE32	109	87	-20.6%	251	LASS3C	41	41	0.3%	106
SE36	65	67	3.8%	423	LASS4C	44	34	-22.7%	64
					Averages	85	65	-23.8%	175

U- Undamped
D- Damped
DD- Damper Drift

Table C.17 Peak Base Shear for MF-1, Nonlinear Analysis Methods.

Acc. History	U kN	D kN	% Change	Acc. History	U kN	D kN	% Change
LA01	5201	2947	-43.3%	BO05	1760	1420	-19.3%
LA02	5871	3517	-40.1%	BO06	1235	1172	-5.1%
LA04	2492	2105	-15.6%	BO13	984	1250	27.0%
LA12	5089	5296	4.1%	BO16	721	506	-29.8%
LA15	3790	3922	3.5%	BO18	875	1234	41.0%
LA18	5992	5339	-10.9%	BO19	1365	1301	-4.7%
LA20	5206	3596	-30.9%	BO20	2189	2060	-5.9%
LA21	7725	6972	-9.7%	BO21	2042	3473	70.1%
LA22	6208	5177	-16.6%	BO22	2836	2985	5.3%
LA23	3912	2261	-42.2%	BO25	2139	2671	24.9%
LA25	5959	5819	-2.4%	BO33	2816	2808	-0.3%
LA28	8467	7834	-7.5%	BO34	3020	3708	22.8%
LA30	7058	5658	-19.8%	BO35	6068	6910	13.9%
LA37	4976	4924	-1.0%	BO36	2070	1454	-29.8%
SE04	5559	1900	-65.8%	NF01	4780	3833	-19.8%
SE05	2971	3913	31.7%	NF02	6103	3665	-39.9%
SE08	2617	5382	105.7%	NF11	1674	1995	19.2%
SE10	3001	2158	-28.1%	NF12	1363	4715	245.9%
SE12	4754	4523	-4.9%	NF15	3155	3665	16.2%
SE18	4043	2151	-46.8%	NF16	6191	4702	-24.0%
SE19	6309	3032	-51.9%	LASS1A	2939	2776	-5.5%
SE21	6845	5418	-20.8%	LASS1B	3355	2391	-28.7%
SE25	6469	4516	-30.2%	LASS1C	2672	2336	-12.6%
SE26	5671	3781	-33.3%	LASS1E	3425	2596	-24.2%
SE30	8170	6767	-17.2%	LASS2A	5696	3413	-40.1%
SE31	10554	8452	-19.9%	LASS3B	2729	2398	-12.1%
SE32	6752	4145	-38.6%	LASS3C	10023	13430	34.0%
SE36	4306	3522	-18.2%	LASS4C	2449	2657	8.5%
				Averages	4333	3796	-4.4%

U- Undamped

D- Damped

Table C.18 Peak Rooftop Displacements and Damper Drift for MF-1, Nonlinear Analysis Methods

Acc. History	U mm	D mm	% Change	DD mm	Acc. History	U mm	D mm	% Change	DD mm
LA01	319	240	-24.7%	416	BO05	32	27	-15.6%	34
LA02	250	276	10.4%	458	BO06	17	15	-12.8%	16
LA04	158	199	26.2%	425	BO13	26	27	5.0%	21
LA12	198	150	-24.2%	203	BO16	15	13	-17.6%	12
LA15	468	366	-21.7%	470	BO18	28	17	-37.9%	19
LA18	497	397	-20.1%	700	BO19	47	33	-30.1%	31
LA20	509	391	-23.1%	723	BO20	49	40	-18.4%	50
LA21	1172	866	-26.1%	1154	BO21	215	107	-50.3%	203
LA22	544	550	1.2%	914	BO22	159	102	-35.9%	154
LA23	501	261	-47.8%	621	BO25	169	91	-46.0%	134
LA25	761	624	-18.0%	917	BO33	75	63	-16.2%	74
LA28	809	639	-21.0%	1198	BO34	62	88	41.5%	72
LA30	445	385	-13.6%	1185	BO35	196	139	-29.0%	239
LA37	680	599	-11.9%	1610	BO36	44	35	-21.2%	35
SE04	148	154	4.0%	229	NF01	478	395	-17.3%	1034
SE05	159	121	-23.7%	110	NF02	273	223	-18.3%	555
SE08	235	149	-36.5%	157	NF11	326	272	-16.4%	789
SE10	293	209	-28.6%	395	NF12	212	149	-29.7%	295
SE12	337	119	-64.9%	167	NF15	579	471	-18.6%	978
SE18	367	180	-51.1%	241	NF16	319	248	-22.3%	440
SE19	438	280	-36.1%	365	LASS1A	636	357	-43.9%	414
SE21	638	632	-1.0%	1500	LASS1B	641	315	-50.9%	505
SE25	371	241	-34.9%	398	LASS1C	509	276	-45.8%	486
SE26	375	261	-30.4%	484	LASS1E	470	242	-48.5%	353
SE30	862	602	-30.1%	713	LASS2A	529	459	-13.2%	1015
SE31	1027	763	-25.7%	845	LASS3B	270	377	39.5%	1173
SE32	485	331	-31.7%	521	LASS3C	280	397	41.9%	3273
SE36	1079	907	-15.9%	1297	LASS4C	287	241	-16.1%	730
					Averages	376	288	-20.8%	563

U- Undamped
D- Damped
DD- Damper Drift

Table C.19 Peak Base Shear for MF-2, Nonlinear Analysis Methods.

Acc. History	U kN	D kN	% Change	Acc. History	U kN	D kN	% Change
LA01	31567	27052	-14.3%	BO05	5623	4342	-22.8%
LA02	28461	28083	-1.3%	BO06	4156	4721	13.6%
LA04	33035	28013	-15.2%	BO13	3556	2396	-32.6%
LA12	21931	20178	-8.0%	BO16	2212	2203	-0.4%
LA15	29685	27888	-6.1%	BO18	4068	3718	-8.6%
LA18	32754	30743	-6.1%	BO19	3859	3026	-21.6%
LA20	32299	29410	-8.9%	BO20	6788	6307	-7.1%
LA21	35315	33666	-4.7%	BO21	11961	9864	-17.5%
LA22	30991	31825	2.7%	BO22	12024	11299	-6.0%
LA23	30177	28610	-5.2%	BO25	8754	8305	-5.1%
LA25	33327	30970	-7.1%	BO33	10165	6632	-34.8%
LA28	35616	34505	-3.1%	BO34	14718	11896	-19.2%
LA30	35166	34423	-2.1%	BO35	19368	16878	-12.9%
LA37	35616	34093	-4.3%	BO36	6359	6311	-0.7%
SE04	19688	14417	-26.8%	NF01	33336	31033	-6.9%
SE05	23186	14646	-36.8%	NF02	30343	29892	-1.5%
SE08	19429	13854	-28.7%	NF11	28558	29510	3.3%
SE10	28532	30158	5.7%	NF12	18348	12042	-34.4%
SE12	20754	14601	-29.6%	NF15	33673	31796	-5.6%
SE18	26759	16543	-38.2%	NF16	29136	28390	-2.6%
SE19	39116	21938	-43.9%	LASS1A	31318	27392	-12.5%
SE21	34566	33402	-3.4%	LASS1B	32097	27850	-13.2%
SE25	30354	27568	-9.2%	LASS1C	32643	28211	-13.6%
SE26	29893	35631	19.2%	LASS1E	30062	21981	-26.9%
SE30	32229	29771	-7.6%	LASS2A	35170	31726	-9.8%
SE31	32521	31182	-4.1%	LASS3B	32237	32115	-0.4%
SE32	28480	26618	-6.5%	LASS3C	33398	32559	-2.5%
SE36	34979	32328	-7.6%	LASS4C	31703	28763	-9.3%
				Averages	24858	22380	-10.9%

U- Undamped

D- Damped

Table C.20 Peak Rooftop Displacements and Damper Drift for MF-2, Nonlinear Analysis Methods

Acc. History	U mm	D mm	% Change	DD mm	Acc. History	U mm	D mm	% Change	DD mm
LA01	667	360	-46.0%	799	BO05	36	32	-13.5%	27
LA02	421	394	-6.5%	544	BO06	26	31	20.4%	21
LA04	339	391	15.3%	753	BO13	34	23	-31.7%	12
LA12	176	192	9.1%	256	BO16	17	19	15.0%	8
LA15	517	387	-25.1%	551	BO18	25	15	-39.3%	16
LA18	785	601	-23.5%	1007	BO19	49	25	-49.7%	22
LA20	740	496	-33.0%	863	BO20	48	32	-33.6%	44
LA21	1051	876	-16.7%	1472	BO21	177	140	-20.9%	102
LA22	620	693	11.7%	1074	BO22	166	148	-10.5%	107
LA23	556	433	-22.2%	785	BO25	135	94	-30.5%	133
LA25	842	618	-26.5%	1034	BO33	97	60	-38.4%	47
LA28	1276	962	-24.6%	1786	BO34	147	75	-49.3%	50
LA30	1035	954	-7.9%	1862	BO35	145	111	-23.5%	205
LA37	1104	918	-16.9%	1930	BO36	48	53	9.9%	25
SE04	214	237	11.0%	266	NF01	843	623	-26.0%	1141
SE05	244	182	-25.4%	198	NF02	569	534	-6.2%	1229
SE08	230	147	-36.1%	160	NF11	429	503	17.5%	998
SE10	427	277	-35.1%	421	NF12	245	161	-34.1%	146
SE12	271	149	-45.1%	183	NF15	876	690	-21.3%	1318
SE18	312	165	-47.3%	155	NF16	474	315	-33.6%	361
SE19	324	248	-23.6%	339	LASS1A	646	371	-42.5%	492
SE21	969	849	-12.4%	1530	LASS1B	720	386	-46.4%	585
SE25	570	377	-33.9%	758	LASS1C	774	401	-48.1%	628
SE26	534	333	-37.6%	620	LASS1E	547	324	-40.7%	436
SE30	733	524	-28.5%	632	LASS2A	1035	683	-34.1%	956
SE31	762	635	-16.6%	842	LASS3B	734	722	-1.6%	2100
SE32	422	346	-18.1%	434	LASS3C	849	766	-9.8%	2605
SE36	1014	743	-26.8%	969	LASS4C	681	445	-34.7%	941
					Averages	495	380	-22.2%	660

U- Undamped
D- Damped
DD- Damper Drift

APPENDIX D

BASIC SAFETY OBJECTIVE OUTPUT

Tables D.1 through D.30 list the output values of peak output parameters results listed in Chapter 6. Values shown reflect the peak rooftop displacements and the peak base shears for the undamped and damped cases. The percent changes for each are listed in Chapter 6 as well as the peak drifts of the NRTMDF for each damped case.

Table D.1 Peak BSO Output Parameters for BF-1, Hard Sites

	Base Shear		Rooftop Displacement		NRTMDF
	Undamped	Damped	Undamped	Damped	Drift
BSE-1	kN	kN	(mm)	(mm)	(mm)
LA20	3322	2732	12	10	27
BO07	2448	1778	9	9	25
SE04	3799	2913	16	10	28
LA12	4066	3511	22	18	44
SE05	2262	2033	8	9	28
SE06	2891	2646	10	10	36
SE12	3190	3156	12	9	26
BSE-2					
LA28	3792	3788	20	18	60
LA30	4217	4142	50	32	79
LA39	3735	3734	16	16	51
LA33	3863	3817	25	19	75
SE39	3921	3857	29	19	59
SE25	3871	3831	26	22	104
SE30	3975	3921	33	23	85

Table D.2 Peak BSO Output Parameters for BF-1, Medium Sites

	Base Shear		Rooftop Displacement		NRTMDF
	Undamped	Damped	Undamped	Damped	Drift
BSE-1	kN	kN	(mm)	(mm)	(mm)
LA13	3743	3738	17	14	49
LA14	3712	2643	15	9	38
LA18	2662	2347	10	8	42
LA02	3728	3484	16	12	53
SE03	3703	3393	14	12	53
SE15	3735	3732	16	14	34
SE18	3728	3727	16	15	60
BSE-2					
LA23	3615	3638	13	14	125
LA24	3005	3134	11	11	88
SE23	3976	3963	33	30	219
LA31	3992	3981	34	32	119
LA32	4028	4001	37	30	145
SE28	4217	4186	50	42	146
SE32	3968	3955	33	29	158

Table D.3 Peak BSO Output Parameters for BF-1, Soft Sites

	Base Shear		Rooftop Displacement		NRTMDF
	Undamped	Damped	Undamped	Damped	Drift
BSE-1	kN	kN	(mm)	(mm)	(mm)
SE01	3778	3772	19	15	33
LA03	3476	3638	13	14	45
LA15	3735	3733	16	15	83
LA09	3740	3572	17	13	52
LA10	3822	3804	22	18	58
LA07	3708	3706	14	13	40
SE07	3800	3790	21	14	67
BSE-2					
LA38	3772	3806	19	24	269
LA40	3782	3798	20	23	151
SE24	3964	3975	34	36	242
LA35	4143	4101	47	37	202
LA36	3956	3915	33	24	137
SE33	4219	3973	53	39	113
SE36	3866	3872	26	28	167

Table D.4 Peak BSO Output Parameters for BF-2, Hard Sites

	Base Shear		Rooftop Displacement		NRTMDF
	Undamped	Damped	Undamped	Damped	Drift
BSE-1	kN	kN	(mm)	(mm)	(mm)
LA20	6547	5658	19	11	24
BO07	5883	4817	14	8	24
SE04	6962	6316	22	15	45
LA12	6449	6236	18	19	67
SE05	6336	5729	17	12	33
SE06	6016	5523	15	12	42
SE12	6006	5287	15	12	37
BSE-2					
LA28	8458	8325	44	28	86
LA30	8362	8730	38	33	114
LA39	8214	7809	33	24	88
LA33	8410	7771	40	26	60
SE39	8470	8142	45	24	90
SE25	8645	8259	54	33	96
SE30	8541	8819	48	35	102

Table D.5 Peak BSO Output Parameters for BF-2, Medium Sites

	Base Shear		Rooftop Displacement		NRTMDF
	Undamped	Damped	Undamped	Damped	Drift
BSE-1	kN	kN	(mm)	(mm)	(mm)
LA13	7089	6127	22	15	39
LA14	6888	5640	21	12	32
LA18	6876	6238	21	16	51
LA02	6269	6062	16	15	31
SE03	6684	6044	19	15	32
SE15	6533	5997	18	15	29
SE18	7157	6300	23	17	43
BSE-2					
LA23	7538	7419	26	25	79
LA24	6539	6827	18	21	46
SE23	8693	8264	56	35	116
LA31	8992	8310	72	36	91
LA32	8854	8511	65	47	115
SE28	8832	8438	63	43	85
SE32	8116	8380	30	39	104

Table D.6 Peak BSO Output Parameters for BF-2, Soft Sites

	Base Shear		Rooftop Displacement		NRTMDF
	Undamped	Damped	Undamped	Damped	Drift
BSE-1	kN	kN	(mm)	(mm)	(mm)
SE01	6330	6681	17	19	52
LA03	6900	6129	21	15	59
LA15	7415	6404	25	17	88
LA09	6186	6944	16	21	76
LA10	7836	7357	28	24	85
LA07	7082	7044	22	22	105
SE07	7914	6698	28	20	60
BSE-2					
LA38	7570	8169	26	31	279
LA40	7898	8069	28	30	159
SE24	8599	8556	51	49	285
LA35	8541	8410	48	41	303
LA36	8490	8390	46	39	207
SE33	9322	8963	89	70	207
SE36	7254	8047	24	29	215

Table D.7 Peak BSO Output Parameters for BF-3, Hard Sites

	Base Shear		Rooftop Displacement		NRTMDF
	Undamped	Damped	Undamped	Damped	Drift
BSE-1	kN	kN	(mm)	(mm)	(mm)
LA20	8458	9026	24	20	25
BO07	5926	6951	17	18	33
SE04	10079	7409	29	20	34
LA12	10431	8291	44	23	44
SE05	9065	7681	26	22	60
SE06	10374	10914	30	25	78
SE12	7548	4824	22	23	42
BSE-2					
LA28	10715	10679	106	70	236
LA30	10618	10366	85	52	130
LA39	10533	10298	67	48	131
LA33	10500	10399	59	43	117
SE39	10464	10458	51	48	102
SE25	10607	10443	83	60	225
SE30	10689	10423	101	55	160

Table D.8 Peak BSO Output Parameters for BF-3, Medium Sites

	Base Shear		Rooftop Displacement		NRTMDF
	Undamped	Damped	Undamped	Damped	Drift
BSE-1	kN	kN	(mm)	(mm)	(mm)
LA13	10385	10386	34	35	117
LA14	8208	9369	24	27	85
LA18	10460	10427	51	32	121
LA02	10374	8561	32	25	70
SE03	9786	8200	28	24	94
SE15	10374	10397	31	33	92
SE18	10448	10379	48	30	90
BSE-2					
LA23	10585	10342	78	51	170
LA24	10455	10433	49	37	203
SE23	10521	10451	64	57	302
LA31	10705	10666	104	67	188
LA32	10533	10545	67	77	256
SE28	10663	10669	95	100	350
SE32	10611	10457	84	61	231

Table D.9 Peak BSO Output Parameters for BF-3, Soft Sites

	Base Shear		Rooftop Displacement		NRTMDF
	Undamped	Damped	Undamped	Damped	Drift
BSE-1	kN	kN	(mm)	(mm)	(mm)
SE01	10404	10365	40	31	154
LA03	10418	10429	45	51	179
LA15	10480	10354	63	47	210
LA09	10399	10402	39	40	219
LA10	10469	10365	59	41	133
LA07	10402	9671	40	28	108
SE07	10461	10376	57	40	155
BSE-2					
LA38	10455	10631	56	66	958
LA40	10637	10379	109	74	1000
SE24	10583	10572	93	84	712
LA35	10574	10551	90	71	805
LA36	10551	10538	84	73	631
SE33	10709	8782	130	100	455
SE36	10463	10397	58	53	489

Table D.10 Peak BSO Output Parameters for BF-4, Hard Sites

	Base Shear		Rooftop Displacement		NRTMDF
	Undamped	Damped	Undamped	Damped	Drift
BSE-1	kN	kN	(mm)	(mm)	(mm)
LA20	7767	6480	39	32	82
BO07	7666	4793	38	22	45
SE04	7954	8118	40	35	62
LA12	10764	9251	53	31	52
SE05	10484	6533	52	31	66
SE06	12294	7788	48	30	65
SE12	12260	8564	64	31	75
BSE-2					
LA28	12860	12778	141	109	261
LA30	12857	12808	141	121	414
LA39	12817	12720	136	97	263
LA33	12795	12664	133	81	263
SE39	12662	12552	116	72	192
SE25	13043	12895	165	107	280
SE30	13285	12153	111	94	181

Table D.11 Peak BSO Output Parameters for BF-4, Medium Sites

	Base Shear		Rooftop Displacement		NRTMDF
	Undamped	Damped	Undamped	Damped	Drift
BSE-1	kN	kN	(mm)	(mm)	(mm)
LA13	12402	11533	82	57	166
LA14	12507	9515	96	47	107
LA18	12283	9201	67	45	105
LA02	12482	10027	93	49	91
SE03	12608	9532	109	47	119
SE15	12333	11022	73	54	91
SE18	12485	8912	87	34	79
BSE-2					
LA23	13460	12890	230	128	283
LA24	13397	14413	198	104	270
SE23	13305	13046	198	152	538
LA31	13523	12870	244	127	301
LA32	13693	12959	283	151	402
SE28	13676	13198	279	193	414
SE32	13588	12921	259	140	361

Table D.12 Peak BSO Output Parameters for BF-4, Soft Sites

	Base Shear		Rooftop Displacement		NRTMDF
	Undamped	Damped	Undamped	Damped	Drift
BSE-1	kN	kN	(mm)	(mm)	(mm)
SE01	12683	12617	118	111	542
LA03	12565	12498	103	94	292
LA15	12688	12564	119	76	329
LA09	12520	12356	97	74	283
LA10	12414	12281	84	65	158
LA07	12774	12534	130	92	212
SE07	12603	12406	77	65	192
BSE-2					
LA38	13209	13150	186	181	1259
LA40	12654	12842	115	137	1254
SE24	13384	13044	215	185	963
LA35	13662	11020	294	235	1129
LA36	13756	13766	231	259	912
SE33	12972	12769	156	132	458
SE36	13397	12719	218	159	510

Table D.13 Peak BSO Output Parameters for BF-5, Hard Sites

	Base Shear		Rooftop Displacement		NRTMDF
	Undamped	Damped	Undamped	Damped	Drift
BSE-1	kN	kN	(mm)	(mm)	(mm)
LA20	6489	4584	97	58	116
BO07	3282	3553	49	46	65
SE04	7781	5841	116	49	128
LA12	4941	3361	74	53	119
SE05	5586	3476	84	58	93
SE06	5713	3509	86	47	90
SE12	6108	3838	91	43	80
BSE-2					
LA28	12423	11983	219	181	475
LA30	11983	12038	193	199	759
LA39	13229	12953	288	247	614
LA33	13388	12303	302	213	528
SE39	13662	12020	322	198	345
SE25	13229	12294	264	213	310
SE30	13217	10553	261	158	254

Table D.14 Peak BSO Output Parameters for BF-5, Medium Sites

	Base Shear		Rooftop Displacement		NRTMDF
	Undamped	Damped	Undamped	Damped	Drift
BSE-1	kN	kN	(mm)	(mm)	(mm)
LA13	10763	6816	161	81	105
LA14	10223	6239	153	88	174
LA18	6969	4755	104	95	120
LA02	11494	6745	172	74	117
SE03	11643	8383	174	111	118
SE15	9370	9140	140	118	157
SE18	8299	5317	124	72	116
BSE-2					
LA23	13862	13775	337	331	516
LA24	14239	13396	378	303	564
SE23	14545	13588	485	372	599
LA31	14545	12878	416	243	402
LA32	14545	13855	452	350	508
SE28	14494	12941	398	247	312
SE32	15219	14310	665	395	470

Table D.15 Peak BSO Output Parameters for BF-5, Soft Sites

	Base Shear		Rooftop Displacement		NRTMDF
	Undamped	Damped	Undamped	Damped	Drift
BSE-1	kN	kN	(mm)	(mm)	(mm)
SE01	12493	12327	223	214	406
LA03	13383	12587	302	228	373
LA15	13481	12684	309	233	469
LA09	13048	12717	252	235	444
LA10	13431	10726	305	161	212
LA07	13229	11939	284	179	243
SE07	14225	10435	377	156	208
BSE-2					
LA38	15263	15163	687	665	1944
LA40	14545	14022	480	416	1894
SE24	15231	14689	656	536	1493
LA35	14454	13512	395	361	1407
LA36	14545	14221	463	409	1318
SE33	15219	14006	643	452	999
SE36	15665	14384	997	694	1203

Table D.16 Peak BSO Output Parameters for EBF-1, Hard Sites

	Base Shear		Rooftop Displacement		NRTMDF
	Undamped	Damped	Undamped	Damped	Drift
BSE-1	kN	kN	(mm)	(mm)	(mm)
LA20	5801	4327	33	25	55
BO07	5173	4085	29	16	36
SE04	6015	6299	34	26	106
LA12	7084	6373	51	36	63
SE05	6986	5518	45	31	89
SE06	6945	4733	42	27	58
SE12	7160	4346	56	24	72
BSE-2					
LA28	8040	7760	117	98	255
LA30	8452	7762	145	98	389
LA39	8373	7556	139	84	277
LA33	7434	7253	75	63	231
SE39	7632	7310	89	67	170
SE25	8388	7653	141	90	228
SE30	8141	7544	124	83	163

Table D.17 Peak BSO Output Parameters for EBF-1, Medium Sites

	Base Shear		Rooftop Displacement		NRTMDF
	Undamped	Damped	Undamped	Damped	Drift
BSE-1	kN	kN	(mm)	(mm)	(mm)
LA13	7432	7018	75	47	122
LA14	7060	6899	50	40	79
LA18	7146	6890	55	40	106
LA02	7435	6975	75	44	88
SE03	7475	6563	78	37	98
SE15	6160	6938	35	41	66
SE18	7195	5847	59	33	67
BSE-2					
LA23	8380	7586	140	86	250
LA24	8005	7305	114	66	281
SE23	8351	8030	138	116	432
LA31	8188	7917	127	108	228
LA32	8321	7898	136	107	379
SE28	9918	8433	245	144	326
SE32	9032	7993	185	114	302

Table D.18 Peak BSO Output Parameters for EBF-1, Soft Sites

	Base Shear		Rooftop Displacement		NRTMDF
	Undamped	Damped	Undamped	Damped	Drift
BSE-1	kN	kN	(mm)	(mm)	(mm)
SE01	7635	7579	89	85	562
LA03	7318	7405	67	73	387
LA15	7491	7322	79	68	200
LA09	7474	7269	78	64	344
LA10	7426	7205	75	60	278
LA07	7812	7285	101	65	218
SE07	7408	7143	73	55	199
BSE-2					
LA38	8059	8121	118	122	1271
LA40	7674	7717	92	95	1156
SE24	8337	7861	137	104	816
LA35	9228	8329	198	136	1165
LA36	8595	7958	155	111	980
SE33	8049	7868	117	105	410
SE36	8045	7986	117	113	519

Table D.19 Peak BSO Output Parameters for SW-1, Hard Sites

	Base Shear		Rooftop Displacement		NRTMDF
	Undamped	Damped	Undamped	Damped	Drift
BSE-1	kN	kN	(mm)	(mm)	(mm)
LA20	6047	4824	24	18	30
BO07	5945	5549	16	17	26
SE04	6108	4671	31	14	25
LA12	6120	4023	30	21	41
SE05	6076	3942	27	19	63
SE06	6108	4370	29	21	47
SE12	6054	4944	25	21	42
BSE-2					
LA28	6758	5062	84	61	207
LA30	6533	5159	65	43	98
LA39	6514	4815	64	36	119
LA33	6563	4671	68	35	118
SE39	6552	4734	67	37	78
SE25	6758	5308	61	39	117
SE30	6820	6263	89	42	134

Table D.20 Peak BSO Output Parameters for SW-1, Medium Sites

	Base Shear		Rooftop Displacement		NRTMDF
	Undamped	Damped	Undamped	Damped	Drift
BSE-1	kN	kN	(mm)	(mm)	(mm)
LA13	6162	4489	34	24	60
LA14	6066	5538	26	28	35
LA18	6234	3979	34	21	65
LA02	6046	6088	24	28	56
SE03	6008	6023	21	22	52
SE15	6183	6100	36	29	35
SE18	6264	6085	43	27	56
BSE-2					
LA23	6342	5239	49	45	162
LA24	6113	6993	30	31	111
SE23	6592	5287	70	51	214
LA31	6776	5527	86	67	184
LA32	6533	6823	65	70	210
SE28	7040	6294	85	58	171
SE32	6383	5454	52	54	180

Table D.21 Peak BSO Output Parameters for SW-1, Soft Sites

	Base Shear		Rooftop Displacement		NRTMDF
	Undamped	Damped	Undamped	Damped	Drift
BSE-1	kN	kN	(mm)	(mm)	(mm)
SE01	6087	6262	28	30	68
LA03	6231	4847	40	33	86
LA15	6279	4385	44	35	120
LA09	6097	7303	28	33	76
LA10	6248	5755	35	28	79
LA07	6101	6171	29	28	91
SE07	6248	4987	41	32	78
BSE-2					
LA38	6328	6433	48	57	395
LA40	6421	6395	56	54	286
SE24	6723	6594	81	70	366
LA35	6839	6621	91	73	337
LA36	6556	6554	67	67	289
SE33	7263	7120	79	71	432
SE36	6357	6341	50	49	296

Table D.22 Peak BSO Output Parameters for SW-2, Hard Sites

	Base Shear		Rooftop Displacement		NRTMDF
	Undamped	Damped	Undamped	Damped	Drift
BSE-1	kN	kN	(mm)	(mm)	(mm)
LA20	178569	177571	28	24	34
BO07	176443	177244	19	23	45
SE04	181004	177031	37	22	38
LA12	184037	177824	49	25	47
SE05	178706	176874	28	21	46
SE06	180027	177568	33	24	52
SE12	177724	176974	24	22	44
BSE-2					
LA28	201660	189983	118	72	273
LA30	196387	188128	97	65	125
LA39	190756	185095	75	53	152
LA33	188644	184114	67	49	122
SE39	186725	186946	59	60	131
SE25	194374	186799	89	60	198
SE30	200999	184905	115	52	159

Table D.23 Peak BSO Output Parameters for SW-2, Medium Sites

	Base Shear		Rooftop Displacement		NRTMDF
	Undamped	Damped	Undamped	Damped	Drift
BSE-1	kN	kN	(mm)	(mm)	(mm)
LA13	181079	180110	38	34	132
LA14	178043	179661	26	32	73
LA18	185819	181835	56	40	134
LA02	180522	178960	35	29	81
SE03	179726	177242	32	23	72
SE15	180172	180705	34	36	116
SE18	185510	180029	55	33	57
BSE-2					
LA23	194184	184877	89	52	178
LA24	186229	182486	58	43	257
SE23	190068	188097	73	65	333
LA31	203128	191275	123	77	186
LA32	190967	191408	76	78	263
SE28	198756	199074	106	108	375
SE32	196837	186931	99	60	220

Table D.24 Peak BSO Output Parameters for SW-2, Soft Sites

	Base Shear		Rooftop Displacement		NRTMDF
	Undamped	Damped	Undamped	Damped	Drift
BSE-1	kN	kN	(mm)	(mm)	(mm)
SE01	183413	181740	47	40	180
LA03	184208	186159	50	57	179
LA15	189160	184515	69	51	224
LA09	182891	182065	45	41	185
LA10	187995	183861	64	48	150
LA07	183168	180784	46	36	140
SE07	187910	183229	64	46	176
BSE-2					
LA38	188037	191660	65	79	1032
LA40	202544	191669	121	79	1058
SE24	198153	193793	104	87	730
LA35	195734	190463	95	74	779
LA36	195167	192324	92	81	628
SE33	211649	199464	157	109	468
SE36	187777	188047	64	65	485

Table D.25 Peak BSO Output Parameters for MF-1, Hard Sites

	Base Shear		Rooftop Displacement		NRTMDF
	Undamped	Damped	Undamped	Damped	Drift
BSE-1	kN	kN	(mm)	(mm)	(mm)
LA20	4175	2903	116	83	108
BO07	2692	2406	74	65	61
SE04	3042	2611	84	88	118
LA12	2640	2380	73	53	55
SE05	3108	2881	86	83	66
SE06	3542	2819	98	81	89
SE12	5260	4245	86	52	62
BSE-2					
LA28	9220	8556	336	287	435
LA30	8738	8146	300	261	678
LA39	10949	9270	464	340	549
LA33	9063	7698	324	243	684
SE39	11139	9587	261	191	346
SE25	8355	6132	272	178	237
SE30	10111	6971	402	213	274

Table D.26 Peak BSO Output Parameters for MF-1, Medium Sites

	Base Shear		Rooftop Displacement		NRTMDF
	Undamped	Damped	Undamped	Damped	Drift
BSE-1	kN	kN	(mm)	(mm)	(mm)
LA13	7125	3515	172	81	110
LA14	6744	3885	203	108	173
LA18	5695	4998	160	138	171
LA02	4053	4621	112	128	183
SE03	5059	4320	140	120	267
SE15	5753	4698	162	130	272
SE18	6453	2931	191	81	146
BSE-2					
LA23	13367	10924	358	266	729
LA24	13746	10526	675	433	1258
SE23	12109	10636	550	441	853
LA31	13997	10476	700	429	701
LA32	13096	11413	623	498	507
SE28	13219	9367	633	347	440
SE32	10638	8644	441	293	450

Table D.27 Peak BSO Output Parameters for MF-1, Soft Sites

	Base Shear		Rooftop Displacement		NRTMDF
	Undamped	Damped	Undamped	Damped	Drift
BSE-1	kN	kN	(mm)	(mm)	(mm)
SE01	9311	8697	343	297	1036
LA03	8340	8673	271	295	743
LA15	9489	8227	356	265	346
LA09	11427	8319	345	197	451
LA10	11580	7880	511	250	521
LA07	8058	6188	258	180	367
SE07	8764	5700	302	160	186
BSE-2					
LA38	15653	15392	1092	995	2618
LA40	16750	16546	1250	1012	2425
SE24	14689	14610	888	794	1890
LA35	15429	13457	654	486	1057
LA36	14694	13923	892	690	1729
SE33	14456	11654	762	516	1031
SE36	15582	14677	1061	877	1233

Table D.28 Peak BSO Output Parameters for MF-2, Hard Sites

	Base Shear		Rooftop Displacement		NRTMDF
	Undamped	Damped	Undamped	Damped	Drift
BSE-1	kN	kN	(mm)	(mm)	(mm)
LA20	13261	10470	168	107	139
BO07	7680	4336	97	76	89
SE04	9607	7798	121	124	158
LA12	5066	4413	64	74	85
SE05	10456	5878	132	87	140
SE06	11076	9010	140	107	138
SE12	9211	6439	116	75	94
BSE-2					
LA28	29871	28498	532	424	634
LA30	31835	31143	694	632	1701
LA39	30324	28768	568	445	804
LA33	33343	32042	843	714	919
SE39	28928	24650	458	313	390
SE25	28416	24728	417	314	580
SE30	26597	19593	345	248	271

Table D.29 Peak BSO Output Parameters for MF-2, Medium Sites

	Base Shear		Rooftop Displacement		NRTMDF
	Undamped	Damped	Undamped	Damped	Drift
BSE-1	kN	kN	(mm)	(mm)	(mm)
LA13	14100	9969	178	123	127
LA14	14029	8556	177	156	180
LA18	20021	13176	253	190	192
LA02	15005	10166	190	163	238
SE03	23372	10821	295	125	177
SE15	18812	11157	238	189	277
SE18	12991	8932	164	81	93
BSE-2					
LA23	32091	29516	719	504	1091
LA24	34497	30262	962	563	1452
SE23	32523	29481	762	501	1253
LA31	29908	28890	535	455	559
LA32	29518	28883	504	454	530
SE28	29533	26680	505	348	393
SE32	27764	23960	383	303	344

Table D.30 Peak BSO Output Parameters for MF-2, Soft Sites

	Base Shear		Rooftop Displacement		NRTMDF
	Undamped	Damped	Undamped	Damped	Drift
BSE-1	kN	kN	(mm)	(mm)	(mm)
SE01	30868	29584	610	509	1544
LA03	30138	29282	553	486	1098
LA15	27984	23319	390	295	364
LA09	28438	26698	419	349	419
LA10	26557	24231	344	306	431
LA07	28438	23760	419	300	634
SE07	20343	12921	257	163	185
BSE-2					
LA38	58180	55414	1771	1560	3191
LA40	69820	63595	2126	1698	3627
SE24	61411	52170	1870	1187	2514
LA35	59037	53949	1798	1413	3007
LA36	64755	53822	1972	1188	3011
SE33	49859	44624	1518	1078	1438
SE36	34818	32172	997	727	939

APPENDIX E

PEER GROUND MOTION OUTPUT

Tables E.1 lists the output values of peak output parameters results listed in Chapter 6 for the analyses of BF-4 utilizing the PEER ground motion suite. Values shown reflect the peak rooftop displacements and the peak base shears for the undamped and damped cases. The percent changes for each are listed in Chapter 6 as well as the peak drifts of the NRTMDF for each damped case.

Table E.1 Peak BSO Ouput Parameters for BF-4, Medium Sites, PEER Motions

U – Undamped, D-Damped	Base Shear		Rooftop Displacement		NRTMDF
	U	D	U	D	Drift
BSE-1	kN	kN	(mm)	(mm)	(mm)
NGA_158IMPVALL.H-AEP_FP	12299	10577	77	53	27
NGA_184IMPVALL.H-EDA_FN	12302	10568	78	53	25
NGA_184IMPVALL.H-EDA_FP	12295	9480	76	47	28
NGA_719SUPERST.B-BRA_FN	12276	11810	71	59	44
NGA_730SPITAK.GUK_FP	12261	9919	67	49	28
NGA_947NORTHR.ARC_FP	12255	10208	66	51	36
NGA_1094NORTHR.SOR_FP	12381	9075	97	46	26
BSE-2					
NGA_1605DUZCE.DZC_FP	12861	12025	213	141	60
NGA_1615DUZCE.1062_FN	12836	12168	207	150	79
NGA_850LANDERS.DSP_FP	12945	11819	233	135	51
NGA_881LANDERS.MVH_FN	13341	11794	330	187	75
NGA_1602DUZCE.BOL_FN	13021	11940	252	156	59
NGA_838LANDERS.BRS_FP	12979	11940	242	151	104
NGA_1776HECTOR.12149_FP	12920	11744	227	125	85

APPENDIX F

BUILDING PUSHOVER CURVES

Nonlinear static pushover curves are developed through the piecewise displacement of the roof level of each undamped model. At each increment of displacement the base shear reaction is determined. Nonlinear static modeling procedures account for the formation of plastic hinging elements within the model through the piecewise displacement using a pattern correlating to the first primary mode of the modal analysis since this represents the predominant seismic behavioral mode. The results are then plotted for each step of the analysis to develop the overall pushover curve for each structure. The pushover curve reflects a rational and convenient measure of the overall nonlinear behavior at the displacement of interest. It enables a measure of system energy as the area under the curve at the specified displacement. Such values are then conveniently incorporated into the energy method calculations and the equivalent damping calculations of Chapter 7. Figures F.1 through F.10 depict the pushover curves developed for each model.

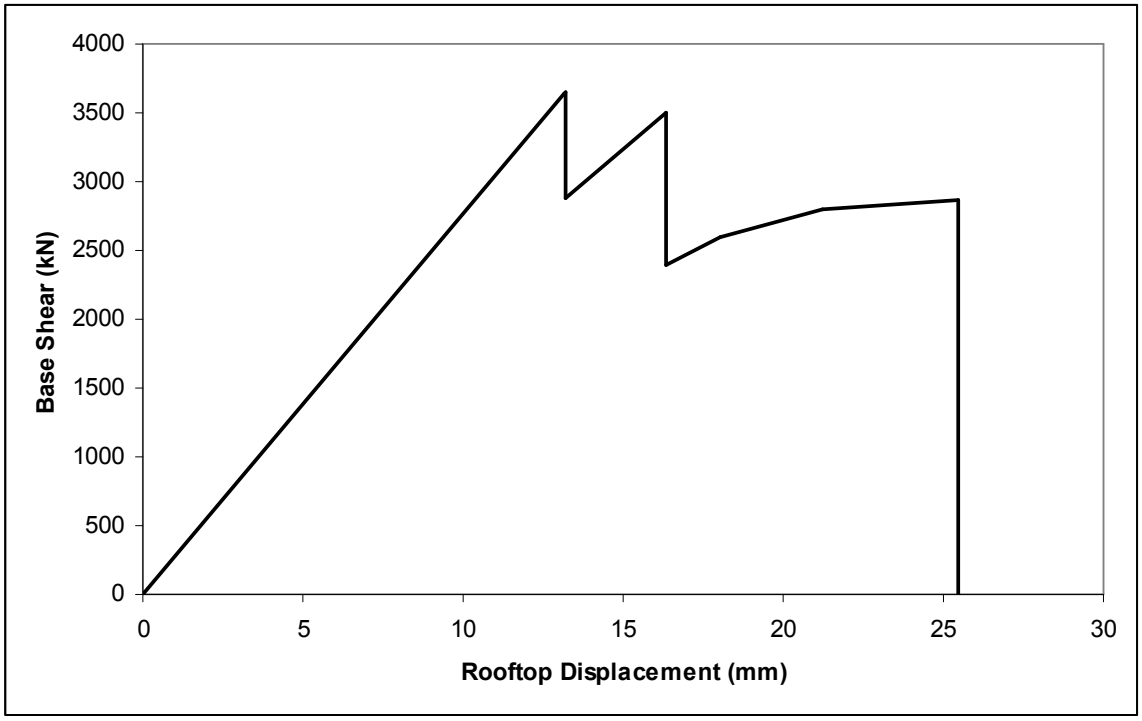

Figure F.1 BF-1 Pushover Curve

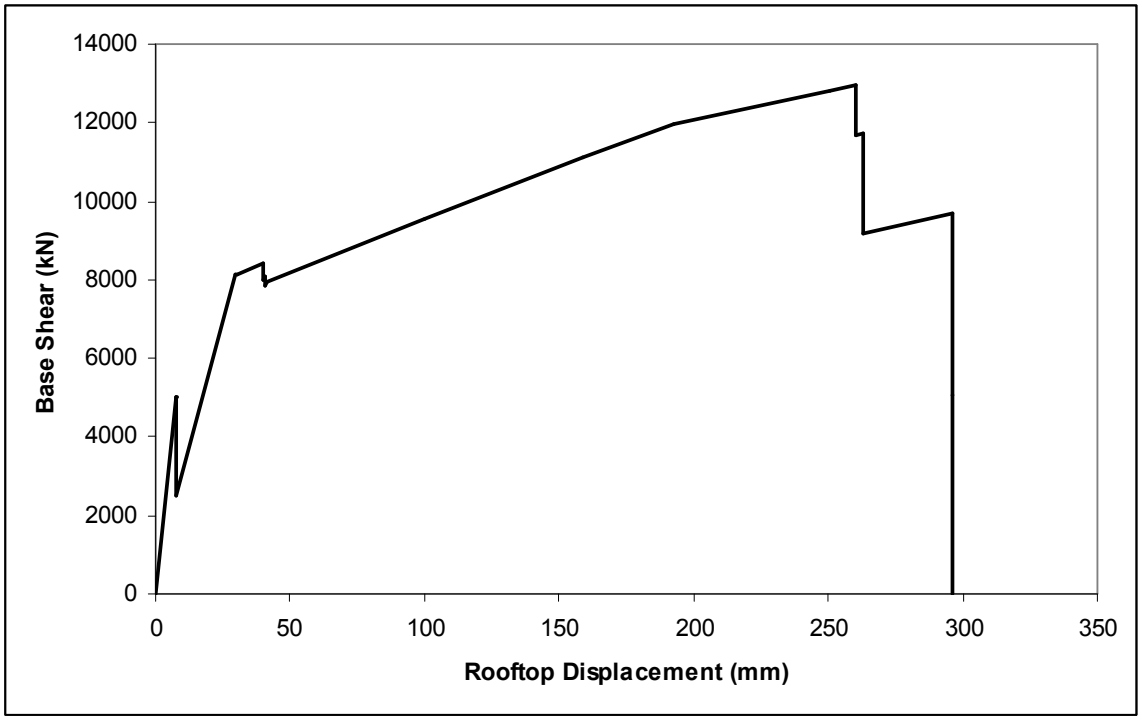

Figure F.2 BF-2 Pushover Curve

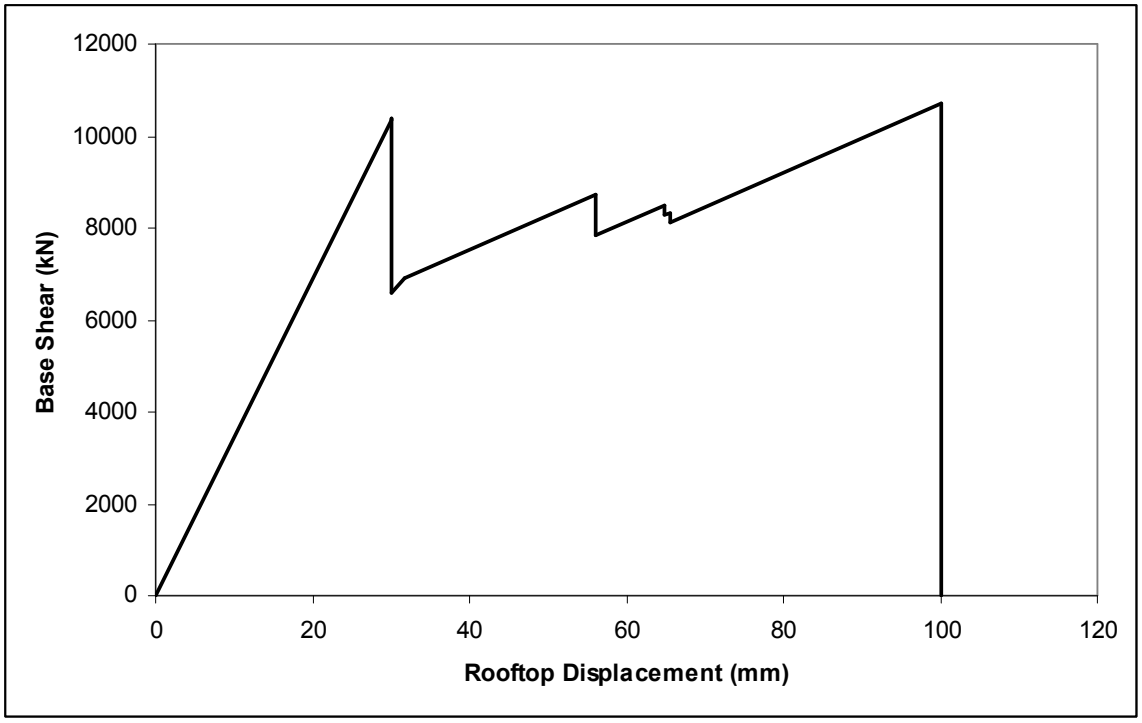

Figure F.3 BF-3 Pushover Curve

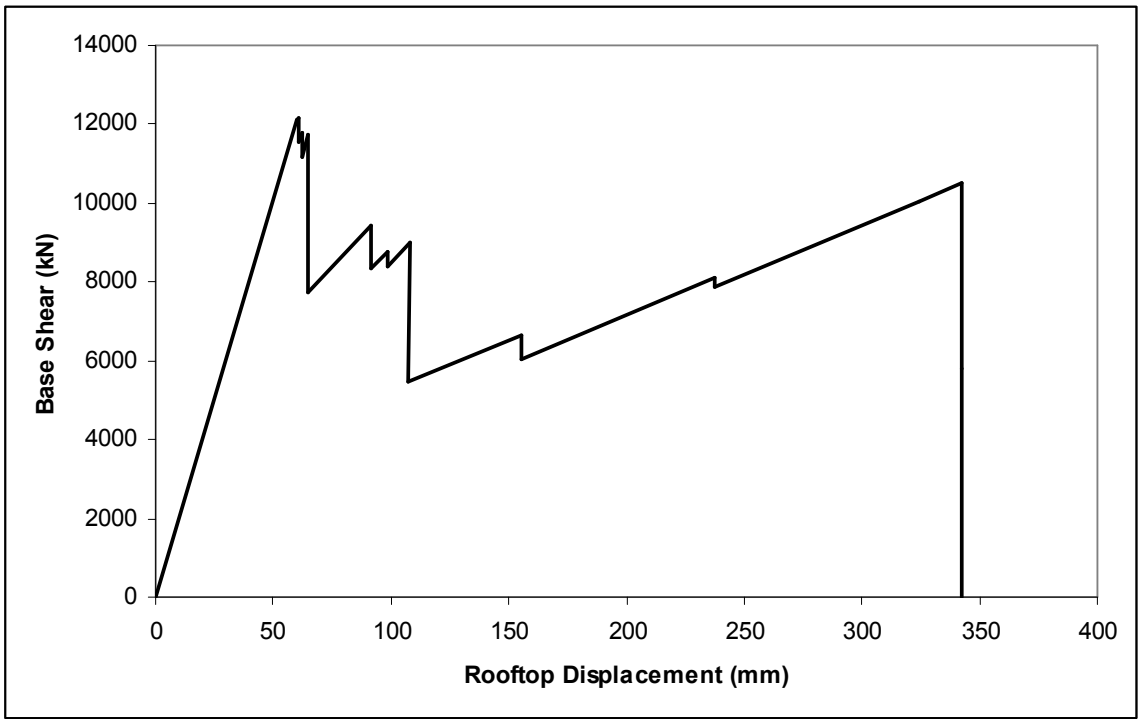

Figure F.4 BF-4 Pushover Curve

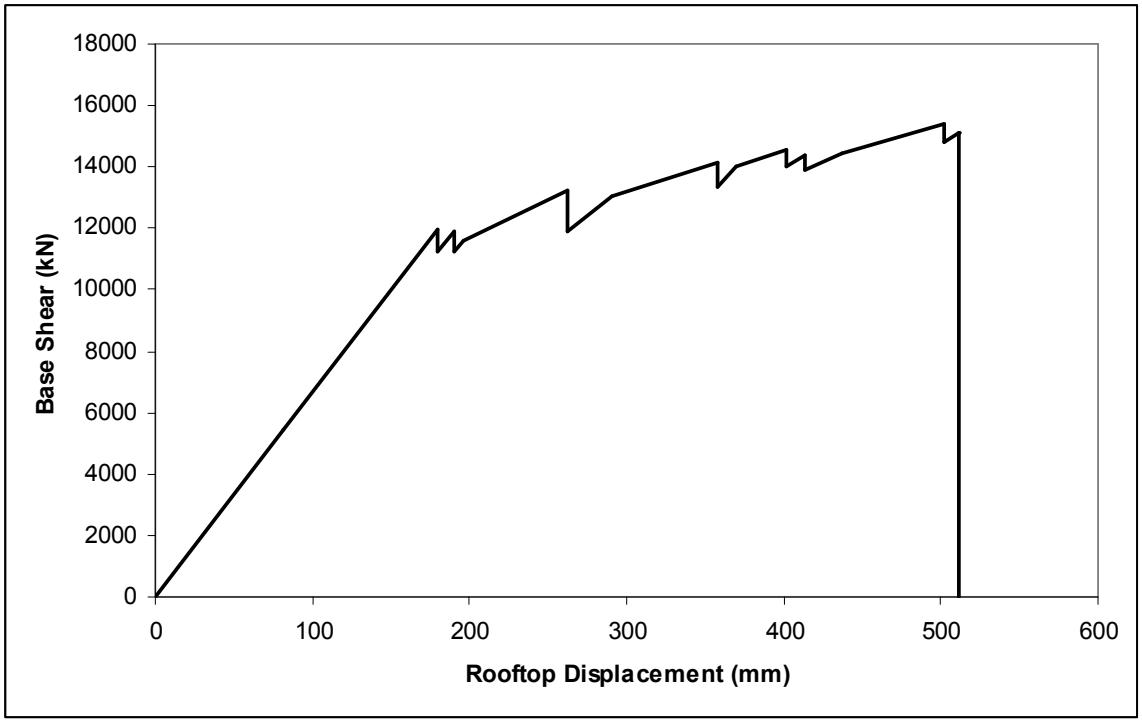

Figure F.5 BF-5 Pushover Curve

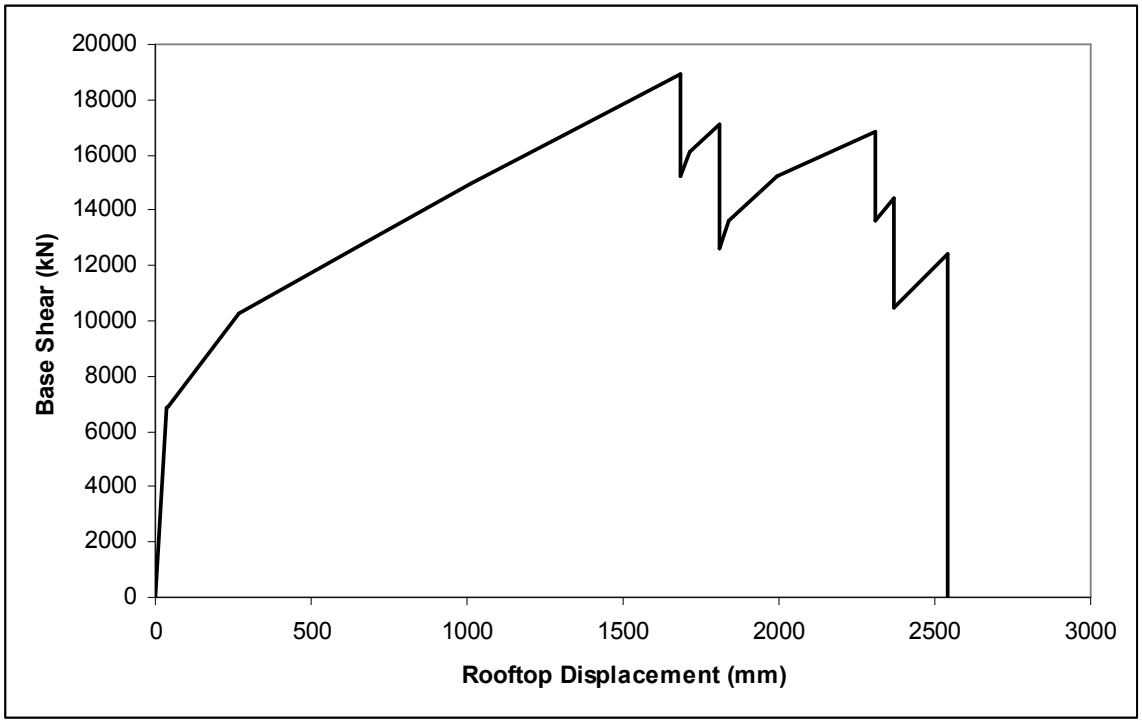

Figure F.6 EBF-1 Pushover Curve

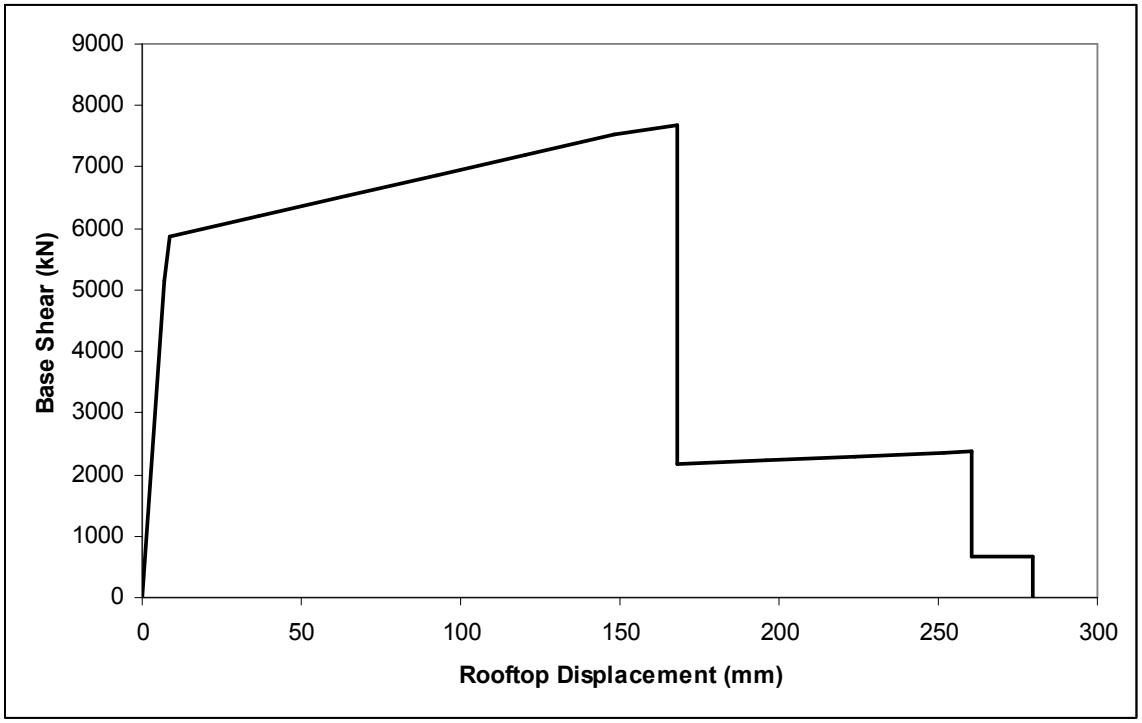

Figure F.7 SW-1 Pushover Curve

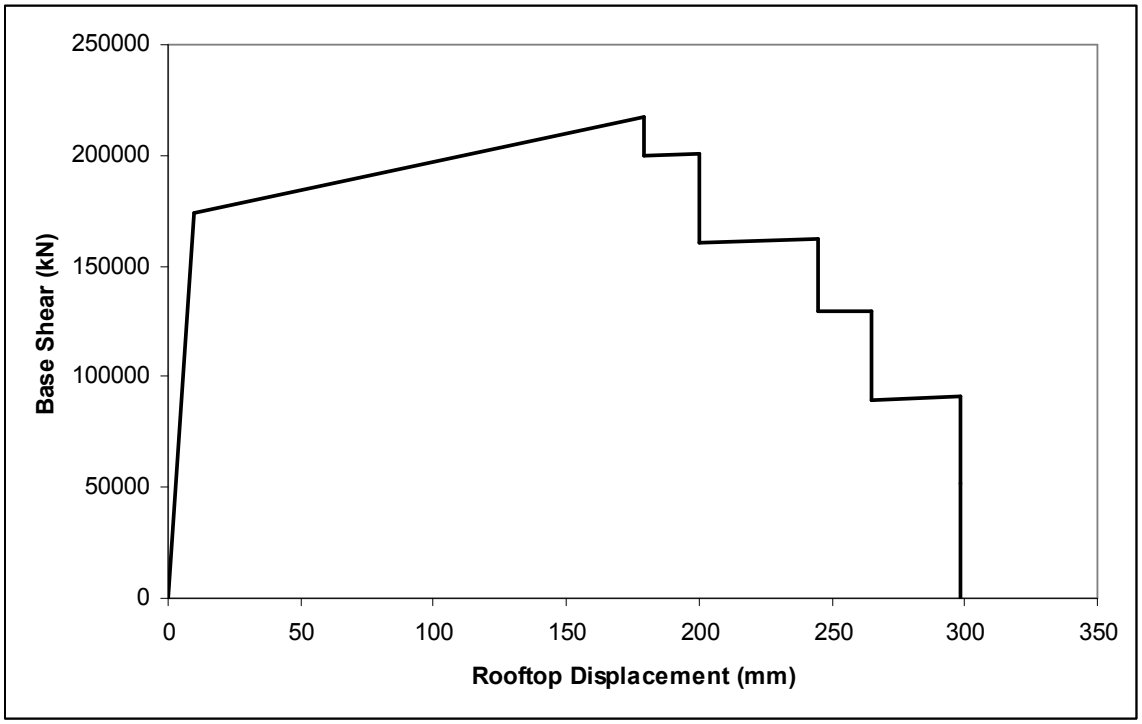

Figure F.8 SW-2 Pushover Curve

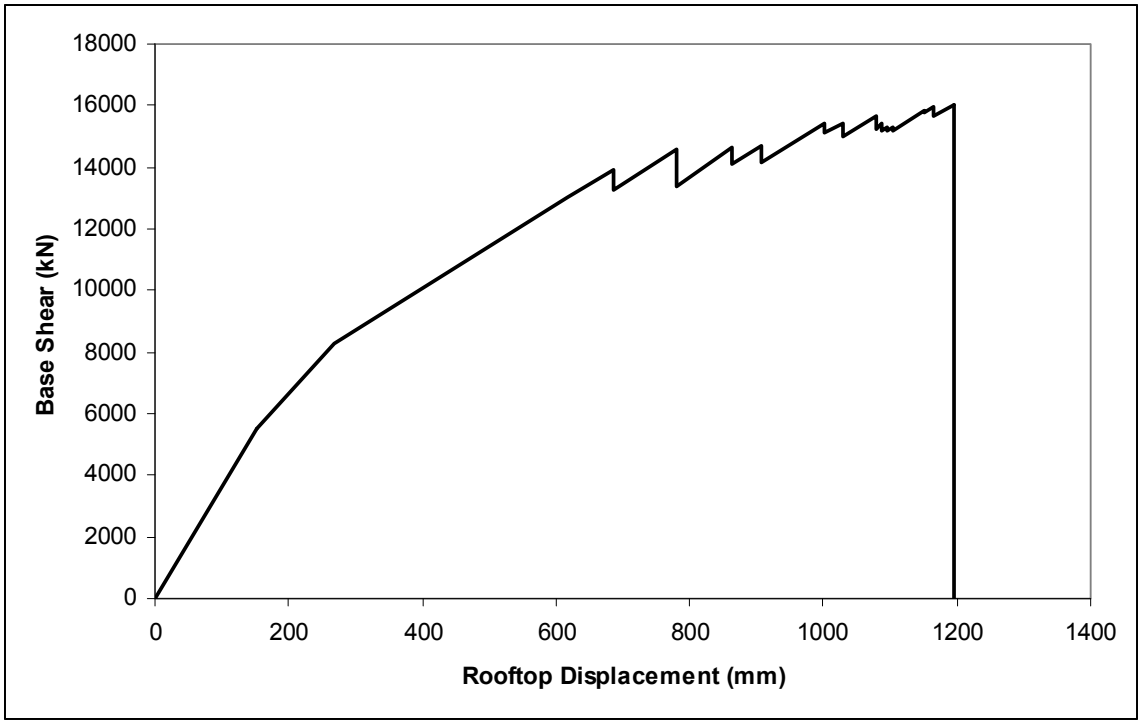

Figure F.9 MF-1 Pushover Curve

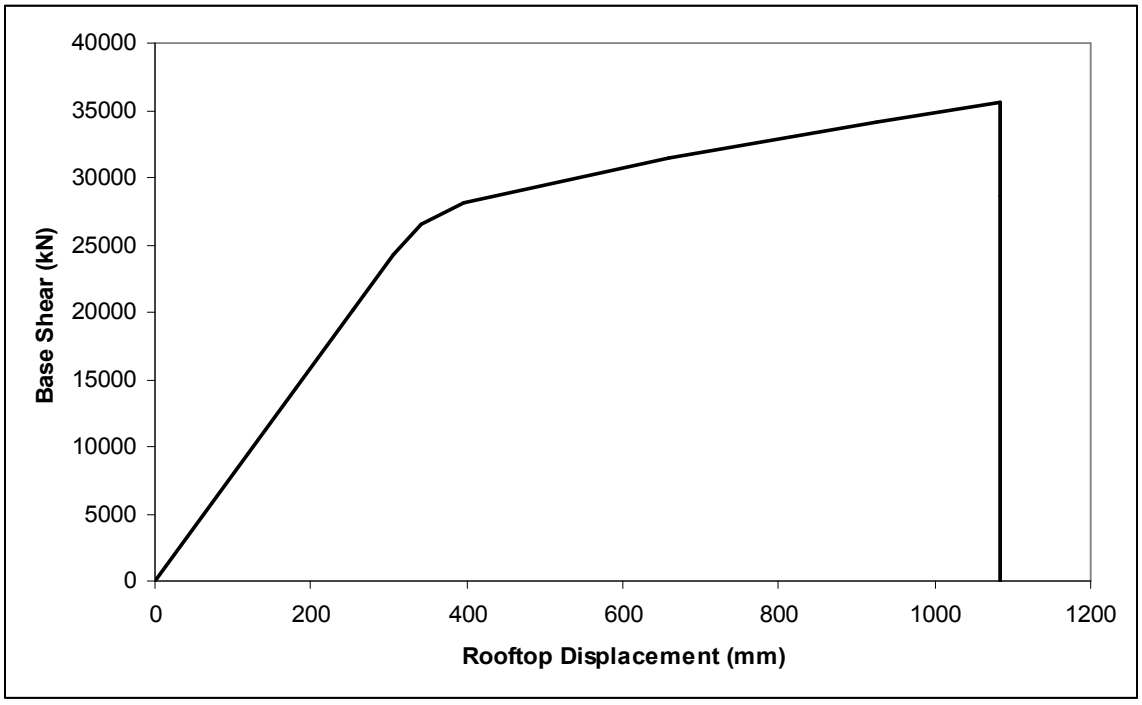

Figure F.10 MF-2 Pushover Curve

APPENDIX G

MODELING VALIDATION AND VERIFICATION

Advancements in desktop computer power and the accompanying development of analysis software have made possible the sophisticated numerical modeling of building structures. Early generations of modeling software followed traditional elastic analysis methods and enabled the rapid evaluation and optimization in structures. Recent developments have enabled the complex nonlinear analysis of building structures and realistic modeling of behaviors accounting for element nonlinearity. While such innovations provide tools enabling engineers to evaluate and design structures which accurately predict system behavior, it is important that the engineer understand in a fundamental sense the basic methods incorporated within analysis applications. In many scenarios, engineers are advised to have a fundamental sense of modeling results prior to even beginning modeling. In other cases, independent verification of modeling results is advised.

For this research, analysis results of SAP2000, ETABS and Perform 3D modeling applications were corroborated with simplified methods developed in the Microsoft Excel application with visual basic algorithms developed to analyze simple, inverted pendulum representations of the building models utilized in this research. Simplified models were developed by assessing the lumped mass and effective stiffness at each story level of each

structure. This information is presented in Appendix A. Figure 3.11 depicts an example of the simplified model for BF-4 with the rooftop damper included.

Corroboration of output between the Microsoft Excel spreadsheets (with visual basic algorithms) and the aforementioned nonlinear analysis applications is demonstrated in Figure G.1. Here, a response history at the rooftop of BF-4 is presented utilizing the N-S component of the El Centro 1940 record. While subtle differences can be observed in the output history, the results are of sufficient equality so as to nearly be superimposed in Figure G.1. For this example, the undamped version of the model was utilized and subjected to the N-S component of the El Centro 1940 accelerogram. Figure G.2 depicts the rooftop history results for a damped version of BF-4, again with the displacement response history displayed for the simplified Microsoft Excel application and ETABS, a nonlinear analysis application. For this, similar results as those demonstrated in Figure G.1 are observed. Specifically, the acceleration histories demonstrate very minor differences, thereby supporting the conclusion that the developed Microsoft Excel algorithm and the selected modeling applications produce practically equal results.

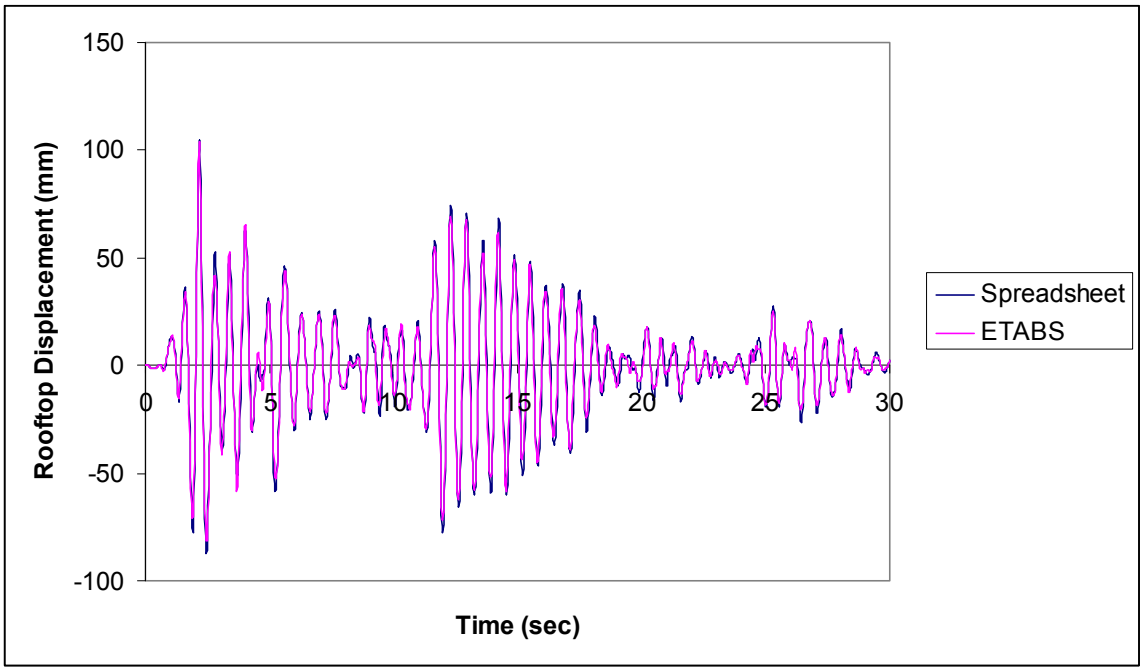

Figure G.1 Rooftop Displacement History Comparison, Undamped BF-4, El Centro 1940 Motion

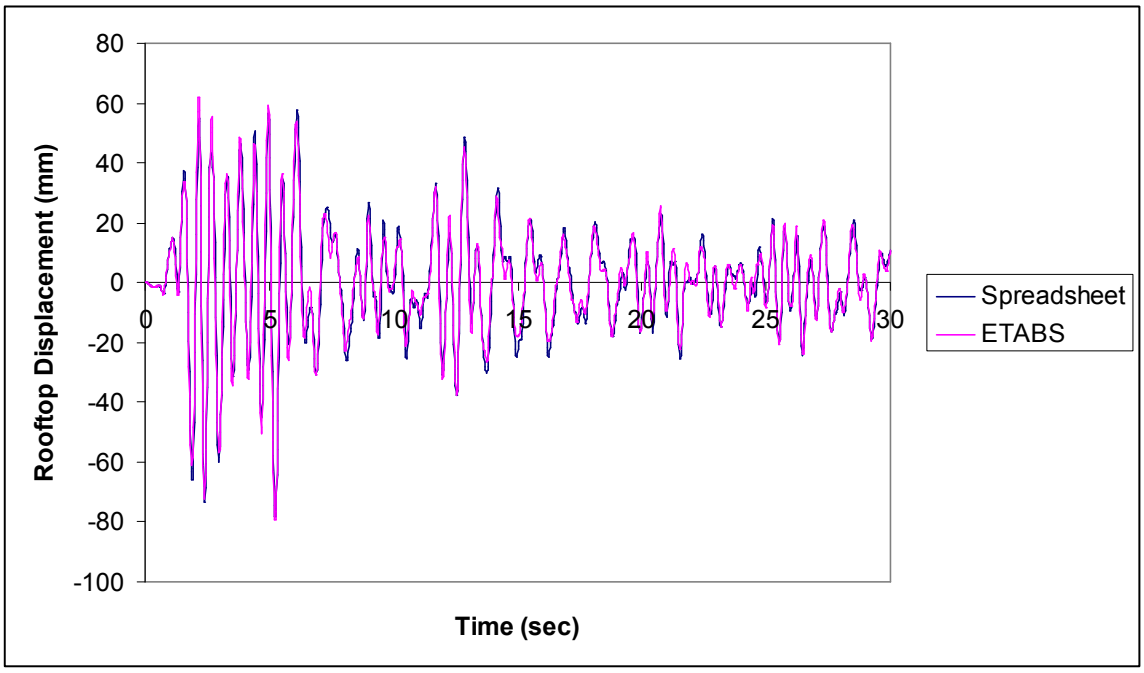

Figure G.2 Rooftop Displacement History Comparison, Damped BF-4, El Centro 1940 Motion

APPENDIX H

ADVANCED NONLINEAR MODELING ISSUES

Appendix H.1 Compression Bracing Nonlinearity

Important concepts are revealed when comparing output parameters of the models where nonlinearity of the base models was incorporated and base models which were analyzed using more conventional linear elastic approaches. For either case, nonlinear modeling of the NRTMDF is essential. The results of the research demonstrate that linear elastic modeling approaches of the NRTMDF serve as a qualitative method to identify whether the approach may be effective for a given structure and site but it does not adequately characterize the actual performance in a quantitative manner. Nonlinear modeling of the base structure can be a meticulous process and the current state-of-the-art for effectively modeling the nonlinearity of braces in compression is an issue of many research endeavors. Davaran and Adelzadeh explored this concept and indicate that cyclic behavior of brace elements in compression is not well understood particularly with respect to factors such as buckling and post buckling behavior.[40] Whether nonlinear modeling of the base structure should be undertaken for any structure under consideration for the approach explored within this research is an issue that should be addressed. Furthermore, if the structure under consideration is a braced frame it must be understood that the true nonlinear behavior, particularly if the braces buckle in compression, may be difficult to capture with analytical models. Even more, code provisions and prescribed

analysis methods do little to address true brace buckling behavior but focus instead on enabling connections to sustain brace buckling behavior without loosing significant capacity. If elastic analysis approaches demonstrate behavior within linear limitations of the base structure, nonlinear modeling of the base structure may not be necessary. If forces are high enough to breach the limits of linear performance, nonlinear modeling of the base structure should be required. Capturing the nonlinear buckling behavior of braces in compression may be considered a form of progressive failure. Upon occurring, phenomena such as soft story or extreme torsional irregularities may be introduced. When considering this, it must be understood that braces in lower period structures may buckle within a smaller time interval than longer period structures by virtue of the structures' inherent dynamic properties. Likewise, longer period structures typically experience greater displacements and therefore greater nonlinear demands. For either case, nonlinear analysis methods capable of modeling buckled braces demonstrate an extreme sensitivity to the time step within the acceleration history. For nonlinear modeling applications to serve effectively, the time step used in the algorithm must be far smaller than the time required for nonlinear behavior to occur (less than 0.02 seconds). As such, when modeling braces in compression, the predicted buckling behavior can be very sensitive to the time step used in the algorithm. This has been observed within the context of this research where competing analysis applications demonstrate a significant difference in the prediction of buckling behavior and therefore a difference in the predicted hysteretic result. Observations of two-dimensional hystereses demonstrate the differences which are further exacerbated when considering three-dimensional hystereses, with time as the third dimension. Figure H.1 depicts a simple two-story

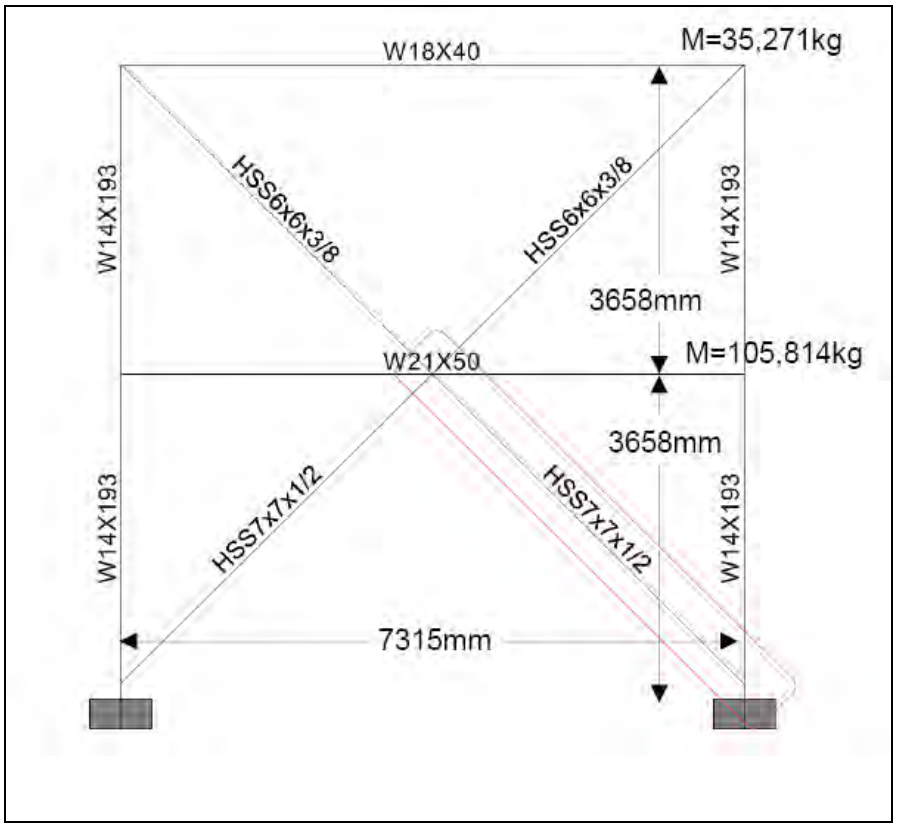

Figure H.1 Simple Braced Frame Structure

braced frame model. Within the context of validation and verification of nonlinear modeling techniques this structure was subjected to the north-south component of the El Centro 1940 ground motion with identical models in SAP 2000 and Perform 3D. This record and the analysis time-step utilized a 0.02 second time interval. Figure H.2 demonstrates the apparent differences in hysteresis loops for a bottom level brace from each model. These differences notwithstanding, the rooftop displacement histories shown in Figures H.3 and H.4 demonstrate obvious but relatively insignificant differences in overall structural behavior. For this case, the differences in behavior between the two analysis applications become resolved by the adjacent brace in the frame, also buckling and contributing to nonlinear behavior and counteracting the differences in the hystereses of Figure H.2. The differences in hystereses reflect the

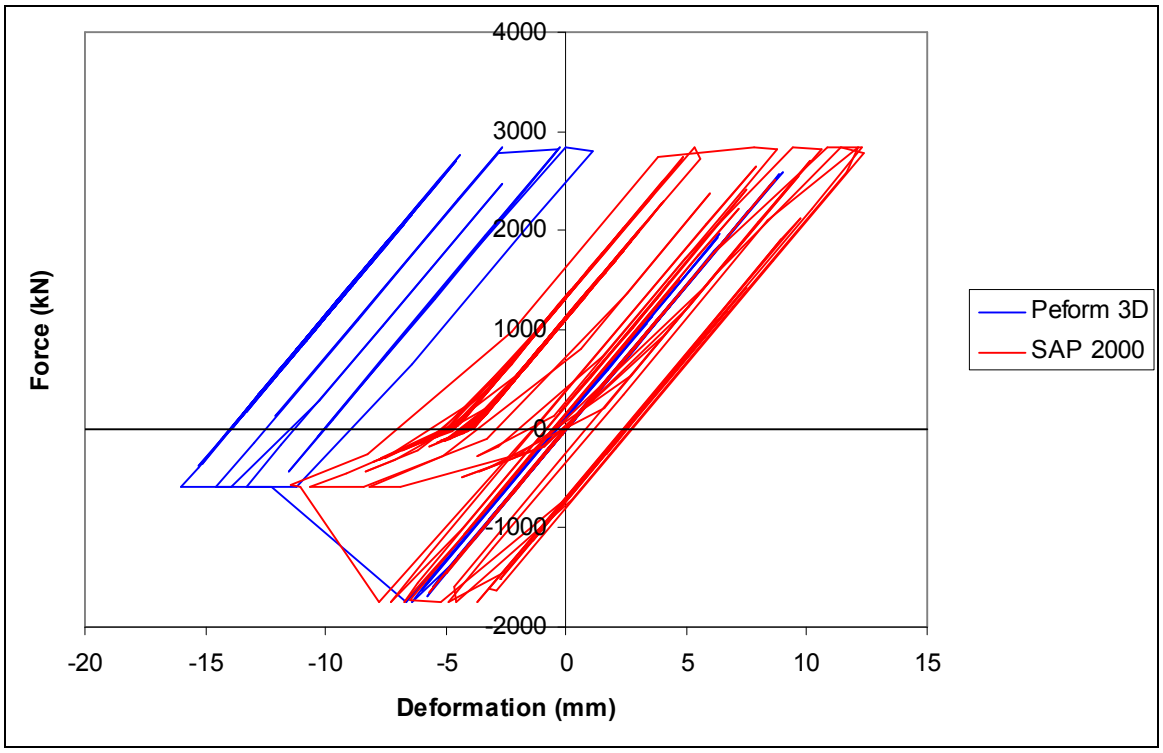

Figure H.2 Nonlinear Brace Behavior Comparison for Perform 3D and SAP2000

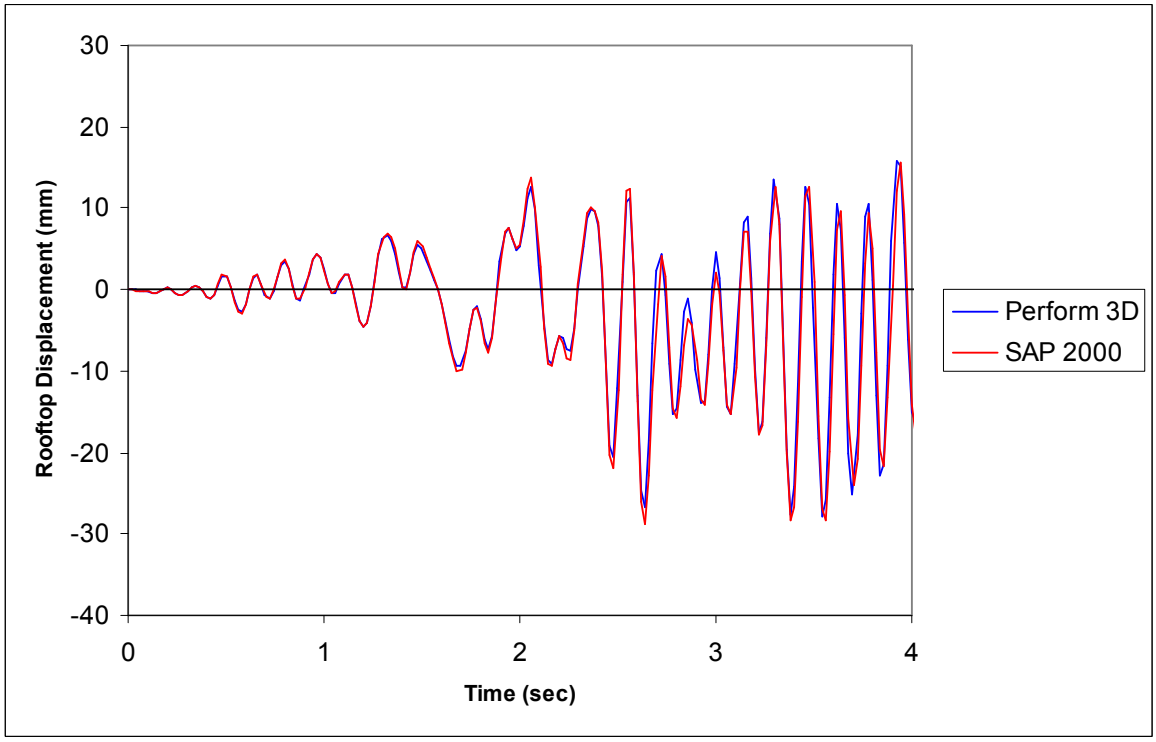

Figure H.3 Simple Brace Frame Rooftop Displacement History, 0 to 4 Seconds, N-S El Centro 1940 Record

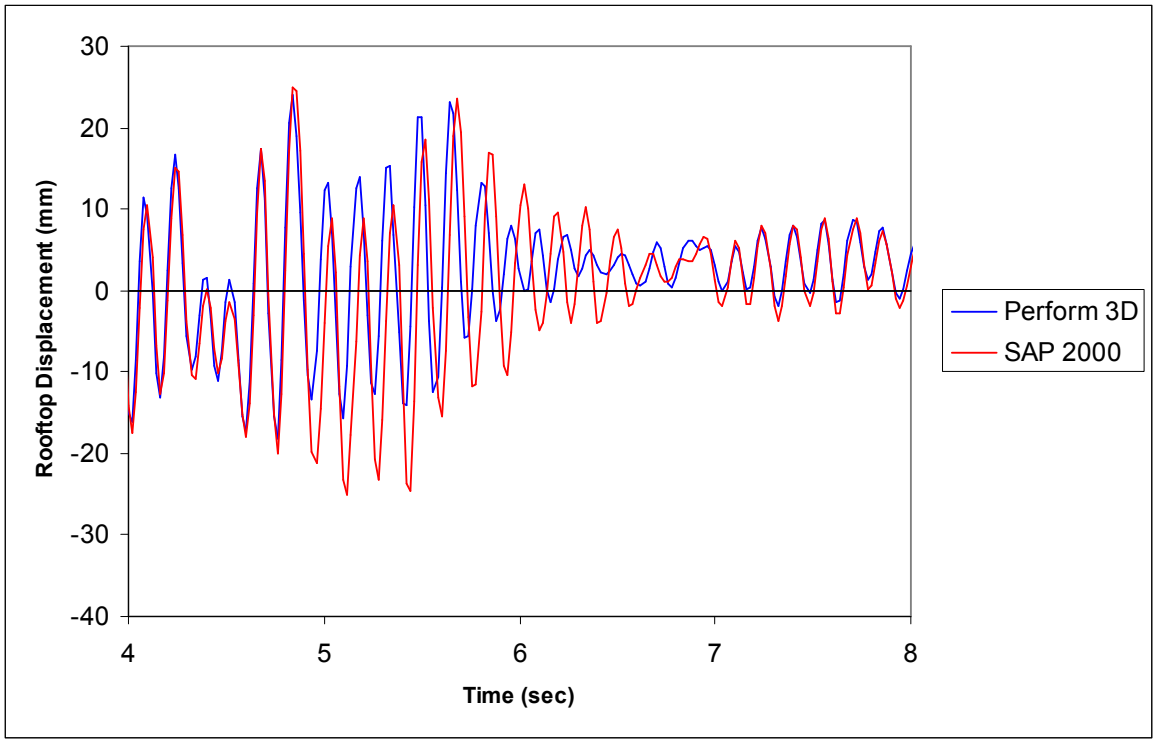

Figure H.4 Simple Braced Frame Rooftop Displacement History, 4 to 8 Seconds, N-S El Centro 1940 Record

numerical sensitivities introduced between the two analysis applications and also demonstrate the uncertainties associated with nonlinear modeling, particularly in consideration of capturing behavior of braces buckling in compression. In a fundamental sense the most critical concept associated with the analysis is the ability to predict whether brace buckling occurs and whether the NRTMDF approach reduces the structural response to the degree that buckling may be prevented.

Appendix H.2 Moment Frame Nonlinearity

In addition to the braced frame comparison of Appendix H.1 a moment frame comparison was conducted between the SAP 2000 and Perform 3D computer applications. Similar to the braced frame study, a simple moment frame model was

developed in each application. Figure H.5 depicts a moment frame model with the sizes and masses indicated accordingly. Figure H.6 demonstrates the hysteretic output between the applications for the second story beam marked in Figure H.5 for the north-south component of the El Centro 1940 record. As depicted, the hysteresis loops between the applications are generally consistent with apparent yet insignificant differences in hysteretic behavior of the beam plastic hinge. The insignificant difference in overall predicted behavior between SAP 2000 and Perform 3D can be observed in the displacement response history of the roof level shown in Figures H.7 and H.8. While the differences between predicted outputs of the SAP2000 and Perform 3D models are apparent, they are far more subtle than those of the braced frame model of Appendix H.1.

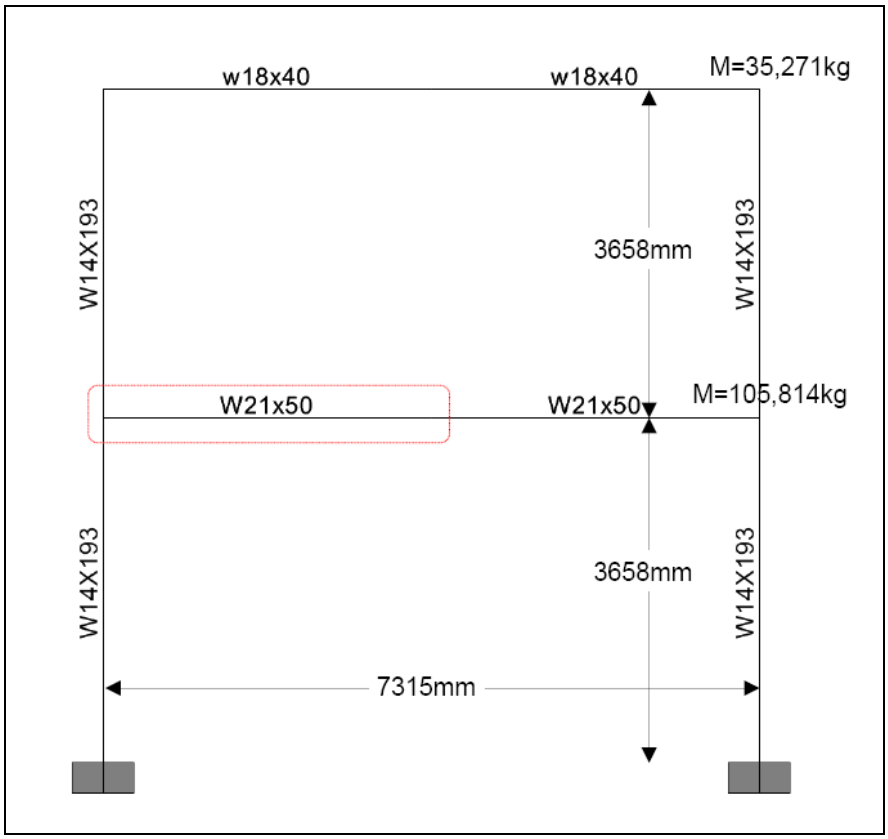

Figure H.5 Simple Moment Frame Structure

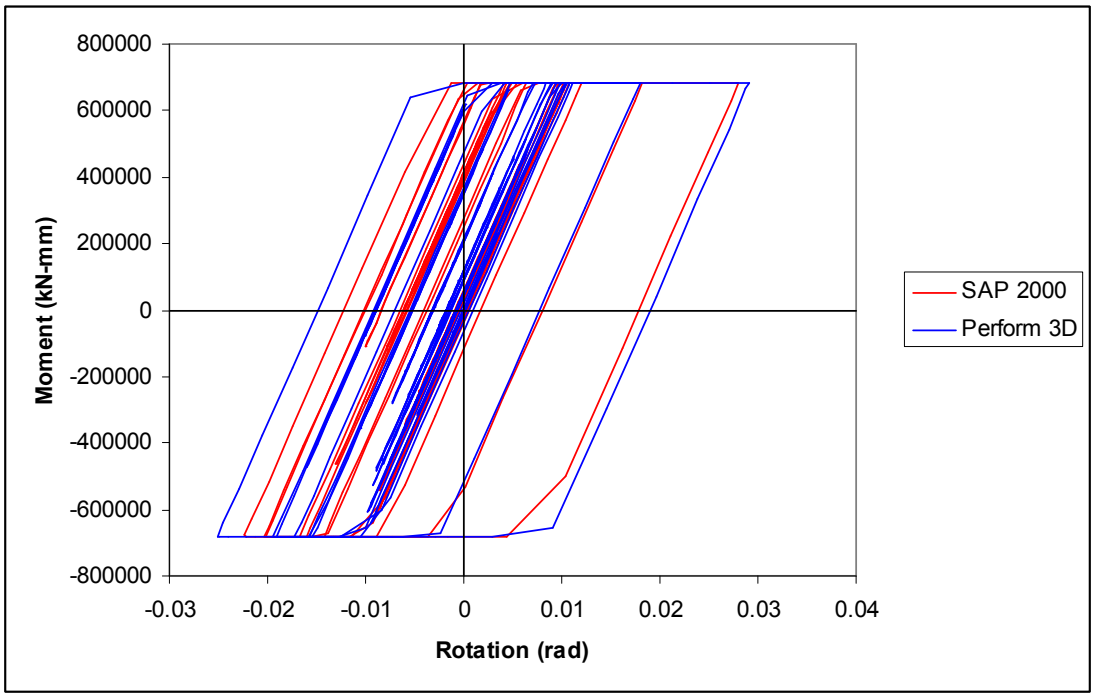

Figure H.6 Nonlinear Beam Comparison Between SAP 2000 and Perform 3D, N-S El Centro 1940 Record

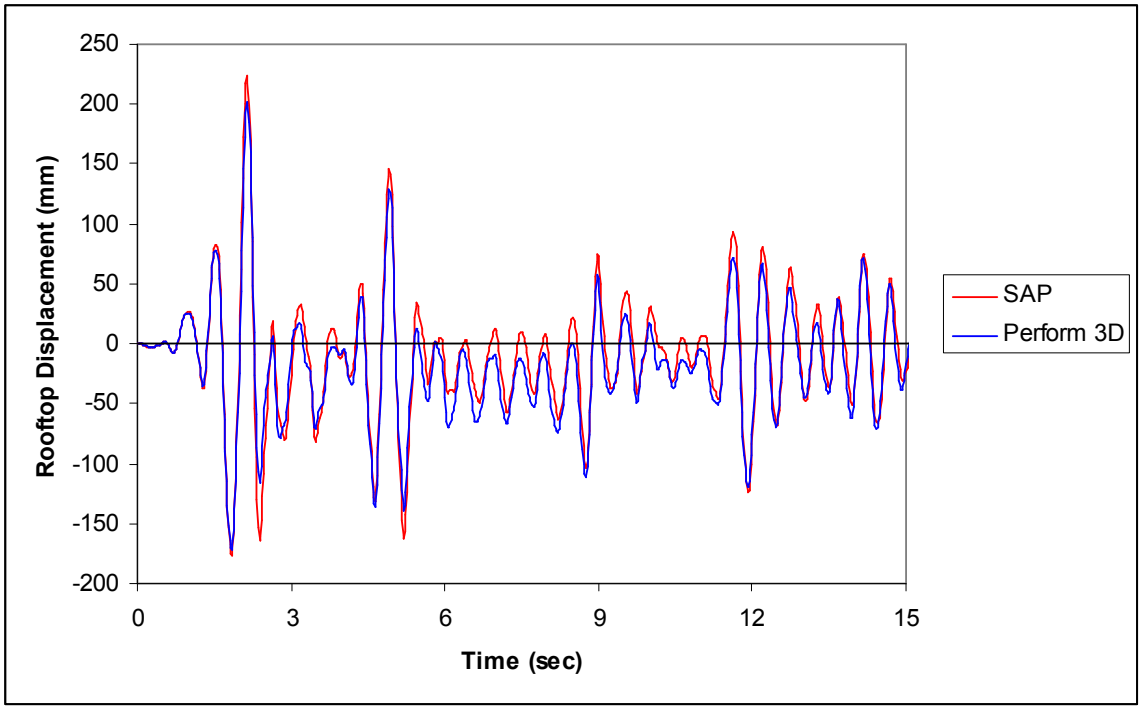

Figure H.7 Simple Moment Frame Rooftop Displacement History, 0 to 15 Seconds, N-S El Centro 1940 Record

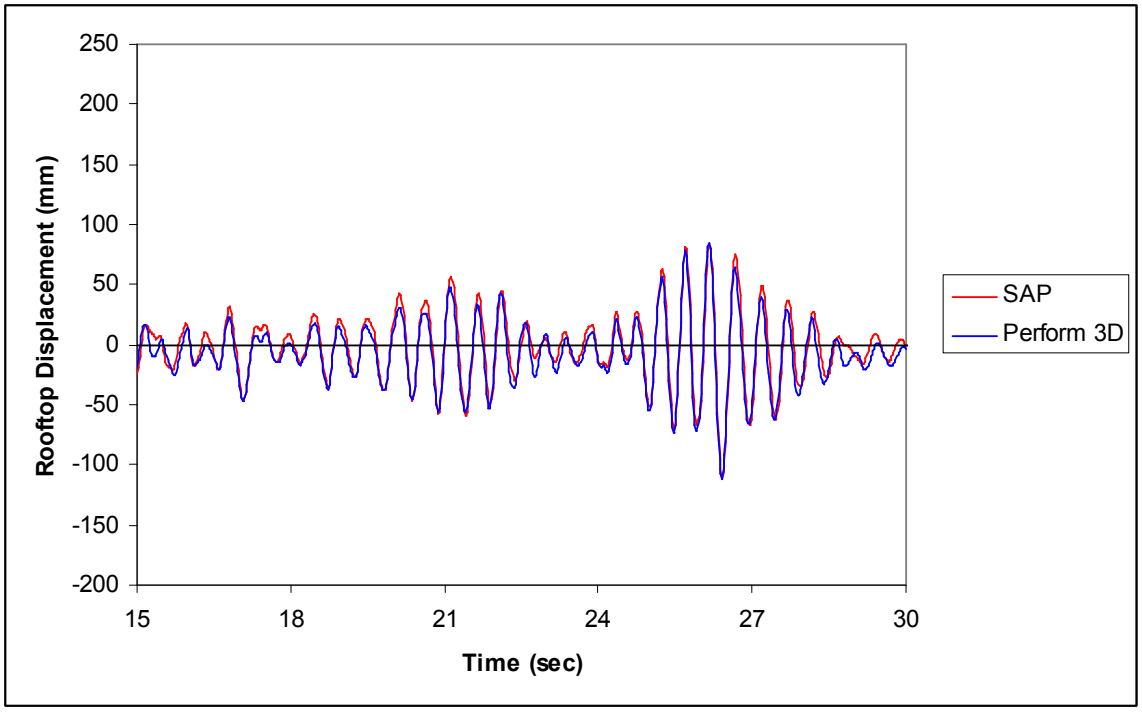

Figure H.8 Simple Moment Frame Rooftop Displacement History 15 to 30 Seconds, N-S El Centro 1940 Record

This is due to the relatively symmetric hysteretic behavior of the moment frame nonlinear hinges which are far less numerically sensitive than those of the braced frame counterpart. Unlike braces acting in compression, hysteretic nonlinearity of moment frame beams does not occur abruptly within the time history analysis. In short, the nonlinear behavior occurs over a greater number of time steps with no abrupt nonlinear transitions without a change of direction within the analysis. This leads to reduced numerical instabilities in the algorithm and therefore a better corroboration between the competing applications.

APPENDIX I

ENERGY METHOD CALCULATIONS

Chapter 7 summarizes the results of the energy analyses utilizing the Park and Ang method. Tables I.1 through I.10 provide the summary of calculations. Also included within Chapter 7 are the Fardis energy calculations, the results of which are summarized in Tables I.11 through I.20.

Table I.1 BF-1 Park and Ang Damage Indices

		Undamped			Damped					Undamped			Damped		
	Record	δ_m mm	Energy kJ	D index	δ_m mm	Energy kJ	D index		Record	δ_m mm	Energy kJ	D index	δ_m mm	Energy kJ	D index
BSE-1	LA20	12	61	0.74	9	56	0.61	BSE-2	LA23	13	70	0.82	14	110	1.02
(Hard)	BO7	9	25	0.46	9	28	0.49	(Med.)	LA24	11	37	0.59	11	82	0.81
	SE04	16	70	0.93	9	55	0.62		SE23	33	170	2.06	30	188	2.01
	LA12	22	85	1.23	18	81	1.06		LA31	34	599	4.00	32	472	3.32
	SE05	8	65	0.61	9	79	0.69		LA32	37	899	5.42	30	537	3.54
	SE06	10	127	0.97	10	109	0.87		SE28	50	1525	8.70	42	1033	6.22
	SE12	12	81	0.81	9	64	0.63		SE32	33	1583	8.27	29	1485	7.71
BSE-2	LA28	20	96	1.22	18	80	1.06	BSE-1	SE01	19	150	1.42	15	102	1.05
(Hard)	LA30	50	1075	6.72	34	514	3.59	(Soft)	LA03	13	87	0.88	14	56	0.79
	LA39	16	104	1.10	15	112	1.09		LA15	16	99	1.08	15	81	0.95
	LA33	25	266	2.17	19	131	1.32		LA09	17	79	1.00	13	73	0.81
	SE39	29	829	4.81	18	487	2.87		LA10	22	298	2.20	18	192	1.55
	SE25	26	645	3.86	21	479	2.96		LA07	14	124	1.11	13	124	1.07
	SE30	33	1678	8.71	24	1048	5.58		SE07	21	342	2.33	15	240	1.63
BSE-1	LA13	17	109	1.14	14	67	0.84	BSE-2	LA38	19	220	1.73	24	177	1.73
(Med.)	LA14	15	57	0.83	9	39	0.54	(Soft)	LA40	20	232	1.81	23	197	1.76
	LA18	10	22	0.47	8	26	0.45		SE24	34	237	2.37	36	202	2.33
	LA02	16	115	1.13	12	112	0.98		LA35	47	1128	6.83	36	573	3.96
	SE03	14	111	1.04	12	84	0.84		LA36	33	270	2.49	24	185	1.77
	SE15	16	176	1.42	14	188	1.39		SE33	53	1947	10.67	39	1201	6.82
	SE18	16	380	2.30	15	339	2.10		SE36	26	217	1.99	28	207	2.01

Table I.2 BF-2 Park and Ang Damage Indices

		Undamped			Damped					Undamped			Damped		
	Record	δ_m mm	Energy kJ	D index	δ_m mm	Energy kJ	D index		Record	δ_m mm	Energy kJ	D index	δ_m mm	Energy kJ	D index
BSE-1	LA20	19	265	0.12	11	203	0.08	BSE-2	LA23	26	415	0.18	21	534	0.18
(Hard)	BO7	14	194	0.09	8	120	0.06	(Med.)	LA24	18	267	0.12	16	399	0.14
	SE04	22	356	0.15	15	225	0.10		SE23	56	1649	0.53	51	1548	0.50
	LA12	18	352	0.14	19	294	0.13		LA31	72	5601	1.36	60	4630	1.12
	SE05	17	522	0.17	12	448	0.13		LA32	65	3075	0.84	62	3312	0.88
	SE06	15	595	0.17	12	568	0.16		SE28	63	7172	1.63	59	6088	1.40
	SE12	15	379	0.13	12	235	0.09		SE32	30	3859	0.86	31	4505	0.99
BSE-2	LA28	44	931	0.35	28	532	0.21	BSE-1	SE01	17	212	0.11	19	301	0.13
(Hard)	LA30	38	1852	0.50	33	1549	0.43	(Soft)	LA03	21	212	0.12	15	226	0.10
	LA39	33	1051	0.33	24	743	0.24		LA15	25	585	0.21	17	371	0.14
	LA33	40	1411	0.43	26	638	0.22		LA09	16	364	0.13	21	386	0.16
	SE39	45	5835	1.30	24	2226	0.52		LA10	28	1160	0.33	24	1081	0.30
	SE25	54	5208	1.21	33	2752	0.66		LA07	22	712	0.22	22	603	0.20
	SE30	48	7650	1.66	35	5491	1.19		SE07	28	2318	0.56	20	1528	0.37
BSE-1	LA13	22	557	0.19	20	497	0.17	BSE-2	LA38	26	787	0.25	31	805	0.28
(Med.)	LA14	21	300	0.14	16	290	0.12	(Soft)	LA40	28	601	0.22	30	827	0.27
	LA18	21	211	0.12	19	164	0.10		SE24	51	1567	0.50	49	1066	0.39
	LA02	16	401	0.14	15	452	0.14		LA35	48	3355	0.83	41	2231	0.59
	SE03	19	476	0.17	16	432	0.15		LA36	46	2050	0.57	39	1660	0.47
	SE15	18	662	0.20	17	762	0.21		SE33	89	15666	3.37	70	8878	1.98
	SE18	23	1732	0.42	19	1422	0.35		SE36	24	882	0.26	29	999	0.31

Table I.3 BF-3 Park and Ang Damage Indices

		Undamped			Damped					Undamped			Damped		
	Record	δ_m mm	Energy kJ	D index	δ_m mm	Energy kJ	D index		Record	δ_m mm	Energy kJ	D index	δ_m mm	Energy kJ	D index
BSE-1	LA20	24	231	0.40	20	263	0.37	BSE-2	LA23	78	3252	2.91	51	1489	1.49
(Hard)	BO7	17	131	0.26	18	203	0.31	(Med.)	LA24	49	913	1.09	37	743	0.86
	SE04	29	366	0.53	20	382	0.45		SE23	64	833	1.19	57	1023	1.24
	LA12	44	482	0.76	23	360	0.46		LA31	104	2891	2.94	67	2140	2.07
	SE05	26	537	0.61	22	553	0.58		LA32	67	1889	1.91	77	1852	1.98
	SE06	30	537	0.65	25	583	0.63		SE28	95	6871	5.46	100	6012	4.94
	SE12	22	363	0.46	23	421	0.50		SE32	84	17748	12.49	61	8044	5.89
BSE-2	LA28	106	2579	2.75	70	1047	1.39	BSE-1	SE01	40	343	0.63	31	316	0.51
(Hard)	LA30	85	2776	2.67	52	1910	1.77	(Soft)	LA03	45	621	0.85	51	565	0.88
	LA39	67	1994	1.97	48	1021	1.15		LA15	63	1268	1.46	47	697	0.93
	LA33	59	1396	1.51	43	990	1.08		LA09	39	875	0.97	40	639	0.82
	SE39	51	4325	3.35	48	2872	2.36		LA10	59	2051	1.94	41	1252	1.23
	SE25	83	5363	4.35	60	3231	2.72		LA07	40	874	0.97	28	699	0.74
	SE30	101	15185	10.98	55	5550	4.19		SE07	57	2880	2.46	40	2161	1.82
BSE-1	LA13	34	528	0.69	35	297	0.54	BSE-2	LA38	56	1571	1.59	66	1775	1.82
(Med.)	LA14	24	292	0.43	27	256	0.44	(Soft)	LA40	109	4360	3.95	74	3077	2.75
	LA18	51	583	0.89	32	249	0.49		SE24	93	1105	1.65	84	1410	1.76
	LA02	32	736	0.80	25	516	0.59		LA35	90	2354	2.45	71	2928	2.63
	SE03	28	436	0.57	24	388	0.49		LA36	84	2199	2.28	73	2616	2.44
	SE15	31	1100	1.03	33	1125	1.06		SE33	130	16239	11.96	100	11282	8.40
	SE18	48	3437	2.73	30	1470	1.26		SE36	58	1281	1.42	53	1917	1.79

Table I.4 BF-4 Park and Ang Damage Indices

		Undamped			Damped					Undamped			Damped		
	Record	δ_m mm	Energy kJ	D index	δ_m mm	Energy kJ	D index		Record	δ_m mm	Energy kJ	D index	δ_m mm	Energy kJ	D index
BSE-1	LA20	39	479	0.66	32	253	0.46	BSE-2	LA23	230	12508	10.04	128	4004	3.72
(Hard)	BO7	38	322	0.56	22	229	0.35	(Med.)	LA24	215	13970	10.84	105	3630	3.27
	SE04	40	444	0.65	35	513	0.65		SE23	198	9272	7.70	152	3497	3.62
	LA12	53	929	1.08	31	433	0.56		LA31	244	11139	9.31	127	3476	3.38
	SE05	52	1183	1.23	31	699	0.73		LA32	283	15545	12.46	151	4685	4.37
	SE06	69	1570	1.63	31	642	0.69		SE28	279	18337	14.19	193	9836	8.01
	SE12	64	969	1.21	31	480	0.59		SE32	259	79509	52.71	140	23050	15.88
BSE-2	LA28	141	2048	2.60	109	1339	1.85	BSE-1	SE01	118	1641	2.14	111	1384	1.90
(Hard)	LA30	141	5734	4.93	121	3417	3.29	(Soft)	LA03	103	1539	1.93	94	960	1.48
	LA39	136	3084	3.21	97	2520	2.50		LA15	119	1362	1.96	95	955	1.48
	LA33	133	3731	3.59	81	1493	1.69		LA09	97	2445	2.45	74	1296	1.51
	SE39	116	4588	3.97	72	3395	2.81		LA10	84	1951	2.01	65	1579	1.60
	SE25	165	11807	9.00	107	5574	4.52		LA07	130	3308	3.30	92	1797	1.99
	SE30	196	21275	15.27	110	11323	8.18		SE07	108	5727	4.63	68	3230	2.67
BSE-1	LA13	82	1112	1.47	57	478	0.83	BSE-2	LA38	186	5388	5.13	181	5849	5.38
(Med.)	LA14	96	1002	1.52	47	398	0.68	(Soft)	LA40	115	2659	2.74	137	4901	4.37
	LA18	67	463	0.91	45	347	0.64		SE24	215	4545	4.87	185	4367	4.48
	LA02	93	1857	2.03	49	1097	1.15		LA35	294	17286	13.66	235	12481	10.08
	SE03	109	3093	2.96	47	1013	1.07		LA36	321	17063	13.77	232	11470	9.41
	SE15	73	2952	2.55	54	1825	1.66		SE33	156	14252	10.46	132	10895	8.11
	SE18	93	4814	3.91	37	2664	2.03		SE36	218	12763	10.10	159	7365	6.13

Table I.5 BF-5 Park and Ang Damage Indices

		Undamped			Damped					Undamped			Damped		
	Record	δ_m mm	Energy kJ	D index	δ_m mm	Energy kJ	D index		Record	δ_m mm	Energy kJ	D index	δ_m mm	Energy kJ	D index
BSE-1	LA20	97	346	0.23	58	216	0.14	BSE-2	LA23	337	6094	1.40	331	4429	1.18
(Hard)	BO7	49	287	0.13	46	188	0.11	(Med.)	LA24	378	5299	1.38	303	3413	1.00
	SE04	116	1074	0.36	49	432	0.15		SE23	485	7371	1.84	372	4626	1.29
	LA12	74	585	0.22	53	331	0.14		LA31	416	8771	1.87	243	5455	1.13
	SE05	84	1224	0.31	58	589	0.18		LA32	452	8598	1.92	350	5483	1.35
	SE06	86	825	0.27	47	501	0.15		SE28	398	12160	2.25	247	6900	1.32
	SE12	91	642	0.26	43	493	0.14		SE32	665	46947	6.96	395	23198	3.57
BSE-2	LA28	219	2359	0.71	181	1645	0.55	BSE-1	SE01	223	1329	0.60	226	1355	0.61
(Hard)	LA30	193	5168	1.00	199	4019	0.87	(Soft)	LA03	302	3539	1.02	231	1372	0.62
	LA39	288	4034	1.05	247	2654	0.80		LA15	309	4278	1.12	233	1479	0.64
	LA33	302	4159	1.09	213	2516	0.72		LA09	252	2810	0.83	244	2572	0.79
	SE39	322	14287	2.35	198	5718	1.08		LA10	305	3158	0.98	158	3413	0.72
	SE25	264	12225	1.99	213	6049	1.15		LA07	284	3493	0.98	179	2233	0.62
	SE30	261	15306	2.36	158	7748	1.24		SE07	377	14588	2.50	152	5274	0.93
BSE-1	LA13	161	765	0.41	81	486	0.22	BSE-2	LA38	687	25702	4.44	673	16521	3.31
(Med.)	LA14	153	896	0.41	88	480	0.23	(Soft)	LA40	480	12958	2.50	429	10384	2.09
	LA18	104	534	0.27	95	375	0.23		SE24	656	6591	2.08	539	7177	1.92
	LA02	172	1696	0.54	74	854	0.25		LA35	395	6229	1.52	372	6823	1.55
	SE03	174	2944	0.70	111	1003	0.34		LA36	463	6770	1.72	419	8220	1.81
	SE15	140	2883	0.62	118	1834	0.45		SE33	643	34981	5.48	456	16999	2.94
	SE18	124	3465	0.66	72	1489	0.32		SE36	997	64259	9.70	679	19773	3.71

Table I.6 EBF-1 Park and Ang Damage Indices

		Undamped			Damped					Undamped			Damped		
	Record	δ_m mm	Energy kJ	D index	δ_m mm	Energy kJ	D index		Record	δ_m mm	Energy kJ	D index	δ_m mm	Energy kJ	D index
BSE-1	LA20	33	234	0.02	25	220	0.02	BSE-2	LA23	140	3265	0.15	86	2198	0.10
(Hard)	BO7	29	160	0.02	16	125	0.01	(Med.)	LA24	114	4627	0.17	66	1424	0.07
	SE04	34	325	0.03	26	313	0.02		SE23	138	1701	0.12	116	1354	0.10
	LA12	51	606	0.04	36	359	0.03		LA31	127	3472	0.15	108	1839	0.10
	SE05	45	591	0.04	31	549	0.03		LA32	136	3696	0.16	107	2123	0.11
	SE06	42	686	0.04	27	516	0.03		SE28	245	12053	0.41	144	5328	0.20
	SE12	56	637	0.05	24	274	0.02		SE32	185	23156	0.62	113	12584	0.34
BSE-2	LA28	117	2151	0.12	98	1502	0.09	BSE-1	SE01	89	800	0.07	85	1071	0.07
(Hard)	LA30	145	3340	0.16	98	2248	0.11	(Soft)	LA03	67	647	0.05	73	796	0.06
	LA39	139	4993	0.19	84	1565	0.08		LA15	79	658	0.06	68	671	0.05
	LA33	75	887	0.06	63	635	0.05		LA09	78	1163	0.07	64	1032	0.06
	SE39	89	2623	0.11	67	2181	0.09		LA10	75	1414	0.08	59	1474	0.07
	SE25	141	5904	0.21	90	3856	0.14		LA07	101	1768	0.10	65	1384	0.07
	SE30	124	15466	0.41	83	8824	0.24		SE07	73	2613	0.10	55	2092	0.08
BSE-1	LA13	75	883	0.06	47	273	0.03	BSE-2	LA38	118	2302	0.12	122	3984	0.16
(Med.)	LA14	50	368	0.04	40	233	0.03	(Soft)	LA40	92	1667	0.09	95	3936	0.14
	LA18	55	486	0.04	40	249	0.03		SE24	137	2025	0.13	104	2727	0.12
	LA02	75	1302	0.07	44	698	0.04		LA35	198	6521	0.26	136	5614	0.20
	SE03	78	1681	0.08	37	527	0.03		LA36	155	5213	0.21	111	4429	0.16
	SE15	35	1000	0.04	41	1198	0.05		SE33	117	6163	0.20	105	6529	0.21
	SE18	59	3501	0.11	33	1788	0.06		SE36	117	2650	0.13	113	2801	0.13

Table I.7 SW-1 Park and Ang Damage Indices

		Undamped			Damped					Undamped			Damped		
	Record	δ_m mm	Energy kJ	D index	δ_m mm	Energy kJ	D index		Record	δ_m mm	Energy kJ	D index	δ_m mm	Energy kJ	D index
BSE-1	LA20	24	299	0.28	18	365	0.27	BSE-2	LA23	49	2281	1.32	45	1629	1.00
(Hard)	BO7	16	257	0.21	17	219	0.20	(Med.)	LA24	30	698	0.49	31	1315	0.78
	SE04	29	612	0.45	16	418	0.28		SE23	70	3298	1.90	51	1693	1.06
	LA12	30	438	0.38	21	533	0.37		LA31	86	5155	2.83	67	4002	2.20
	SE05	27	981	0.60	19	692	0.42		LA32	65	3163	1.81	70	3554	2.02
	SE06	29	916	0.59	21	836	0.50		SE28	108	14702	7.26	65	8664	4.29
	SE12	25	777	0.50	21	522	0.36		SE32	52	9126	4.42	54	11630	5.56
BSE-2	LA28	84	2931	1.82	61	1331	0.96	BSE-1	SE01	28	446	0.37	30	439	0.37
(Hard)	LA30	65	2957	1.72	43	2395	1.33	(Soft)	LA03	40	904	0.64	33	508	0.42
	LA39	64	1967	1.26	36	1244	0.77		LA15	44	1826	1.08	35	760	0.55
	LA33	68	3715	2.08	35	1054	0.69		LA09	28	826	0.54	33	748	0.53
	SE39	67	8720	4.32	37	3358	1.73		LA10	41	2105	1.19	29	1294	0.76
	SE25	84	9790	4.91	44	4035	2.08		LA07	29	1115	0.67	28	1082	0.65
	SE30	89	16969	8.17	42	7327	3.55		SE07	41	3765	1.94	32	2559	1.34
BSE-1	LA13	34	618	0.48	24	650	0.44	BSE-2	LA38	48	1643	1.02	57	2368	1.40
(Med.)	LA14	26	449	0.36	28	478	0.38	(Soft)	LA40	56	1960	1.21	54	3603	1.94
	LA18	40	663	0.54	25	411	0.33		SE24	81	2101	1.43	70	2551	1.57
	LA02	24	775	0.49	28	958	0.60		LA35	91	8954	4.57	73	6747	3.47
	SE03	21	539	0.37	22	1048	0.60		LA36	67	3586	2.01	67	3804	2.11
	SE15	36	1943	1.09	29	1797	0.98		SE33	127	34277	16.19	97	21979	10.47
	SE18	43	3841	1.98	27	2821	1.43		SE36	50	1779	1.10	49	2847	1.57

Table I.8 SW-2 Park and Ang Damage Indices

		Undamped			Damped					Undamped			Damped		
	Record	δ_m mm	Energy kJ	D index	δ_m mm	Energy kJ	D index		Record	δ_m mm	Energy kJ	D index	δ_m mm	Energy kJ	D index
BSE-1	LA20	28	1188	0.17	24	1079	0.15	BSE-2	LA23	89	16273	0.70	52	8329	0.40
(Hard)	BO7	19	727	0.12	23	1145	0.14	(Med.)	LA24	58	5209	0.39	43	4179	0.29
	SE04	37	2104	0.23	22	2221	0.15		SE23	73	4070	0.46	65	4938	0.42
	LA12	49	2712	0.31	25	1596	0.16		LA31	123	15147	0.88	77	11312	0.57
	SE05	28	2533	0.19	21	2754	0.15		LA32	76	9225	0.54	78	9084	0.55
	SE06	33	2639	0.22	24	2445	0.16		SE28	106	32776	1.00	108	33434	1.02
	SE12	24	1731	0.16	22	2286	0.15		SE32	99	101281	1.81	60	45167	0.90
BSE-2	LA28	118	12474	0.81	72	4913	0.46	BSE-1	SE01	47	1884	0.28	39	1974	0.24
(Hard)	LA30	97	15835	0.74	65	11268	0.50	(Soft)	LA03	50	3033	0.31	55	3370	0.35
	LA39	75	9880	0.54	53	5235	0.36		LA15	69	6262	0.46	54	4614	0.36
	LA33	67	6754	0.46	49	5096	0.34		LA09	45	4290	0.30	42	3529	0.28
	SE39	59	22557	0.61	60	17687	0.56		LA10	64	9970	0.48	52	7582	0.38
	SE25	89	25286	0.81	60	17861	0.56		LA07	46	4585	0.31	33	3657	0.23
	SE30	115	84364	1.69	52	30973	0.68		SE07	64	13529	0.53	41	11943	0.38
BSE-1	LA13	38	2613	0.24	34	1551	0.21	BSE-2	LA38	65	9094	0.47	72	10332	0.53
(Med.)	LA14	26	1305	0.16	32	1369	0.20	(Soft)	LA40	121	23714	0.97	94	18610	0.75
	LA18	56	2821	0.35	40	1434	0.24		SE24	104	5358	0.65	87	7757	0.58
	LA02	35	3731	0.24	29	2903	0.20		LA35	95	10952	0.66	80	15542	0.64
	SE03	32	2445	0.21	23	2394	0.16		LA36	92	10626	0.65	79	13551	0.61
	SE15	34	5527	0.26	36	6575	0.28		SE33	157	82071	1.89	110	58733	1.35
	SE18	55	19095	0.54	33	8855	0.30		SE36	64	6457	0.44	60	10999	0.47

Table I.9 MF-1 Park and Ang Damage Indices

		Undamped			Damped					Undamped			Damped		
	Record	δ_m mm	Energy kJ	D index	δ_m mm	Energy kJ	D index		Record	δ_m mm	Energy kJ	D index	δ_m mm	Energy kJ	D index
BSE-1	LA20	116	463	0.11	83	189	0.08	BSE-2	LA23	645	8489	0.86	394	4097	0.48
(Hard)	BO7	74	197	0.07	65	183	0.06	(Med.)	LA24	675	7998	0.86	433	5336	0.56
	SE04	84	381	0.08	88	564	0.09		SE23	550	3627	0.60	441	3149	0.49
	LA12	73	404	0.08	53	235	0.05		LA31	700	16243	1.19	429	7294	0.63
	SE05	86	741	0.10	83	587	0.09		LA32	623	8774	0.85	498	4909	0.60
	SE06	98	760	0.11	81	528	0.09		SE28	633	15888	1.12	347	6138	0.52
	SE12	146	840	0.15	63	379	0.07		SE32	441	15184	0.94	293	10338	0.63
BSE-2	LA28	336	4126	0.44	287	1831	0.31	BSE-1	SE01	343	1950	0.36	297	2335	0.34
(Hard)	LA30	300	4523	0.42	261	2288	0.30	(Soft)	LA03	271	1542	0.28	295	1671	0.31
	LA39	464	4945	0.57	340	2355	0.37		LA15	356	3067	0.41	265	1126	0.26
	LA33	324	2504	0.36	243	1578	0.26		LA09	499	9855	0.79	266	2495	0.32
	SE39	478	10665	0.80	210	4202	0.33		LA10	511	12914	0.91	250	2888	0.32
	SE25	272	7395	0.50	178	3643	0.29		LA07	258	2660	0.32	180	1967	0.22
	SE30	402	9630	0.70	213	5149	0.37		SE07	302	9430	0.61	160	3549	0.27
BSE-1	LA13	219	1422	0.24	81	378	0.08	BSE-2	LA38	1092	21905	1.73	995	17958	1.50
(Med.)	LA14	203	1031	0.21	108	427	0.11	(Soft)	LA40	1250	35807	2.38	1012	23614	1.73
	LA18	160	933	0.17	138	370	0.13		SE24	888	15384	1.32	794	10766	1.07
	LA02	112	1144	0.14	128	679	0.13		LA35	1000	21284	1.63	718	12461	1.07
	SE03	140	1569	0.18	120	878	0.13		LA36	892	16109	1.35	690	9831	0.95
	SE15	162	2930	0.25	130	1106	0.15		SE33	762	27330	1.66	516	15687	1.02
	SE18	191	2181	0.24	81	1259	0.11		SE36	1061	30935	2.04	877	21589	1.54

Table I.10 MF-2 Park and Ang Damage Indices

		Undamped			Damped					Undamped			Damped		
	Record	δ_m mm	Energy kJ	D index	δ_m mm	Energy kJ	D index		Record	δ_m mm	Energy kJ	D index	δ_m mm	Energy kJ	D index
BSE-1	LA20	168	1197	0.18	107	677	0.11	BSE-2	LA23	719	23485	1.08	504	21531	0.85
(Hard)	BO7	97	713	0.10	76	502	0.08	(Med.)	LA24	962	37508	1.55	563	31563	1.08
	SE04	121	2264	0.15	124	1348	0.14		SE23	762	43549	1.47	501	23073	0.87
	LA12	64	962	0.08	74	884	0.08		LA31	535	17401	0.80	455	13329	0.66
	SE05	132	2690	0.17	87	1617	0.11		LA32	504	20161	0.82	454	15675	0.70
	SE06	140	2647	0.18	107	1840	0.13		SE28	505	29977	1.00	348	16915	0.62
	SE12	116	1584	0.14	75	1001	0.09		SE32	383	60919	1.43	303	39997	0.99
BSE-2	LA28	532	10598	0.68	424	7471	0.52	BSE-1	SE01	610	12641	0.79	509	14774	0.73
(Hard)	LA30	694	31367	1.20	632	24196	1.01	(Soft)	LA03	553	10577	0.70	486	9567	0.62
	LA39	568	16700	0.82	445	9202	0.57		LA15	390	5050	0.45	295	3855	0.34
	LA33	843	26509	1.25	714	19059	1.00		LA09	419	13325	0.62	349	7983	0.46
	SE39	458	30009	0.95	313	18790	0.62		LA10	344	15473	0.59	306	8736	0.44
	SE25	417	26849	0.86	314	14600	0.55		LA07	419	29083	0.90	300	13092	0.51
	SE30	345	23463	0.73	248	16574	0.52		SE07	257	12989	0.47	163	9798	0.32
BSE-1	LA13	178	2624	0.21	122	1328	0.14	BSE-2	LA38	1771	81602	3.08	1560	69037	2.66
(Med.)	LA14	177	3522	0.23	156	1308	0.17	(Soft)	LA40	2126	189422	5.31	1699	125600	3.79
	LA18	253	2398	0.28	190	1253	0.20		SE24	1870	133363	4.09	1187	83457	2.57
	LA02	190	4150	0.25	163	2832	0.20		LA35	1798	159330	4.48	1413	107142	3.20
	SE03	295	12035	0.49	125	3009	0.17		LA36	1972	165172	4.74	1188	110111	3.05
	SE15	238	7721	0.36	189	4531	0.25		SE33	1518	159680	4.23	1078	104803	2.85
	SE18	164	5313	0.25	81	3807	0.14		SE36	997	40055	1.63	727	30234	1.21

Table I.11 BF-1 Fardis Damage Indices

		Undamped			Damped					Undamped			Damped		
	Record	E_d	dE_h	D_E	E_d	dE_h	D_E		Record	E_d	dE_h	D_E	E_d	dE_h	D_E
BSE-1	LA20	24	61	1.23	24	56	1.16	BSE-2	LA23	24	70	1.35	24	110	1.88
(Hard)	BO7	24	25	0.74	24	28	0.78	(Med.)	LA24	24	37	0.91	24	82	1.51
	SE04	24	70	1.35	24	55	1.15		SE23	24	170	2.69	24	188	2.93
	LA12	24	85	1.55	24	81	1.49		LA31	24	599	8.44	24	472	6.73
	SE05	24	65	1.28	24	79	1.47		LA32	24	899	12.46	24	537	7.60
	SE06	24	127	2.11	24	109	1.87		SE28	24	1525	20.84	24	1033	14.25
	SE12	24	81	1.49	24	64	1.27		SE32	24	1583	21.62	24	1485	20.31
BSE-2	LA28	24	96	1.69	24	80	1.48	BSE-1	SE01	24	150	2.42	24	102	1.77
(Hard)	LA30	24	1075	14.82	24	514	7.30	(Soft)	LA03	24	87	1.58	24	56	1.16
	LA39	24	104	1.80	24	112	1.91		LA15	24	99	1.74	24	81	1.50
	LA33	24	266	3.97	24	131	2.17		LA09	24	79	1.47	24	73	1.38
	SE39	24	829	11.51	24	487	6.93		LA10	24	298	4.41	24	192	2.98
	SE25	24	645	9.06	24	479	6.83		LA07	24	124	2.07	24	124	2.07
	SE30	24	1678	22.89	24	1048	14.45		SE07	24	342	4.99	24	240	3.62
BSE-1	LA13	24	109	1.87	24	67	1.31	BSE-2	LA38	24	220	3.36	24	177	2.78
(Med.)	LA14	24	57	1.18	24	39	0.94	(Soft)	LA40	24	232	3.52	24	197	3.06
	LA18	24	22	0.70	24	26	0.75		SE24	24	237	3.58	24	202	3.12
	LA02	24	115	1.95	24	112	1.90		LA35	24	1128	15.52	24	573	8.09
	SE03	24	111	1.90	24	84	1.54		LA36	24	270	4.02	24	185	2.89
	SE15	24	176	2.77	24	188	2.93		SE33	24	1947	26.49	24	1201	16.50
	SE18	24	380	5.50	24	339	4.96		SE36	24	217	3.32	24	207	3.19

Table I.12 BF-2 Fardis Damage Indices

		Undamped			Damped					Undamped			Damped		
	Record	E_d	dE_h	D_E	E_d	dE_h	D_E		Record	E_d	dE_h	D_E	E_d	dE_h	D_E
BSE-1	LA20	62	265	0.07	31	203	0.04	BSE-2	LA23	106	415	0.11	100	534	0.12
(Hard)	BO7	39	194	0.05	21	120	0.03	(Med.)	LA24	61	267	0.07	73	399	0.09
	SE04	79	356	0.09	44	225	0.05		SE23	353	1649	0.40	177	1548	0.31
	LA12	58	352	0.08	66	294	0.07		LA31	486	5601	1.08	191	4630	0.81
	SE05	54	522	0.10	32	448	0.08		LA32	424	3075	0.65	275	3312	0.63
	SE06	43	595	0.11	34	568	0.10		SE28	414	7172	1.30	244	6088	1.06
	SE12	43	379	0.08	32	235	0.05		SE32	138	3859	0.66	213	4505	0.80
BSE-2	LA28	253	931	0.25	124	532	0.13	BSE-1	SE01	54	212	0.05	67	301	0.07
(Hard)	LA30	207	1852	0.37	164	1549	0.31	(Soft)	LA03	76	212	0.06	47	226	0.05
	LA39	162	1051	0.23	94	743	0.15		LA15	100	585	0.13	56	371	0.08
	LA33	224	1411	0.31	110	638	0.14		LA09	49	364	0.08	78	386	0.09
	SE39	258	5835	1.02	97	2226	0.39		LA10	122	1160	0.23	97	1081	0.21
	SE25	332	5208	0.95	164	2752	0.50		LA07	84	712	0.15	82	603	0.13
	SE30	288	7650	1.32	177	5491	0.94		SE07	126	2318	0.42	68	1528	0.27
BSE-1	LA13	84	557	0.12	47	497	0.10	BSE-2	LA38	108	787	0.17	148	805	0.18
(Med.)	LA14	75	300	0.08	32	290	0.06	(Soft)	LA40	125	601	0.14	135	827	0.18
	LA18	75	211	0.06	51	164	0.05		SE24	312	1567	0.37	294	1066	0.28
	LA02	52	401	0.08	45	452	0.09		LA35	288	3355	0.64	227	2231	0.44
	SE03	67	476	0.10	44	432	0.09		LA36	266	2050	0.43	216	1660	0.35
	SE15	61	662	0.13	43	762	0.14		SE33	641	15666	2.73	473	8878	1.59
	SE18	87	1732	0.31	53	1422	0.25		SE36	92	882	0.18	134	999	0.21

Table I.13 BF-3 Fardis Damage Indices

		Undamped			Damped					Undamped			Damped		
	Record	E_d	dE_h	D_E	E_d	dE_h	D_E		Record	E_d	dE_h	D_E	E_d	dE_h	D_E
BSE-1	LA20	104	231	0.34	67	263	0.32	BSE-2	LA23	542	3252	3.63	317	1489	1.75
(Hard)	BO7	51	131	0.18	53	203	0.25	(Med.)	LA24	301	913	1.21	207	743	0.94
	SE04	147	366	0.52	71	382	0.44		SE23	422	833	1.30	363	1023	1.39
	LA12	259	482	0.77	90	360	0.44		LA31	761	2891	3.59	447	2140	2.51
	SE05	119	537	0.64	82	553	0.60		LA32	444	1889	2.28	529	1852	2.36
	SE06	157	537	0.69	105	583	0.66		SE28	707	6871	7.09	757	6012	6.39
	SE12	82	363	0.43	90	421	0.50		SE32	595	17748	16.70	394	8044	7.73
BSE-2	LA28	761	2579	3.31	473	1047	1.56	BSE-1	SE01	230	343	0.61	160	316	0.49
(Hard)	LA30	610	2776	3.29	320	1910	2.13	(Soft)	LA03	263	621	0.90	312	565	0.92
	LA39	443	1994	2.37	289	1021	1.30		LA15	413	1268	1.68	284	697	1.00
	LA33	384	1396	1.76	247	990	1.21		LA09	221	875	1.07	230	639	0.88
	SE39	318	4325	4.30	289	2872	2.95		LA10	385	2051	2.34	237	1252	1.43
	SE25	586	5363	5.58	385	3231	3.40		LA07	226	874	1.08	136	699	0.81
	SE30	761	15185	14.62	345	5550	5.43		SE07	368	2880	3.07	227	2161	2.24
BSE-1	LA13	184	528	0.72	190	297	0.52	BSE-2	LA38	353	1571	1.87	435	1775	2.16
(Med.)	LA14	97	292	0.39	127	256	0.40	(Soft)	LA40	761	4360	4.91	503	3077	3.42
	LA18	311	583	0.93	172	249	0.45		SE24	686	1105	1.89	598	1410	2.05
	LA02	167	736	0.88	107	516	0.60		LA35	659	2354	2.98	480	2928	3.26
	SE03	139	436	0.57	97	388	0.48		LA36	595	2199	2.75	493	2616	2.99
	SE15	160	1100	1.20	173	1125	1.24		SE33	761	16239	15.56	757	11282	11.11
	SE18	289	3437	3.46	156	1470	1.52		SE36	371	1281	1.64	331	1917	2.15

Table I.14 BF-4 Fardis Damage Indices

		Undamped			Damped					Undamped			Damped		
	Record	E_d	dE_h	D_E	E_d	dE_h	D_E		Record	E_d	dE_h	D_E	E_d	dE_h	D_E
BSE-1	LA20	150	479	0.21	104	253	0.12	BSE-2	LA23	1596	12508	4.58	903	4004	1.62
(Hard)	BO7	146	322	0.16	50	229	0.09	(Med.)	LA24	1486	13970	5.01	765	3630	1.45
	SE04	157	444	0.20	122	513	0.21		SE23	1360	9272	3.47	1055	3497	1.51
	LA12	288	929	0.41	94	433	0.17		LA31	1712	11139	4.19	900	3476	1.45
	SE05	273	1183	0.48	98	699	0.26		LA32	2043	15545	5.72	1050	4685	1.89
	SE06	448	1570	0.67	97	642	0.24		SE28	2007	18337	6.59	1325	9836	3.63
	SE12	411	969	0.46	97	480	0.19		SE32	1834	79509	25.96	975	23050	7.70
BSE-2	LA28	984	2048	1.03	793	1339	0.73	BSE-1	SE01	848	1641	0.85	804	1384	0.75
(Hard)	LA30	982	5734	2.20	864	3417	1.42	(Soft)	LA03	748	1539	0.77	667	960	0.56
	LA39	950	3084	1.34	699	2520	1.07		LA15	852	1362	0.76	677	955	0.56
	LA33	933	3731	1.54	550	1493	0.68		LA09	699	2445	1.04	497	1296	0.60
	SE39	832	4588	1.78	474	3395	1.26		LA10	578	1951	0.84	422	1579	0.66
	SE25	1134	11807	4.18	781	5574	2.07		LA07	916	3308	1.40	651	1797	0.82
	SE30	1341	21275	7.27	799	11323	3.90		SE07	790	5727	2.12	441	3230	1.19
BSE-1	LA13	564	1112	0.57	325	478	0.28	BSE-2	LA38	1274	5388	2.20	1239	5849	2.33
(Med.)	LA14	685	1002	0.58	220	398	0.21	(Soft)	LA40	826	2659	1.16	957	4901	1.92
	LA18	436	463	0.31	208	347	0.19		SE24	1481	4545	2.01	1267	4367	1.87
	LA02	657	1857	0.84	245	1097	0.44		LA35	2142	17286	6.31	1642	12481	4.59
	SE03	793	3093	1.29	220	1013	0.41		LA36	2403	17063	6.34	1614	11470	4.26
	SE15	488	2952	1.12	298	1825	0.69		SE33	1078	14252	4.94	925	10895	3.82
	SE18	660	4814	1.78	137	2664	0.90		SE36	1507	12763	4.63	1097	7365	2.76

Table I.15 BF-5 Fardis Damage Indices

		Undamped			Damped					Undamped			Damped		
	Record	E_d	dE_h	D_E	E_d	dE_h	D_E		Record	E_d	dE_h	D_E	E_d	dE_h	D_E
BSE-1	LA20	315	346	0.10	113	216	0.05	BSE-2	LA23	3068	6094	1.30	2979	4429	1.08
(Hard)	BO7	81	287	0.05	70	188	0.04	(Med.)	LA24	3632	5299	1.30	2602	3413	0.88
	SE04	453	1074	0.21	81	432	0.07		SE23	5192	7371	1.83	3546	4626	1.20
	LA12	183	585	0.10	93	331	0.06		LA31	4182	8771	1.82	1843	5455	1.00
	SE05	234	1224	0.19	113	589	0.09		LA32	4699	8598	1.89	3251	5483	1.25
	SE06	244	825	0.14	74	501	0.07		SE28	3922	12160	2.19	1886	6900	1.18
	SE12	279	642	0.13	62	493	0.07		SE32	8156	46947	7.21	3881	23198	3.54
BSE-2	LA28	1545	2359	0.57	1092	1645	0.40	BSE-1	SE01	1590	1329	0.45	1484	1355	0.43
(Hard)	LA30	1228	5168	0.85	1303	4019	0.73	(Soft)	LA03	2589	3539	0.90	1650	1372	0.46
	LA39	2404	4034	0.92	1893	2654	0.66		LA15	2685	4278	1.00	1714	1479	0.49
	LA33	2594	4159	0.97	1468	2516	0.57		LA09	1958	2810	0.69	1736	2572	0.63
	SE39	2865	14287	2.26	1292	5718	0.93		LA10	2636	3158	0.86	861	3413	0.57
	SE25	2110	12225	1.87	1463	6049	1.00		LA07	2362	3493	0.85	1067	2233	0.46
	SE30	2075	15306	2.25	834	7748	1.10		SE07	3615	14588	2.43	815	5274	0.79
BSE-1	LA13	867	765	0.25	221	486	0.10	BSE-2	LA38	8569	25702	4.68	8156	16521	3.48
(Med.)	LA14	782	896	0.25	261	480	0.11	(Soft)	LA40	5106	12958	2.50	4176	10384	2.02
	LA18	364	534	0.13	301	375	0.10		SE24	7990	6591	2.24	5961	7177	1.95
	LA02	989	1696	0.38	183	854	0.14		LA35	3876	6229	1.46	3404	6823	1.45
	SE03	1015	2944	0.54	413	1003	0.20		LA36	4858	6770	1.70	4080	8220	1.74
	SE15	657	2883	0.47	464	1834	0.31		SE33	7770	34981	5.67	4693	16999	2.92
	SE18	516	3465	0.52	174	1489	0.21		SE36	15505	64259	10.64	8711	19773	3.98

Table I.16 EBF-1 Fardis Damage Indices

		Undamped			Damped					Undamped			Damped		
	Record	E_d	dE_h	D_E	E_d	dE_h	D_E		Record	E_d	dE_h	D_E	E_d	dE_h	D_E
BSE-1	LA20	95	234	0.00	54	220	0.00	BSE-2	LA23	907	3265	0.05	473	2198	0.03
(Hard)	BO7	75	160	0.00	24	125	0.00	(Med.)	LA24	697	4627	0.05	330	1424	0.02
	SE04	102	325	0.01	60	313	0.00		SE23	891	1701	0.04	710	1354	0.03
	LA12	220	606	0.01	114	359	0.01		LA31	798	3472	0.05	649	1839	0.03
	SE05	173	591	0.01	86	549	0.01		LA32	874	3696	0.05	639	2123	0.03
	SE06	154	686	0.01	63	516	0.01		SE28	1871	12053	0.14	938	5328	0.06
	SE12	258	637	0.01	53	274	0.00		SE32	1296	23156	0.20	690	12584	0.11
BSE-2	LA28	716	2151	0.04	564	1502	0.03	BSE-1	SE01	498	800	0.02	469	1071	0.02
(Hard)	LA30	949	3340	0.05	566	2248	0.03	(Soft)	LA03	336	647	0.01	380	796	0.02
	LA39	903	4993	0.06	458	1565	0.02		LA15	424	658	0.02	338	671	0.01
	LA33	395	887	0.02	303	635	0.01		LA09	415	1163	0.02	312	1032	0.02
	SE39	497	2623	0.03	332	2181	0.03		LA10	391	1414	0.02	280	1474	0.02
	SE25	912	5904	0.07	508	3856	0.04		LA07	592	1768	0.03	320	1384	0.02
	SE30	772	15466	0.13	451	8824	0.08		SE07	382	2613	0.03	249	2092	0.02
BSE-1	LA13	394	883	0.02	189	273	0.01	BSE-2	LA38	726	2302	0.04	761	3984	0.05
(Med.)	LA14	209	368	0.01	142	233	0.01	(Soft)	LA40	519	1667	0.03	542	3936	0.04
	LA18	251	486	0.01	141	249	0.01		SE24	882	2025	0.04	619	2727	0.04
	LA02	395	1302	0.02	168	698	0.01		LA35	1419	6521	0.09	878	5614	0.07
	SE03	416	1681	0.02	121	527	0.01		LA36	1032	5213	0.07	671	4429	0.05
	SE15	107	1000	0.01	150	1198	0.01		SE33	721	6163	0.06	622	6529	0.06
	SE18	275	3501	0.03	96	1788	0.02		SE36	719	2650	0.04	686	2801	0.04

Table I.17 SW-1 Fardis Damage Indices

		Undamped			Damped					Undamped			Damped		
	Record	E_d	dE_h	D_E	E_d	dE_h	D_E		Record	E_d	dE_h	D_E	E_d	dE_h	D_E
BSE-1	LA20	119	299	0.19	83	365	0.18	BSE-2	LA23	273	2281	0.96	248	1629	0.73
(Hard)	BO7	67	257	0.14	73	219	0.13	(Med.)	LA24	153	698	0.35	163	1315	0.56
	SE04	150	612	0.32	71	418	0.19		SE23	410	3298	1.40	283	1693	0.78
	LA12	156	438	0.26	101	533	0.25		LA31	513	5155	2.10	386	4002	1.62
	SE05	134	981	0.43	86	692	0.29		LA32	377	3163	1.33	408	3554	1.49
	SE06	150	916	0.42	100	836	0.35		SE28	667	14702	5.39	377	8664	3.17
	SE12	123	777	0.35	99	522	0.25		SE32	295	9126	3.26	306	11630	4.10
BSE-2	LA28	503	2931	1.35	350	1331	0.71	BSE-1	SE01	140	446	0.25	153	439	0.26
(Hard)	LA30	377	2957	1.27	233	2395	0.97	(Soft)	LA03	214	904	0.46	171	508	0.30
	LA39	366	1967	0.93	189	1244	0.56		LA15	240	1826	0.79	187	760	0.39
	LA33	393	3715	1.53	188	1054	0.49		LA09	145	826	0.38	171	748	0.38
	SE39	387	8720	3.19	196	3358	1.26		LA10	223	2105	0.87	148	1294	0.54
	SE25	503	9790	3.63	239	4035	1.52		LA07	147	1115	0.48	140	1082	0.46
	SE30	538	16969	6.05	231	7327	2.61		SE07	223	3765	1.42	164	2559	0.97
BSE-1	LA13	178	618	0.34	118	650	0.30	BSE-2	LA38	266	1643	0.75	322	2368	1.03
(Med.)	LA14	129	449	0.25	141	478	0.26	(Soft)	LA40	316	1960	0.89	302	3603	1.43
	LA18	216	663	0.38	125	411	0.23		SE24	483	2101	1.06	410	2551	1.16
	LA02	119	775	0.35	140	958	0.42		LA35	549	8954	3.39	426	6747	2.56
	SE03	100	539	0.25	107	1048	0.43		LA36	389	3586	1.49	388	3804	1.56
	SE15	189	1943	0.79	146	1797	0.71		SE33	801	34277	12.00	594	21979	7.76
	SE18	232	3841	1.45	139	2821	1.04		SE36	281	1779	0.80	272	2847	1.15

Table I.18 SW-2 Fardis Damage Indices

		Undamped			Damped					Undamped			Damped		
	Record	E_d	dE_h	D_E	E_d	dE_h	D_E		Record	E_d	dE_h	D_E	E_d	dE_h	D_E
BSE-1	LA20	4010	1188	0.11	3318	1079	0.09	BSE-2	LA23	15345	16273	0.54	8475	8329	0.29
(Hard)	BO7	2540	727	0.07	3092	1145	0.09	(Med.)	LA24	9452	5209	0.28	6764	4179	0.21
	SE04	5715	2104	0.16	2945	2221	0.09		SE23	12265	4070	0.34	10814	4938	0.32
	LA12	7872	2712	0.22	3493	1596	0.10		LA31	22266	15147	0.70	13161	11312	0.44
	SE05	4105	2533	0.13	2836	2754	0.10		LA32	12932	9225	0.41	13261	9084	0.42
	SE06	5028	2639	0.15	3315	2445	0.11		SE28	18844	32776	0.78	19090	33434	0.80
	SE12	3423	1731	0.10	2905	2286	0.09		SE32	17366	101281	1.41	9962	45167	0.68
BSE-2	LA28	21108	12474	0.64	12202	4913	0.35	BSE-1	SE01	7425	1884	0.20	6235	1974	0.17
(Hard)	LA30	17021	15835	0.58	10836	11268	0.38	(Soft)	LA03	7994	3033	0.23	9401	3370	0.27
	LA39	12776	9880	0.41	8632	5235	0.26		LA15	11595	6262	0.35	8215	4614	0.25
	LA33	11215	6754	0.34	7926	5096	0.25		LA09	7052	4290	0.22	6465	3529	0.19
	SE39	9812	22557	0.46	9973	17687	0.42		LA10	10739	9970	0.36	7745	7582	0.27
	SE25	15489	25286	0.63	9866	17861	0.42		LA07	7250	4585	0.22	5560	3657	0.17
	SE30	20590	84364	1.32	8495	30973	0.51		SE07	10677	13529	0.40	7293	11943	0.30
BSE-1	LA13	5768	2613	0.17	5086	1551	0.14	BSE-2	LA38	10770	9094	0.36	13448	10332	0.43
(Med.)	LA14	3645	1305	0.10	4772	1369	0.13	(Soft)	LA40	21804	23714	0.77	13456	18610	0.51
	LA18	9155	2821	0.25	6302	1434	0.17		SE24	18378	5358	0.51	15050	7757	0.45
	LA02	5376	3731	0.17	4282	2903	0.13		LA35	16522	10952	0.52	12558	15542	0.46
	SE03	4817	2445	0.14	3090	2394	0.10		LA36	16090	10626	0.50	13945	13551	0.48
	SE15	5129	5527	0.18	5504	6575	0.20		SE33	29149	82071	1.51	19393	58733	1.05
	SE18	8931	19095	0.41	5029	8855	0.21		SE36	10579	6457	0.32	10777	10999	0.37

Table I.19 MF-1 Fardis Damage Indices

		Undamped			Damped					Undamped			Damped		
	Record	E_d	dE_h	D_E	E_d	dE_h	D_E		Record	E_d	dE_h	D_E	E_d	dE_h	D_E
BSE-1	LA20	241	463	0.03	126	189	0.01	BSE-2	LA23	5307	8489	0.63	2373	4097	0.29
(Hard)	BO7	100	197	0.01	76	183	0.01	(Med.)	LA24	5711	7998	0.65	2769	5336	0.36
	SE04	128	381	0.02	139	564	0.03		SE23	4097	3627	0.41	2855	3149	0.30
	LA12	96	404	0.02	51	235	0.01		LA31	6059	16243	0.90	2730	7294	0.41
	SE05	134	741	0.03	124	587	0.03		LA32	5023	8774	0.62	3490	4909	0.40
	SE06	174	760	0.03	118	528	0.02		SE28	5151	15888	0.83	1914	6138	0.31
	SE12	383	840	0.05	71	379	0.02		SE32	2856	15184	0.64	1432	10338	0.39
BSE-2	LA28	1813	4126	0.25	1376	1831	0.15	BSE-1	SE01	1875	1950	0.19	1465	2335	0.17
(Hard)	LA30	1492	4523	0.24	1164	2288	0.15	(Soft)	LA03	1240	1542	0.14	1450	1671	0.15
	LA39	3106	4945	0.37	1847	2355	0.20		LA15	2000	3067	0.23	1192	1126	0.12
	LA33	1707	2504	0.20	1017	1578	0.12		LA09	3502	9855	0.54	1206	2495	0.16
	SE39	3261	10665	0.54	779	4202	0.17		LA10	3632	12914	0.63	1076	2888	0.16
	SE25	1249	7395	0.30	568	3643	0.14		LA07	1135	2660	0.16	582	1967	0.10
	SE30	2452	9630	0.45	796	5149	0.20		SE07	1509	9430	0.37	462	3549	0.13
BSE-1	LA13	841	1422	0.10	118	378	0.02	BSE-2	LA38	11764	21905	1.49	10269	17958	1.27
(Med.)	LA14	732	1031	0.08	209	427	0.03	(Soft)	LA40	14352	35807	2.07	10531	23614	1.44
	LA18	461	933	0.06	346	370	0.04		SE24	8691	15384	1.08	7366	10766	0.85
	LA02	227	1144	0.05	295	679	0.04		LA35	10344	21284	1.36	6304	12461	0.82
	SE03	354	1569	0.07	258	878	0.04		LA36	8751	16109	1.10	5927	9831	0.72
	SE15	475	2930	0.12	305	1106	0.05		SE33	6915	27330	1.28	3696	15687	0.71
	SE18	652	2181	0.11	119	1259	0.04		SE36	11279	30935	1.70	8546	21589	1.24

Table I.20 MF-2 Fardis Damage Indices

		Undamped			Damped					Undamped			Damped		
	Record	E_d	dE_h	D_E	E_d	dE_h	D_E		Record	E_d	dE_h	D_E	E_d	dE_h	D_E
BSE-1	LA20	1112	1197	0.06	453	677	0.03	BSE-2	LA23	15849	23485	0.98	9207	21531	0.71
(Hard)	BO7	373	713	0.03	227	502	0.02	(Med.)	LA24	23928	37508	1.52	10962	31563	0.95
	SE04	583	2264	0.06	610	1348	0.05		SE23	17235	43549	1.39	9127	23073	0.74
	LA12	162	962	0.02	218	884	0.02		LA31	10125	17401	0.67	7768	13329	0.51
	SE05	691	2690	0.07	300	1617	0.04		LA32	9212	20161	0.69	7753	15675	0.55
	SE06	775	2647	0.07	449	1840	0.05		SE28	9247	29977	0.86	4778	16915	0.47
	SE12	536	1584	0.05	223	1001	0.03		SE32	5735	60919	1.29	3629	39997	0.85
BSE-2	LA28	10038	10598	0.54	6883	7471	0.38	BSE-1	SE01	12420	12641	0.66	9366	14774	0.60
(Hard)	LA30	15037	31367	1.09	13090	24196	0.90	(Soft)	LA03	10667	10577	0.57	8665	9567	0.48
	LA39	11111	16700	0.69	7492	9202	0.43		LA15	5934	5050	0.30	3437	3855	0.19
	LA33	19916	26509	1.18	15692	19059	0.89		LA09	6748	13325	0.48	4794	7983	0.31
	SE39	7855	30009	0.82	3872	18790	0.47		LA10	4672	15473	0.44	3711	8736	0.29
	SE25	6700	26849	0.72	3903	14600	0.40		LA07	6749	29083	0.76	3568	13092	0.36
	SE30	4707	23463	0.59	2427	16574	0.38		SE07	2616	12989	0.33	1055	9798	0.21
BSE-1	LA13	1257	2624	0.09	594	1328	0.04	BSE-2	LA38	28371	81602	2.46	28371	69037	2.24
(Med.)	LA14	1244	3522	0.11	959	1308	0.06	(Soft)	LA40	28371	189422	4.40	28371	125600	3.25
	LA18	2534	2398	0.13	1423	1253	0.07		SE24	28371	133363	3.39	28371	83457	2.50
	LA02	1423	4150	0.12	1050	2832	0.09		LA35	28371	159330	3.86	28371	107142	2.92
	SE03	3453	12035	0.34	619	3009	0.08		LA36	28371	165172	3.96	28371	110111	2.97
	SE15	2237	7721	0.22	1410	4531	0.13		SE33	28371	159680	3.86	28016	104803	2.87
	SE18	1067	5313	0.13	258	3807	0.08		SE36	25150	40055	1.60	16105	30234	1.11

APPENDIX J

GROUND MOTION SCALING FACTORS

Chapter 3 summarizes the ground motions utilized for the Basic Safety Objective analyses for the linear and nonlinear analysis methods of Chapter 6. To address a broad-based approach for a realistic ground motion suite, motions for Basic Safety Earthquake 1 and Basic Safety Earthquake 2 were selected for hard, medium and soft conditions as characterized in contemporary building codes. Following code prescribed procedures, the ground motions were scaled to match the code prescribed design spectrum. The results of this scaling can be observed in Figures 3.23 through 3.34. Table J.1 summarizes the scale factors utilized to modify the selected ground motions to coincide with the design spectra.

Table J.1 Scaling Factors of Acceleration Records for Basic Safety Objective

Suite	Record	Scale Factor	Suite	Record	Scale Factor
BSE-1 Hard	LA20	0.227	BSE-2 Medium	LA23	1.293
	BO7	3.170		LA24	0.730
	SE04	0.567		SE23	1.148
	LA12	0.364		LA31	0.639
	SE05	0.541		LA32	0.622
	SE06	0.613		SE28	0.799
	SE12	0.429		SE32	0.907
BSE-2 Hard	LA28	0.417	BSE-1 Soft	SE01	2.289
	LA30	0.670		LA03	1.025
	LA39	0.862		LA15	0.755
	LA33	0.557		LA09	0.701
	SE39	0.946		LA10	1.007
	SE25	0.732		LA07	1.171
	SE30	0.471		SE07	1.087
BSE-1 Medium	LA13	0.387	BSE-2 Soft	LA38	1.202
	LA14	0.348		LA40	1.401
	LA18	0.322		SE24	1.715
	LA02	0.450		LA35	0.920
	SE03	0.773		LA36	0.852
	SE15	1.142		SE33	1.289
	SE18	0.526		SE36	0.983

REFERENCES

1. FEMA, and NEHRP (2006). *Next-Generation Performance-Based Seismic Design Guidelines Program Plan for New and Existing Buildings – FEMA 445*, Federal Emergency Management Agency, Washington, D.C.

2. American Society of Civil Engineers, and Structural Engineering Institute (2005). *Minimum Design Loads for Buildings and Other Structures - ASCE* **7**, American Society of Civil Engineers.

3. Daniels, M. A. (2006). *Performance of Eight Buckling Restrained Braces, M. Sc. Thesis,* University of Utah Department of Civil and Environmental Engineering, Salt Lake City, UT.

4. Romero, P., and Reaveley, L. D., and Miller, P. J., and Okahashi, T. (2006). *Full Scale Testing of WC Series Buckling-Restrained Braces*, University of Utah Department of Civil and Environmental Engineering, Salt Lake City, UT.

5. Ross, T. (2009). *Perforated Plate Dampers with Added Secondary Stiffness, Ph.D Dissertation,* University of Utah Department of Civil and Environmental Engineering, Salt Lake City, UT.

6. Goel, S. C., and Chao, S. H. (2008). *Performance-Based Plastic Design Volume 1 – Earthquake Resistant Steel Structures (Draft Copy)*, ICC.

7. Okada (2007). "Energy Balance Seismic Design –Application of Seismic Design Based on Energy Balance in Steel Construction", *Steel Construction Today and Tomorrow,* 18, 10-15.

8. Naeim, F., and Kelley, J. M. (1999) *Design of Seismic Isolated Structures: From Theory to Practice*, Wiley, New York.

9. Chopra, A. K. (1995). *Dynamics of Structures Chapter 20 Earthquake Dynamics of Base Isolated Buildings*, 683-702, Prentice Hall, Upper Saddle River, New Jersey.

10. Johnson, J. G. (1999). *A New Approach to Passive Tuned Mass Dampers, M. Sc. Thesis,* University of Utah Department of Civil and Environmental Engineering, Salt Lake City, UT.

11. Johnson, J. G., and Pantelides, C. P., and Reaveley, L. D. (2003). "A Rooftop Tuned Mass Damper Frame", *Earthquake Engineering & Structural Dynamics*, 32, 965-984.

12. Chopra, A. K. (1995). *Dynamics of Structures Chapter 12 Dynamic Analysis and Response of Linear Systems*, 429-466, Prentice Hall, Upper Saddle River, New Jersey.

13. Chopra, A. K. (1995). *Dynamics of Structures Chapter 12.2 Vibration Absorber or Tuned Mass Dampers*, 432, Prentice Hall, Upper Saddle River, New Jersey.

14. Robinson, J. K., and Gamble, S. L., and Myslimaj, B. M. (2007). "Supplemental Damping and Using Tuned Sloshing Dampers", *Structure Magazine*, June, 2007, 14-18.

15. Brock, J. E. (1946). "A Note on the Damped Vibration Absorber", *Journal of Applied Mechanics*, ASME 13, A-284.

16. Den Hartog, J. P. (1956). *Mechanical* Vibrations, 4th Ed., McGraw-Hill, New York.

17. Kaynia, A. M. and Veneziano, D., Biggs, J. M. (1981). "Seismic Effectiveness of Tuned Mass Dampers", *Journal of the Structural Division*, ASCE (107), 1465-1484.

18. Sladek, J. R., and Klingner, R. E. (1983). "Effect of Tuned Mass Dampers on Seismic Response", *Journal of Structural Engineering*, ASCE (109), 2004-2009.

19. Wong, K. F., and Johnson, J. G. (2009). "Seismic Energy Dissipation of Inelastic Structures with Multiple Tuned Mass Dampers", *Journal of Engineering Mechanics*, 135(4), 265-275.

20. Nawrotski, P. (2006). "Tuned-Mass Systems for the Seismic Retrofit of Buildings", *Seventh International Congress on Advances in Civil Engineering*, Istanbul, Turkey.

21. Villaverde, R. (1998). "Roof Isolation System to Reduce Seismic Response of Buildings: A Preliminary Assessment", *Earthquake Spectra*, 14(3), 521-532.

22. Villaverde, R., and Aguirre, M., and Hamilton, C. (2005). "Aseismic Roof Isolation System Built with Steel Oval Elements: Exploratory Study", *Earthquake Spectra*, 21(1), 225-241.

23. Modern Steel Construction (2009), "The Addition at 185 Berry Street (China Basin Landing) – San Francisco", *Modern Steel Construction*, May.

24. International Conference of Building Officials (1988, 1991, 1994, 1997). *Uniform Building Code UBC*, International Conference of Building Officials, Whittier, California.

25. International Code Council (2000, 2003, 2006). *International Building Code IBC*, International Code Council, Whittier, California.

26. SAC Joint Venture Steel Project Phase 2, (1997). "Develop Suites of Time Histories", *Project 5.4.1, Draft Report*, http://nisee.berkeley.edu/data/strong_motion/sacsteel/draftreport.html.

27. Hussain, S. and Van Benshoten, P., and Al Satari, M., and Lin, S. (2005). "Buckling Restrained Braced Frame (BRBF) Structures: Analysis, Design and Approvals Issues", *Nippon Steel News*, 333.

28. American Society of Civil Engineers, and Structural Engineering Institute (2006). *Seismic Rehabilitation of Existing Buildings – ASCE 41*, American Society of Civil Engineers.

29. Pacific Earthquake Engineering Research Center, "PEER Ground Motion Database", http://peer.berkeley.edu/peer_ground_motion_database.

30. Park, Y., and Ang, A. (1985). "Mechanistic Seismic Damage Model for Reinforced Concrete", *Journal of Structural Engineering*, ASCE 111(4), 722-739.

31. Amador Teran-Gilmore (2004). **"**On the Use of Spectra to Establish Damage Control in Regular Frames during Global Predesign", *Earthquake Spectra*, 20(3), 995-1020.

32. Park, Y., and Ang, A., and Wen, Y. (1985). "Seismic Damage Analysis of Reinforced Concrete Buildings", *Journal of Structural Engineering*, ASCE 111(4), 740-757.

33. Fardis, M. (1995). "Damage Measures and Failure Criteria for Reinforced Concrete Members", *10th European Conference on Earthquake Engineering*, Vienna, Austria, 1377-1382.

34. Priestley, and Seible, and Calvi (1996). *Seismic Design and Retrofit of Bridges Chapter 4 Modeling and Analysis*, 173-177, Wiley, New York.

35. Fahnestock, and Ricles, and Sause (2007). "Experimental Evaluation of Large-Scale Buckling-Restrained Braced Frame", *Journal of Structural Engineering* - ASCE, September*,* 1205-1214.

36. Bray, J, and Rodriguez-Marek, A. (2004). "Characterization of Forward-Directivity Ground Motions in the Near-Fault Region", *Soil Dynamics and Earthquake Engineering*, 24, 815-828.

37. American Institute of Steel Construction (2006). *AISC Seismic Design Manual Appendix T Qualifying Cyclic Tests of Buckling-Restrained Braces*, American Institute of Steel Construction.

38. Mahoney, M. (2011). "The Japan Earthquake & Tsunami and What They Mean for the U.S.", March 17, http://nthmp.tsunami.gov/taw/downloads/japan-earthquake-3-17-2011.pdf.

39. Cohen, J. M. (1991). "Cladding Design: Whose Responsibility", *Journal of Performance Constructed Facilities*, 5(3), 208-217.

40. Davaran, A. and Adelzadeh, M. (2009). "An Improved Non-Linear Physical Modeling Method for Brace Elements", Sharif University of Technology Civil Engineering, 16(1), 58-64, (2009).